NASA Conference Publication 3163
Part 2

Tenth Workshop for Computational Fluid Dynamic Applications in Rocket Propulsion

Compiled by
R. W. Williams
George C. Marshall Space Flight Center
Marshall Space Flight Center, Alabama

Proceedings of a workshop held at
NASA George C. Marshall Space Flight Center
Huntsville, Alabama
April 28–30, 1992

NASA
National Aeronautics and
Space Administration
Office of Management
Scientific and Technical
Information Program
1992

TABLE OF CONTENTS

TABLE OF CONTENTS (Continued)

TABLE OF CONTENTS (Continued)

TABLE OF CONTENTS (Continued)

TABLE OF CONTENTS (Continued)

N92-32246

Current Status of the Development of an Ignition Transient Model for Solid Rocket Motors

Gary D. Luke
Aerojet ASRM Division
Sacramento, California
and
Harry A. Dwyer
University of California
Davis, California

An ignition transient model for solid rocket motors is currently being developed jointly by the Aerojet ASRM Division and the University of California at Davis. Though the CFD code will be general enough to predict the start transient for most solid rocket motors, the particular motive for the development of this code stems from the desire to analyze the flow field within the Advanced Solid Rocket Motor (ASRM) for the Space Shuttle with all its geometric complexity. The star grain configuration in the head end of the ASRM coupled with the multiport igniter creates a formidable problem which can only be modeled accurately using a three dimensional Navier-Stokes code if one wishes to preserve both volume and burning surface area as a function of axial position down the bore. The actual physical geometry is crucial in modeling the multiple wave interactions occurring within the combustion chamber as well as in predicting the correct amount of mass, momentum, and energy injected as a function of time and space at the propellant surface.

The primary objectives of the CFD code are to calculate the pressure rise rate, the thrust rise rate, and the maximum chamber pressure which occurs during the first second of the ASRM action time. And, more specifically, to determine the relative difference between the ignition transients produced using a single port igniter and that produced by a multiport igniter.

An implicit, three dimensional, time accurate, finite volume method is being developed to solve this problem. Current plans are to use an ADI technique, with replacement, to solve the set of analytically linearized full Navier-Stokes equations. However, to gain an understanding of which features of the code need more attention than others, and to provide an inexpensive, quick tool for studying the time accuracy of the selected solution algorithm, a one dimensional version of the code was written first. The various features of the one dimensional code were validated by comparing the numerical results to analytical results for problems where exact solutions were available. Then the one dimensional code was used to perform some sensitivity studies to help develop an understanding of the complex wave interactions occurring within the solid rocket motor.

This presentation will discuss the results obtained from the one dimensional code and the plans for the development of the 3-D code.

Part 2.

ASRM
LOCKHEED • AEROJET • RUST

CURRENT STATUS OF THE DEVELOPMENT OF AN IGNITION TRANSIENT MODEL FOR SOLID ROCKET MOTORS

Gary D. Luke
Aerojet ASRM Division
Sacramento, California
and
Harry A. Dwyer
University of California
Davis, California

1992 Workshop for
Computational Fluid Dynamic Applications in
Rocket Propulsion

ASRM
LOCKHEED • AEROJET • RUST

OBJECTIVES

- Develop Ignition Transient Model(s) to Characterize the Start Transient for Solid Rocket Motors

- Determine Relative Differences Between the Ignition Transients Produced Using Single (RSRM) and Multiport (ASRM) Igniters

DEFINITION OF PROBLEM

NEED TO ACCURATELY PREDICT:

- Instantaneous Pressure Rise Rate
- Corresponding Thrust Rise Rate
- Maximum Chamber Pressure
- Details of Flow Field in Head End Where Fins and Igniter are Located for RSRM and ASRM

LOCKHEED • AEROJET • RUST

THREE PART MODELING APPROACH

1. Preliminary Analysis with Existing General 3-D Navier-Stokes Solver (CONTINUSYS Code)
2. Develop 1-D "Engineering Workhorse" Ignition Transient Code
3. Develop "Full" 3-D Ignition Transient Code Using Same Methodology as 1-D Code

LOCKHEED • AEROJET • RUST

Only 1-D Code Discussed Today

PURPOSE OF 1-D CODE

- Provide Quick, Efficient Tool for Performing Sensitivity Studies
- Establish Bounds for Problem Through Parametric Studies
- Evaluate Various Numerical Schemes Prior to Incorporation into 3-D Code
- Determine Which Factors are Most Influential, Requiring More Attention During Development of 3-D Code

ASRM
LOCKHEED • AEROJET • RUST

DESCRIPTION OF NUMERICAL MODEL

- Implicit, Time Dependent, Finite Volume Method
- Modular Format for Flexibility
- Currently Contains Centered Scheme with Explicit Artificial Dissipation
- System of Equations Solved Using Alternating Direction Implicit (ADI) with Replacement (Essentially a Direct Solver for 1-D Case)

ASRM
LOCKHEED • AEROJET • RUST

Governing Equations in Integral Form

Continuity

$$\frac{\partial}{\partial t} \iiint_V \rho dV + \iint_S \rho \vec{u} \cdot \vec{n} dA = \iint_{A_p} \dot{r} \rho_p dA_p$$

X-Momentum

$$\frac{\partial}{\partial t} \iiint_V \rho \vec{u} dV + \iint_S \rho \vec{u} (\vec{u} \cdot \vec{n}) dA = -\vec{n} \iint_S p dA - \iint_W \tau_w dA_w - \iint_S \tau_{xx} dA$$

Energy

$$\frac{\partial}{\partial t} \iiint_V \rho e \, dV + \iint_S [\rho e + P](\vec{u} \cdot \vec{n}) dA = \iint_W q_w dA_w + \iint_S q_x dA + \iint_{A_p} \dot{r} \rho_p H_p dA_p$$

where $e = C_v T + u^2/2$

Equation of State

$$P = \rho RT$$

LOCKHEED • AEROJET • RUST

Linearized Form of Discrete Equations

$$- \frac{A_{i-1/2}}{2}\left[\bar{\bar{J}}^{n}_{i-1}\right]\left(\Delta \hat{U}^{n+1}_{i-1}\right) + \left\{ \frac{A_i \Delta X_i}{\Delta t}\left[\bar{\bar{I}}\right] + \left(\frac{A_{i+1/2} - A_{i-1/2}}{2}\right)\left[\bar{\bar{J}}^{n}_{i}\right]\right\}\left(\Delta \hat{U}^{n+1}_{i}\right) + \frac{A_{i+1/2}}{2}\left[\bar{\bar{J}}^{n}_{i+1}\right]\left(\Delta \hat{U}^{n+1}_{i+1}\right)$$

$$= \left[\hat{S}^n_i\right] + \frac{A_{i-1/2}}{2}\left[\hat{F}^n_i + \hat{F}^n_{i-1}\right] - \frac{A_{i+1/2}}{2}\left[\hat{F}^n_{i+1} + \hat{F}^n_i\right]$$

where: $\hat{U} \equiv$ primitive variable vector $= \begin{bmatrix} \rho \\ \rho u \\ \rho e \end{bmatrix}$ $\hat{F} \equiv$ flux vector $= \begin{bmatrix} \rho u \\ \rho u^2 + P \\ (\rho e + P)u \end{bmatrix}$

$\bar{\bar{J}} \equiv$ Jacobian Matrix $= \left[\frac{\partial \hat{F}}{\partial \hat{U}}\right]$

$$\hat{S} = \begin{bmatrix} \left[\dot{r}\, \rho_p\, A_p\right]^n_i \\ -\left[\frac{f}{2}\rho u^2 \frac{u}{|u|} A_w\right]^n_i - \left\{\left[\mu \frac{\partial u}{\partial x} A\right]^n_{i+1/2} - \left[\mu \frac{\partial u}{\partial x} A\right]^n_{i-1/2}\right\} + P^n_i\left[A_{i+1/2} - A_{i-1/2}\right] \\ \left[h\,(T - T_w)\, A_w\right]^n_i + \left\{\left[-k \frac{\partial T}{\partial x} A\right]^n_{i+1/2} - \left[-k \frac{\partial T}{\partial x} A\right]^n_{i-1/2}\right\} + \left[\dot{r}\, \rho_p\, H_p\, A_p\right]^n_i \end{bmatrix}$$

Analytically Linearized Using Newton's Method

LOCKHEED • AEROJET • RUST

Artificial Dissipation
2nd Order Terms Required to Dampen Out Oscillations Occurring at Steep Gradients

- **Continuity Equation:**

$$\eta \frac{\partial \rho}{\partial x}$$

- **Momentum Equation:**

$$\tau_{xx} = (\mu_R + \mu_A)\frac{\partial u}{\partial x}, \mu_A = \frac{\rho u \Delta x}{R_e}$$

- **Energy Equation:**

$$q_x = -(k_R + k_A)\frac{\partial T}{\partial x}, k_A = \frac{\rho C_p u \Delta x}{P_e}$$

R = Real, A = Artificial

Pe = Peclet Number (Re*Pr)
Re = Reynold's Number
Pr = Prandtl Number

LOCKHEED • AEROJET • RUST

FEATURES OF 1-D CODE

- Heat Transfer
- Friction
- Variable Area
- Mass Injection Through Side Walls

ASRM
LOCKHEED • AEROJET • RUST

BOUNDARY CONDITIONS

- ENTRANCE BOUNDARY CONDITIONS
  - Solid Wall
  - All Static Conditions Specified
  - Reservoir Conditions Specified
  - Solid Wall with Mass and Energy Source
- EXIT PLANE BOUNDARY CONDITIONS
  - Solid Wall
  - Static Pressure Specified
  - Frictionless, Constant Area Extension for Supersonic Outflow
  - Linear Extrapolation for Supersonic Outflow
- SIDE WALL BOUNDARY CONDITIONS
  - Impermeable
  - Specified Mass/Energy Injection Rate
  - Burning Propellant Surface

LOCKHEED • AEROJET • RUST

VALIDATION BY COMPARISON TO EXACT 1-D SOLUTIONS

- Fanno Flow
- Rayleigh-Line Flow
- Isentropic Nozzle Flow
- Mass Injection Through Walls of Constant Area Duct
- Shock Tube Problem

LOCKHEED • AEROJET • RUST

Flow Through Constant Area Duct With Friction

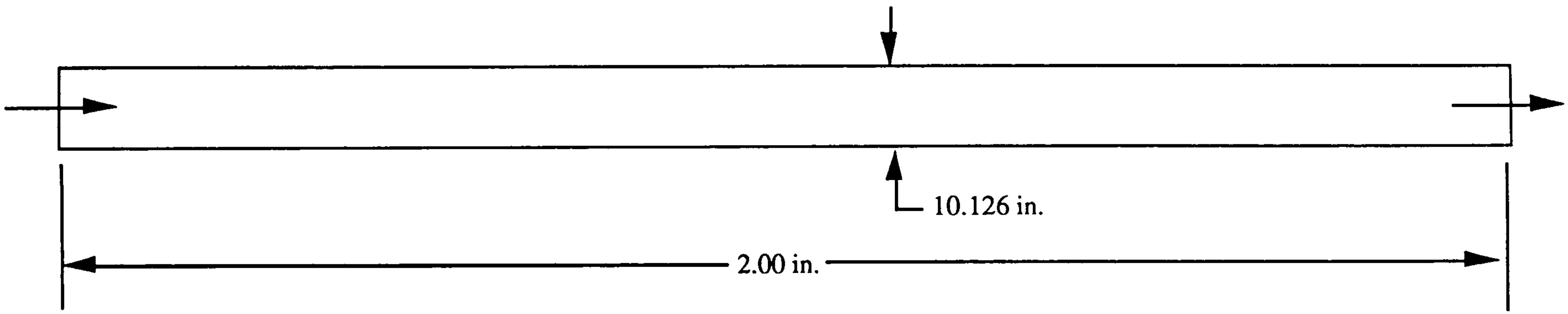

Inlet Boundary Conditions:

Reservoir Conditions

P_r = 3,000 psia

T_r = 700°R

V_r = 0 ft/sec

Outlet Boundary Condition:

Static Pressure Specified

$P_{ex} = P_a = 1,673$ psia

Initial Conditions:

P_i = 3,000 psia

T_i = 700°R

V_i = 0 ft/sec

For: $1 \leq i \leq I\ MAX$

Additional Input Required

$\gamma = 1.4$

$R = 53.35 \frac{ft\ lbf}{lbm\ °R}$

$f = 0.00325$ (Darcy-Weisbach)

$L/D \approx 20$

LOCKHEED • AEROJET • RUST

FLOW THROUGH CONSTANT AREA DUCT WITH FRICTION

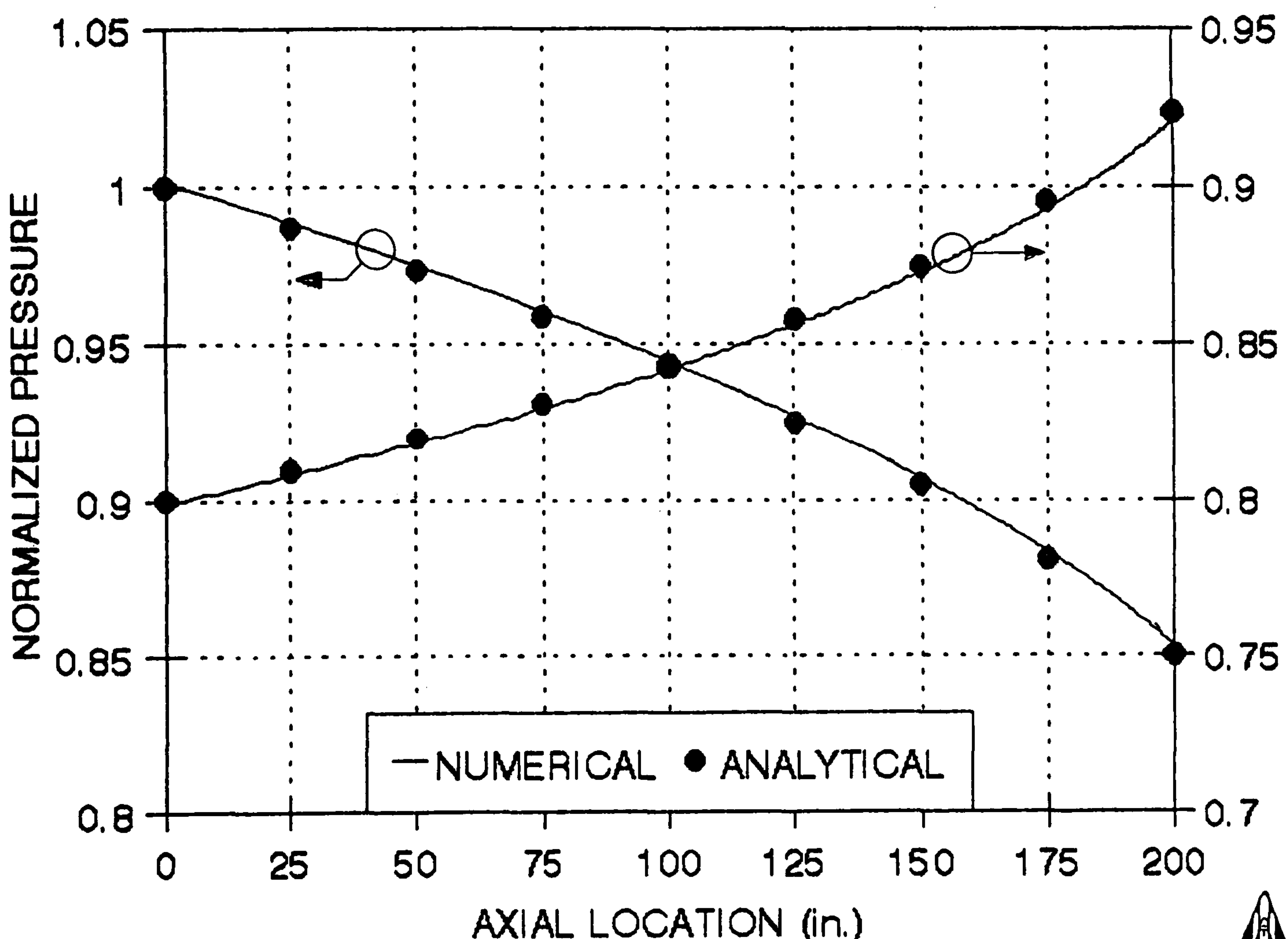

Numerical results from AJITC1D Code using 200 cells
Analytical results interpolated from Fanno Flow Tables

ASRM LOCKHEED • AEROJET • RUST

FLOW THROUGH CONSTANT AREA DUCT WITH FRICTION

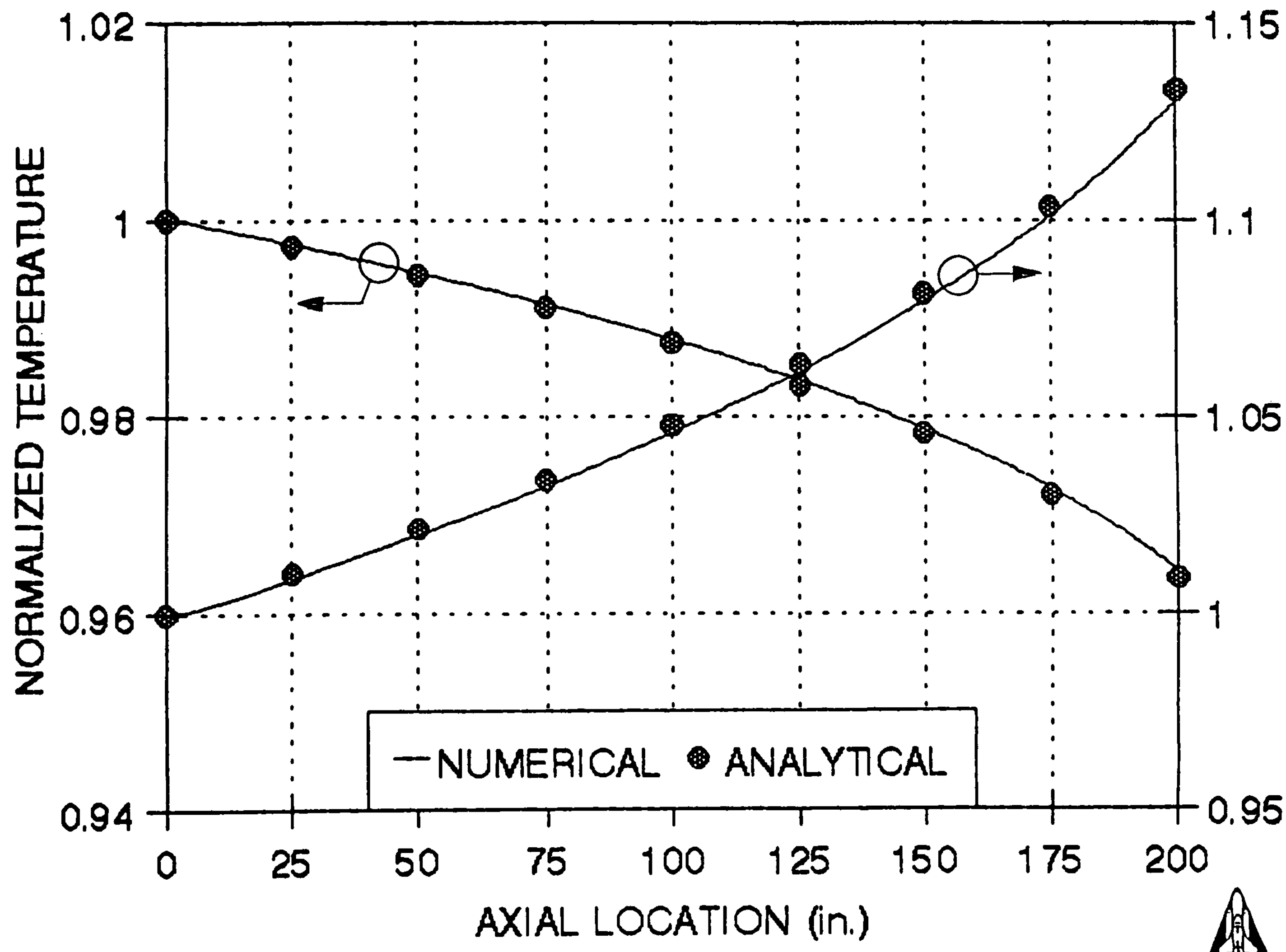

Numerical results from AJITC1D Code using 200 cells
Analytical results interpolated from Fanno Flow Tables

ASRM LOCKHEED • AEROJET • RUST

ISENTROPIC FLOW THROUGH A NOZZLE
NOZZLE CONFIGURATION

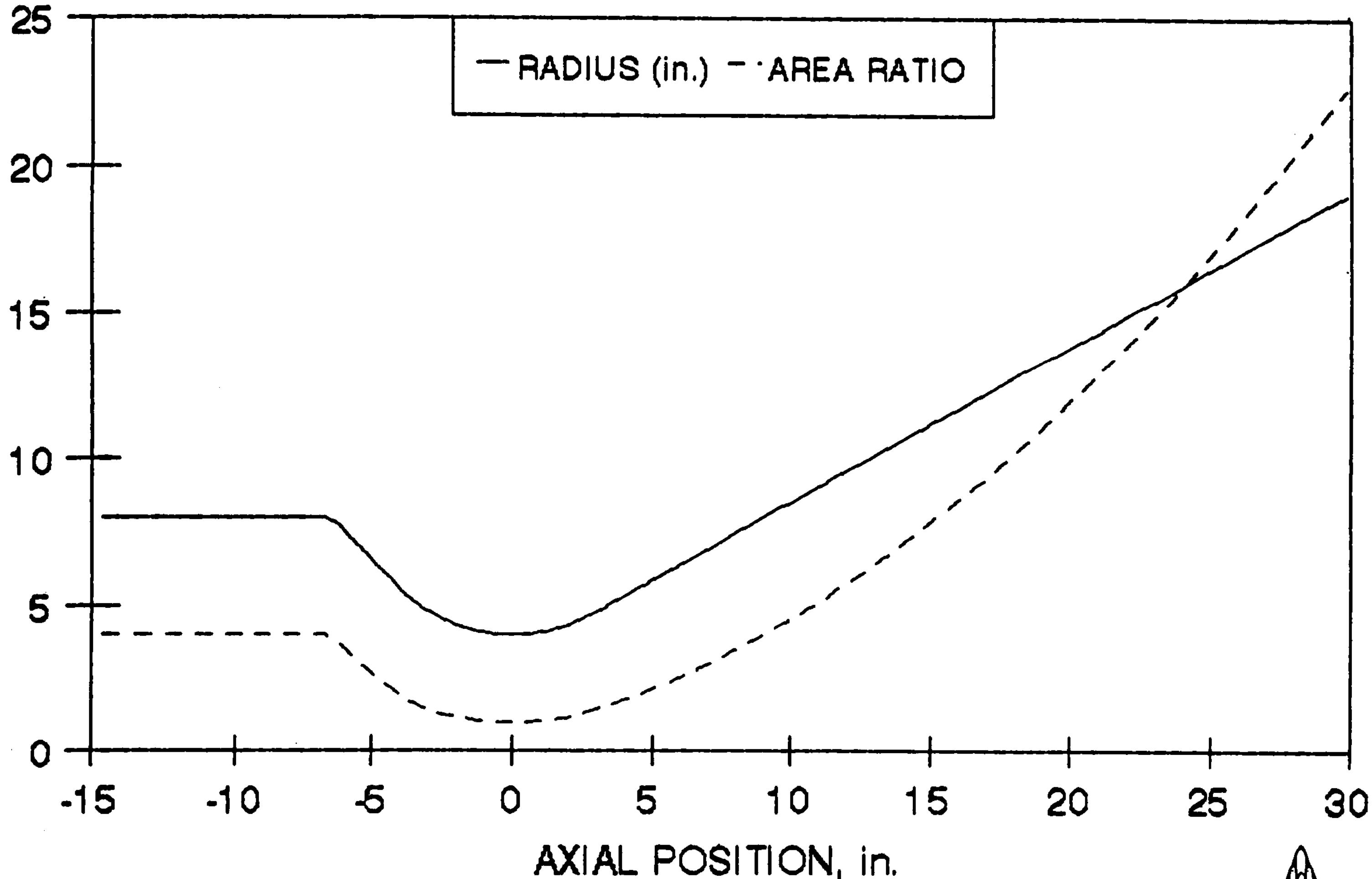

Numerical results from AJITC1D Code using 145 cells
Analytical results from 1-D Isentropic Tables

ASRM LOCKHEED • AEROJET • RUST

ISENTROPIC FLOW THROUGH A NOZZLE

PRESSURE vs AXIAL POSITION

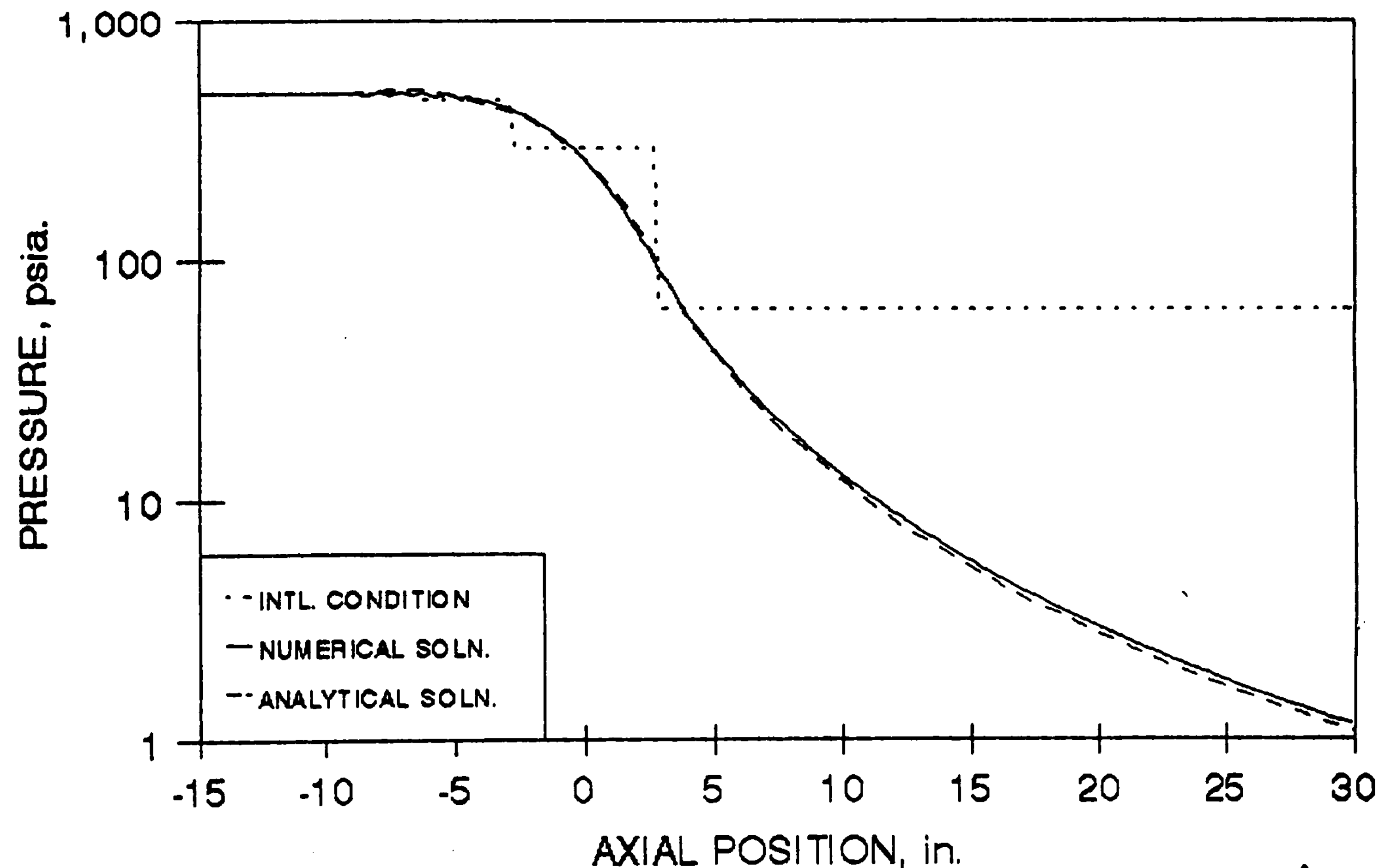

Numerical results from AJITC1D Code using 145 cells
Analytical results from 1-D Isentropic Tables

ASRM LOCKHEED • AEROJET • RUST

ISENTROPIC FLOW THROUGH A NOZZLE
TEMPERATURE vs AXIAL POSITION

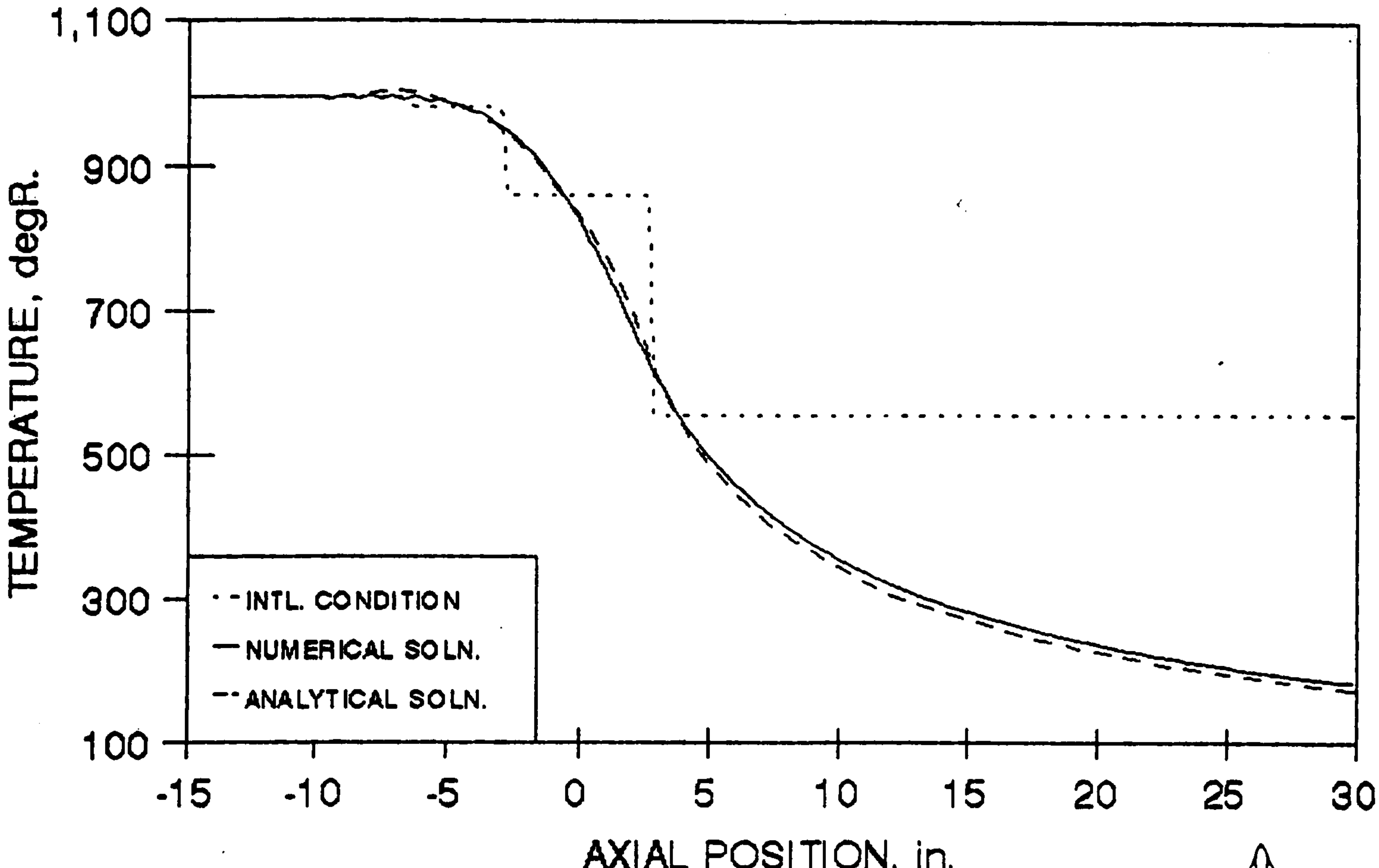

Numerical results from AJITC1D Code using 145 cells
Analytical results from 1-D Isentropic Tables

ASRM LOCKHEED • AEROJET • RUST

Radial Mass Injection Into Constant Area Duct

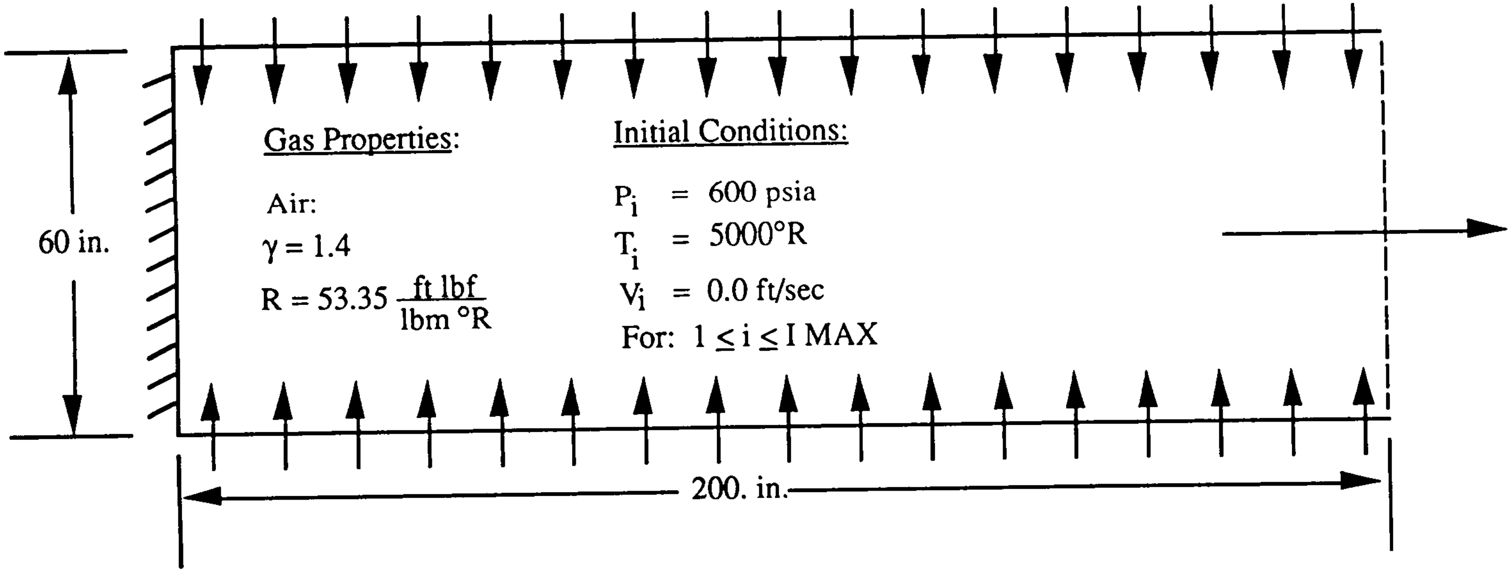

Gas Properties:

Air:

$\gamma = 1.4$

$R = 53.35 \frac{ft\ lbf}{lbm\ °R}$

Initial Conditions:

$P_i = 600$ psia

$T_i = 5000°R$

$V_i = 0.0$ ft/sec

For: $1 \leq i \leq I\ MAX$

Left Boundary Condition:

Solid Wall

∴ Reflective Boundary Condition Used

Right Boundary Condition:

Static Pressure Specified

$P_{ex} = P_a = 600$ psia

Lateral Surface Boundary Conditions:

$\dot{w}' = 0.3855 \frac{lbm}{sec\ in.^2}$

$A_w = 37,700\ in.^2$

$\dot{w} = 14,533$ lbm/sec

$T_t = 6000°R$

LOCKHEED • AEROJET • RUST

RADIAL MASS INJECTION INTO CONSTANT AREA DUCT

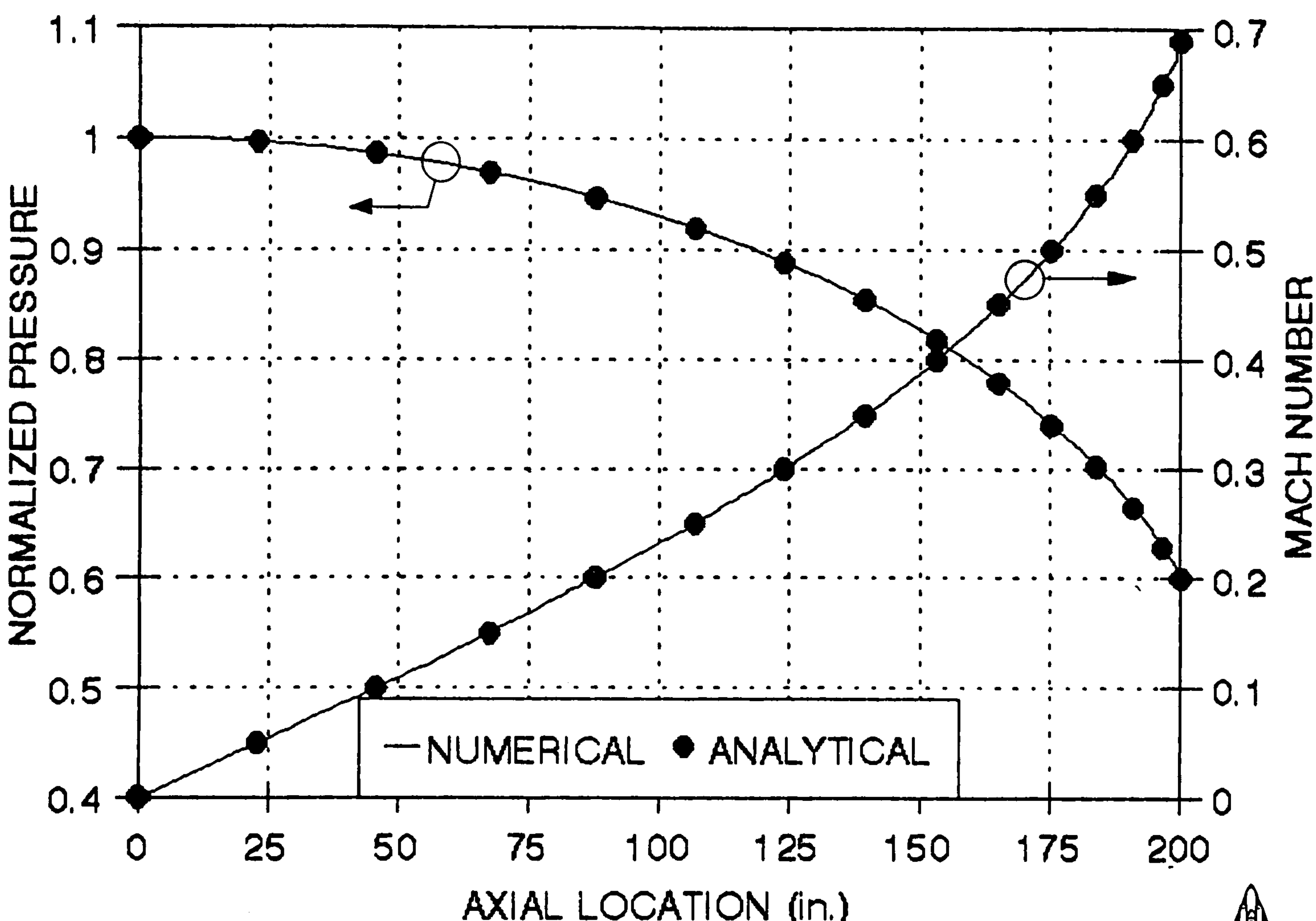

Numerical results from AJITC1D Code using 200 cells
Analytical results from 1-D formulas in Shapiro's

ASRM
LOCKHEED • AEROJET • RUST

RADIAL MASS INJECTION INTO CONSTANT AREA DUCT

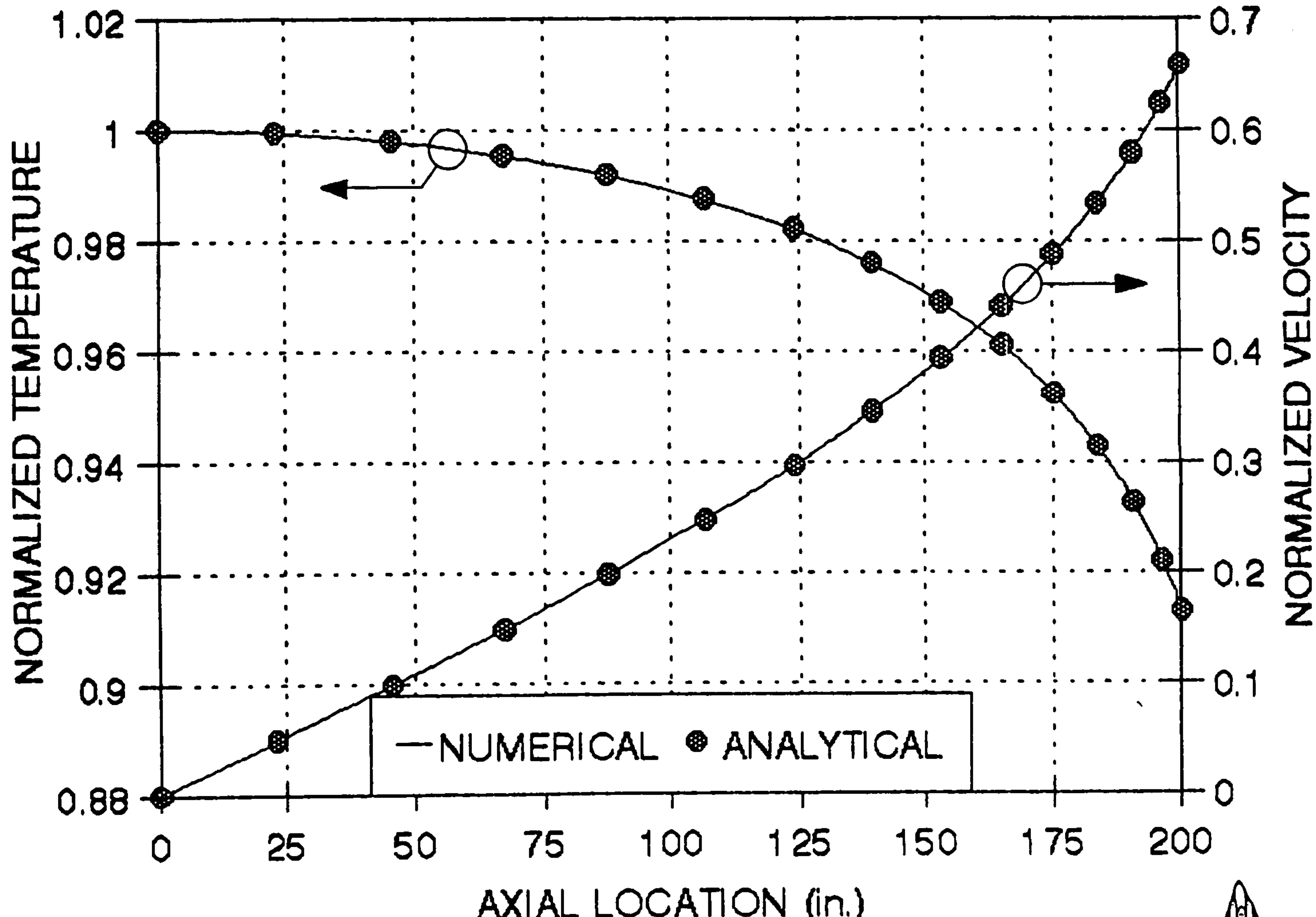

Numerical results from AJITC1D Code using 200 cells
Analytical results from 1-D formulas in Shapiro's

ASRM LOCKHEED • AEROJET • RUST

ONE DIMENSIONAL SHOCK TUBE PROBLEM

PRESSURE vs AXIAL POSITION PRIOR TO SHOCK REFLECTION, t = 0.5 milliseconds

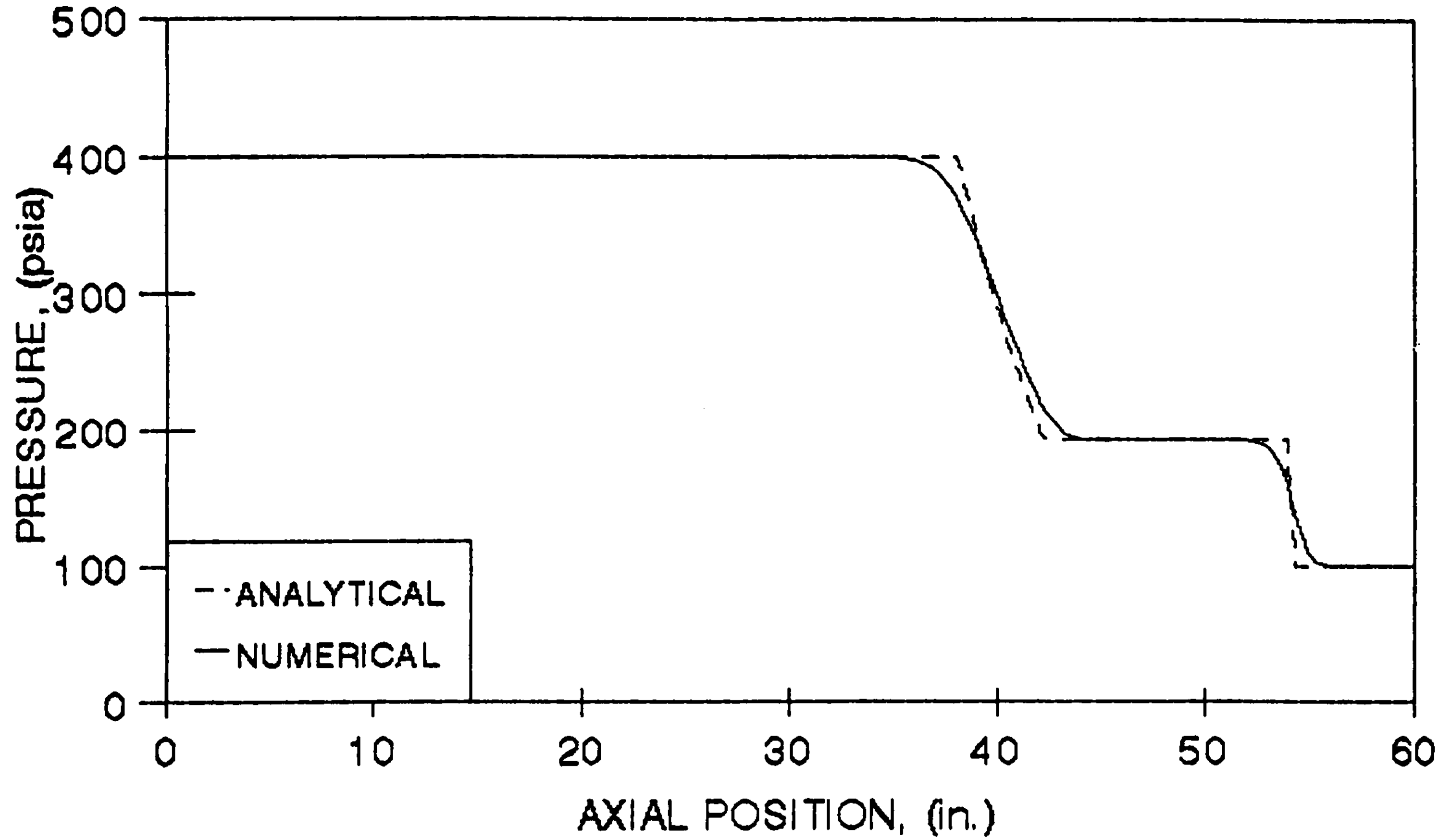

DIAPHRAGM ORIGINALLY LOCATED AT X/L = 0.75
LEFT: P = 400 psia, T = 530 degR, V = 0 ft/sec
RIGHT: P = 100 psia, T = 530 degR, V = 0 ft/sec

ASRM
LOCKHEED • AEROJET • RUST

ONE DIMENSIONAL SHOCK TUBE PROBLEM

PRESSURE vs AXIAL POSITION AS SHOCK CONTACTS WALL, t = 1.0 milliseconds

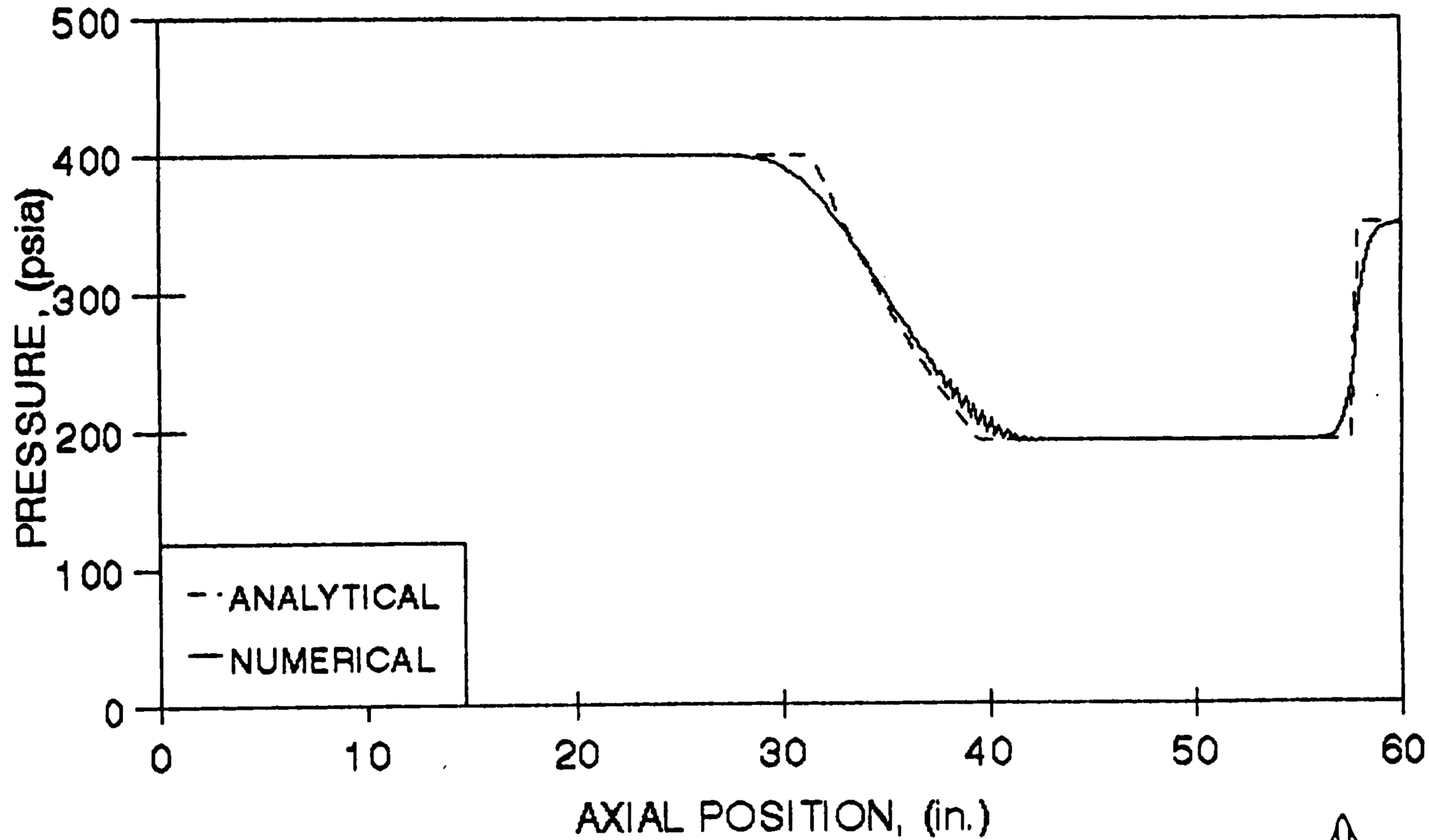

DIAPHRAGM ORIGINALLY LOCATED AT X/L = 0.75
LEFT: P = 400 psia, T = 530 degR, V = 0 ft/sec
RIGHT: P = 100 psia, T = 530 degR, V = 0 ft/sec

ASRM
LOCKHEED • AEROJET • RUST

ONE DIMENSIONAL SHOCK TUBE PROBLEM

PRESSURE vs AXIAL POSITION NEAR STEADY STATE, t = 835 milliseconds

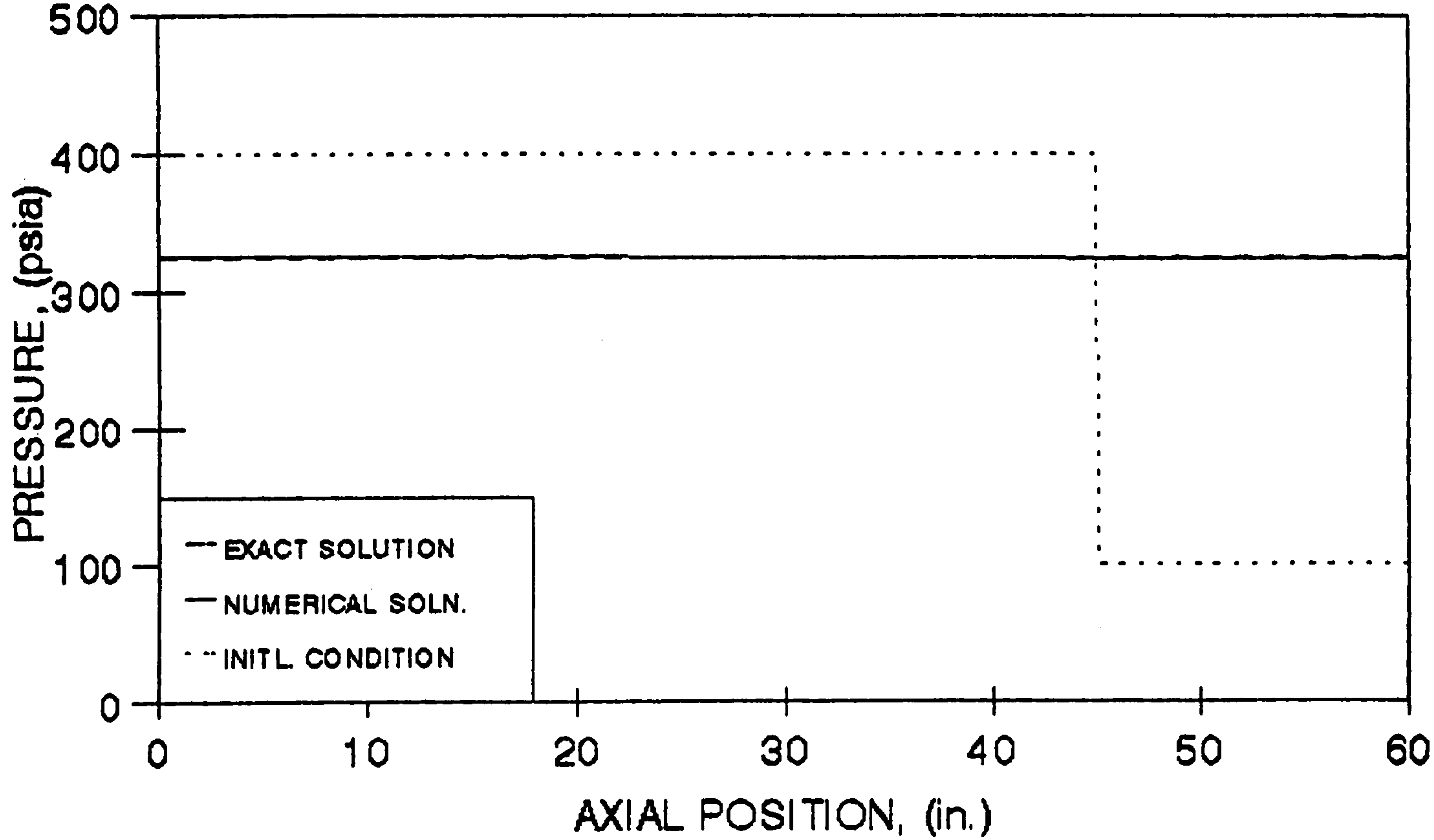

DIAPHRAGM ORIGINALLY LOCATED AT X/L = 0.75
LEFT: P = 400 psia, T = 530 degR, V = 0 ft/sec
RIGHT: P = 100 psia, T = 530 degR, V = 0 ft/sec

ONE DIMENSIONAL SHOCK TUBE PROBLEM

TEMPERATURE vs AXIAL POSITION PRIOR TO SHOCK REFLECTION, t = 0.5 milliseconds

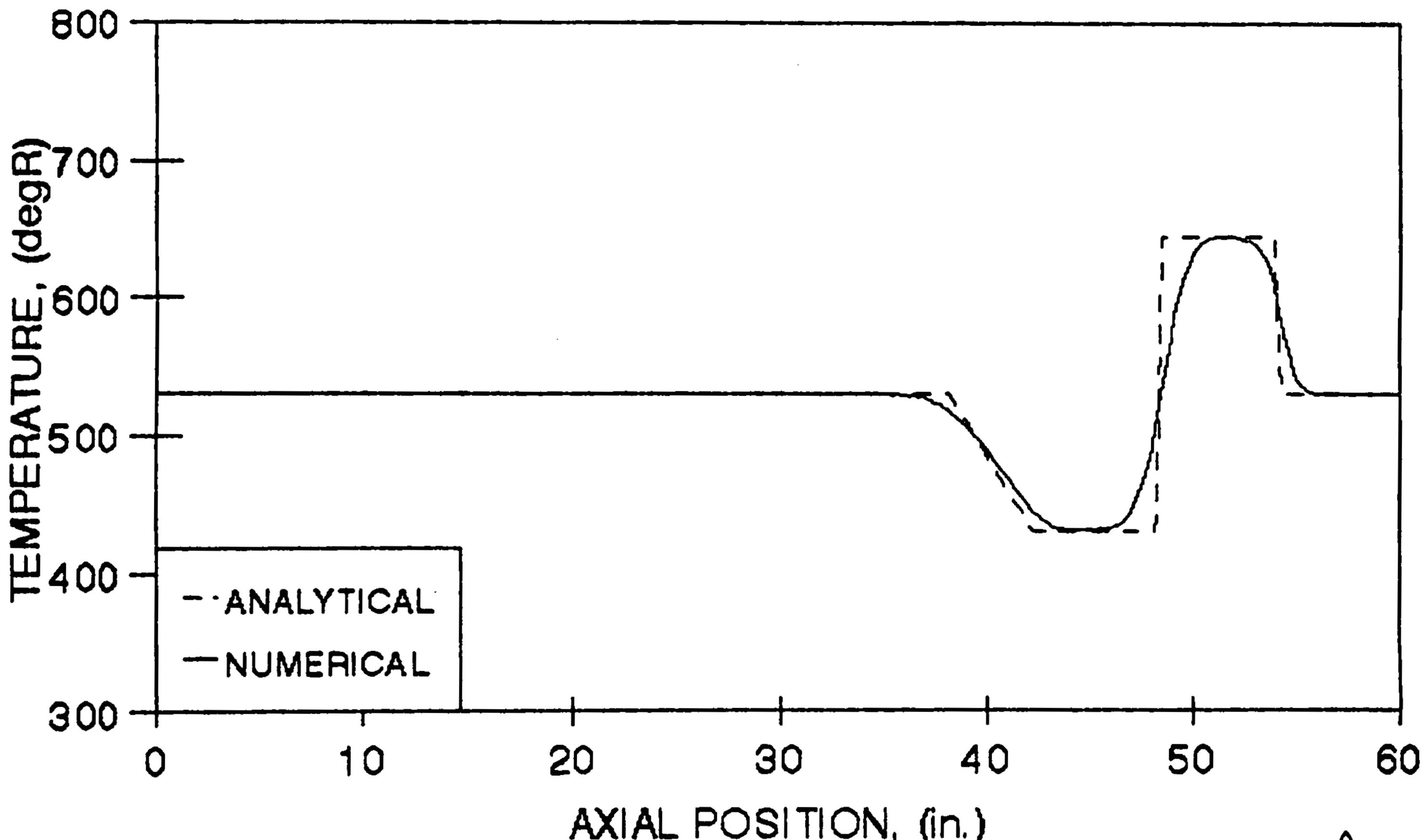

DIAPHRAGM ORIGINALLY LOCATED AT X/L = 0.75
LEFT: P = 400 psia, T = 530 degR, V = 0 ft/sec
RIGHT: P = 100 psia, T = 530 degR, V = 0 ft/sec

ASRM
LOCKHEED • AEROJET • RUST

ONE DIMENSIONAL SHOCK TUBE PROBLEM

TEMPERATURE vs AXIAL POSITION AS SHOCK CONTACTS WALL, t = 1.0 milliseconds

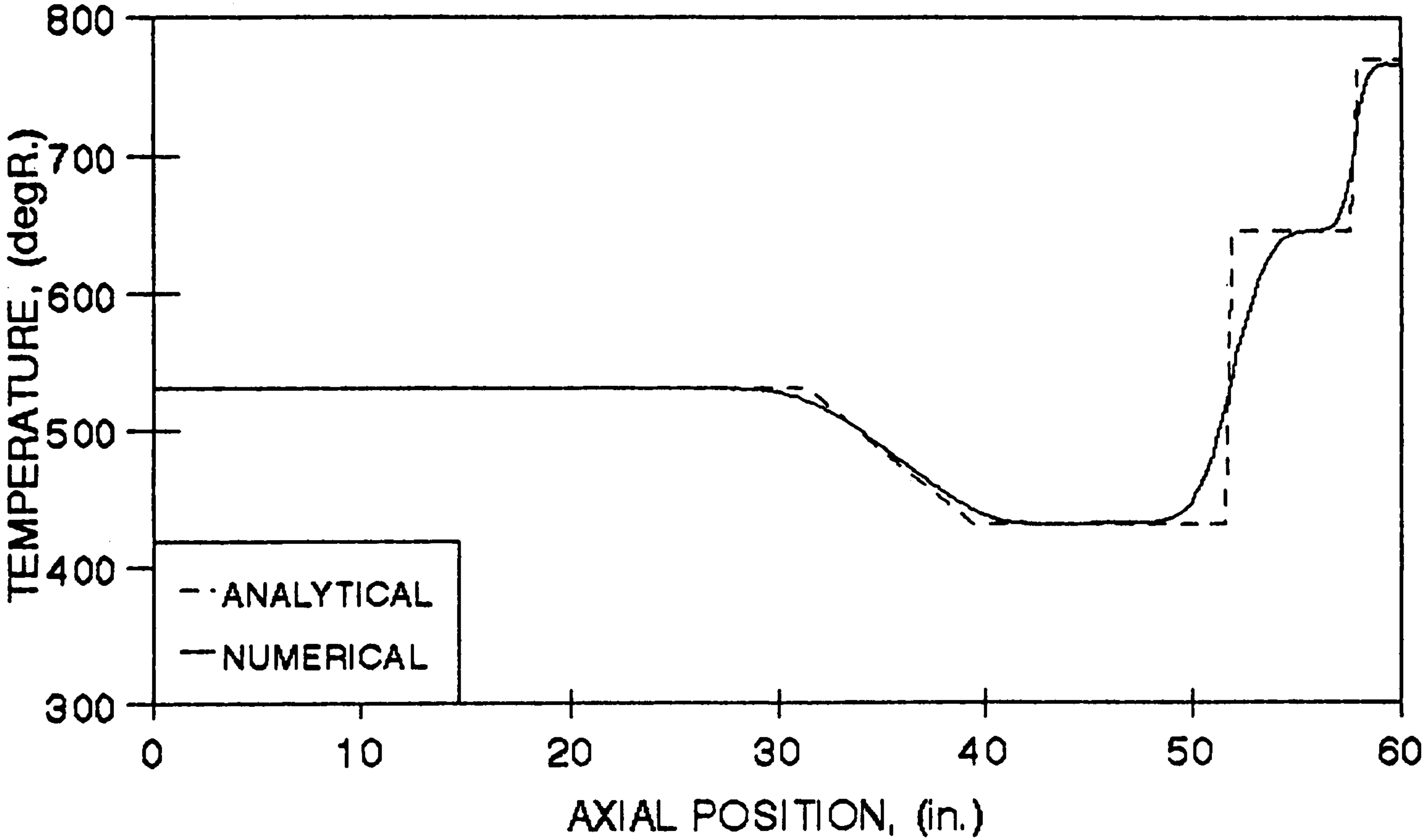

DIAPHRAGM ORIGINALLY LOCATED AT X/L = 0.75
LEFT: P = 400 psia, T = 530 degR, V = 0 ft/sec
RIGHT: P = 100 psia, T = 530 degR, V = 0 ft/sec

ASRM
LOCKHEED • AEROJET • RUST

ONE DIMENSIONAL SHOCK TUBE PROBLEM

TEMPERATURE vs AXIAL POSITION NEAR STEADY STATE, t = 835 milliseconds

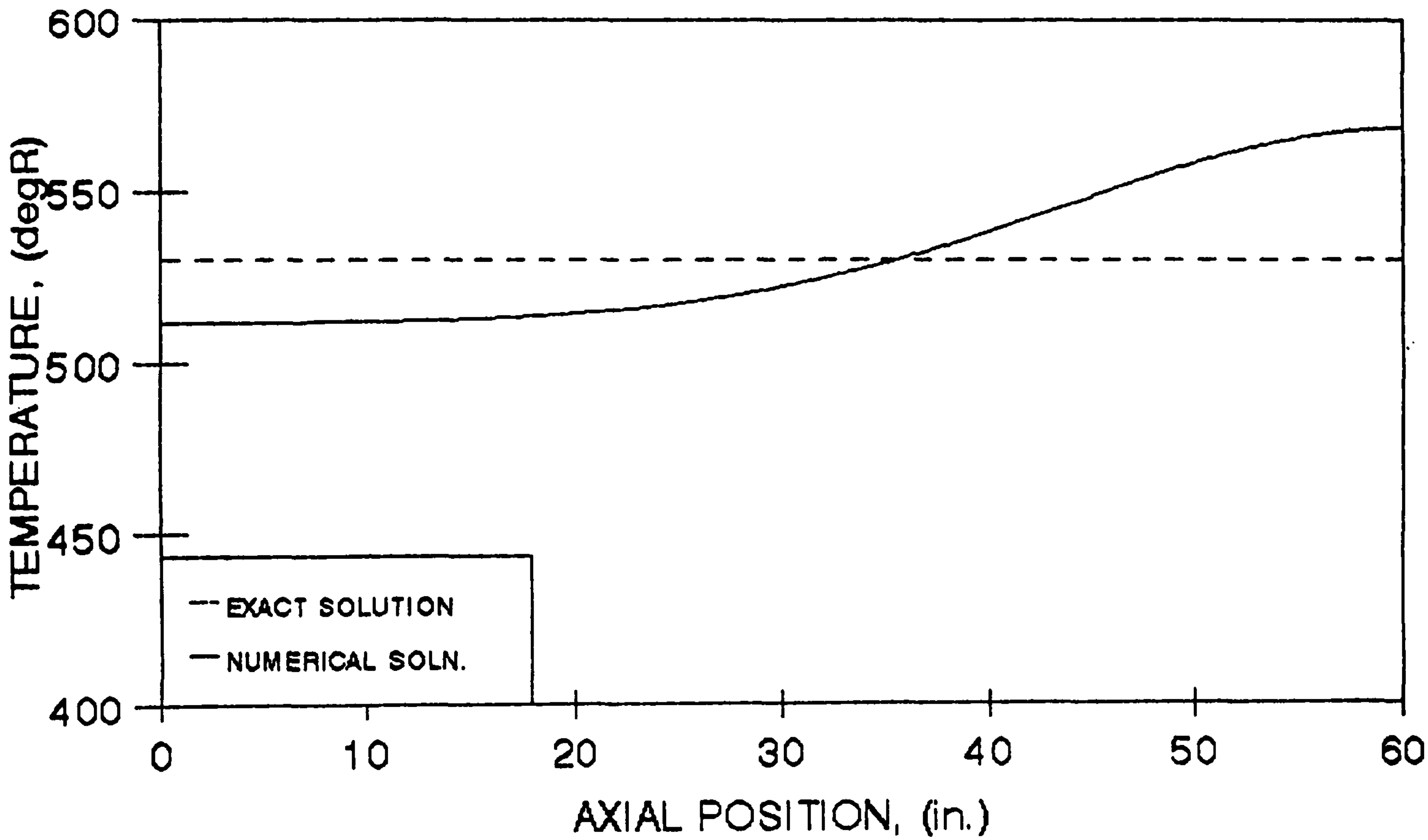

DIAPHRAGM ORIGINALLY LOCATED AT X/L = 0.75
LEFT: P = 400 psia, T = 530 degR, V = 0 ft/sec
RIGHT: P = 100 psia, T = 530 degR, V = 0 ft/sec

ASRM
LOCKHEED • AEROJET • RUST

PRELIMINARY SENSITIVITY STUDIES

MAXIMUM HEAD END dP/dt AS A FUNCTION OF DUCT LENGTH AND NOZZLE CONTRACTION RATIO

- General Results Obtained Using a Cylindrical Duct with a Closed Aft End and an Increasing Mass Flow Rate Entering at the Head End:
  - as the Duct Length Increased, the Maximum dP/dt at the Head End Increased
  - Closer Examination Revealed Sinusoidal Behavior Due to Complex Wave Interactions

- General Results Obtained Using a Cylindrical Duct with a Nozzle Attached at the Aft End:
  - as the Nozzle Contraction Ratio Increased, the Maximum dP/dt at the Head End Increased
  - Contraction Ratio of 2.5:1 (ASRM) Produced Results within 10% of Worst Case Solid Wall

ASRM
LOCKHEED • AEROJET • RUST

PRELIMINARY RESULTS FROM THE AJITC1D CODE

VERIFICATION OF SHOCK STEEPENING AS A CONSEQUENCE OF AN INCREASING MASS FLOW RATE

TIME (msec)

— (1) 14.33 ··· (2) 24.83 - - (3) 34.78 — (4) 44.36 ··· (5) 53.65 - - (6) 62.71 — (7) 71.58 ··· (8) 80.29

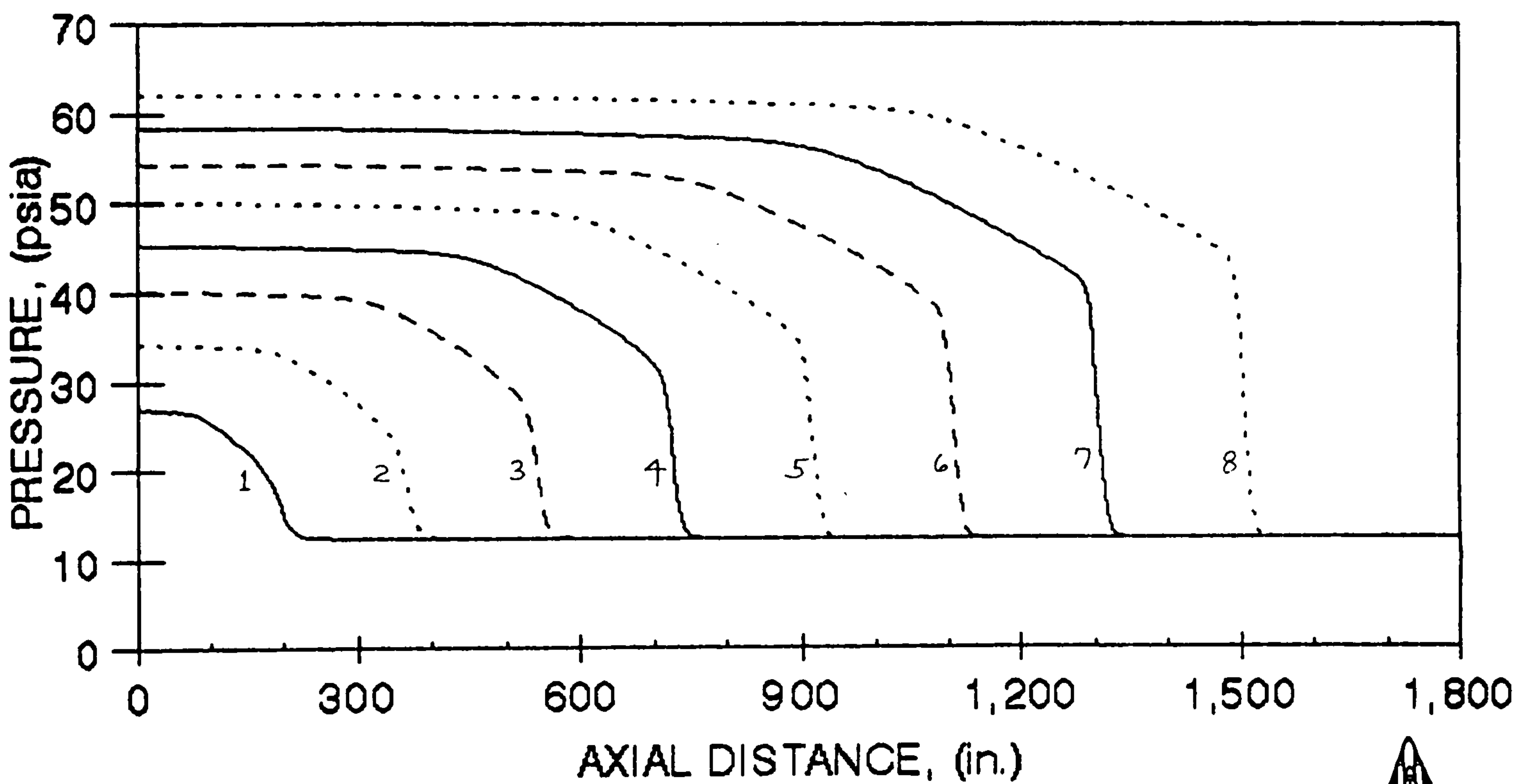

IGNITER PRESSURE RISE RATE = 75,000 psi/sec

ASRM LOCKHEED • AEROJET • RUST

PRELIMINARY RESULTS FROM THE AJITC1D CODE

VERIFICATION OF SHOCK STEEPENING AS A CONSEQUENCE OF AN INCREASING MASS FLOW RATE

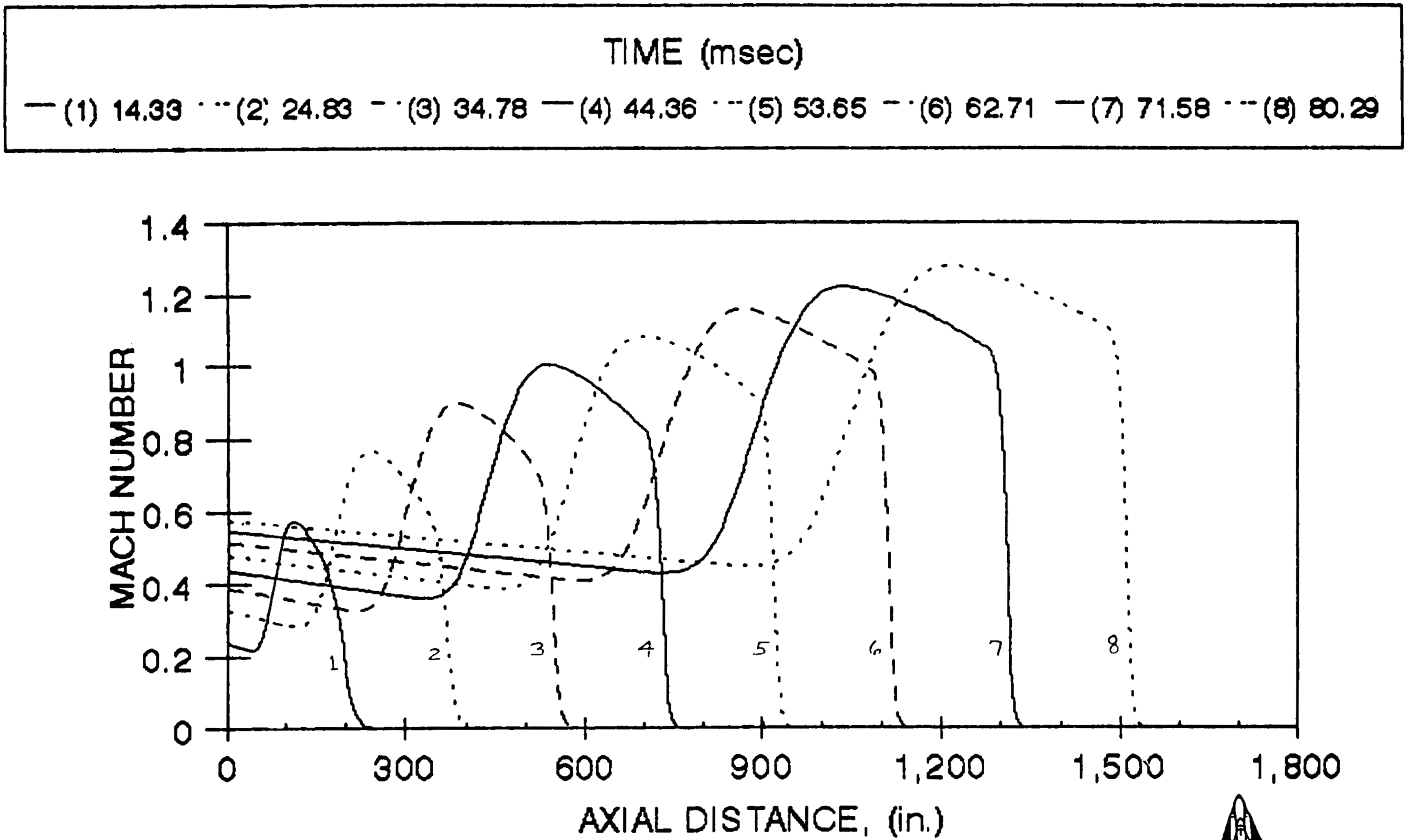

IGNITER PRESSURE RISE RATE = 75,000 psi/sec

LOCKHEED • AEROJET • RUST

PRELIMINARY RESULTS FROM THE AJITC1D CODE

MAXIMUM dP/dt AS A FUNCTION OF THE TOTAL DUCT LENGTH AND THE IGNITER MASS FLOW RATE

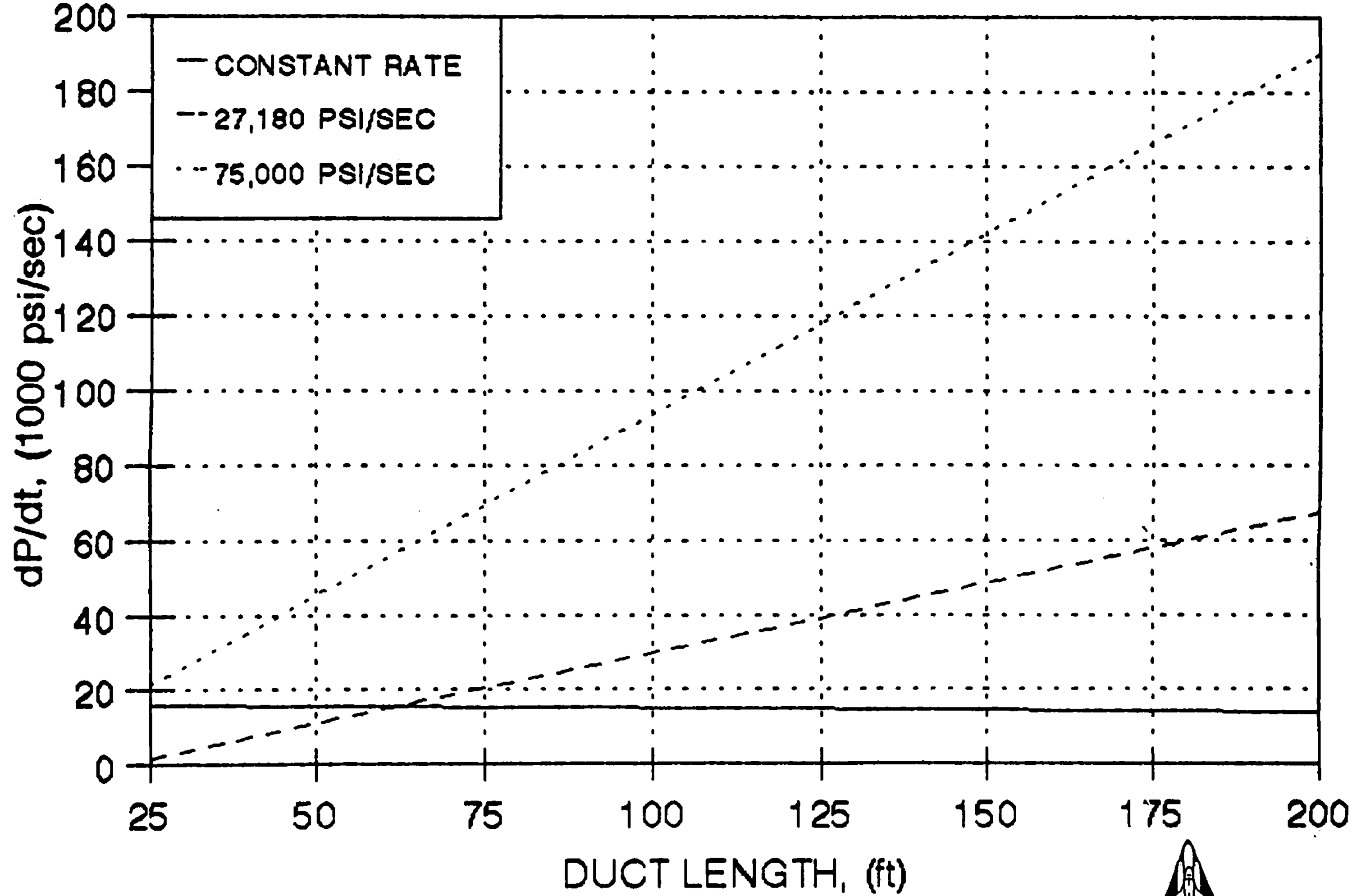

ASRM

PRELIMINARY RESULTS FROM THE AJITC1D CODE

MAXIMUM dP/dt AS A FUNCTION OF THE TOTAL DUCT LENGTH AND THE IGNITER MASS FLOW RATE

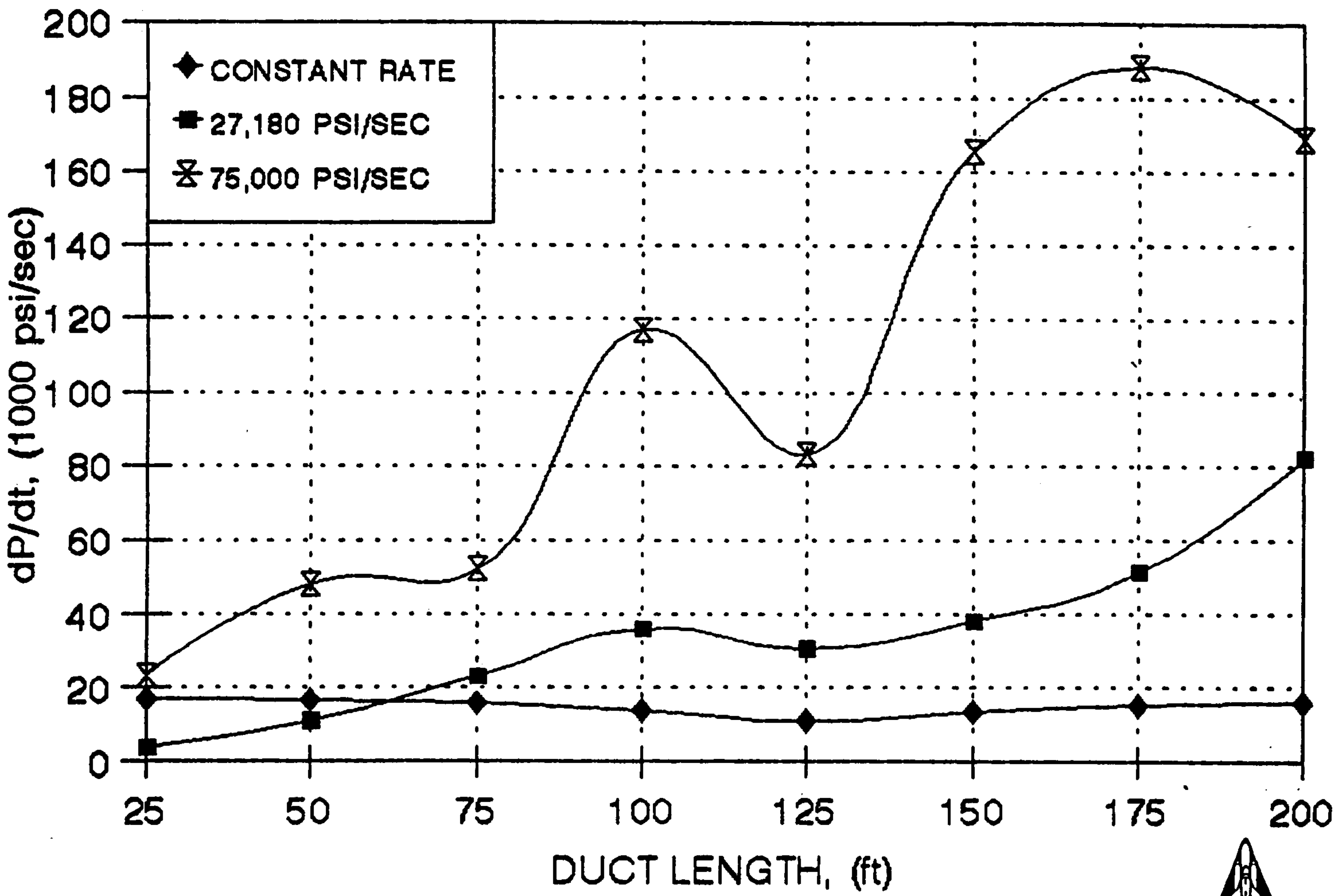

PRELIMINARY RESULTS FROM THE AJITC1D CODE

MAXIMUM dP/dt AS A FUNCTION OF THE DOWNSTREAM BOUNDARY CONDITION SPECIFIED

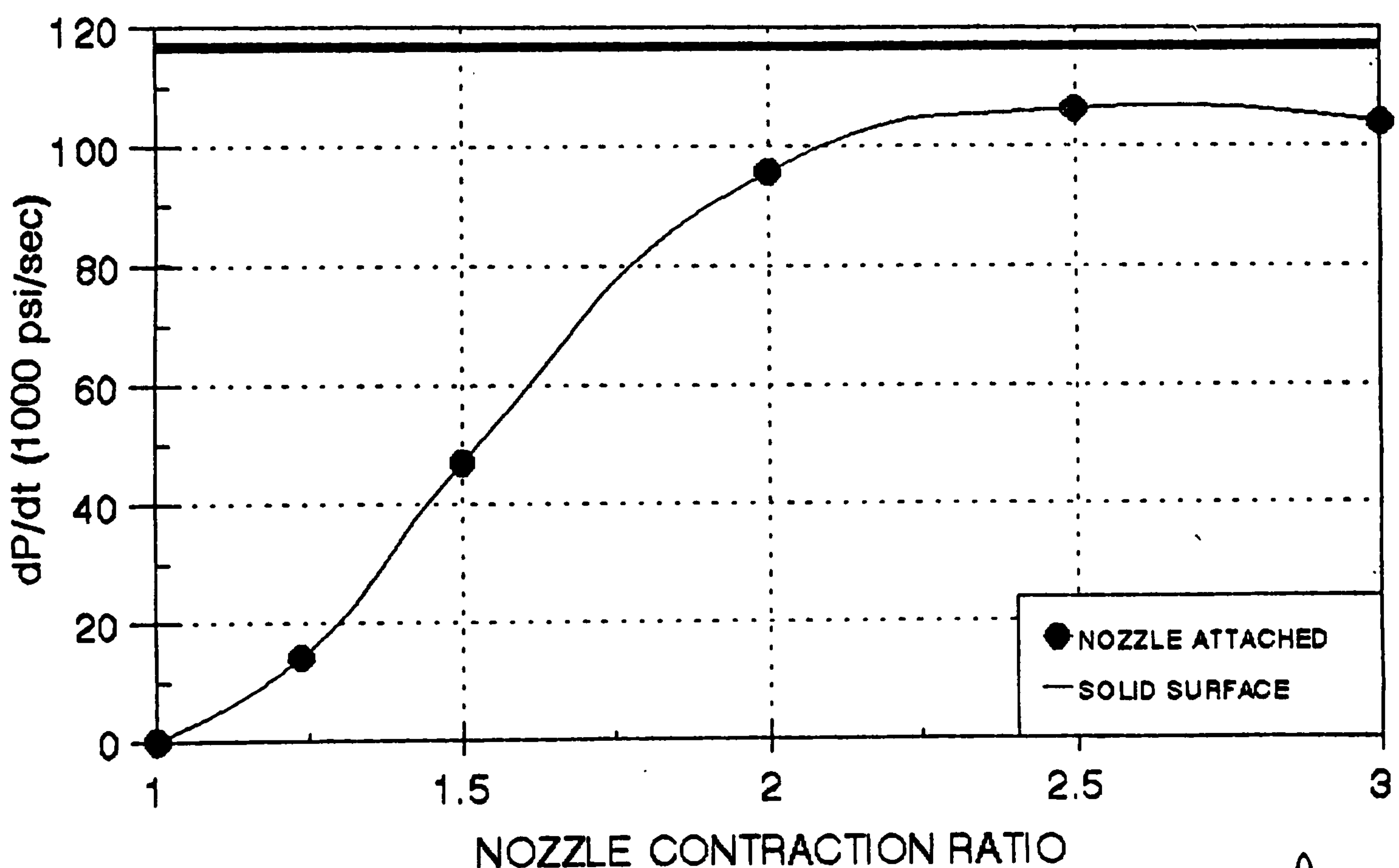

RESULTS OBTAINED USING AN INCREASING IGNITER FLOW RATE (75,000 PSI/SEC)

ASRM
LOCKHEED • AEROJET • RUST

CURRENT STATUS OF 1-D CODE

- **ALL FEATURES OF CODE VALIDATED INDIVIDUALLY BY COMPARISONS TO EXACT ANALYTICAL SOLUTIONS**
- **BURNING SURFACE BOUNDARY CONDITION ADDED**
- **FOR IMMEDIATE PARAMETRIC STUDY TO ESTABLISH BOUNDS:**
  - SIMPLE PERCENT OF PROP. LIT VS T AND X LOGIC ADDED
  - CAN BE ADJUSTED TO MATCH SINGLE PORT RSRM DATA (LOWER LIMIT FOR ASRM)
  - WORST CASE UPPER LIMIT OBTAINED BY ALLOWING FINS TO IGNITE AS INITIAL PULSE PASSES

Lockheed GenCorp Aerojet
ASRM DIVISION

FUTURE PLANS FOR 1-D CODE

- **NEED FLAME SPREADING MODEL FOR "FINNED" ZONE**
  - DERIVE FROM RSRM DATA (LOTS OF VARIABLES)
  - INCORPORATE RESULTS FROM AUBURN UNIVERSITY HEAD END COLD FLOW TEST SERIES (EXTRAPOLATION PROBLEM)
  - CALCULATE MASS ADDITION RATE USING CONTINUSYS CODE (LIMITED TO INVISCID CALCULATIONS WITH USER SUPPLIED IGNITION TEMPERATURE)
- **ADD EROSIVE BURNING MODEL**
  - PENN STATE FUNDED FOR TEST PROGRAM

Lockheed GenCorp Aerojet ASRM DIVISION

ASRM

PLANS FOR 3-D IGNITION TRANSIENT MODEL

- **EXTEND 1-D ADI TECHNIQUE TO 3-D**
- **USE EXISTING GRID GENERATORS AND COORDINATE TRANSFORMATION ROUTINES**
- **PROBABLY NOT FEASIBLE TO RUN FULL 3-D MODEL (EVEN WITH 22 PLANES OF SYMMETRY)**
  - COMPLICATED GEOMETRY IN HEAD END
  - EXTREMELY LONG DOMAIN (L/D > 20)
  - MUST CALCULATE THROUGH ENTIRE 1ST SECOND
- **NEED TO DEVELOP TRANSITION FROM 3-D TO AXISYMMETRIC GEOMETRY**
  - MUST PRESERVE WAVE MECHANICS

Lockheed GenCorp Aerojet
ASRM DIVISION

3

N92-32247

SRMAFTE Facility Checkout Model Flow Field Analysis

Richard A. Dill, ERC Incorporated
Harold R. Whitesides, ERC Incorporated

Abstract

The Solid Rocket Motor Air Flow Equipment (SRMAFTE) facility was constructed for the purpose of evaluating the internal propellant, insulation, and nozzle configurations of solid propellant rocket motor designs. This makes the characterization of the facility internal flow field very important in assuring that no facility induced flow field features exist which would corrupt the model related measurements. In order to verify the design and operation of the facility, a three-dimensional computational flow field analysis was performed on the facility checkout model setup.

The facility checkout model entails a straight constant diameter pipe in place of a specific solid propellant rocket motor internal component. This configuration was to provide a simple internal flow field for evaluation of any facility induced effects.

One-dimensional estimates of the checkout model flow field were available for comparison to the measurement data collected for the checkout model but the CFD results provided a comparative estimate in regions where one-dimensional estimates were not valid.

Since the facility was too large and complex to perform a complete three-dimensional analysis from end to end, the facility was divided into three major zones for analysis. 1) The header pipes, metering nozzle, nozzle exit, and diffuser. 2) The adapter chamber, transition, checkout model section, and checkout model nozzle. 3) The model nozzle exit, diffuser and muffler. The three-dimensional numerical calculation of the flow field was performed by Fluent/BFC. This code solves the full Navier-Stokes equations of fluid flow cast in a staggered grid formulation. The SIMPLER numerical algorithm is used in the solution process. The code utilizes wall functions instead of physically resolving the boundary layer and the standard k-e turbulence model is used to close the system fluid dynamic equations.

The checkout model measurement data, one-dimensional and three-dimensional estimates were compared and the design and proper operation of the facility was verified. The proper operation of the metering nozzles, adapter chamber transition, model nozzle and diffuser were verified. The one-dimensional and three-dimensional flow field estimates along with the available measurement data are compared in this presentation.

SRMAFTE FACILITY CHECKOUT MODEL FLOW FIELD ANALYSIS

Richard A. Dill and R. Harold Whitesides
ERC, Inc.

Tenth Annual CFD Working Group Meeting

Session 8

NASA/MSFC

April 29, 1992

OBJECTIVES

- VERIFY CHECKOUT MODEL SYSTEM DESIGN AND OPERATIONAL PERFORMANCE PARAMETERS INCLUDING TWO AND 3-D EFFECTS

  1) ASYMMETRIC FLOW EFFECTS CREATED BY THE MANIFOLD SYSTEM
  2) METERING NOZZLE PERFORMANCE AND EXPANSION SECTION FLOW FIELD
  3) ASYMMETRIC FLOW FIELD IN THE ADAPTER CHAMBER
  4) UNIFORMITY OF FLOW IN THE CHECKOUT MODEL CHAMBER
  5) MODEL NOZZLE REGION FLOW FIELD
  6) DIFFUSER FLOW FIELD INCLUDING SHOCKS

- COMPARE FACILITY CHECKOUT MODEL TEST DATA WITH CFD RESULTS AS VERIFICATION OF THE CFD CODE

ERC, Inc. 4/29/92

CFD METHODOLOGY

- GOVERNING EQUATIONS ARE THE 3-D ENSEMBLE-AVERAGED NAVIER STOKES EQUATIONS IN CONSERVATION FORM
- CLOSURE OF THE EQUATIONS BY THE STANDARD TWO-EQUATION $\kappa-\varepsilon$ MODEL OF TURBULENCE
- WALL FUNCTIONS USED TO DETERMINE NEAR WALL GRADIENTS
- DISCRETIZATION METHOD
    - GOVERNING EQUATIONS ARE WRITTEN IN COMPONENT FORM USING CONTRAVARIANT VELOCITY COMPONENTS
    - THIS ALLOWS THE USE OF A BOUNDARY FITTED CURVILINEAR COORDINATE SYSTEM
    - NUMERICAL METHOD IS FINITE VOLUME BASED
    - STAGGERED GRID STORAGE SYSTEM IS USED
    - CONVECTION AND DIFFUSION FLUXES ARE APPROXIMATED USING A POWER-LAW SCHEME
    - TIME DERIVATIVES ARE CALCULATED USING A FULLY IMPLICIT FIRST ORDER SCHEME
- PRESSURE-VELOCITY COUPLING IS ACCOMPLISHED BY USING THE SIMPLER ALGORITHM
- SOLVER USES LINEARIZED BLOCK IMPLICIT SCHEME

ERC, Inc. 4/29/92

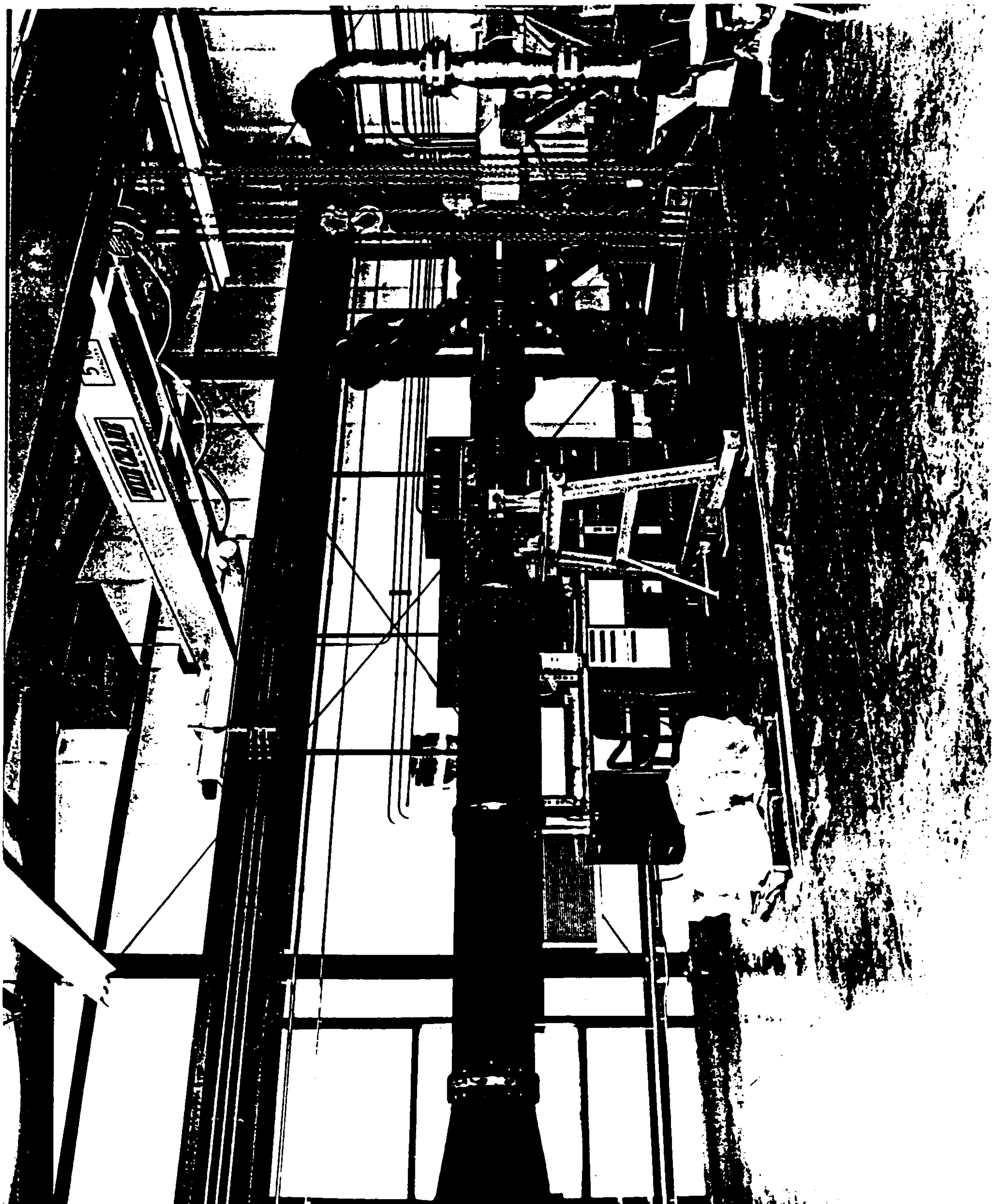

Checkout Model Cutaway

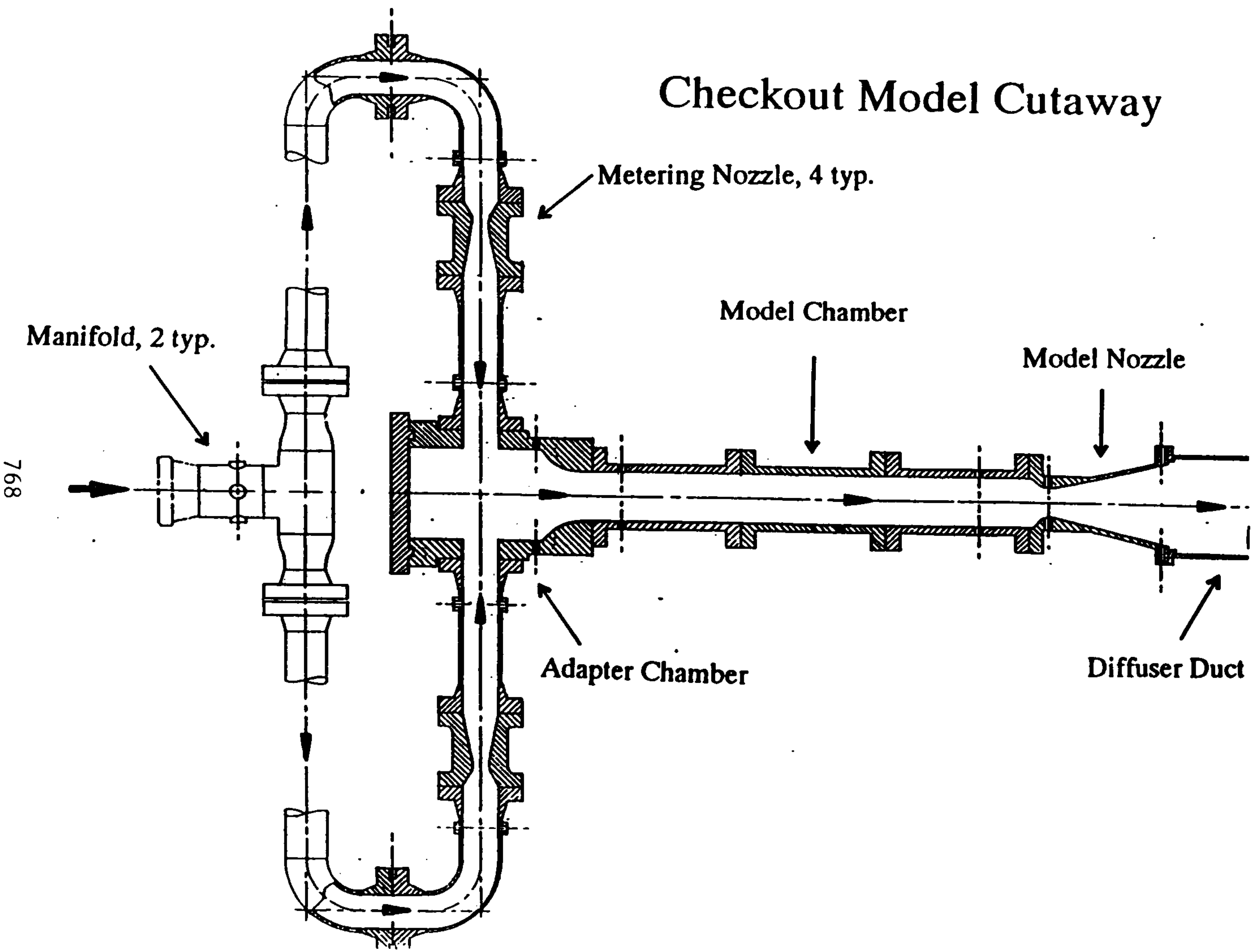

BOUNDARY CONDITIONS USED FOR THE CHECKOUT MODEL HEADER PIPES AND METERING NOZZLE

- **INLET CONDITIONS**

STAGNATION PRESSURE (psia)	:	1200
STAGNATION TEMPERATURE (°R)	:	530
TURBULENCE INTENSITY (%)	:	10
TURBULENCE LENGTH SCALE (m)	:	0.146

- **GENERAL CONDITIONS MODELED**

IDEAL GAS LAW USED		
RATIO OF SPECIFIC HEATS	:	1.4
MOLECULAR WEIGHT	:	28.966
DYNAMIC VISCOSITY (lbm/ft-sec)	:	1.245×10^{-5}

- **EXIT CONDITION**

STATIC PRESSURE (psia)	:	600

ERC, Inc. 4/29/92

COMPUTATIONAL GRID FOR MANIFOLD SYSTEM AND METERING NOZZLE

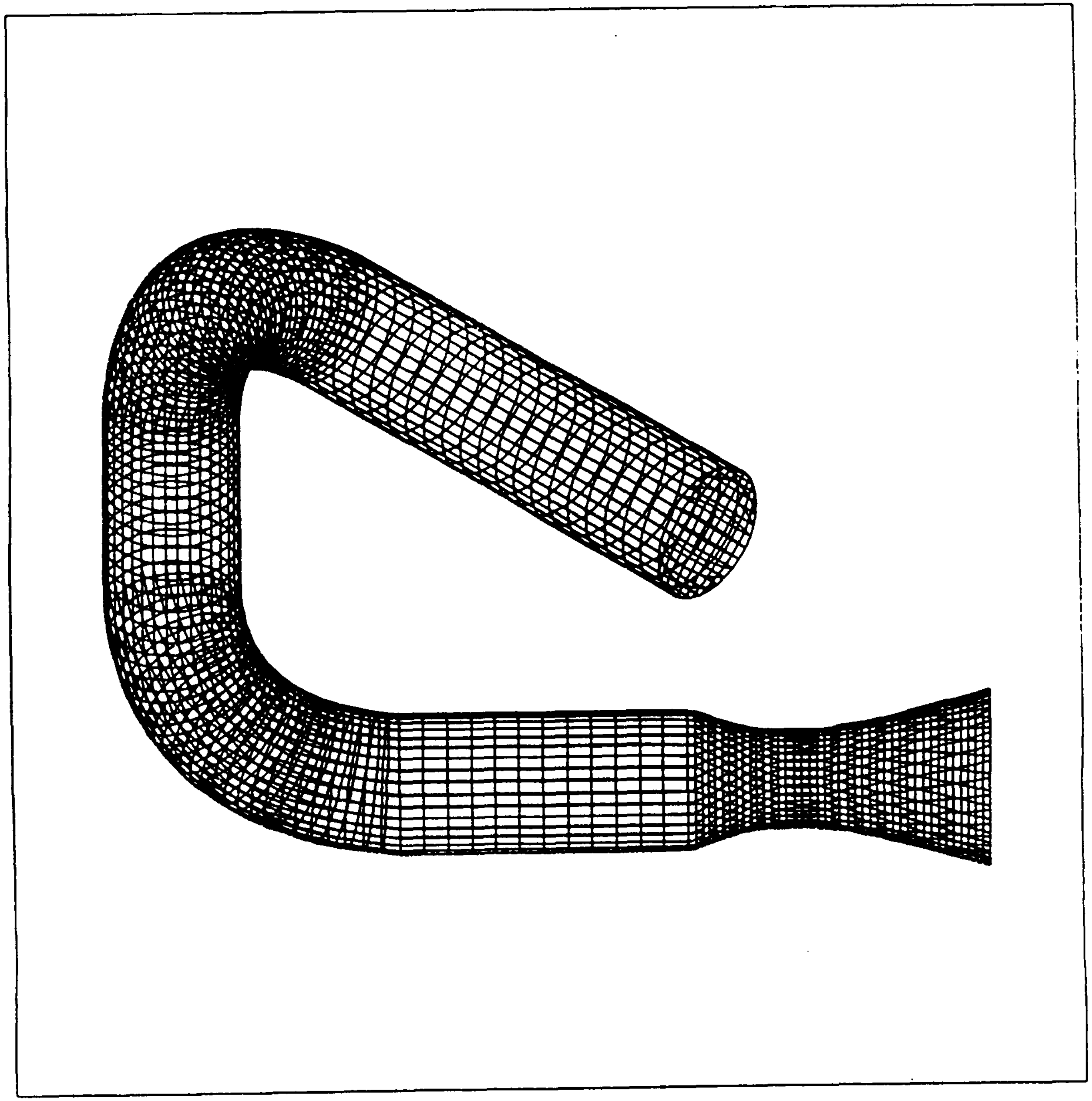

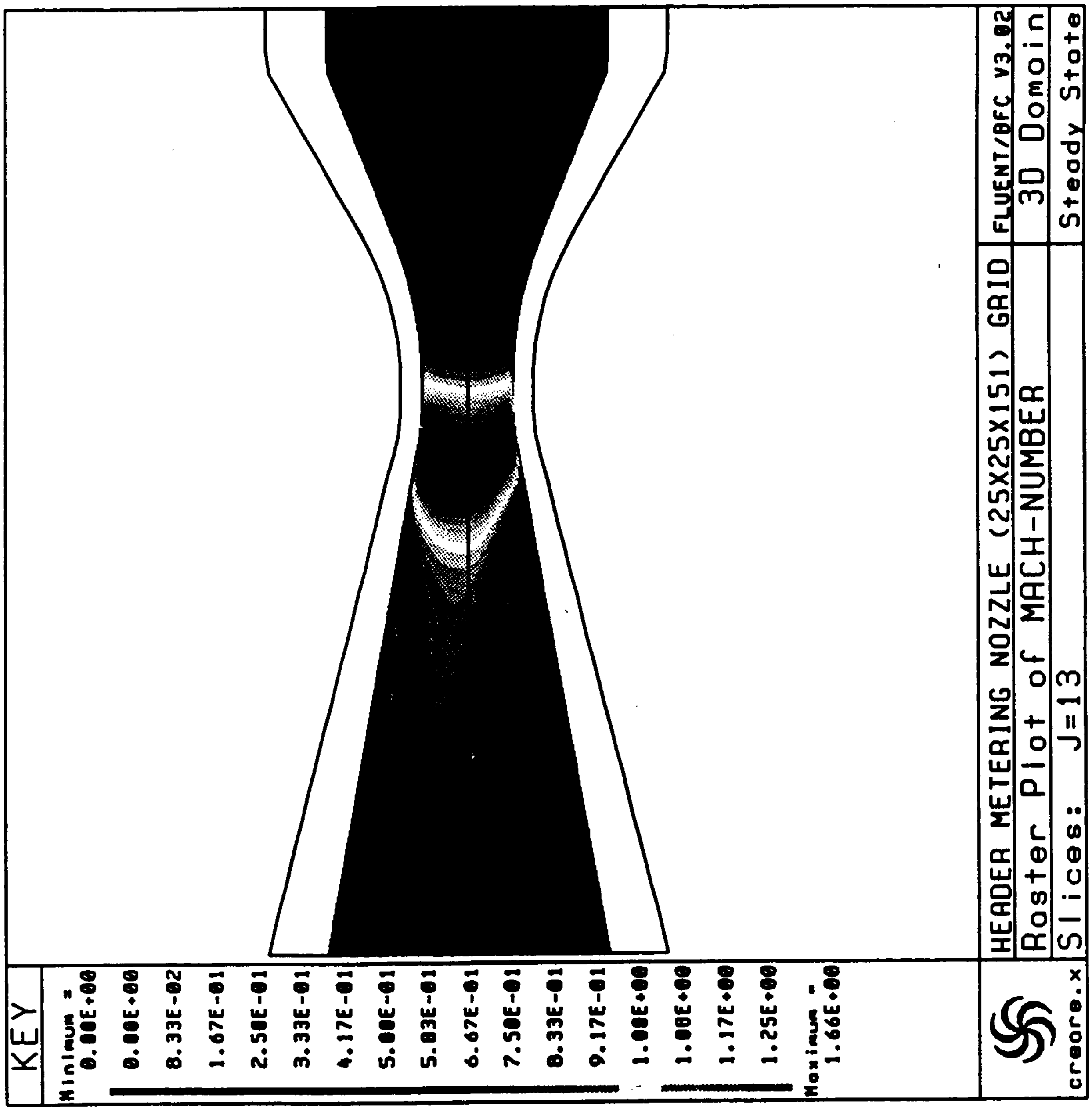

HEADER METERING NOZZLE (25X25X151) GRID
Raster Plot of MACH-NUMBER
Slices: J=13
FLUENT/BFC V3.02
3D Domain
Steady State
creare.x
KEY
Minimum = 0.00E+00
0.00E+00
8.33E-02
1.67E-01
2.50E-01
3.33E-01
4.17E-01
5.00E-01
5.83E-01
6.67E-01
7.50E-01
8.33E-01
9.17E-01
1.00E+00
1.08E+00
1.17E+00
1.25E+00
Maximum = 1.66E+00

Metering Nozzle Radial Pressure Ratio Profile

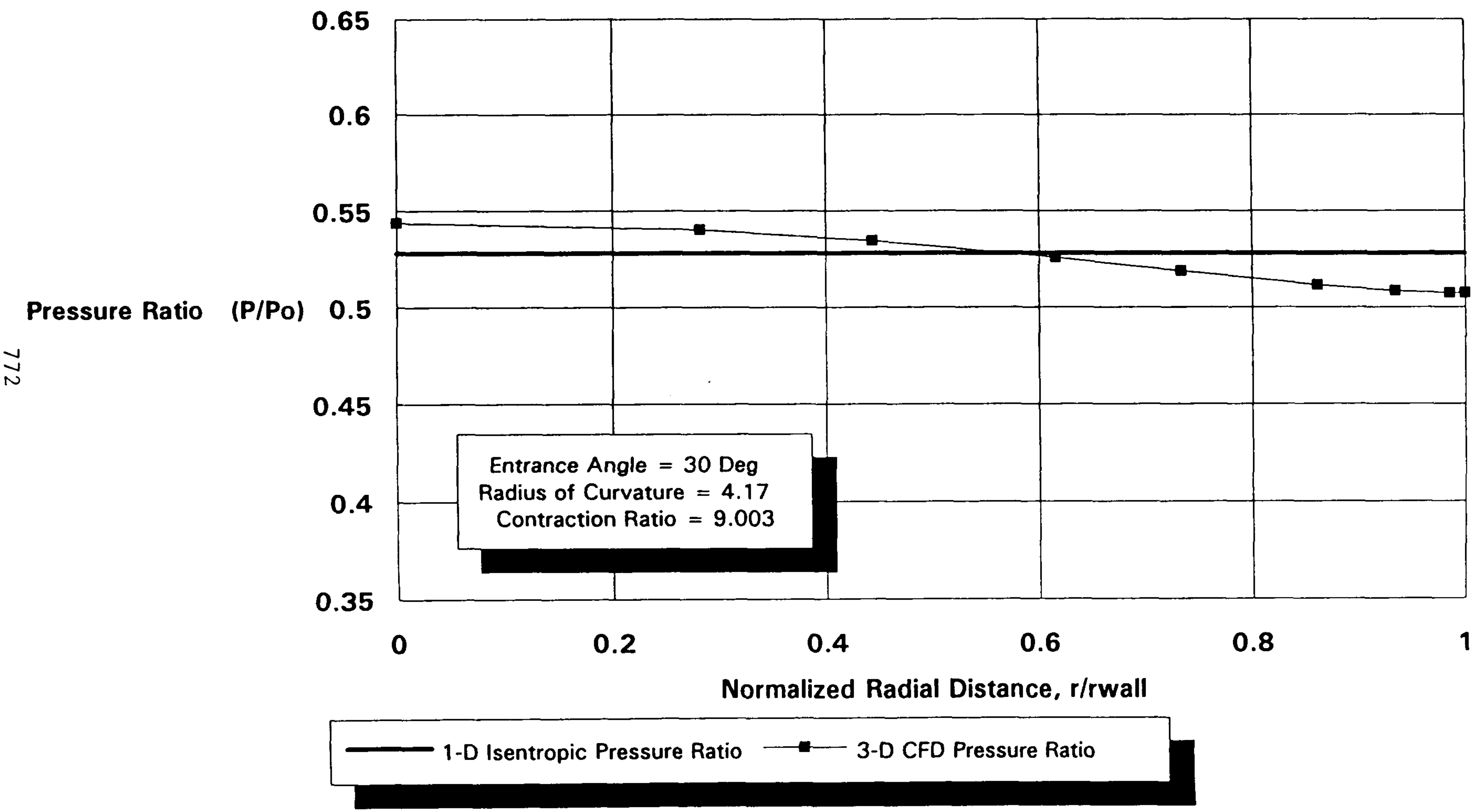

ERCI - 1/8/92

BOUNDARY CONDITIONS USED FOR THE CHECKOUT MODEL ADAPTER, SPOOL PIECES AND MODEL NOZZLE

- **INLET CONDITIONS**

STAGNATION PRESSURE (psia)	:	610
STAGNATION TEMPERATURE (°R)	:	530
TURBULENCE INTENSITY (%)	:	10
TURBULENCE LENGTH SCALE (m)	:	0.146

- **GENERAL CONDITIONS MODELED**

IDEAL GAS LAW USED		
RATIO OF SPECIFIC HEATS	:	1.4
MOLECULAR WEIGHT	:	28.966
DYNAMIC VISCOSITY (lbm/ft-sec)	:	1.245×10^{-5}

- **EXIT CONDITION**

SUPERSONIC OUTLET BOUNDARY CONDITION

ERC, Inc. 4/29/92

CHECKOUT MODEL CHAMBER COMPUTATIONAL GRID

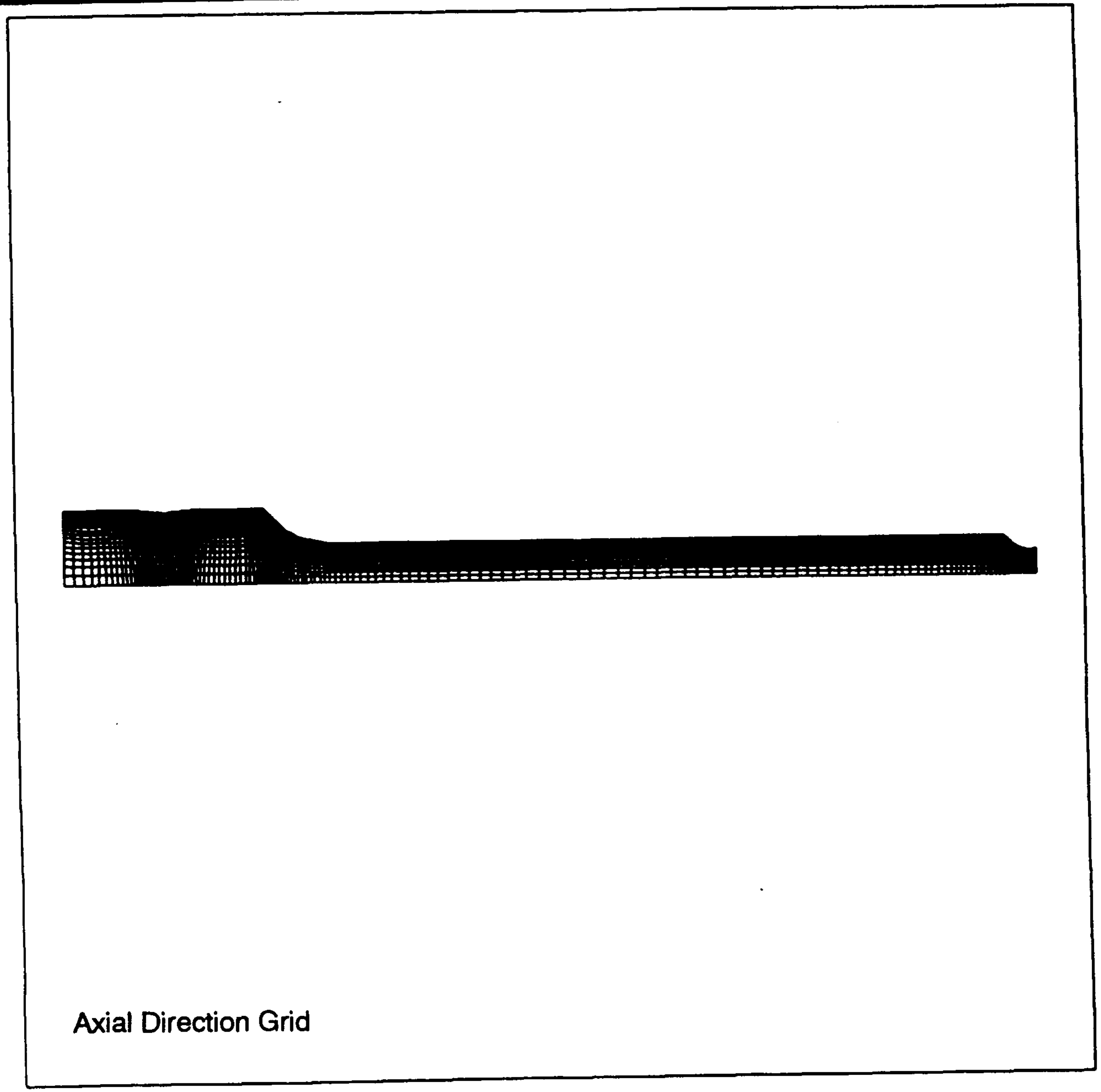

CHECKOUT MODEL CHAMBER COMPUTATIONAL GRID

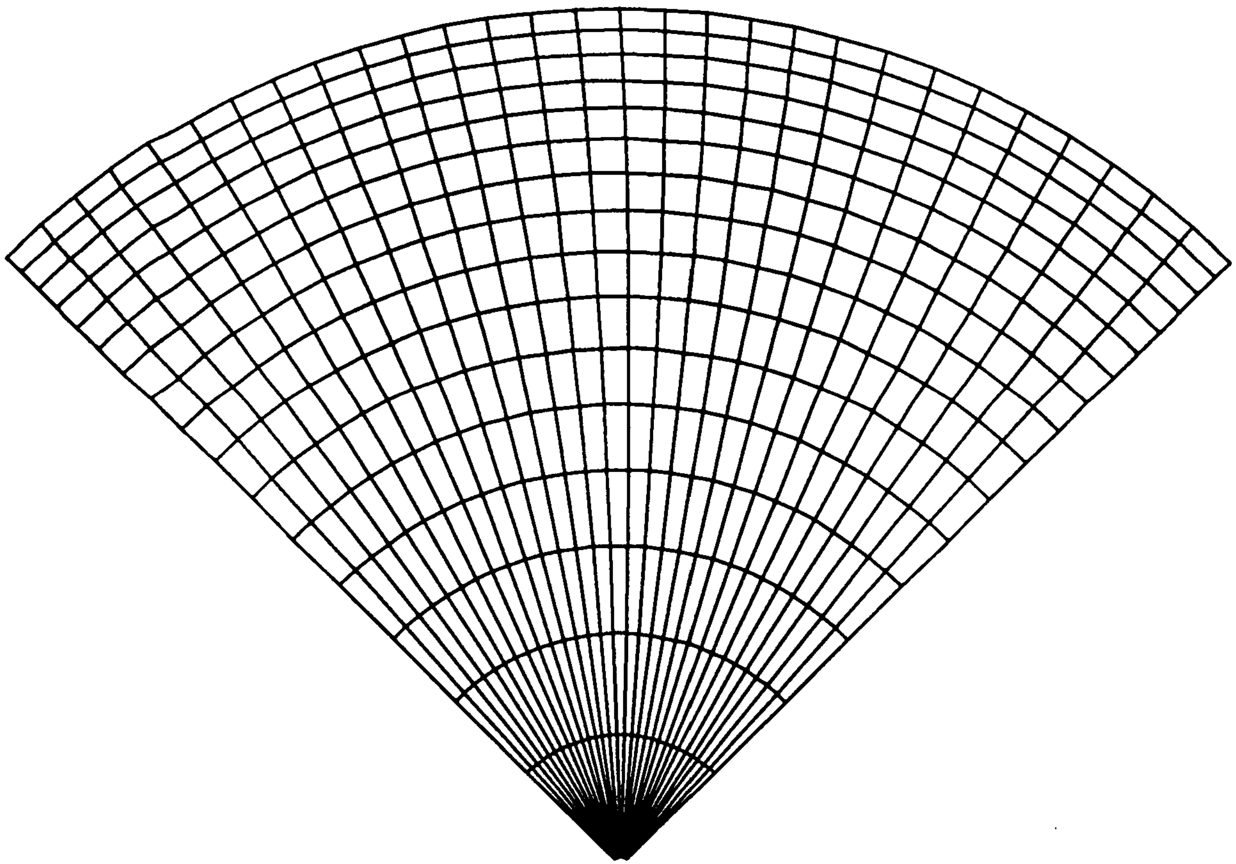

Cross-Section of a Single Axial Station

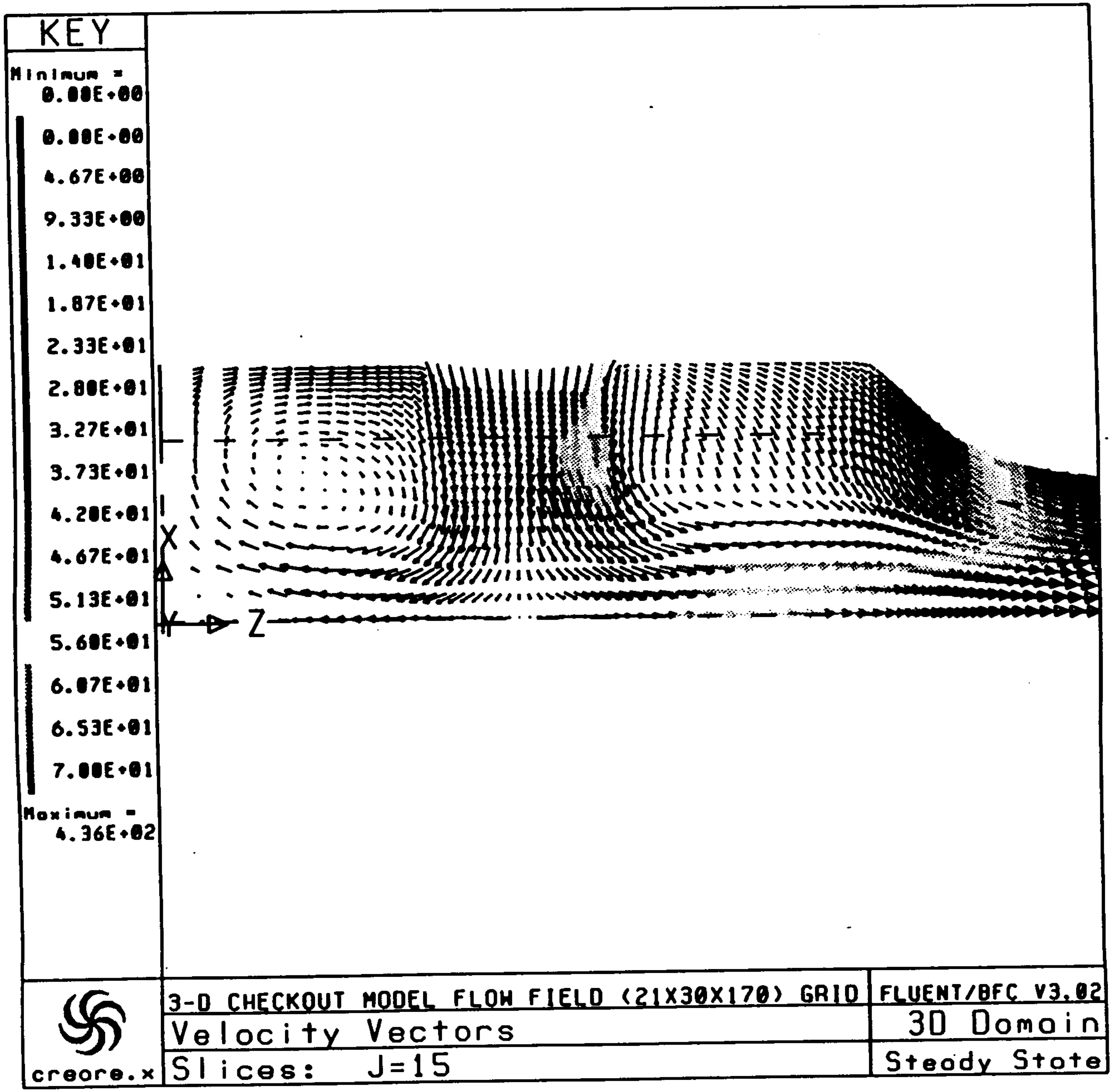
KEY
Minimum = 0.00E+00
0.00E+00
4.67E+00
9.33E+00
1.40E+01
1.87E+01
2.33E+01
2.80E+01
3.27E+01
3.73E+01
4.20E+01
4.67E+01
5.13E+01
5.60E+01
6.07E+01
6.53E+01
7.00E+01
Maximum = 4.36E+02
X
Z
creare.x
3-D CHECKOUT MODEL FLOW FIELD (21X30X170) GRID
Velocity Vectors
Slices: J=15
FLUENT/BFC V3.02
3D Domain
Steady State

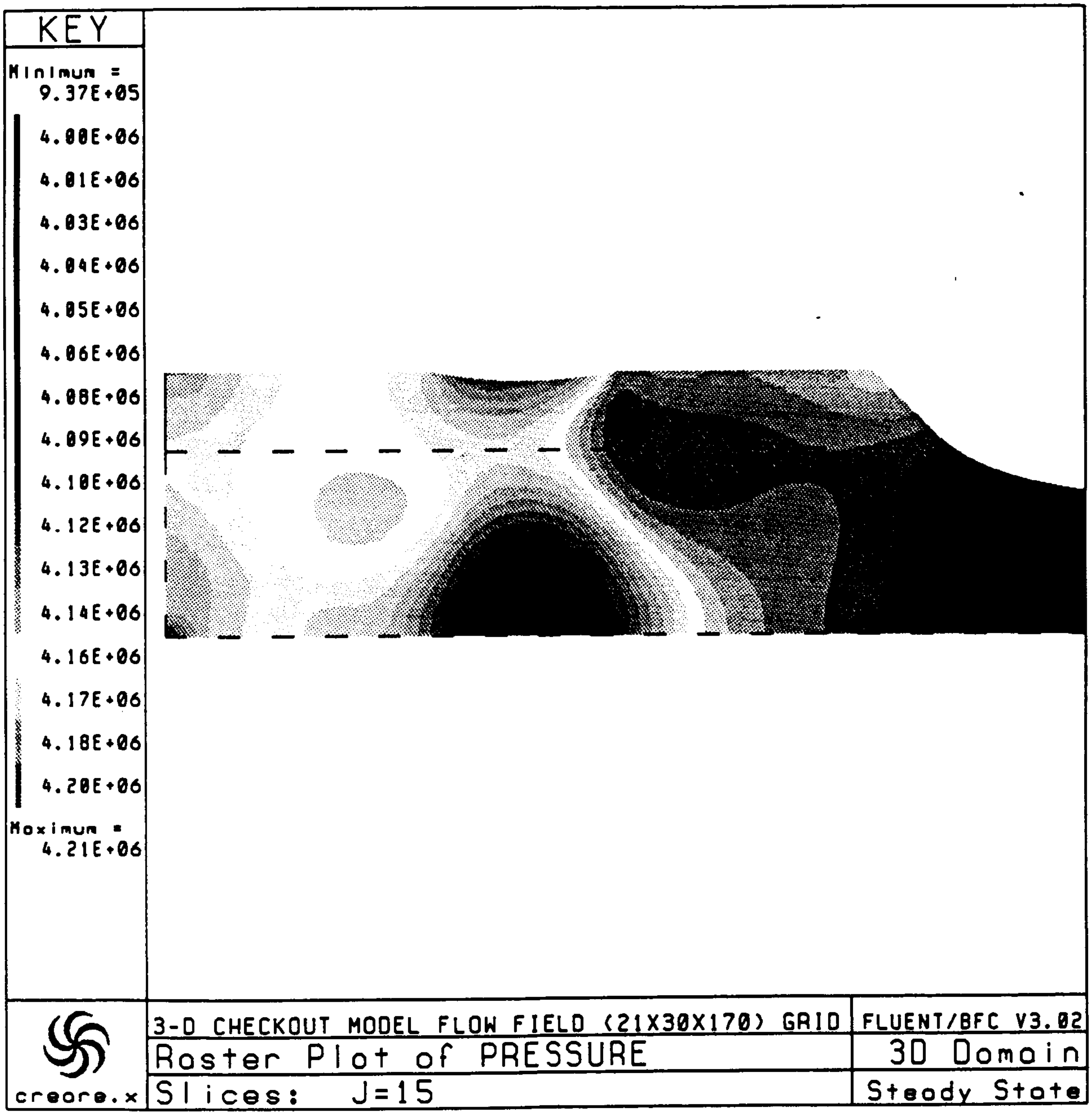
KEY
Minimum =
9.37E+05
4.00E+06
4.01E+06
4.03E+06
4.04E+06
4.05E+06
4.06E+06
4.08E+06
4.09E+06
4.10E+06
4.12E+06
4.13E+06
4.14E+06
4.16E+06
4.17E+06
4.18E+06
4.20E+06
Maximum =
4.21E+06
creare.x
3-D CHECKOUT MODEL FLOW FIELD (21X30X170) GRID
FLUENT/BFC V3.02
Raster Plot of PRESSURE
3D Domain
Slices: J=15
Steady State

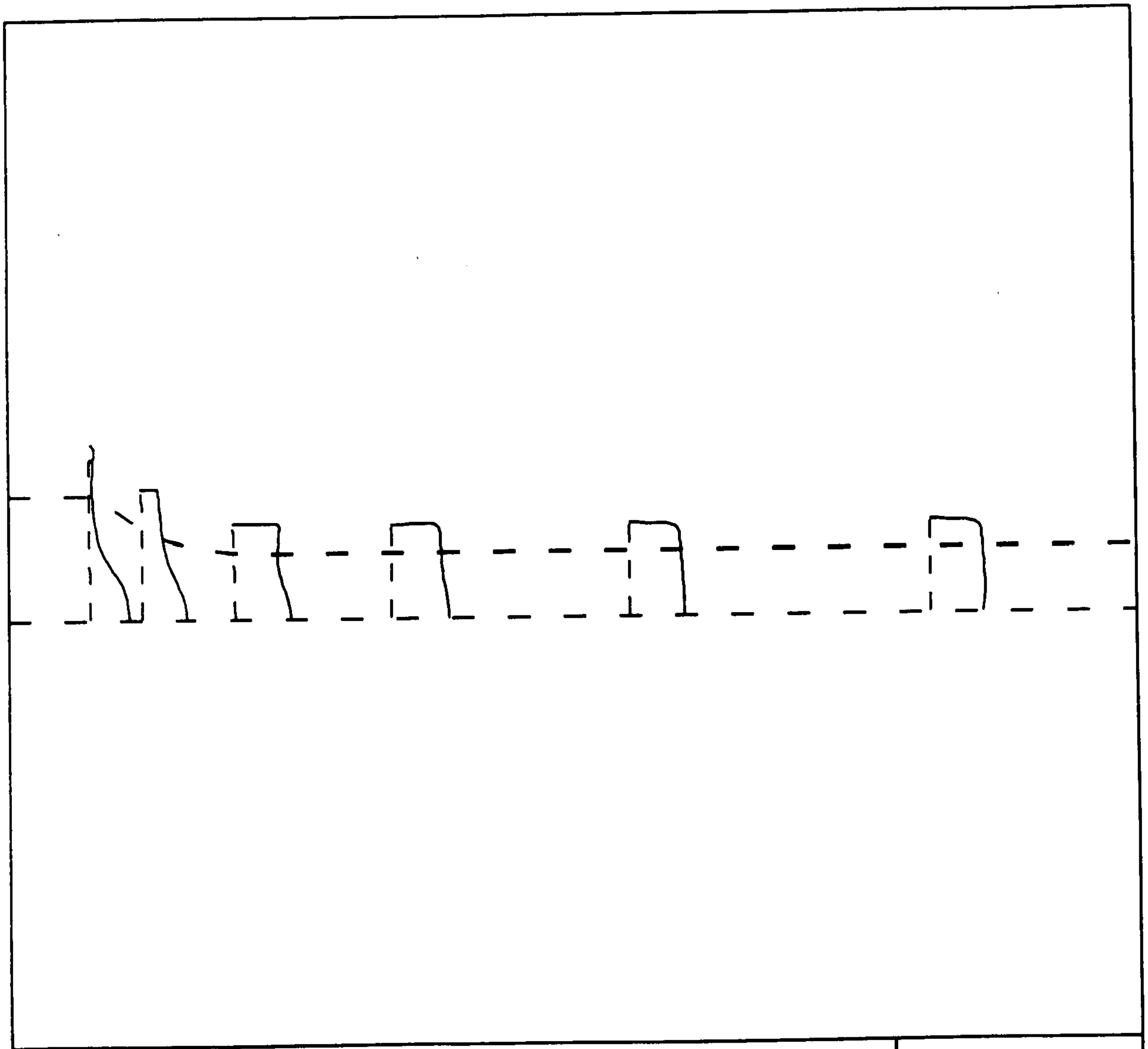

creare.x	3-D CHECKOUT MODEL FLOW FIELD (21X30X170) GRID	FLUENT/BFC V3.02
	Profiles of W-VELOCITY	3D Domain
	Slices: J=15	Steady State

Pressure Ratio and Mach Number Profiles at Model Nozzle Throat Plane

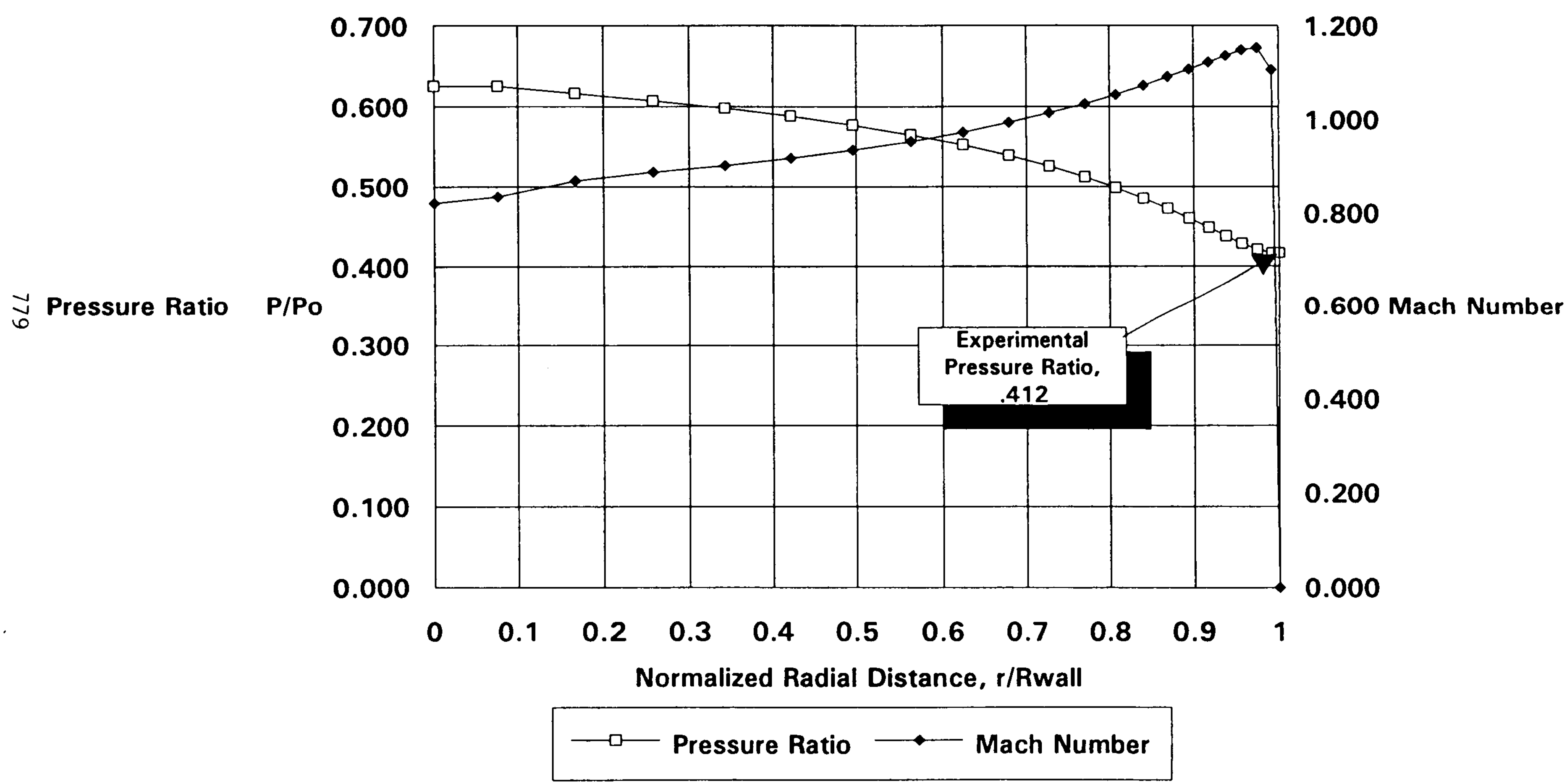

BOUNDARY CONDITIONS USED FOR THE SRMAFTE DIFFUSER

- **INLET CONDITIONS**

STAGNATION PRESSURE (psia)	:	150
STAGNATION TEMPERATURE (°R)	:	530
TURBULENCE INTENSITY (%)	:	5
TURBULENCE LENGTH SCALE (m)	:	0.108

- **GENERAL CONDITIONS MODELED**

IDEAL GAS LAW USED		
RATIO OF SPECIFIC HEATS	:	1.4
MOLECULAR WEIGHT	:	28.966
DYNAMIC VISCOSITY (lbm/ft-sec)	:	1.245×10^{-5}

- **EXIT CONDITION**

STATIC PRESSURE (psia)	:	15

ERC, Inc. 4/29/92

COMPUTATIONAL GRID FOR THE DIFFUSER

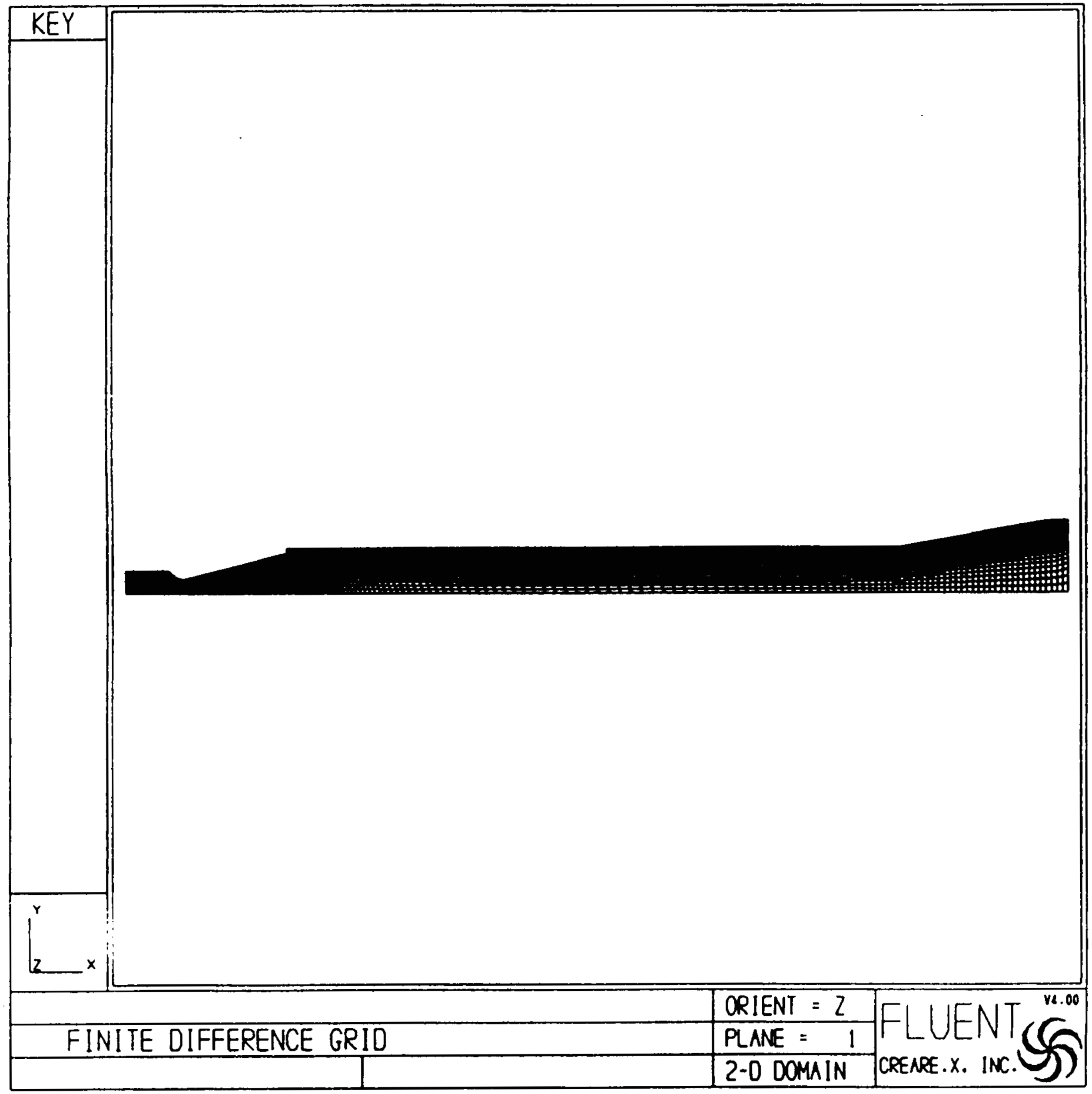

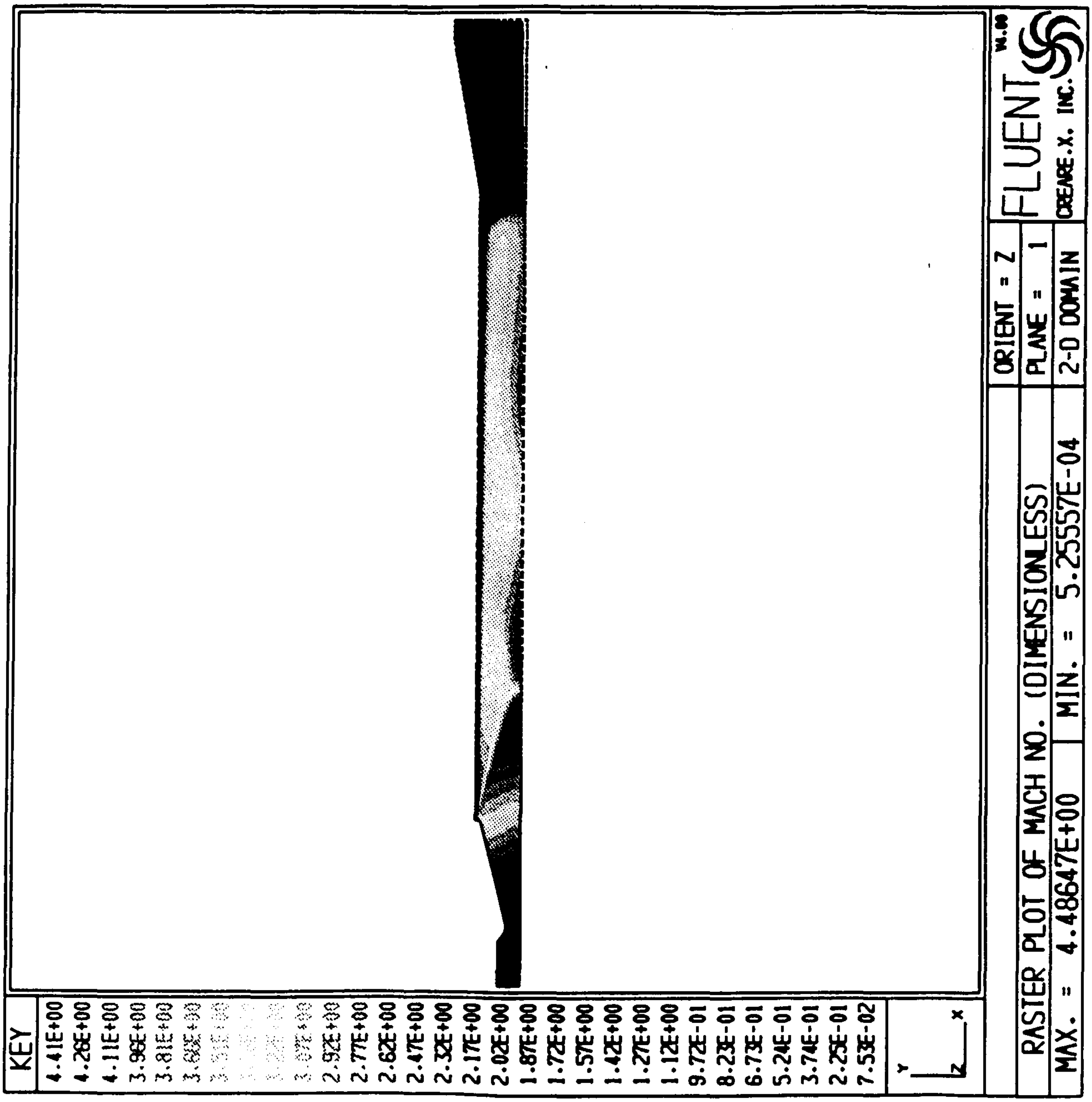
KEY
4.41E+00
4.26E+00
4.11E+00
3.96E+00
3.81E+00
3.66E+00
3.51E+00
3.07E+00
2.92E+00
2.77E+00
2.62E+00
2.47E+00
2.32E+00
2.17E+00
2.02E+00
1.87E+00
1.72E+00
1.57E+00
1.42E+00
1.27E+00
1.12E+00
9.72E-01
8.23E-01
6.73E-01
5.24E-01
3.74E-01
2.25E-01
7.53E-02
Y
X
Z
RASTER PLOT OF MACH NO. (DIMENSIONLESS)
MAX. = 4.48647E+00
MIN. = 5.25557E-04
ORIENT = Z
PLANE = 1
2-D DOMAIN
FLUENT V4.00
CREARE.X. INC.

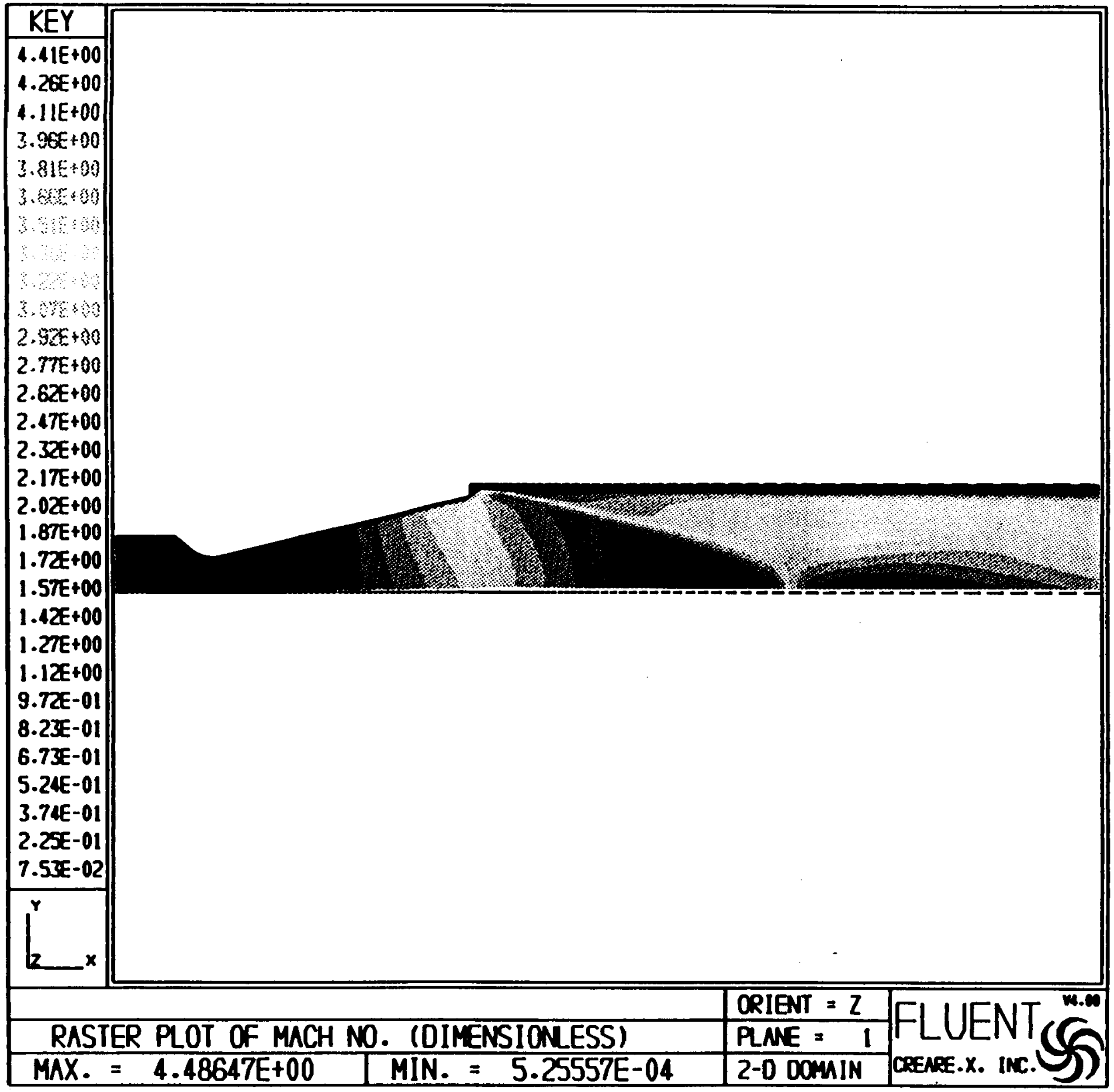
KEY
4.41E+00
4.26E+00
4.11E+00
3.96E+00
3.81E+00
3.66E+00
3.51E+00
3.07E+00
2.92E+00
2.77E+00
2.62E+00
2.47E+00
2.32E+00
2.17E+00
2.02E+00
1.87E+00
1.72E+00
1.57E+00
1.42E+00
1.27E+00
1.12E+00
9.72E-01
8.23E-01
6.73E-01
5.24E-01
3.74E-01
2.25E-01
7.53E-02
Y
Z
X
RASTER PLOT OF MACH NO. (DIMENSIONLESS)
MAX. = 4.48647E+00
MIN. = 5.25557E-04
ORIENT = Z
PLANE = 1
2-D DOMAIN
FLUENT
V4.00
CREARE.X. INC.

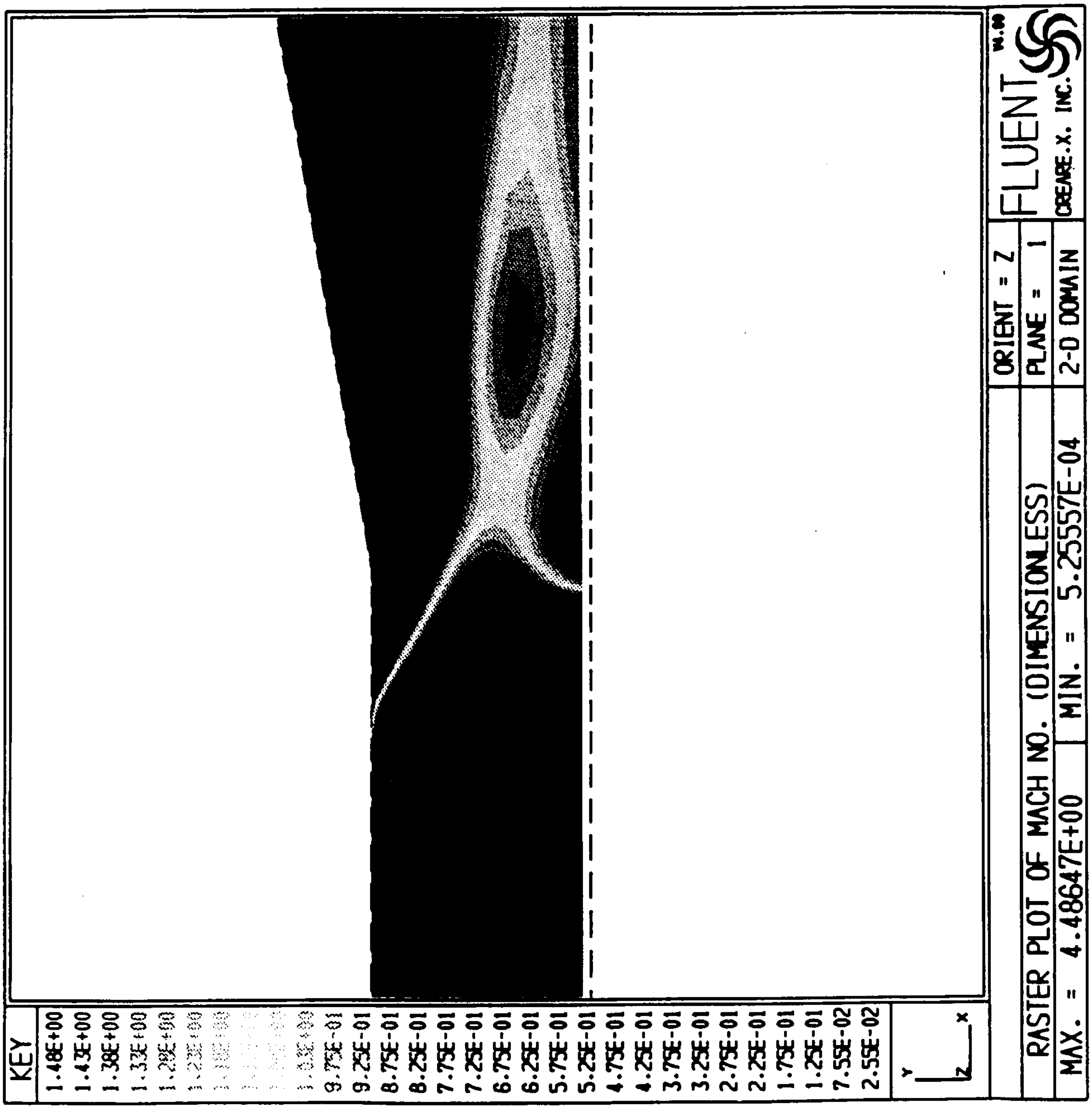
KEY
1.48E+00
1.43E+00
1.38E+00
1.33E+00
1.28E+00
1.23E+00
9.75E-01
9.25E-01
8.75E-01
8.25E-01
7.75E-01
7.25E-01
6.75E-01
6.25E-01
5.75E-01
5.25E-01
4.75E-01
4.25E-01
3.75E-01
3.25E-01
2.75E-01
2.25E-01
1.75E-01
1.25E-01
7.55E-02
2.55E-02
Y
X
Z
RASTER PLOT OF MACH NO. (DIMENSIONLESS)
MAX. = 4.48647E+00
MIN. = 5.25557E-04
ORIENT = Z
PLANE = 1
2-D DOMAIN
FLUENT V4.00
CREARE.X. INC.

Diffuser Performance Map

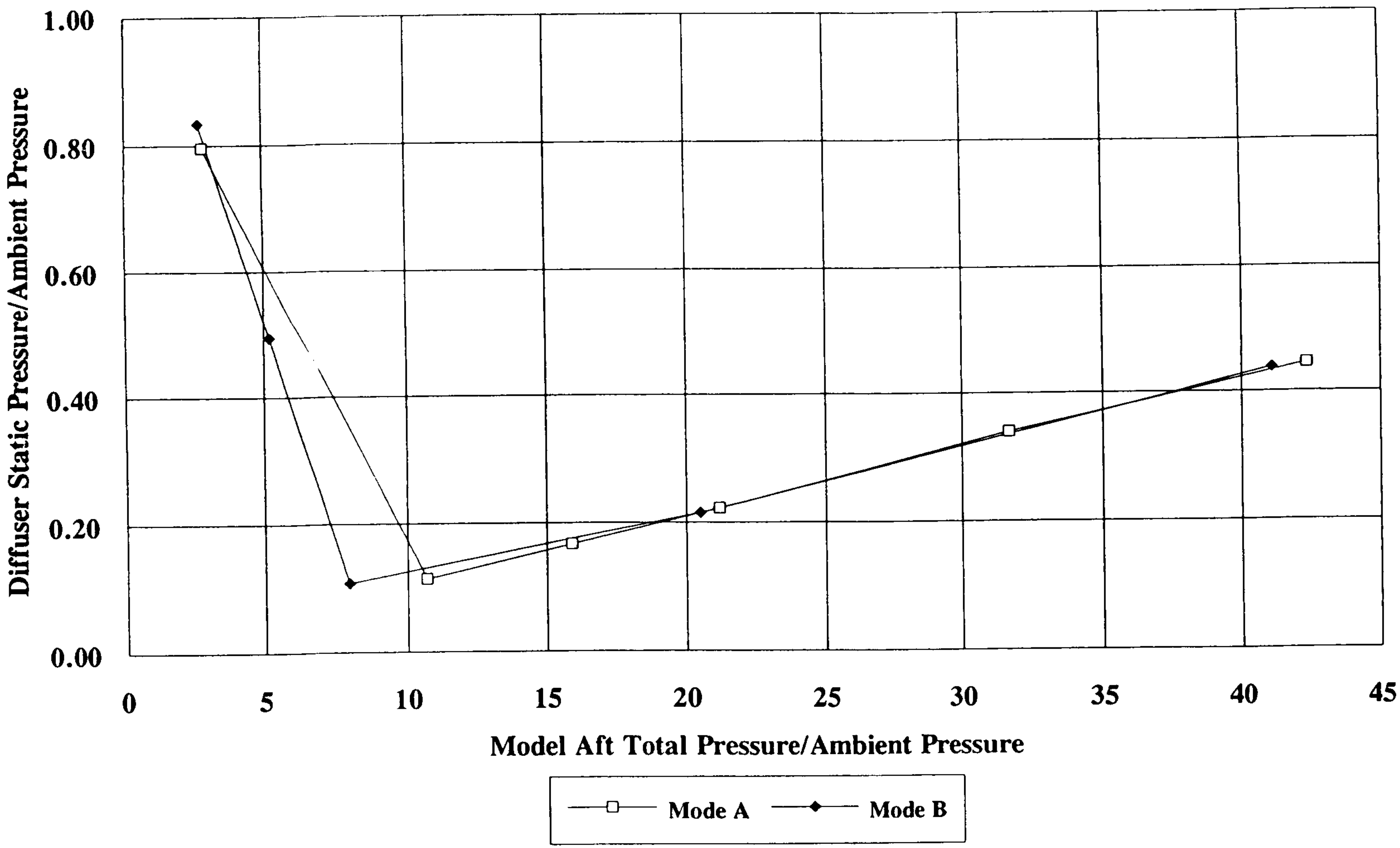

CONCLUSIONS

THE CFD ANALYSES OF THE CHECKOUT MODEL, MANIFOLD SYSTEM AND DIFFUSER CONFIRMED THE DESIGN AND VERIFIED THAT:

1) THE FLOW CHOKES IN BOTH THE METERING AND MODEL NOZZLE AND THE MANIFOLD SYSTEM SHOULD PERFORM AS EXPECTED.

2) THE ADAPTER AND TRANSITION SECTION PERFORM WELL IN DELIVERING A UNIFORM FLOW PROFILE TO THE MODEL NOZZLE.

3) THE PREDICTED SHOCK STRUCTURE IN THE DIFFUSER INDICATES THE DESIGN SHOULD PERFORM AS EXPECTED.

ERC, Inc. 4/29/92

N92-32248

A Comparative Study of the Effects of Inhibitor Stub Length on Solid Rocket Motor Combustion Chamber Pressure Oscillations: RSRM at T=80 Seconds, Preliminary Results

D. Chasman, D. Burnette, J. Holt
Rockwell International, Space Systems Division
Huntsville, Alabama 35806
R. Farr
NASA Science and Engineering Laboratory
George C. Marshall Space Flight Center

ABSTRACT

Results from a continuing, time-accurate computational study of the combustion gas flow inside the Space Shuttle Redesigned Solid Rocket Motor (RSRM) are presented. These CFD analyses duplicate unsteady flow effects which interact in the RSRM to produce pressure oscillations, and resulting thrust oscillations, at nominally 15, 30 and 45 Hz. Results of Navier-Stokes computations made at mean pressure and flow conditions corresponding to 80 seconds after motor ignition both with and without a protruding, rigid inhibitor at the forward joint cavity are presented here.

Previous studies by the authors have demonstrated that combustion chamber pressure oscillations in the RSRM are generated by flow/acoustic interactions which occur at the three field joint cavities [1,2,3]. Edge-tone, Hole-tone and Organ pipe-tone are all acoustic sources that play part in these interactions[4,5,6]. By constructive interference proccesses, the different acoustic sources interact, amplifying the pressure oscillation level at some instant during the RSRM burn (i.e. T+80 sec). This behavior is representitive of an aerodynamic whistle of Class III [7,8].

However, the question remained as to whether the cavities alone are the main acoustic generators or whether protruding inhibitors dominate the system. With this in mind, two simulations have been conducted. The first simulation represent a full scale model of the RSRM with a rigid inhibitor perturbing the flow at the forward joint, while the second simulation was conducted without an inhibitor. All other flow conditions and grain geometries were kept constant for both simulations.

Fig. 1 shows a comparison of results between the two simulations. A full-length density contour plot of the simulation with forward inhibitor is shown in Fig. 1a., while that without the inhibitor is shown in Fig. 1d.. In both plots the shear layer which developed from the burning surfaces is apparent. High density values, corresponding to areas of high pressure amplitude, appear in red.

Details of the forward field joint area are shown for both simulations in Figs. 1b. and 1e.. Both show intense, but different, shear flow activity indicative of vortex dynamics. Streamlines shown in Fig. 1c. and Fig. 1f. single out individual vortices and further illustrate the difference between the two simulations.

Fig. 2 illustrates a comparison of pressure data time histories for three points common to both simulations. It can be seen that 30 Hz oscillations are evident in the midsection of the chamber, while 15 Hz is found at both the head and aft ends, with the head end being 180 degrees out of phase with the aft end. These results indicate classic organ pipe acoustics are found in both simulations. However, there is a marked difference in the peak-to-peak amplitude of these pressure oscillations. These preliminary results show pressure amplitude in the case **without** the inhibitor are about 14% of total chamber pressure, while those in the case **with** the inhibitor are only 10% of the total pressure.

While calculated peak-to-peak pressure amplitude values are significally higher than levels measured during actual firing and flight, we feel these results can nevertheless be used for comparative analyses of the effects of inhibitor stub height on RSRM combustion chamber acoustic pressure amplitudes. Specifically, these findings demonstrate that the inhibitors alone are not the dominant factor in amplifying combustion chamber pressure oscillations, but rather are included in secondary acoustic/flow interactions occuring at the three field joint cavities. Our results indicate that inhibitors, when present, actually act to damp such oscillations.

References

1. D., R. Farr, T. Nesman, D. Burnette,and Chasman, D., " **Time-Accurate Navier-Stokes Computations of Low Speed Flow Over Cavities: No Slip vs. Blowing Walls"**, Fourth International Symposium on Computational Fluid Dynamics, Davis California, September 1991.

2. R. Farr, T. Nesman, Chasman, D., and D. Burnette, " **Time-Accurate Navier-Stokes Computations of Pressure Oscillation in the RSRM, 80 seconds after Ignition"**, Fourth International Symposium on Computational Fluid Dynamics, Davis California, September 1991.

3. Burnette, D., J. M. O'Farrell, J. Holt, R. A. Farr, T. Nesman " **Time Accurate Navier-Stokes Computations of Solid Rocket Motor Internal Field Joint Cavity Flows"**, TABES 91 Paper No. 91-269, Seventh Annual Technical and Business Exhibition and Symposium, Huntsville Alabama, May 1991.

4. Powell, A., **"On The Edgetone"**, J. Acoust. Soc. of America, Vol. 33, No. 4, pp. 395-409, 1961.

5. Powell, A., **"Nature of the Feedback Mechanism in Some Fluid Flows Producing Sound"**, 4th International Congress on Acoustics, No. 022, Copenhagen, Aug. 1962.

6. Rossiter, J. E. , **"Wind Tunnel Experiments on the Flow over Rectangular Cavities at Subsonic and Transonic Speeds"**, Royal Aircraft Establishment Technical Report No. 64037, October 1964.

7. Chanaud, R.C. and Powell, A., **"Some Experiments Concerning the Hole and Ring Tone"**, J. Acoust. Soc. of America, Vol. 37, NO. 5, pp 902-911, May 1965.

8. Chanaud, R.C., **"Aerodynamic Whistles"**, Scientific American, January 1970.

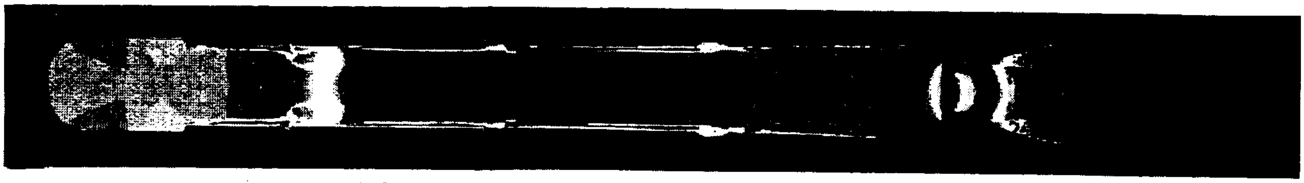

a) Simulation With Forward Inhibitor (Density)

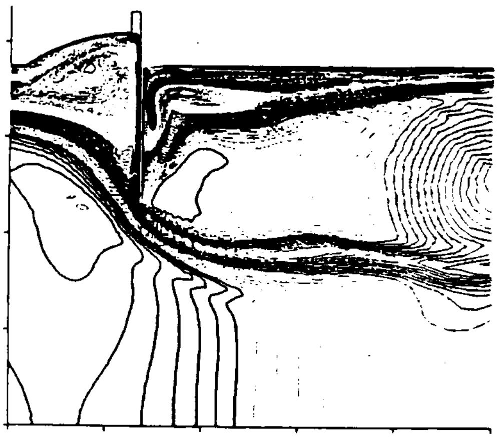

b) Density Detail
With Forward Inhibitor

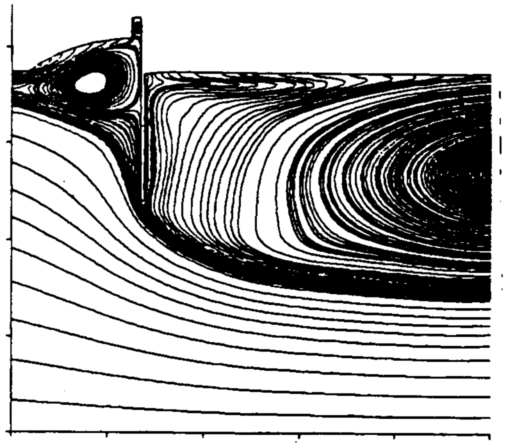

c) Streamline Detail
With Forward Inhibitor

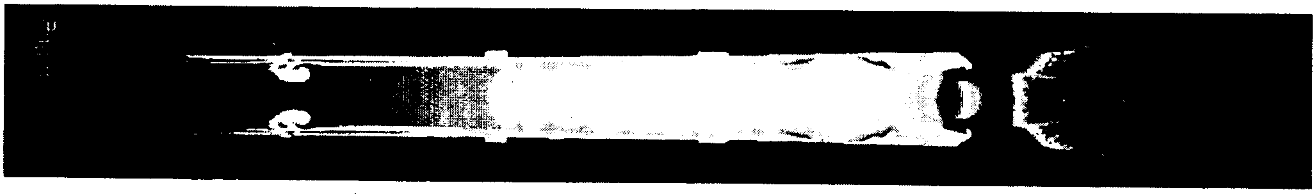

d) Simulation Without Forward Inhibitor (Density)

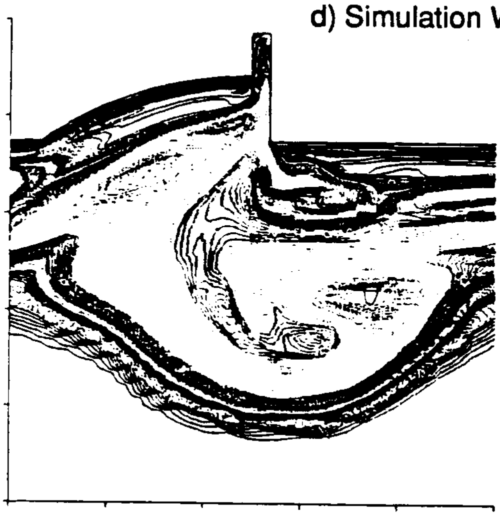

e) Density Detail
Without Forward Inhibitor

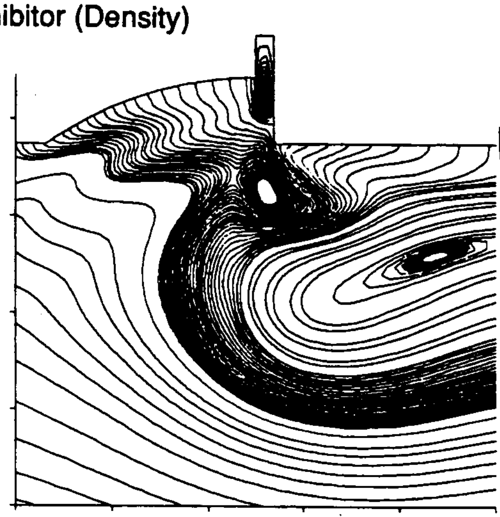

f) Streamline Detail
Without Forward Inhibitor

Figure 1. Simulations With and Without Forward Inhibitor

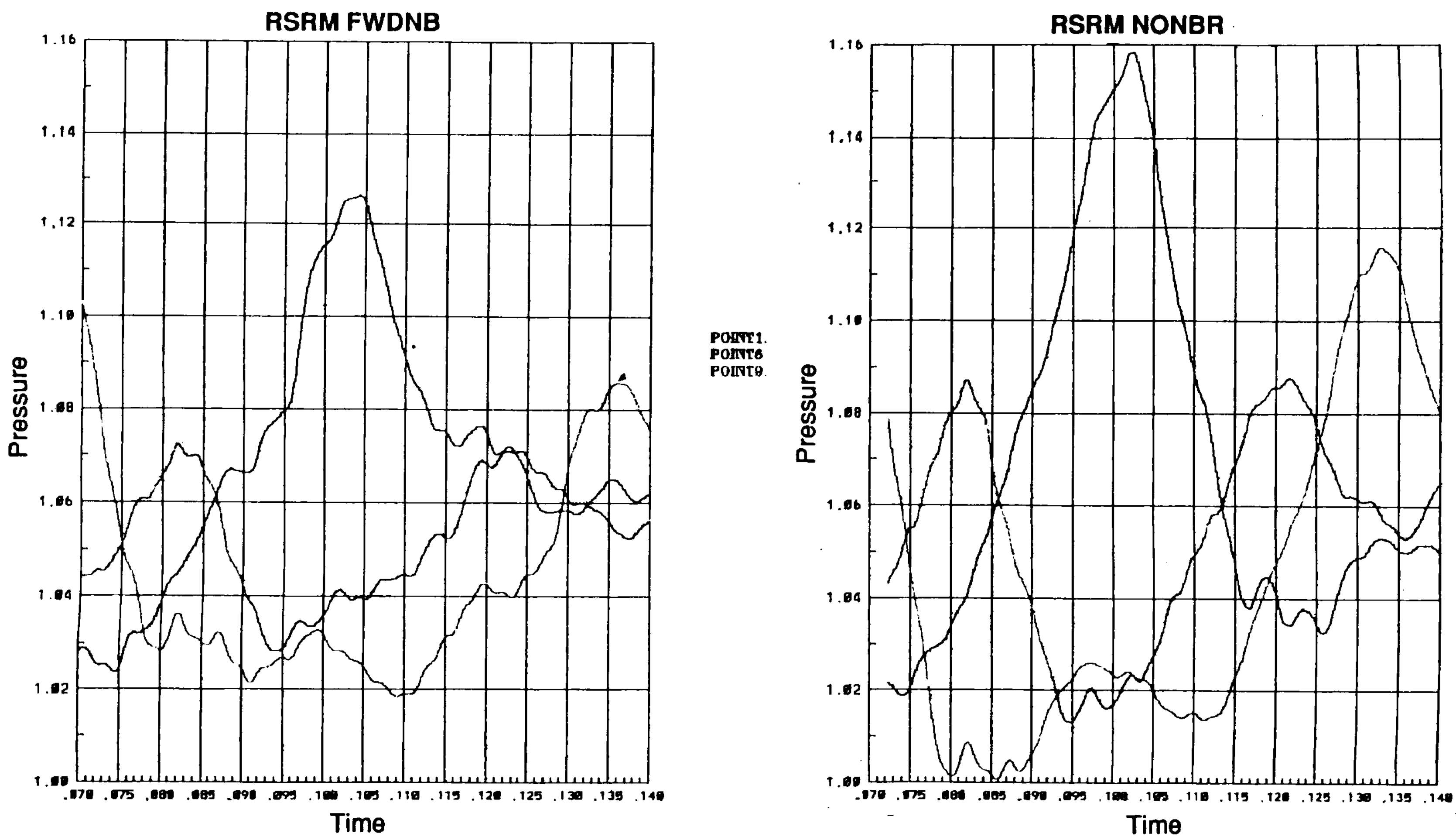

a) Simulation with FWD inhibitor

b) Simulation without FWD inhibitor

Figure 2. Pressure data history of selected points in the RSRM chamber at T + 80 sec:

i. Point 1 is located in the head end
ii. Point 6 is located in the middle
iii. Point 9 is located in the aft end

Rockwell International

Space Systems Division

Huntsville Operations

N92-32249

Overview of the relevant CFD work at Thiokol Corporation

Pawel Chwalowski & Hai-Tien Loh
Thiokol Corporation, M/S L63, P.O. Box 707,
Brigham City, Utah 84302-0707

The use of computational fluid dynamics (CFD) in supporting the rocket propulsion designs at Thiokol Corporation has continuously increased in the past few years. An in-house developed proprietary advanced CFD code called SHARP© is a primary tool for many flow simulations and design analyses. The SHARP code is a time dependent, two-dimensional (2-D) axisymmetric numerical solution technique for the compressible Navier-Stokes equations. The solution technique in SHARP uses a vectorizable implicit, second order accurate in time and space, finite-volume scheme based on the following: 1) an upwind flux-difference splitting of a Roe-type approximated Riemann solver, 2) Van Leer's flux vector splitting, and 3) a fourth order artificial dissipation scheme with a preconditioning to accelerate the flow solution. Turbulence is simulated by an algebraic model, and ultimately the k-ε model. Some other capabilities of the code are 2-D two-phase Lagrangian particle tracking and cell blockages. Extensive development and testing has been conducted on the three-dimensional (3-D) version of the code with flow, combustion, and turbulence interactions.

The SHARP code has been applied in many areas of the solid rocket motor (SRM) design involving internal and external flow analysis. However, the internal flow analysis inside the motor and in the nozzle region are the most frequent. Usually, the results from these CFD analyses become the boundary conditions for thermal and structural computations. In the case of the internal nozzle flow calculations, SHARP computes the convective heat transfer coefficients and temperature distribution along the nozzle wall for the thermal erosion predictions, and the pressure distribution for the structural predictions. The pressure loads on the propellant grain surfaces inside the SRM obtained from SHARP are used as a boundary conditions to predict propellant grain deformation and displacement.
The 2-D two-phase Lagrangian particle tracking gives the ability to predict solid particle impingement on the exit cone. Also, SHARP prediction of the slag accumulation in the aft dome region of the SRM agrees with the actual static test data.

The emphasis in the presentation will be put on the specific applications of SHARP in SRM design.

© SHock wave And Recirculation Program is a copyrighted acronym owned by Thiokol Corporation.

OVERVIEW OF THE RELEVANT CFD WORK AT THIOKOL CORPORATION

SPACE OPERATIONS

Pawel Chwalowski

CFD Workshop

April 28, 1992

Thiokol CORPORATION
SPACE OPERATIONS

AGENDA

- CFD Tools Used at Thiokol Corp.
- Description of the Primary CFD Code
- Applications in the Solid Rocket Motor (SRM) Design

CFD TOOLS

PHOENICS (versions 1.4 and 1.5)

- -well developed and tested for many incompressible and/or subsonic flow cases (includes heat conduction, multiphase flow, reactive flow, etc.)
- -works well for incompressible and/or subsonic flow
- -finite volume SIMPLE scheme (Semi-Implicit Method for Pressure Linked Equation)
- -exhibits problems for high speed compressible and turbulent modeling
- -lacks flexibility in BFC gridding

SHARP

- -developed in-house by Thiokol; considered proprietary
- -2D version extensively tested and operational
- -3D version in development and testing

SHARP 2D DESCRIPTION

- Flow Modeling
  - 2D Planar/Axisymmetric Compressible Code
  - 2D Lagrangian Particle Tracking
- Solution Algorithm
  - Upwind Roe Flux Difference Splitting
  - Upwind Van Leer's Flux Vector Splitting
  - Central Difference with Artificial Dissipation

SHARP 2D DESCRIPTION (cont.)

Features

- Finite Volume / Second Order Accuracy in Time
- Use of Preconditioning to Accelerate Flow Solution
- Cell Blockage
- Baldwin-Lomax Algebraic Turbulence Model (Ultimately k-ε Model)
- Unstructured Grid in Testing

SHARP 3D CODE

SHARP 3D in Development and Testing with Flow, Combustion, and Turbulence Interaction

APPLICATIONS IN SRM DESIGN

Internal Flow Modeling

Nozzle Flow

-heat transfer coefficients and temperature distribution along nozzle wall are calculated for the thermal erosion analysis

-pressure along nozzle wall is calculated for the structural analysis

-aluminum oxide particle motion is predicted and better understood

Thiokol CORPORATION
SPACE OPERATIONS

SHARP Results
Internal Flow Modeling
Nozzle Flow
Pressure Contour (N/m^2)

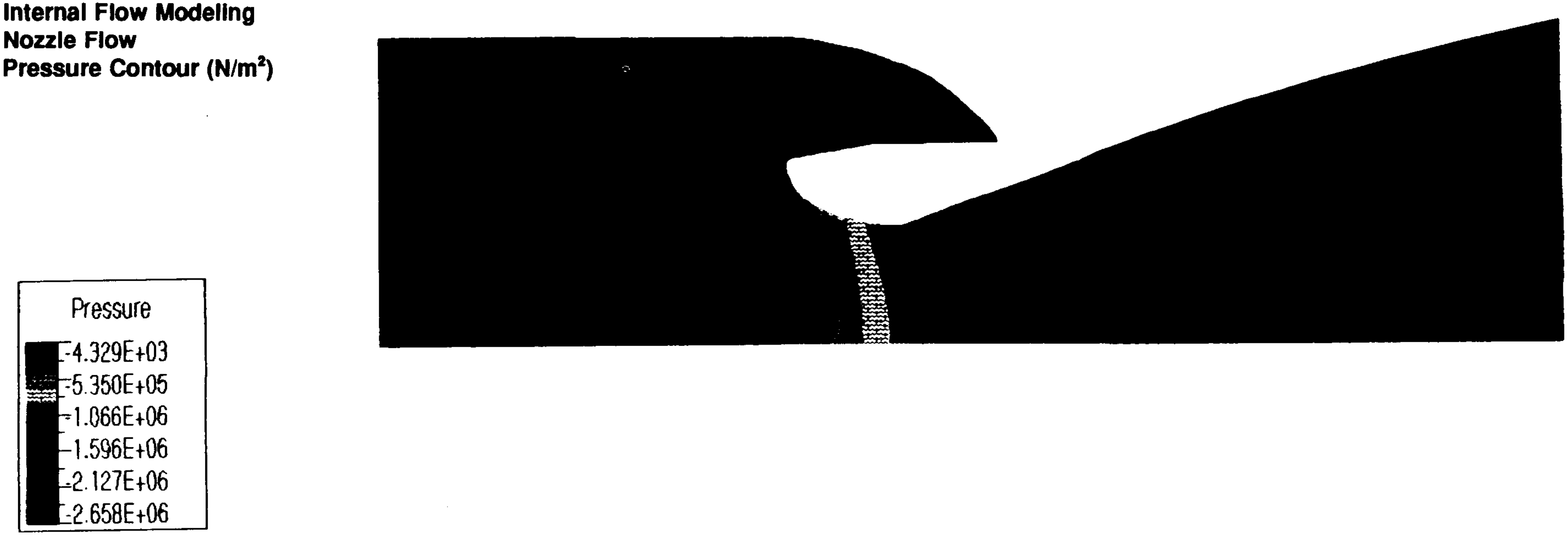

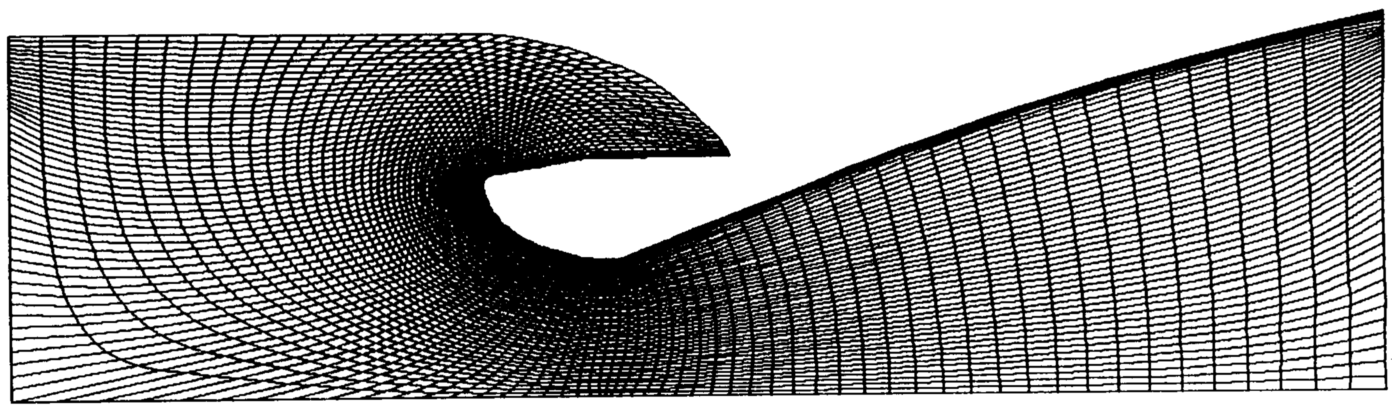

Thiokol CORPORATION
SPACE OPERATIONS

INFORMATION ON THIS PAGE WAS PREPARED TO SUPPORT AN ORAL PRESENTATION AND CANNOT BE CONSIDERED COMPLETE WITHOUT THE ORAL DISCUSSION

SHARP Results
Internal Flow Modeling
Nozzle Flow
Mach Contour
Temperature Contour (K)

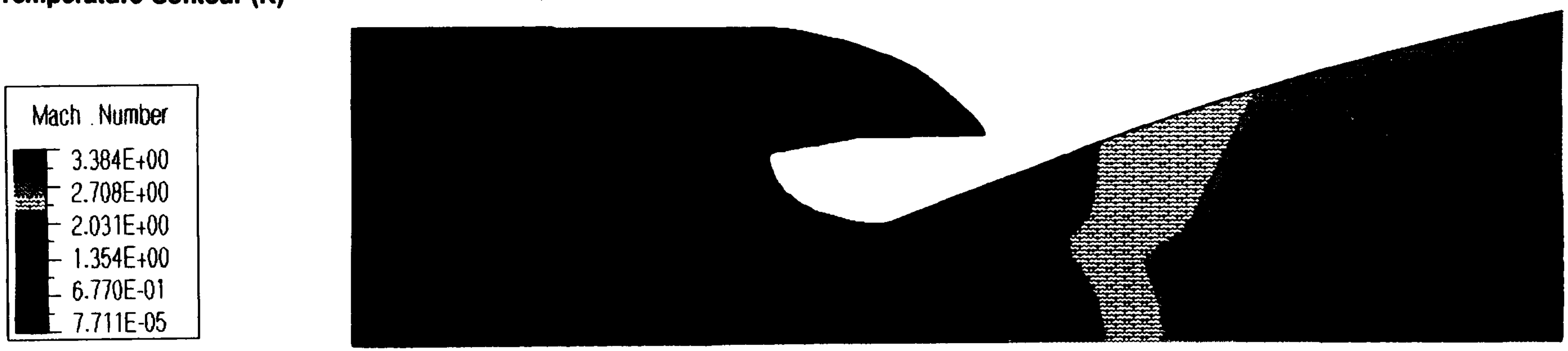

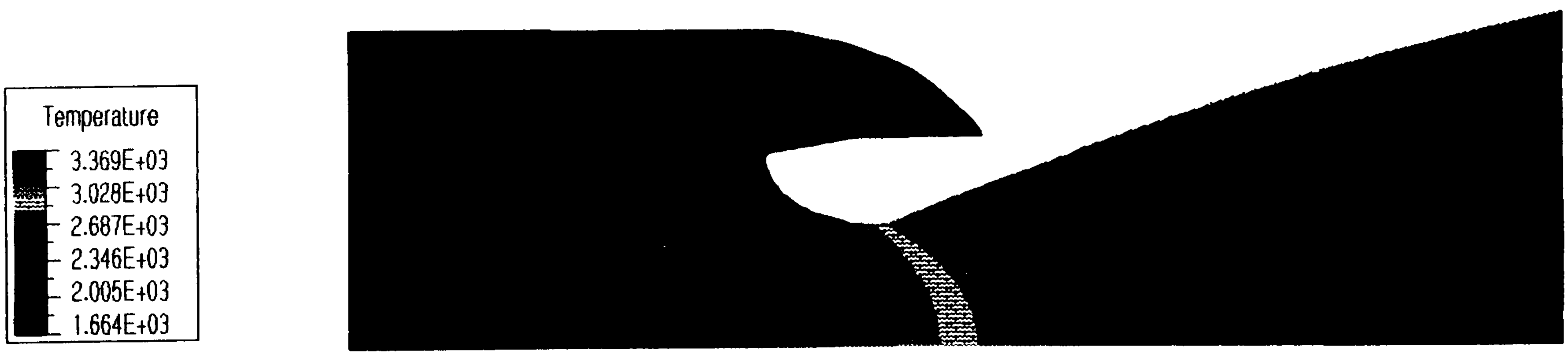

Thiokol CORPORATION
SPACE OPERATIONS

INFORMATION ON THIS PAGE WAS PREPARED TO SUPPORT AN ORAL PRESENTATION AND CANNOT BE CONSIDERED COMPLETE WITHOUT THE ORAL DISCUSSION

SHARP Results
Internal Flow Modeling
Nozzle Flow

Shuttle SRM Aluminum Oxide Particle Motion At Different Burn Times

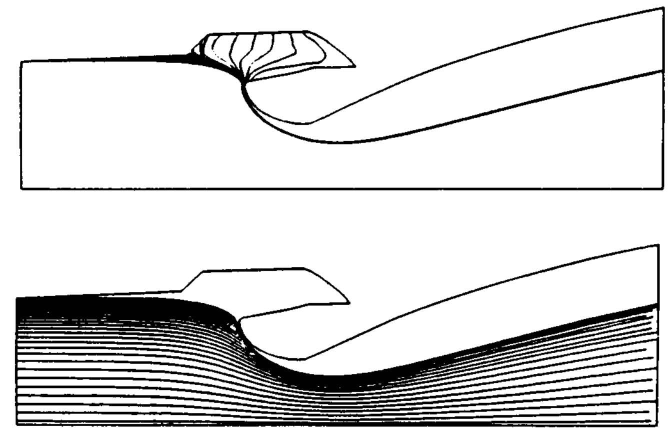

a) 35 seconds

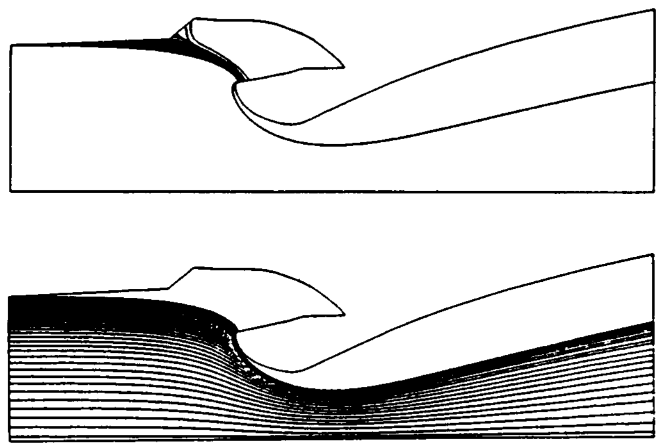

b) 52 seconds

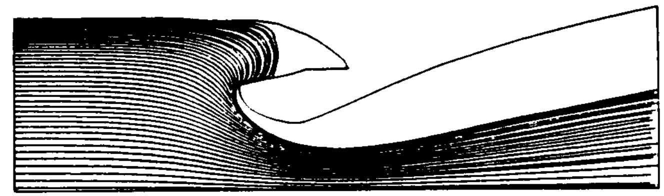

c) 79 seconds

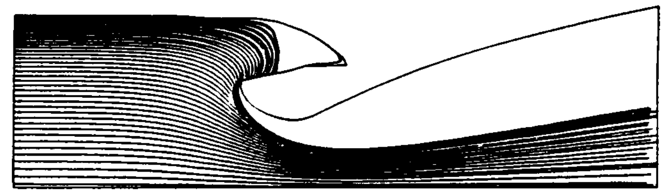

d) 111 seconds

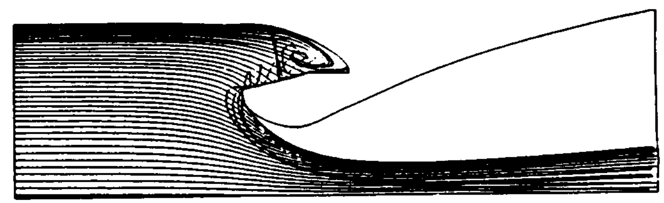

e) 120 seconds

Thiokol CORPORATION
SPACE OPERATIONS

INFORMATION ON THIS PAGE WAS PREPARED TO SUPPORT AN ORAL PRESENTATION AND CANNOT BE CONSIDERED COMPLETE WITHOUT THE ORAL DISCUSSION

APPLICATIONS IN SRM DESIGN (cont.)

Internal Flow Modeling (cont.)

Chamber Internal Flow

-pressure loads on the propellant grain surfaces are calculated to predict propellant grain deformation and displacement

Internal Flow Modeling
Shuttle SRM Internal Flow
Pressure Contour (psi)

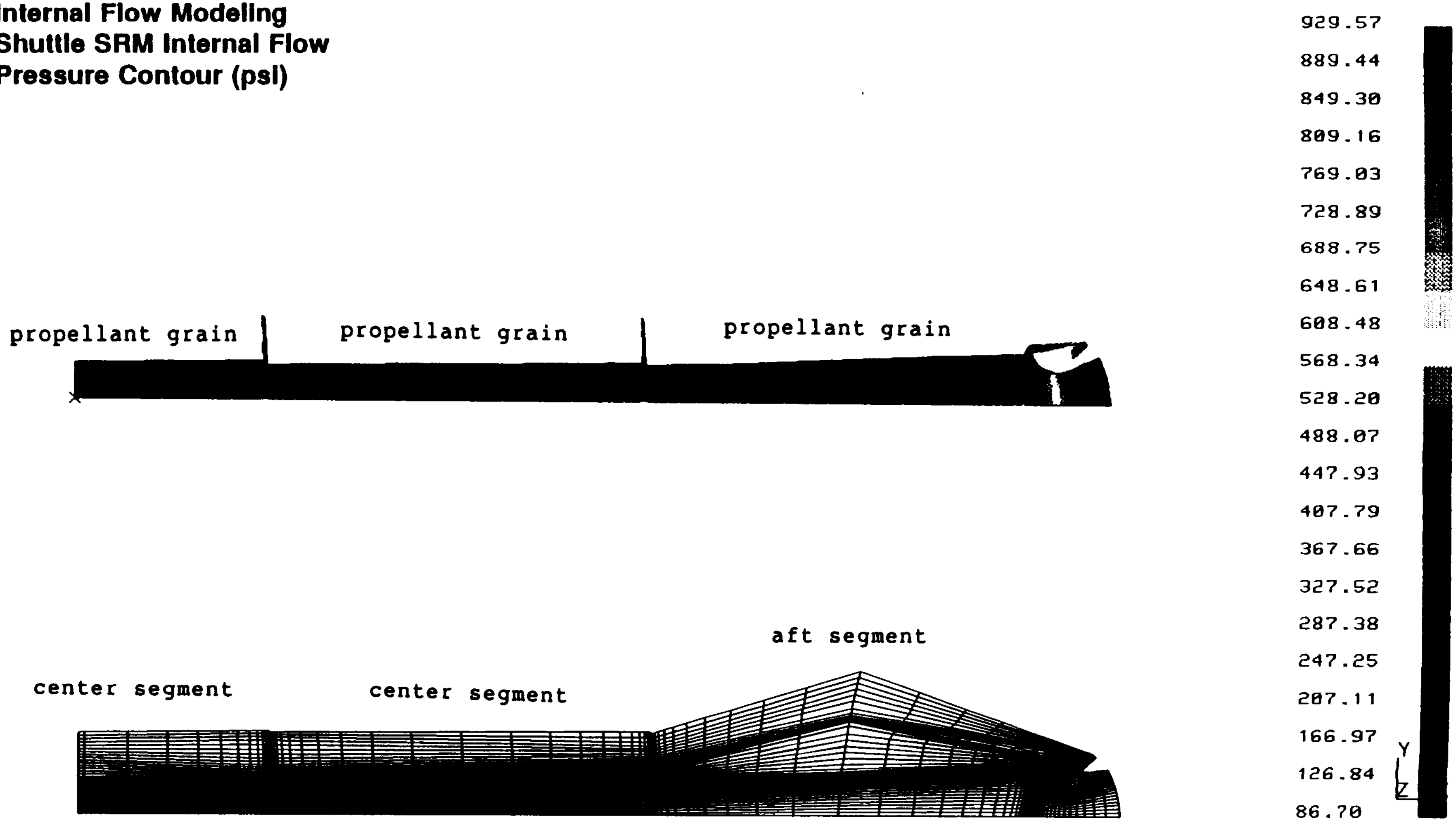

Thiokol CORPORATION
SPACE OPERATIONS

Internal Flow Modeling
Shuttle SRM Internal Flow
Velocity Vector Contour (ft/sec)

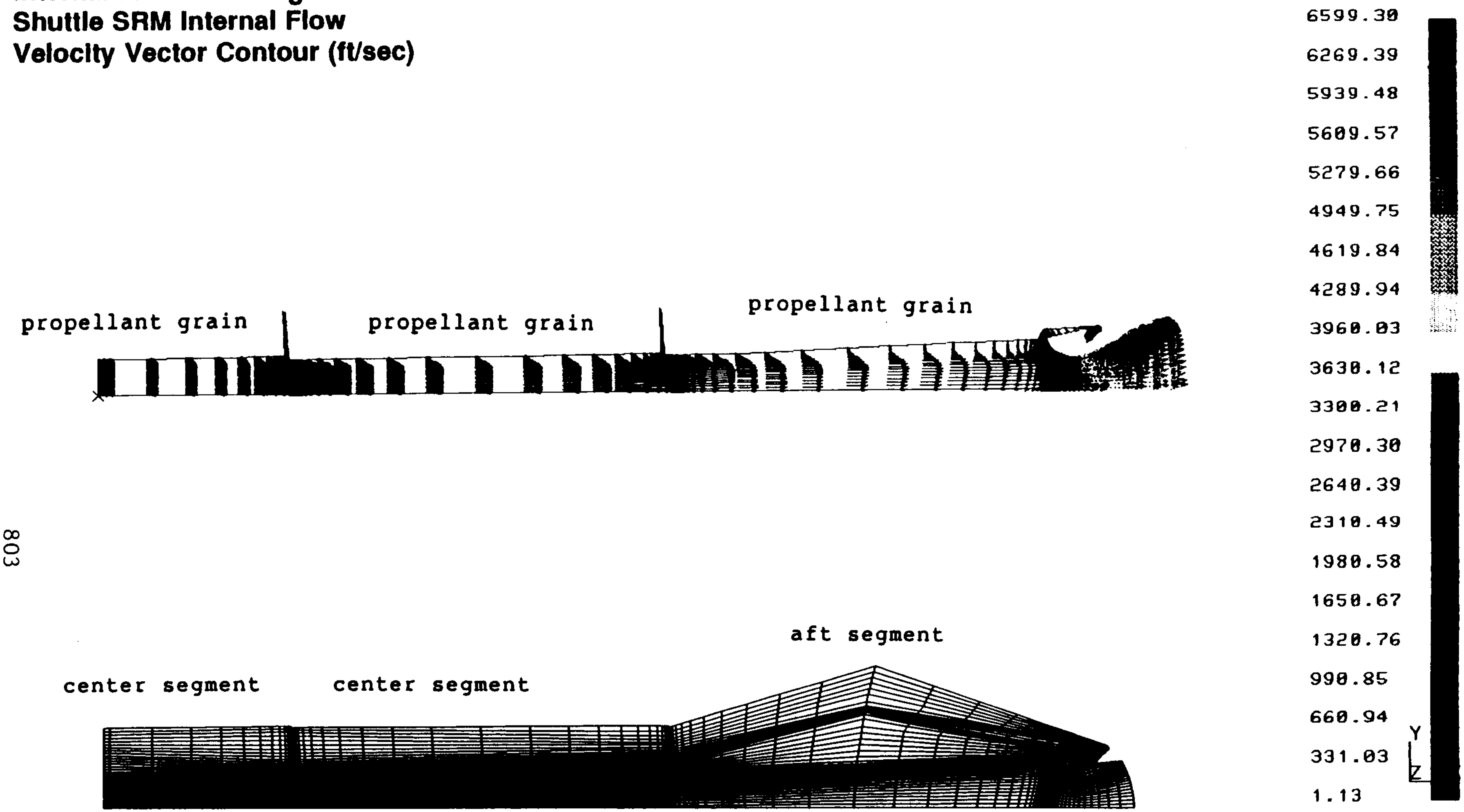

Internal Flow Modeling
Shuttle SRM Internal Flow Pressure Differential In The Slot Area Between Center And Aft Segments (psi)

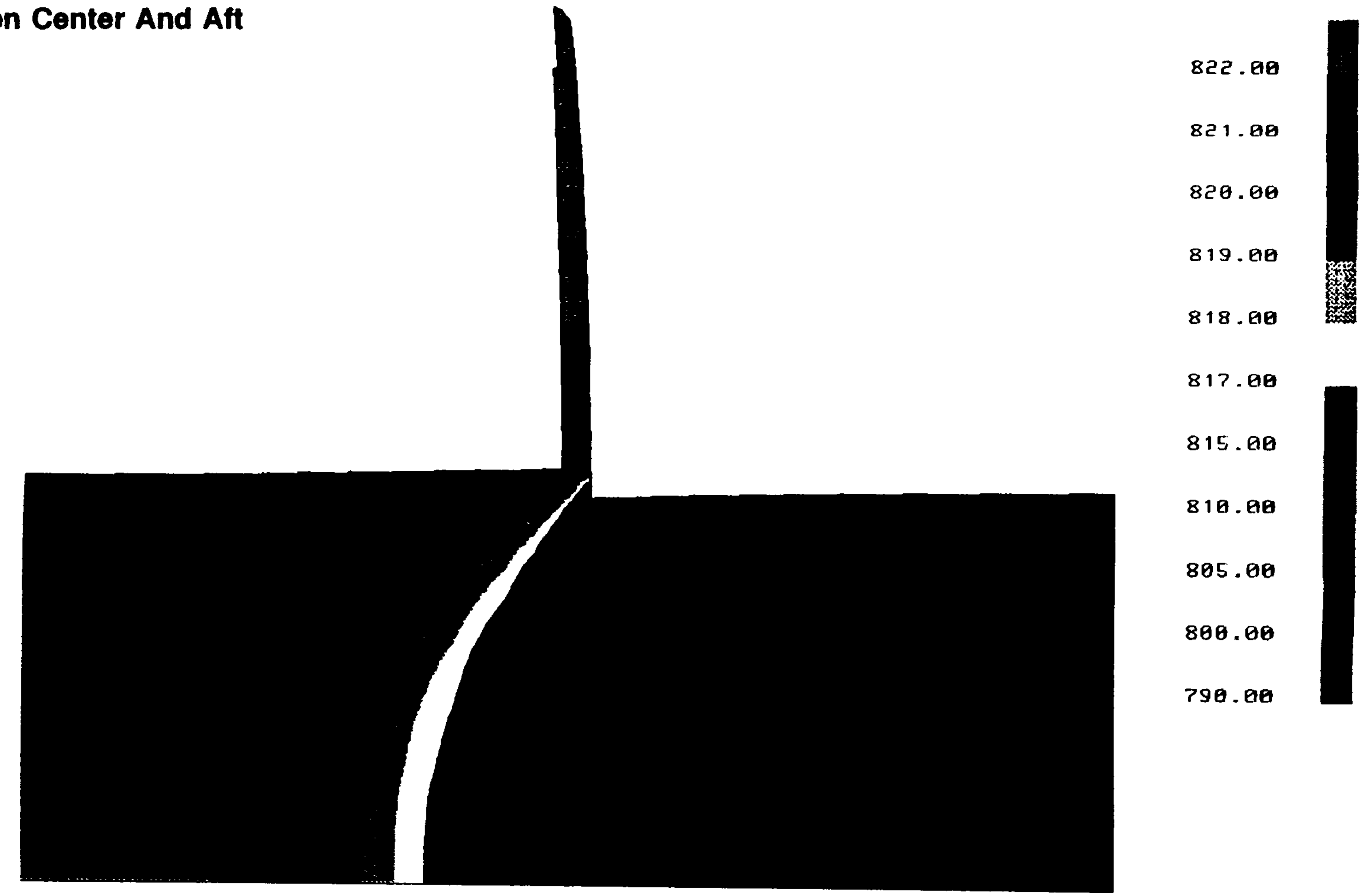

Thiokol CORPORATION
SPACE OPERATIONS

Internal Flow Modeling
Shuttle SRM Internal Flow

Velocity Vectors In The Slot Area Between Center And Aft Segments (ft/sec)

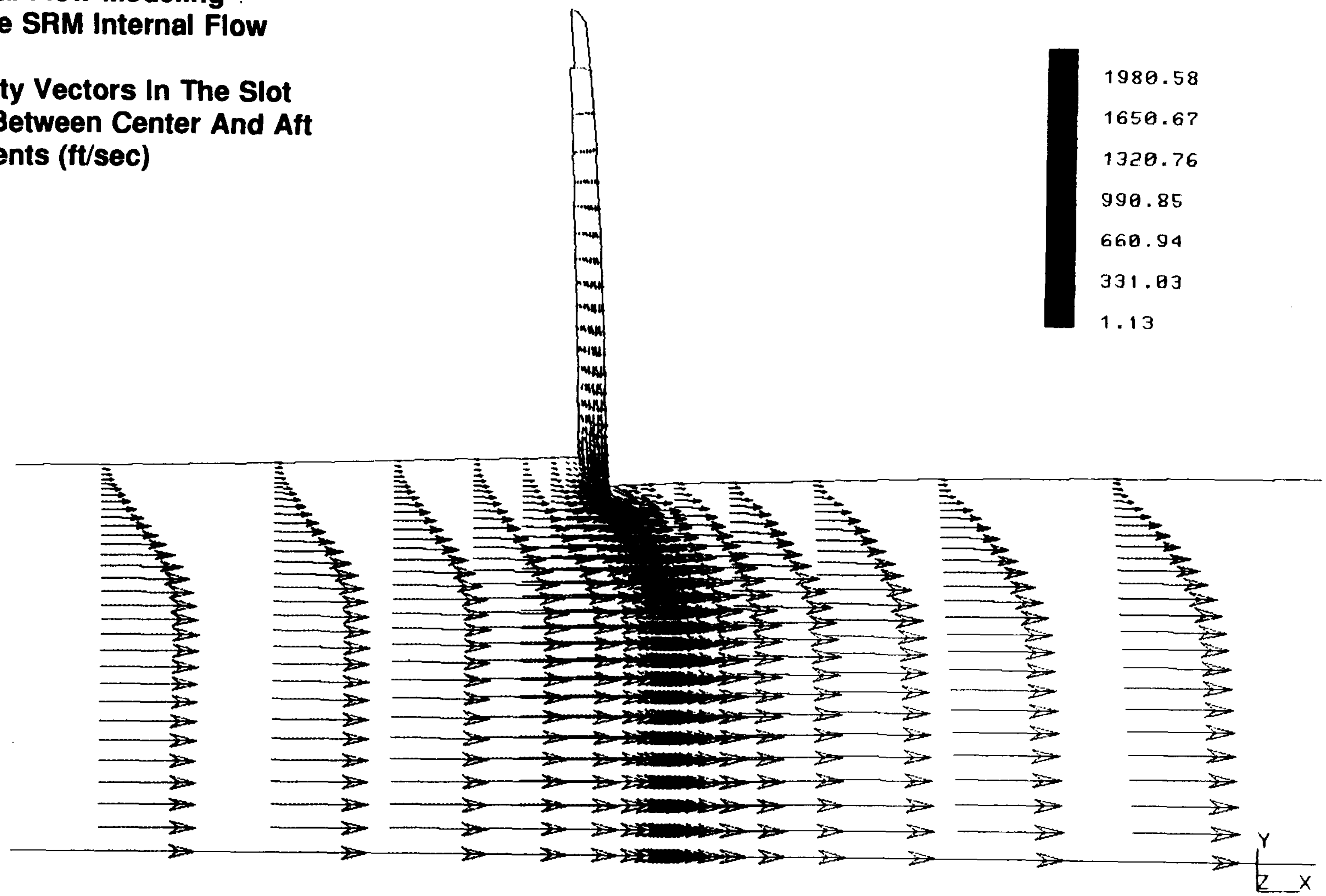

Thiokol CORPORATION
SPACE OPERATIONS

INFORMATION ON THIS PAGE WAS PREPARED TO SUPPORT AN ORAL PRESENTATION AND CANNOT BE CONSIDERED COMPLETE WITHOUT THE ORAL DISCUSSION

SUMMARY

-efficient algorithm was developed / runs well on computer workstations

-SHARP 2D was extensively tested

-SHARP demonstrates capabilities in SRM design and flow analysis

-turbulent combustion development and testing is in progress

Thiokol CORPORATION
SPACE OPERATIONS

N92-32250

Submitted for the CFD Workshop - 1992

A Status of the Activities of the NASA/Marshall Space Flight Center Combustion Devices Technology Team

Kevin Tucker

The Consortium for Computational Fluid Dynamics (CFD) Applications in Propulsion Technology was established to focus CFD applications in propulsion. Specific areas of effort include developing the CFD technology required to address rocket propulsion issues, validating the technology, and applying the validated technology to design problems; all under peer review by experts in the field.

The Combustion Devices Technology Team was formed to implement the above objectives in the broad area of combustion-driven flows. In an effort to bring CFD to bear in the design environment, the team has focused its efforts on the Space Transportation Main Engine nozzle. The main emphasis has been on the film cooling scheme used to cool the nozzle wall. Benchmark problems have been chosen to validate CFD film cooling capabilities. CFD simulations of the subscale nozzle (to be tested 8/92) have been made. Also, CFD predictions of the base flow resulting from this type of nozzle have been made. A status of these calculations will be presented along with future plans.

NASA
National Aeronautics and
Space Administration

A STATUS OF THE ACTIVITIES OF THE MSFC COMBUSTION DEVICES TECHNOLOGY TEAM

KEVIN TUCKER
APRIL 29, 1992

National Aeronautics and
Space Administration

Combustion-Driven Flow Analysis Technology

Overview

- Combustion Driven Flow Team Participants
- Background
- Programs
  - STME Nozzle Film Cooling
  - NLS Base Heating
- Summary

NASA
National Aeronautics and
Space Administration

Combustion-Driven Flow Analysis Technology

Participants

- NASA/Marshall Space Flight Center (MSFC)
- NASA/Ames Research Center (ARC)
- NASA/Lewis Research Center (LeRC)
- Air Force (Phillips Lab)
- Aerojet
- Pratt & Whitney (P&W)
- Rocketdyne (Rkdn)
- SECA
- Computational Fluid Dynamics (CFD) Research Corporation
- United Technology Research Center (UTRC)
- Calspan - University of Buffalo Research Center (CUBRC)
- Calspan - AEDC Operations
- W. J. Shafer Associates
- Remtech
- University of Tennessee Space Institute (UTSI)
- Pennsylvania State University
- The University of Alabama (UA)
- The University of Alabama in Huntsville (UAH)

C-2

National Aeronautics and
Space Administration

Combustion-Driven Flow Analysis Technology

Background

STME Nozzle

- TQM activity identified TCA issues which could benefit from enhanced analytical capabilities
  - Evaluated issues based on:
    - -- Need for improved design methodology (engine contractors)
    - -- Potential for CFD impact in near to mid-term (CFD specialists)
  - Identified nine generic technology issues in injector, chamber, and nozzle
  - Identified major technology/development in STME TCA
    - -- Nozzle film cooling
    - -- Integral fuel mixer
    - -- High aspect ratio coolant channels
  - Compared general technology issues with STME TCA concerns
  - Chose STME film/dump cooled nozzle for team focus
  - Identified validation/verification requirements for supersonic film cooling

Combustion-Driven Flow Analysis Technology

Background

NLS Base Heating

- Base heating is a concern on every launch vehicle

- The hydrogen-rich film/dump coolant causes additional complexities/concerns
  - Dumping low energy hydrogen into the base region put the program out of historical database
  - Resulting high heating rate environments are based on conservative assumptions
  - Subscale tests with base and/or afterburning don't scale well

- CFD is being used to augment classical analysis and testing

- Extensive code validation plan has been developed

National Aeronautics and Space Administration

Combustion-Driven Flow Analysis Technology

Program - STME Nozzle Film Cooling

- Issues
  - Capability of the film to adequately cool the nozzle skirt
    - -- Effect of accelerating core flow on film integrity
    - -- Conditions at which film should be injected
  - Effect of film coolant/injector delivery system on performance
    - -- Shock losses
  - Environment definition in nozzle/MCC joint area

- Task Description
  - Validate CFD codes for supersonic film cooling
  - Use validated codes as design tool for subscale (40K) nozzle
  - Verify film cooling performance in subscale nozzle
  - Use validated codes in design of full scale nozzle

National Aeronautics and Space Administration

Combustion-Driven Flow Analysis Technology

Program - STME Nozzle Film Cooling

- Results to Date
  - Film cooling benchmark calculations complete
  - Analysis of film coolant network for subscale nozzle complete
  - Preliminary primary injector analysis complete
  - Analysis of cases from subscale test matrix underway; to be completed 8/92

- Impact
  - Demonstration of CFD as a nozzle design tool successful
  - Subscale secondary injector redesigned using CFD
  - Confidence gained in film cooling early in subscale design
  - Large film cooling analytical/test database being developed

National Aeronautics and Space Administration

Combustion-Driven Flow Analysis Technology

Film Cooling Benchmark

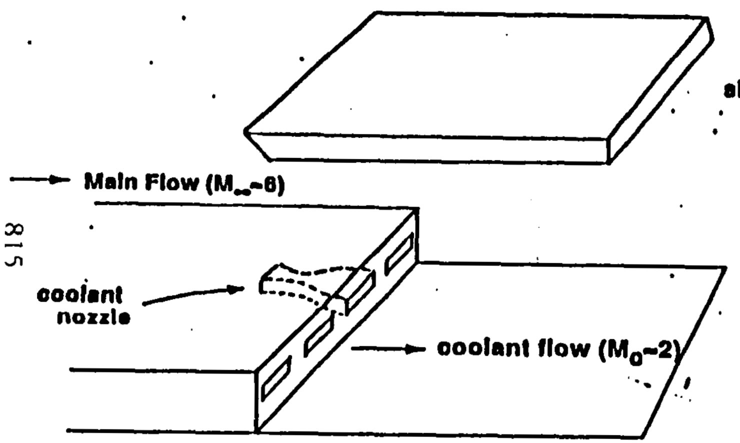

Case 45:
Matched Pressure Condition
Shock Generator Angle = 0°

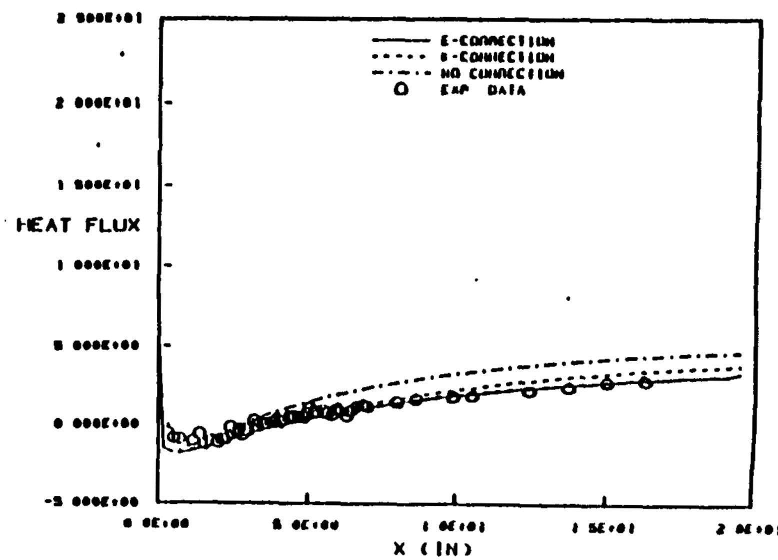

HOLDEN FILM COOLING TEST CASE 45 WITH TURBU INLET DATA
-- MODEL COMPARISONS (HEAT FLUX UNIT = BTU/FT2/SEC)

STME Subscale Nozzle

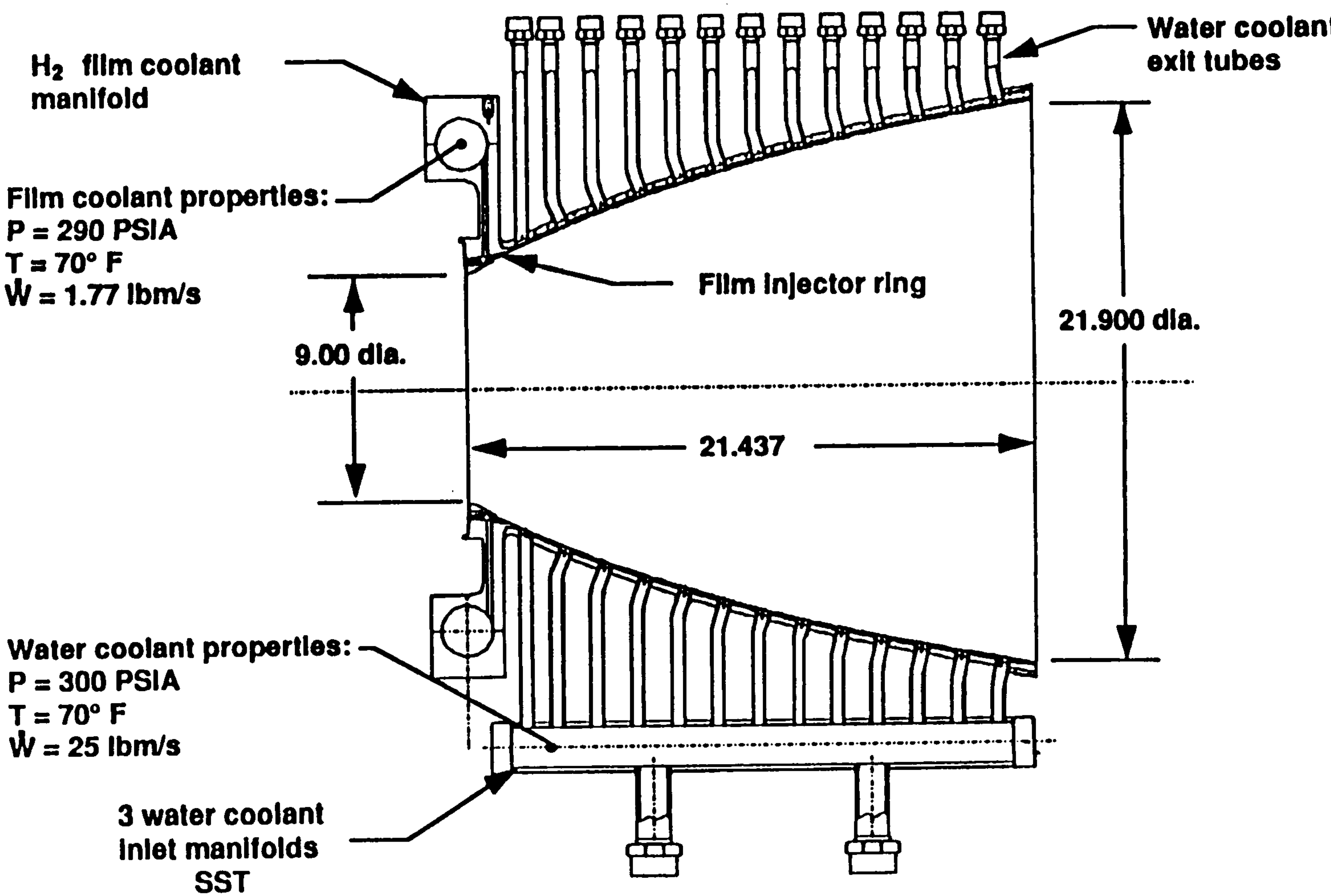

CORE/SECONDARY COOLANT FLOW INTERACTION

Interaction Pressure Contours Indicate a Step–Induced Shock

CORE/SECONDARY COOLANT FLOW INTERACTION

Velocity Vectors / H_2 Mass Fraction Contours Show Vortex Mixing

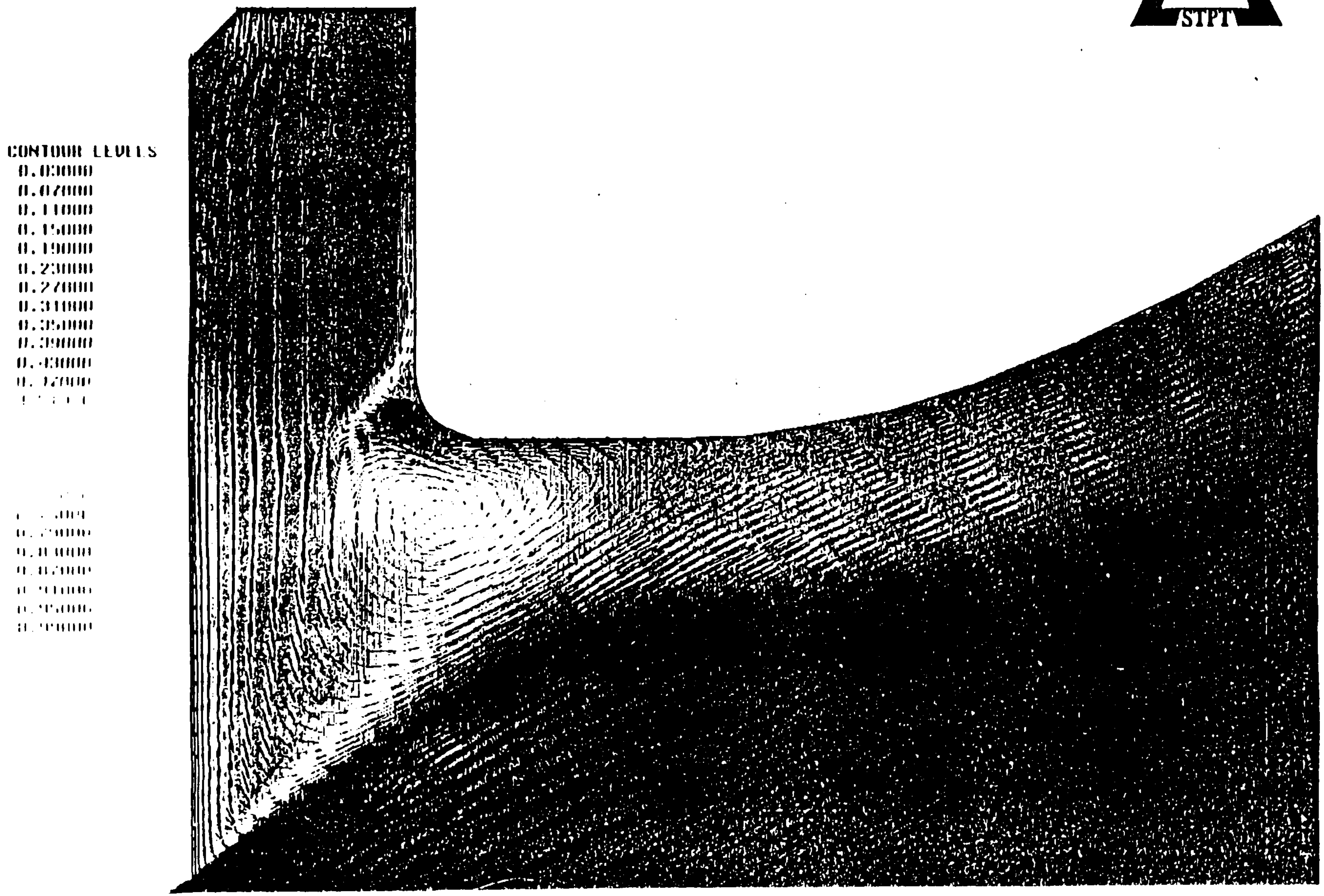

CORE/SECONDARY COOLANT FLOW INTERACTION

Interaction Temperature Contours Indicate Entrainment of Core Gases

CORE/SECONDARY COOLANT FLOW INTERACTION

H_2 Mass Fraction Contours Indicate Vortex and Diffusion Mixing

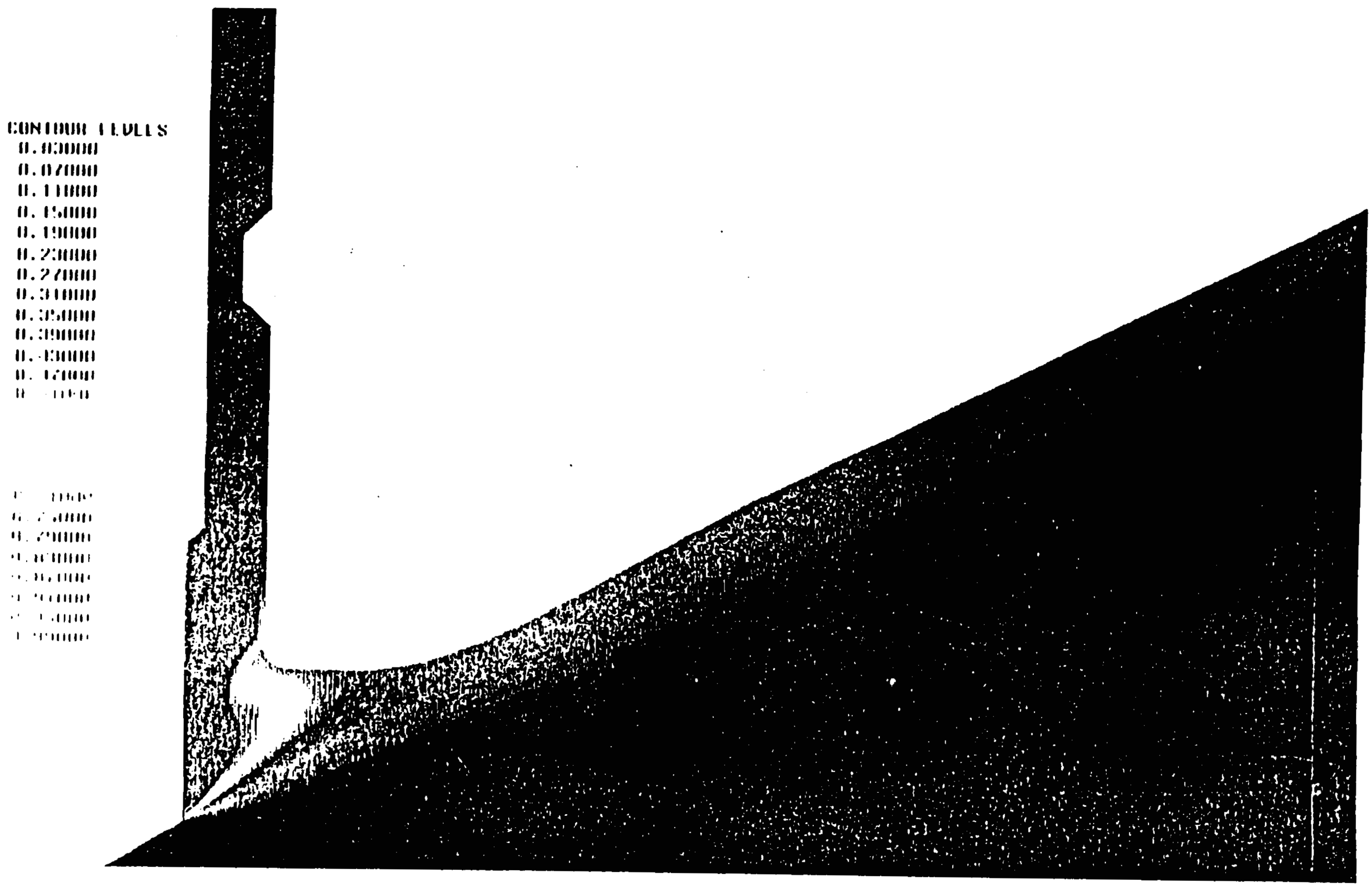

TEMPERATURE DISTRIBUTION
DEGREES RANKINE

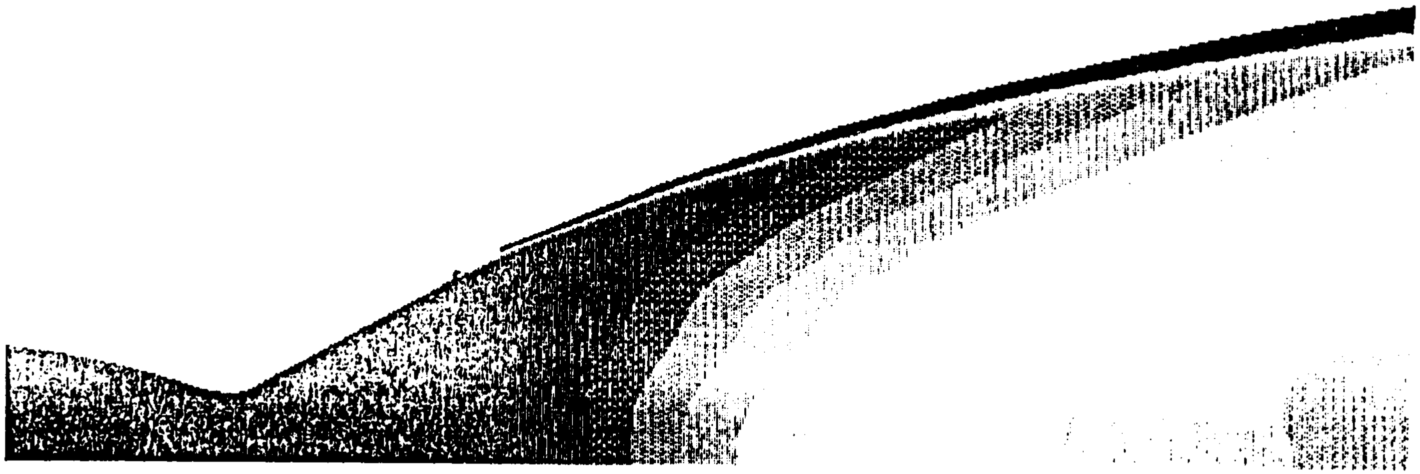

NASA
National Aeronautics and Space Administration

Combustion-Driven Flow Analysis Technology

Program - NLS Base Heating

- Issues
  - CFD has not been used extensively for base environments
  - Codes must be assessed for vehicle base flows
  - Decisions must be made on where, how, and when CFD codes will be used to supplement current predictive techniques

- Task Description
  - Establish validation plan based on physical processes involved in base heating
  - Perform single nozzle analyses for the following:
    - Engineering models
    - Support for subscale model design and subsequent scaling
  - Perform 3D/axisymmetric clustered nozzle calculations
  - Perform all nozzle analyses at altitudes spanning vehicle trajectory

NASA
National Aeronautics and Space Administration

Combustion-Driven Flow Analysis Technology

Program - NLS Base Heating

- Results to Date
  - STME single nozzle "demonstration" calculations at low and high altitudes complete (4 codes)
  - Benchmark calculations well underway in-house and at Rocketdyne
    - -- Backward facing step
    - -- MOC/Inviscid plume
    - -- S-1C single nozzle
    - -- 4-nozzle cluster
  - Preliminary NLS/STME single nozzle calculations to be completed by 5/92
  - Preliminary 3D NLS/STME base calculation to be completed by 5/92

- Impact
  - Results of "demonstration" calculations delivered to ED64 for heat flux calculations
  - The 3D analyses are pushing computer limits; job turnaround is slow

NLS 1.5 Stage Base

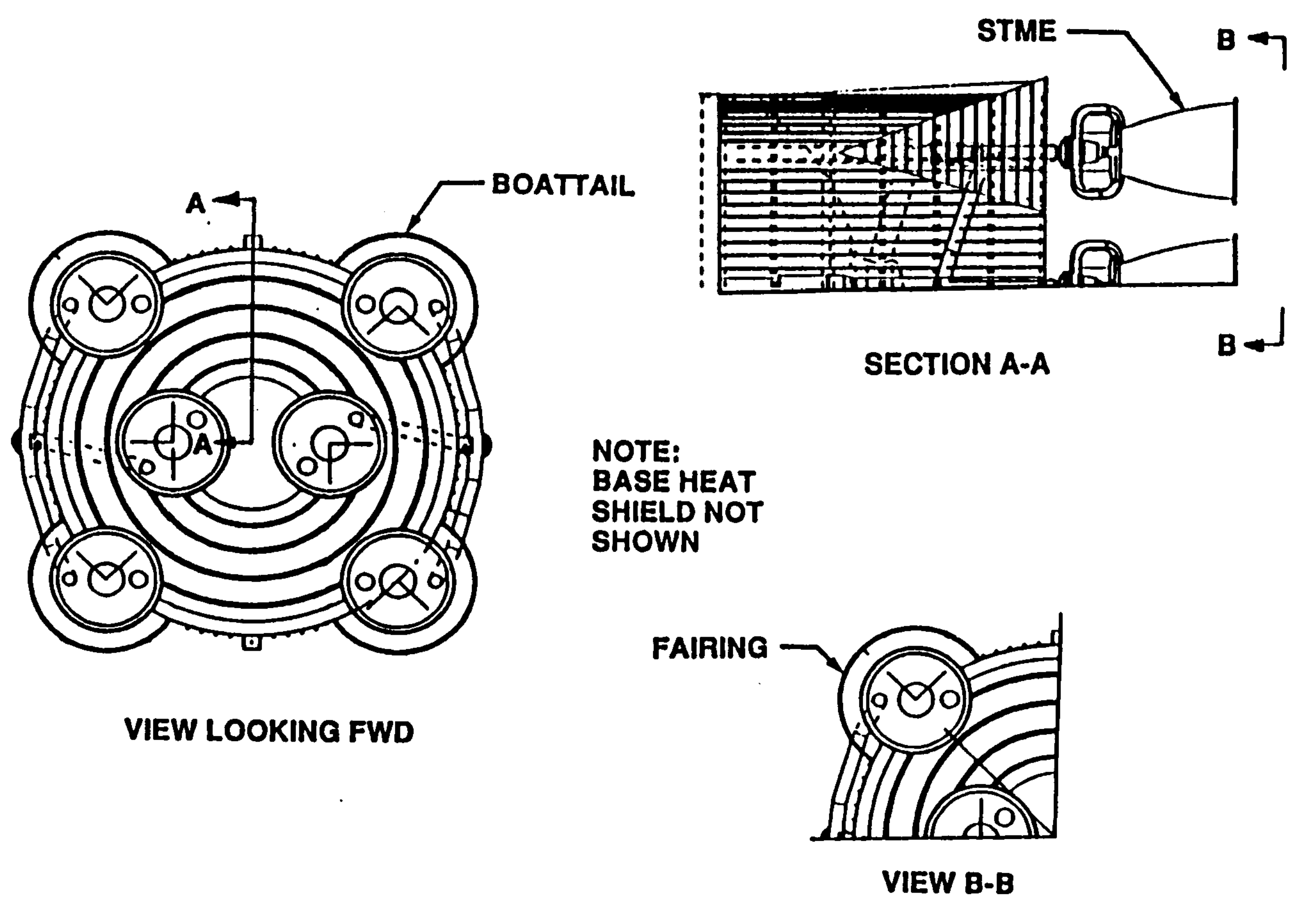

Combustion-Driven Flow Analysis Technology

Backward-Facing Step Benchmark

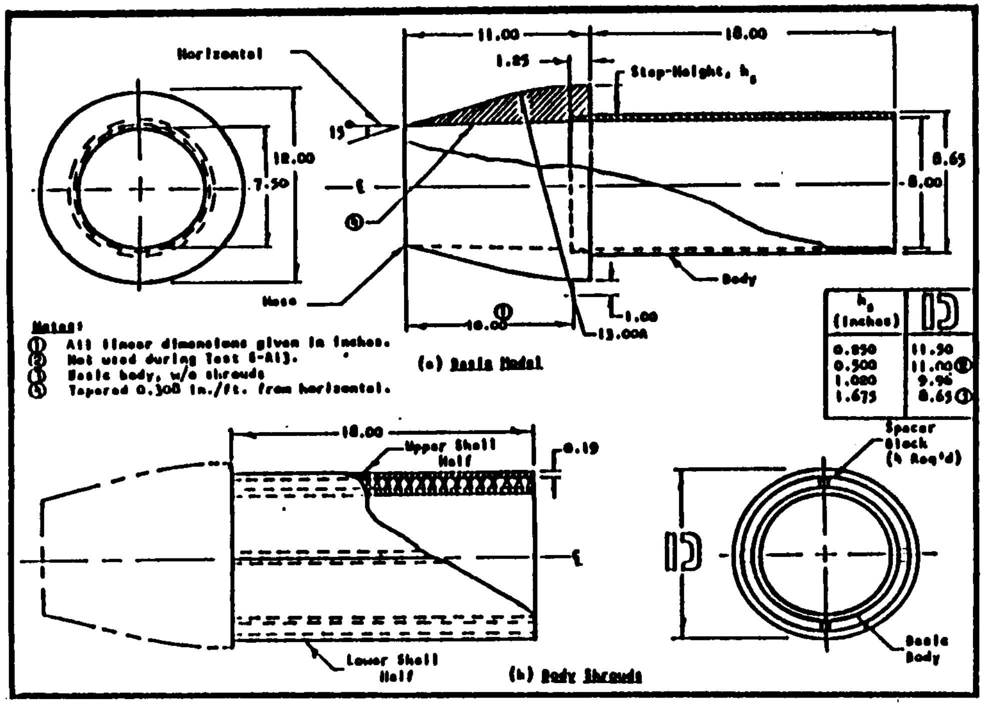

MODEL DIMENSIONS AND COMPONENT DESIGNATIONS

Notes:
1. All linear dimensions given in inches.
2. Not used during Test 6-A13.
3. Basic body, w/o shrouds
4. Tapered 0.308 in./ft. from horizontal.

h_s (inches)	D
0.250	11.50
0.500	11.00
1.000	9.96
1.675	8.65

Flow Benchmark (Backstep flow M = 2.996, H = 1.02

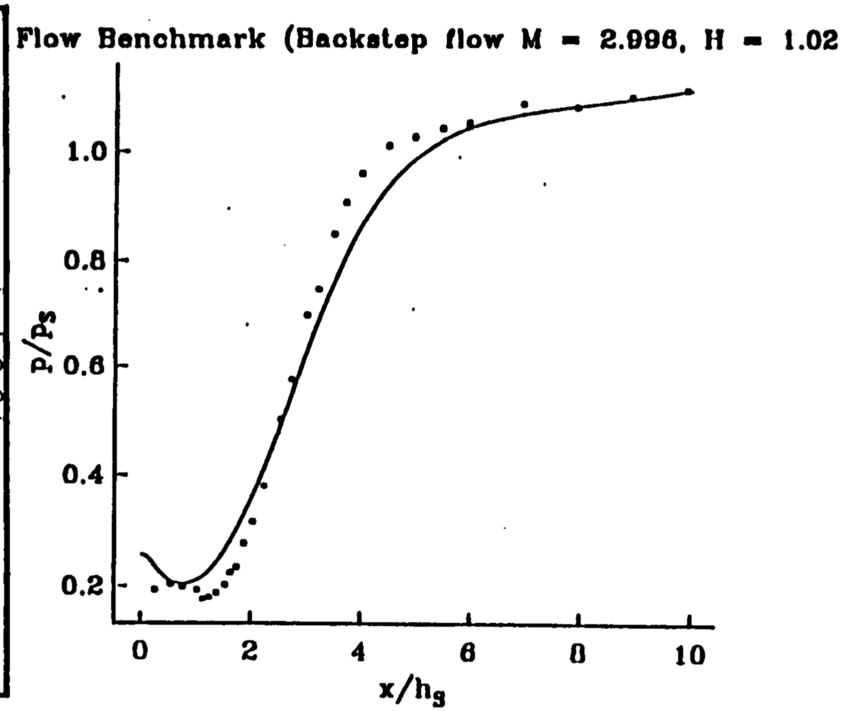

Combustion-Driven Flow Analysis Technology

Clustered Nozzle Benchmark

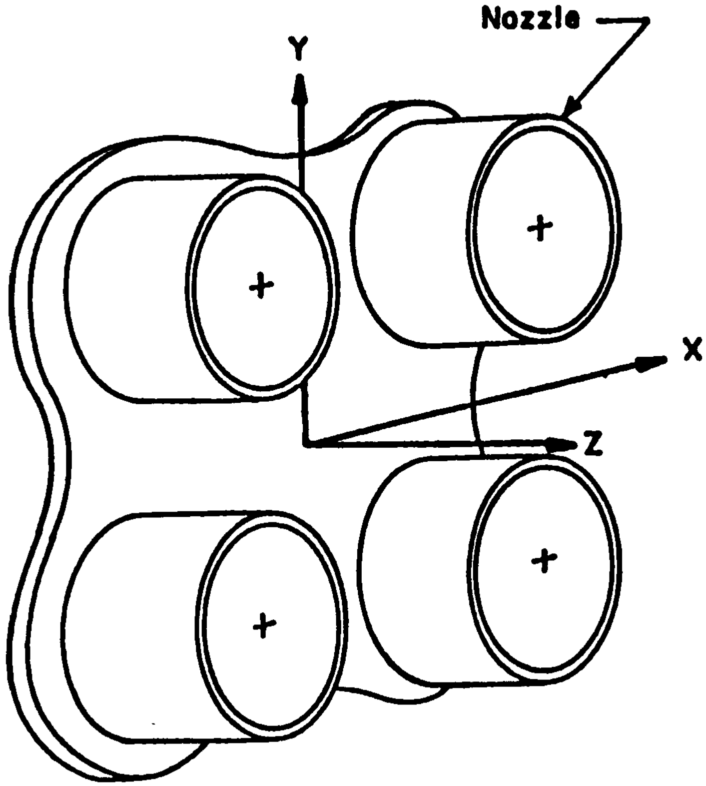

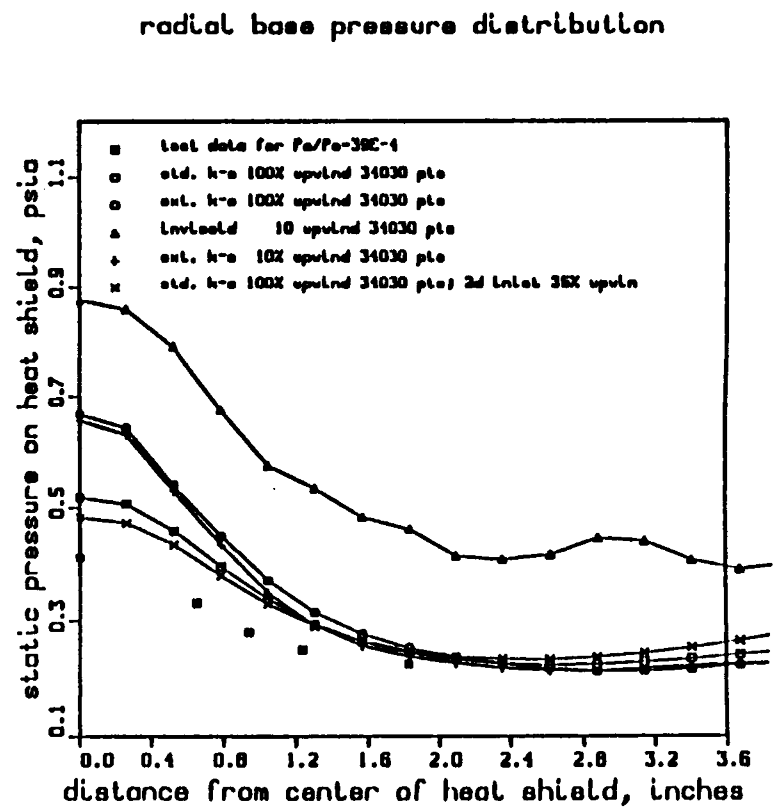

NASA
National Aeronautics and
Space Administration

Combustion-Driven Flow Analysis Technology

Summary

- **Technology program geared toward STME TCA issues**
  - **Supported by government, industry, and universities**
- **CFD codes being validated for and applied to NLS/STME**
- **CFD contributing to STME design improvements**
- **Usefulness of analytical tools being enhanced via technology, experience, and peer review of results**

N92-32251

CFD Analysis of the STME Nozzle Flowfield

Anantha Krishnan
CFD Research Corporation, Huntsville, AL
and
Kevin Tucker
NASA MSFC, Huntsville, AL

The Space Transporter Main Engine (STME) uses a gas generator cycle to cool the nozzle wall by a film-dump of the turbine exhaust. The ability to cool the skirt is a key concern in the design of the STME. CFD calculations were undertaken to predict the film cooling effectiveness and performance sensitivities for various design configurations, operating points and inlet conditions. The results in this study were obtained for the subscale nozzle. The computations were performed using REFLEQS.

The computational analysis showed that a chemical equilibrium model was necessary to obtain correct predictions of the specific impulse. The frozen composition model underpredicts the ISP by about 6%. It was also observed that the coolant film was successful in maintaining the nozzle wall well below the stagnation temperature of the core flow. The effect of the coolant flow on the performance of the engine was found to be negligible. The computed heat fluxes at the wall were in good agreement with the empirical data obtained by Pratt & Whitney.

Further test data from Pratt & Whitney are forthcoming for the subscale nozzle. Calculations will be performed to determine cooling efficiencies and nozzle performance over a range of conditions and the model predictions will be compared with experimental data.

CFD Research Corporation
3325-D Triana Blvd. ■ Huntsville, AL 35805 ■ (205) 536-6576 ■ FAX: (205) 536-6590

CFDRC

CFD ANALYSIS OF THE STME FLOWFIELD

by
Ananta Krishnan
CFD Research Corporation

and
Kevin Tucker
NASA - MSFC

Tenth Annual CFD Workshop
NASA - MSFC
April 28-30, 1992

INTRODUCTION

CFDRC

- The STME Uses a Gas Generator Cycle to Cool the Nozzle Wall by a Film Dump of the Turbine Exhaust.
- The Film Dump is Split into a Subsonic Stream and Supersonic Stream Injected at Different Locations on the Nozzle Wall.
- CFD Calculations were Undertaken to Predict Film Cooling Effectiveness and Performance Sensitivies for Various Design Configurations and Operating Points.
- The Calculations were Done for the Subscale Nozzle.

STME SUBSCALE NOZZLE ASSEMBLY

CFDRC

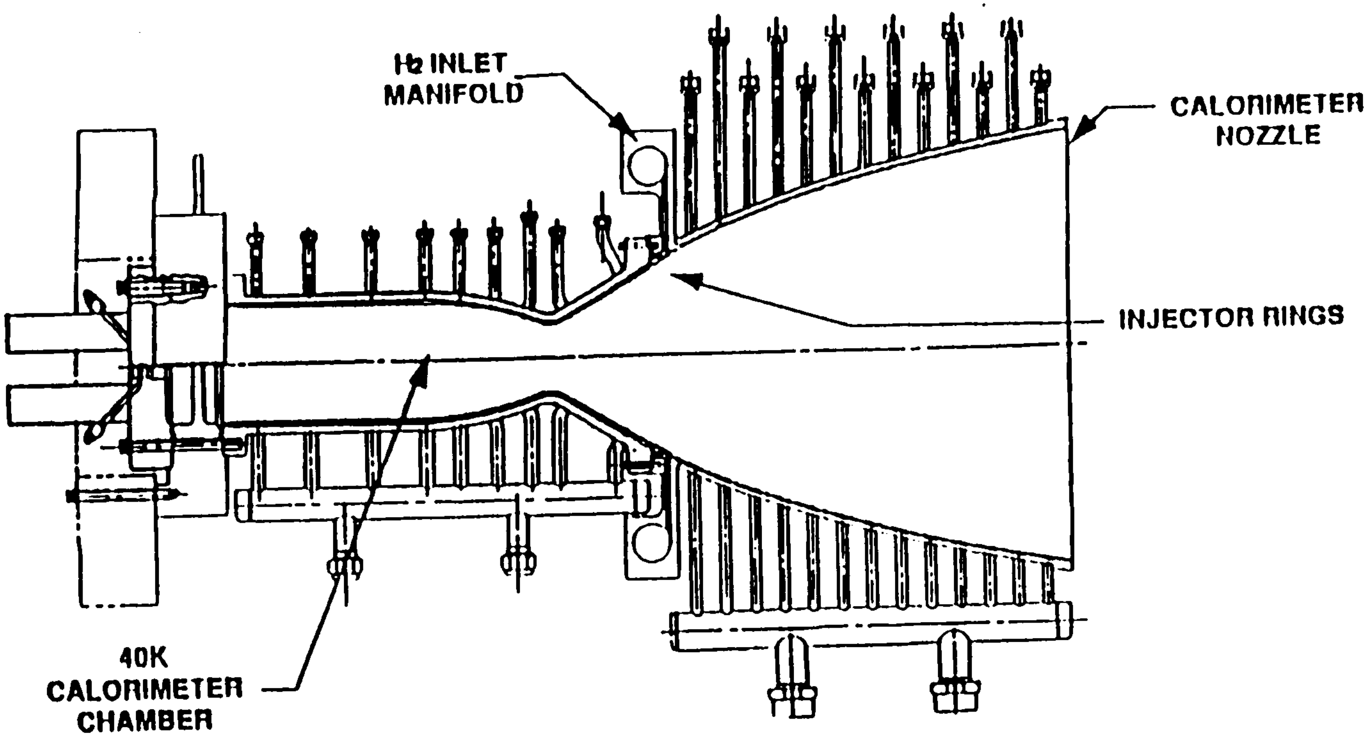

COOLANT INJECTOR DESIGN

CFDRC

Supply Coolant Splits between Injector Ring and Primary Coolant

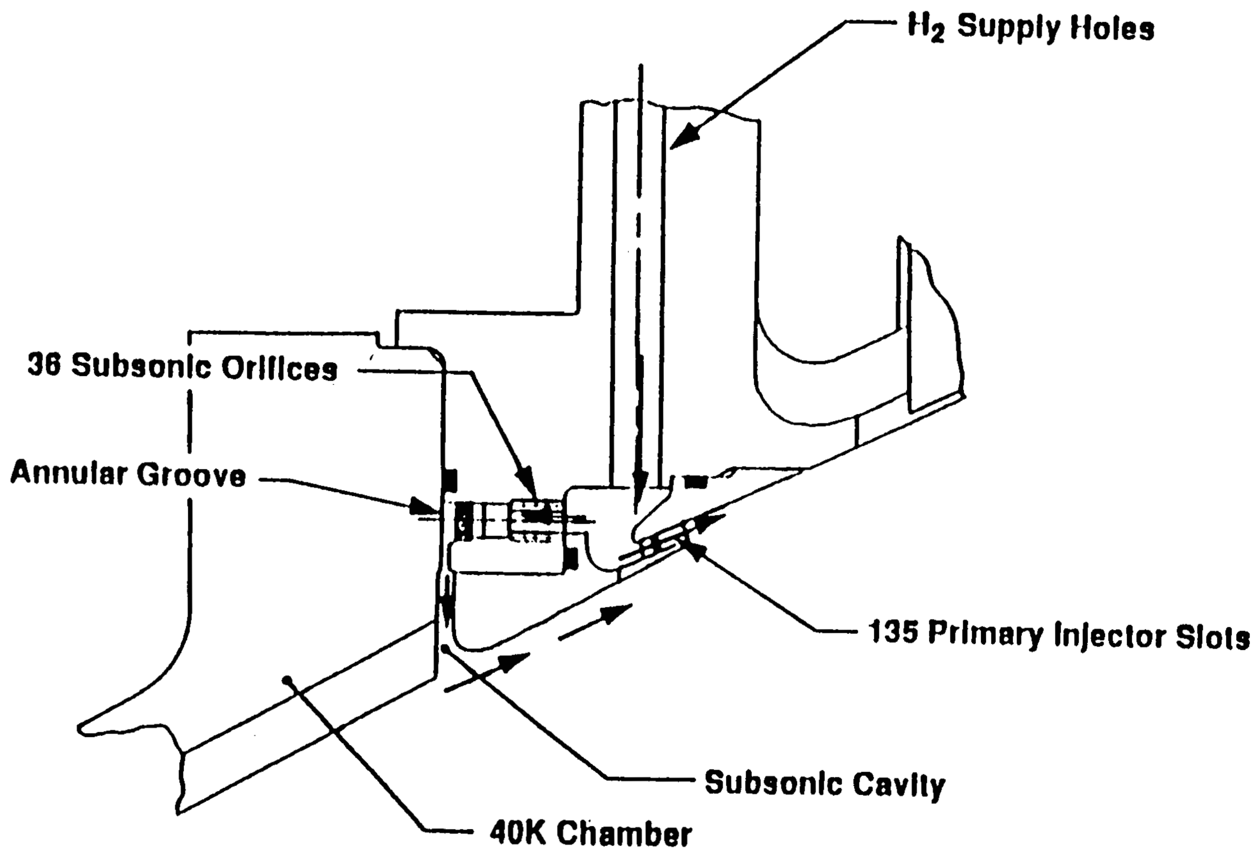

CFD METHODOLOGY

CFDRC

- REFLEQS Code has been Adapted for Rocket Thrust Chambers
- Solving for Reynolds Average Navier-Stokes Equations with
  - k-ε Turbulence Model
  - Chemical Equilibrium
  - BFC Grid (210x58)
  - Colocated Variables and Solving for Cartesian Velocity Components (strong conservation form)
  - Implicit Solver for Skew Grids
  - Finite Volume Discretization
- Validated for Large Number of Benchmark Problems (REFLEQS Validation Manual)

STME NOZZLE COMPUTATIONAL GRID

CFDRC

- Structured 210 x 58 Grid

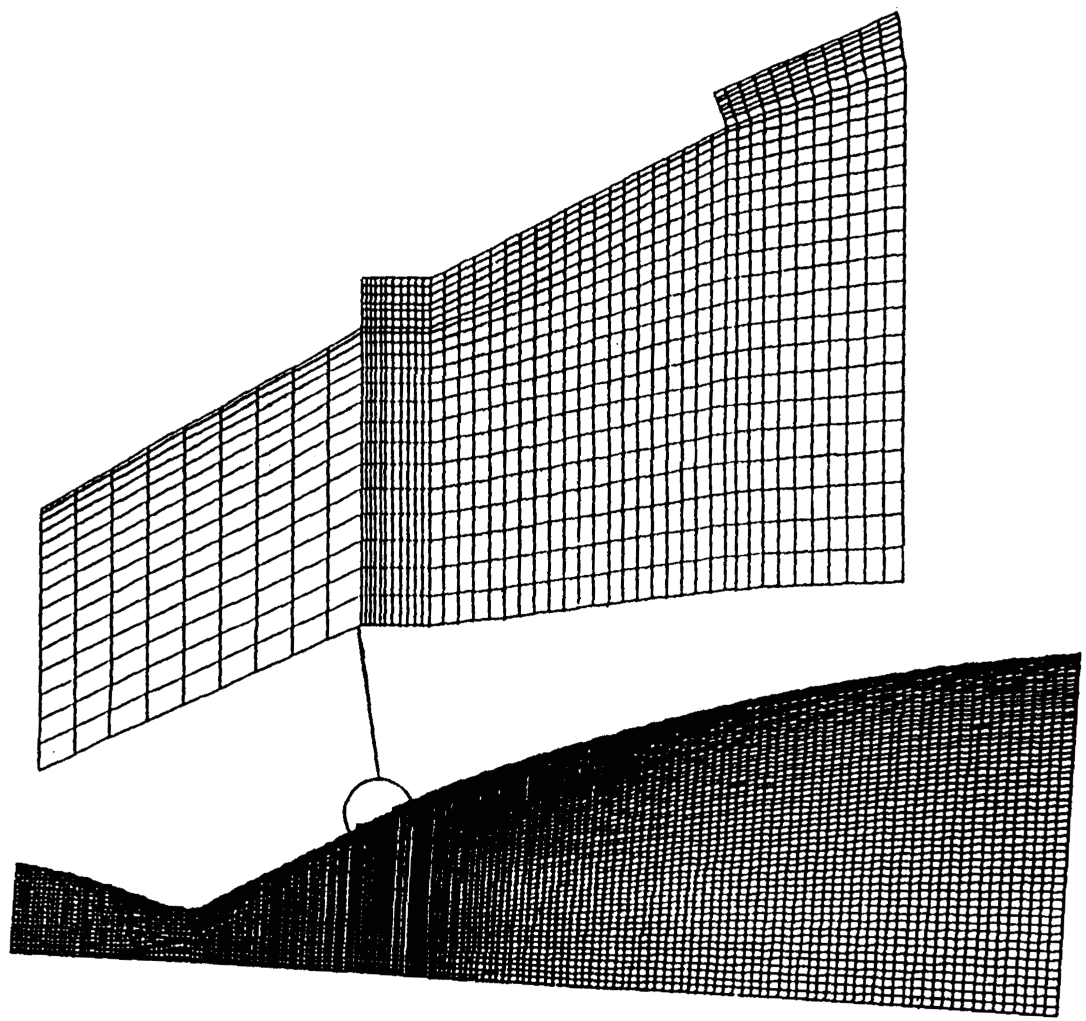

Table 1. Inlet Conditions

Mass Flow Rate (lb/sec)	Pressure (Psia)	Temperature (°R)	Velocity (ft/sec)	Mach Number	Area of c/s (in^2)
82.91	2189.9	6683.4	1096.08	0.219	23.469

Table 2. Subsonic Injector

Mass Flow Rate (lb/sec)	Pressure (Psia)	Temperature (°R)	Velocity (ft/sec)	Mach Number	Area of c/s (in^2)
0.254	59.13	523.9	876.9	0.205	1.98

Table 3. Sonic and Supersonic Injectors

Mass Flow Rate (lb/sec)	Pressure (Psia)	Temperature (°R)	Velocity (ft/sec)	Mach Number	Area of c/s (in^2)
1.51	60.9	568.53	4456.0	1.0	2.448
1.51	48.0	377.14	5277.0	1.454	1.740
1.22	57.6	568.53	4456.0	1.0	2.092
1.22	46.1	377.14	5277.0	1.454	1.464
1.82	73.47	568.53	4456.0	1.0	2.448
1.82	53.98	372.74	5423.0	1.503	1.794

CASES CONSIDERED

CFDRC

Case	Chemistry	Coolant Flow	Coolant Exit Condition
✓ 1.	Frozen Composition	Nominal	Sonic
✓ 2.	Equilibrium Model	Nominal	Sonic
3.	Equilibrium Model	Nominal	Supersonic
4.	Equilibrium Model	Minimum	Sonic
5.	Equilibrium Model	Minimum	Supersonic
6.	Equilibrium Model	Maximum	Sonic
7.	Equilibrium Model	Maximum	Supersonic
8.	Equilibrium Model (no subsonic flow)	Nominal	Sonic
9.	Equilibrium Model	(no primary injector flow)	
10.	Equilibrium Model (T_W=1060°R)	Nominal	Sonic
11.	Equilibrium Model (T_W=1060°R)	Nominal	Supersonic

SUBSCALE NOZZLE CALCULATIONS

CFDRC

Temperature Distribution (°K) - Frozen Composition Model

XY PLANE 1
TEMP CONTOURS
FMIN 2.878E+02
FMAX 3.711E+03
CONTOUR LEVELS

1	2.878E+02
2	4.694E+02
3	6.511E+02
4	8.328E+02
5	1.015E+03
6	1.196E+03
7	1.378E+03
8	1.560E+03
9	1.741E+03
10	1.923E+03
11	2.105E+03
12	2.286E+03
13	2.468E+03
14	2.650E+03
15	2.831E+03
16	3.013E+03
17	3.195E+03
18	3.376E+03
19	3.558E+03
20	3.740E+03

OK>

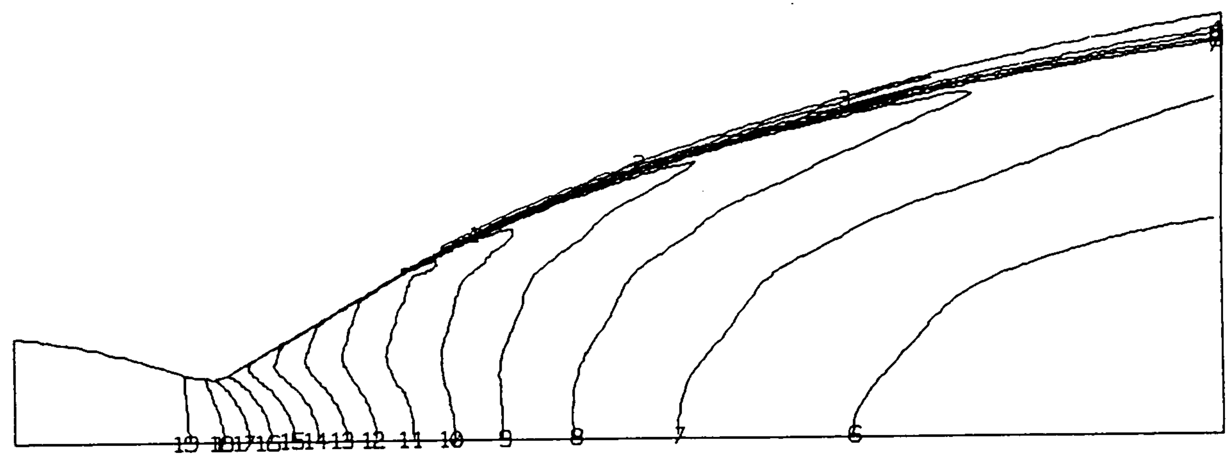

SUBSCALE NOZZLE CALCULATIONS

Temperature Distribution (°K) - Chemical Equilibrium Model

XY PLANE 1
TEMP CONTOURS
FMIN 2.918E+02
FMAX 3.712E+03
CONTOUR LEVELS

1	2.918E+02
2	4.726E+02
3	6.534E+02
4	8.342E+02
5	1.015E+03
6	1.196E+03
7	1.377E+03
8	1.557E+03
9	1.738E+03
10	1.919E+03
11	2.100E+03
12	2.280E+03
13	2.461E+03
14	2.642E+03
15	2.823E+03
16	3.004E+03
17	3.184E+03
18	3.365E+03
19	3.546E+03
20	3.727E+03

OK>

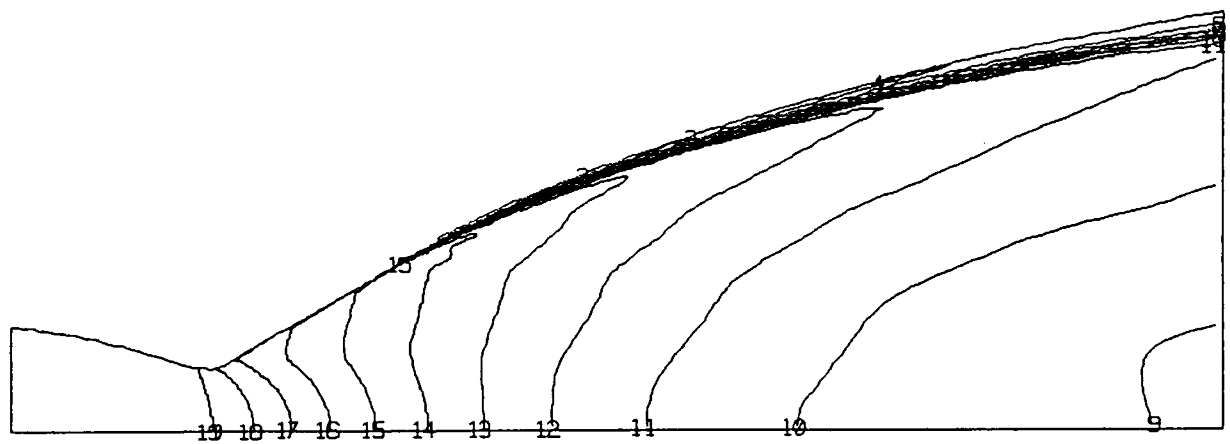

SUBSCALE NOZZLE CALCULATIONS

Pressure Distribution (Pa) - Chemical Equilibrium Model

XY PLANE 1
PRES CONTOURS
FMIN 1.860E+04
FMAX 1.462E+07
CONTOUR LEVELS

1	2.711E+04
3	4.533E+04
5	6.356E+04
7	8.178E+04
9	1.000E+05
11	2.000E+05
13	4.000E+05
15	6.000E+05
17	8.000E+05
19	1.000E+06
21	4.425E+06
23	1.128E+07

OK>

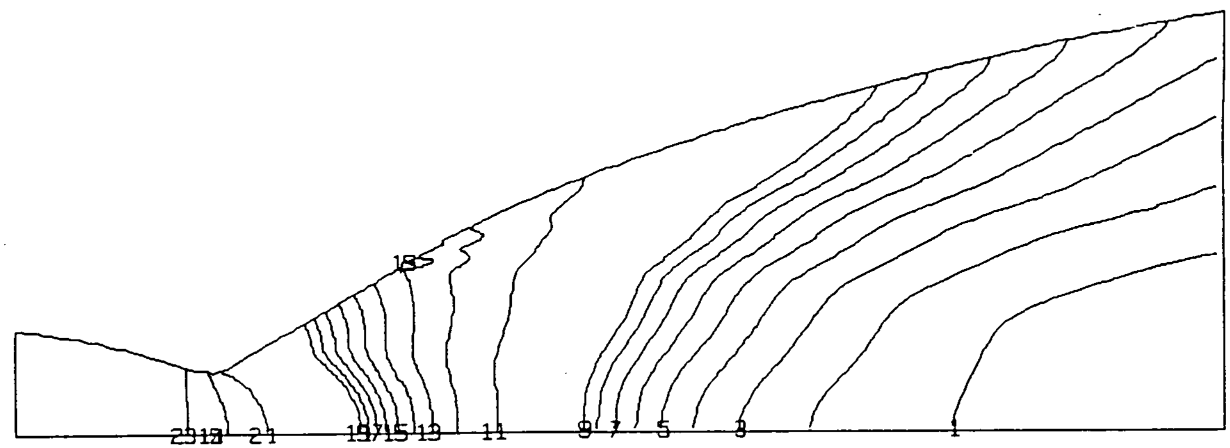

SUBSCALE NOZZLE CALCULATIONS

CFDRC

Pressure Distribution (Pa) - Chemical Equilibrium Model

XY PLANE 1
PRES CONTOURS
FMIN 2.583E+05
FMAX 6.213E+05

CONTOUR	LEVELS
1	2.922E+05
2	3.344E+05
3	3.767E+05
4	4.189E+05
5	4.611E+05
6	5.033E+05
7	5.456E+05
8	5.878E+05
9	6.300E+05

OK>

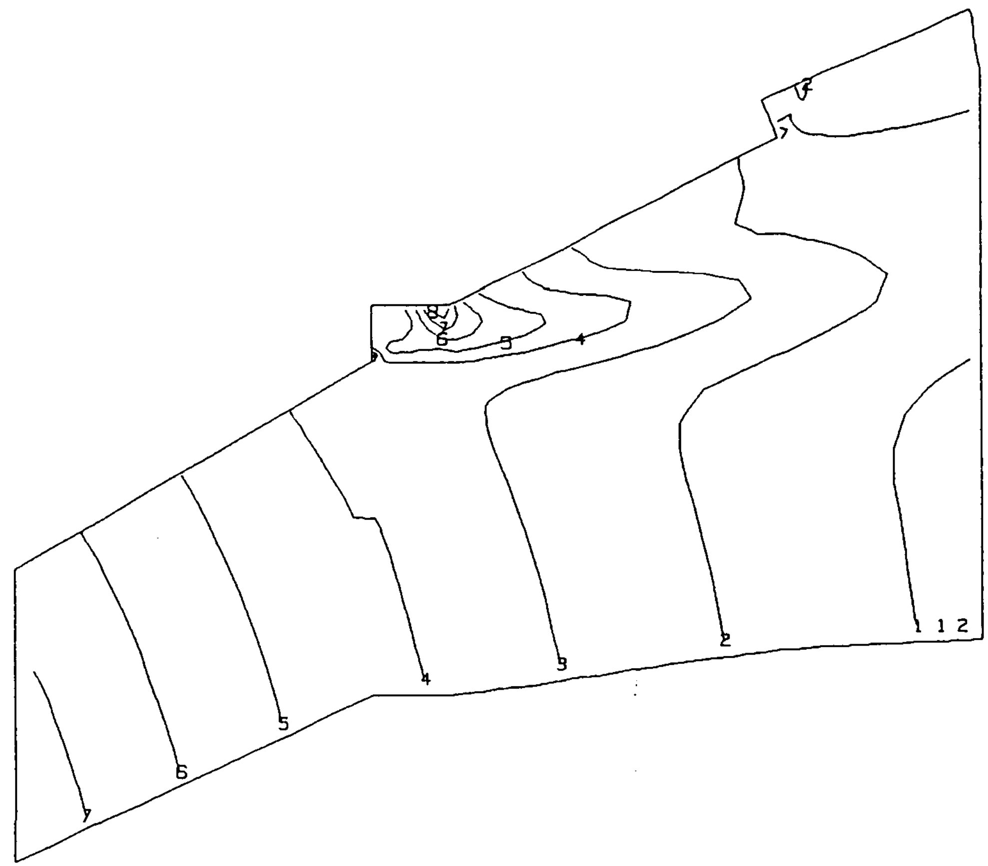

SUBSCALE NOZZLE CALCULATIONS

CFDRC

Mach Number - Chemical Equilibrium Model

XY PLANE 1
MACH CONTOURS
FMIN 1.127E-01
FMAX 4.181E+00

CONTOUR LEVELS	
1	2.201E-01
2	4.401E-01
3	6.602E-01
4	8.803E-01
5	1.100E+00
6	1.320E+00
7	1.540E+00
8	1.761E+00
9	1.981E+00
10	2.201E+00
11	2.421E+00
12	2.641E+00
13	2.861E+00
14	3.081E+00
15	3.301E+00
16	3.521E+00
17	3.741E+00
18	3.961E+00
19	4.181E+00

OK>

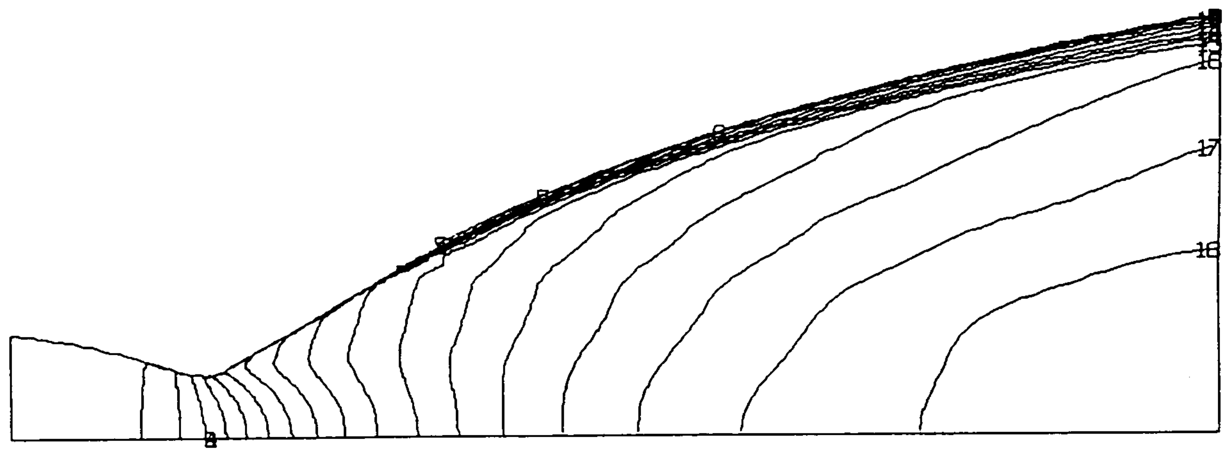

COMPUTATIONAL RESULTS FOR THE SUB-SCALE NOZZLE FILM COOLING

CFDRC

Model	Primary Injector Type	Mass Flow Rate (1bm/sec)	ISP
Frozen Composition	Nominal, Sonic	84.67	407.7
Equilibrium Model	Nominal, Sonic	84.67	434.2
Equilibrium Model	Nominal, Supersonic	84.67	433.8
Equilibrium Model	Minimum, Sonic	84.38	434.6
Equilibrium Model	Minimum, Supersonic	84.38	434.3
Equilibrium Model	Maximum, Sonic	84.98	433.7
Equilibrium Model	Maximum, Supersonic	84.98	433.3
Equilibrium Model	Nominal, Sonic No Subsonic Flow	84.42	434.3
Equilibrium Model	Subsonic Flow No Sonic Flow	83.16	435.5
Equilibrium Model Wall at 1060°R	Nominal, Sonic	84.67	432.3
Equilibrium Model Wall at 1060°R	Nominal, Supersonic	84.67	431.9

HEAT FLUX VS. X FOR T_{WALL} =1060°R

Nominal, Sonic

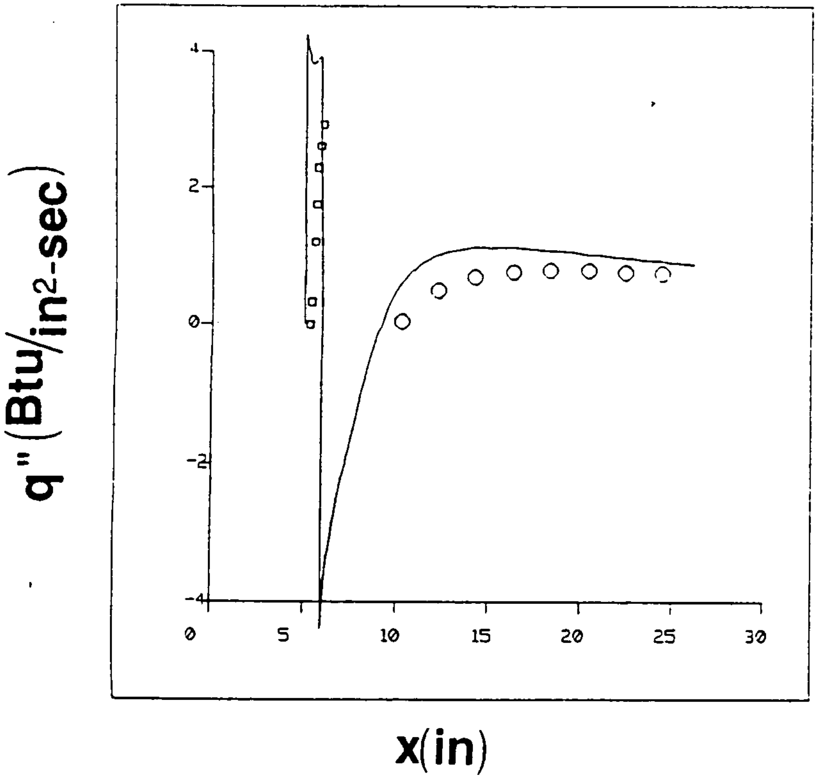

Nominal, Supersonic

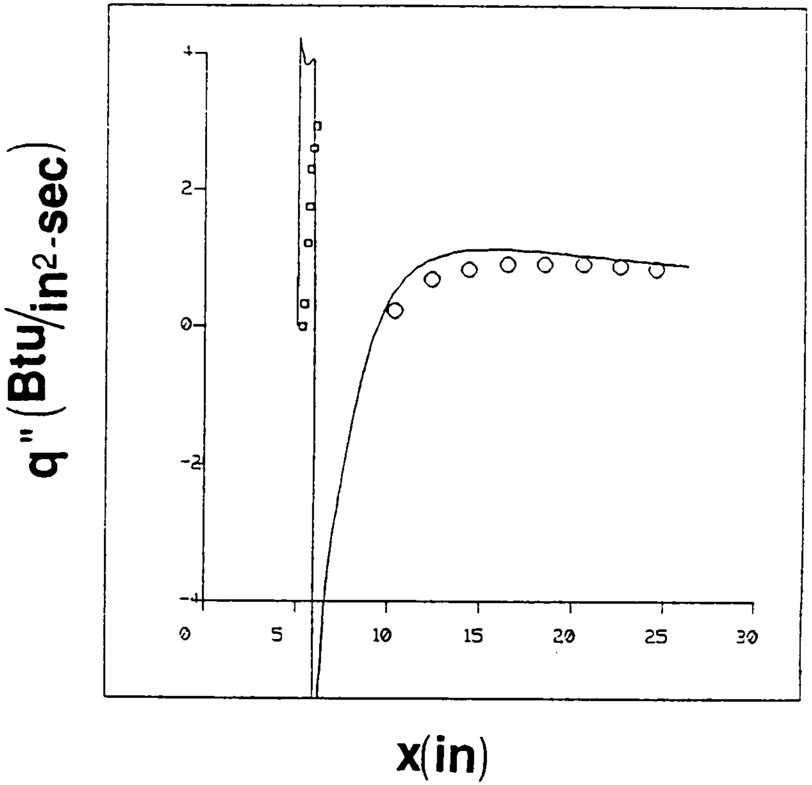

○○○ - P&W Analysis for Primary Injector

□□□ - P&W Analysis for Secondary Injector

CONCLUSIONS

Computations were Performed for the Subscale STME Film Cooling. The Main Conclusions of this Analysis were:

1. Chemistry Needs to be Considered to Predict the ISP Correctly

2. The Coolant Film is Successful in Maintaining the Nozzle Wall Well Below the Stagnation Temperature of the Core Flow

3. Computed Heat Fluxes at the Wall were in Good Agreement with (P&W) Empirical Data

4. The Nozzle Performance is Relatively Insensitive to the Coolant Injection

N92-32252

NLS Nozzle Base Flow Characteristics

J. J. Erhart
Pratt & Whitney
West Palm Beach, FL

ABSTRACT

The flow characteristics of the NLS nozzle base area need to be determined in order for heat transfer rates to be estimated. The objective of this work is to calculate these flow characteristics using CFD. A Full Navier-Stokes code in an axisymmetric mode using a k-ε turbulent model with wall functions is applied. Calculations were completed at an altitude of 3,250 and 80,000 feet in the flight trajectory. The results show flow features which can affect vehicle design. Calibration of a 3-D case with data is underway.

PRECEDING PAGE BLANK NOT FILMED

NOZZLE BASE CFD ANALYSIS

PRATT & WHITNEY
DEPENDABLE ENGINES

John J. Erhart

Wednesday, April 29, 1992

MSFC CFD Workshop

OUTLINE

- o Motivation
- o Approach
- o Geometry and Flow Boundary Conditions
- o Results
- o Summary

MOTIVATION

Understand Base Flow Phenomena

- o Parameters Influencing Transport Of Hydrogen Into Base Of Nozzle.

- o Define Typical Base Flow Environment
  - □ Streaklines
  - □ H_2
  - □ Mach Number
  - □ Pressure

APPROACH

- o Simplify Geometry – Single Axisymmetric Nozzle With Largest Base Height.

- o Two Altitudes – Different Plume Shapes.

GEOMETRY & FLOW BOUNDARY CONDITIONS

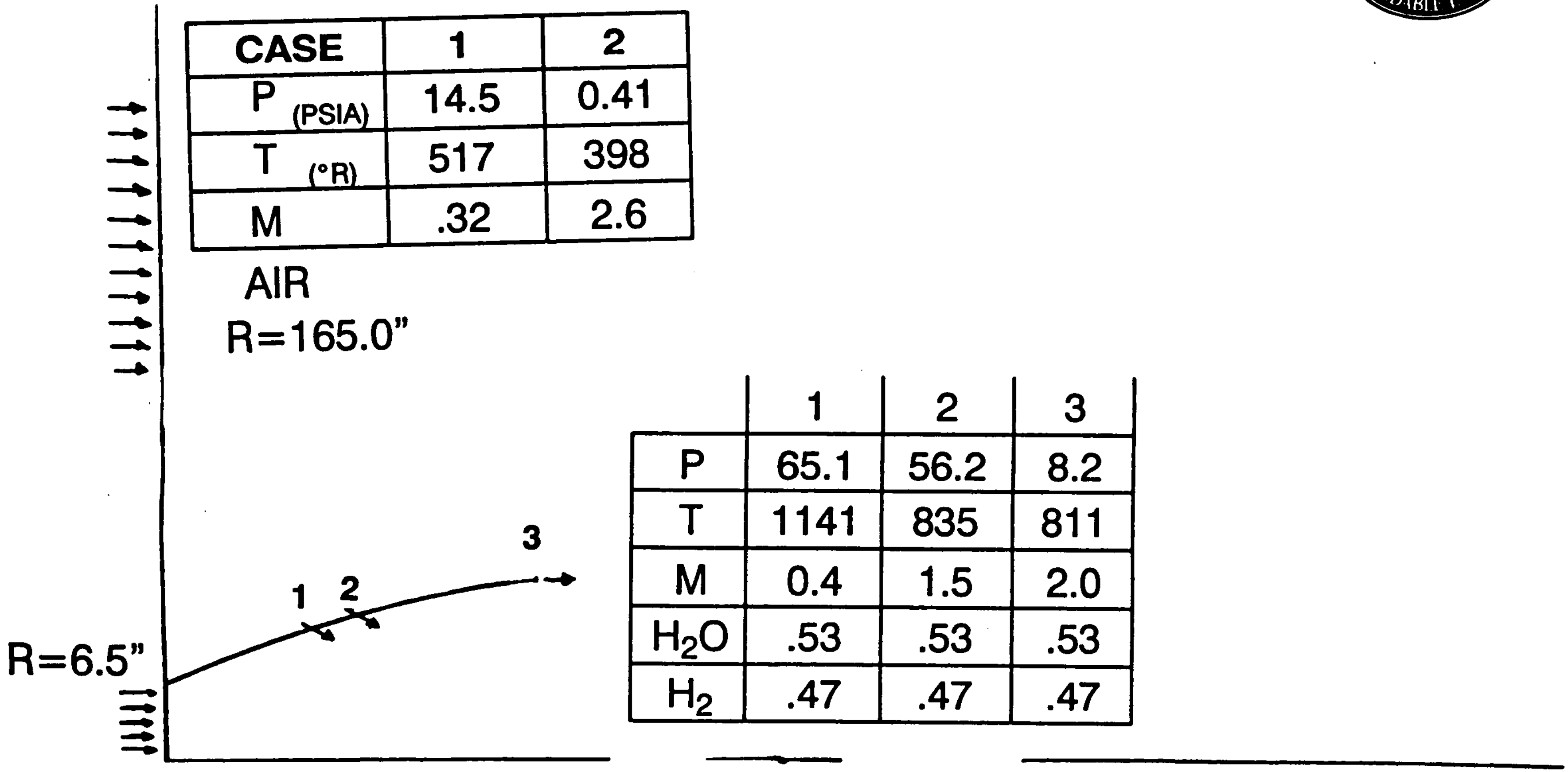

CASE	1	2
P (PSIA)	14.5	0.41
T (°R)	517	398
M	.32	2.6

AIR
R=165.0"

	1	2	3
P	65.1	56.2	8.2
T	1141	835	811
M	0.4	1.5	2.0
H_2O	.53	.53	.53
H_2	.47	.47	.47

P = 1300 PSIA
T = 6336°R
H_2O = .986

P = 4.9 PSIA
M = 4.04
AR = 45
R = 43.6"

HIGH & LOW ALTITUDE – STREAKLINES

Base H_2 Concentration Function Of Nozzle Plume And Bluff Body Recirculation Interaction

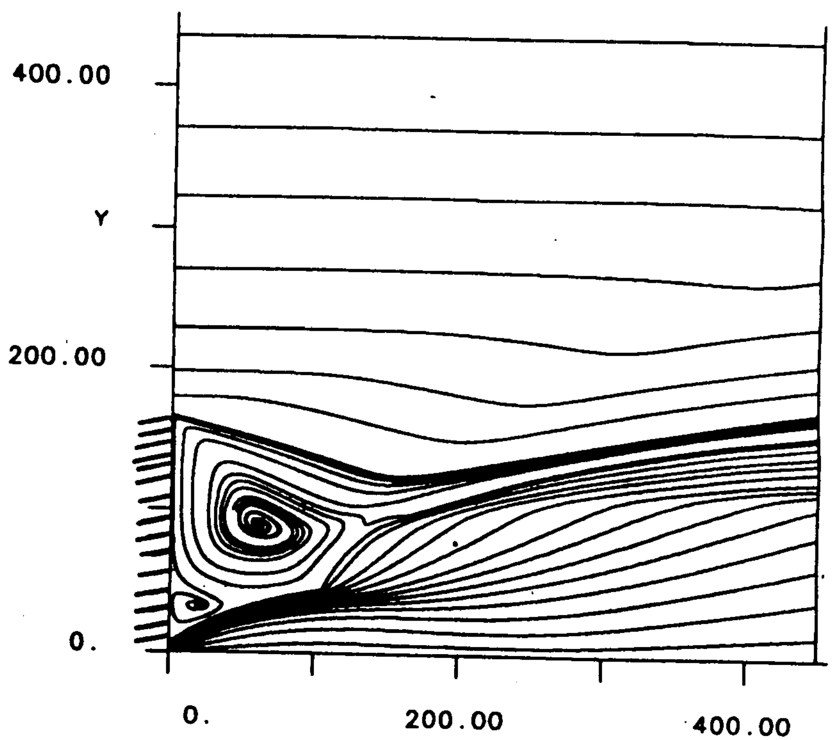

High Altitude

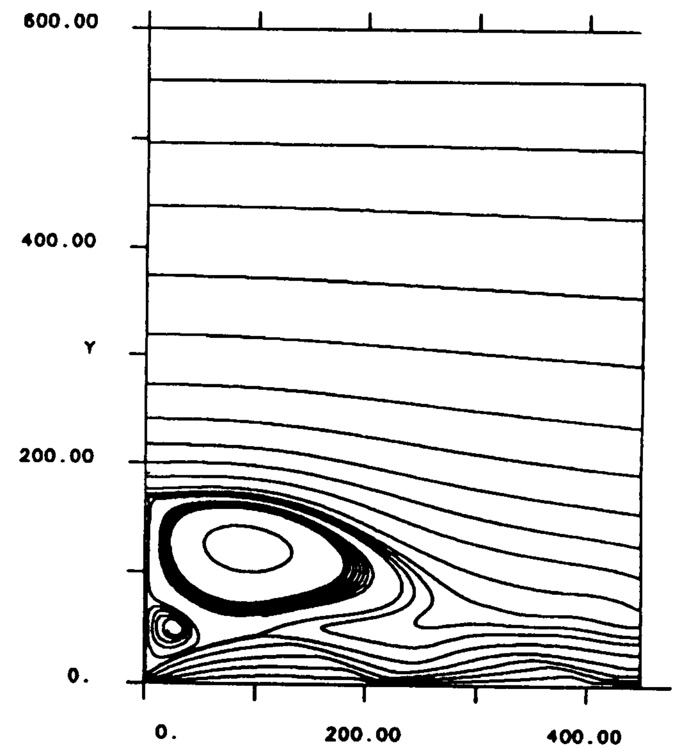

Low Altitude

RESULTS

H_2


CONTOUR L
0.00000
0.00300
0.00600
0.00900
0.01200
0.01500
0.01800
0.02100
0.02400
0.02700
0.03000

RESULTS

Mach Number

mach number at nozzle base region

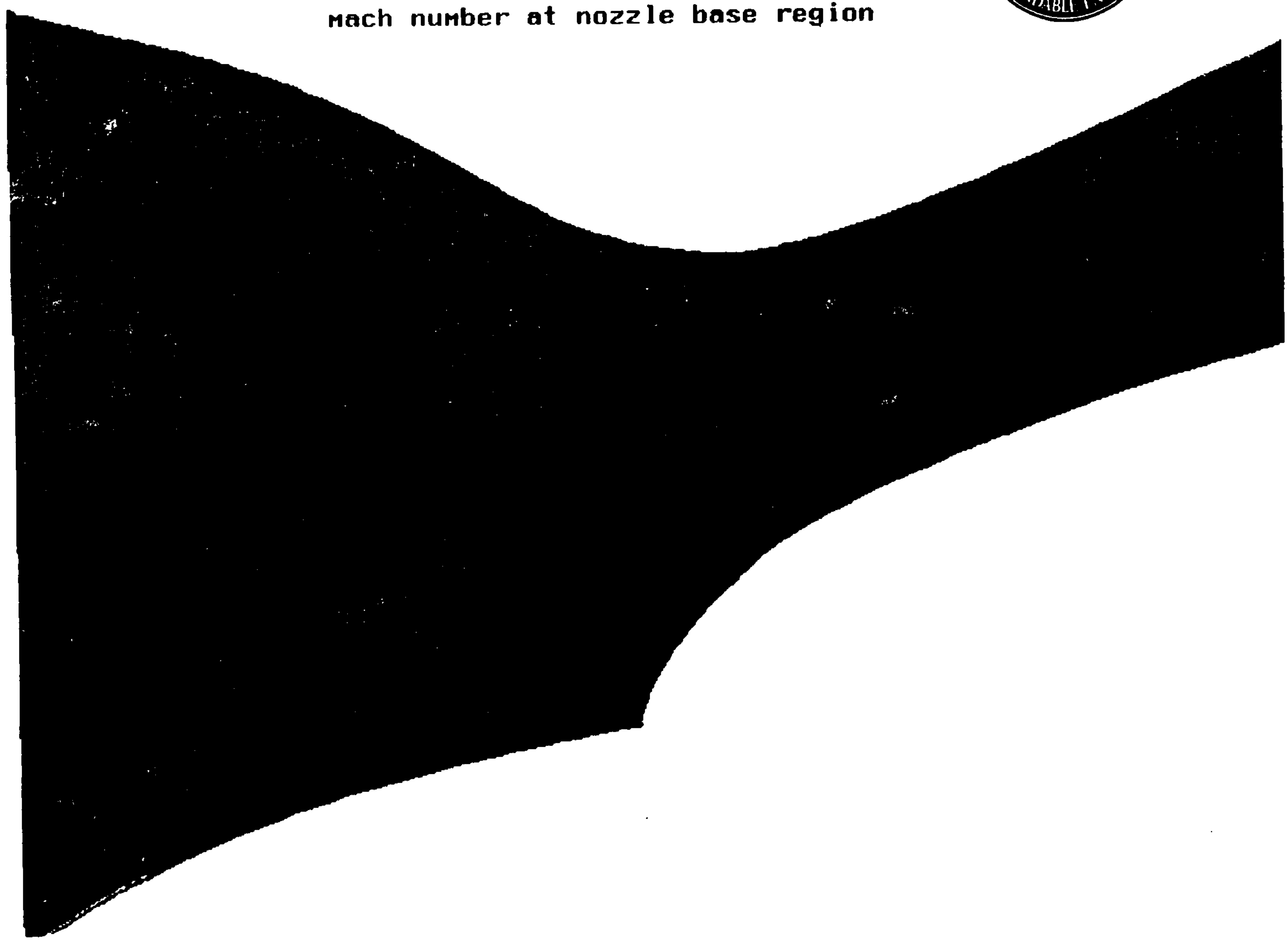

CONTOUR LEVELS
0.00000
0.10000
0.20000
0.30000
0.40000
0.50000
0.60000
0.70000
0.80000
0.90000
1.00000
1.10000
1.20000
1.30000
1.40000
1.50000
1.60000
1.70000
1.80000
1.90000
2.00000

RESULTS

Pressure

CONTOUR LEVELS	
0.00020	.014
0.00060	
0.00100	.069
0.00140	
0.00180	.125
0.00220	
0.00260	.181
0.00300	
0.00340	.236
0.00380	
0.00420	.292
0.00460	
0.00500	.347
0.00540	
0.00580	.403
PSF 10^{-4}	PSI

RESULTS

H_2 – Low Altitude

CONTOUR LEVELS
0.00000
0.00300
0.00600
0.00900
0.01200
0.01500
0.01800
0.02100
0.02400
0.02700
0.03000

RESULTS

Mach Number – Low Altitude

CONTOUR LEVELS
0.00000
0.10000
0.20000
0.30000
0.40000
0.50000
0.60000
0.70000
0.80000
0.90000
1.00000
1.10000
1.20000
1.30000
1.40000
1.50000
1.60000
1.70000
1.80000
1.90000
2.00000

RESULTS

Pressure – Low Altitude

CONTOUR LEVE
0.19000
0.19100
0.19200
0.19300
0.19400
0.19500
0.19600
0.19700
0.19800
0.19900
0.20000
0.20100
0.20200
0.20300
0.20400
0.20500
0.20600
0.20700
0.20800
0.20900
0.21000

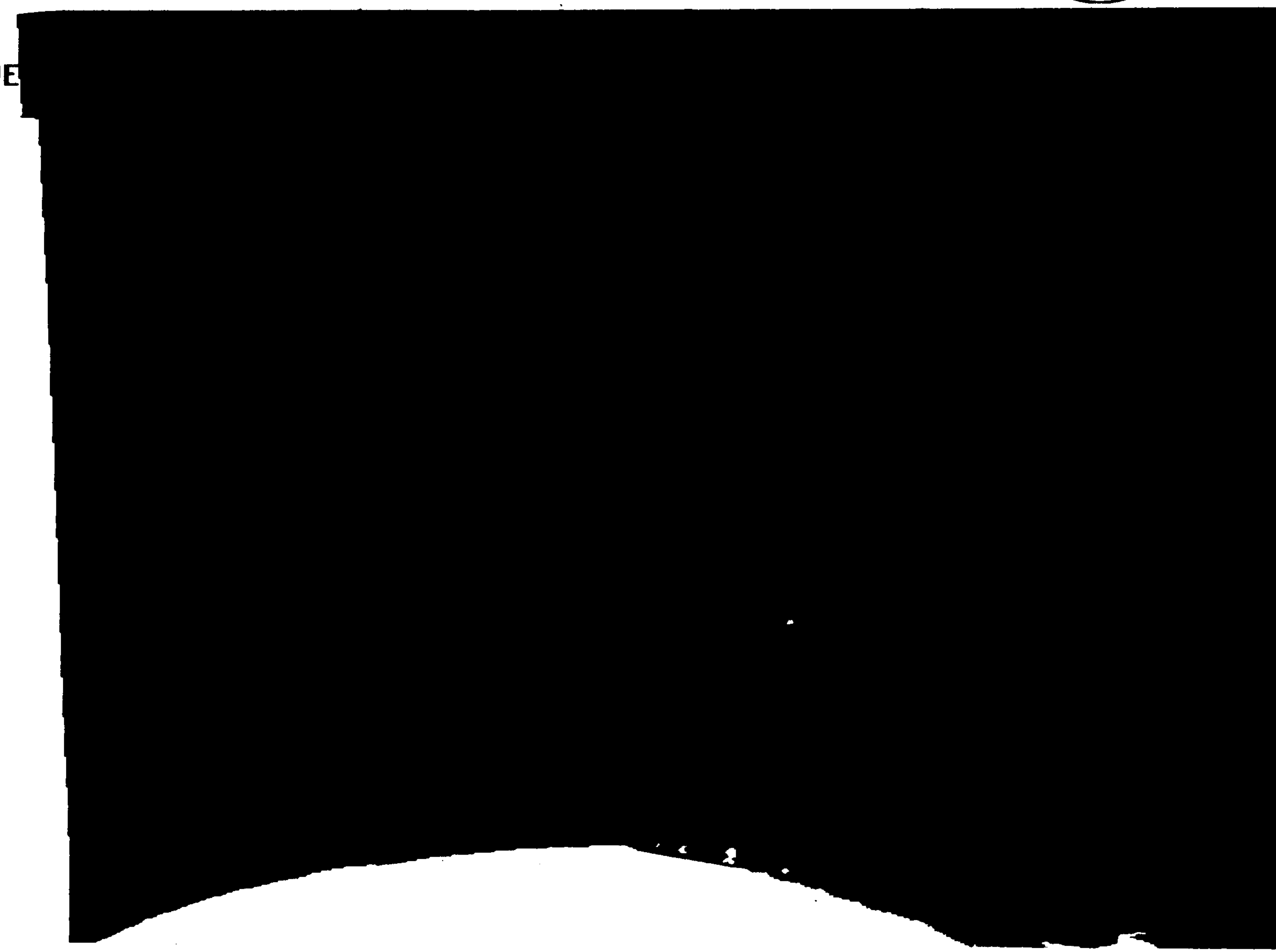

SUMMARY

- o H_2 Transport Into The Base Is A Function Of Configuration And Flight Conditions.

	Low Altitude	High Altitude
Recirculation Region	Stronger	Weaker
H_2 Transport Into Base	Trace	$\sim$1 – 1.5%
Pressure	$\sim$13.9 PSIA	$\sim$0.2 PSIA

N92-32253

HEAT TRANSFER IN ROCKET ENGINE COMBUSTION CHAMBERS AND NOZZLES

P. G. Anderson*, Y.S. Chen†, and R.C. Farmer*

Abstract

Complexities of liquid rocket engine heat transfer which involve the injector faceplate and regeneratively and film cooled walls are being investigated by computational analysis. A conjugate heat transfer analysis will be used to describe localized heating phenomena associated with particular injector configurations and coolant channels and film coolant dumps. These components are being analyzed, and the analyses verified with appropriate test data. Finally, the component analyses will be synthesized into an overall flowfield/heat transfer model. The FDNS code is being used to make the component analyses. Particular attention is being given to the representation of the thermodynamic properties of the fluid streams and to the method of combining the detailed models to represent overall heating. Unit flow models of specific coaxial injector elements have been developed and will be described. Film cooling simulations of film coolant flows typical of the subscale STME being experimentally studied by Pratt and Whitney have been made, and these results will be presented. Other film coolant experiments have also been simulated to verify the CFD heat transfer model being developed by SECA. The status of this entire study will be presented, and its relevance as a new design tool will be demonstrated.

* SECA, Inc., 3313 Bob Wallace Avenue, Suite 202, Huntsville, AL

† Engineering Sciences, Inc., 4920 Corporate Drive, Suite K, Huntsville, AL

HEAT TRANSFER IN ROCKET ENGINE COMBUSTION CHAMBERS AND NOZZLES

P. G. Anderson, Y. S. Chen, and R. C. Farmer

SECA, Inc.

OUTLINE OF STUDY

- NAVIER-STOKES FLOW SOLVER
- TWO-EQUATION TURBULENCE MODELS WITH COMPRESSIBILITY CORRECTIONS AND WALL FUNCTION APPROACH
- HOLDEN'S TEST CASE #45
  - Slot Jet Nozzle Flowfield
  - Film Cooling Analysis
- GASL TEST CASE #41

- **k-EQ. CORRECTION:**

$$\frac{\partial \rho k}{\partial t} + \frac{\partial \rho k U_j}{\partial X_j} = \frac{\partial}{\partial X_j}\left[\left(\mu + \frac{\mu_t}{\sigma_k}\right)\frac{\partial k}{\partial X_j}\right] + \mu_t\left[\frac{\partial U_i}{\partial X_j} + \frac{\partial U_j}{\partial x_i}\right]\frac{\partial U_i}{\partial X_j} - \rho \varepsilon \left(1 + \alpha M_t^2\right)$$

- **ε-EQ. CORRECTION:**

$$\frac{\partial \rho \varepsilon}{\partial t} + \frac{\partial \rho \varepsilon U_j}{\partial X_j} = \frac{\partial}{\partial X_j}\left[\left(\mu + \frac{\mu_t}{\sigma_\varepsilon}\right)\frac{\partial \varepsilon}{\partial X_j}\right] + \frac{C^*_{\varepsilon 1} \varepsilon \mu_t}{k}\left[\frac{\partial U_i}{\partial X_j} + \frac{\partial U_j}{\partial x_i}\right]\frac{\partial U_i}{\partial X_j} - \rho C_{\varepsilon 2}\frac{\varepsilon^2}{k}$$

where

$$\alpha = 1, \qquad M_t = \frac{k}{a^2}$$

$$C^*_{\varepsilon 1} = 1.44\left(1 + 0.08 M^{0.25}\right), \qquad C_{\varepsilon 2} = 1.92, \qquad M = \frac{V_{total}}{a}$$

- **HEAT TRANSFER WALL FUNCTION:**

(Integration of Near Wall Energy Balance-- Viegas et al. 1985)

Heat Flux Source Term:

$$q_w = [h_w - h - Pr_t (u - u_w)^2 / 2] (\tau_w / Pr_t u)$$
$$= [h_w - h - Pr_t (u - u_w)^2 / 2] (\rho u_\tau / Pr_t u^+)$$

where

$$u^+ = ln\left[\frac{(y^+ + 11)^{4.02}}{(y^{+^2} - 7.37 y^+ + 83.3)^{0.79}}\right] + 0.563 \, tan^{-1}(0.12 y^+ - 0.441) - 3.81$$

$$Pr_t = 0.9$$

For Adiabatic Wall Boundary Condition,

$$h_w = h + Pr_t (u - u_w)^2 / 2$$

- **HOLDEN'S TEST CASE #45**
  - SLOT JET NOZZLE (H = 0.12)

    $Re = 4.51 \times 10^4$ per inch

    $\lambda = 0.0945$

    Mesh: 61 x 11 x 31

  - FILM COOLING ANALYSIS

    $Re = 7.00 \times 10^5$ / in

    Mesh: 101 x 81

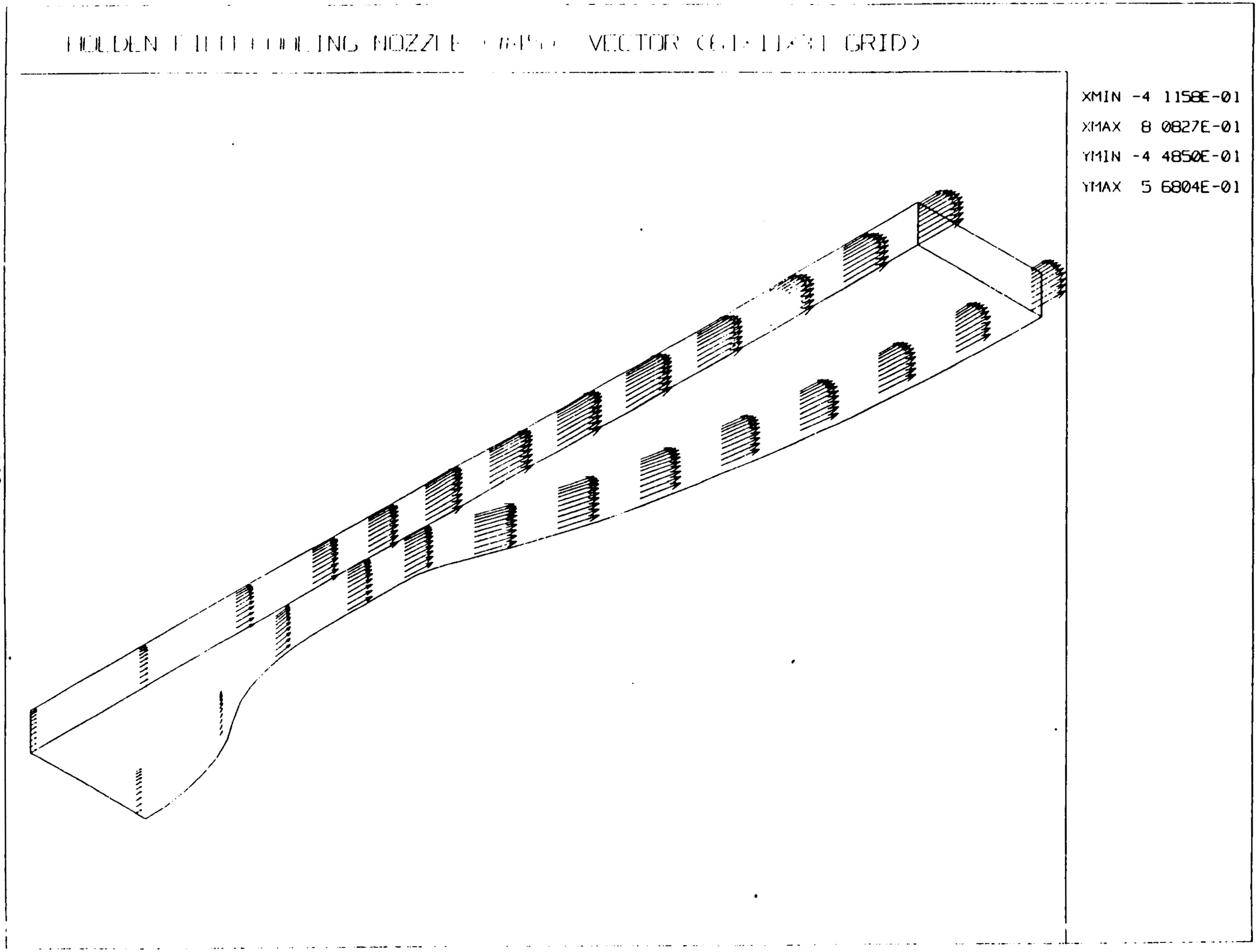

ORIGINAL PAGE IS
OF POOR QUALITY

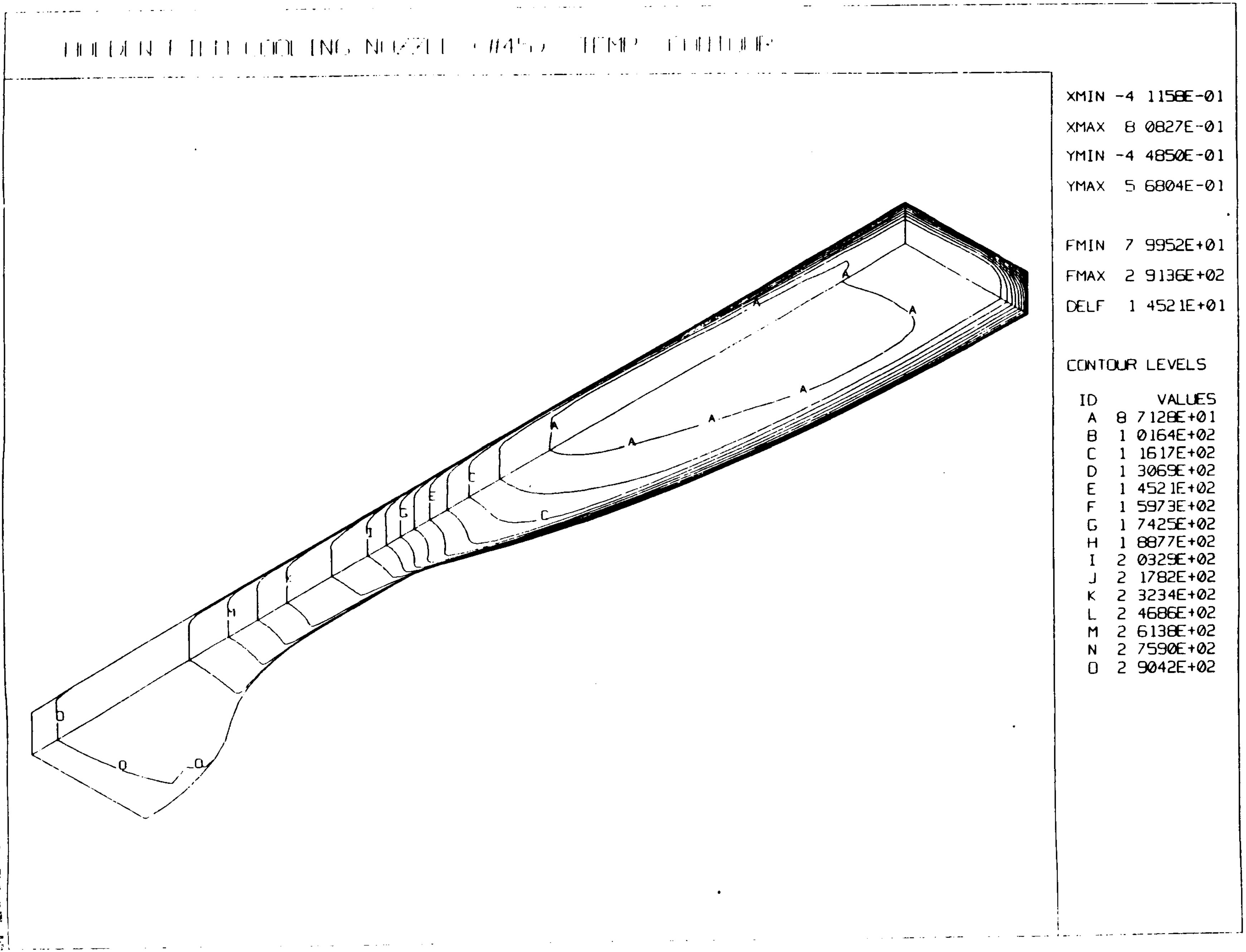
XMIN -4 1158E-01
XMAX 8 0827E-01
YMIN -4 4850E-01
YMAX 5 6804E-01
FMIN 7 9952E+01
FMAX 2 9136E+02
DELF 1 4521E+01
CONTOUR LEVELS
ID VALUES
A 8 7128E+01
B 1 0164E+02
C 1 1617E+02
D 1 3069E+02
E 1 4521E+02
F 1 5973E+02
G 1 7425E+02
H 1 8877E+02
I 2 0329E+02
J 2 1782E+02
K 2 3234E+02
L 2 4686E+02
M 2 6138E+02
N 2 7590E+02
O 2 9042E+02

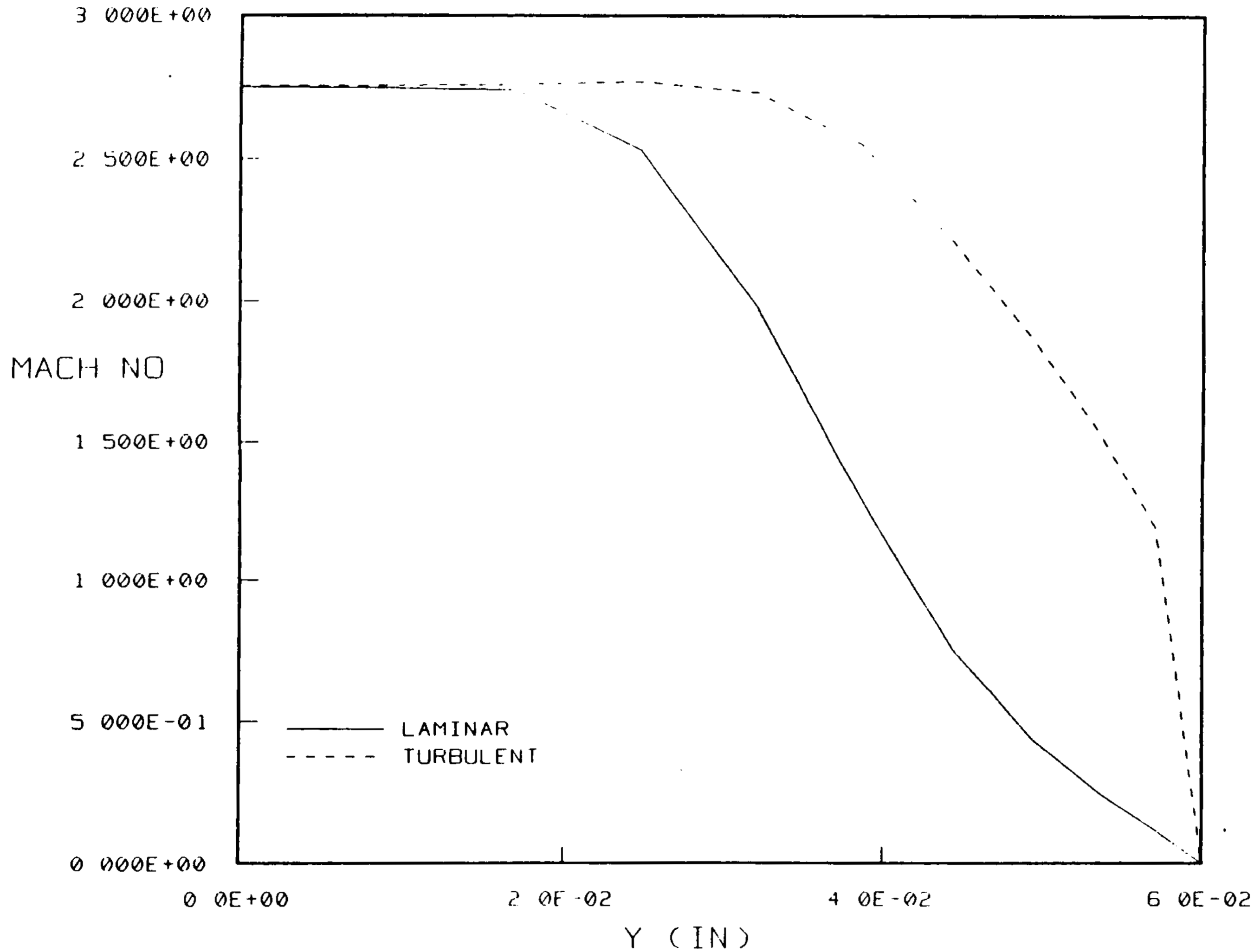

HOLDEN TEST CASE 45 COOLING JET NOZZLE EXIT MACH NUMBER
PROFILE COMPARISONS

HOLDEN FILM COOLING TEST CASE 45 VECTOR & HE-CONTOUR

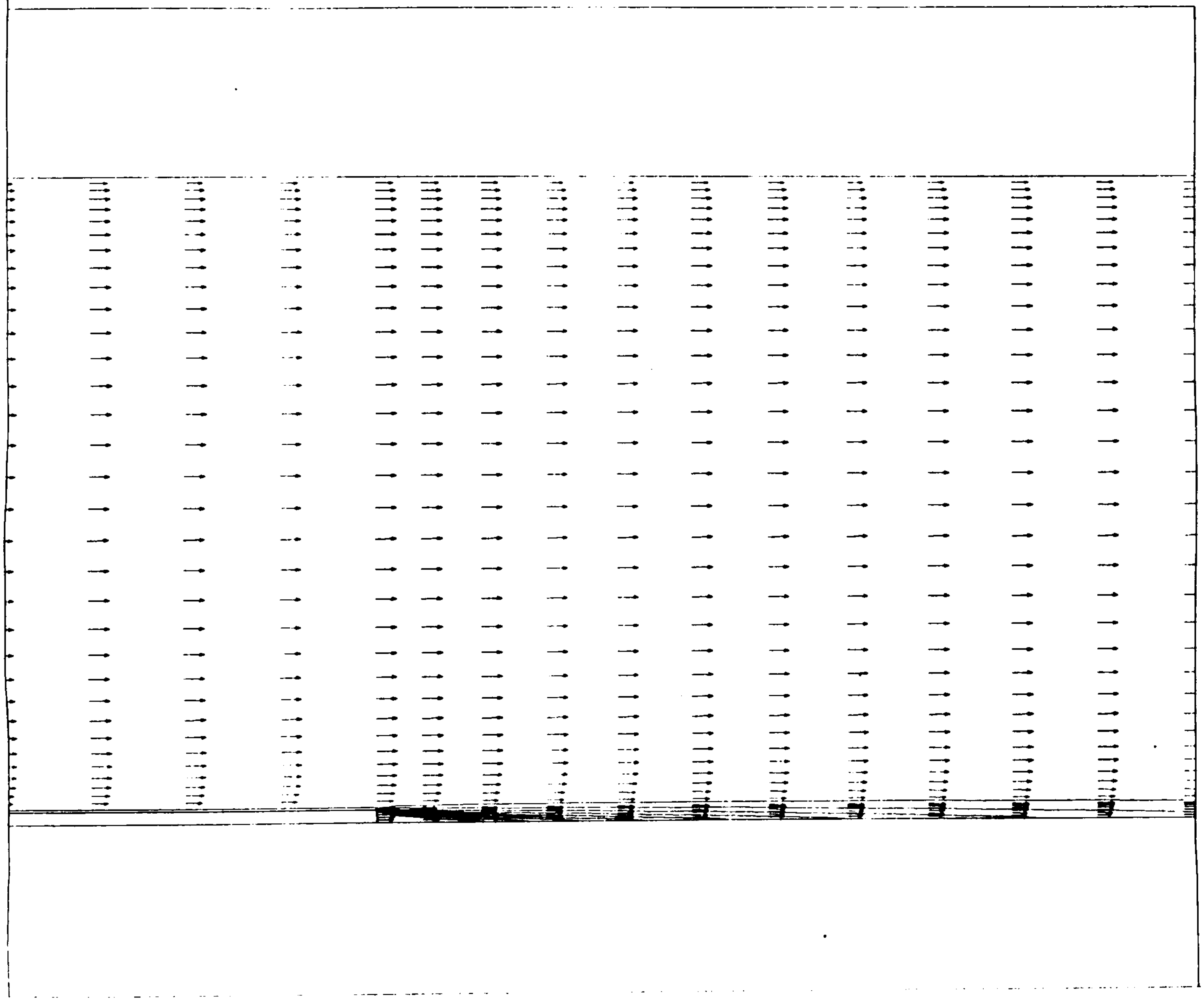

XMIN -3 3952E+00
XMAX 7 5834E+00
YMIN -1 5818E+00
YMAX 7 5671E+00

FMIN 0 0000E+00
FMAX 1 0000E+00
DELF 1 0000E-01

CONTOUR LEVELS

ID	VALUES
A	0 0000E+00
B	1 0000E-01
C	1 9999E-01
D	2 9999E-01
E	3 9999E-01
F	4 9999E-01
G	5 9999E-01
H	6 9999E-01
I	7 9999E-01
J	8 9999E-01
K	9 9999E-01

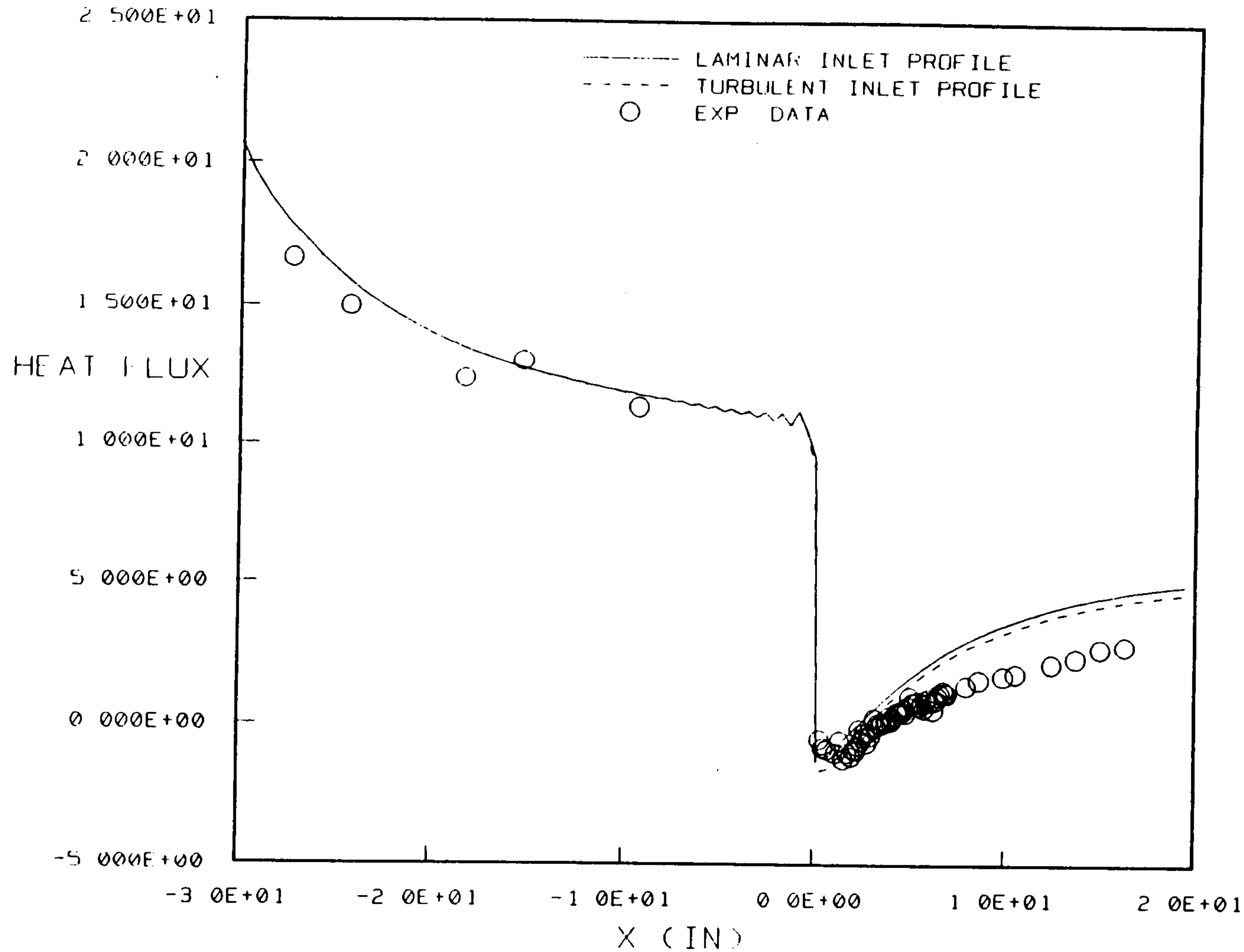

HOLDEN FILM COOLING TEST CASE 45 WITHOUT MODEL CORRECTION
(HEAT FLUX UNIT BTU/FT2/SEC)

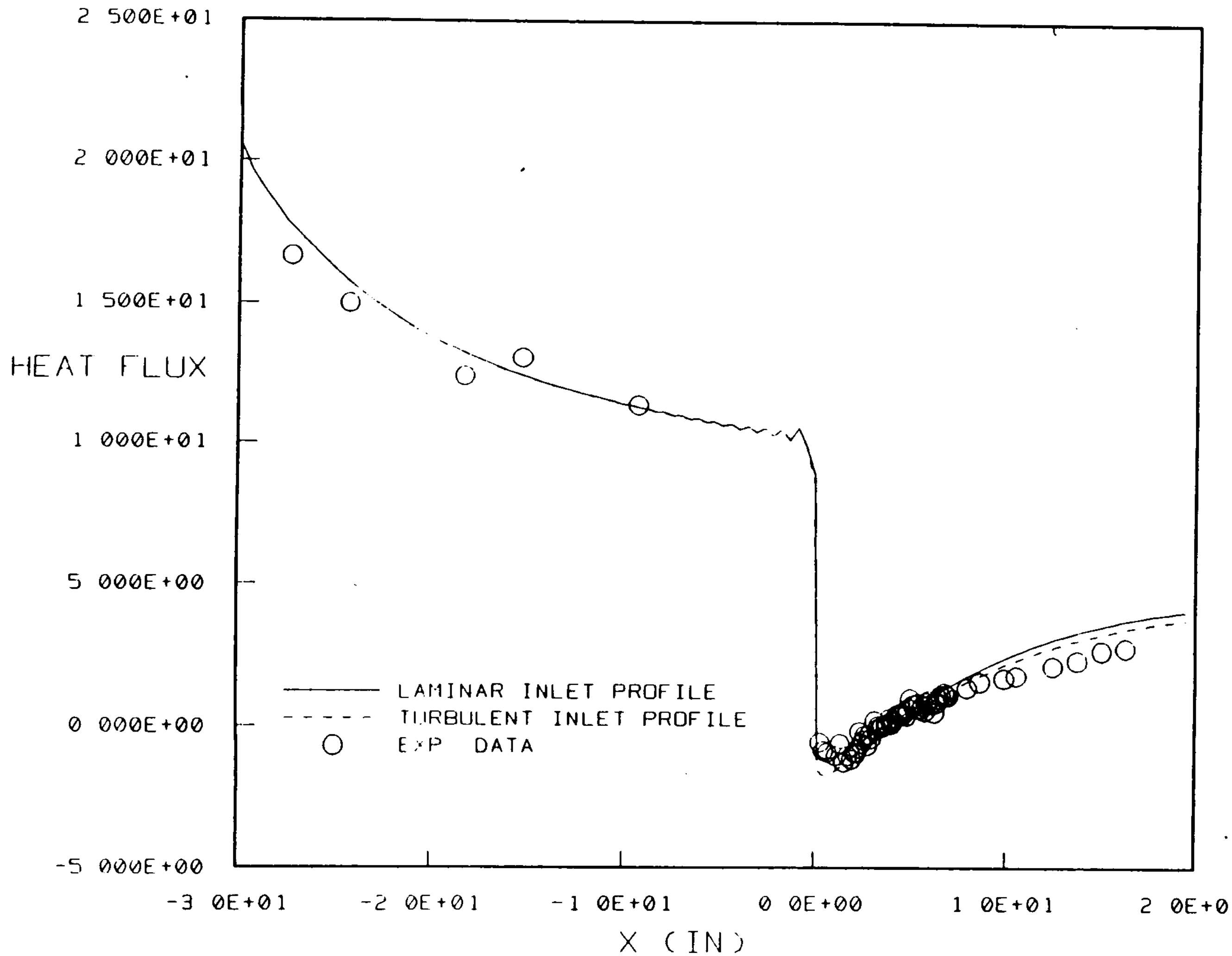

HOLDEN FILM COOLING TEST CASE 45 WITH K-CORRECTED MODEL
(HEAT FLUX UNIT BTU/FT2/SEC)

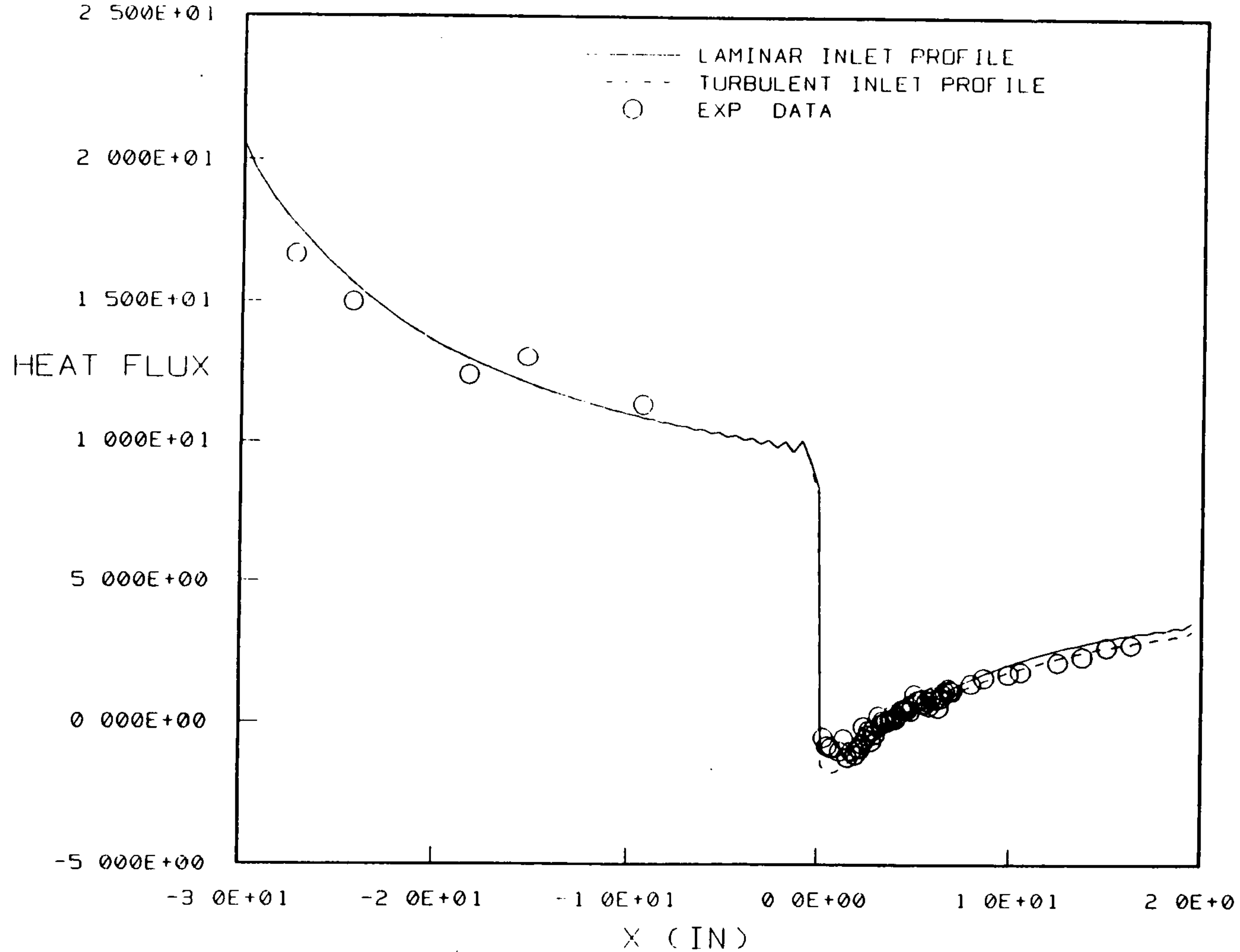

HOLDEN FILM COOLING TEST CASE 45 WITH E-CORRECTED MODEL
(HEAT FLUX UNIT = BTU/FT2/SEC)

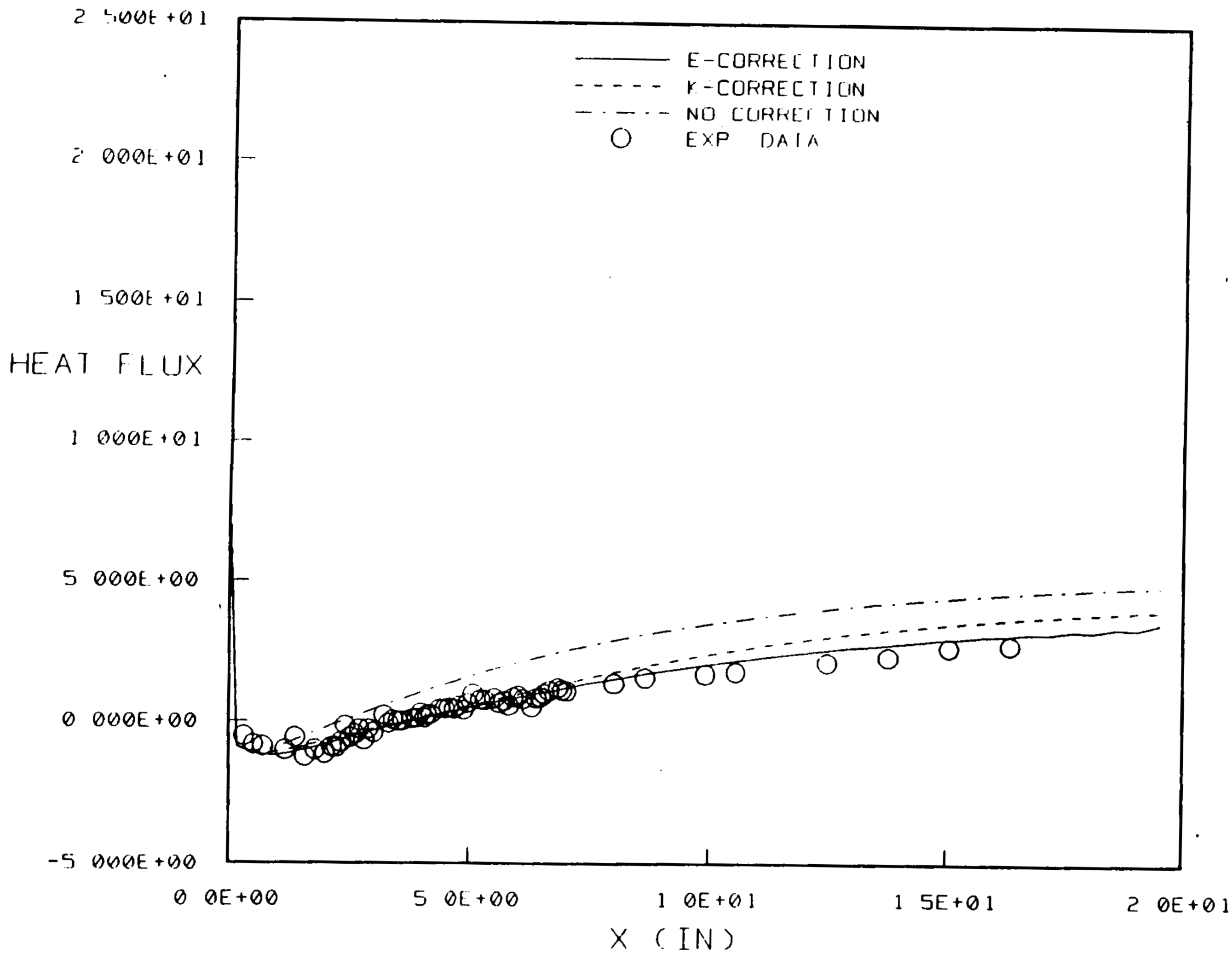

HOLDEN FILM COOLING TEST CASE 45 WITH LAMINAR INLET DATA
- MODEL COMPARISONS (HEAT FLUX UNIT = BTU/FT2/SEC)

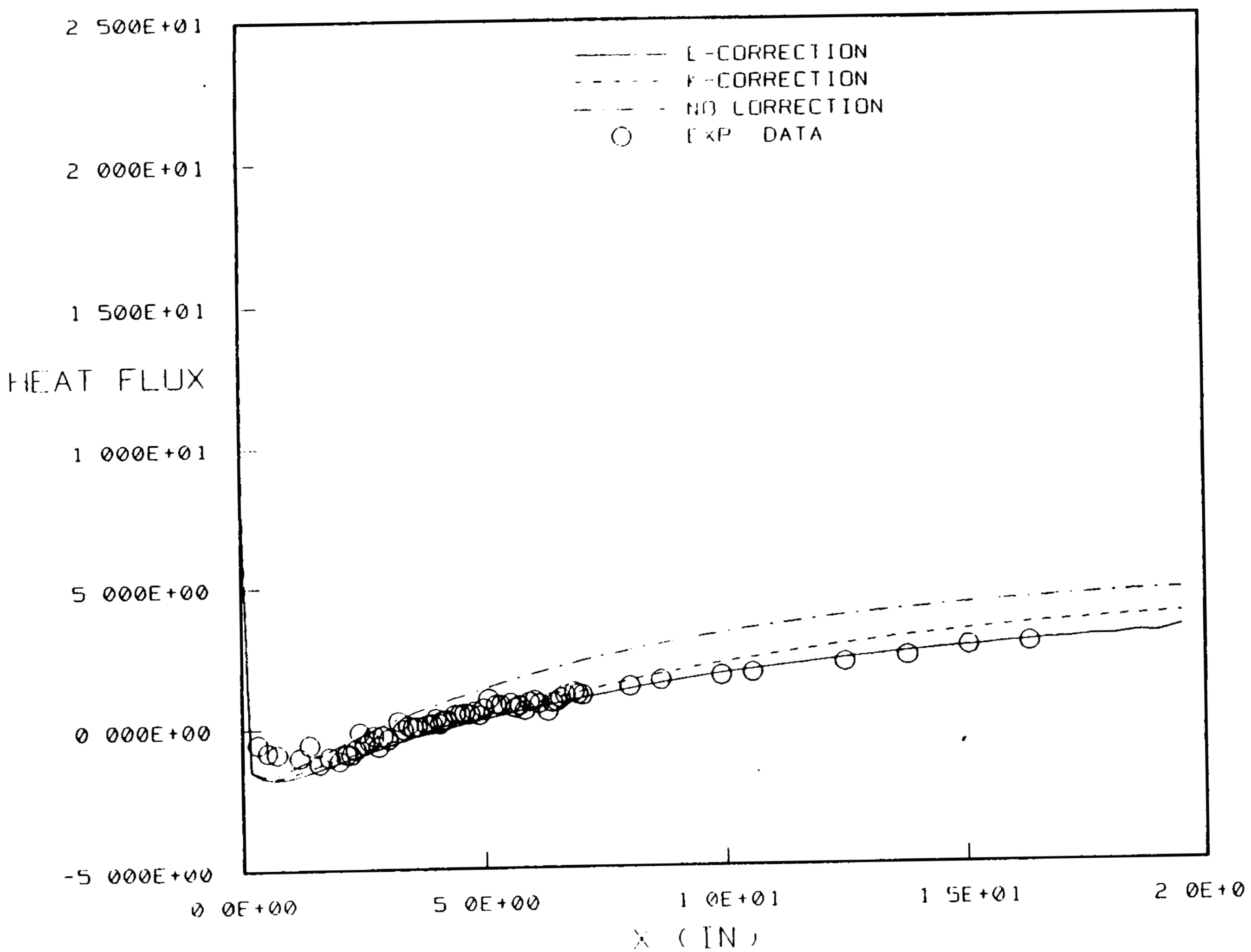

HOLDEN FILM COOLING TEST CASE 45 WITH TURBU INLET DATA
MODEL COMPARISONS (HEAT FLUX UNIT = BTU/FT2/SEC)

- **GASL TEST CASE #41**

$Re = 1.74 \times 10^5$ per inch

$M_{air} = 3.84$

$P_{air} = 5.7$ psia

$T_{air} = 2000\ ^oR$

$M_{H2} = 2.50$ (Fully Developed Laminar Profile)

$Re_{H2} = 2.557 \times 10^4$

$P_{H2} = 16.6$ psia

$T_{H2} = 233\ ^oR$

Mesh: 101 x 81

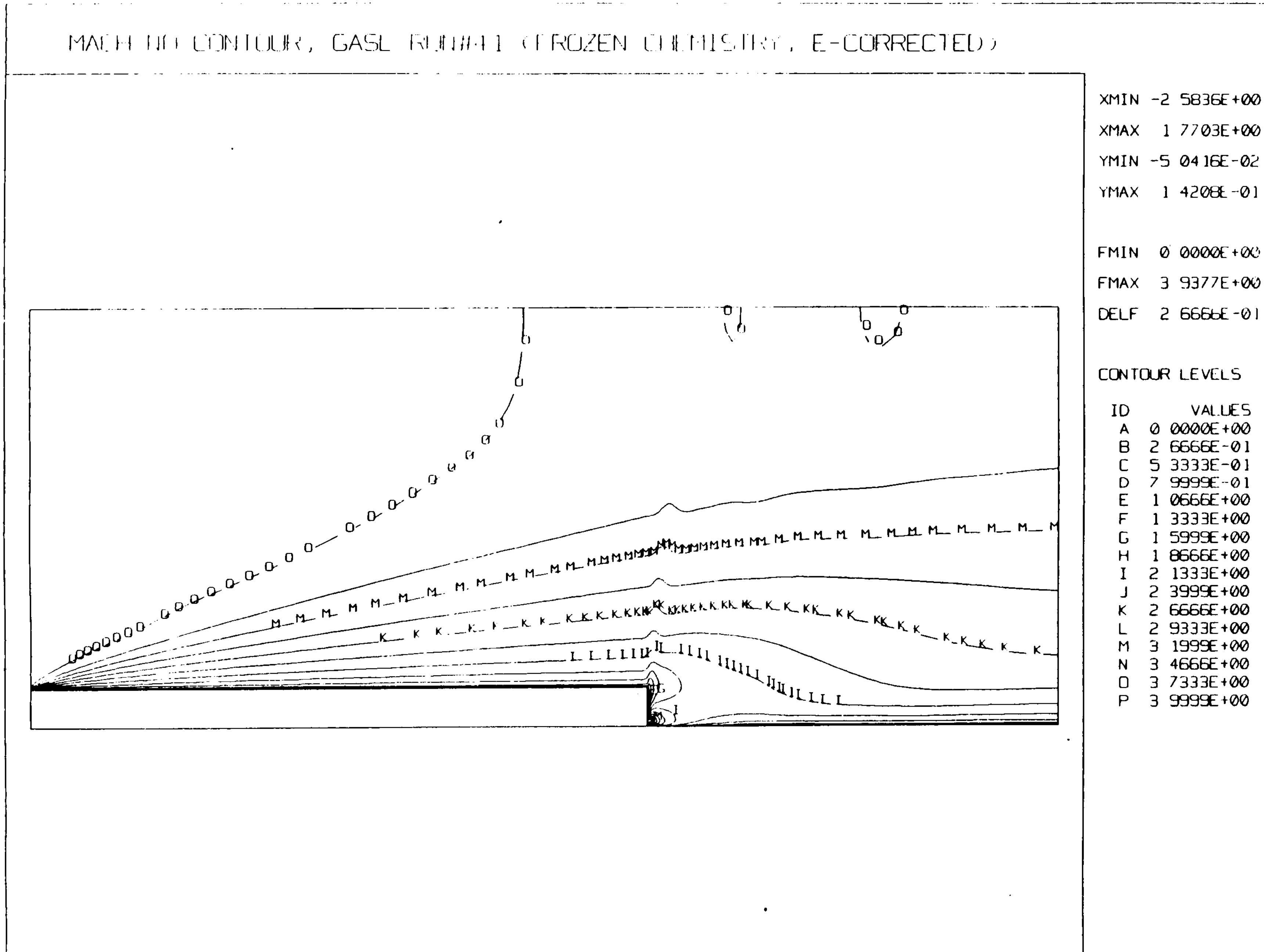
MACH NO CONTOUR, GASL RUN#1 (FROZEN CHEMISTRY, E-CORRECTED)
XMIN -2 5836E+00
XMAX 1 7703E+00
YMIN -5 0416E-02
YMAX 1 4208E-01
FMIN 0 0000E+00
FMAX 3 9377E+00
DELF 2 6666E-01
CONTOUR LEVELS
ID VALUES
A 0 0000E+00
B 2 6666E-01
C 5 3333E-01
D 7 9999E-01
E 1 0666E+00
F 1 3333E+00
G 1 5999E+00
H 1 8666E+00
I 2 1333E+00
J 2 3999E+00
K 2 6666E+00
L 2 9333E+00
M 3 1999E+00
N 3 4666E+00
O 3 7333E+00
P 3 9999E+00

VELOCITY VECTORS, CASE RUN#11 (FROZEN CHEM., F-CORRECTED)

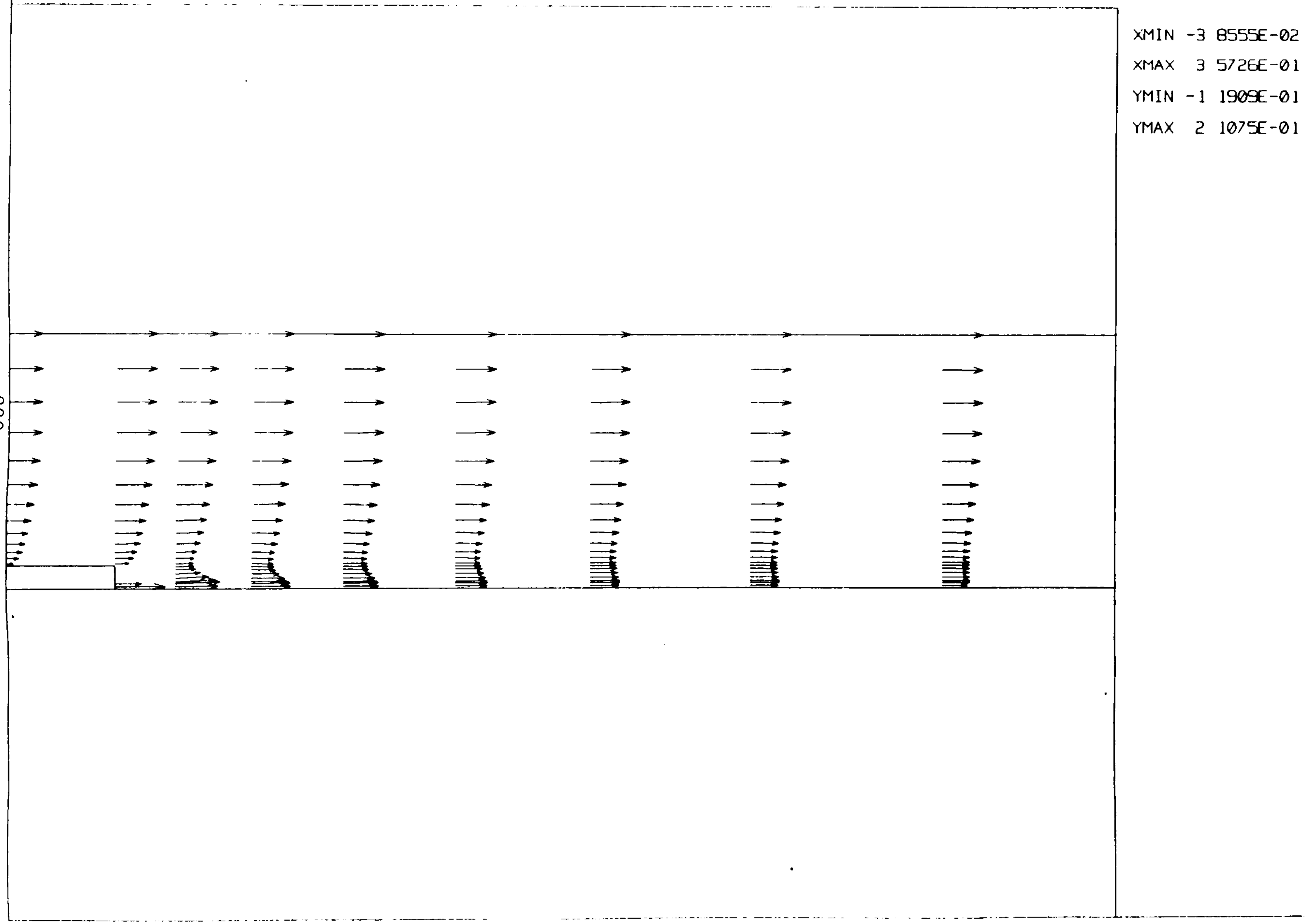

ORIGINAL PAGE IS
OF POOR QUALITY

SPECIES CONCENTRATION OF HYDROGEN (FROZEN CHEM., E-CORRECT)

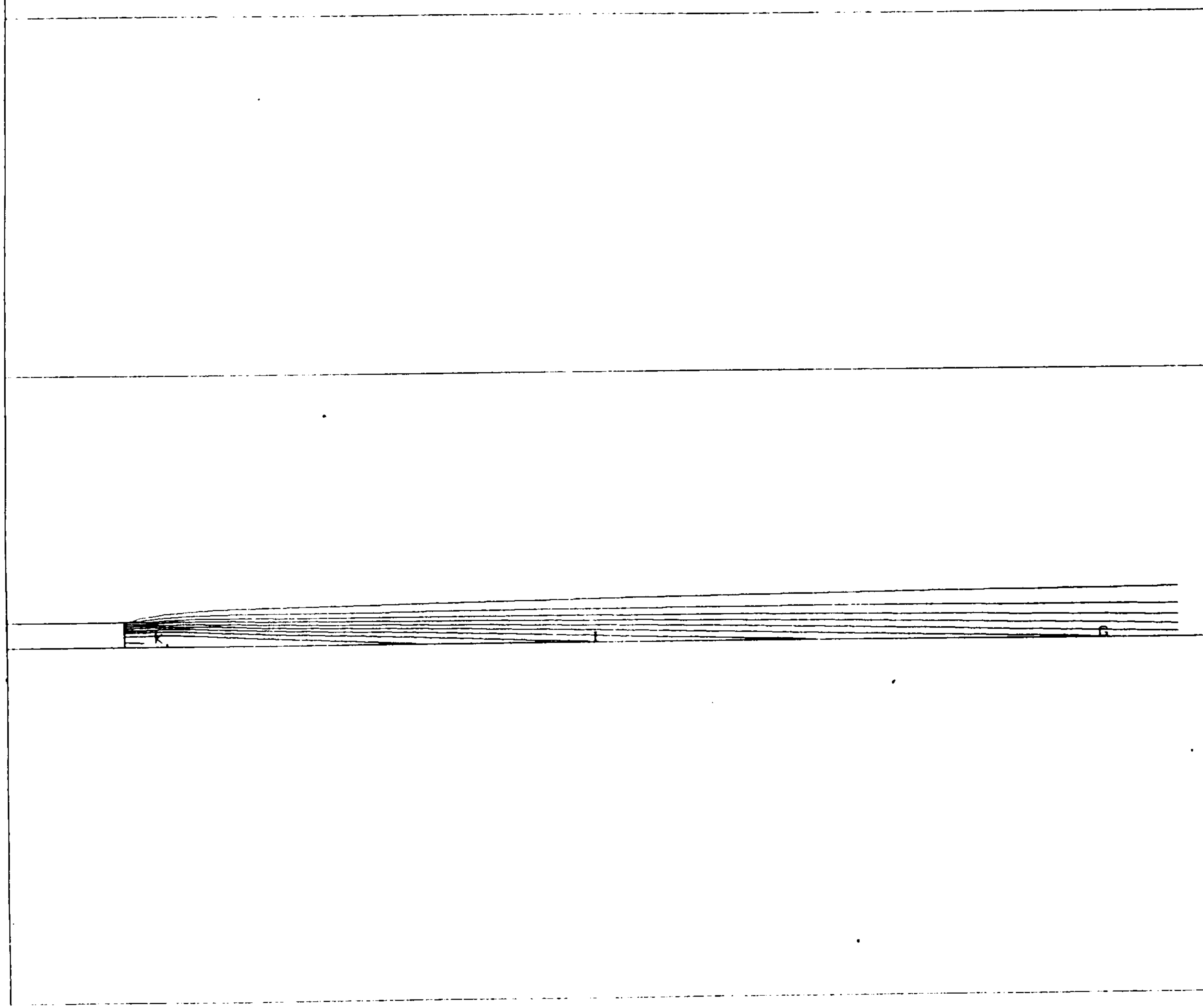

XMIN	-3 8555E-02
XMAX	3 5726E-01
YMIN	-1 1909E-01
YMAX	2 1075E-01
FMIN	0 0000E+00
FMAX	1 0000E+00
DELF	1 0000E-01

CONTOUR LEVELS

ID	VALUES
A	0 0000E+00
B	1 0000E-01
C	1 9999E-01
D	2 9999E-01
E	3 9999E-01
F	4 9999E-01
G	5 9999E-01
H	6 9999E-01
I	7 9999E-01
J	8 9999E-01
K	9 9999E-01

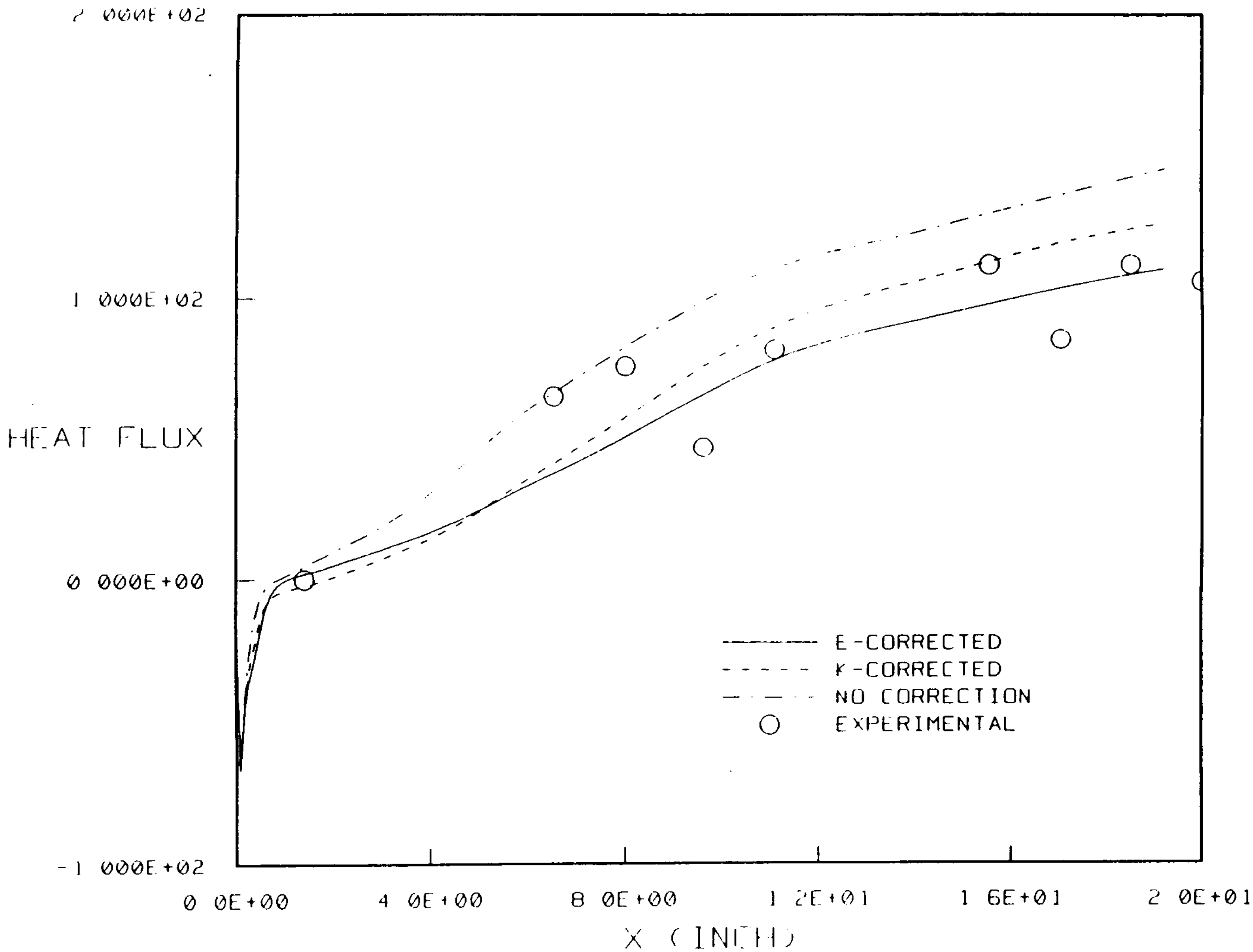

HEAT FLUX FOR CASE RUN#41 (FROZEN CHEMISTRY, HIGH RE K-E)

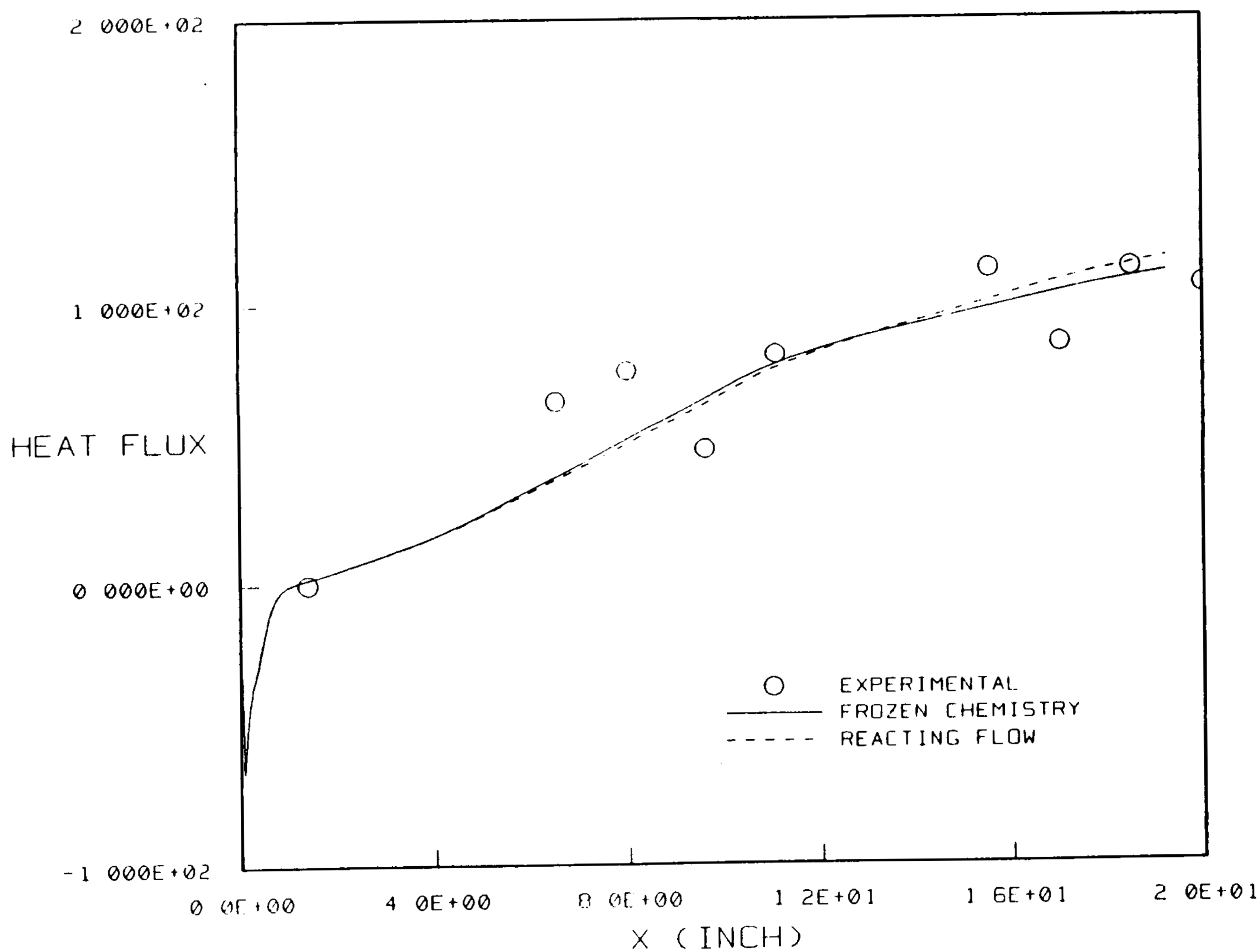

HEAT FLUX FOR GASL RUN# [illegible] (HIGH K-E [illegible], E-CORRECTED)

ORIGINAL PAGE IS
OF POOR QUALITY

CASE RUN#[illegible] MASS FRACTION OF [illegible] (HIGH RE K-E, E CORRECTED)

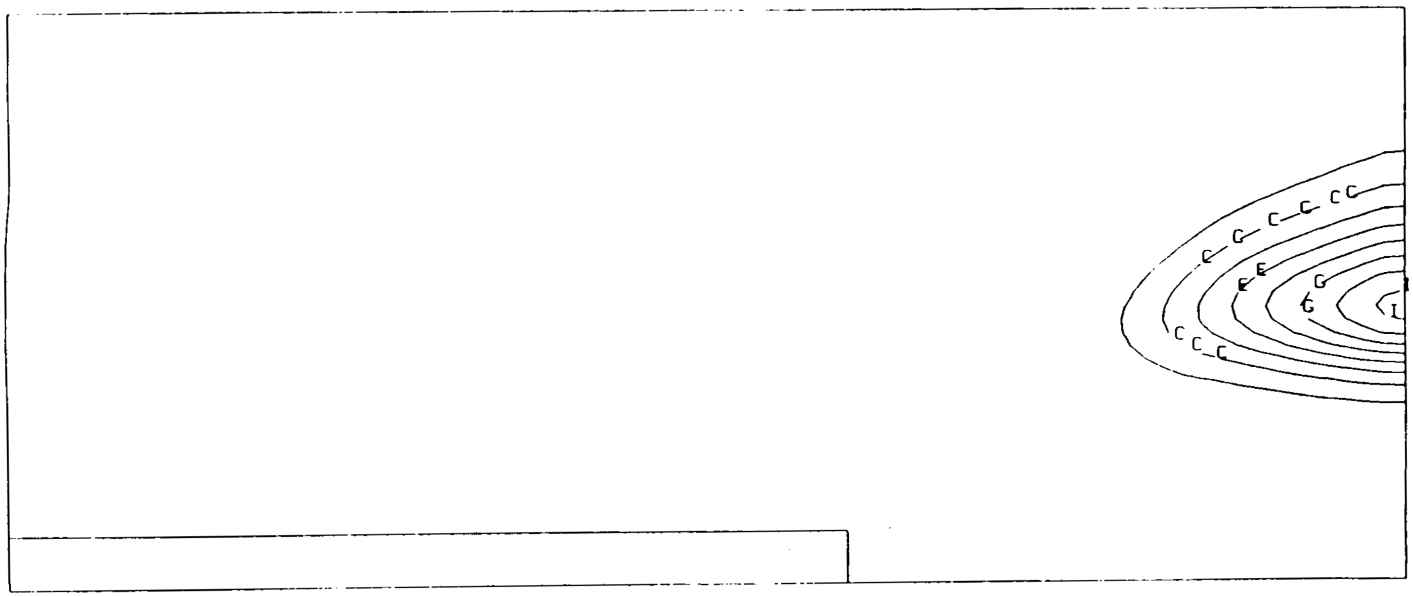

XMIN -2 5836E+00
XMAX 1 7703E+00
YMIN -5 0416E-02
YMAX 1 4208E-01

FMIN 0 0000E+00
FMAX 8 3315E-02
DELF 1 0000E-02

CONTOUR LEVELS

ID	VALUES
A	0 0000E+00
B	1 0000E-02
C	2 0000E-02
D	3 0000E-02
E	4 0000E-02
F	5 0000E-02
G	6 0000E-02
H	7 0000E-02
I	8 0000E-02
J	9 0000E-02
K	1 0000E-01

CONCLUSIONS

- COOLING JET EXIT BOUNDARY CONDITIONS ARE IMPORTANT FOR FILM COOLING ANALYSIS
- 3-D COMPUTATION OF COOLING JET NOZZLE FLOWFIELD PROVIDES THE NEEDED JET EXIT BOUNDARY CONDITIONS
- COMPRESSIBILITY CORRECTIONS FOR TWO-EQUATION TURBULENCE MODELS ARE EFFECTIVE FOR FILM COOLING ANALYSIS

APPLICATION TO STME NOZZLE FLOW

- Mesh Size: 18,000 Grid Points
  40,000 Grid Points
  (2nd case in progress)
- Two-Equation Turbulence Model With Compressibility Correction
- Finite-Rate Chemistry
  (6 Species, 9 Reaction)

Subscale Nozzle Operating Conditions:

Nozzle: $Re = 2.95 \times 10^5$ (1/in)
Mass Flow Rate = 82.6 (lbm/sec)
$P_c = 2190$ psia
$T_c = 6700$ °R
$M_{in} = 0.225$
$\gamma_{in} = 1.1925$ (Equilibrium Chem.)

Subsonic Jet: $\dot{m} = 0.254$ lbm/sec ; $P = 59.13$ psia
Sonic Jet: $\dot{m} = 1.51$ lbm/sec ; $P = 60.90$ psia
$T_{jet} = 530$ °R

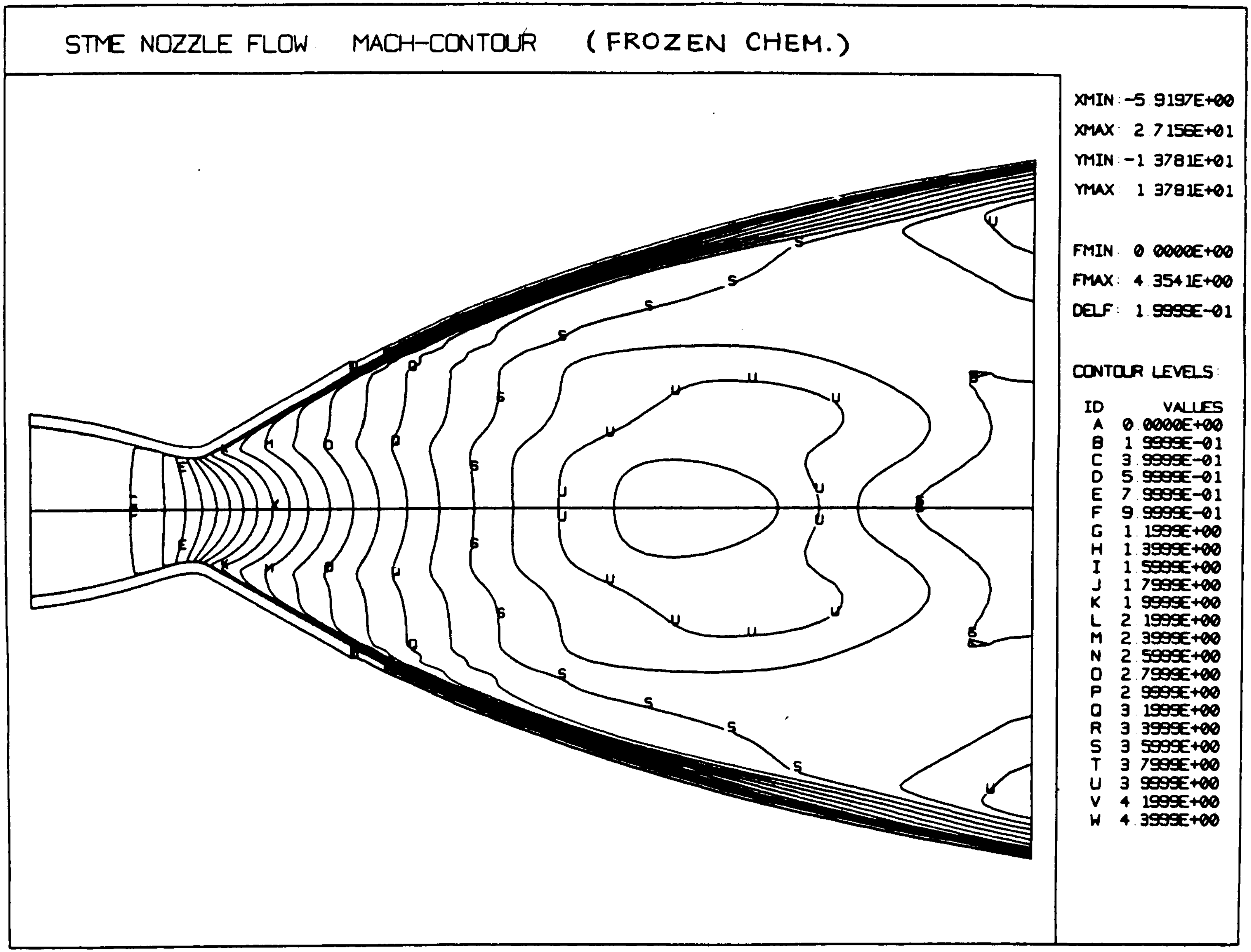
STME NOZZLE FLOW MACH-CONTOUR (FROZEN CHEM.)
XMIN: -5.9197E+00
XMAX: 2.7156E+01
YMIN: -1.3781E+01
YMAX: 1.3781E+01
FMIN: 0.0000E+00
FMAX: 4.3541E+00
DELF: 1.9999E-01
CONTOUR LEVELS:
ID VALUES
A 0.0000E+00
B 1.9999E-01
C 3.9999E-01
D 5.9999E-01
E 7.9999E-01
F 9.9999E-01
G 1.1999E+00
H 1.3999E+00
I 1.5999E+00
J 1.7999E+00
K 1.9999E+00
L 2.1999E+00
M 2.3999E+00
N 2.5999E+00
O 2.7999E+00
P 2.9999E+00
Q 3.1999E+00
R 3.3999E+00
S 3.5999E+00
T 3.7999E+00
U 3.9999E+00
V 4.1999E+00
W 4.3999E+00

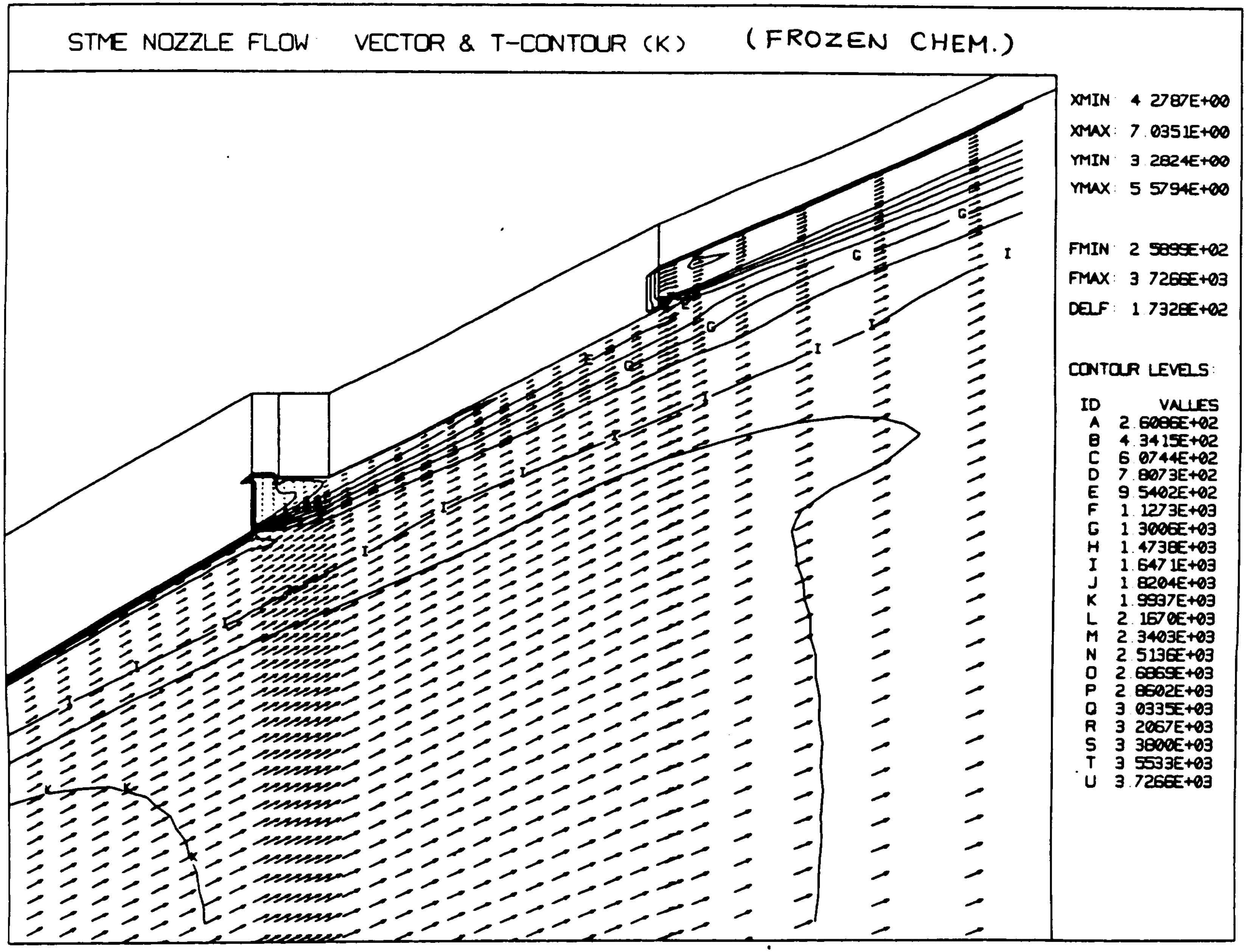
STME NOZZLE FLOW VECTOR & T-CONTOUR (K) (FROZEN CHEM.)
XMIN: 4.2787E+00
XMAX: 7.0351E+00
YMIN: 3.2824E+00
YMAX: 5.5794E+00
FMIN: 2.5899E+02
FMAX: 3.7266E+03
DELF: 1.7328E+02
CONTOUR LEVELS:
ID VALUES
A 2.6086E+02
B 4.3415E+02
C 6.0744E+02
D 7.8073E+02
E 9.5402E+02
F 1.1273E+03
G 1.3006E+03
H 1.4738E+03
I 1.6471E+03
J 1.8204E+03
K 1.9937E+03
L 2.1670E+03
M 2.3403E+03
N 2.5136E+03
O 2.6869E+03
P 2.8602E+03
Q 3.0335E+03
R 3.2067E+03
S 3.3800E+03
T 3.5533E+03
U 3.7266E+03

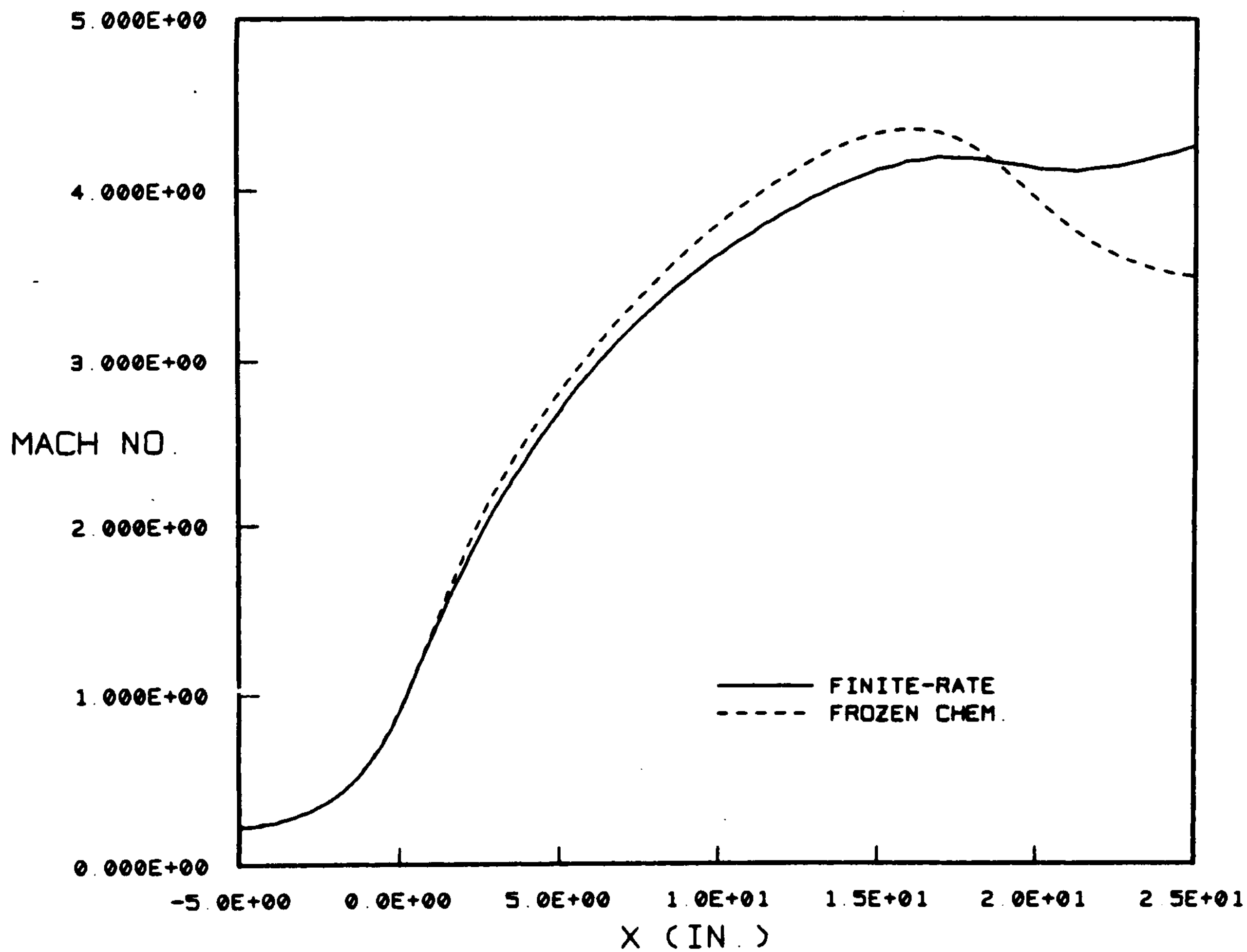

SUBSCALE STME NOZZLE CENTER-LINE MACH NUMBER DISTRIBUTION

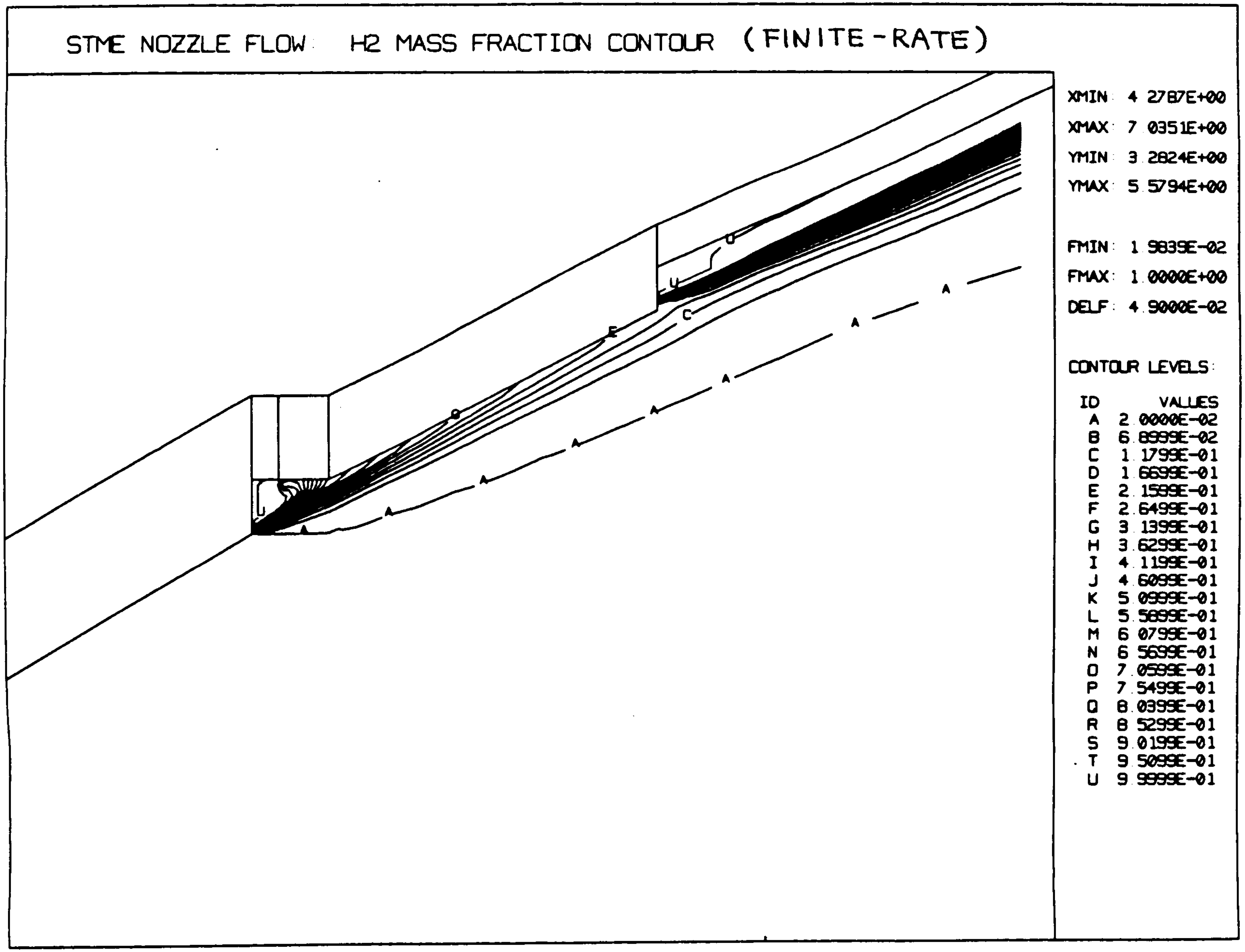
STME NOZZLE FLOW: H2 MASS FRACTION CONTOUR (FINITE-RATE)
XMIN: 4.2787E+00
XMAX: 7.0351E+00
YMIN: 3.2824E+00
YMAX: 5.5794E+00
FMIN: 1.9839E-02
FMAX: 1.0000E+00
DELF: 4.9000E-02
CONTOUR LEVELS:
ID VALUES
A 2.0000E-02
B 6.8999E-02
C 1.1799E-01
D 1.6699E-01
E 2.1599E-01
F 2.6499E-01
G 3.1399E-01
H 3.6299E-01
I 4.1199E-01
J 4.6099E-01
K 5.0999E-01
L 5.5899E-01
M 6.0799E-01
N 6.5699E-01
O 7.0599E-01
P 7.5499E-01
Q 8.0399E-01
R 8.5299E-01
S 9.0199E-01
T 9.5099E-01
U 9.9999E-01

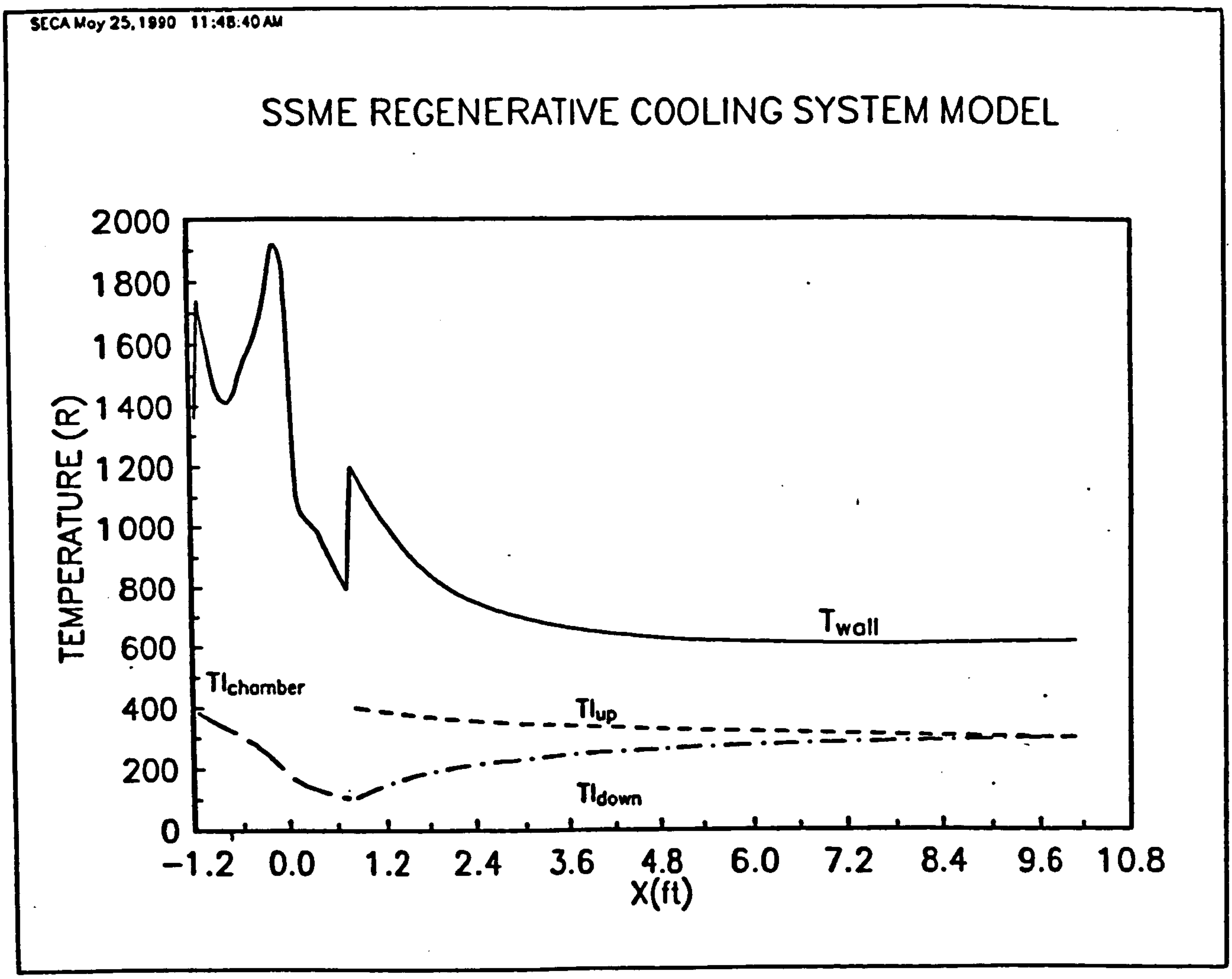

SSME MCC and Nozzle Wall Heating

HEAT-FLUX

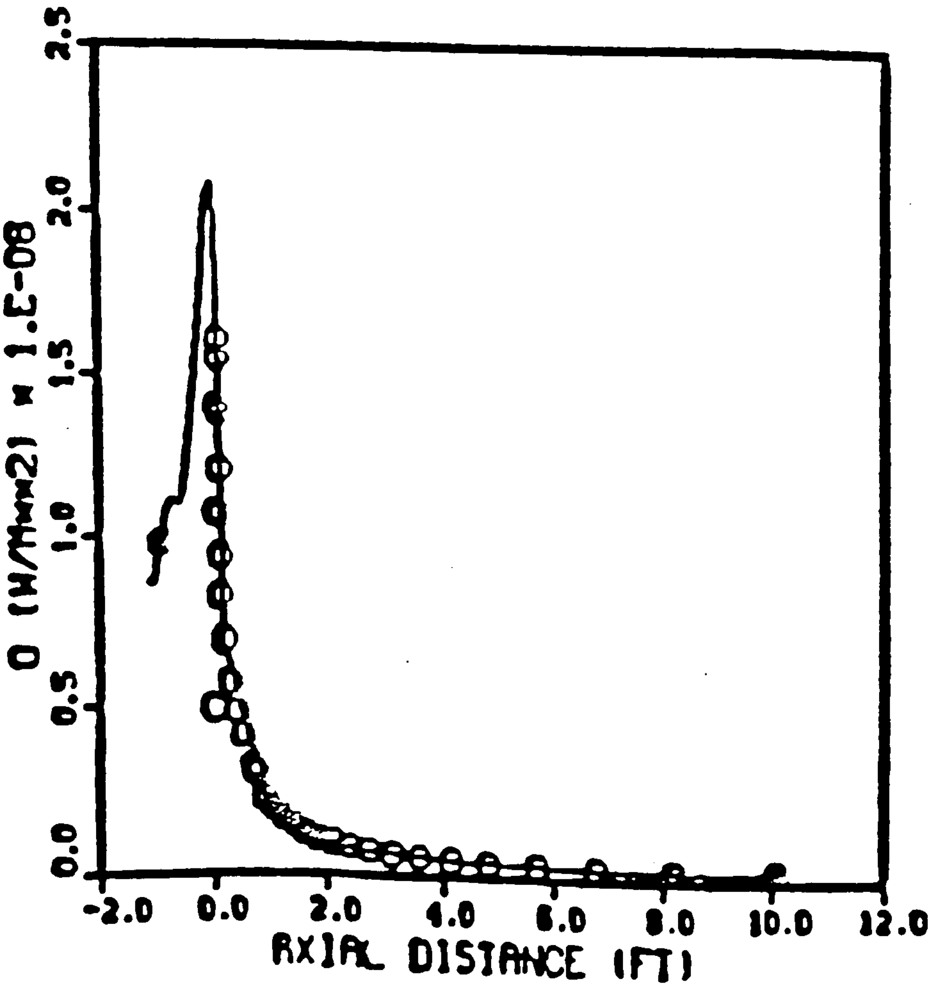

Q (W/MM2) * 1.E-08
0.0
0.5
1.0
1.5
2.0
2.5
-2.0
0.0
2.0
4.0
6.0
8.0
10.0
12.0
AXIAL DISTANCE (FT)

Case 2 Cooling Jets Mesh System:

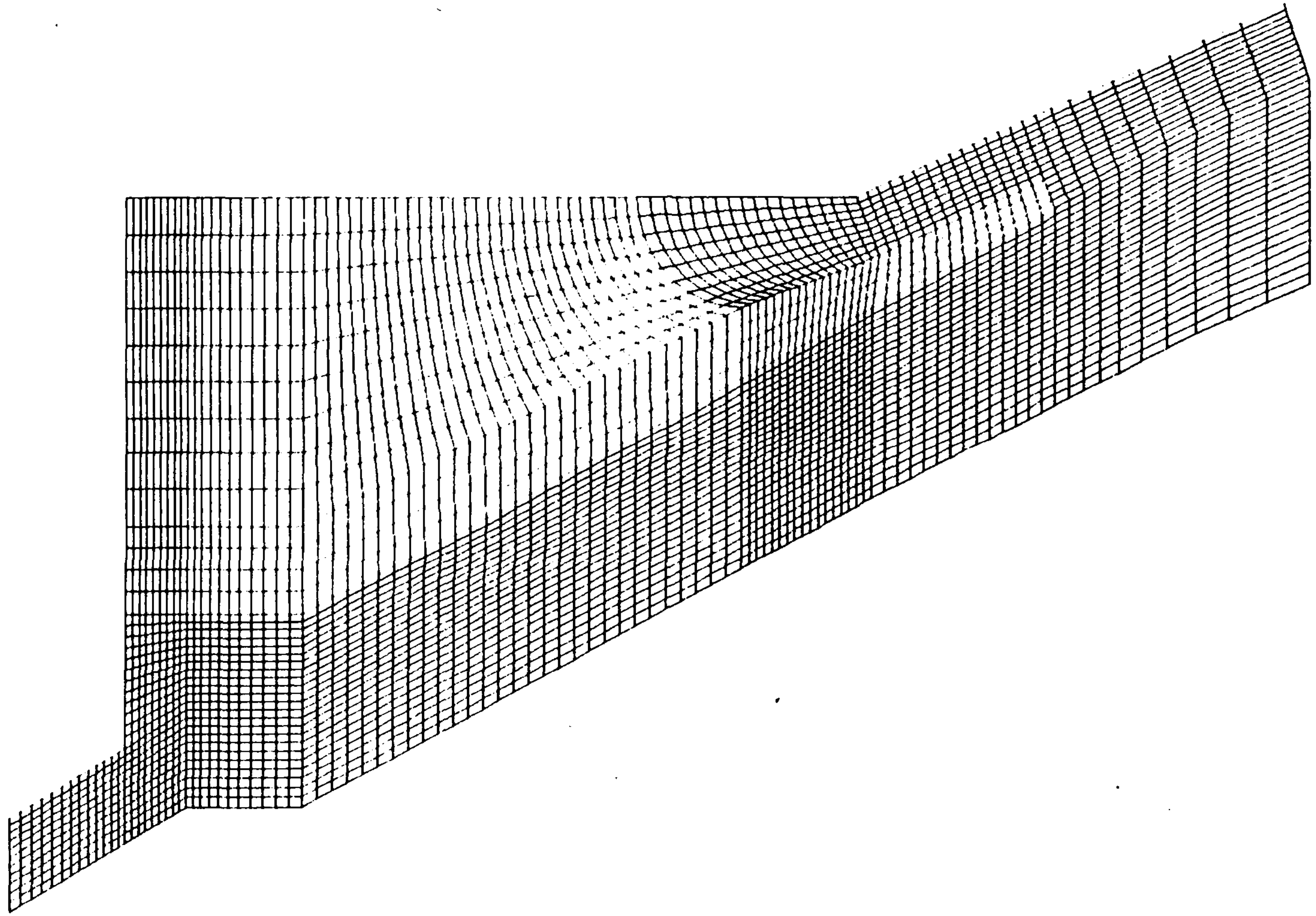

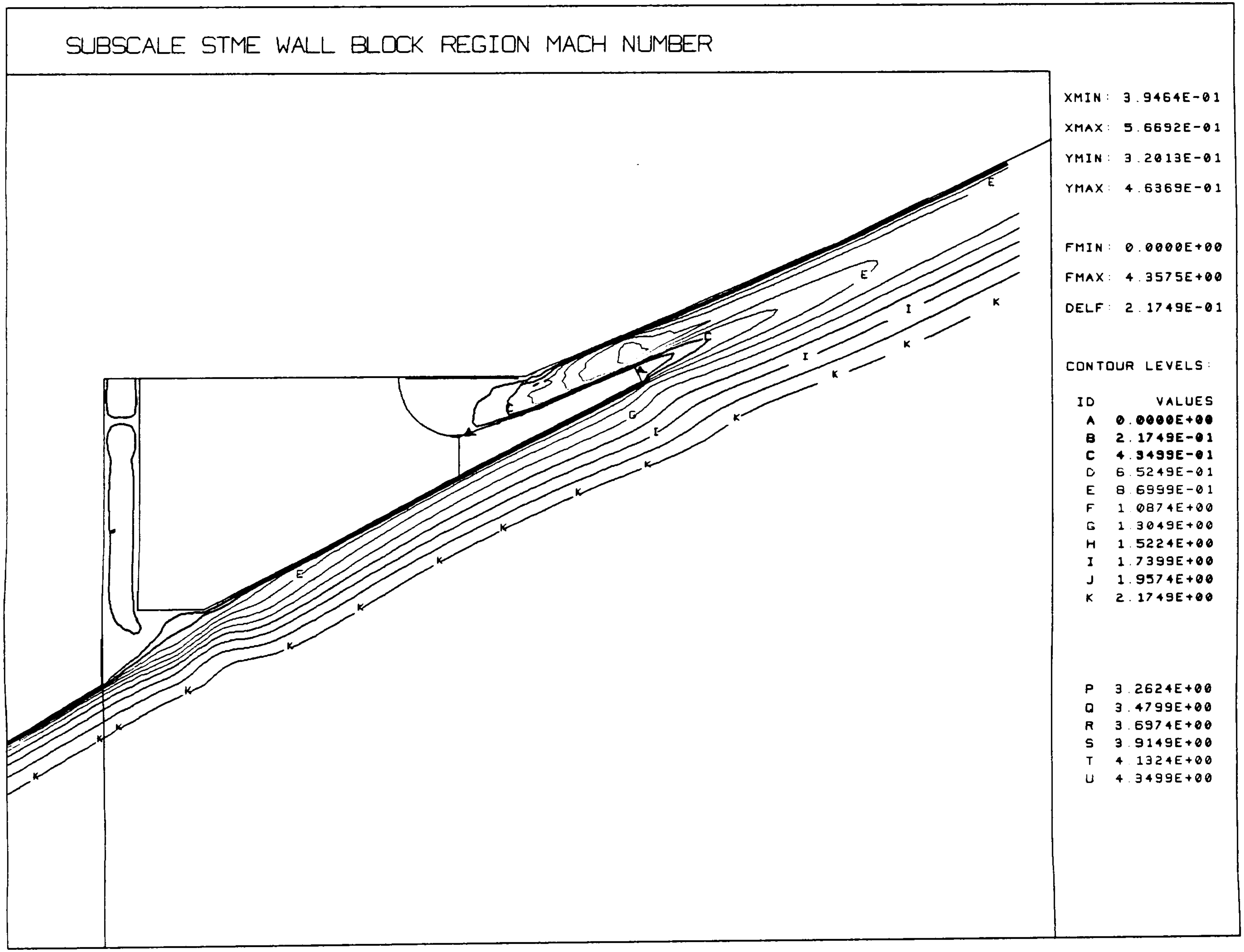
SUBSCALE STME WALL BLOCK REGION MACH NUMBER
XMIN: 3.9464E-01
XMAX: 5.6692E-01
YMIN: 3.2013E-01
YMAX: 4.6369E-01
FMIN: 0.0000E+00
FMAX: 4.3575E+00
DELF: 2.1749E-01
CONTOUR LEVELS:
ID VALUES
A 0.0000E+00
B 2.1749E-01
C 4.3499E-01
D 6.5249E-01
E 8.6999E-01
F 1.0874E+00
G 1.3049E+00
H 1.5224E+00
I 1.7399E+00
J 1.9574E+00
K 2.1749E+00
P 3.2624E+00
Q 3.4799E+00
R 3.6974E+00
S 3.9149E+00
T 4.1324E+00
U 4.3499E+00

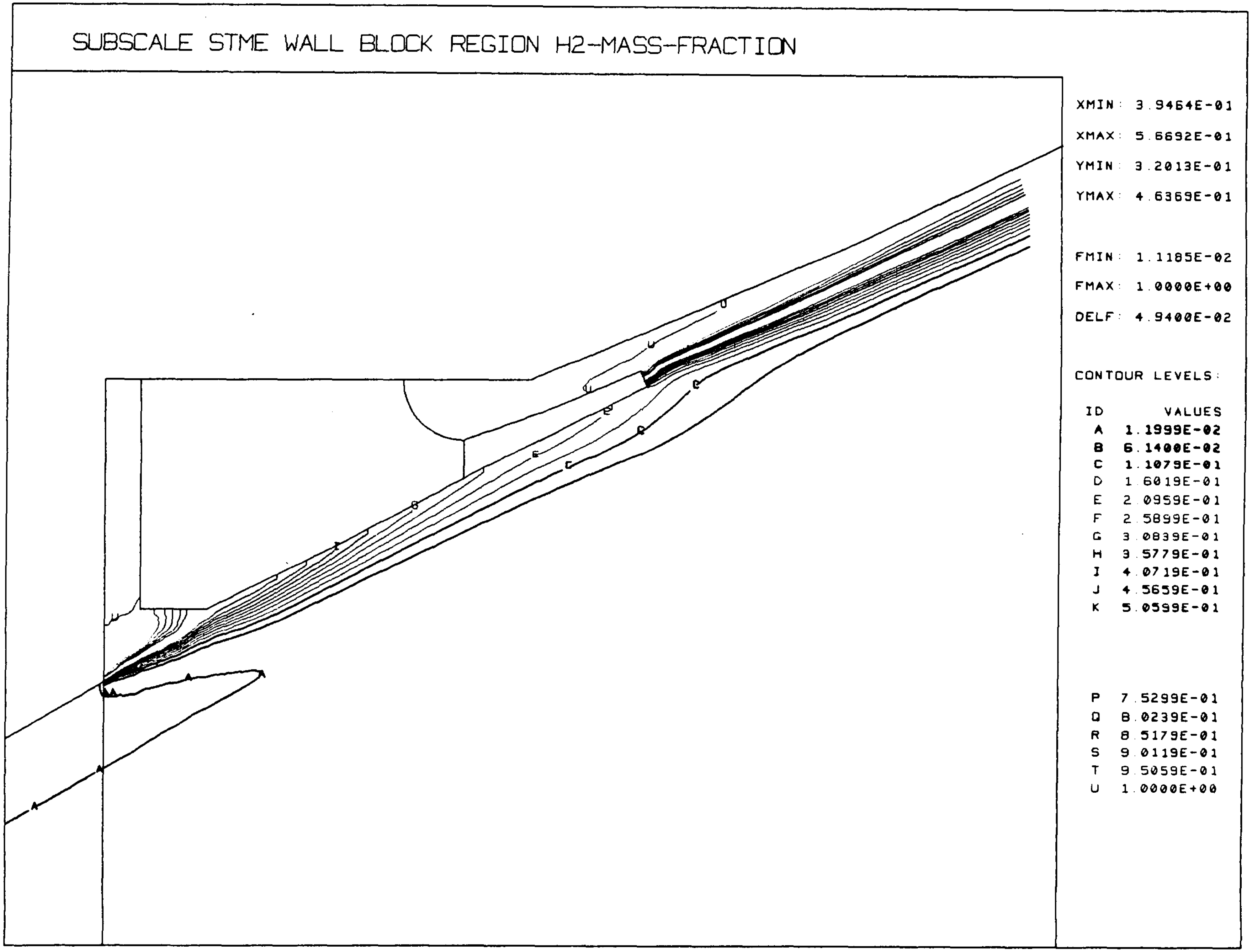

SUBSCALE STME WALL BLOCK REGION H2-MASS-FRACTION
XMIN: 3.9464E-01
XMAX: 5.6692E-01
YMIN: 3.2013E-01
YMAX: 4.6369E-01
FMIN: 1.1185E-02
FMAX: 1.0000E+00
DELF: 4.9400E-02
CONTOUR LEVELS:
ID VALUES
A 1.1999E-02
B 6.1400E-02
C 1.1079E-01
D 1.6019E-01
E 2.0959E-01
F 2.5899E-01
G 3.0839E-01
H 3.5779E-01
I 4.0719E-01
J 4.5659E-01
K 5.0599E-01
P 7.5299E-01
Q 8.0239E-01
R 8.5179E-01
S 9.0119E-01
T 9.5059E-01
U 1.0000E+00

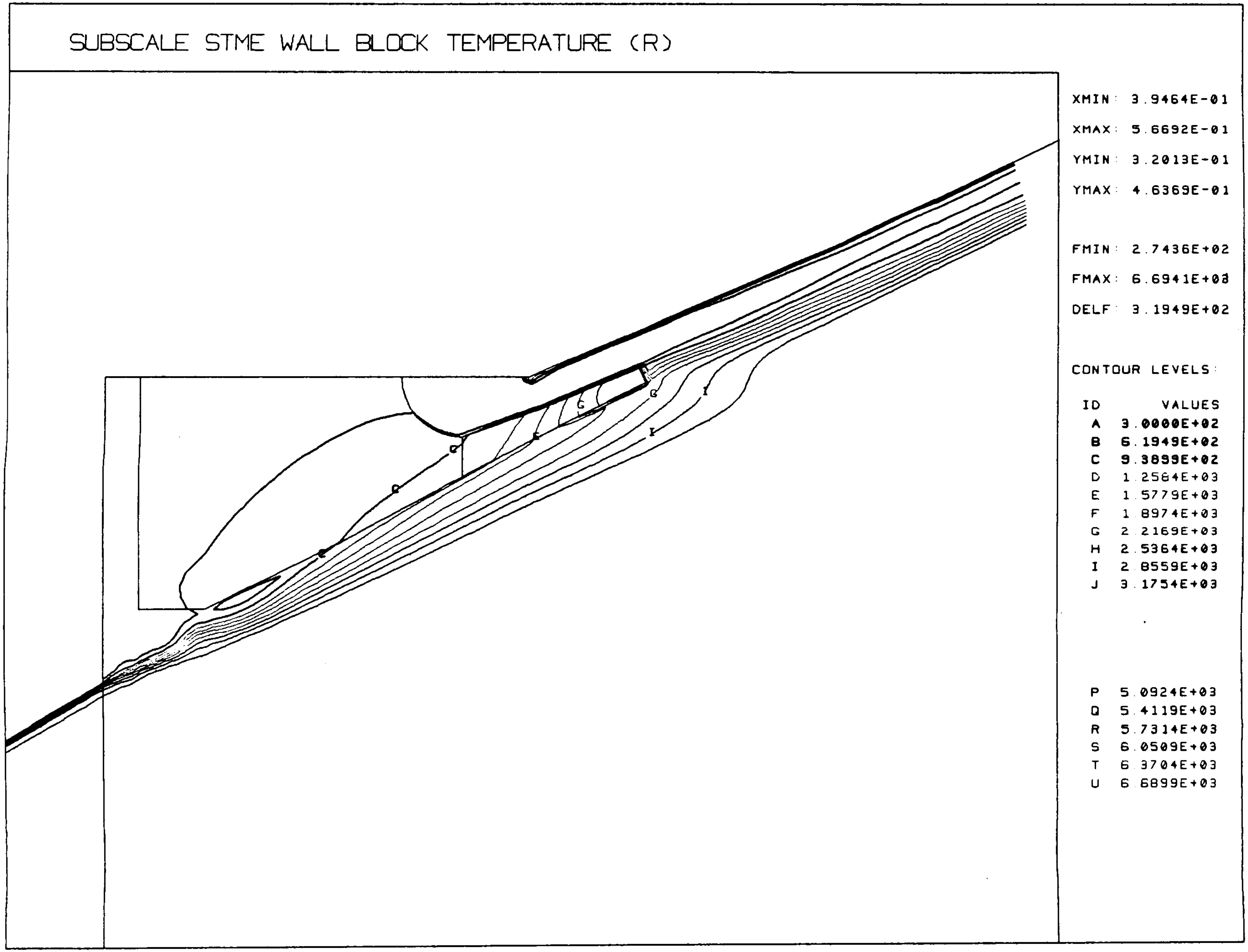
SUBSCALE STME WALL BLOCK TEMPERATURE (R)
XMIN: 3.9464E-01
XMAX: 5.6692E-01
YMIN: 3.2013E-01
YMAX: 4.6369E-01
FMIN: 2.7436E+02
FMAX: 6.6941E+03
DELF: 3.1949E+02
CONTOUR LEVELS:
ID VALUES
A 3.0000E+02
B 6.1949E+02
C 9.3899E+02
D 1.2564E+03
E 1.5779E+03
F 1.8974E+03
G 2.2169E+03
H 2.5364E+03
I 2.8559E+03
J 3.1754E+03
P 5.0924E+03
Q 5.4119E+03
R 5.7314E+03
S 6.0509E+03
T 6.3704E+03
U 6.6899E+03
G
I

N92-32254

APPLICATION OF COMPUTATIONAL FLUID DYNAMICS TO THE DESIGN OF THE FILM COOLED STME SUBSCALE NOZZLE FOR THE NATIONAL LAUNCH SYSTEM.

By

Joseph L. Garrett
Government Engine and Space Propulsion
Pratt and Whitney
West Palm Beach, Florida

ABSTRACT

A status of CFD calculations for the STME film/dump cooled nozzle design will be presented, with an emphasis on the timely impact of CFD in the design of the sub-scale nozzle coolant system. The following aspects of the sub-scale coolant delivery system were analyzed with CFD:

1. Design trade study of a mechanical flow splitting device for uniform distribution of the subsonic cavity flow.
2. Design trade study of the subsonic cavity lip to achieve coolant film integrity.
3. Analysis of the primary flow interaction with the core/secondary coolant streams.

All design calculations were performed with the Generalized Aerodynamic Simulation Program (GASP), a 3-D, multi-block, generalized Navier-Stokes code capable of solving with frozen, finite-rate or equilibrium chemical kinetics.

The initial design of the subsonic cavity flow used square posts to distribute the sonic orifice jets into a uniform flow. Calculations for this design indicated that an unacceptable mal-distribution of film occurred. Design modifications involving curved and slotted posts were computed in an effort to uniformly distribute the secondary coolant flow. Analysis of these configurations showed that although the flowfield improved in uniformity, it was still unacceptable, especially at higher feed pressures. Results from these studies were then incorporated into a design that resulted in the insertion of a porous metal ring into the subsonic cavity. Subsequent water flow model studies showed that this concept was successful in uniformly distributing flow exiting the cavity.

In addition to the design of the subsonic cavity, CFD was also used to analyze the secondary coolant lip and the primary flow interaction with the core/secondary coolant streams. A series of calculations were first performed to modify the subsonic cavity lip contour. The flow over the modified lip was then computed simultaneously with the primary injectors to determine the impact of the subsonic coolant stream on the primary slot jets.

Pressure, temperature, velocity and coolant mass fraction contours will be presented for these configurations.

APPLICATION OF CFD TO THE DESIGN OF THE FILM COOLED STME SUBSCALE NOZZLE

Joseph L. Garrett
Pratt & Whitney, GESP
West Palm Beach, Florida

Presented At 10^{th} Annual Workshop For
CFD Applications In Rocket Propulsion –NASA MSFC
April 29, 1992

ACKNOWLEDGEMENTS

- NASA MSFC Consortium For CFD In Combustion Driven Flows.
- National Aerodynamic Simulation Facility For CRAY YMP Computing Resources.
- CRAY Research For CRAY YMP Computing Resources.

OUTLINE

- Analysis Of Secondary Coolant Cavity
- Support Of Secondary Subsonic Lip Design
- Analysis Of Core/Secondary/Primary Flow Interactions
- Summary

CFD CODE USED

General Aerodynamic Simulation Program

- 3–D, 2–D or Axisymetric
- Parabolized & Full Navier–Stokes
- Explicit & Implicit Time Integration
- Finite–Rate, Frozen & Equilibrium Chemistry
- Algebraic & 2–Equation Turbulence Models
- Memory Management Techniques

STPT

ANALYSIS OF SECONDARY COOLANT CAVITY

Geometry Orientation

Subscale Thrust Chamber Assembly

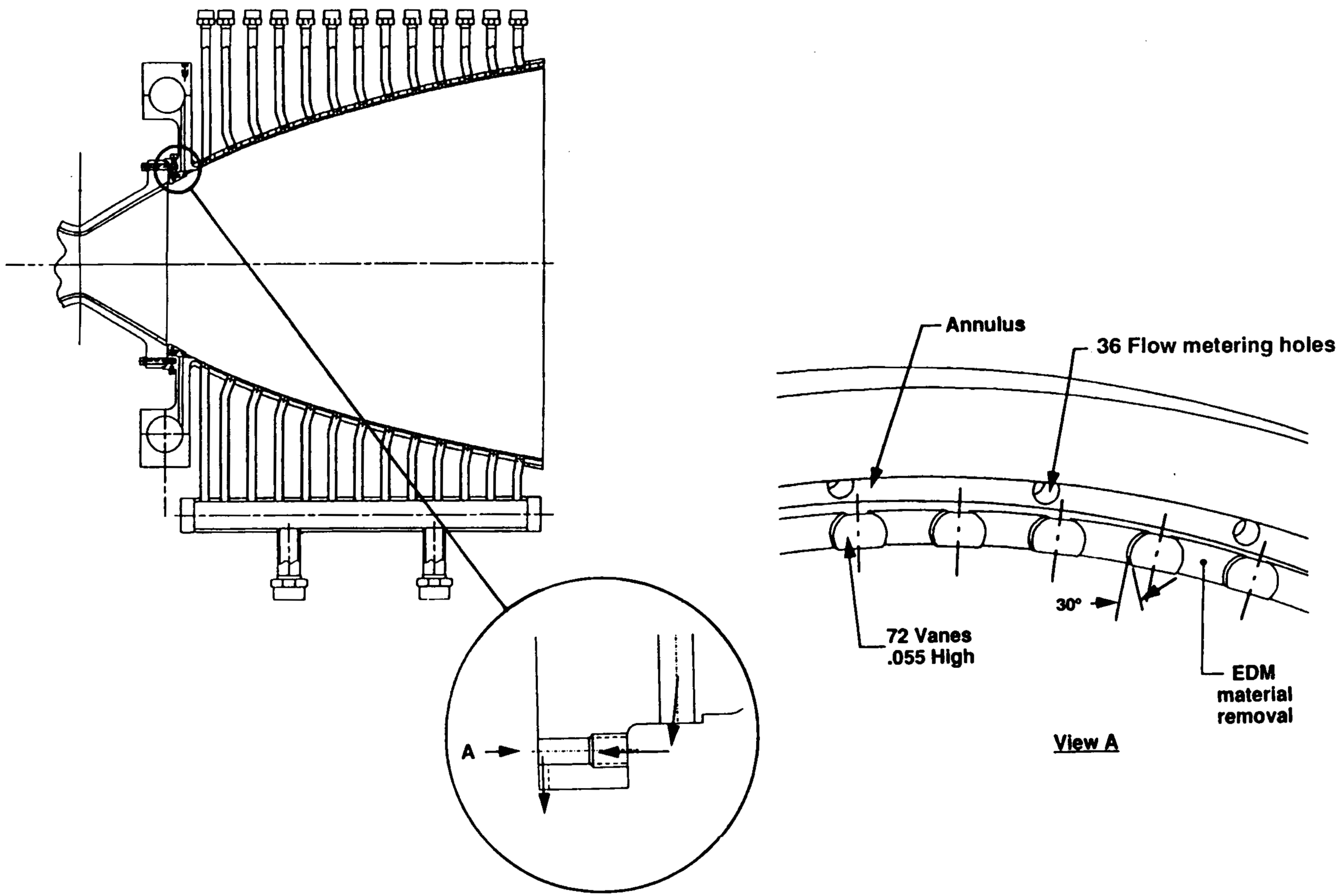

ANALYSIS OF SECONDARY COOLANT CAVITY

Curve Post Design, Low P

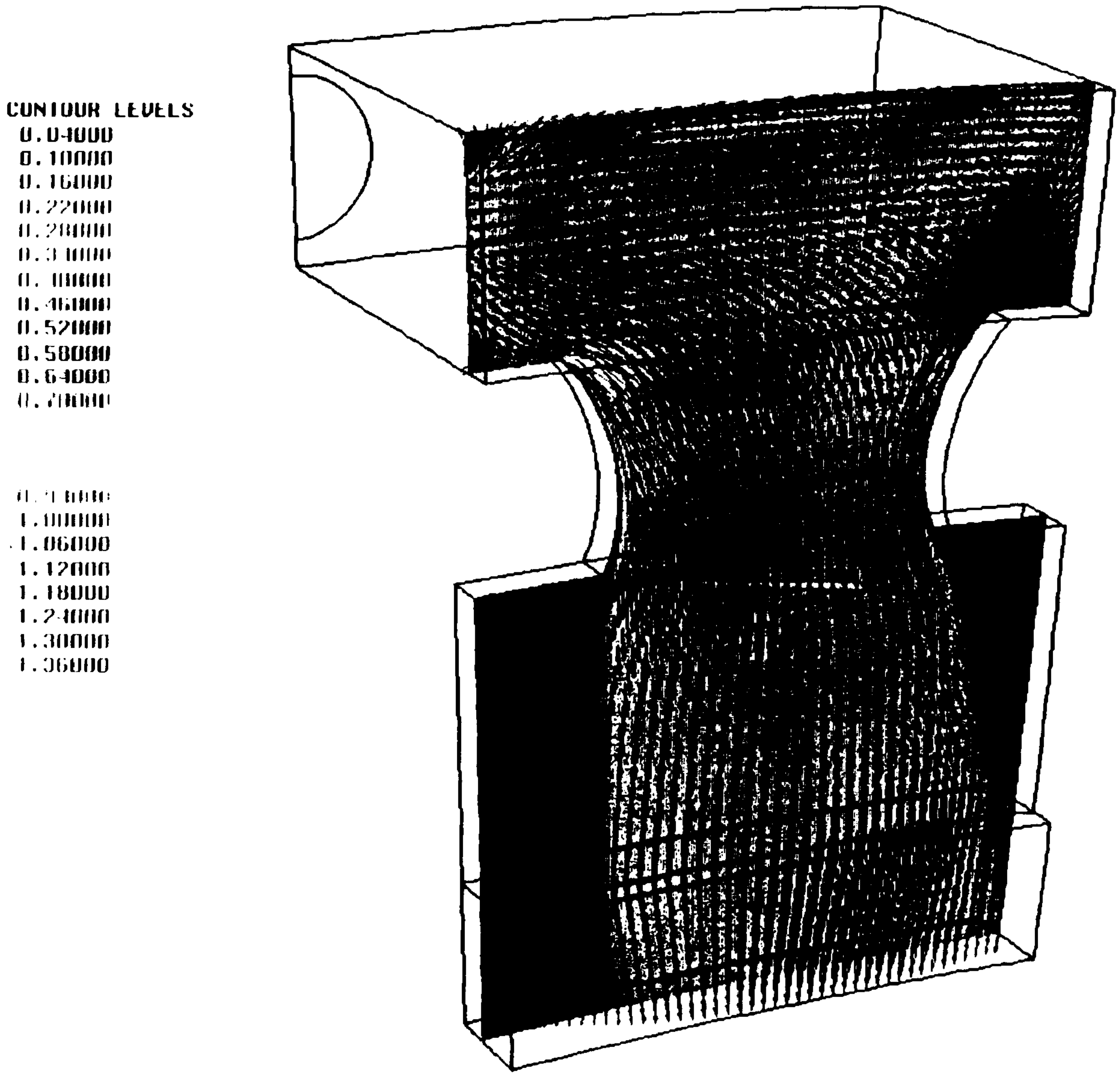

ANALYSIS OF SECONDARY COOLANT CAVITY

Slotted Post Design, Low P

CONTOUR LEVELS
0.04000
0.10000
0.16000
0.22000
0.28000
0.34000
0.40000
0.46000
0.52000
0.58000
0.64000
0.70000

[illegible]
1.00000
1.06000
1.12000
1.18000
1.24000
1.30000
1.36000

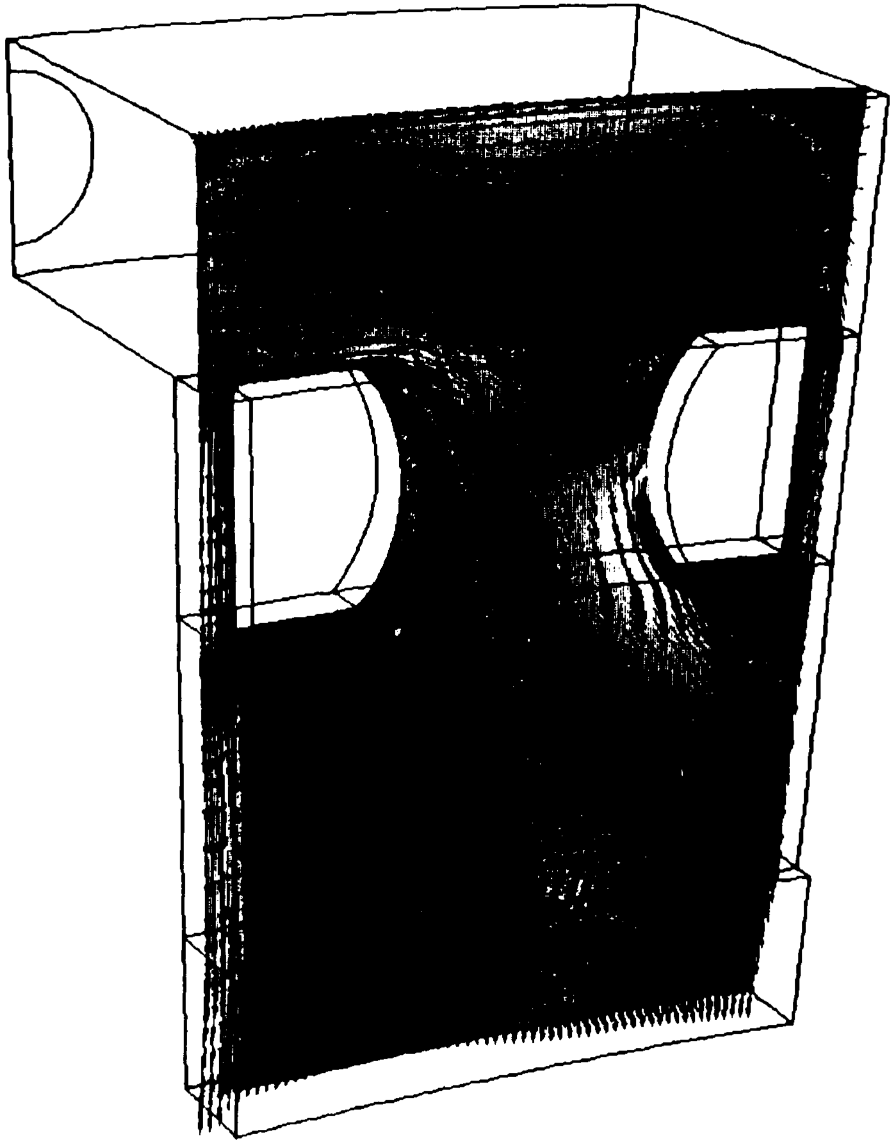

ANALYSIS OF SECONDARY COOLANT CAVITY

Comparison of Exit Solutions

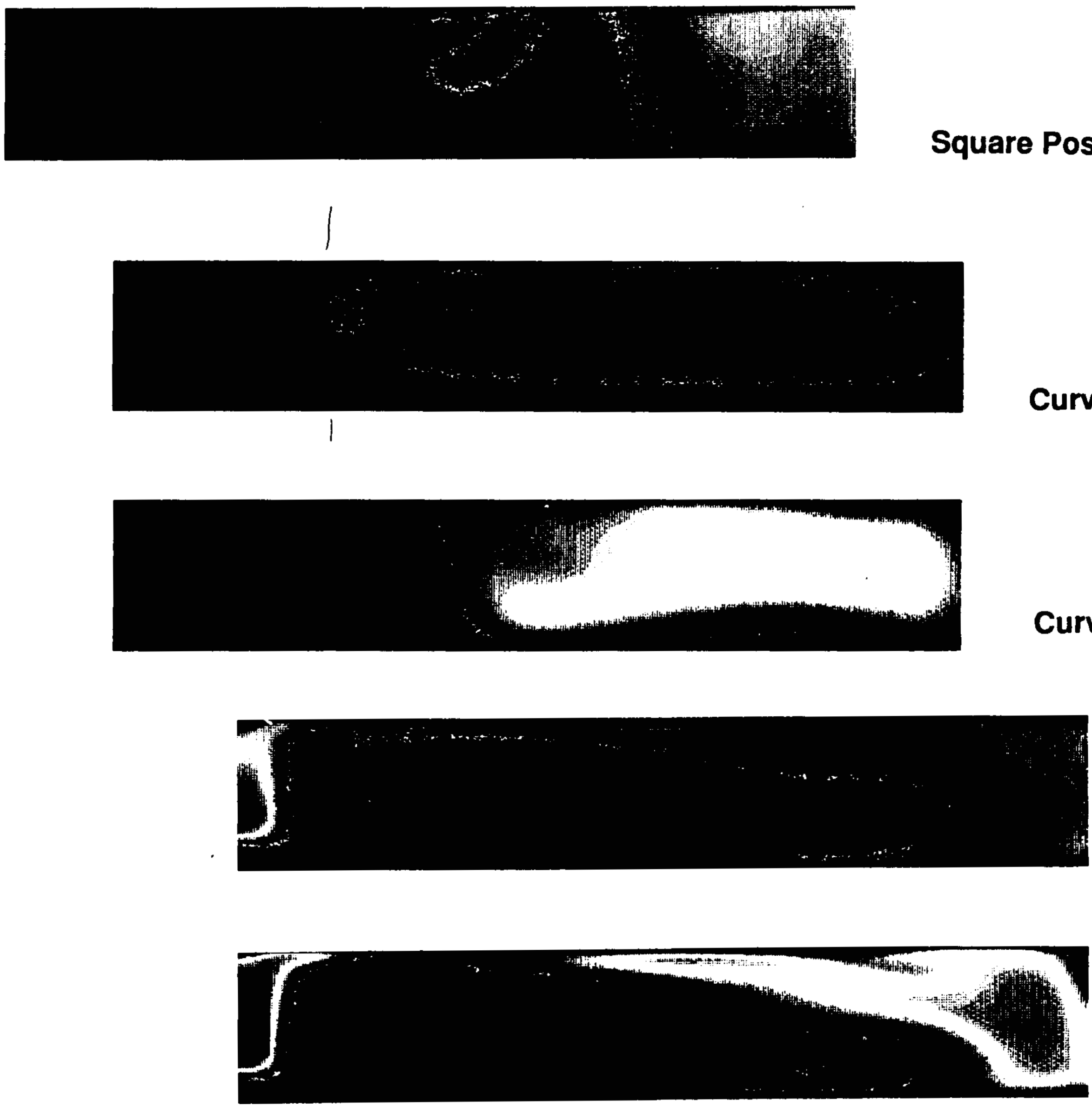

CONTOUR LEVELS
0.04000
0.10000
0.16000
0.22000
0.28000
0.34000
0.40000
0.46000
0.52000
0.58000
[illegible]

0.82000
0.88000
0.94000
1.00000
1.06000
1.12000
1.18000

C-3

ANALYSIS OF SECONDARY COOLANT CAVITY

Design Solution: Porous Stainless Steel Filter

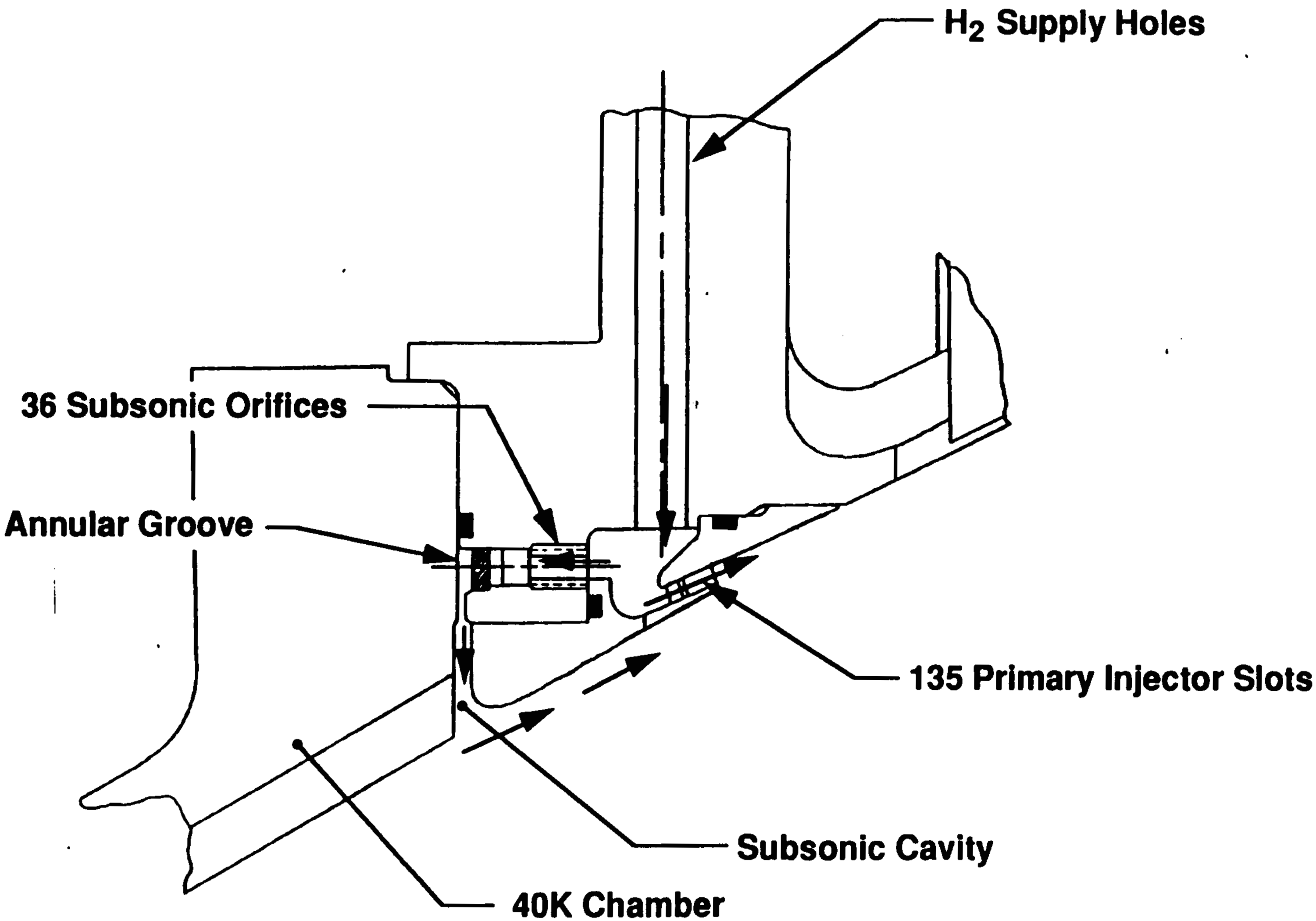

SUBSCALE CORE/FILM COOLANT INTERACTION

Previous Assumptions

- o Algebraic Turbulence Model
- o Equilibrium Chemistry in the Chamber
- o Frozen Chemistry in the Interaction Region
- o Chamber $P_O = 2250$ psi, $T_O = 6500\,^{\circ}R$
- o Injector $P_O = 70$ psi, $T_O = 530\,^{\circ}R$
- o Chamber Walls Fixed at $T = 1440\,^{\circ}R$
- o Injector Walls are Adiabatic

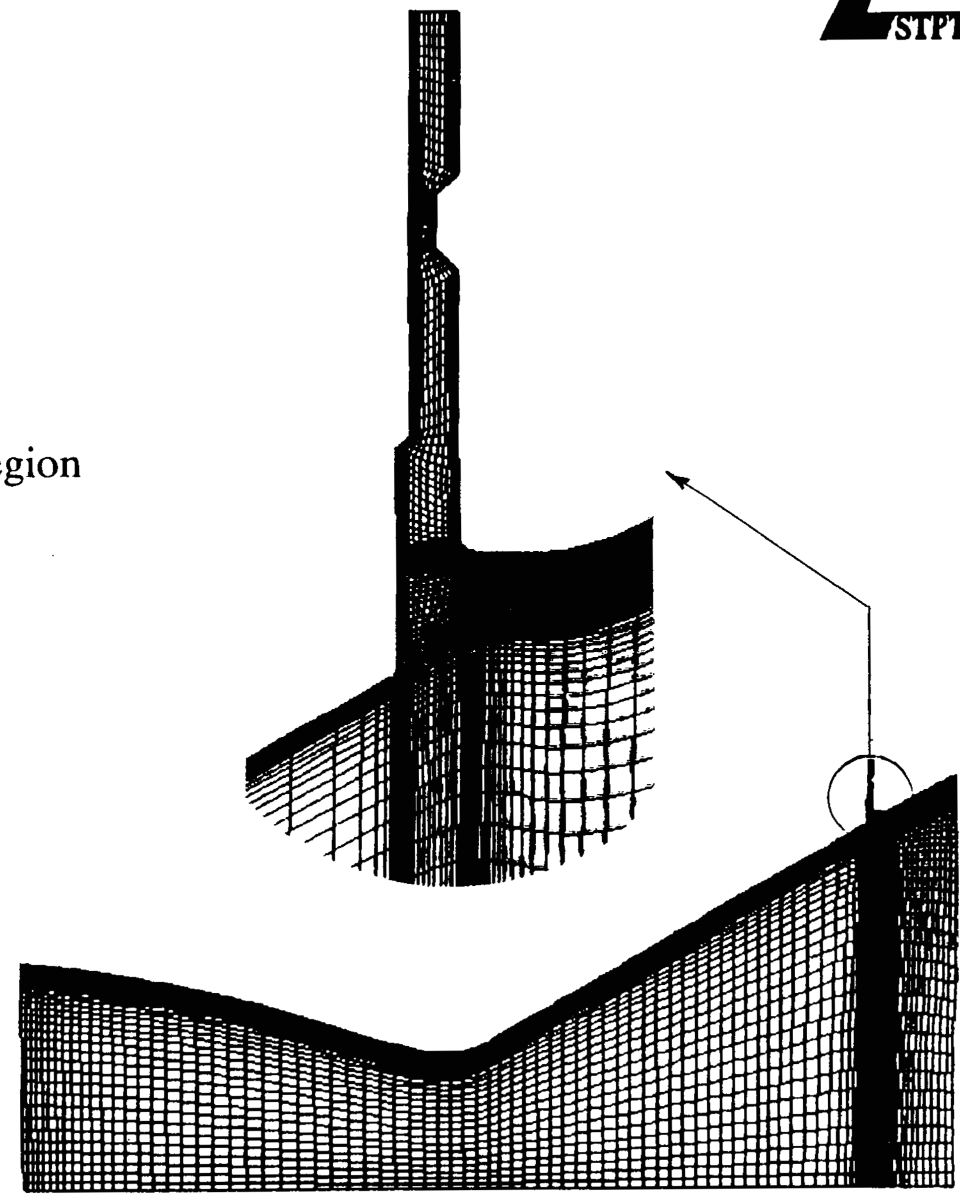

CORE/SECONDARY COOLANT FLOW INTERACTION

H_2 Mass Fraction Contours Indicate Vortex and Diffusion Mixing

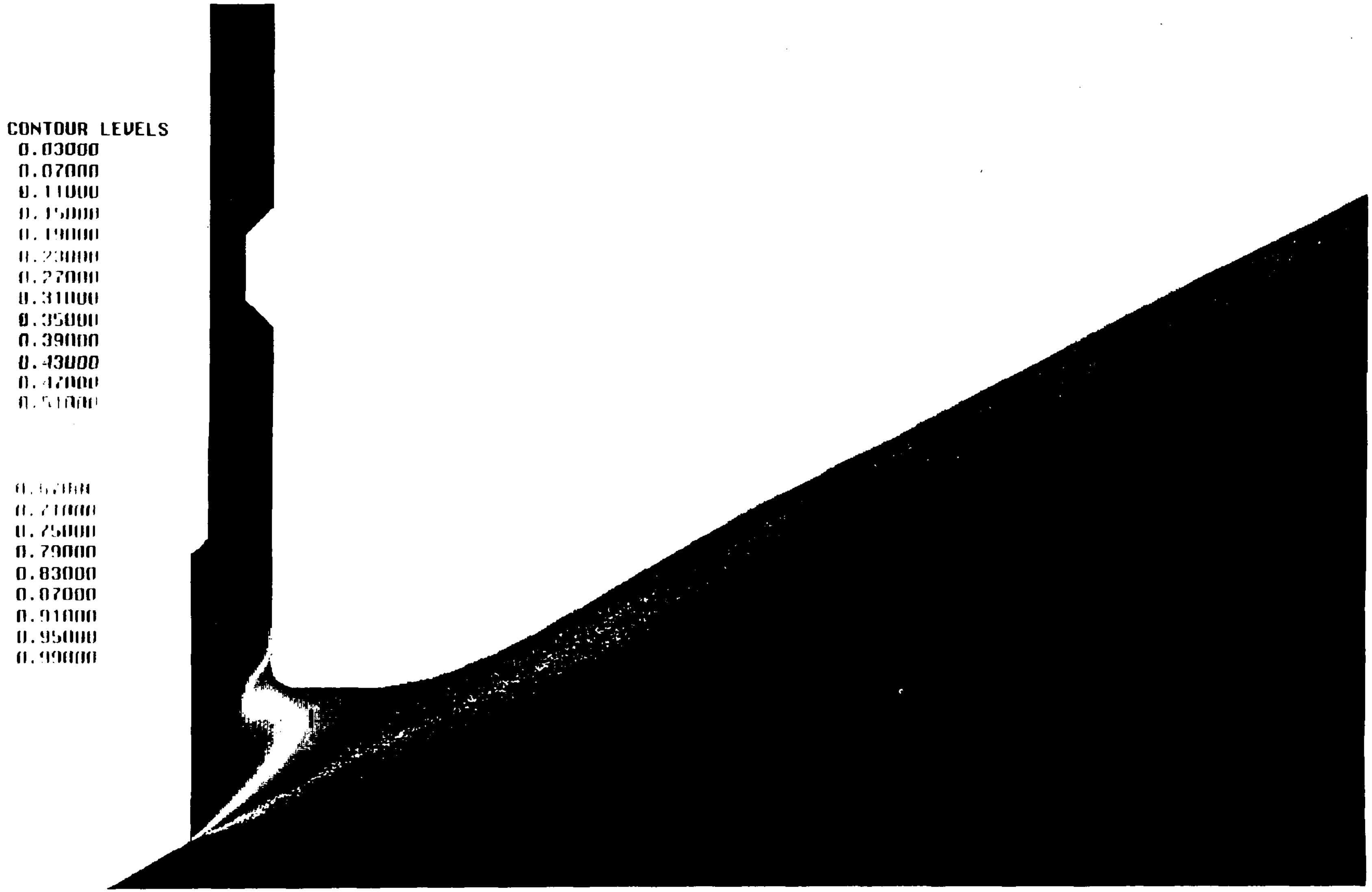

CORE/SECONDARY COOLANT FLOW INTERACTION

Velocity Vectors / H_2 Mass Fraction Contours Show Vortex Mixing

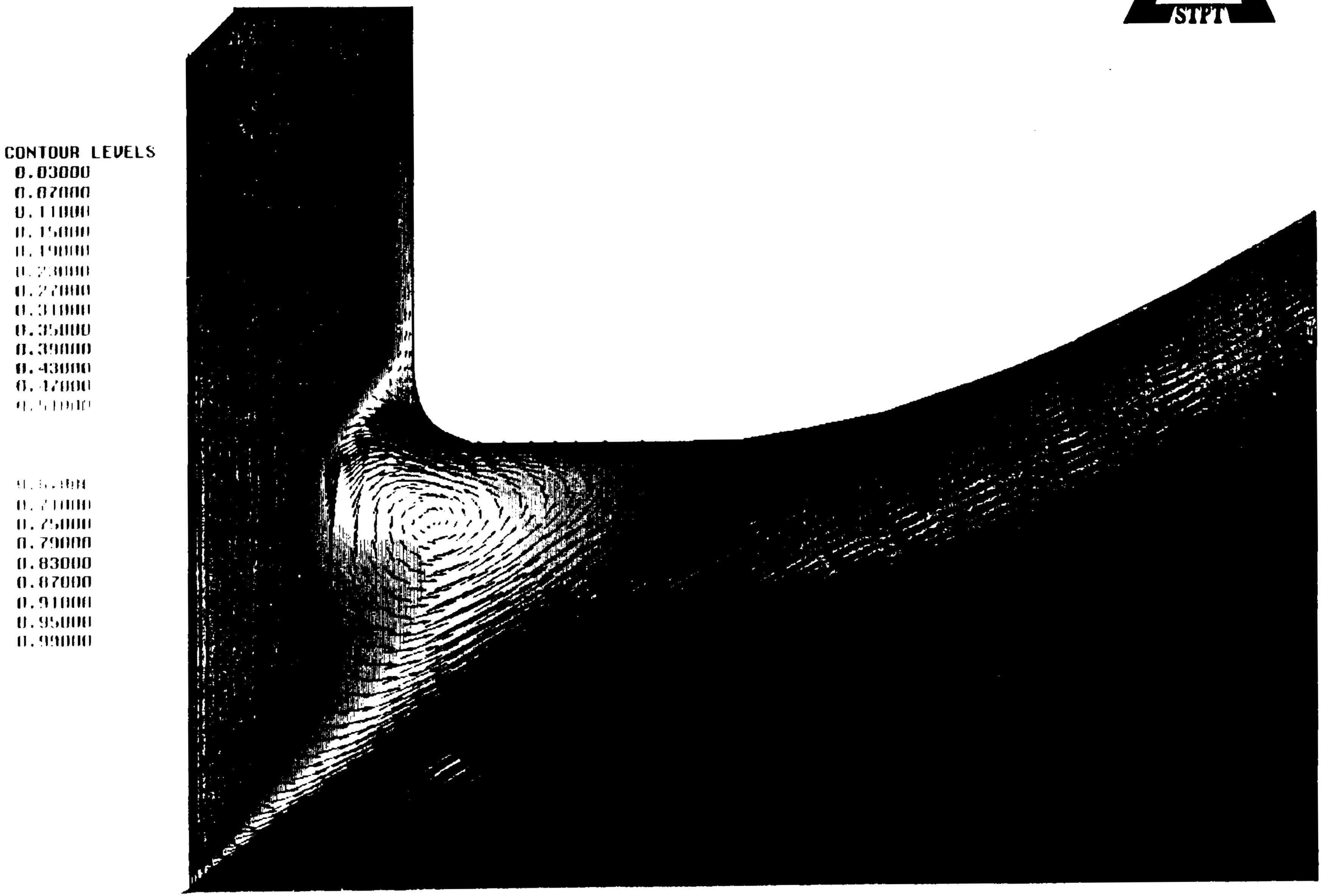

COMPARISON OF OLD & NEW SECONDARY SLOT

Pertinent Geometry And Inflow Conditions

Parameter	Old Slot	New Slot
R_{lip}	0.005"	0.070"
$\dot{m}$	0.210 lbm/sec	0.352 lbm/sec
P_o	70 psi	94.26 psi
T_o	530 R	535.5 R
M	0.20	0.05
P	68.06 psi	94.1 psi
T	525.8 R	535.25 R
ϱ	7.536×10^{-4} slug/ft^3	1.023×10^{-3} slug/ft^3
γ	1.4	1.386

COMPARISON OF OLD & NEW SUBSONIC SLOT

New Conditions Result In Substantial Improvement in Film Effectiveness

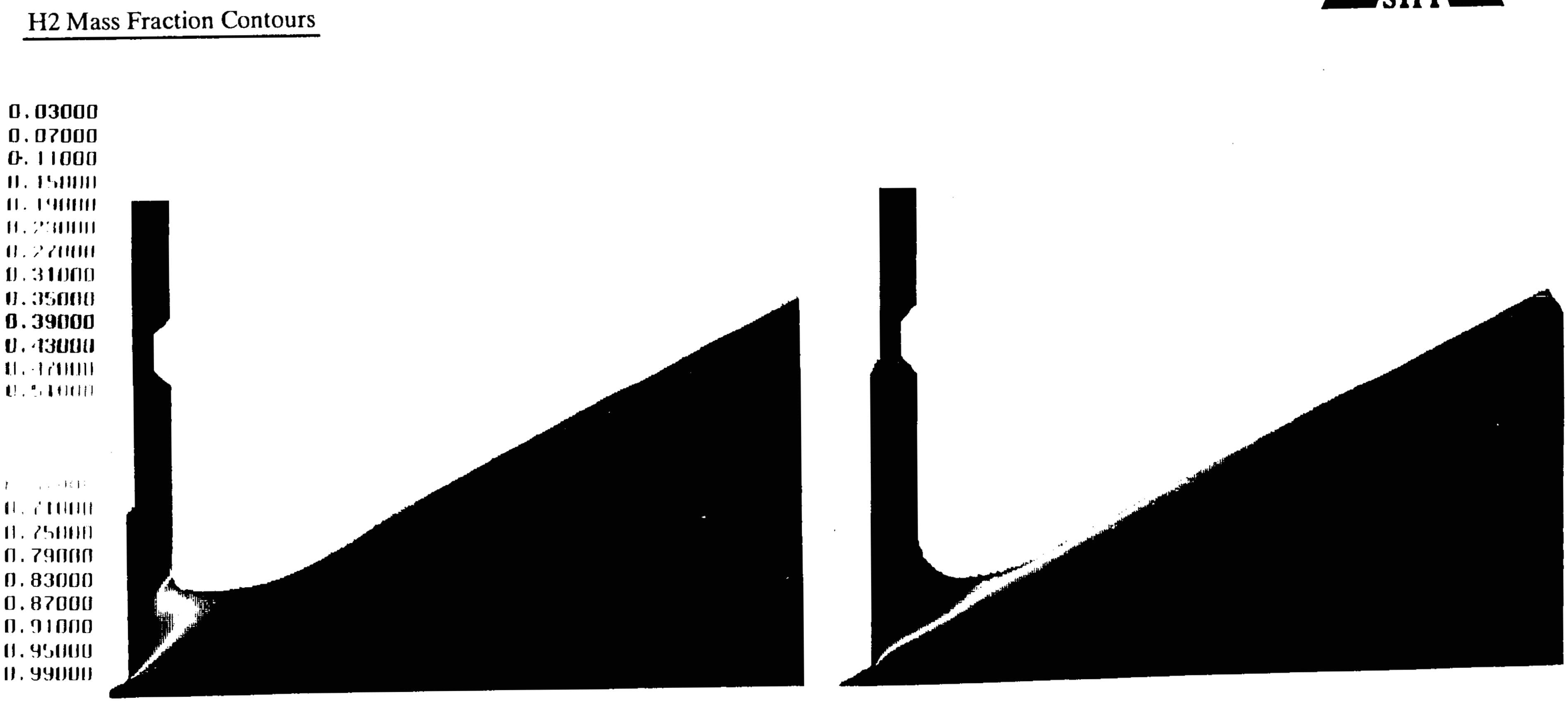

Note: Increasing Lip Radius and Flow Rate Result in Diminishing the Impact of Vortex Mixing

COMPARISON OF OLD & NEW SUBSONIC SLOT

New Conditions Indicate Dramatic Improvement In Film Cooling

Temperature Contours (R)

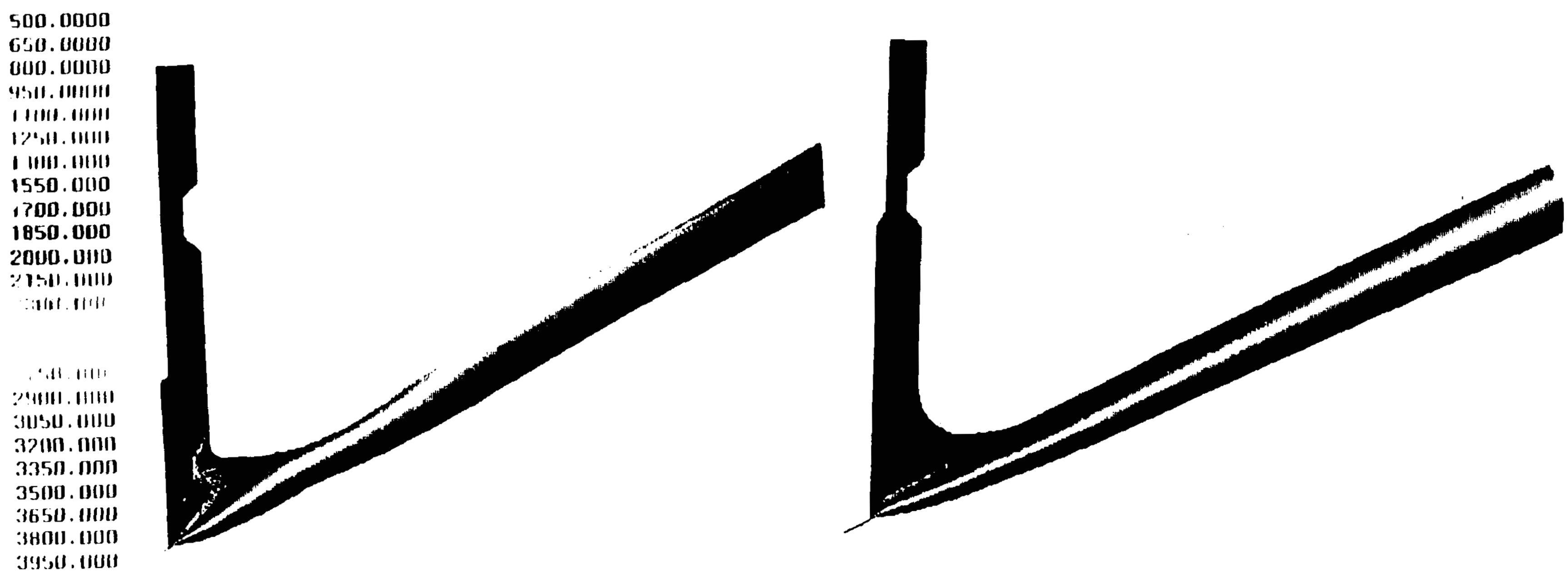

Note: Backside Cooling Over The Last 1/3 of Injector Ring Would Further Reduce Temperature Load

COMPARISON OF OLD & NEW SUBSONIC SLOT

Penalty For High Mass Flow Rate Is Increased Shock Strength

STPT

Pressure Contours (psi)

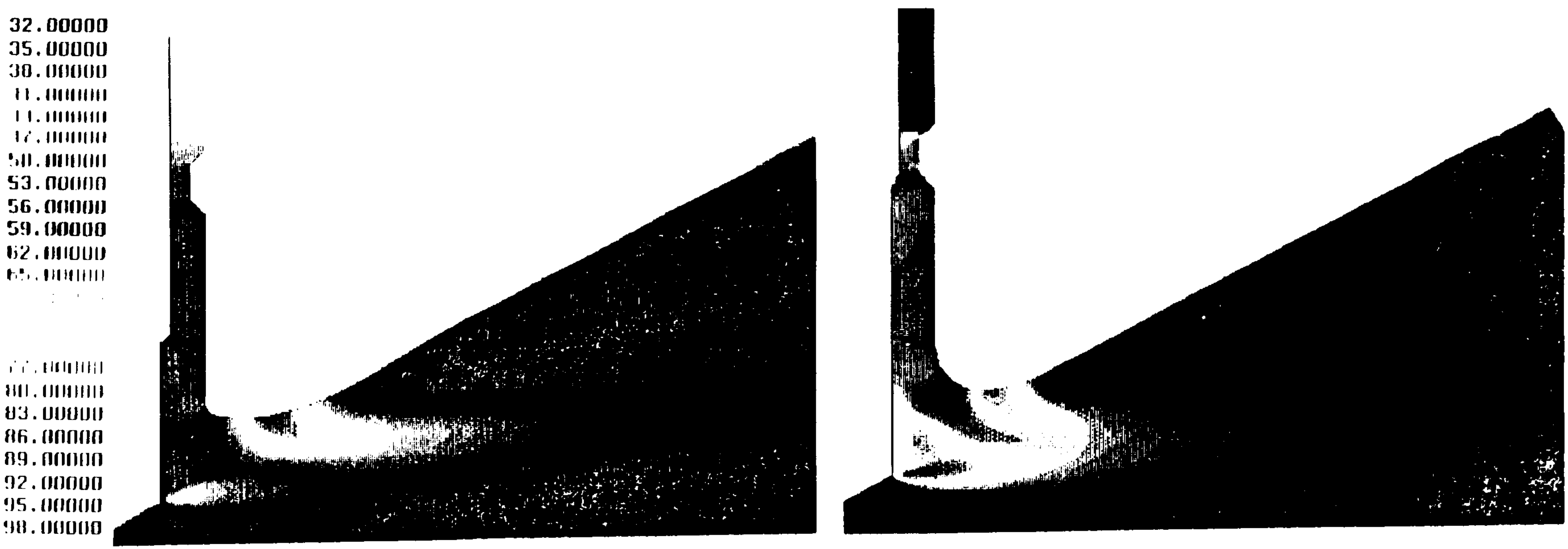

Note: Increased Flow Rate has Small Impact on Pressure Sensed by the Primary Lip

SUBSCALE CORE/FILM COOLANT INTERACTION

Imposed Boundary Values For High $\dot{m}$ Case

Property	Core Inflow	Subsonic Inflow	Primary Inflow
P_o	2250 psi	94.26 psi	———
T_o	6780 R	535.5 R	———
M	0.2233	0.05	1.456
P	2187.38 psi	94.1 psi	55.5 psi
T	6735.0 R	535.25 R	372.1 R
ϱ	1.448×10^{-2} slug/ft^3	1.023×10^{-3} slug/ft^3	8.677×10^{-4} slug/ft^3
γ	1.134	1.386	1.386
$\dot{m}$	84.21 lbm/sec	0.352 lbm/sec	1.773 lbm/sec

MESH SIZE: 75x61, 25x69, 59x81, 36x118, 36x118; 19,575 Grid Points

SUBSCALE CORE/FILM COOLANT INTERACTION

New Conditions Produce Less Mixing Of Secondary Film

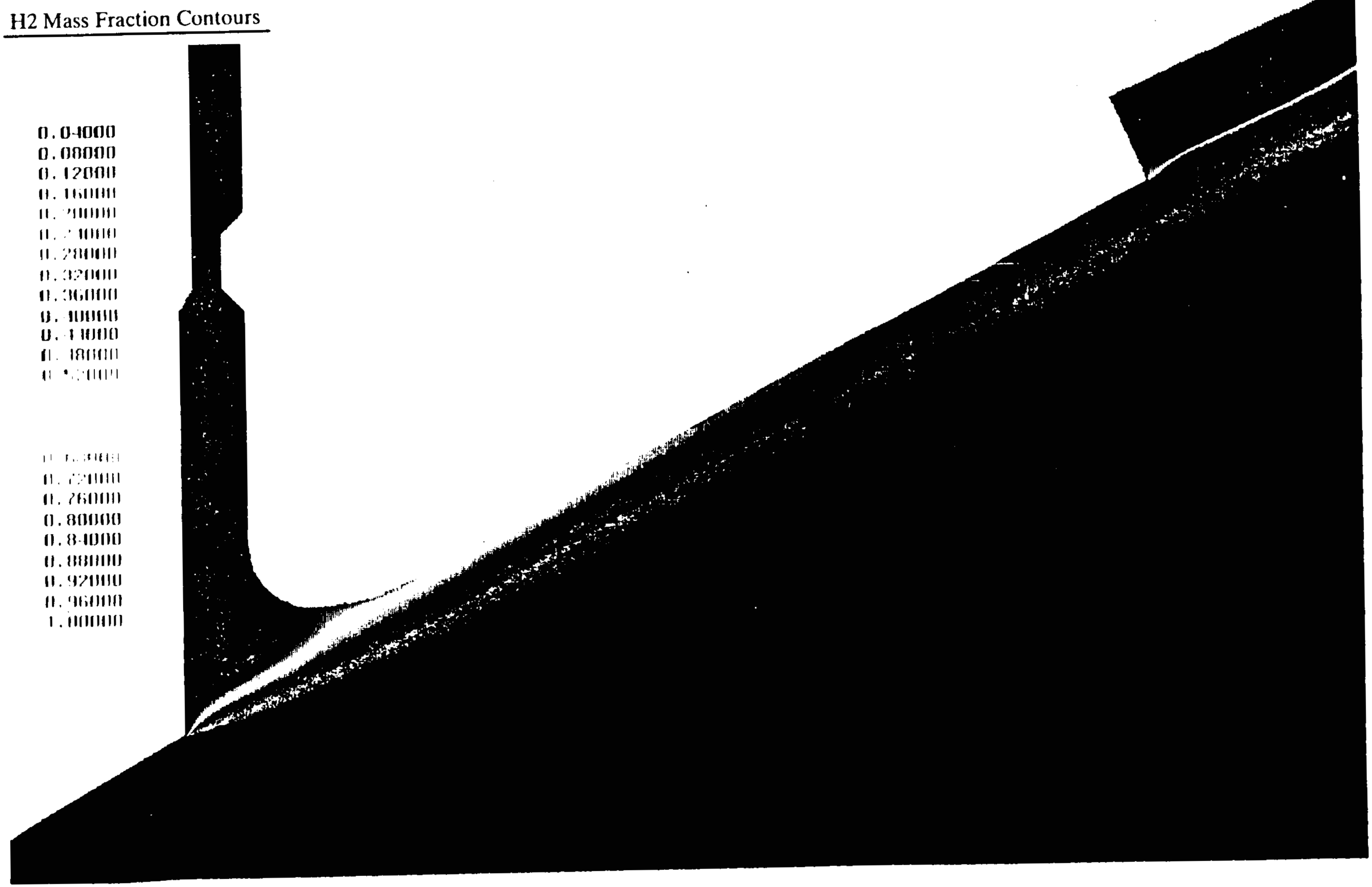

SUBSCALE CORE/FILM COOLANT INTERACTION

Secondary Film Layer Provides Adequate Cooling for Injector Ring

Temperature Contours (R)

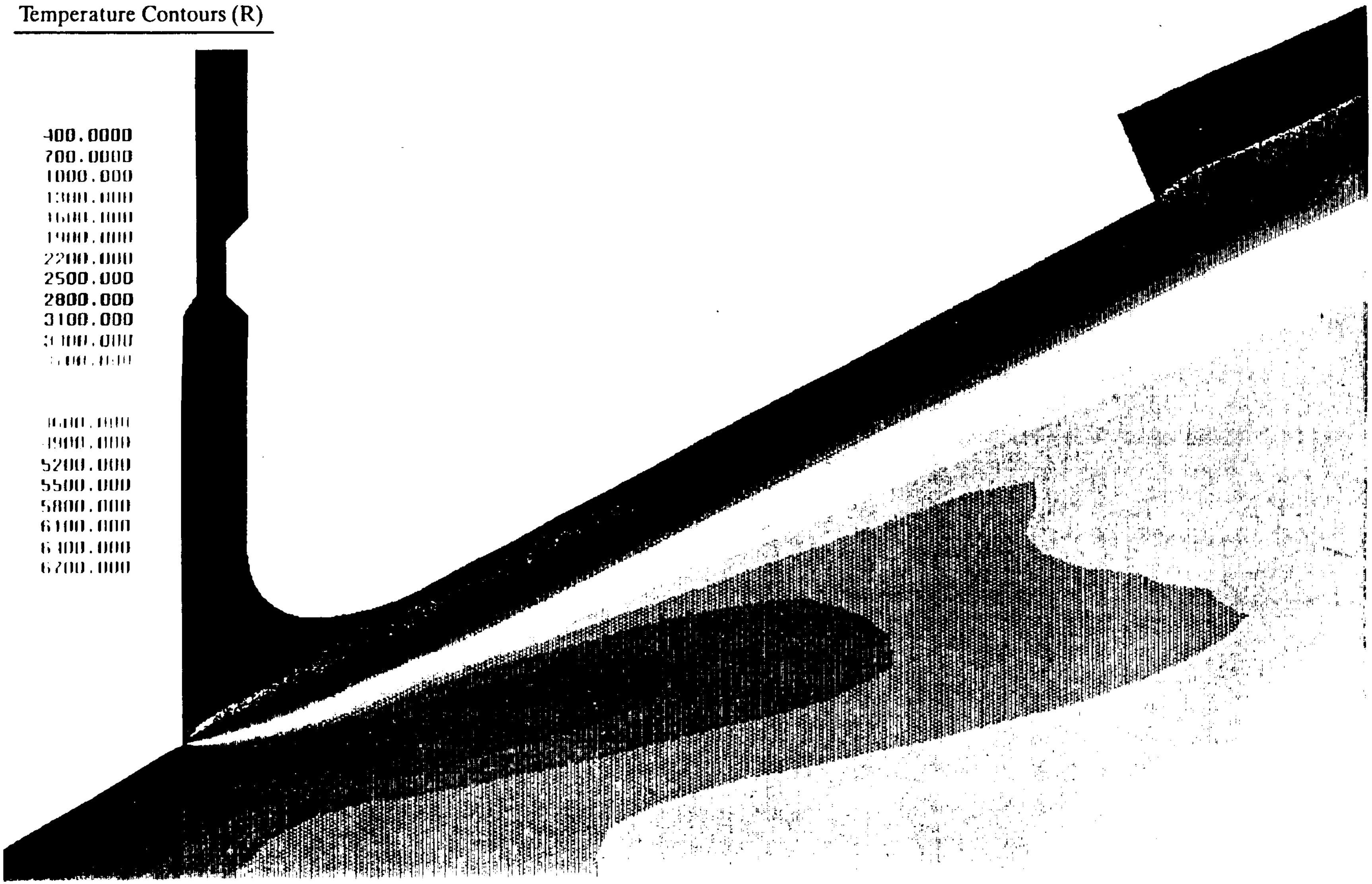

SUBSCALE CORE/FILM COOLANT INTERACTION

Normal & Tangential Injection Produce Complex Shock & Expansion Waves

Pressure Contours (psi)

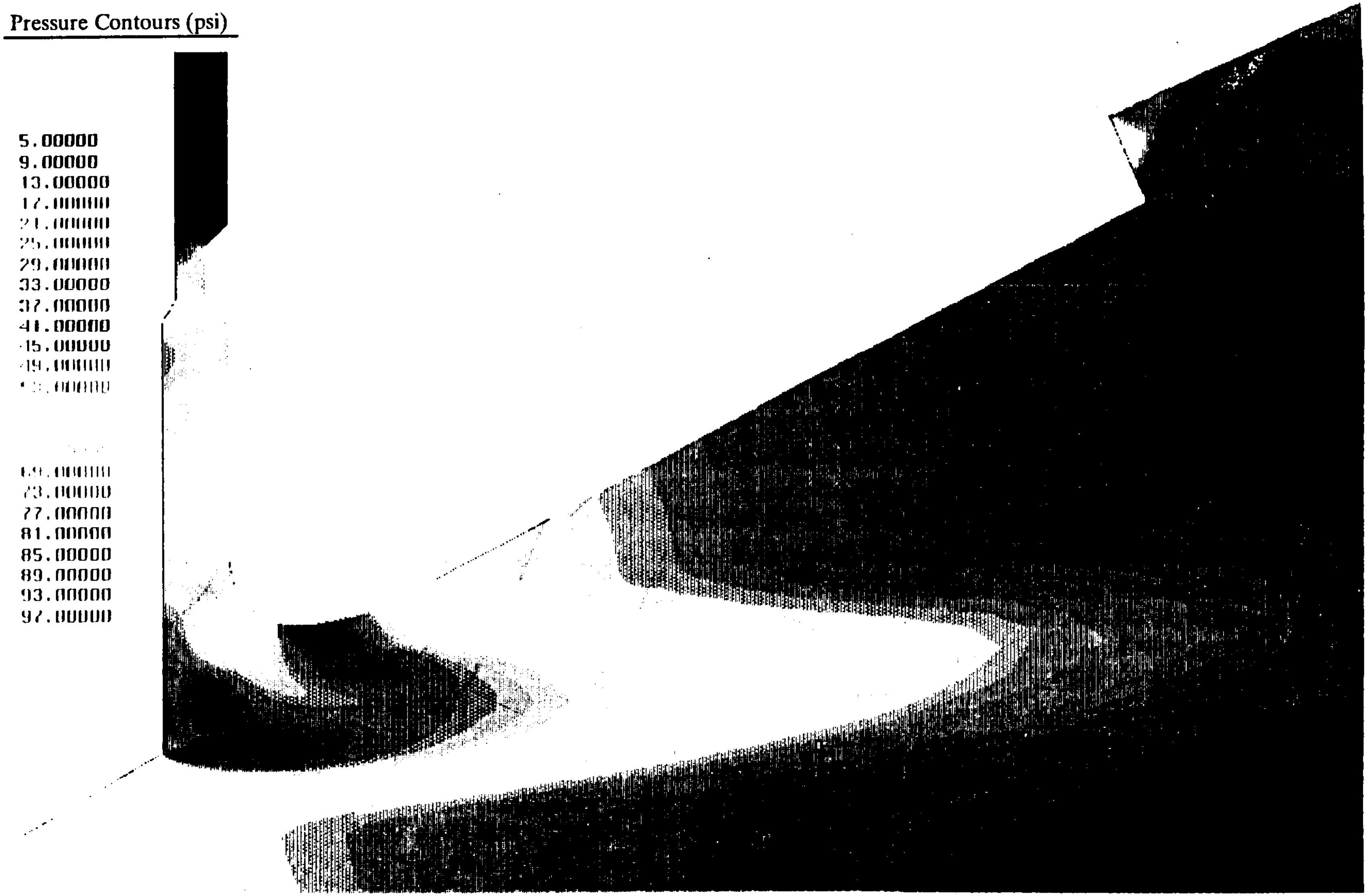

SUBSCALE CORE/FILM COOLANT INTERACTION

Integrity of Primary Jet Maintained

Note: Mixing of Jet with the core Indicates Exhaust Film is Less than 50% H_2

SUBSCALE CORE/FILM COOLANT INTERACTION

Primary Film Layer Provides Adequate Cooling For Nozzle Skirt

Temperature Contours (R)

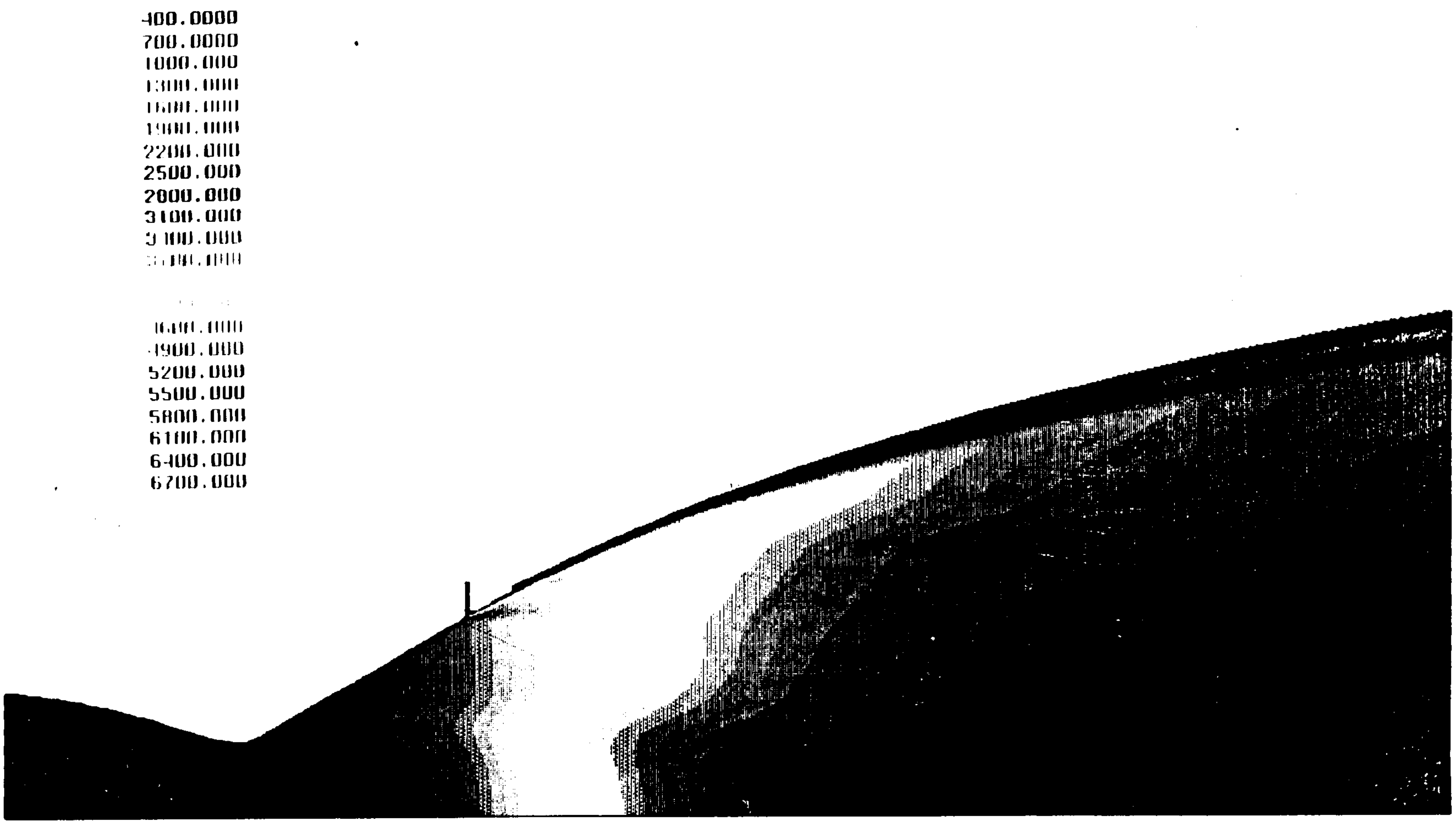

SUBSCALE CORE/FILM COOLANT INTERACTION

Nozzle Geometry & Film Injection Produce Shock Losses

Pressure Contours (psi)

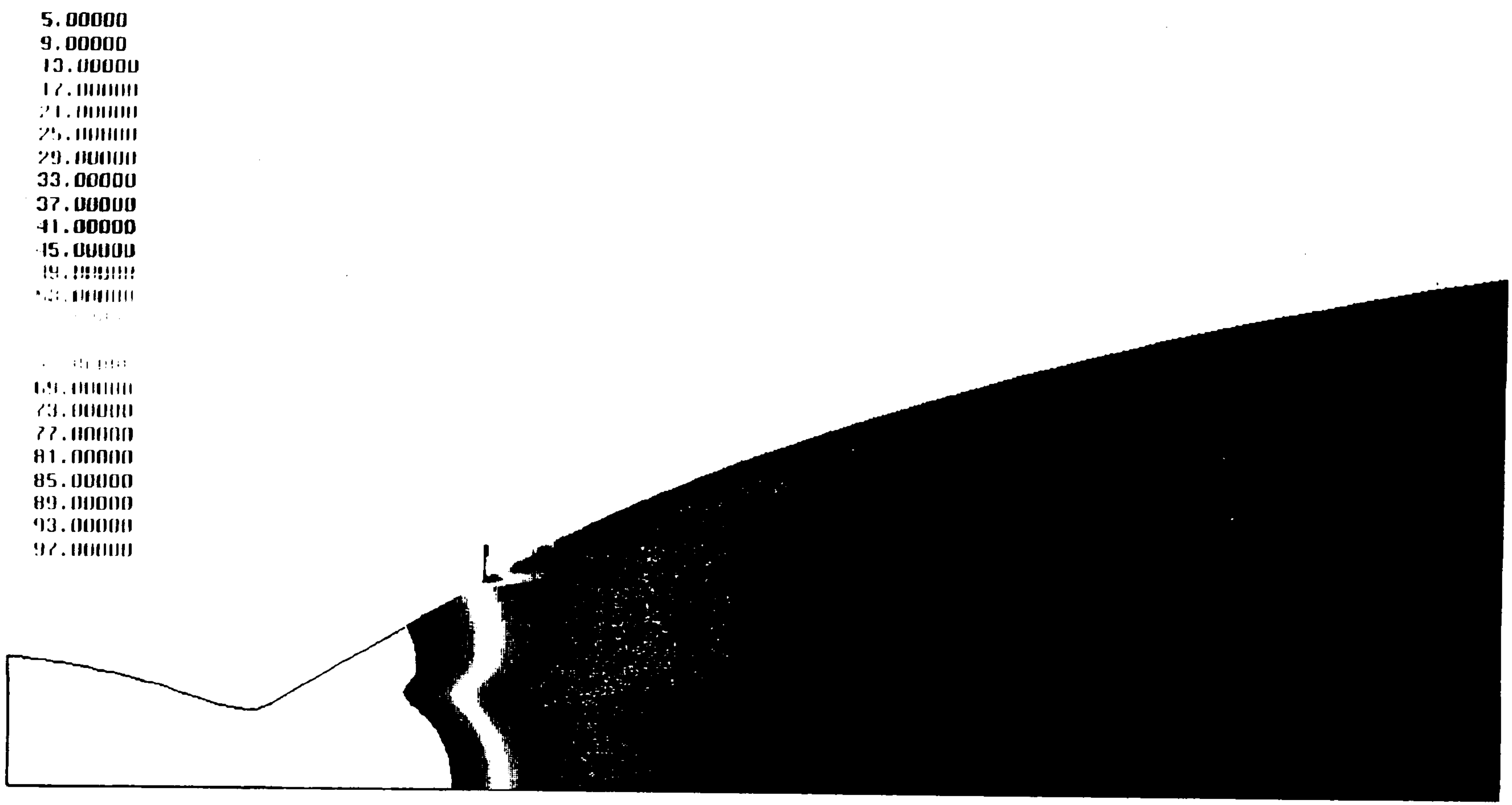

Note: Performance Losses to be Quantified

SUMMARY

- CFD Impacted The Design Of The Secondary Cavity Coolant Distribution System.

- CFD Used To Minimize Temperature Loads On The Injector Ring.

FUTURE WORK

- Validate GASP With Subscale Nozzle Test Data.

- Evaluate / Enhance Fullscale Design (Scaling Methodology).

N92-32255

COMPUTATIONAL FLUID DYNAMICS ANALYSIS OF SPACE SHUTTLE MAIN ENGINE MULTIPLE PLUME FLOWS AT HIGH-ALTITUDE FLIGHT CONDITIONS

by

N. S. Dougherty, J. B. Holt, B. L. Liu and S. L. Johnson
Rockwell International
Space System Division
Huntsville, Alabama 35806

ABSTRACT

for the Consideration of
WORKSHOP FOR COMPUTATIONAL FLUID DYNAMIC APPLICATIONS IN ROCKET PROPULSION
APRIL 28-30, 1992

Computational fluid dynamics (CFD) analysis is providing verification of Space Shuttle flight performance details and is being applied to Space Shuttle main engine multiple plume interaction flow field definition. Advancements in real-gas CFD methodology described herein have allowed definition of exhaust plume flow details at Mach 3.5 and 107,000 ft. The specific objective of the study includes the estimate of flow properties at oblique shocks between plumes and plume recirculation into the Orbiter base so that base heating and base pressure can be model accurately. The approach utilizes the Rockwell USA Real Gas Three-Dimensional Navier-Stokes (USARG3D) Code for the analysis. The code has multi-zonal capability to detail the geometry of the plumes and base region and utilizes finite-rate chemistry to compute the plume expansion angle and relevant flow properties at altitude correctly. Through an improved definition of the base recirculation flow properties, heating and aerodynamic design environments of the Space Shuttle Vehicle can be further updated.

Results of IRAD work in progress indicate that at this altitude the plumes intersect and produce oblique shocks. At the hottest spot of the oblique shock between Engines 2 and 3, the recovery pressure and temperature were found to be 216 psfa and 5000 °F. There the flow resembles a location of a source flow with a discriminating streamline driving hot gas back into the base. Considerable exhaust gas is forced back toward the thermal shield of the Orbiter base between Engines 2 and 3, although Engine 1 flow is aspirated. The highest base temperature at the lower center of the heat shield reaches 2500 °F. Future work is planned to integrate the base flow solution to the integrated vehicle forebody flow for a total 'nose-to-plume' solution. With the vertical tail and OMS pods effects included later, it is expected that there may be recirculation of Engine 1 flow, also.

Computational Fluid Dynamics Analysis of Space Shuttle Vehicle and Exhaust Plume Flows at High Altitude Flight Conditions

by

N.S. Dougherty, J.B. Holt, B.L. Liu, and S.L. Johnson
Rockwell International
Space Systems Division
Huntsville, Alabama 35806

April 21, 1992

Work Sponsored in part by NASA Johnson Space Center

Rockwell International
Space Systems Division
Huntsville Operations

Rockwell International

Space Systems Division

SPACE SHUTTLE SURFACE GRID

Huntsville Operations

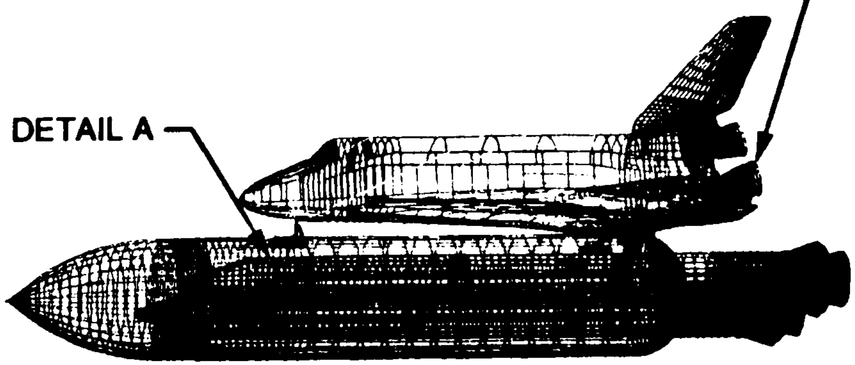

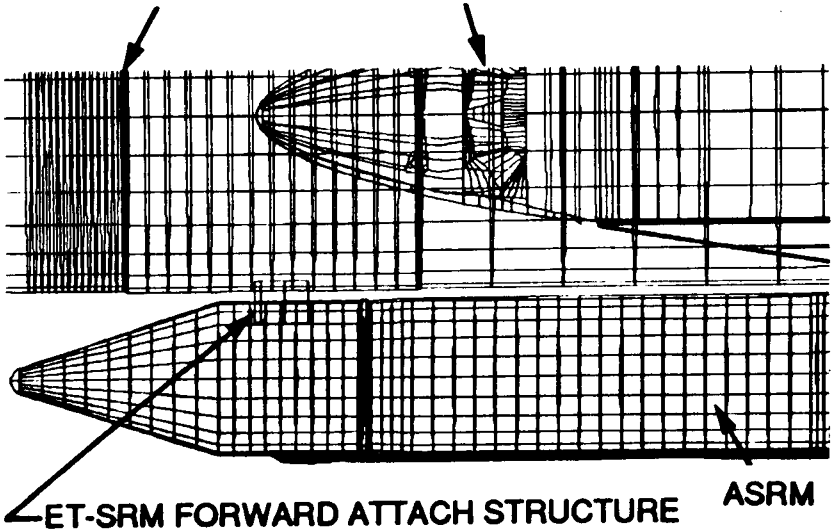

Detail A (Rotated To Planview)

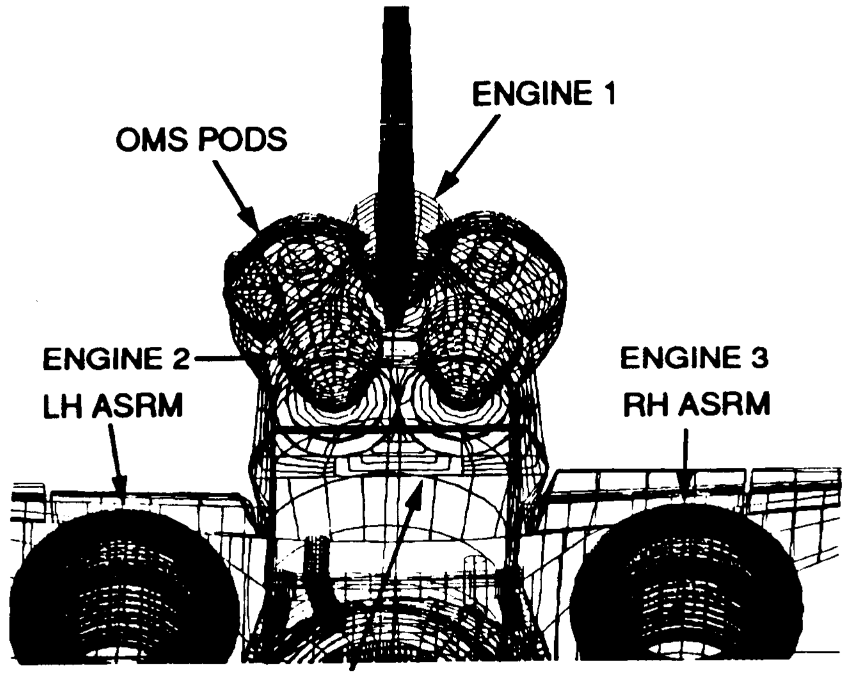

Detail B (View Looking Forward)

OBJECTIVE

Refined definition of Space Shuttle Vehicle airloading and base recirculation plume effects to reduce small uncertainties that remain at high altitude conditions to improve payload managers' margin for

- the vehicle as it flies today

- will fly after 1994 with ASRM's

APPROACH

Space Shuttle ascent computational fluid dynamics (CFD) simulations are being extended to 'nose-to-plume'

Present effort:

at Mach 3.5 and 107,000 ft

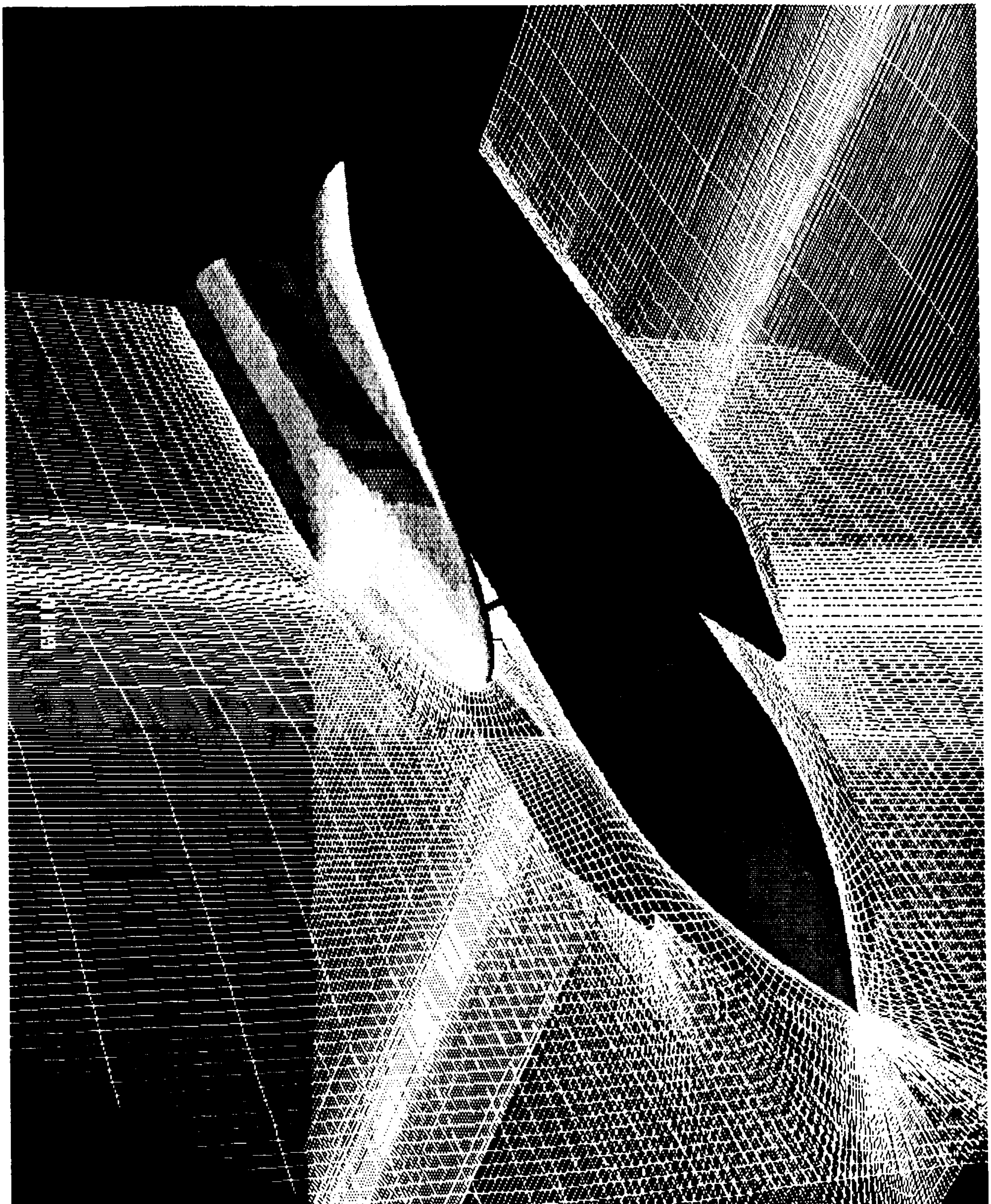

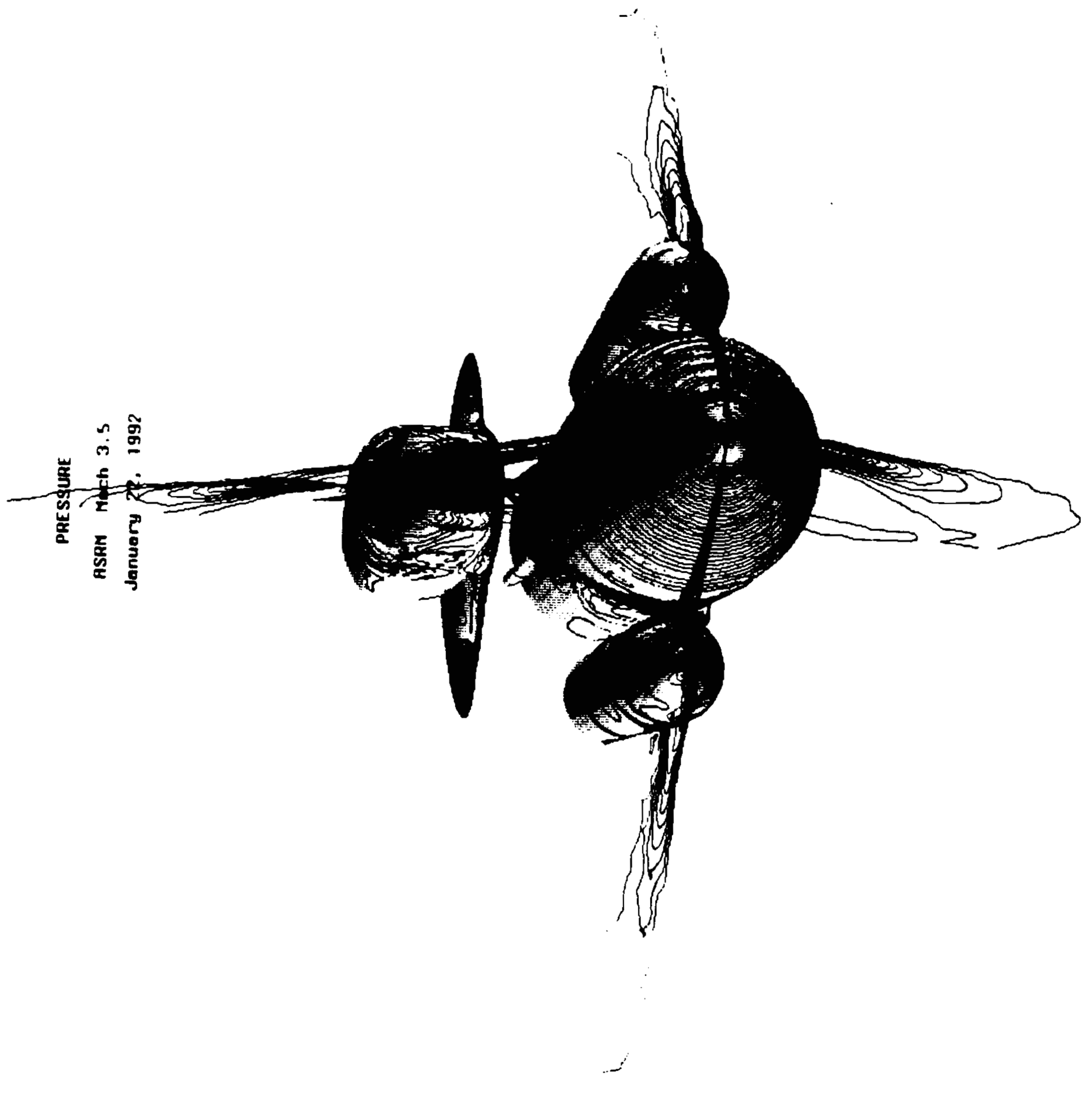
PRESSURE
ASRM Mach 3.5
January
1992

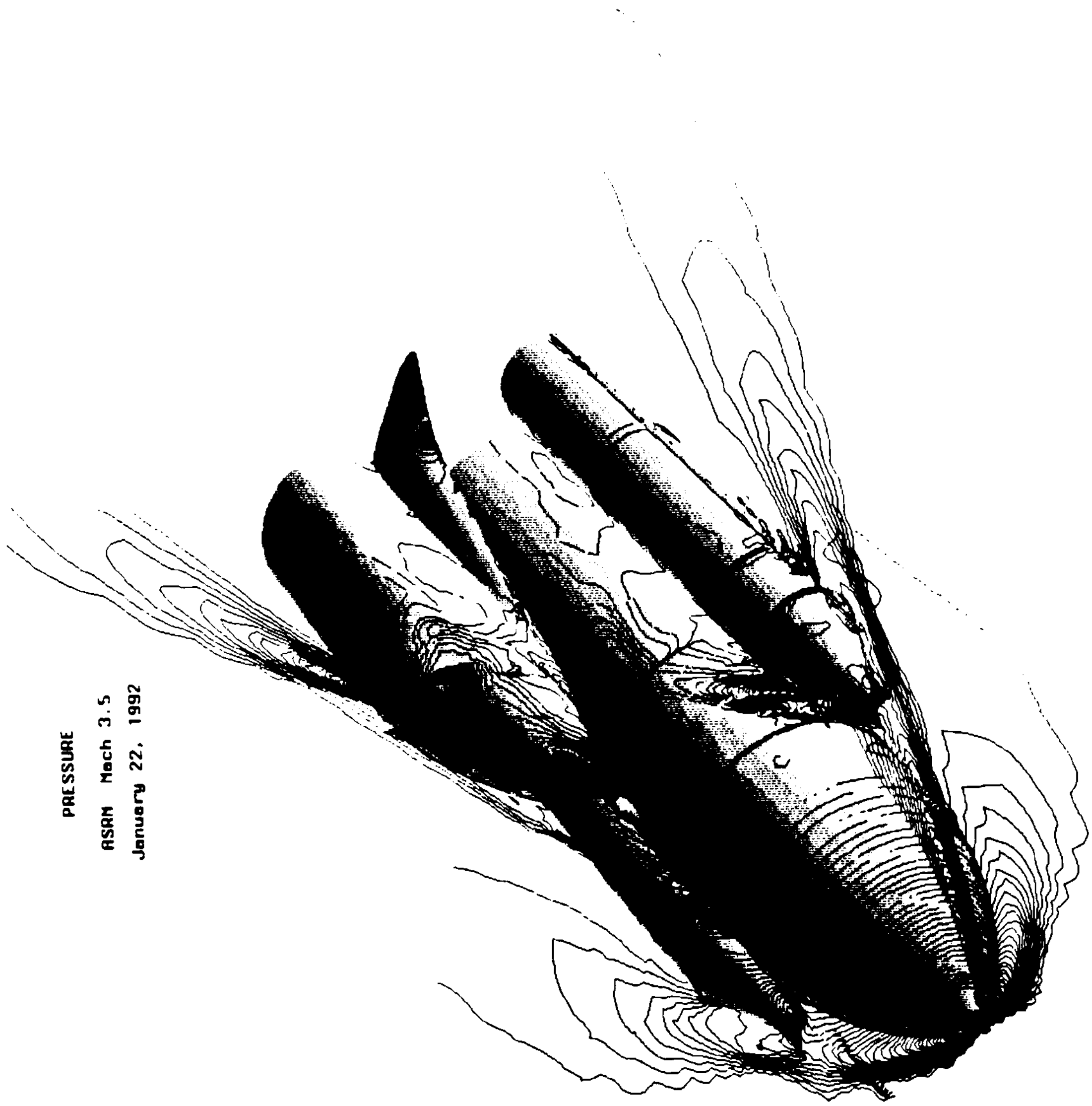
PRESSURE
ASRM Mach 3.5
January 22, 1992


PRESSURE
ASRM Mach 3.5
January 22, 1992

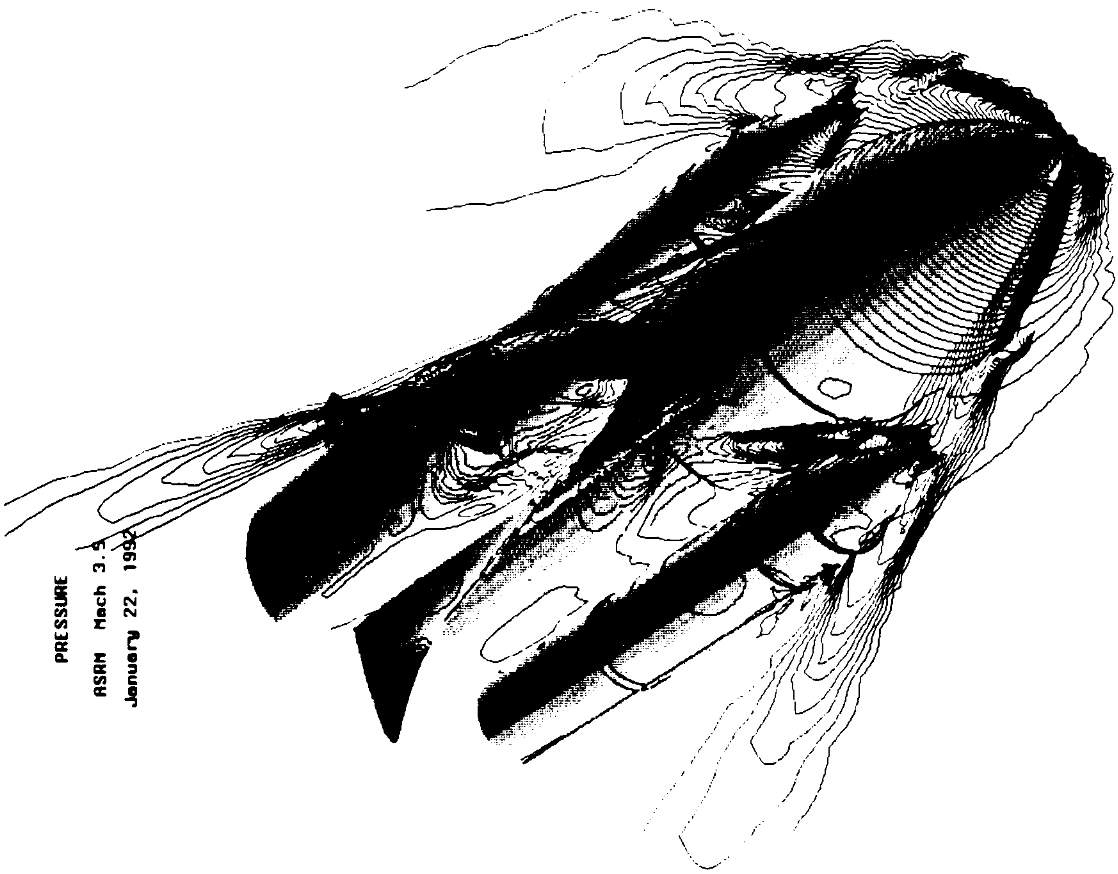
PRESSURE
ASRM Mach 3.5
January 22, 1992

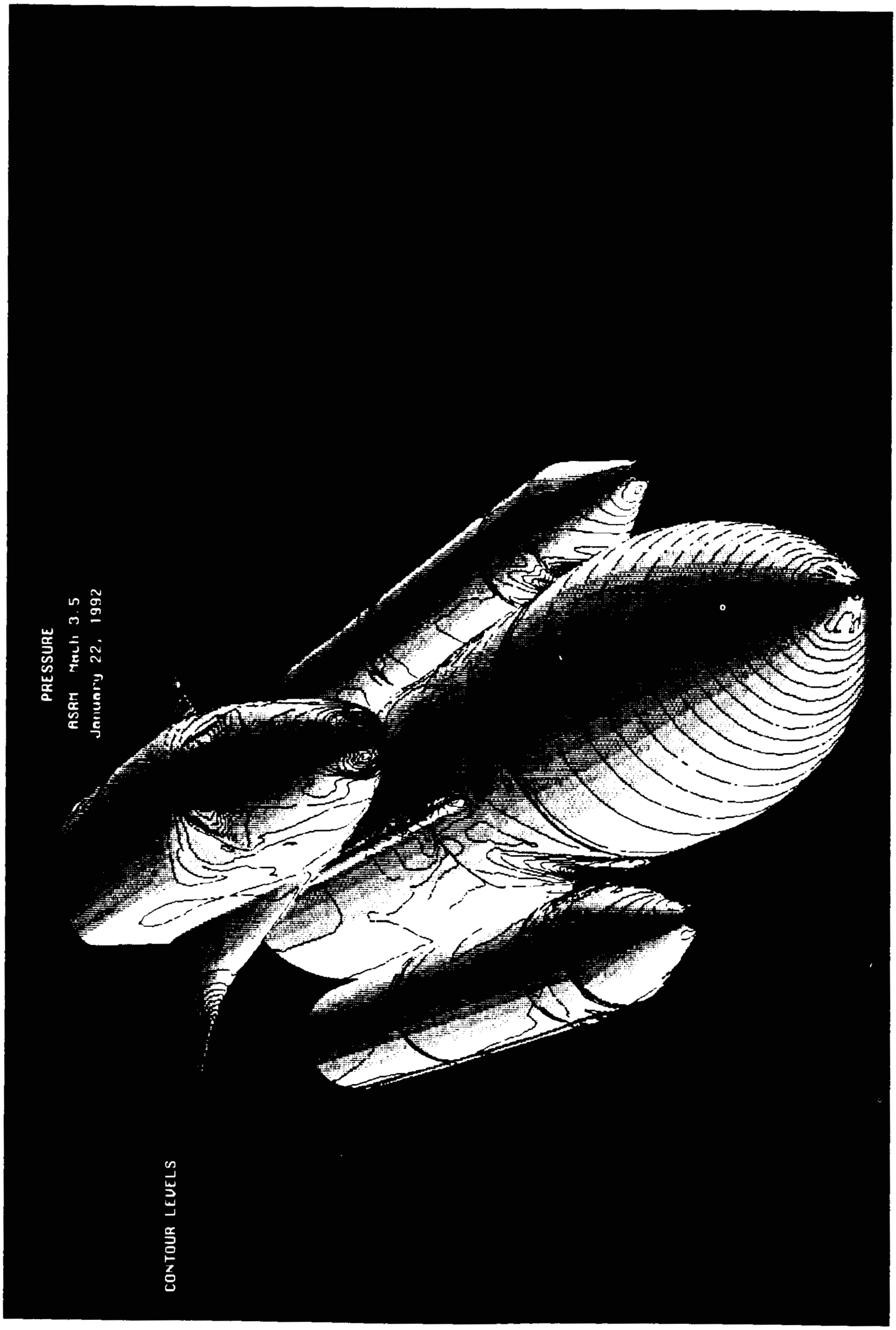
PRESSURE
ASRM Mach 3.5
January 22, 1992
CONTOUR LEVELS


Mach 3.5
22, 1992

ET FOREBODY PRESSURE

ET SURFACE ADJACENT TO ASRM

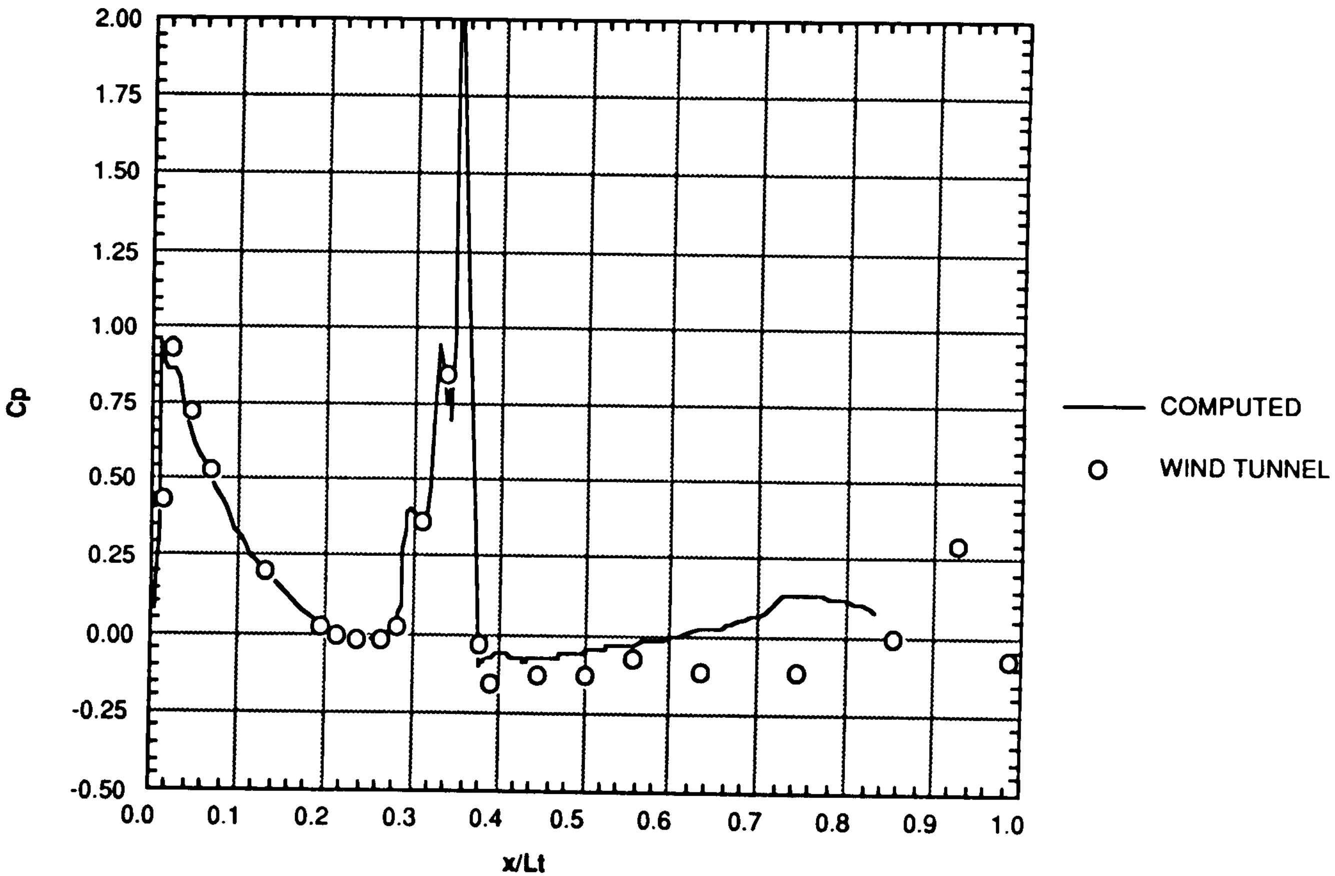

Rockwell International

Space Systems Division

ORBITER FOREBODY PRESSURE

Huntsville Operations

ORBITER CANOPY AND CARGO BAY DOORS

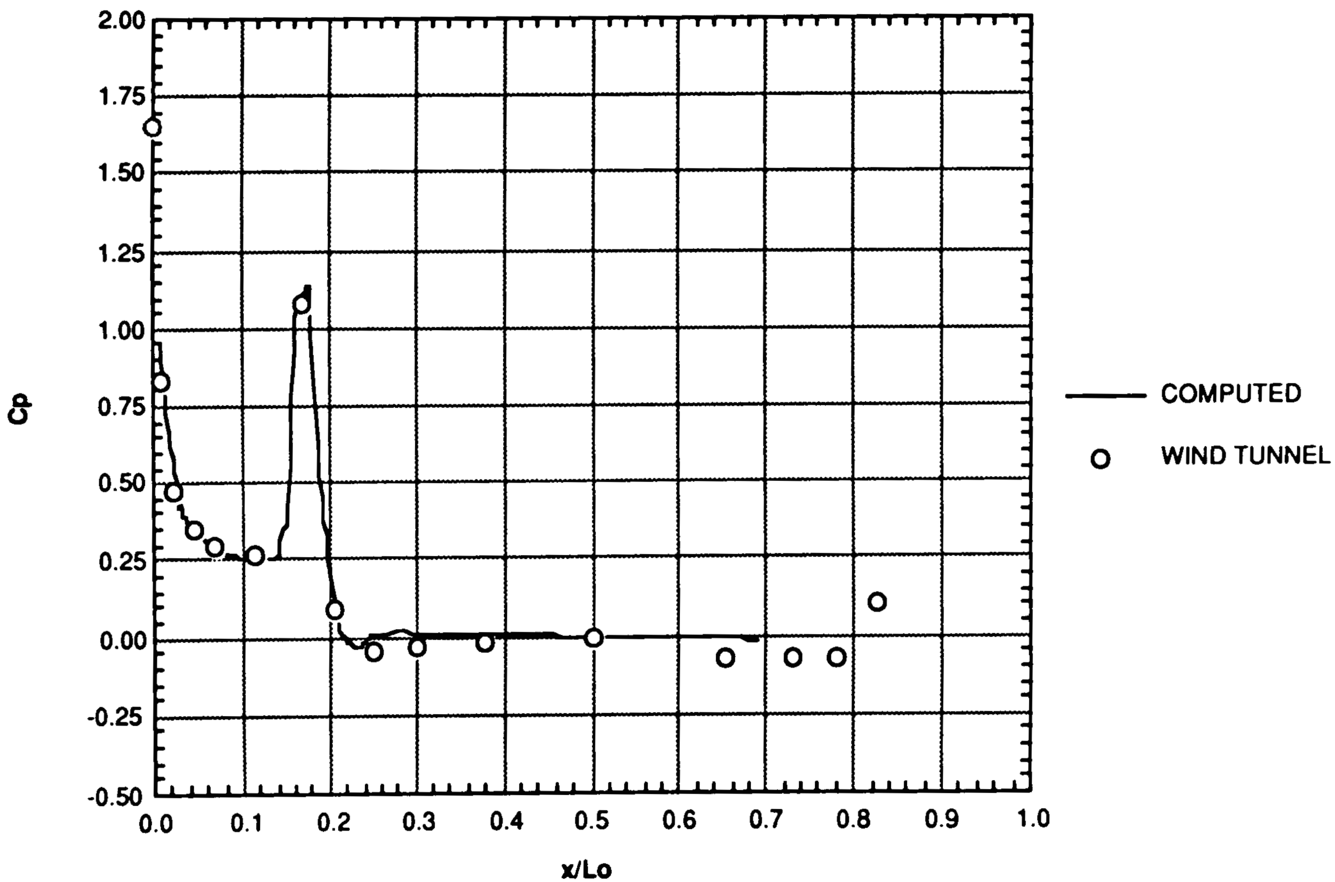

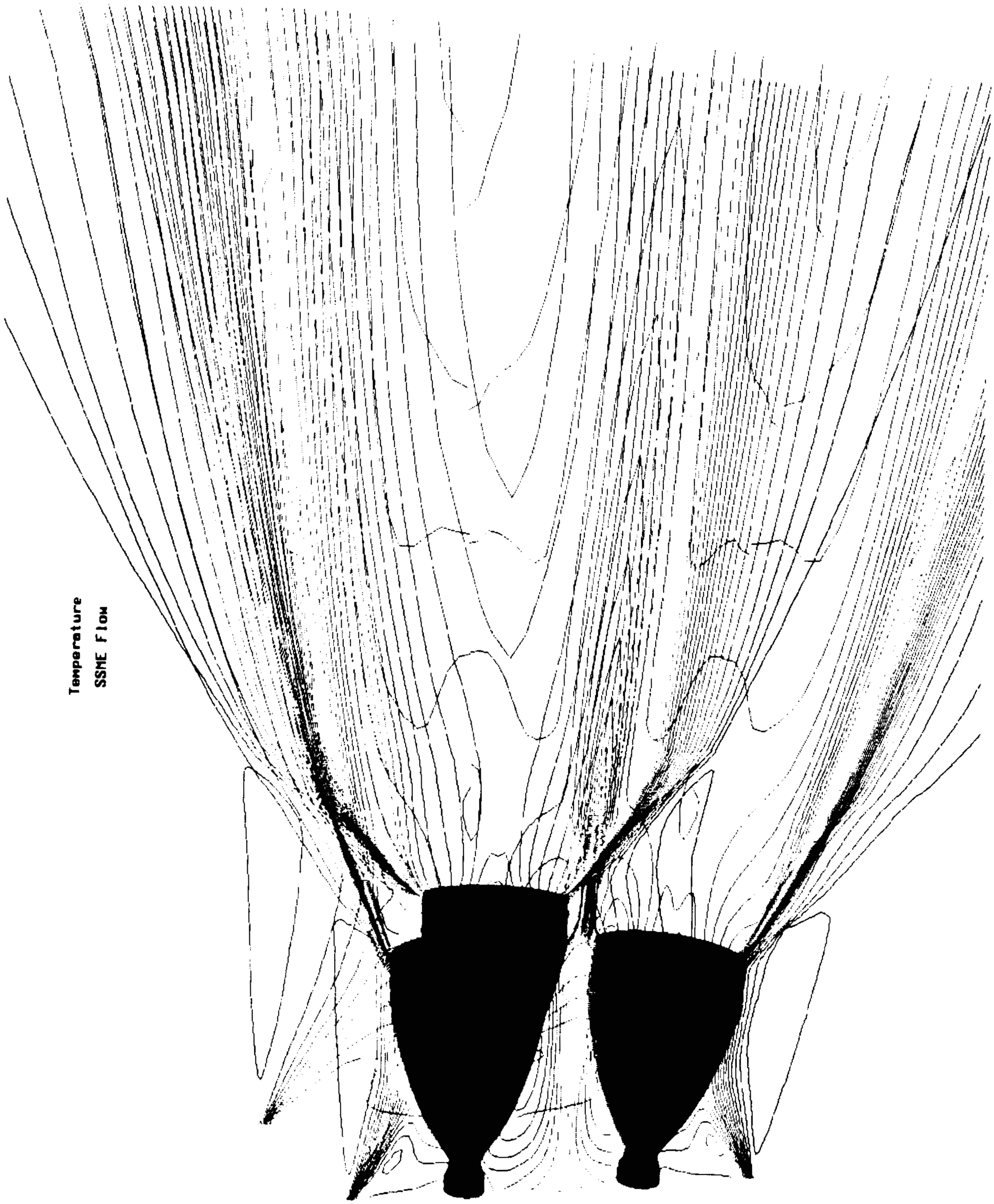
Temperature
SSME Flow

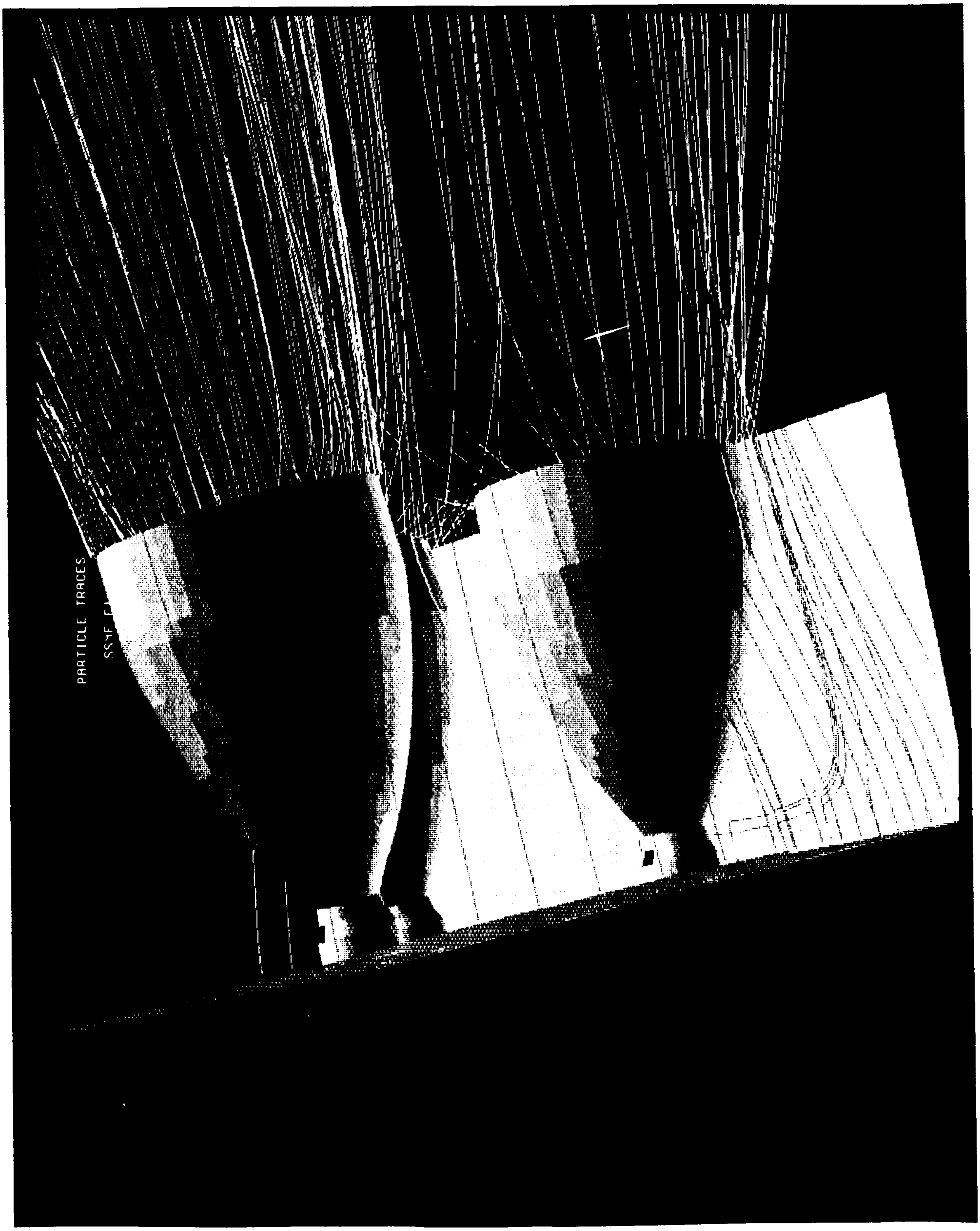
PARTICLE TRACES

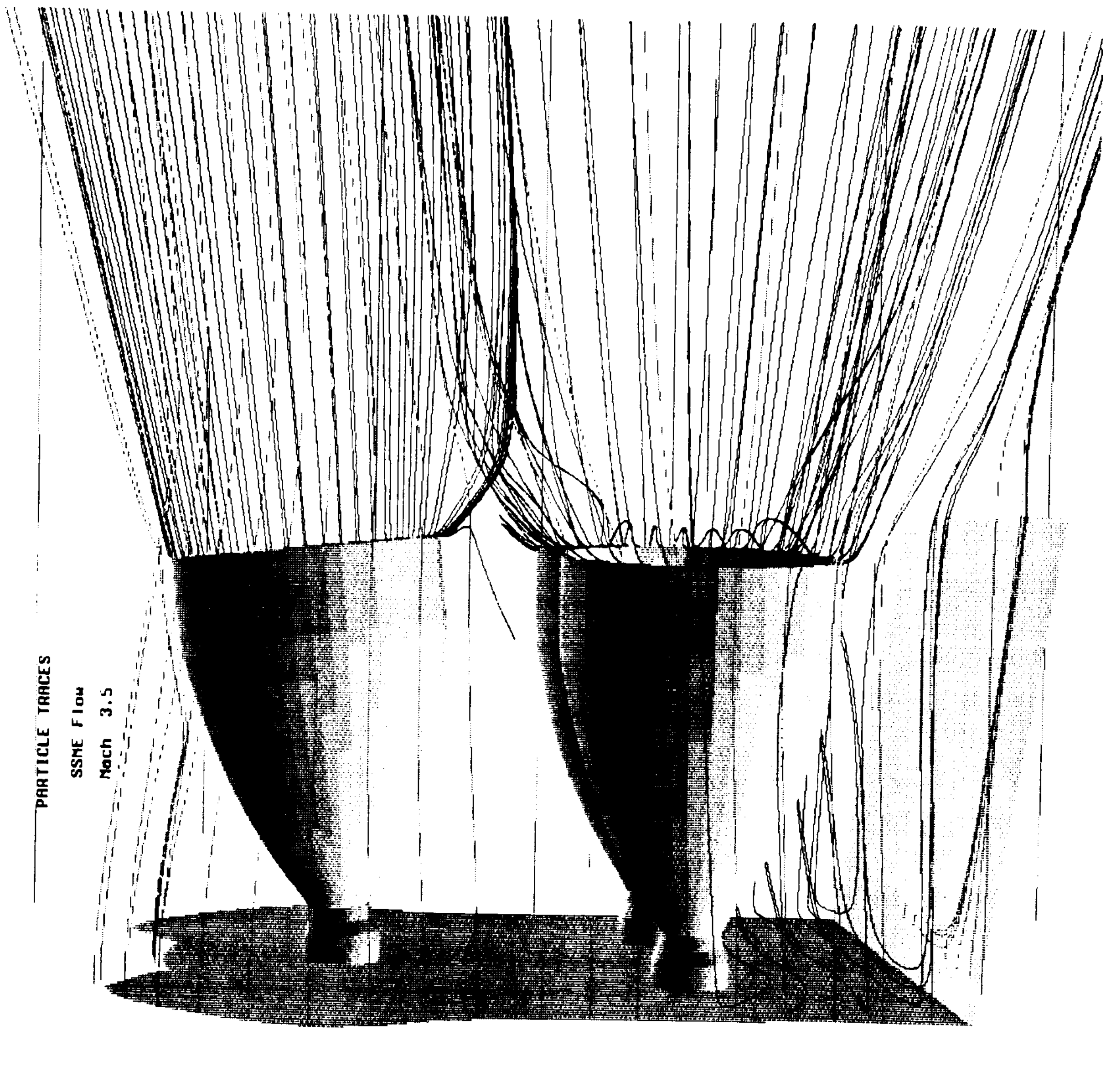
PARTICLE TRACES
SSME Flow
Mach 3.5

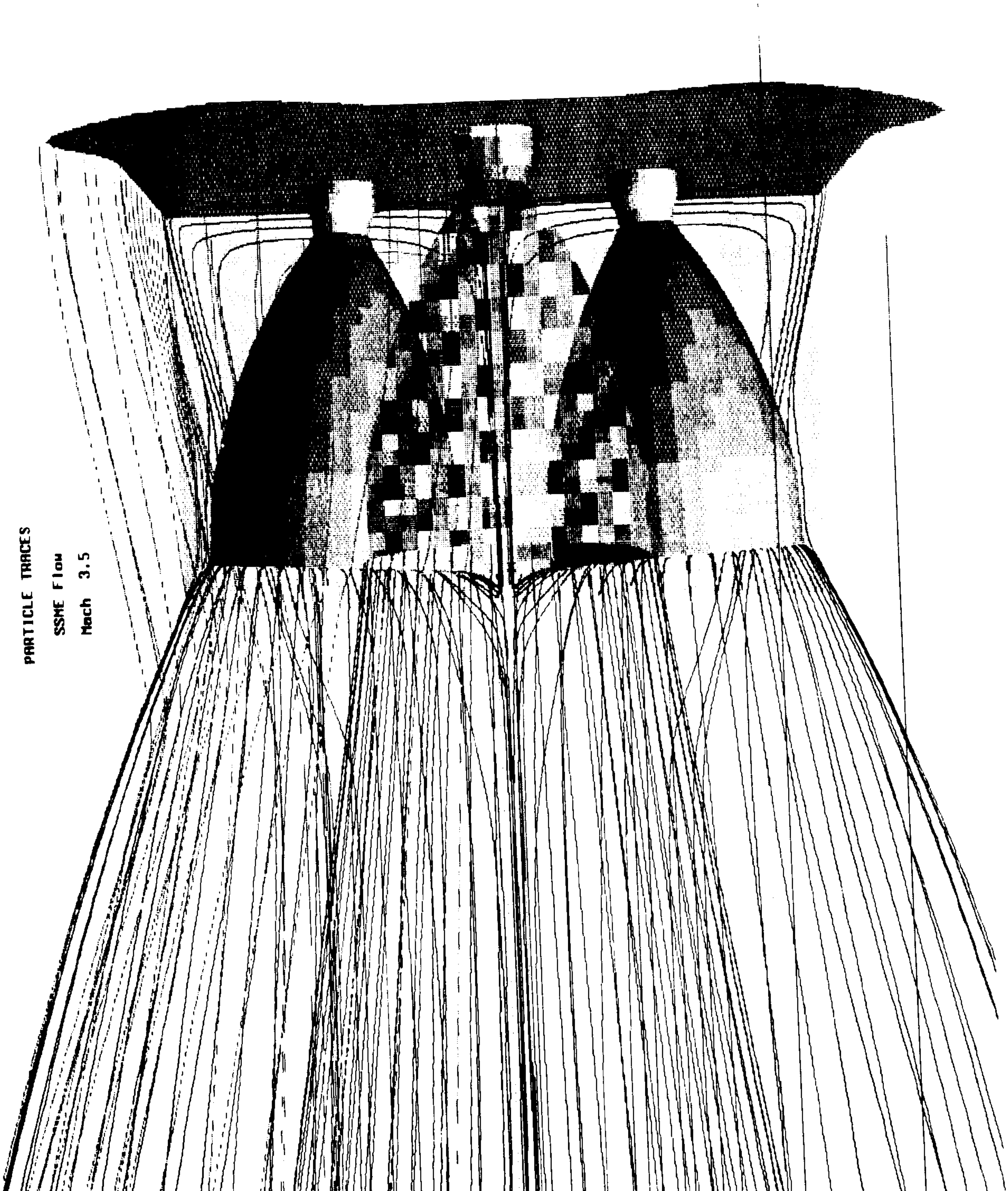
PARTICLE TRACES
SSME Flow
Mach 3.5

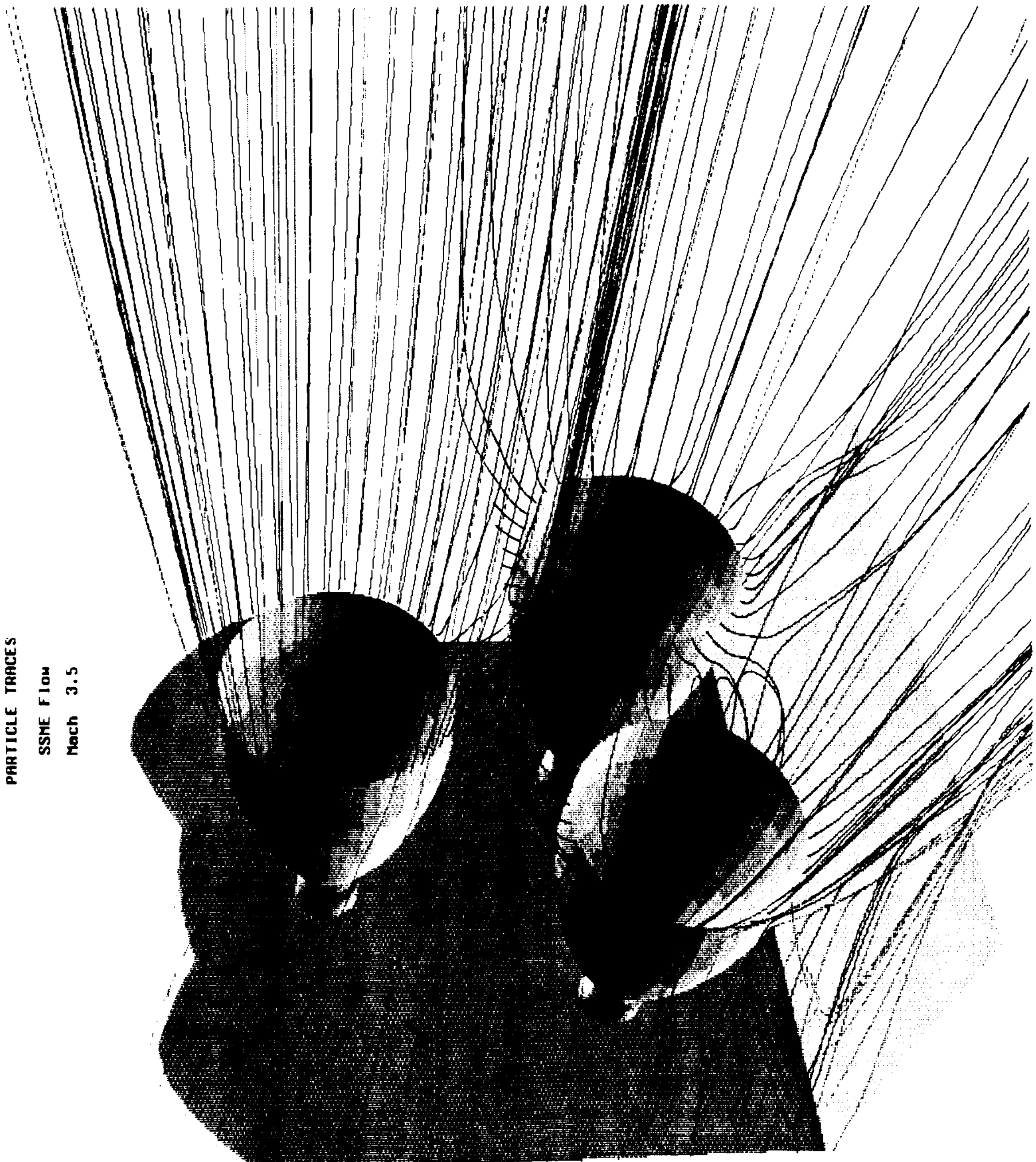
PARTICLE TRACES
SSME Flow
Mach 3.5

Rockwell International
Space Systems Division

ORBITER BASE HEATING MECHANISM

Huntsville Operations

CONDITIONS:
FREE-STREAM MACH NUMBER = 3.5
ALTITUDE = 107,000 FT, PRESSURE = 17.5 PSFA, TEMPERATURE = -20°F

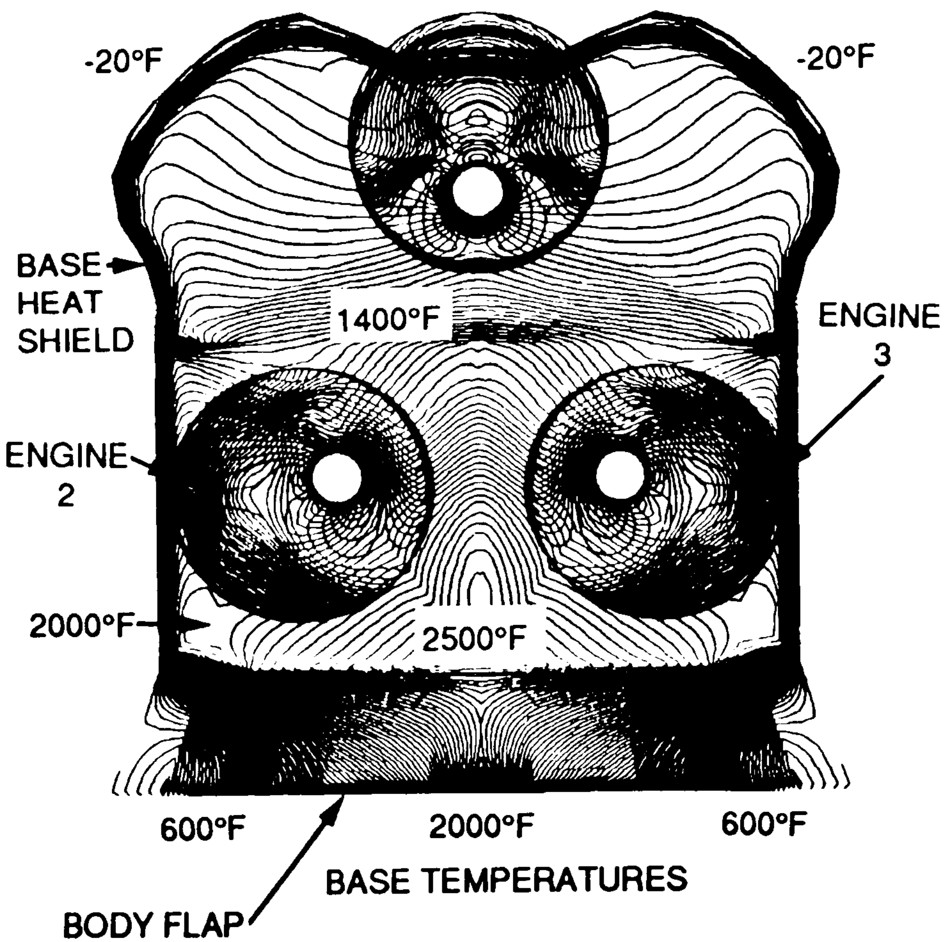

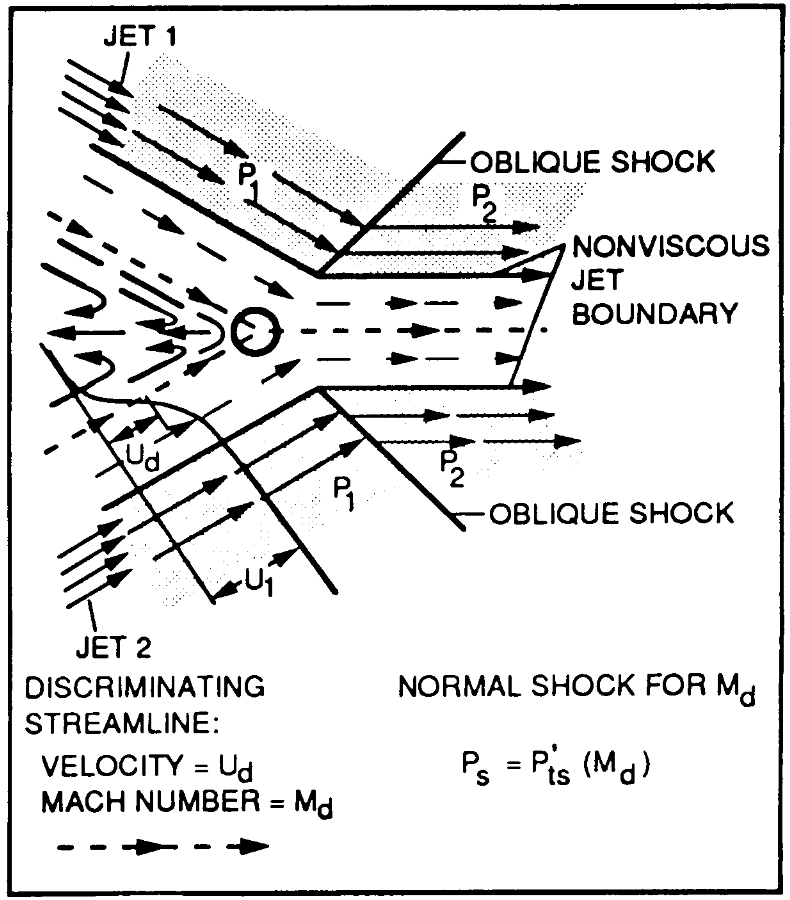

CONCLUSIONS

- Space Shuttle forebody pressures in the CFD simulation confirm the wind tunnel data
- Space Shuttle CFD simulation provides much greater detail on forebody pressures and temperatures and shows no adverse effects with ASRM's
- Space Shuttle Main Engine exhaust plumes CFD simulation shows base recirculation flow details and good agreement with Orbiter base heat shield pressure/temperature data

Direct Numerical Simulation of a Combusting Droplet with Convection

P. Y. Liang
CFD Technology Center,
Rocketdyne Division, Rockwell International
Canoga Park, California

The evaporation and combustion of a single droplet under forced and natural convection has been studied numerically from first principles using a numerical scheme that solves the time-dependent multi-phase and multi-species Navier-Stokes equations and tracks the sharp gas-liquid interface cutting across an arbitrary Eulerian grid. The flow fields both inside and outside of the droplet are resolved in a unified fashion. Additional governing equations model the inter-phase mass, energy and momentum exchange. Test cases involving iso-octane, n-hexane and n-propanol droplets show reasonable comparision with experimental data regarding parameters such as breakup mode, evaporation rate and flame stand-off distance. The partially validated code is thus readied to be applied to more demanding droplet combustion situations where substantial drop deformation render classical models inadequate.

DIRECT NUMERICAL SIMULATION OF A COMBUSTION DROPLET WITH CONVECTION

PAK-YAN LIANG

ROCKWELL INTERNATIONAL CORPORATION
ROCKETDYNE DIVISION

Rockwell International
Rocketdyne Division

CFD 92-030-009/D2/PYL

OBJECTIVE

STUDY THE EVAPORATION AND COMBUSTION OF A SINGLE DROPLET UNDER FORCED AND NATURAL CONVECTION FROM FIRST PRINCIPLES

Rockwell International
Rocketdyne Division

CFD 92-030-008/D2/PYL

SIGNIFICANCE

DIRECT MODELING OF BOTH DROPLET <u>AND</u> AMBIENT IN UNIFIED CFD MODEL REMOVES CONSTRAINTS DUE TO ASSUMPTIONS OF

- SPHERICAL SYMMETRY
- SMALL CONVECTIVE EFFECTS
- LOW EVAPORATION RATE (NO BLOWING)
- SHARP FLAME FRONT (INSTANTANEOUS AND COMPLETE COMBUSTION)

Rockwell International
Rocketdyne Division

CFD 92-030-007/D2/PYL

Control Volume Next to Droplet Surface

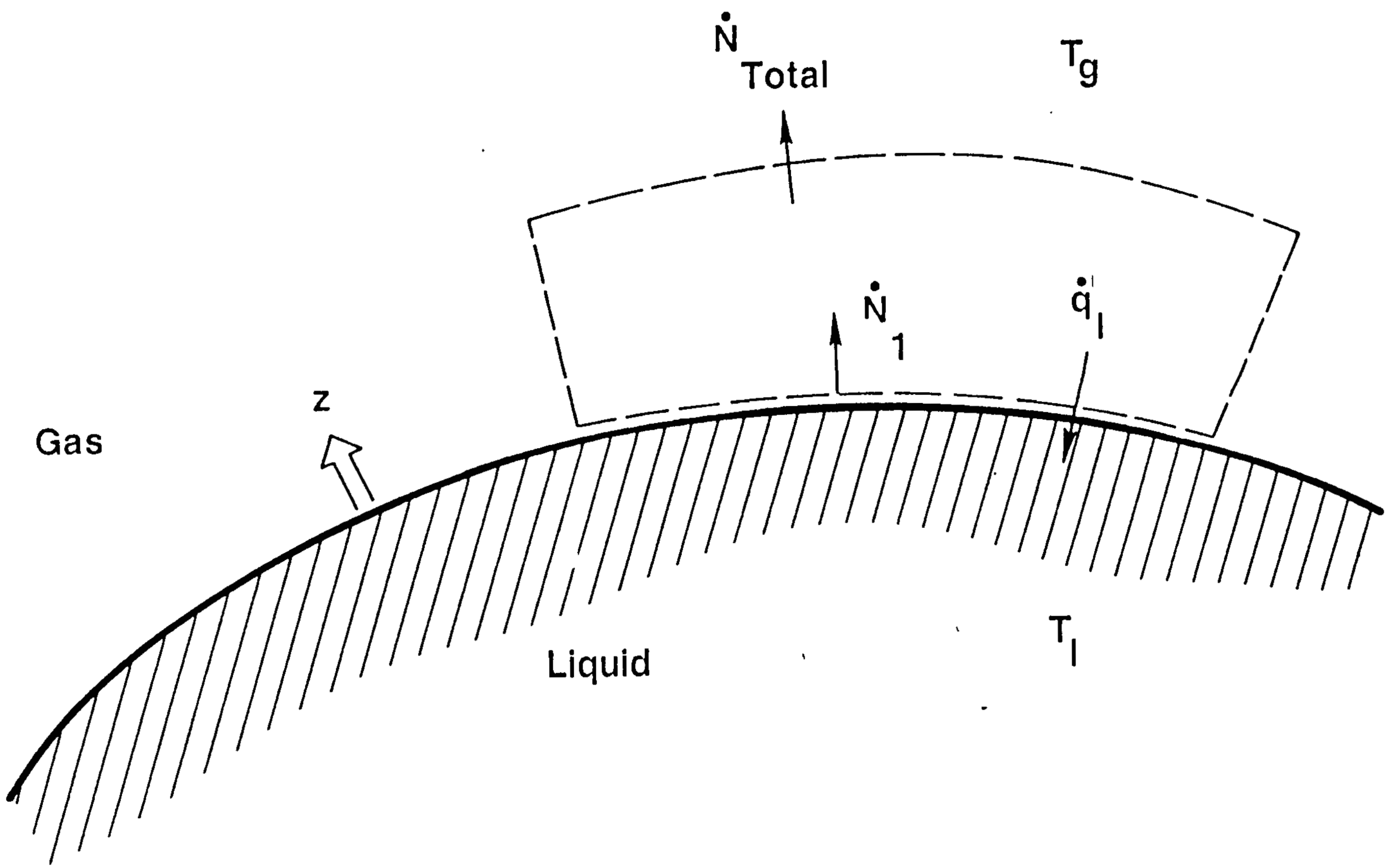

Rockwell International
Rocketdyne Division

Governing Equations

- Continuity equation integrated twice to yield

$$\dot{N}_1 \quad (\Delta z) = c \ \mathfrak{D} \ln \left(\frac{1 - X_1 gas}{1 - X_1 surface} \right)$$

or

$$\dot{m}_{vap} = \frac{c \ \mathfrak{D} \ \hat{M}_1 \ A_s}{\Delta z} \ \ln \left(\frac{1 - X_{1gas}}{1 - X_1 surface} \right)$$

- Assuming $N_{total} \approx N_1$

Governing Equations

- Final heat-up rate equation for multi-species

$$V_\ell \left(c_\ell \hat{M}_1\right)\left(\frac{c_{p_{1_v}}}{\hat{M}_1}\right)\frac{dT_\ell}{dt} = \frac{k\,\xi\,A_s\left(T_g - T_\ell\right)}{\left(\Delta z\right)\left(e^{\xi} - 1\right)} - \dot{m}_{vap}\left(\frac{\Delta H_{vap}}{\hat{M}_1}\right)$$

where

$$\xi \equiv \frac{\dot{N}_1 \; c_{p_{1_v}}\left(\Delta z\right)}{k} = \frac{\dot{m}_{vap}}{A_s}\left(\frac{c_{p_{1_v}}}{\hat{M}_1}\right)\frac{\left(\Delta z\right)}{k}$$

- Equation for single species

$$\dot{m}_{vap} = A_s\,E_p\left(p_{vap} - p\right)\left(\frac{\hat{M}_1}{2\pi R T_\ell}\right)^{1/2}$$

Governing Equations

- Energy equation integrated twice to yield

$$\dot{q}_\ell \left[e^{\dot{N}_1 c_{p_{1_v}} (\Delta z)/k} - 1 \right] = \dot{N}_1 c_{p_{1_v}} \left(T_g - T_\ell \right)$$

where $\dot{q}_\ell$ is in turn given by

$$\dot{q}_\ell = \frac{V_\ell}{A_s} c_\ell c_{p_{1_\ell}} \frac{dT_\ell}{dt} + \dot{N}_1 \left(\Delta H_{vap} \right)$$

ARICC-ST MODELS

- FULL NAVIER-STOKES IN BOTH GAS AND LIQUID PHASES
- TWO PHASE, VOLUME-OF-FLUID, WITH SURFACE TRACKING
- VARIABLE TEMPERATURE IN BOTH PHASES
- INTER-PHASE MASS AND HEAT TRANSFER (EVAPORATION) AND SURFACE TENSION

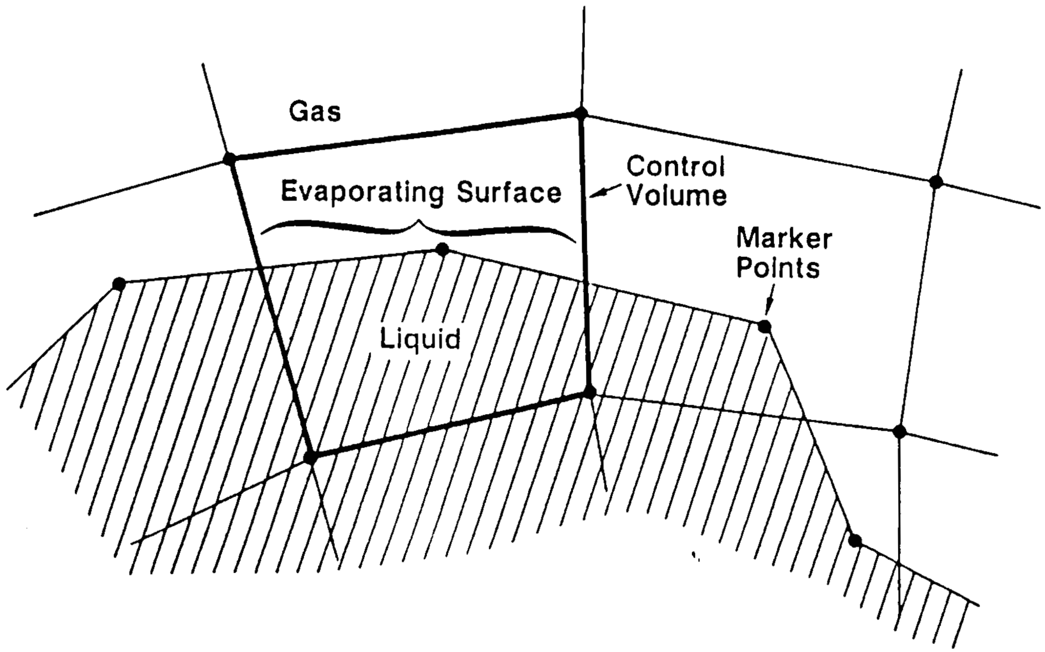

Fig. 1 Schematic of Partitioned Computational Volume with Evaporating Free Surface Segments

Fig. 2 Bag Mode Breakup of Simulated (a & c) and Experimental (b) Droplet Due to Shock Wave Passage. (c) was done with evaporation and ignition.

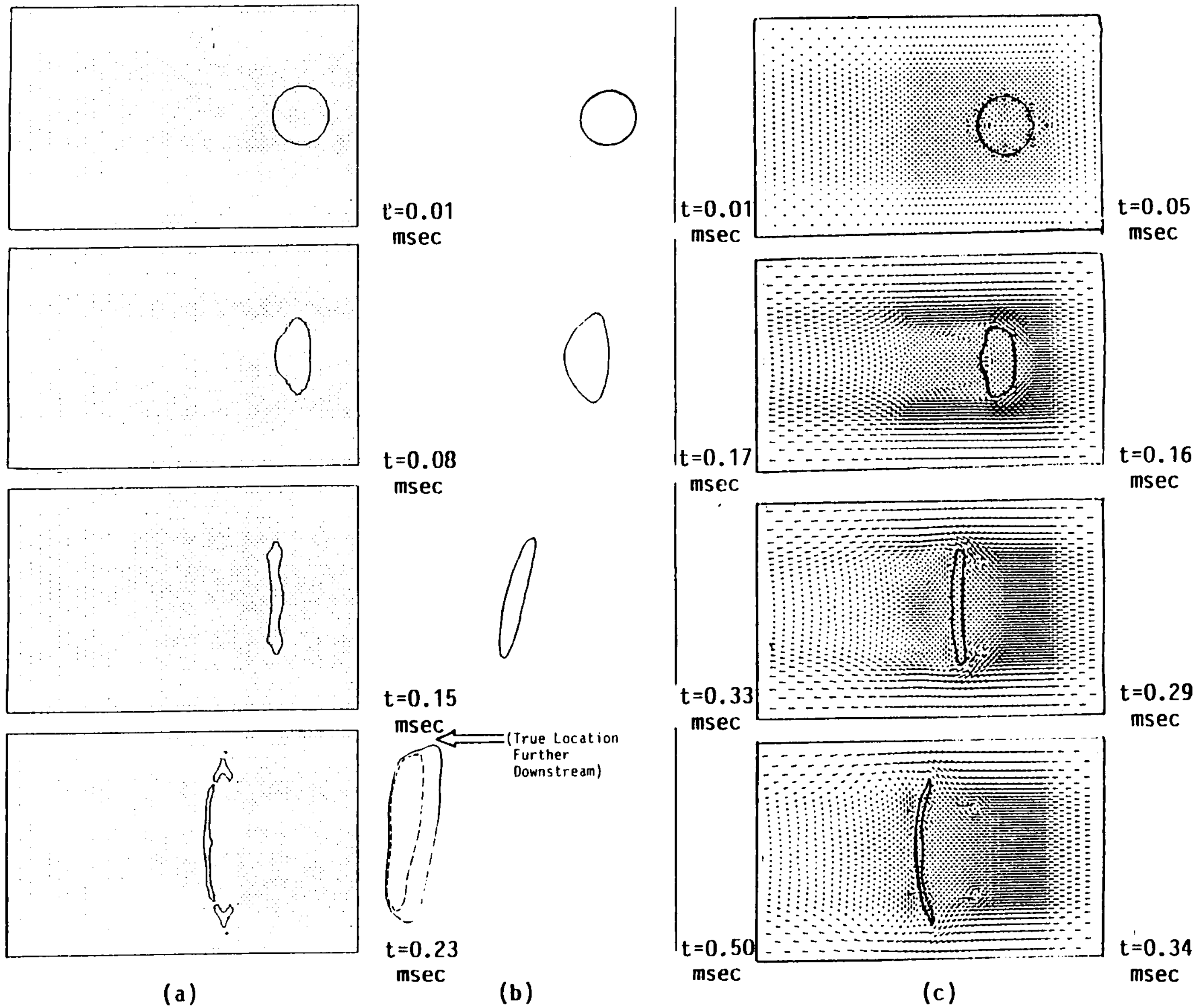

Table 1. Highlight of Problem Parameters for Combusting Droplet With Convection Simulations

	Forced Convection	Natural Convection
Liquid	n-Hexane (C_6H_{14})	n-Propanol (C_3H_7OH)
MW	86.178	60.096
Surface tension (dynes/cm)	14.4 (at 333 K)	23.04 (at 293 K)
Density (g/cc)	.521 (at 423 K)	.804 (at 293 K)
Viscosity (poise)	$.21554 \times 10^{-2}$ (at 342 K)	$.464 \times 10^{-2}$ (at 370 K)
Conductivity (ergs/cm-s-K)	1.1076×10^{4} (at 342 K)	1.4255×10^{4} (at 370 K)
Vapor pressure (mmHg)	exp(15.84-2698/(T-48.78))	exp(17.54-3166/(T-80.15))
Latent heat (ergs/g)	$3.165 \times 10^{9}((1-T_r)/(1-T_{r,ref}))^{.375}$ $T_r = T/T_{crit}$, $T_{crit}=507.6$	$6.952 \times 10^{9}((1-T_r)/(1-T_{r,ref}))^{.375}$ $T_{crit}=536.7$
Initial drop diam. (cm)	.1815	.210
Initial drop temp (K)	355.0	293.0
Ambient	N_2	Air
Initial temp. (K)	470.0	293.0
Pressure (atm.)	13.6	3
Prandtl number	.714	.75
Viscosity (poise)	1.925×10^{-4} (at 470 K)	1.813×10^{-4} (at 293 K)
Grid size	30 x 100	35 x 105

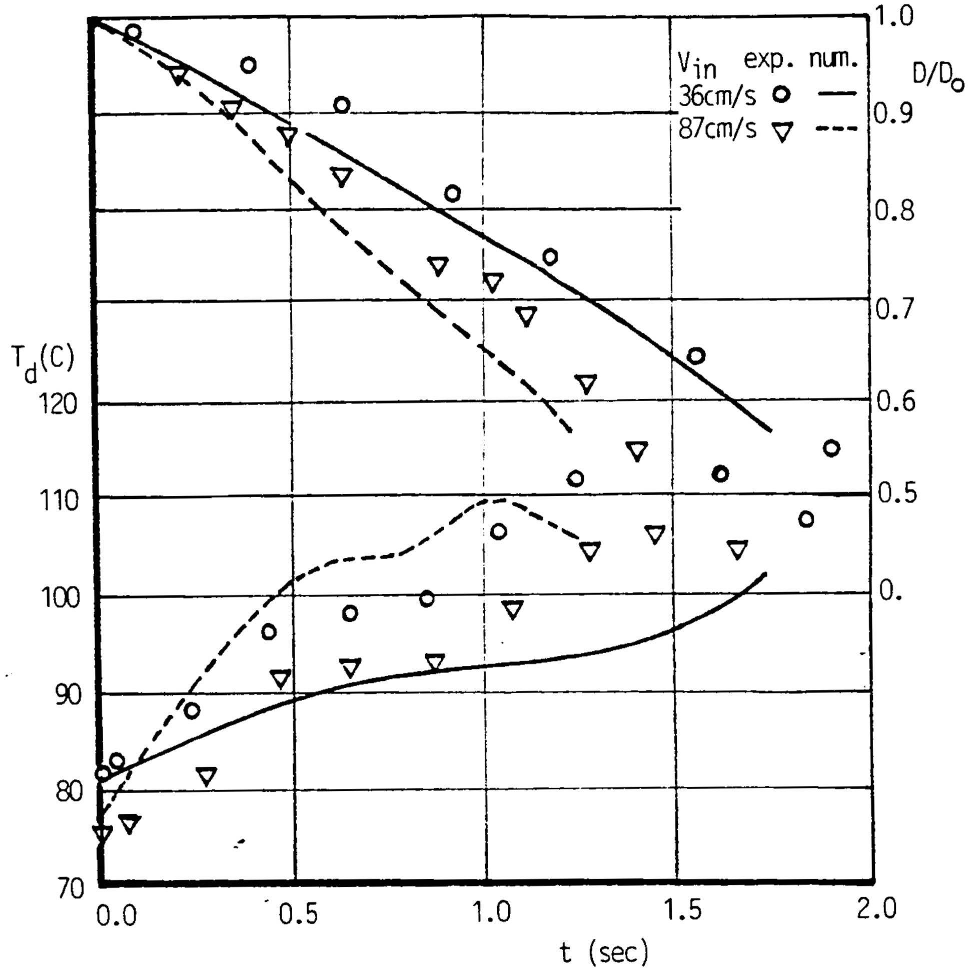

Fig. 3 Numerical vs Experimental Drop Diameter and Drop Center Temperature Histories in Forced Convection

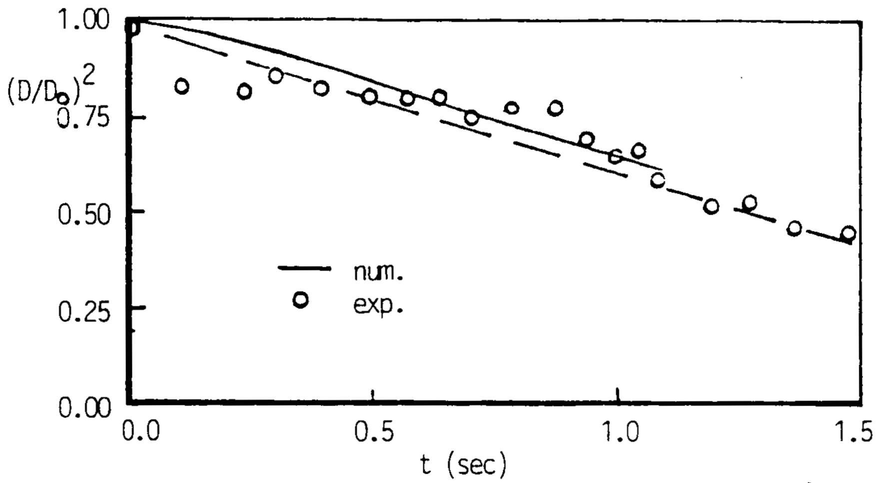

Fig. 4 Numerical vs Experimental Drop Diameter Histories in Natural Convection. Dashed line is reference D^2-law

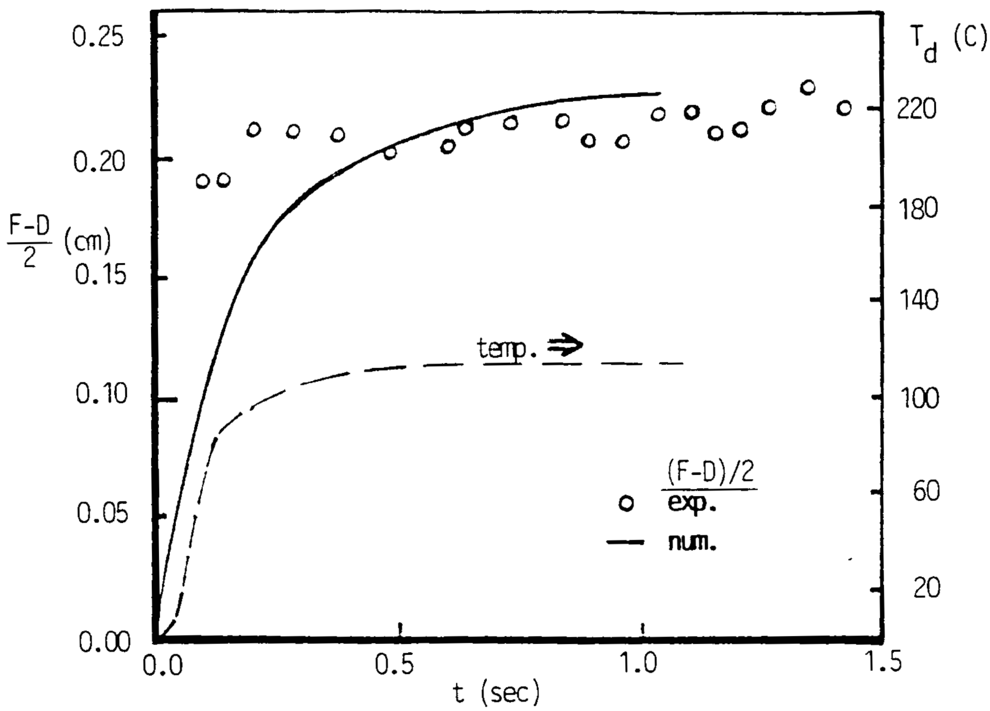

Fig. 5 Flame Stand-off Distance and Drop Center Temperature vs Time in Natural Convection

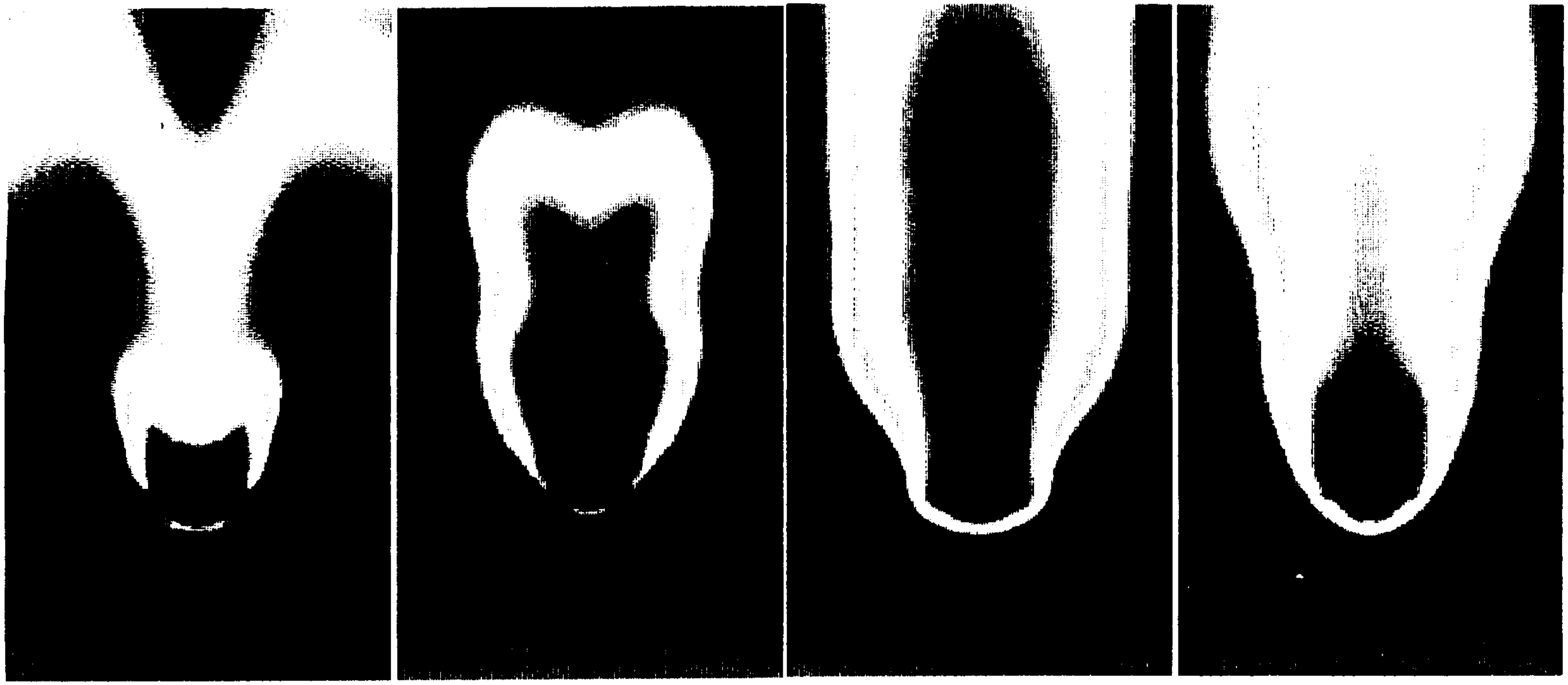

Fig. 6 Sequence of Simulated Temperature Contours in Grey Scale Showing Initial Transient of n-Propanol Droplet Combusting with Natural Convection. (white Tmax=2500 K, black Tmin=300 K)

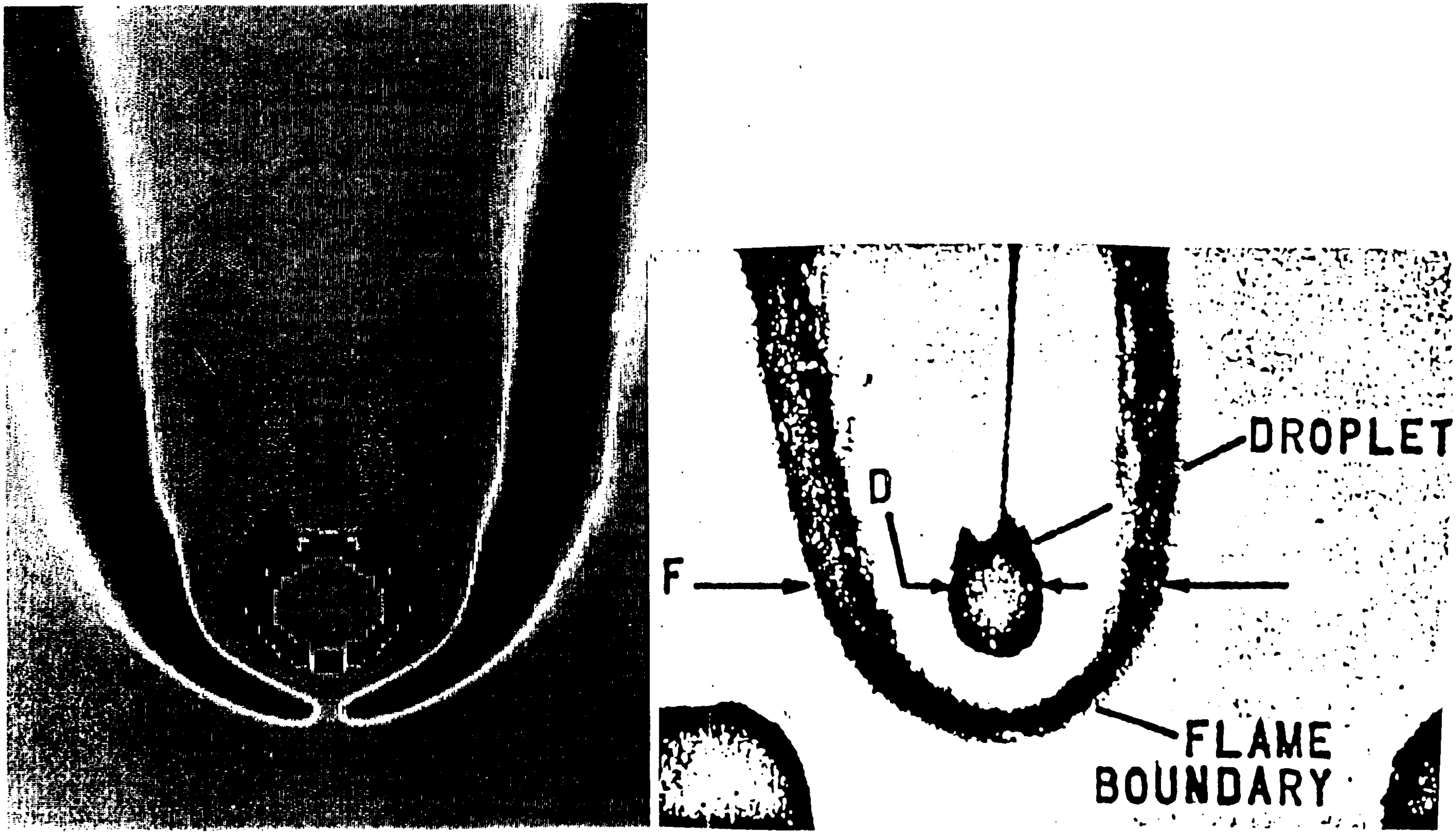

(a) (b)

Fig. 7 Comparision of Simulated Density Gradient Contours (a) with Experimental Schlieren Photograph (b) of Combusting Droplet from Rush et al (Ref. 11)

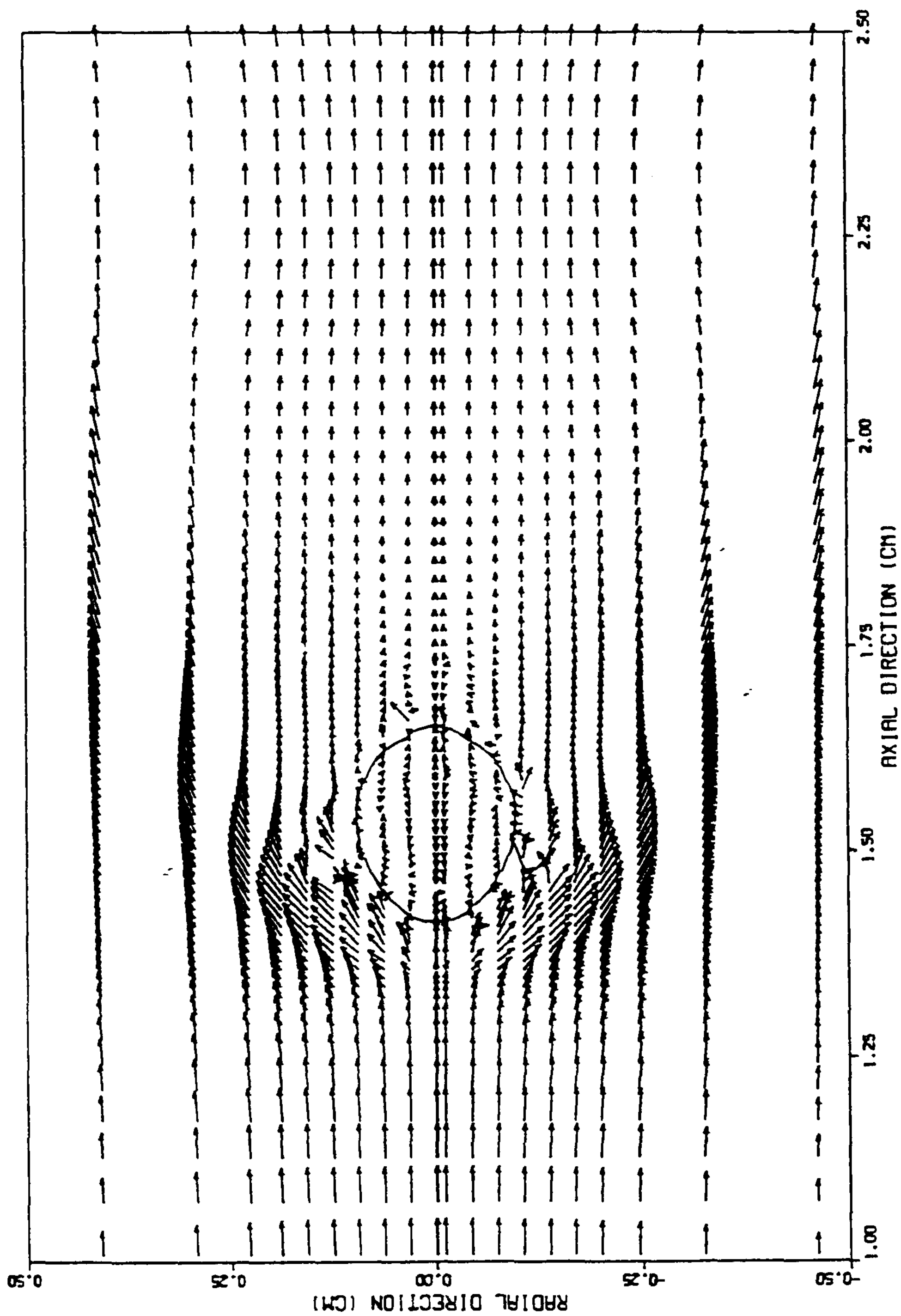

t = .110 sec

Fig.8 Close-up View of Velocity Vector Plot from n-Propanol Drop Combustion Under Natural Convection Simulation

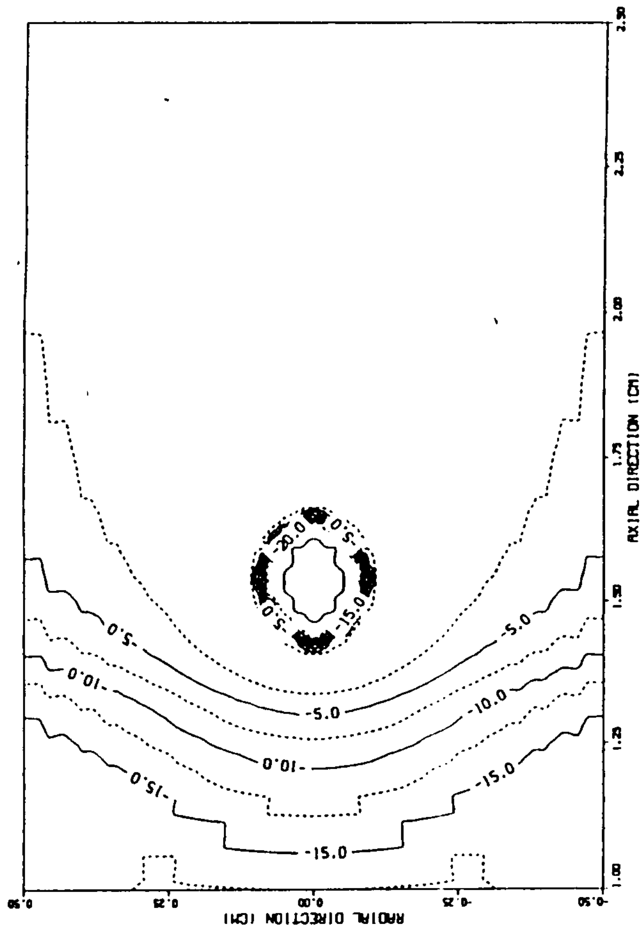

(a) water

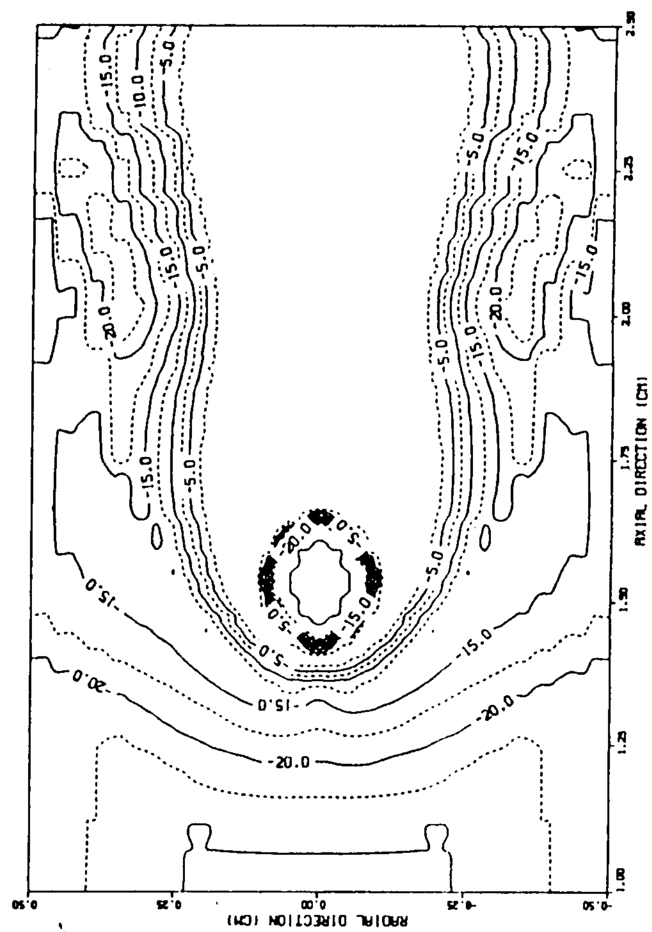

(b) propanol

t = .110 sec

Fig. 9 Log_{10} Species Concentration Contours from n-Propanol Drop Combustion Under Natural Convection Simulation

CONCLUSIONS

- SIMULATIONS OF DEFORMING, EVAPORATING AND COMBUSTING DROPS PERFORMED WITHOUT EMPIRICAL INPUTS

- REASONABLE COMBUSTION RATE, EVAPORATION RATE AND TEMPERATURE DISTRIBUTION OBTAINED

- EFFECT OF EVAPORATION ON BREAKUP MODE REQUIRE MANY MORE PARAMETRIC STUDIES

- DETAILS OF INTERNAL RECIRCULATING FLOWFIELD REQUIRE LARGE GRID CONCENTRATION AROUND BOUNDARY LAYER

Rockwell International
Rocketdyne Division

CFD 92-030-006/D2/PYL

N92-32257

A NUMERICAL MODEL FOR ATOMIZATION-SPRAY COUPLING IN LIQUID ROCKET THRUST CHAMBERS

by

M. G. Giridharan, A. Krishnan, J. J. Lee and A. J. Przekwas
CFD Research Corporation, Hunstville, AL 35802
and

K. Gross
NASA Marshall Space Flight Center, Hunstville, AL 35802

The physical process of atomization is an important consideration in the stable operation of liquid rocket engines. Many spray combustion CFD codes do not include an atomization sub-model but assume arbitrary drop size distributions, drop initial locations and velocities. It has been shown that the results of spray combustion models are extremely sensitive to the assumed droplet initial conditions. Furthurmore, the atomization process itself is a strong function of the local conditions of the liquid and gas flow. Thus it is important to account for the strong mutual coupling between the liquid phase, the spray dynamics and the gas flow. A method of coupling an atomization model with the spray model in a REFLEQS CFD code will be presented. This method is based on a novel Jet-Embedding technique in which the equations governing the liquid jet core are solved separately using the surrounding gas phase conditions. The droplet initial conditions are calculated using a stability analysis appropriate for the atomization regime of liquid jet break-up.

This novel coupling model is used to analyze the SSME fuel preburner single injector flow. Results of the diffusion flame characteristics in a single injection element will be presented. The effect of relative velocity, mixture ratio and droplet initial conditions will be shown. The predictions of present atomization model is compared with that of the widely used CICM correlation. The results are also compared with the predictions of volume-of-fluid method.

CFD Research Corporation
3325-D Triana Blvd. ■ Huntsville, AL 35805 ■ (205) 536-6576 ■ FAX: (205) 536-6590

CFDRC

A NUMERICAL MODEL FOR ATOMIZATION-SPRAY COUPLING IN LIQUID ROCKET THRUST CHAMBERS

by
M.G. Giridharan, J.J. Lee, A. Krishnan and A.J. Przekwas
CFD Research Corporation

and
K. Gross
Marshall Space Flight Center

10th Annual CFD Workshop
NASA - MSFC
April 30, 1992

OUTLINE

CFDRC

- Introduction
- Atomization-Spray Coupling Model
- Validation
- Demonstration Results
- Conclusions

INTRODUCTION

CFDRC

- Importance of an Atomization-Spray Coupling Model
- Two Approaches:
  - Interface Capturing - VOF Methodology
  - Interface Fitting - Jet-Embedding
- Atomization Models
  - Meyer's Model
  - Linear Dispersion Equation
- Spray Model
  - Eulerian/Lagrangian Particle Tracking

Temperature Distribution in the Thrust Chamber

Ud = Vd = 25.0 m/s, Dd = 25 Microns

Isp = 318.6 seconds

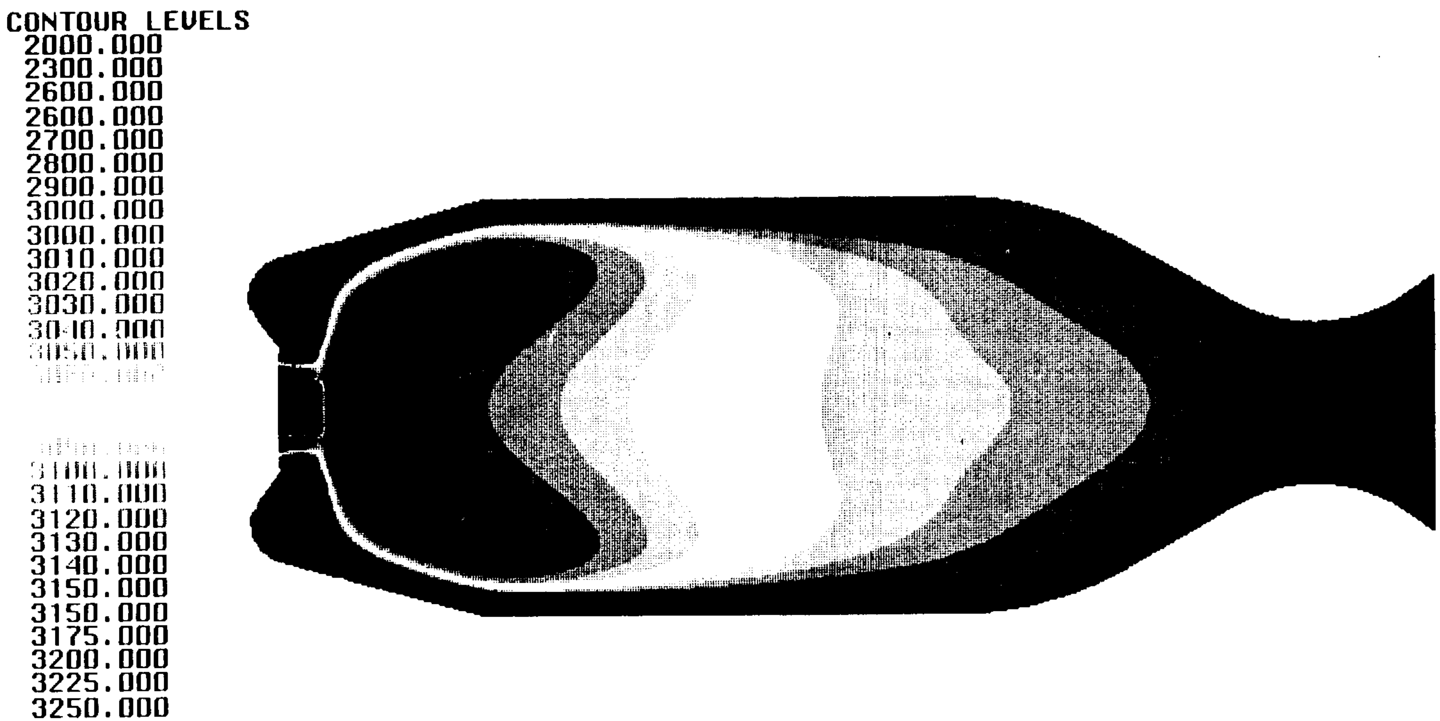

Temperature Distribution in the Thrust Chamber

Ud = Vd = 25.0 m/s, Dd = 100 Microns

Isp = 313.8 seconds

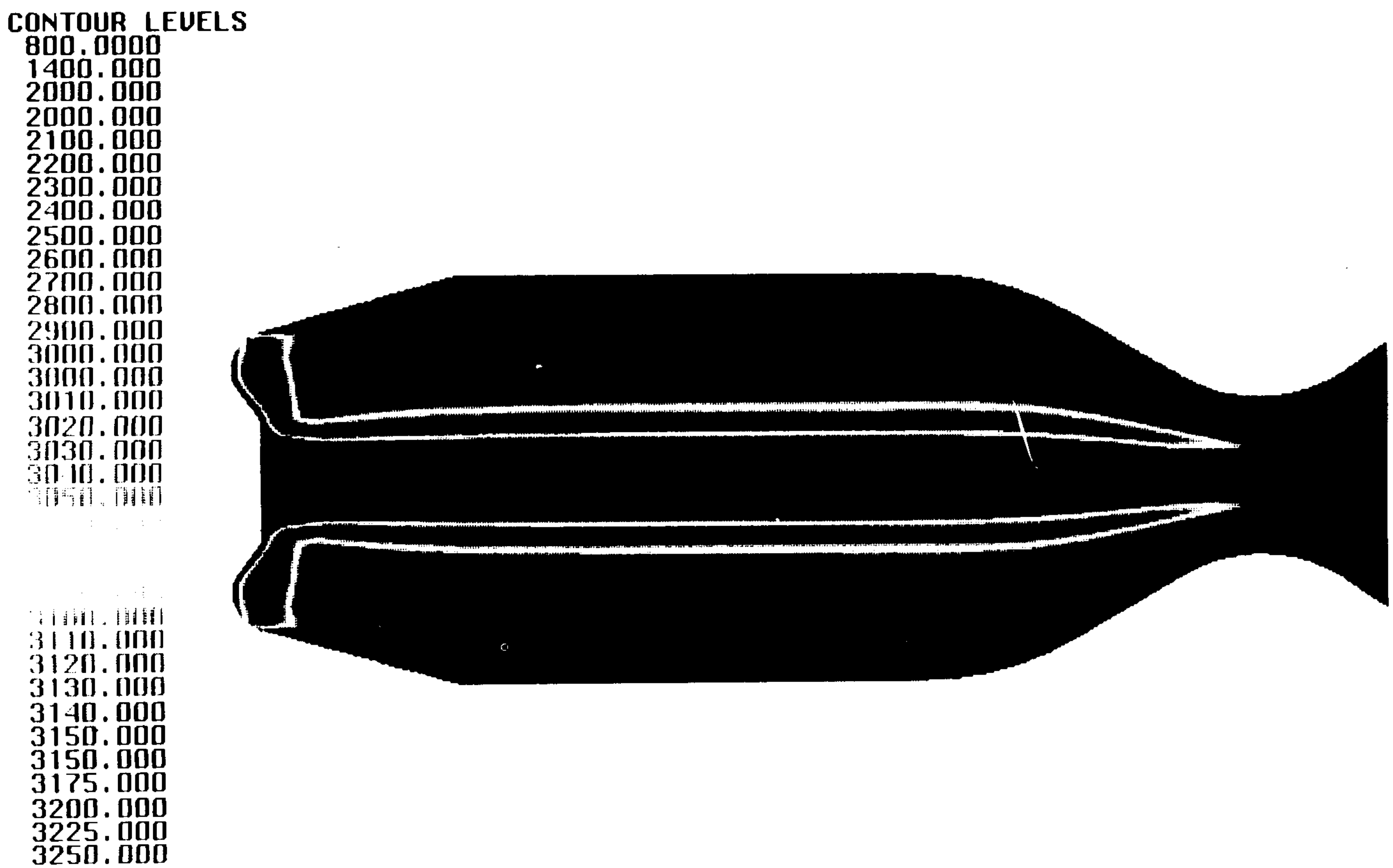

ATOMIZATION MODELS

CFDRC

Meyers Model

- Energy Balance at the Interface

Linear Theory

- Dispersion Relationship: Growth Rate = F (λ, r, s, Re, We)

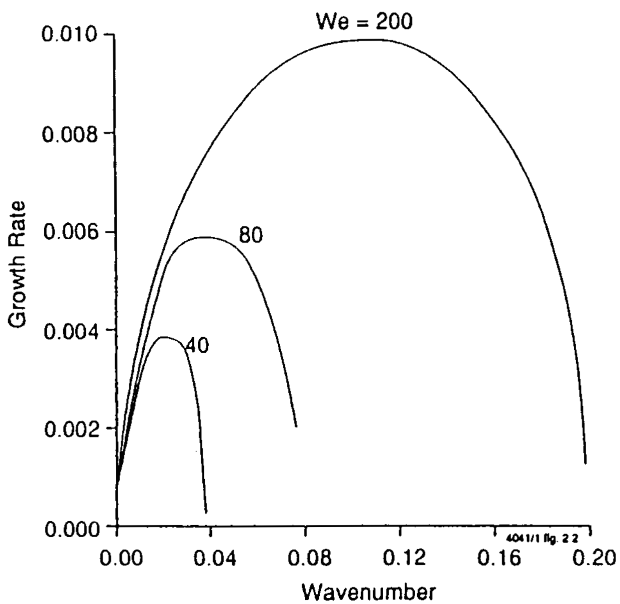

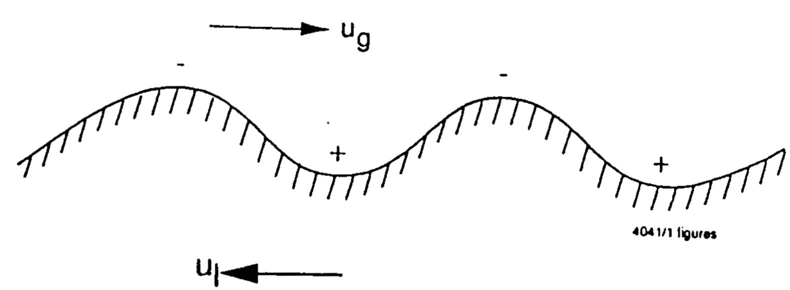

Wavy-wall Analogy

PR-92-15/14

SPRAY MODEL

CFDRC

- Improved Version of PSI-CELL Model
- Deterministic Droplet Tracking
- Coupled Droplet Source/Sink Terms for the Gas Phase
- Droplet Boundary Conditions
    - Wall - Zero Normal Momentum
    - Symmetry - Reflection

PR-92-15/15

COUPLING MODEL (jet-embedding technique)

CFDRC

LIQUID PHASE CALCULATION:

- Obtain Shape and Velocity of Intact Liquid Core

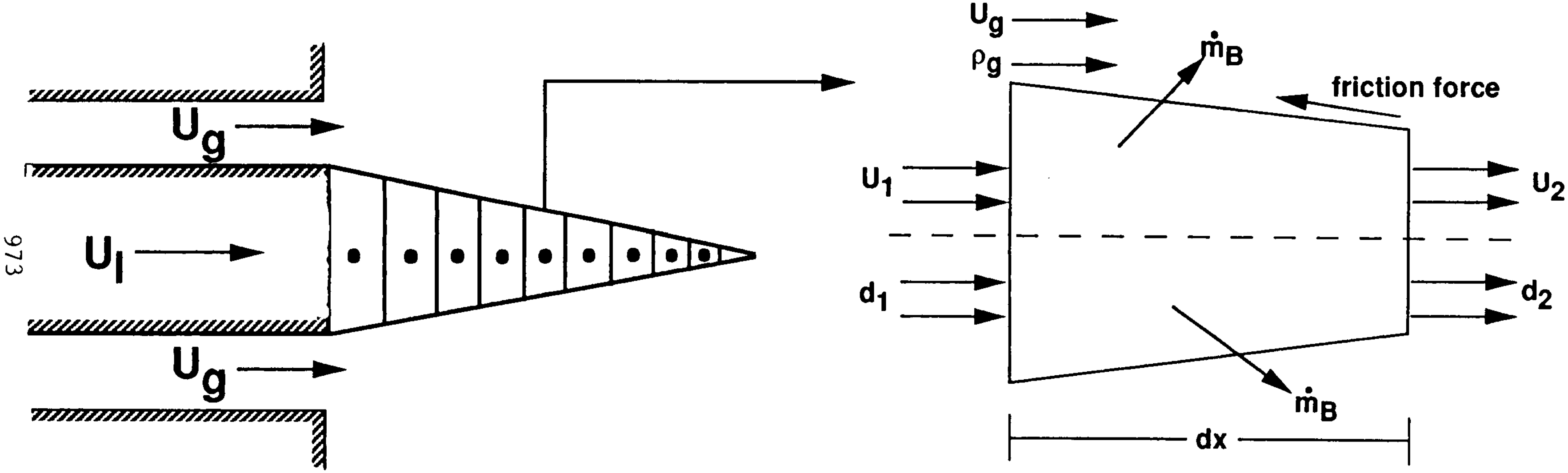

- Space-MarchingTechnique

PR-92-15/04

COUPLING MODEL

CFDRC

GAS PHASE CALCULATION:

- REFLEQS CFD Code
- Gas Phase Grid is Adapted to the Shape of the Core
- Interface Modeled as Sliding Wall
- Combustion Model:
  - Instantaneous Chemistry Model

PR 92-15/05

FLOW CHART OF COUPLING PROCEDURE

CFDRC

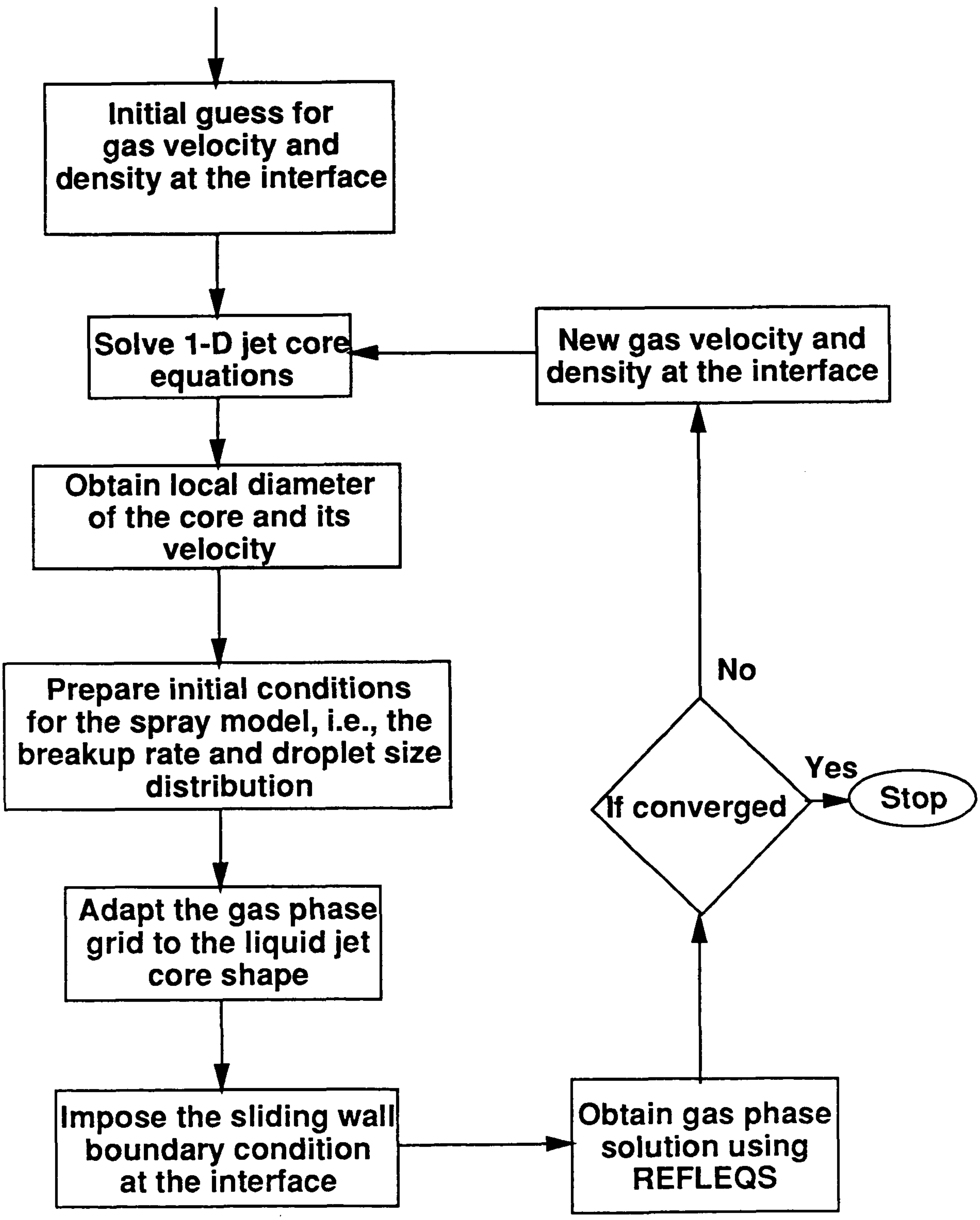

4041-09/91 prog.

PR-92-15/09

VALIDATION

CFDRC

Experimental Data

- Low Speed Water Jet Experiments by Chigier (1990)
- Reynolds Number: 1460-9300
- Weber Number: 50-200
- Jet Intact Core Length from Photographs
- Drop Size (PDPA)

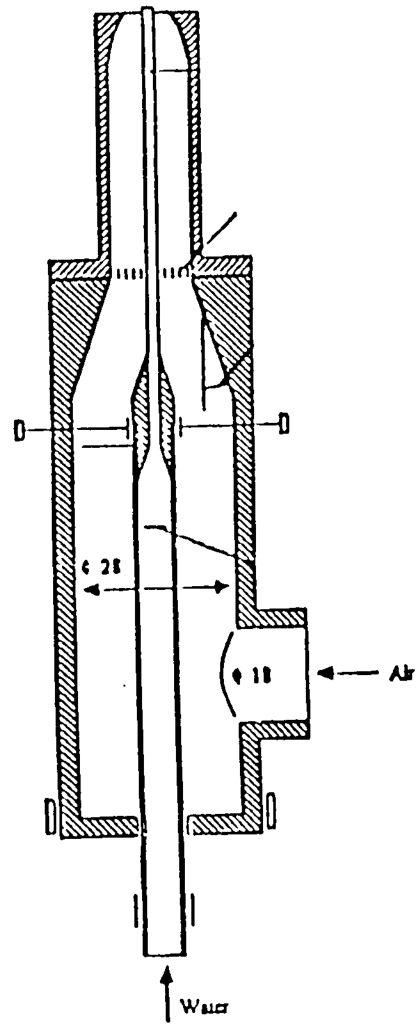

VALIDATION (CONTINUED)

Comparison of Predictions with Experimental Data

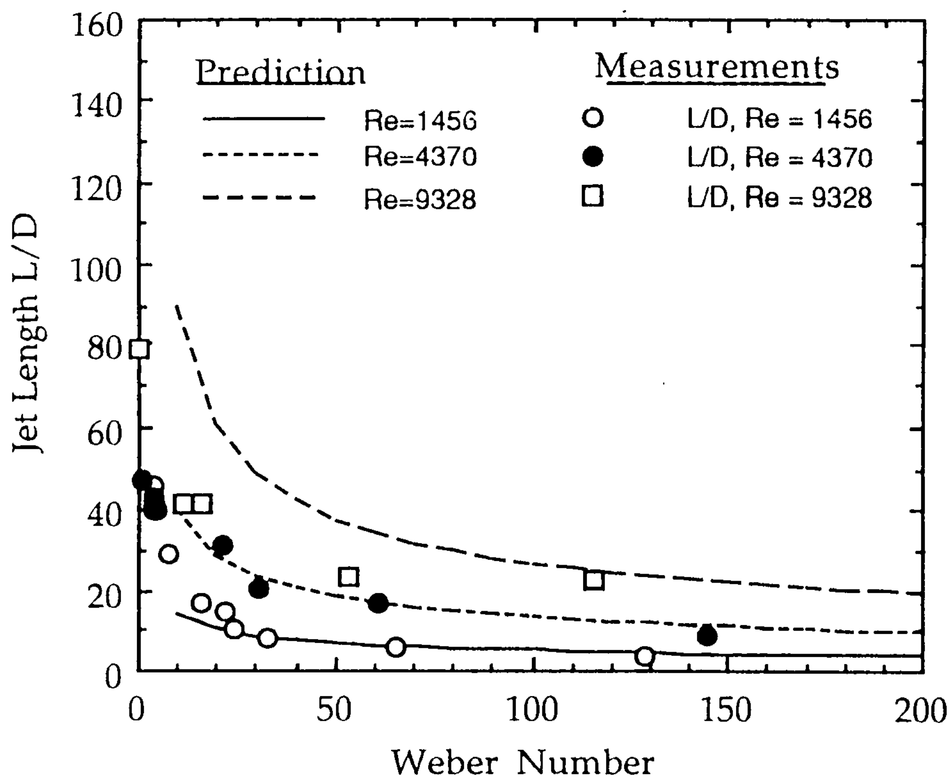

Intact Core Length

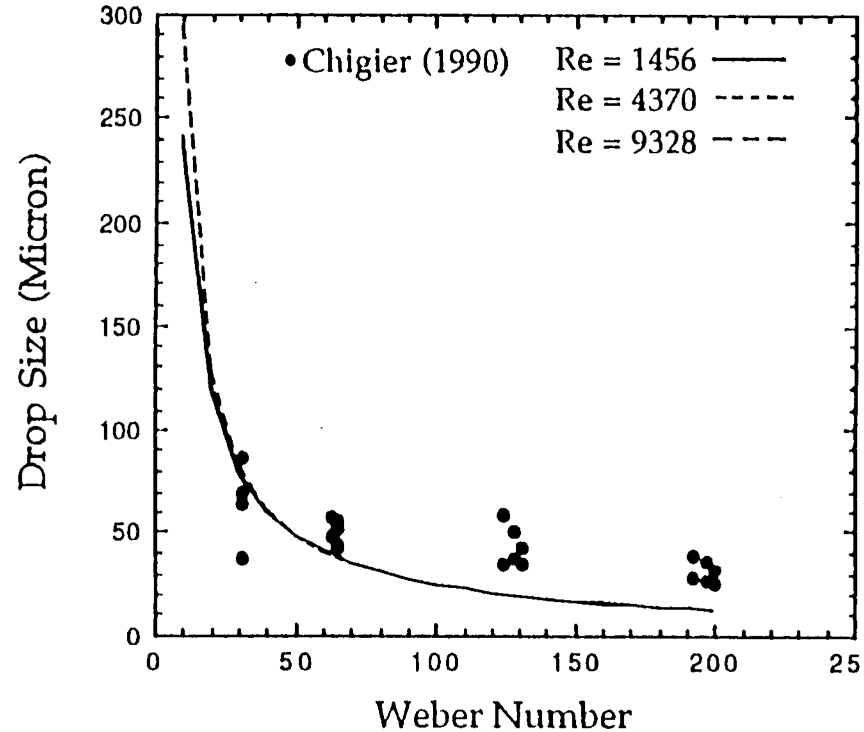

Drop Size

DEMONSTRATION CASE

CFDRC

SSME Preburner Flow Field

Operating Condition

	Oxidizer (LOX)	Fuel (GH_2)
$\dot{m}$, kg/sec	0.1498	0.1805
u_o, m/sec	25	213
ρ_o, kg/m^3	1122	91
T, °K	106	70

Coaxial Injection Element

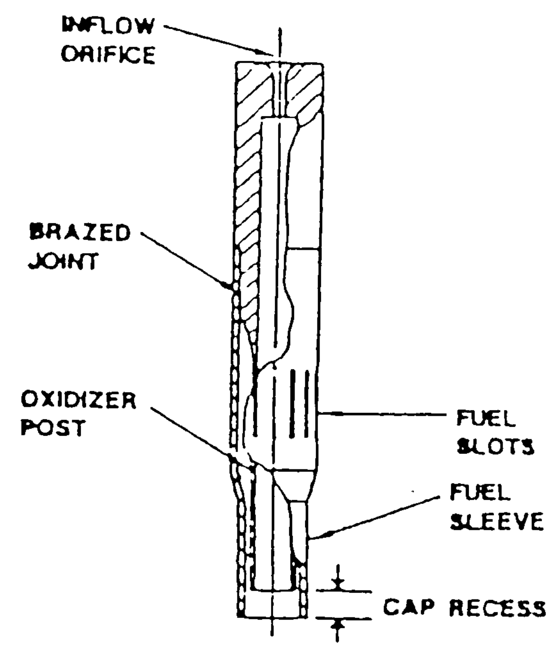

BOUNDARY CONDITIONS

CFDRC

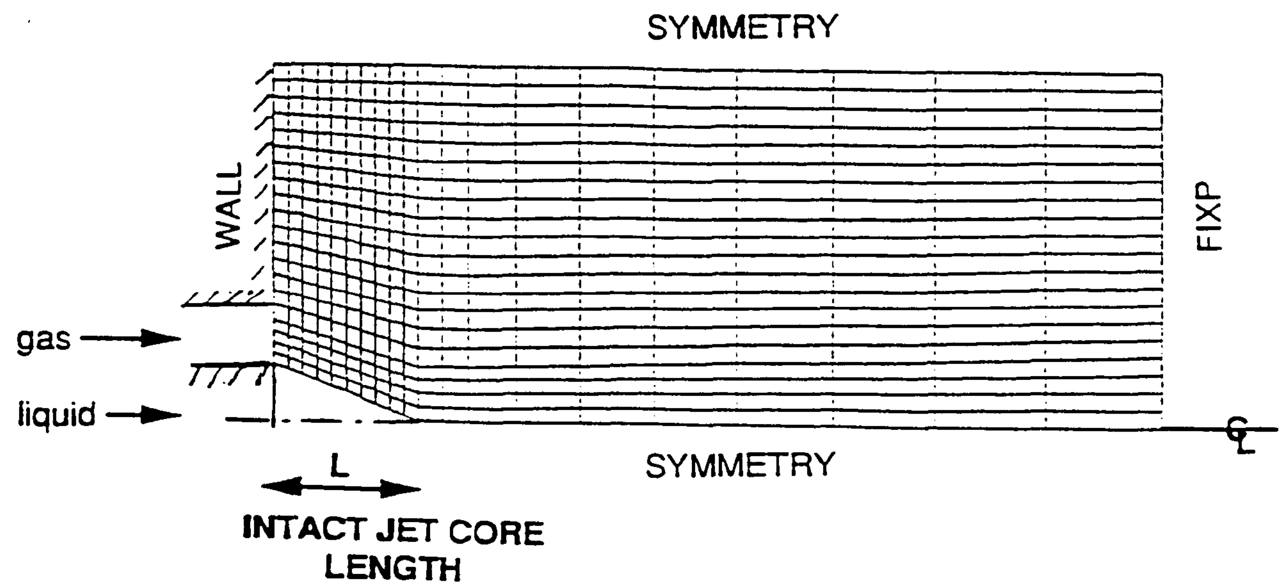

Eulerian Gas Grid
40 x 20

RESULTS

CFDRC

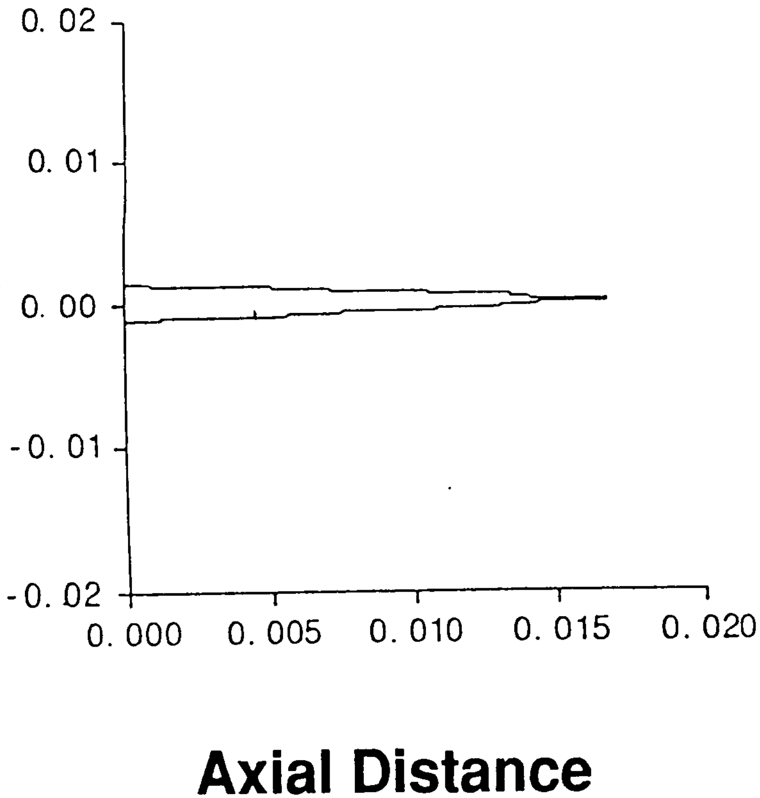

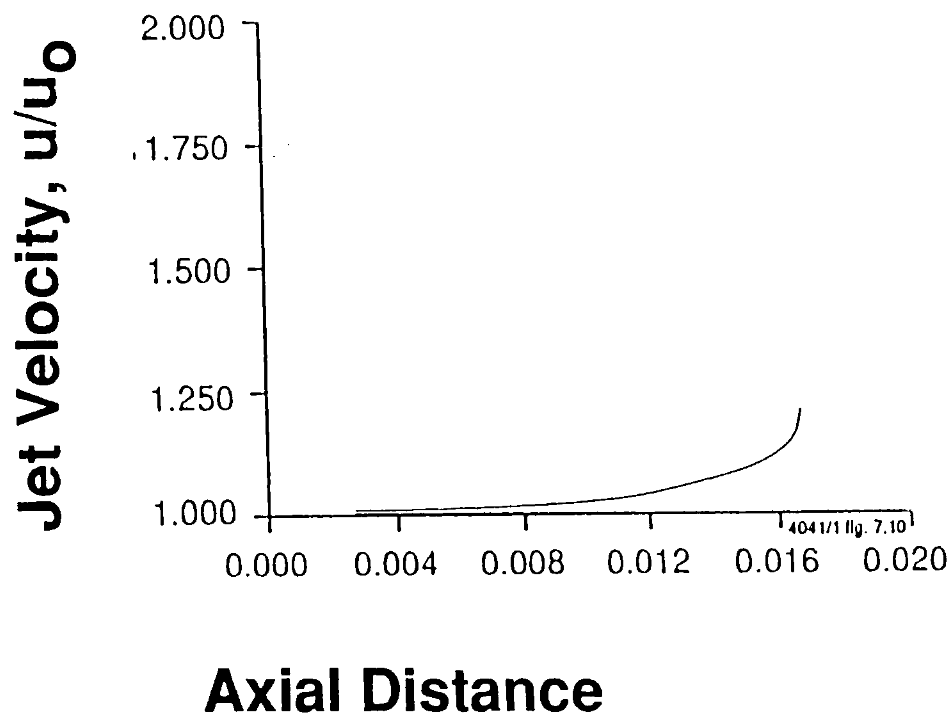

RESULTS (CONTINUED)

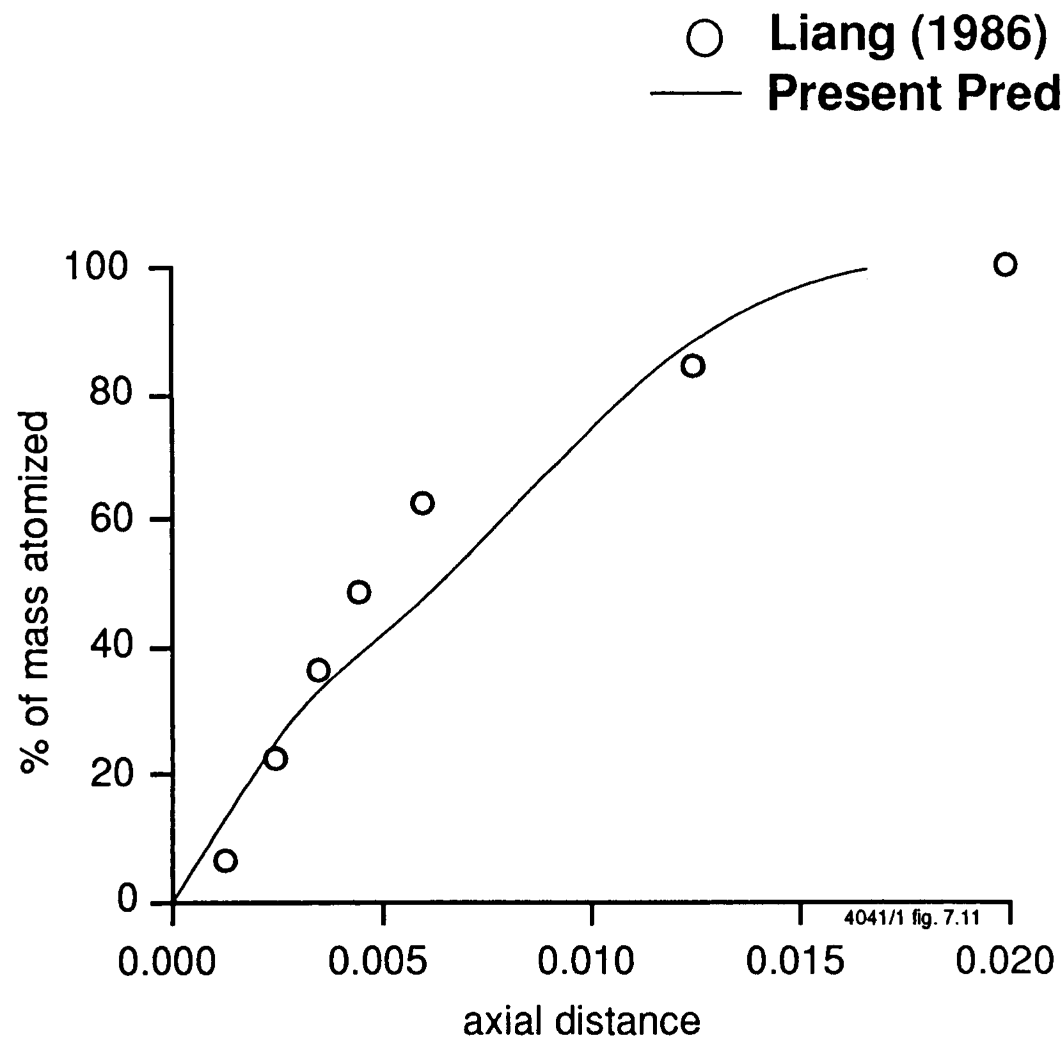

Ug = 200.0 m/s, Ul = 25.0 m/s, Tg = 200 K
(CICM Correlation)

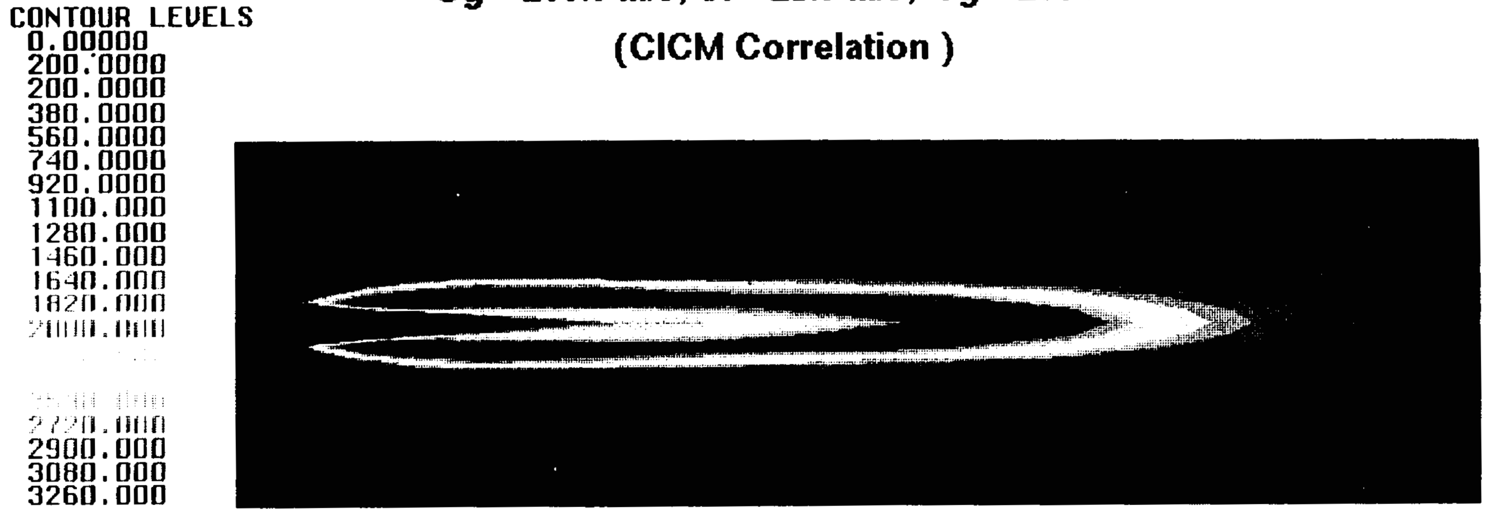

Temperature Distribution

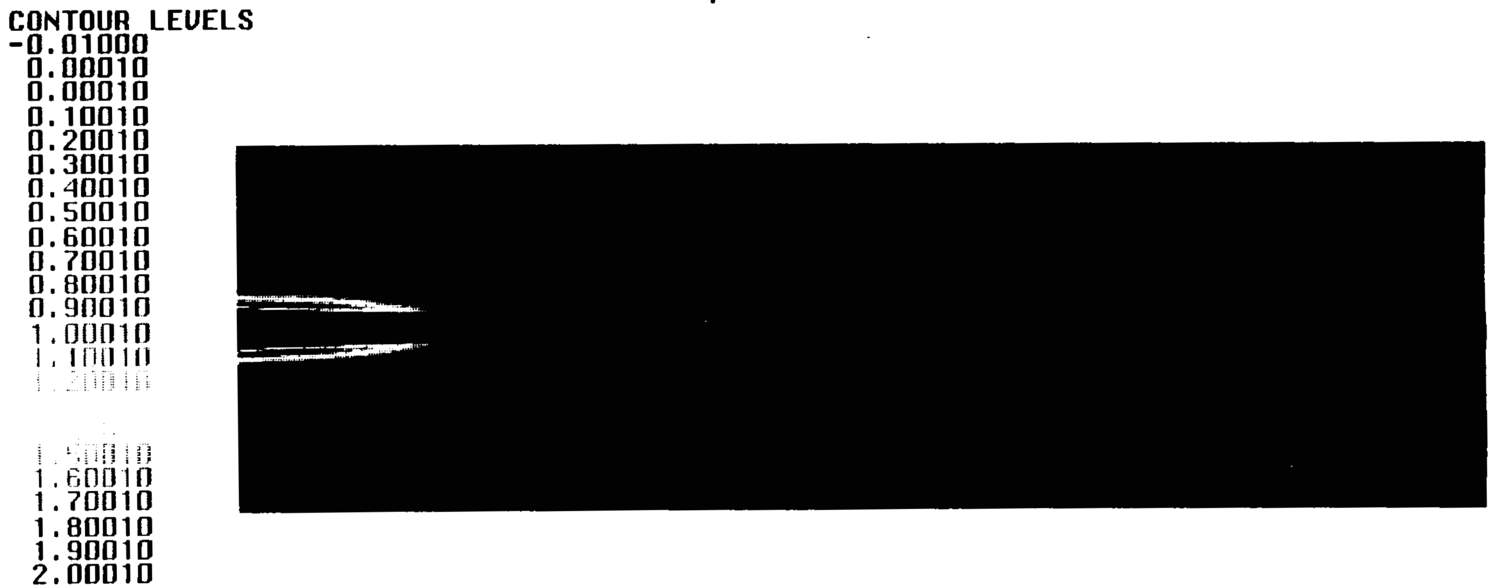

Oxygen Mass Source (gms/sec) Distribution

ORIGINAL PAGE IS
OF POOR QUALITY

Ug = 200.0 m/s, Ul = 25.0 m/s, Tg = 200 K

(Linear Surface Wave Model)

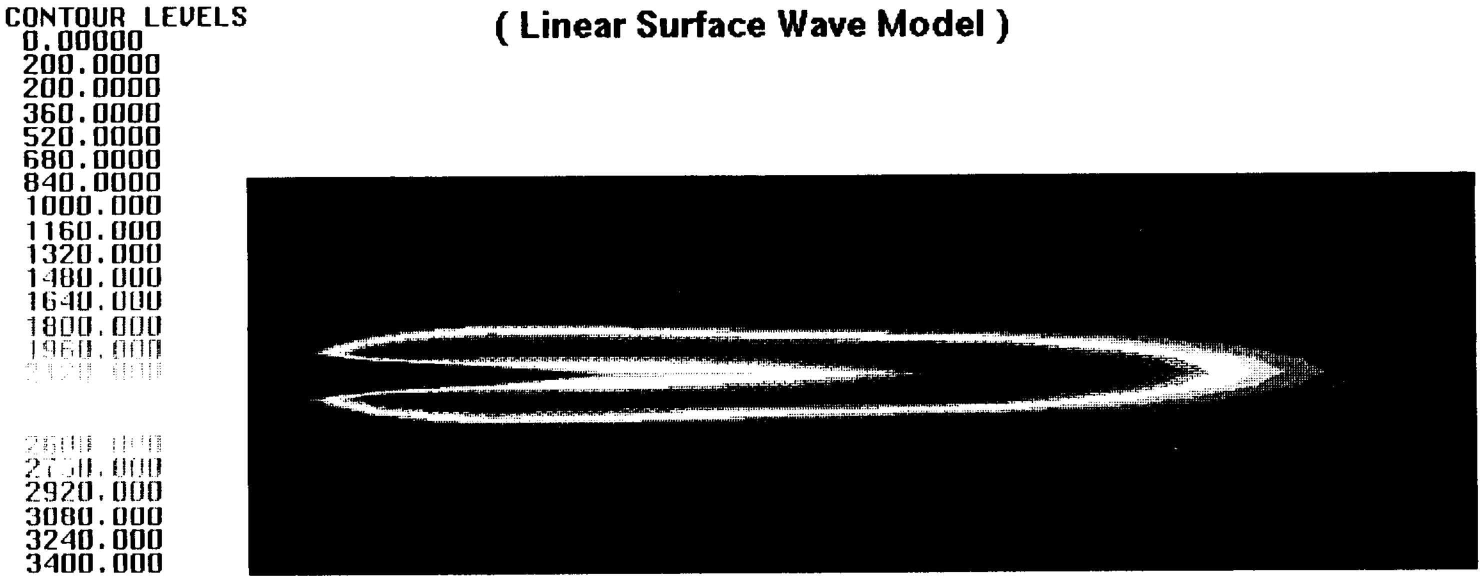

Temperature Distribution

Oxygen Mass Source (gms/sec) Distribution

Ug = 150.0 m/s, Ul = 25.0 m/s, Tg = 200 K

(CICM Model)

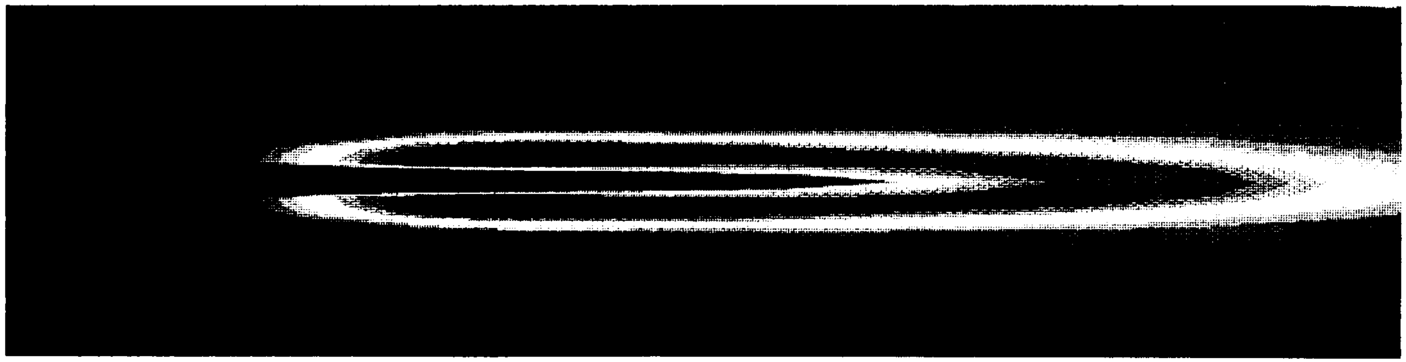

Temperature Distribution

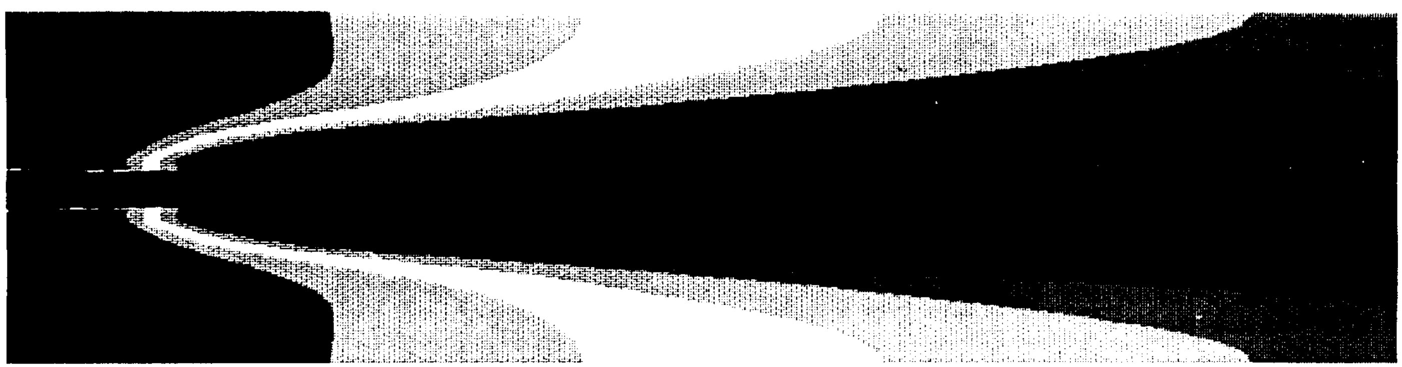

Passive Scalar (Hydrogen) Concentration Distribution

CONCLUSIONS

CFDRC

- Developed a New Jet-Embedding Technique to Couple Atomization and Spray Models
- Predictions have been Validated with Water Jet Data
- Coupling Model has been Successfully Employed to SSME Single Injector Flow and Could be Extended to Multi-Injector Flow
- Computationally Efficient Tool for Rocket Injector Flow Analysis

Numerical Modeling for Dilute and Dense Sprays

C.P. Chen, Y.M. Kim, H.M. Shang, and J.P. Ziebarth
University of Alabama in Huntsville

T.S. Wang
NASA Marshall Space Flight Center

Abstract

Numerical modelings of fuel-droplet spray combustion finds useful applications for the assessment of the engine performance & stability characteristics. With our on-going studies on turbulent reacting flows, we have successfully implemented a numerical model for spray-combustion calculations. In this model, the governing gas-phase equations in Eulerian coordinate are solved by a time-marching multiple pressure correction procedure based on the operator-splitting technique. The droplet-phase equations in Lagrangian coordinate are solved by a stochastic discrete particle technique. In order to simplify the calculation procedure for the circulating droplets, the effective conductivity model is utilized. This vaporization model includes the effects of variable thermophysical properties, non-unitary Lewis number in the gas-film, the Stefan flow effect, and the effect of internal circulation and transient liquid heating. The $k - \epsilon$ models are utilized to characterize the time and length scales of the gas-phase in conjunction with turbulent modulation by droplets and droplet dispersion by turbulence. This method entails random sampling of instantaneous gas flow properties and the stochastic process requires a large number of computational parcels to produce the satisfactory dispersion distributions even for rather dilute sprays.

The present study has made two major improvements in spray combustion modelings. Firstly, we have developed a probability density function approach in multi-dimensional space to represent a specific computational particle. Advantages of a parcel PDF tracking method is to reduce the number of computational parcels representing the spray dynamics as well as to obtain grid- independent solutions for two-phase flows. Secondly, we incorporate the TAB Taylor Analogy Breakup model for handling the dense spray effects. These breakup models is based on the reasonable assumption that atomization and drop breakup are indistinguishable processes within a dense spray near the nozzle exit. Accordingly, atomization is prescribed by injecting drops which have a characteristic size equal to the nozzle exit diameter.

Example problems include the nearly homogeneous and inhomogeneous turbulent particle dispersion, and the non-evaporating, evaporating, and burning dense sprays. Comparison with experimental data will be discussed in detail.

NUMERICAL MODELING FOR DILUTE AND DENSE SPRAYS

Y.M. Kim, H.M. Shang, C.P. Chen, and J.P. Ziebarth
University of Alabama in Huntsville
and
T.S. Wang
NASA/Marshall Space Flight Center

10th Workshop for CFD Applications in Rocket Propulsion
April 28-30, 1992
NASA/Marshall Space Flight Center

MOTIVATION

- To attain a prediction capability to assess the performance and the stability characteristics of liquid-fueled engines.
- To appraise the physical submodels as well as to evaluate numerical procedures for prediction of spray-combusting flows.
- To gain fundamental understanding of the effects of vaporization, swirl, initial size distribution, and droplet dispersion.
- To provide reliable distribution of drop size and velocity.
- To develop an efficient, accurate, and stable numerical model spray combustion.

APPROACH

- Stochastic Particle Tracking Technique
  - Delta function stochastic separated flow(SSF) model
  - Deterministic dispersion width transport(DDWT) model
  - Stochastic dispersion width transport(SDWT) model
- Incorporation of Dense Spray Effects
  - Taylor analogy breakup(TAB) model.
  - Drop collision and coalescence model
- Eulerian-Lagrangian Formulation
  - Multiple pressure correction
  - Non-iterative for transient calculation
  - Applicable to all-speed flows

ISSUES

- Turbulene effects on droplets and turbulece modulation by droplets.
- Incorporation of dense spray effects and primary atomization model.
- Vaporization at subcritical and supercritical condition.
- Numerical accuracy, stability, and efficiency for the fast transient spray-combusting flows.

GROUP/WIDTH DISPERSION MODEL

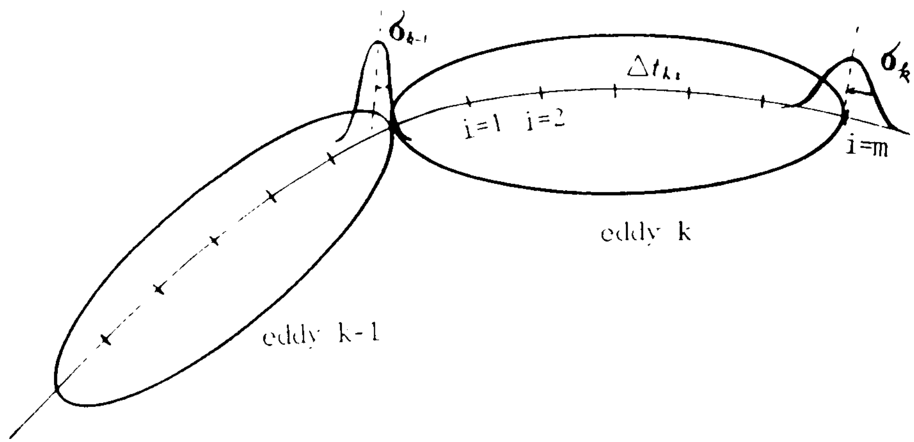

Turbulence-induced displacement and velocity:

$$\frac{dv'_k}{dt} = \frac{u'_k - v'_k}{\tau_k}$$

$$\frac{dx'_k}{dt} = v'_k$$

Particle fluctuating locations and velocities:

$$x'_{ki} = u'_{krms}\Delta t_{ki} + (v'_{k(i-1)} - u'_{krms})\tau_{k(i-1)}(1 - e^{\frac{-\Delta t_{ki}}{\tau_{k(i-1)}}})$$

$$v'_{ki} = u'_{krms} + (v'_{k(i-1)} - u'_{krms})e^{\frac{-\Delta t_{ki}}{\tau_{k(i-1)}}}$$

Time step to interact with k^{th} eddy:

$$\sum_{i=1}^{m} \Delta t_{ki} = \Delta t_k$$

Variance of a computational particle pdf within the k^{th} eddy:

$${\sigma_k}^2 = {\sigma_{k-1}}^2 + \left(\sum_{i=1}^{m} {x'}_{ki}\right)^2$$

Normalized particle variance:

$$\hat{\sigma}_{yk} = K \frac{\sigma_{yk}}{\sqrt{N_t}}$$

$\frac{\sigma_{yk}}{\sqrt{N_t}}$ = **statistical uncertainty in the mean particle position**
K = **correction factor to account for undersampling**
N_t = **total number of computational particles**
σ_{k-1} = **existing variance of the particle pdf**

Cumulative pdf distribution at any point in coordinate y:

$$P(y) = \int_{-y}^{y} \frac{1}{\sqrt{2\pi}\hat{\sigma}_{yk}} e^{\frac{-(y-y_p)^2}{2\hat{\sigma}_{yk}^2}} \, dy$$

Symmetric cumulative distribution function:

$$P(y) = 0.5[erf(\frac{y - y_p}{\sqrt{2}\hat{\sigma}_{yk}}) + erf(\frac{y + y_p}{\sqrt{2}\hat{\sigma}_{yk}})]$$

Two ways to calculate the mean position of parcel:

- **Deterministic Dispersion Width Transport(DDWT) model**
- **Stochastic Dispersion Width Transport(SDWT) model**

Numerical Implementations of Collision Model

- **Mean collision rate between each pair of "parcels" coexisting in a given numerical cell:**

$$\nu = \frac{N_1}{Vol}\pi(r_1 + r_2)^2 \mid v_1 - v_2 \mid / N_2$$

- **Probability(Poisson distribution) occuring n collisions in time Δt:**

$$P_n = e^{-\overline{n}}\frac{\overline{n}^n}{n!} \quad (\overline{n} = \nu\Delta t, \quad P_o = e^{-\overline{n}} \quad : \quad probability \ \ of \ \ no \ \ collision)$$

- **Stochastic collision sampling procedure:**

$$XX < P_o \Rightarrow \quad no \ \ collision$$

$$XX > P_o \Rightarrow \quad collision \ \ (collision \ \ parameter, \quad b = \sqrt{YY}(r_1 + r_2) \ \ )$$

$$b < b_{cr} \Rightarrow \quad coalescence \quad , \quad b \geq b_{cr} \Rightarrow \quad grazing \ \ collision$$

$$b_{cr} = f(drop \ \ radii, \ \ surface \ \ tension, \ \ relative \ \ velocity)$$

$$XX, \ \ YY \quad : \quad 1st \ \ and \ \ 2nd \ \ random \ \ number$$

BREAKUP MODEL

- **Taylor Analogy Breakup Model**
  - *analogy between an oscillating & distorting drop and spring-mass system*
  - *gas aerodynamic f.-surface tension f.-liquid viscous f.*
- **Two Extra Equations**(y_p, y'_p)
  - $y_p \rightarrow$ *deformation and* $y'_p \rightarrow$ *oscillation*
  - *functions of We, viscous damping time, and oscillation frequency*
- **Oscillation amplitude, frequency,** y_p**, and** $y'_p \rightarrow \mathbf{t}_{br}$

$$t^n < t_{br} < t^{n+1} \quad : \quad breakup$$

$$Energy\ \ conservation \quad \rightarrow \quad r_{32} = \frac{r}{1 + \frac{8K}{20} + \frac{\rho_l r^3}{\sigma} y'^2 \frac{(6K-5)}{120}}$$

chi – squared distribution for product drops(r_{br})

$$Mass\ \ conservation \rightarrow N^{n+1} = N^n \left(\frac{r^n}{r_{br}}\right)^3$$

random velocity components normal to the relative velocity

VALIDATION CASES

- Particle Turbulent Dispersion(Snyder et. al.)
- Particle Laden Turbulent Round Jet(Yuu et. al.)
- Non-Evaporating Solid-Cone Spray(Hiroyasu et. al.)
- Non-Evaporating Hollow-Cone Spray(Shearer et. al.)
- Evaporating and Burning Spray(Yokota et. al.)

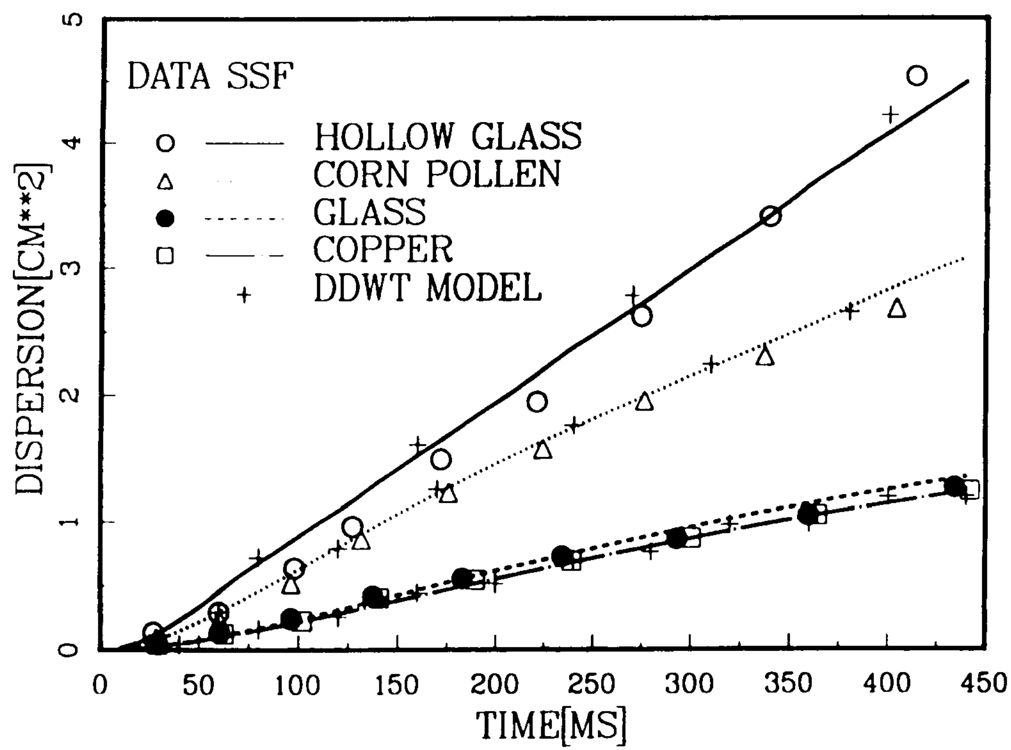

Figure 1. Particle dispersion of a nearly-homogeneous flow for SSF model(5000 particles) and DDWT model.

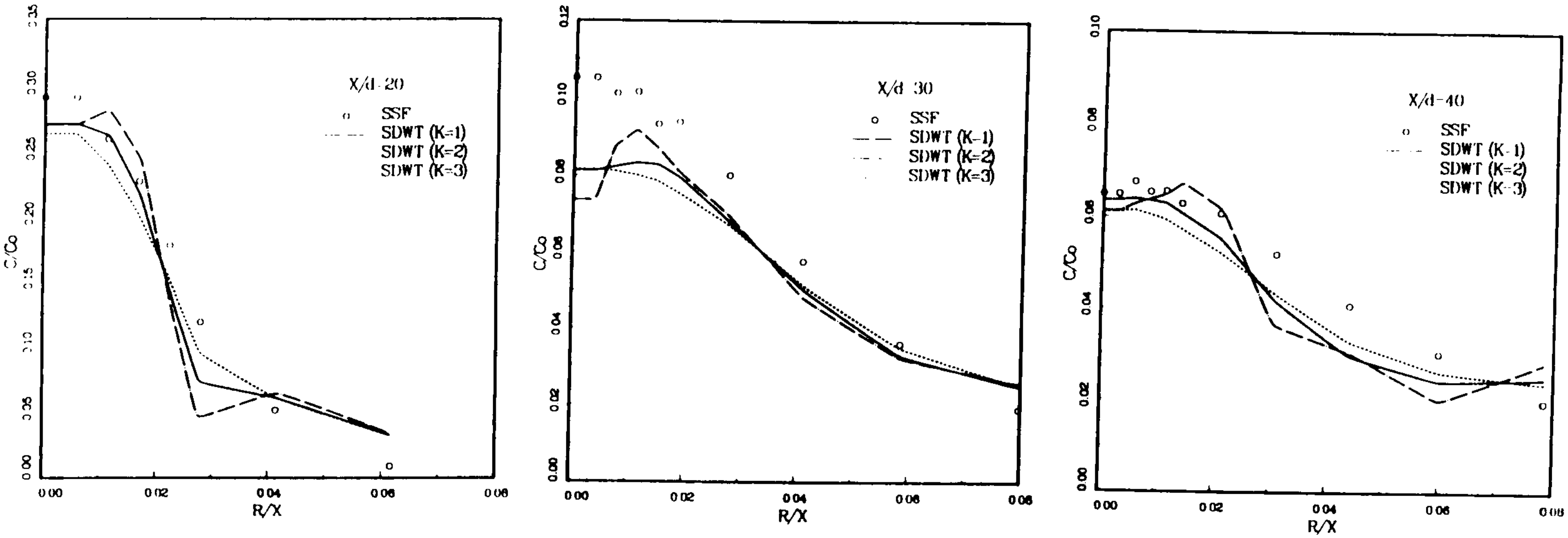

Figure 2. Normalized particle concentration distribution of particle laden round jet for SSF model(10,000 particles) and SDWT model(50 parcels) with various correction factors.

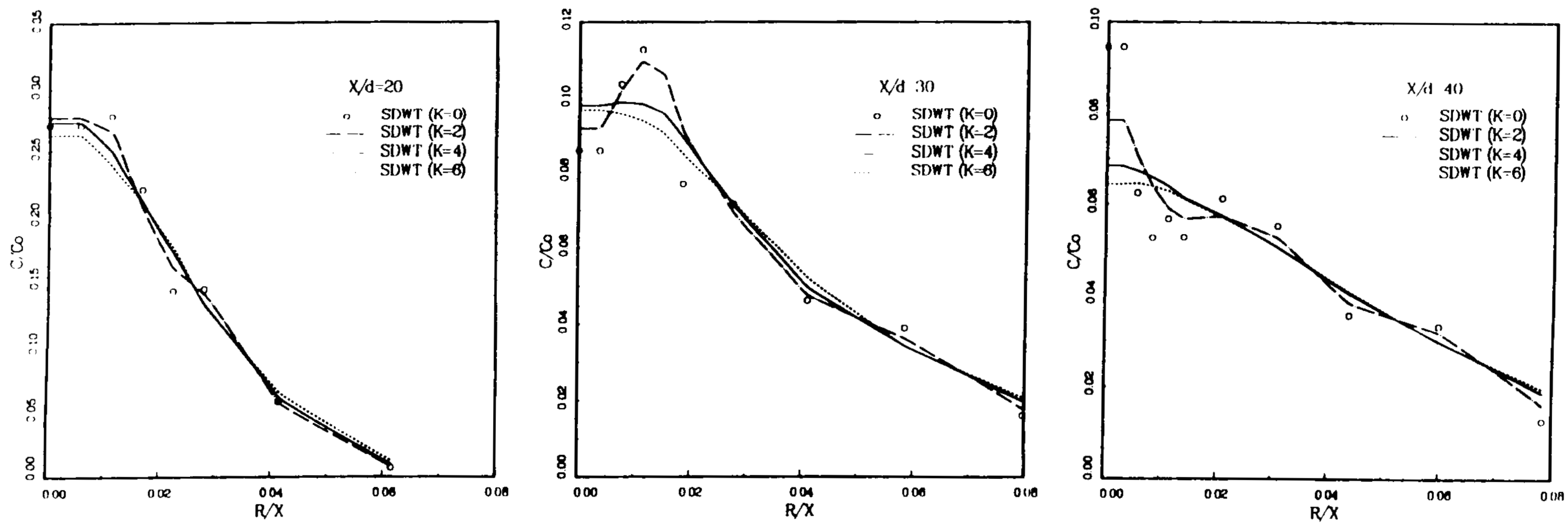

Figure 3. Normalized particle concentration distribution of particle laden round jet for SDWT model(200 parcels) with various correction factors.

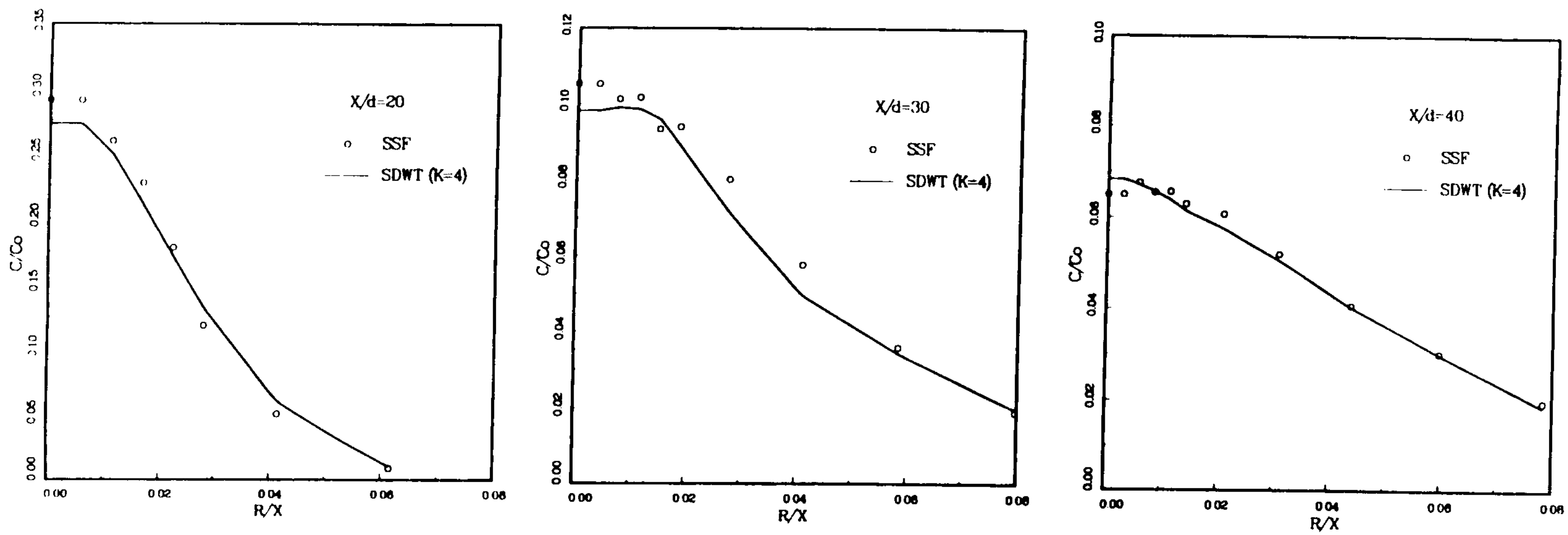

Figure 4. Normalized particle concentration distribution of particle laden round jet for SSF model(10,000 particles) and SDWT model(200 parcels).

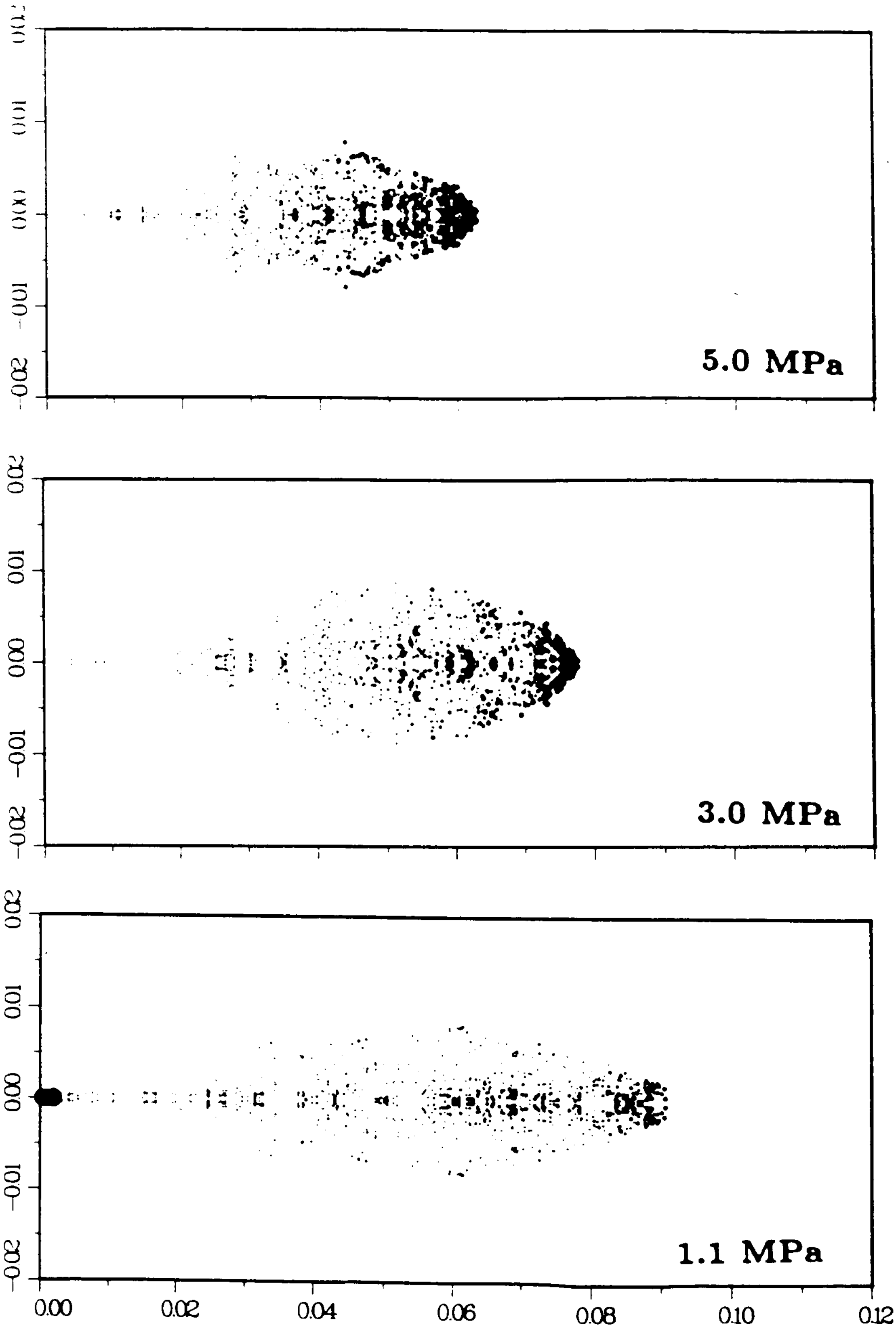

Figure 4.22 Spray parcel distribution in a solid-cone spray($t = 3.0ms$)

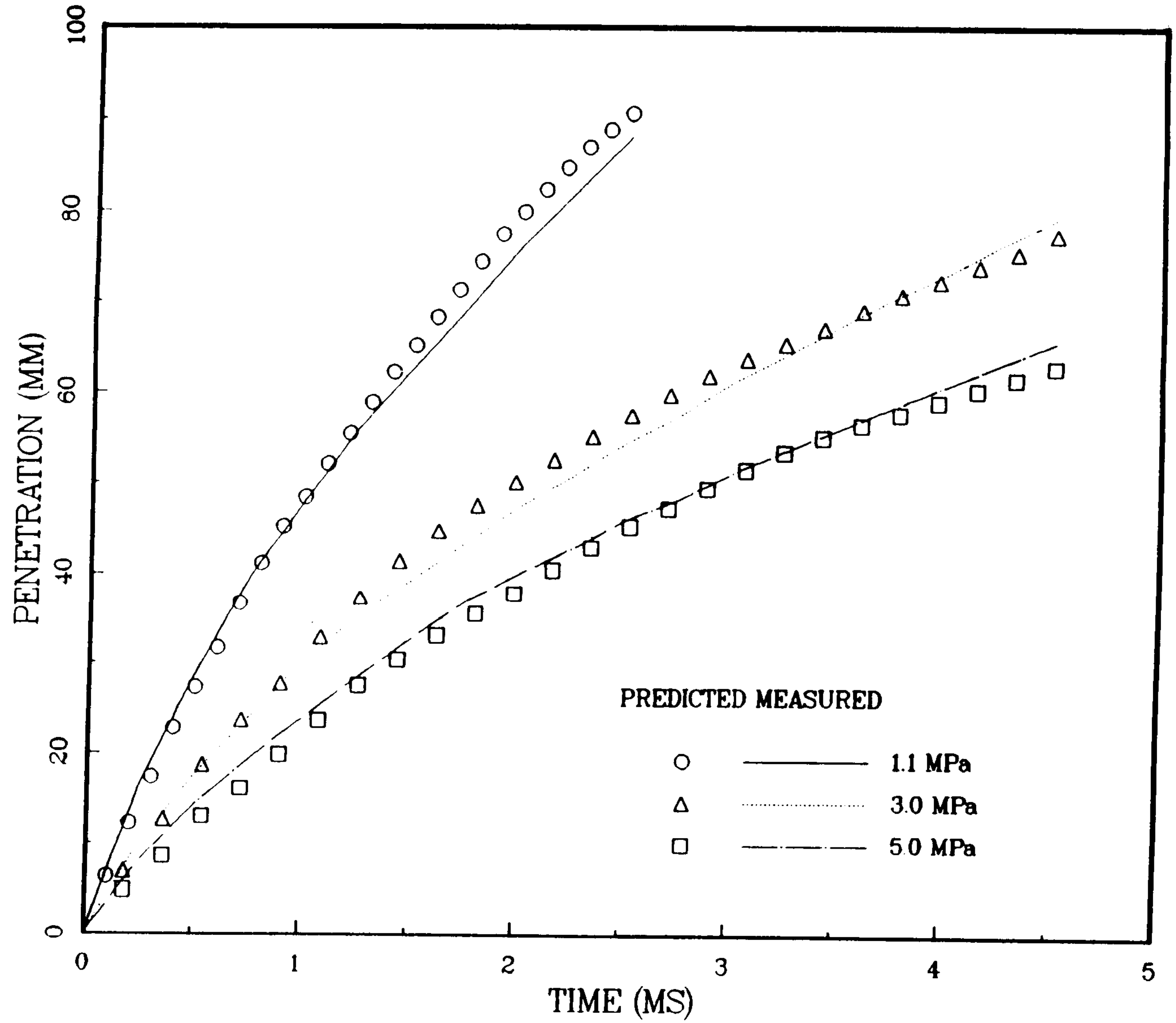

Figure 4.23 Spray tip penetration versus time in a solid-cone spray

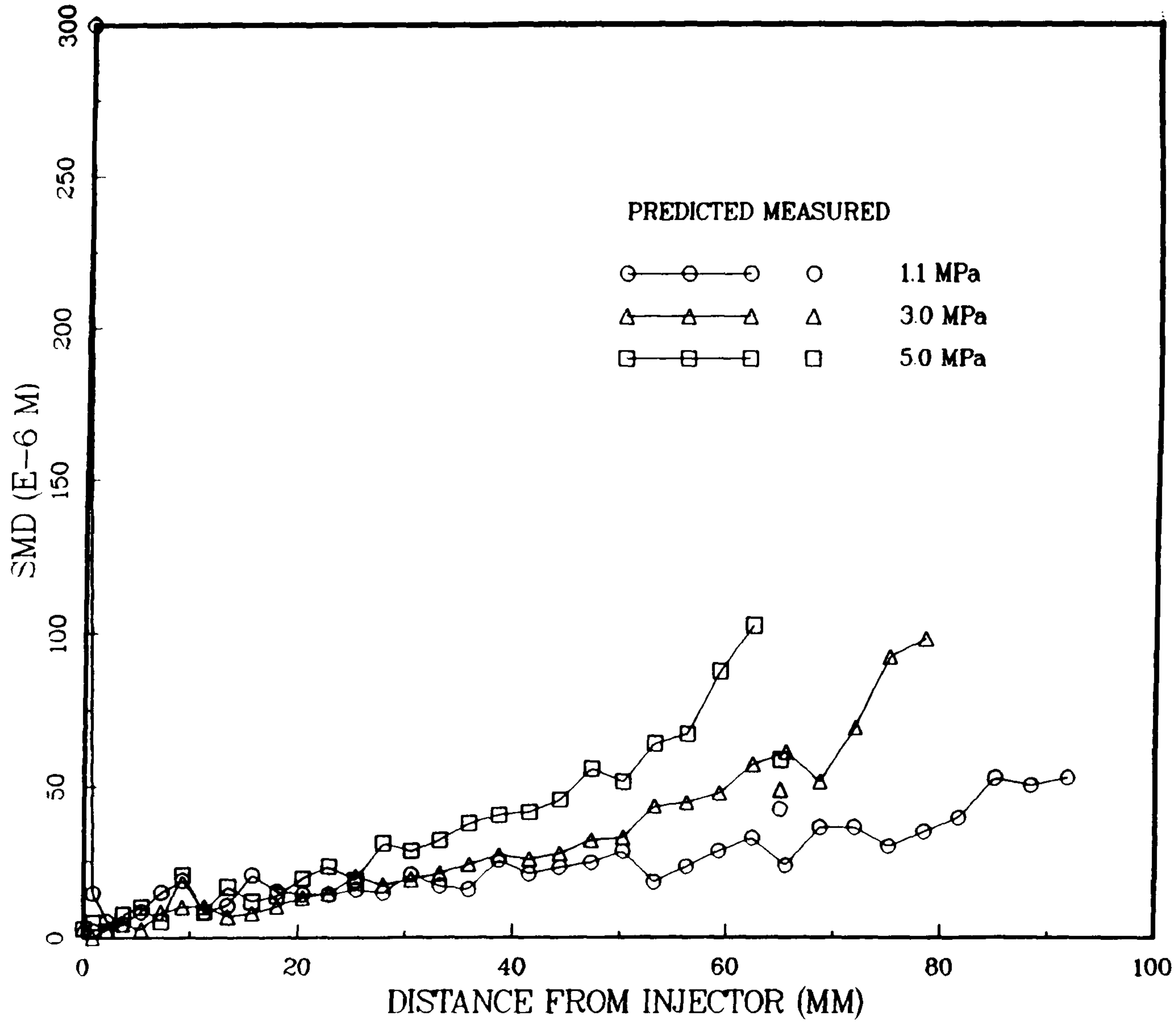

Figure 4.24 Sauter mean diameter versus distance from the injector

SAUTER MEAN DIAMETER

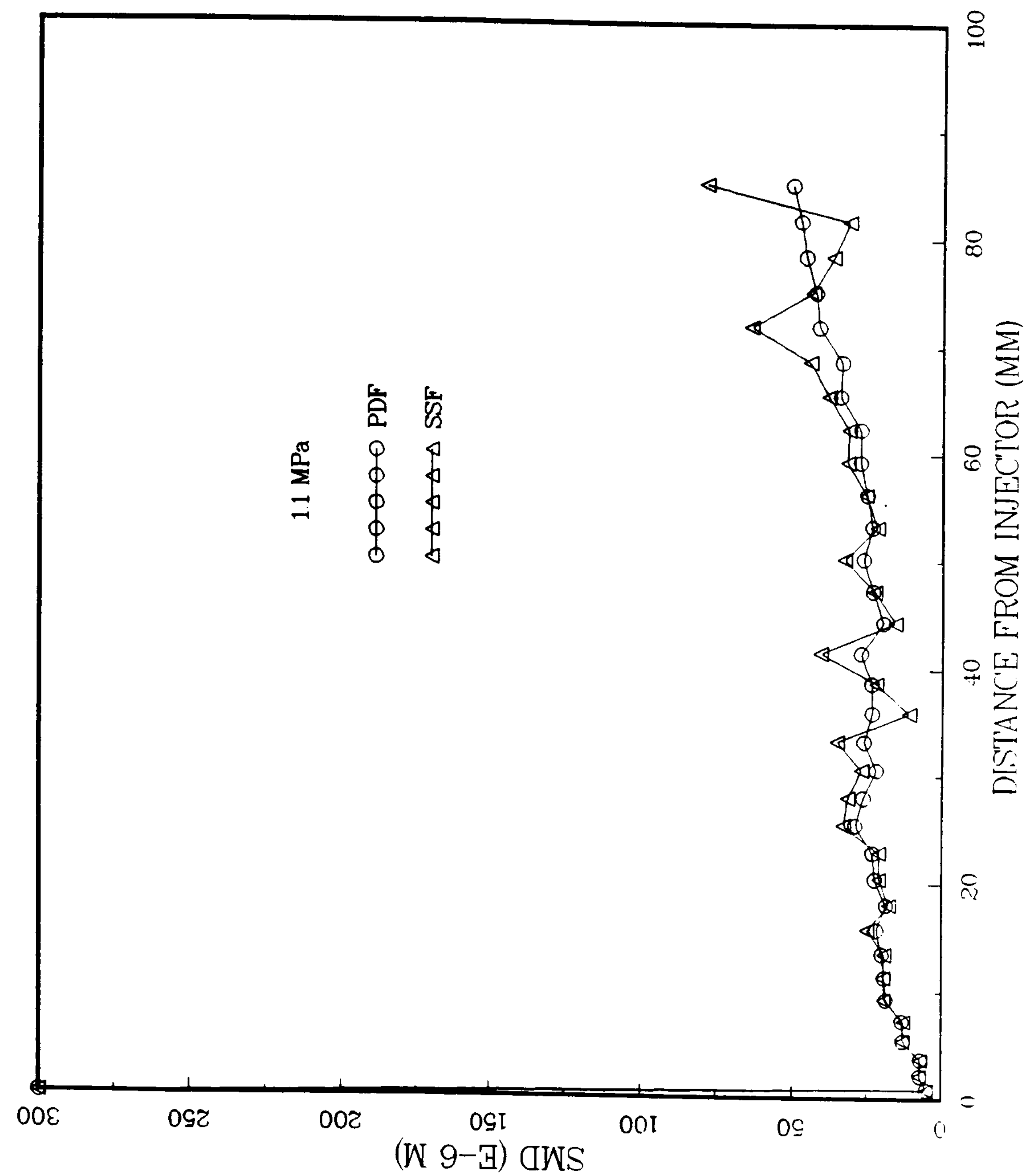

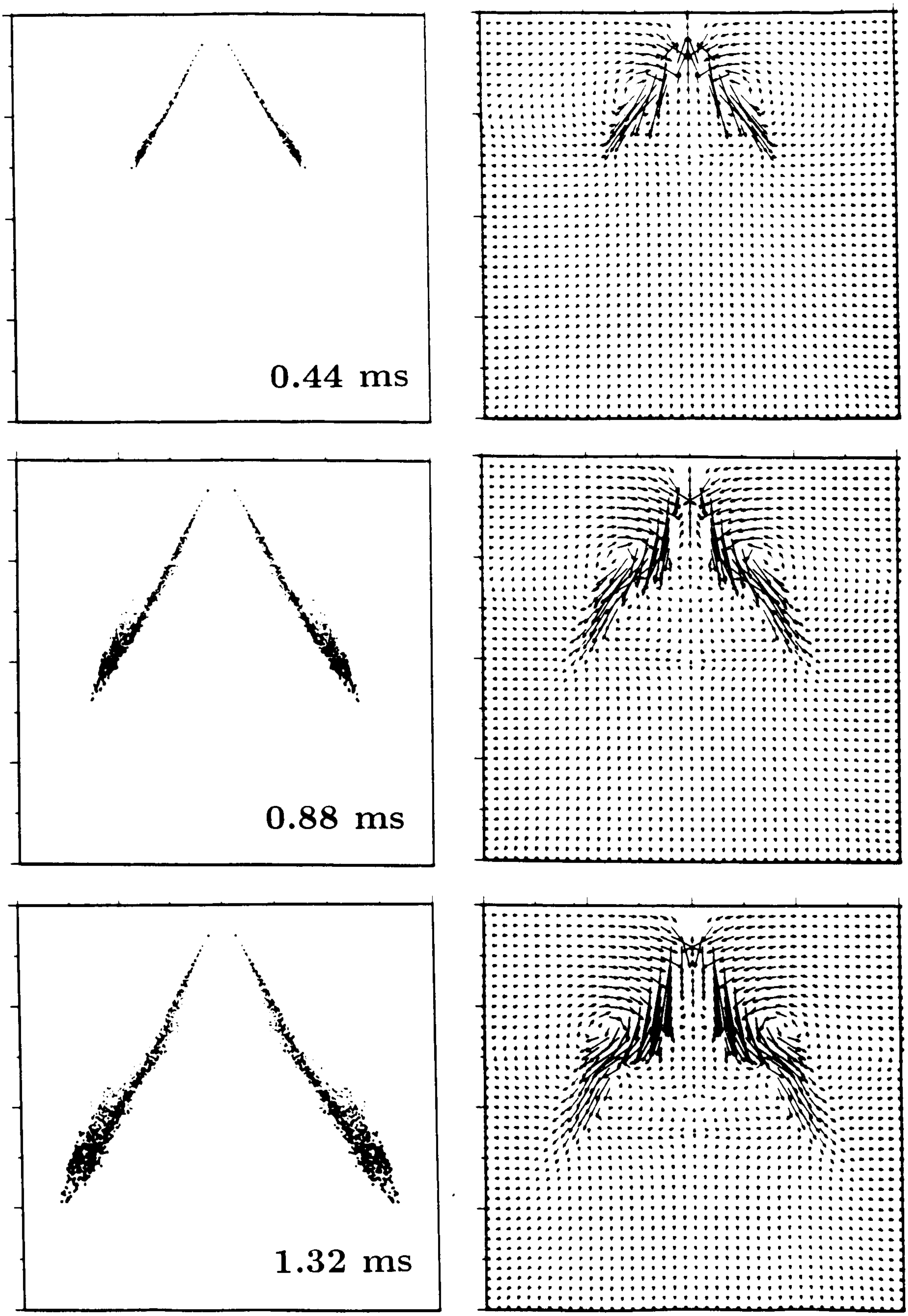

Figure 4.25 Spray parcel distribution and velocity vectors in a hollow-cone spray

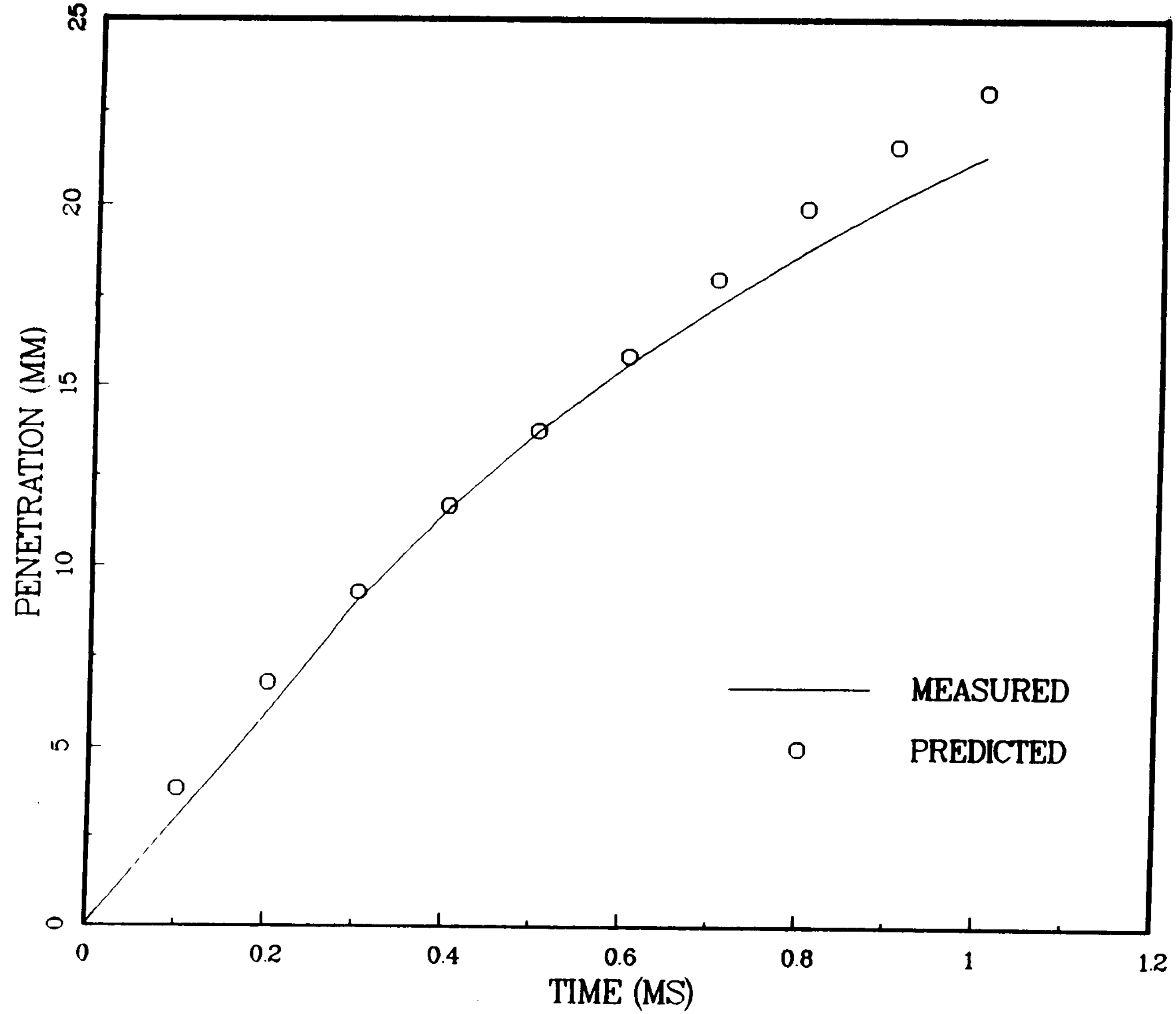

Figure 4.26 Spray tip penetration versus time in a hollow-cone spray

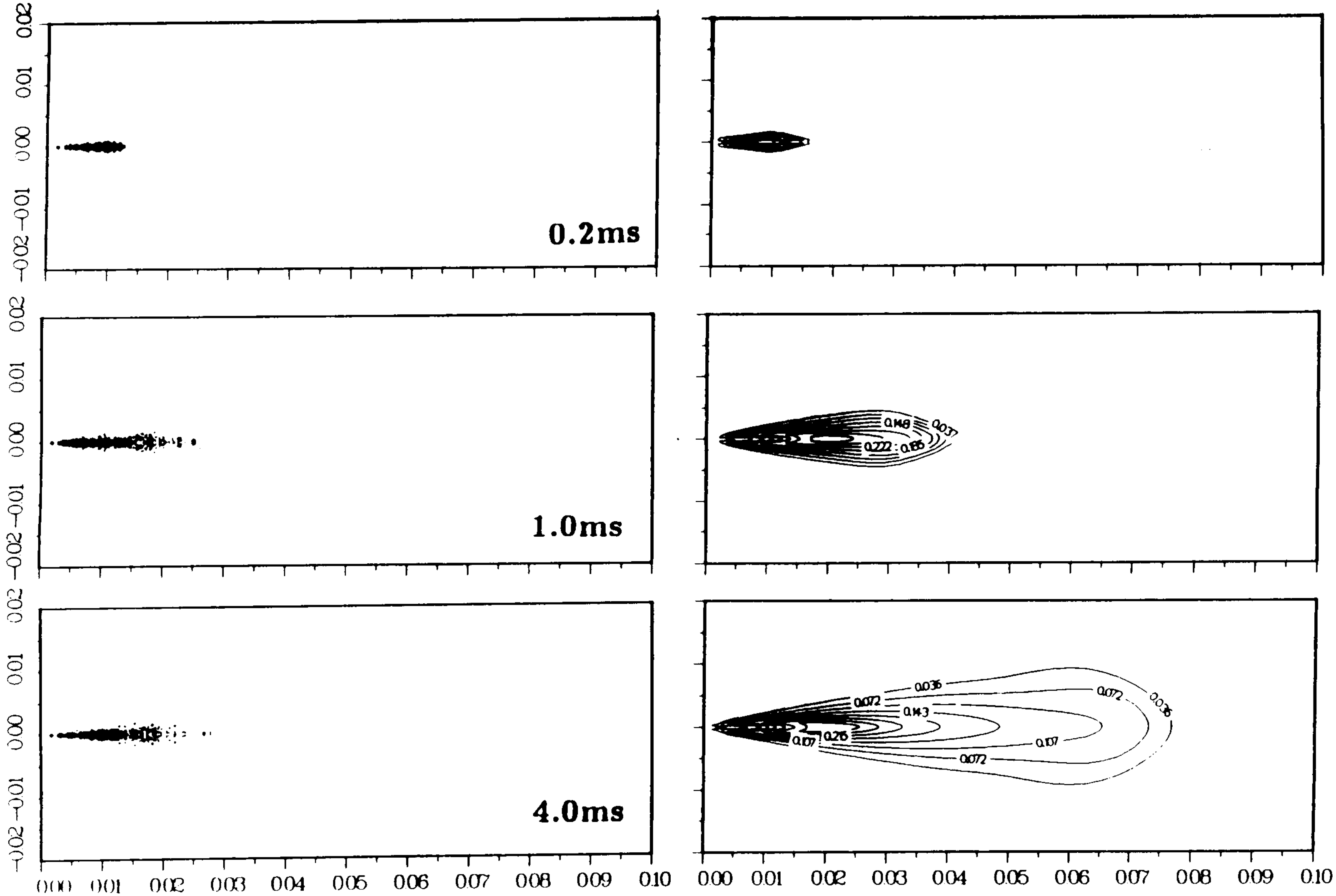

Figure 4.27 Spray parcel distribution and contours of fuel mass fraction in an evaporating spray

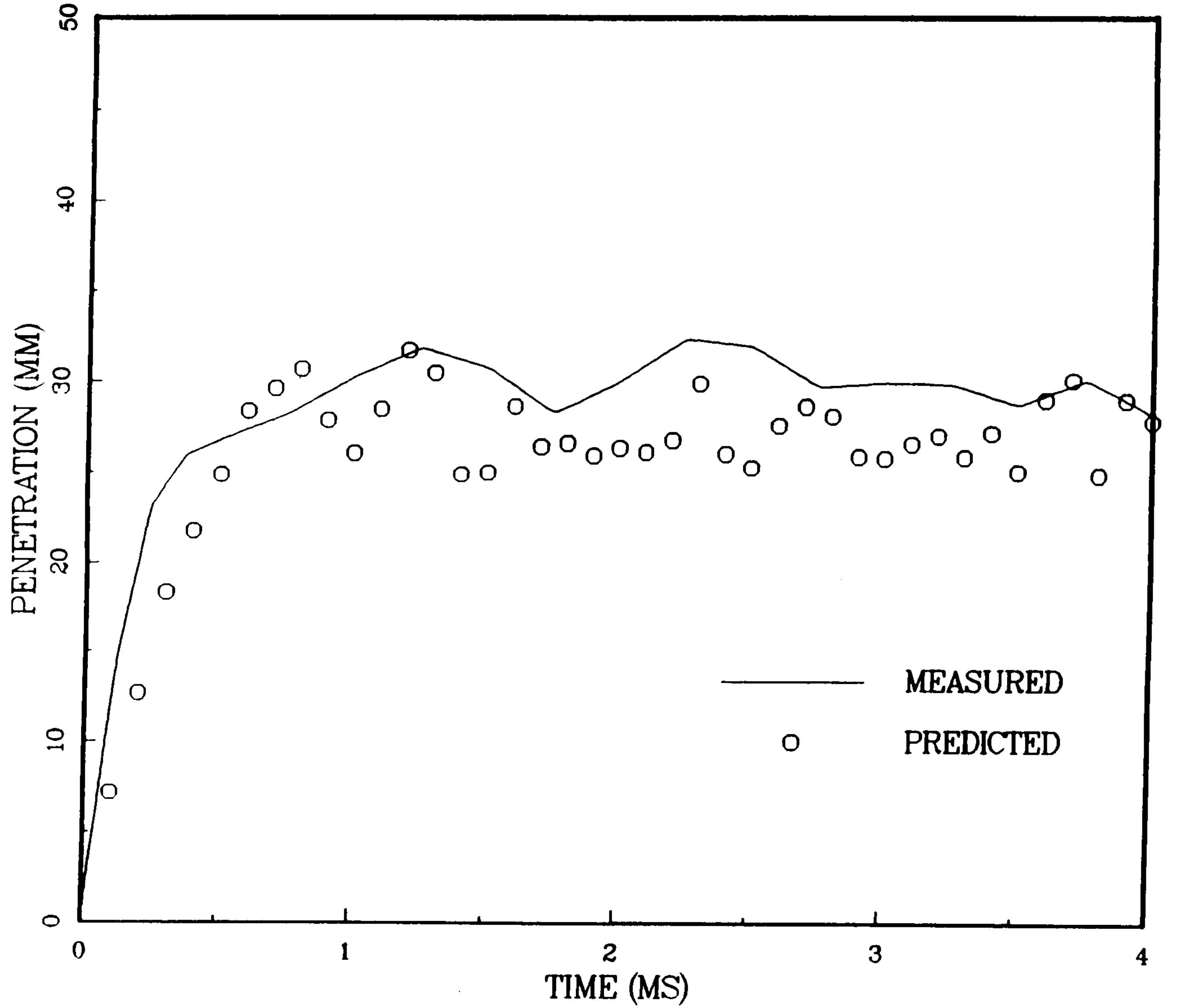

Figure 4.28 Spray tip penetration versus time in an evaporating spray

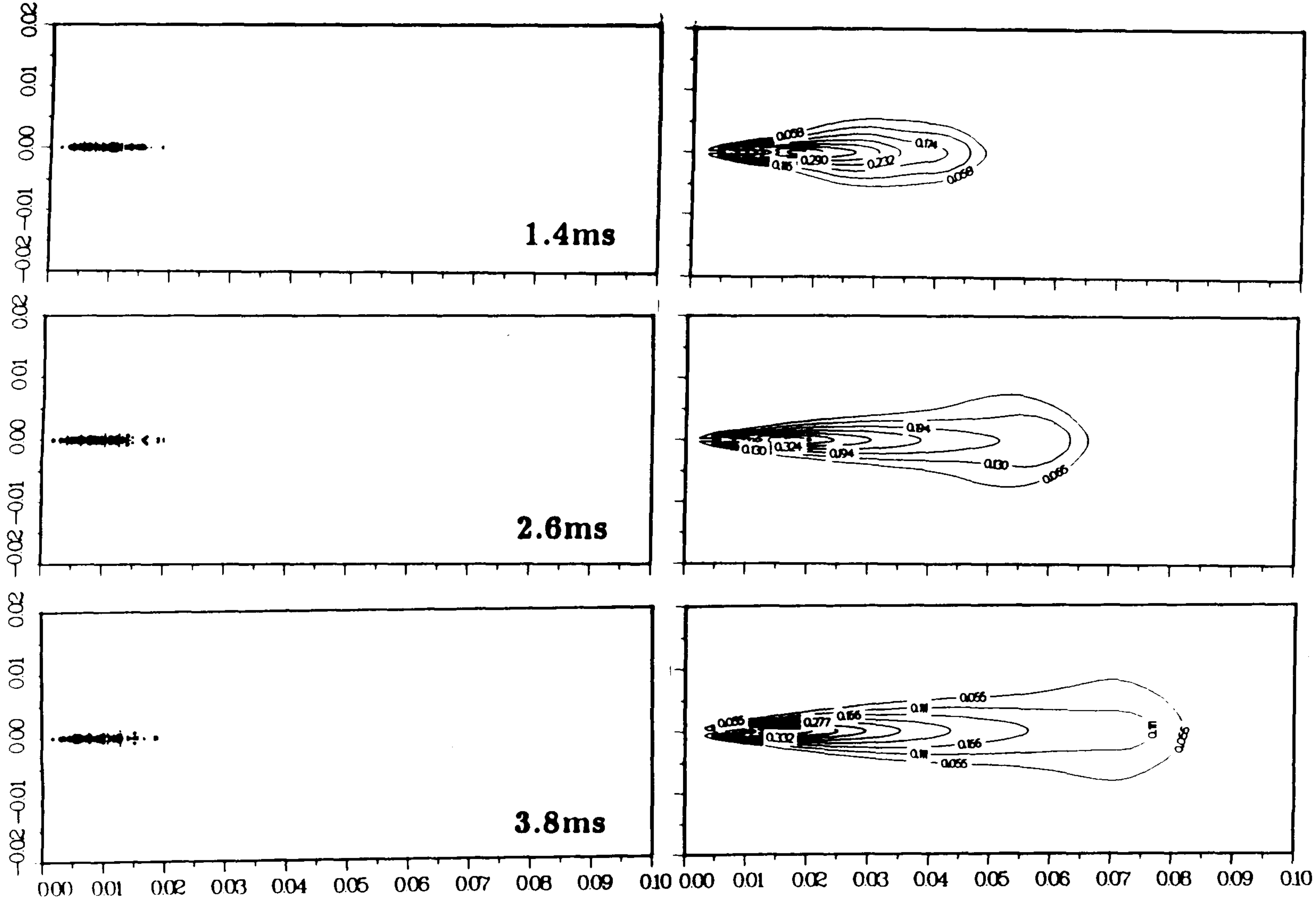

Figure 4.29 Spray parcel distribution and contours of fuel mass fraction in a burning spray

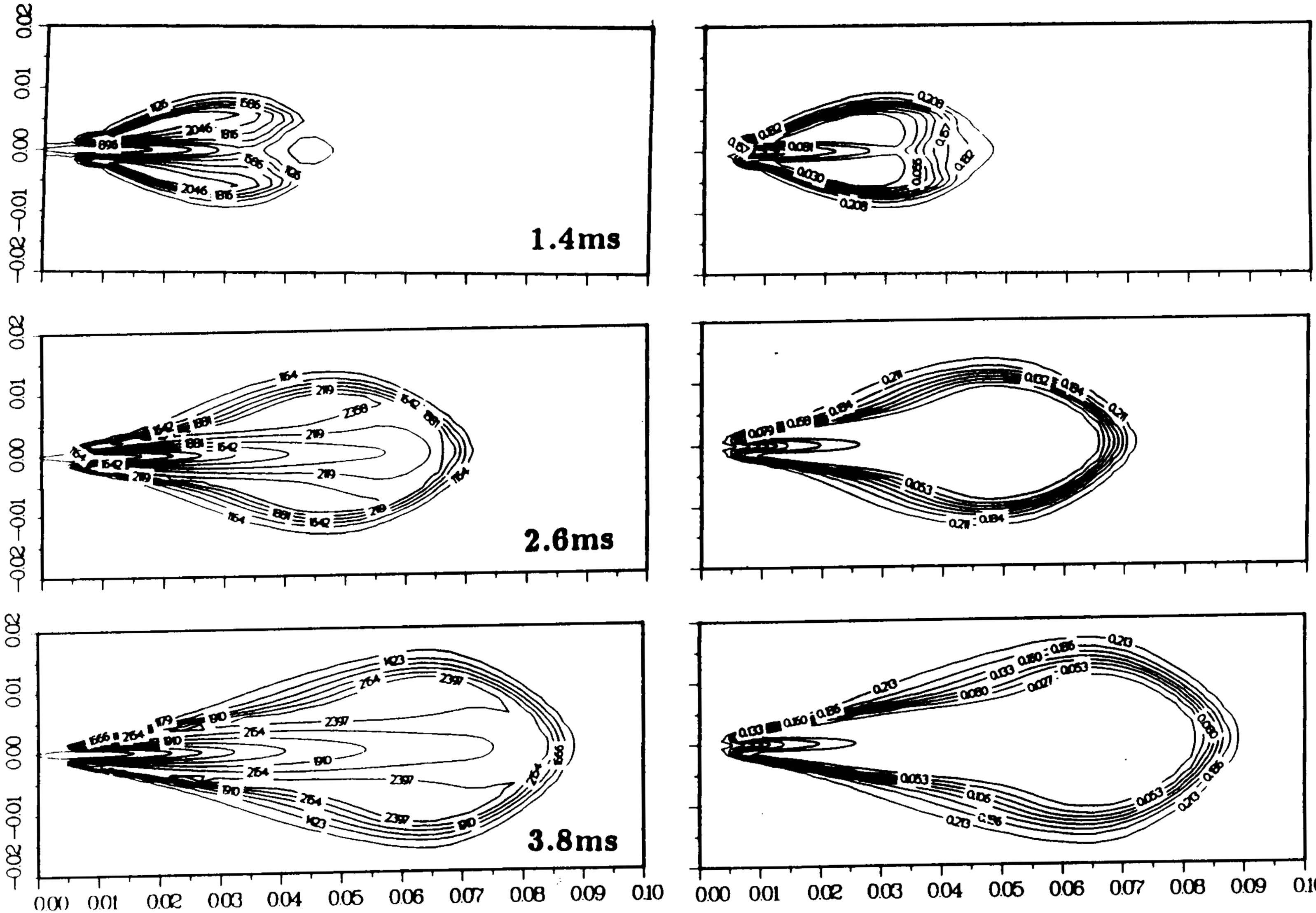

Figure 4.30 Contours of temperature and oxygen mass fraction in a burning spray

SUMMARIES

- **Efficient Particle Dispersion Modeling by DDWT and SDWT.**
- **Good Agreement with Experiment for Dense Spray Cases.**
- **Extension of SDWT to Evaporating and Burning Dense sprays.**
- **Implementation of Volume of Fluid(VOF) method.**
- **Incorporation of Supercritical Vaporization Model.**

N92-32259

Modeling of SSME Fuel Preburner ASI

P. Y. Liang
CFD Technology Center
Rocketdyne Division, Rockwell International Corporation
Canoga Park, California

The Augmented Spark Ignitor (ASI) is a LOX/H2/electrical spark system that functions as an ignition source and sustainer for stable combustion. It is used in the SSME preburner combustor, the SSME main combustion chamber, the J-1 and J-2 engines as well as proposed designs of the Space Transportation Main Engine (STME) main combustor and gas generators. In the SSME it is a long circular cylindrical chamber located along the Main Combustor centerline with a truncated conical dome at the top, which contains two oblique LOX injection ports and two spark plugs offset at 90 degrees. Hydrogen injection is through a number of nearly tangential slots downstream which creates a swirl flow intended to cool the ASI chamber walls. Past incidents of erosion of the ASI spark plugs have often led to the need for replacement of these very costly devices. Thus it is desirable to understand the complex reactive flow field within the ASI both during the initial ignition transient and during the main stage steady state combustion (no sparking).

While it is impossible to perform direct optical diagnostics to measure the internal flow field of the ASI under hot-fire conditions, recent advances in CFD-based combustion modeling have made it feasible to characterize the flow through time-accurate simulations. This paper documents an undertaking.to characterize the flow of the ASI. The code consists of a marriage of the Implicit-Continuous-Eulerian/Arbitrary-Lagrangian-Eulerian (ICE-ALE) Navier-Stokes solver with the Volume-of-Fluid (VOF) methodology for tracking of two immiscible fluids with sharp discontinuities. Spray droplets are represented by discrete numerical parcels tracked in a Lagrangian fashion. Numerous physical sub-models are also incorporated to describe the processes of atomization, droplet collision, droplet breakup, evaporation, and droplet and gas phase turbulence. An equilibrium chemistry model accounting for 8 active gaseous species is also used. Taking advantage of the symmetry plane, half of the actual ASI is modeled with a 3-dimensional grid that geometrically resolves the LOX ports, the spark plug locations, and the hydrogen injection slots. The pertinent features and formulations of these submodels will be briefly described in the paper.

MODELING OF SSME FUEL PREBURNER ASI

PAK-YAN LIANG

ROCKWELL INTERNATIONAL CORPORATION
ROCKETDYNE DIVISION

Rockwell International
Rocketdyne Division

CFD 92-030-005/D2/PYL

OBJECTIVES

- APPLY NEWLY COMPLETED ARICC -3D CODE TO REAL LIFE COMBUSTION HARDWARE

- VALIDATE ATOMIZATION MODEL (PREVIOUSLY ANCHORED FOR COAXIAL INJECTORS) IN TRANSVERSE (NOMINALLY IMPINGING) INJECTION MODE

Rockwell International
Rocketdyne Division

CFD 92-030-004/D2/PYL

SIGNIFICANCE

- EROSION AND REPLACEMENT OF ASI SPARK PLUGS EXTREMELY COSTLY
- DESIRABLE TO UNDERSTAND REACTIVE FLOWFIELD INSIDE ASI DURING IGNITION TRANSIENT AND MAIN STAGE
- DIAGNOSTICS WITHIN ASI VERY DIFFICULT
- MAY REPLACE ONE SPARK PLUG WITH SEEDING DEVICE FOR PLUME MEASUREMENTS IN TESTS

Rockwell International
Rocketdyne Division

CFD 92-030-003/D2/PYL

MODEL PARAMETERS

- COARSE GRID (11 x 13 x 26) REPRESENTS 180° SECTOR
- CYCLIC BOUNDARIES AT J = 1 & J = 13
- CONSTANT PRESSURE OUTFLOW (5501 PSI) AT 4.84 IN. FROM TOP
- MULTI-PHASE MODEL RESOLVES LOX JET, 8 SPECIES (O, H, O_2, H_2, HO_2, H_2O_2, H_2O, OH) EQUILIBRIUM CHEMISTRY AND ABOUT 5000 DROPLETS
- K-ε TURBULENCE MODEL
- SIMULATION TIME = 1 MS COLD FLOW + 1 MS SPARK IGNITION
  + 2 MS HOT FIRE TRANSIENT TO STEADY-STATE

Rockwell International
Rocketdyne Division

CFD 92-030-002/D2/PYL

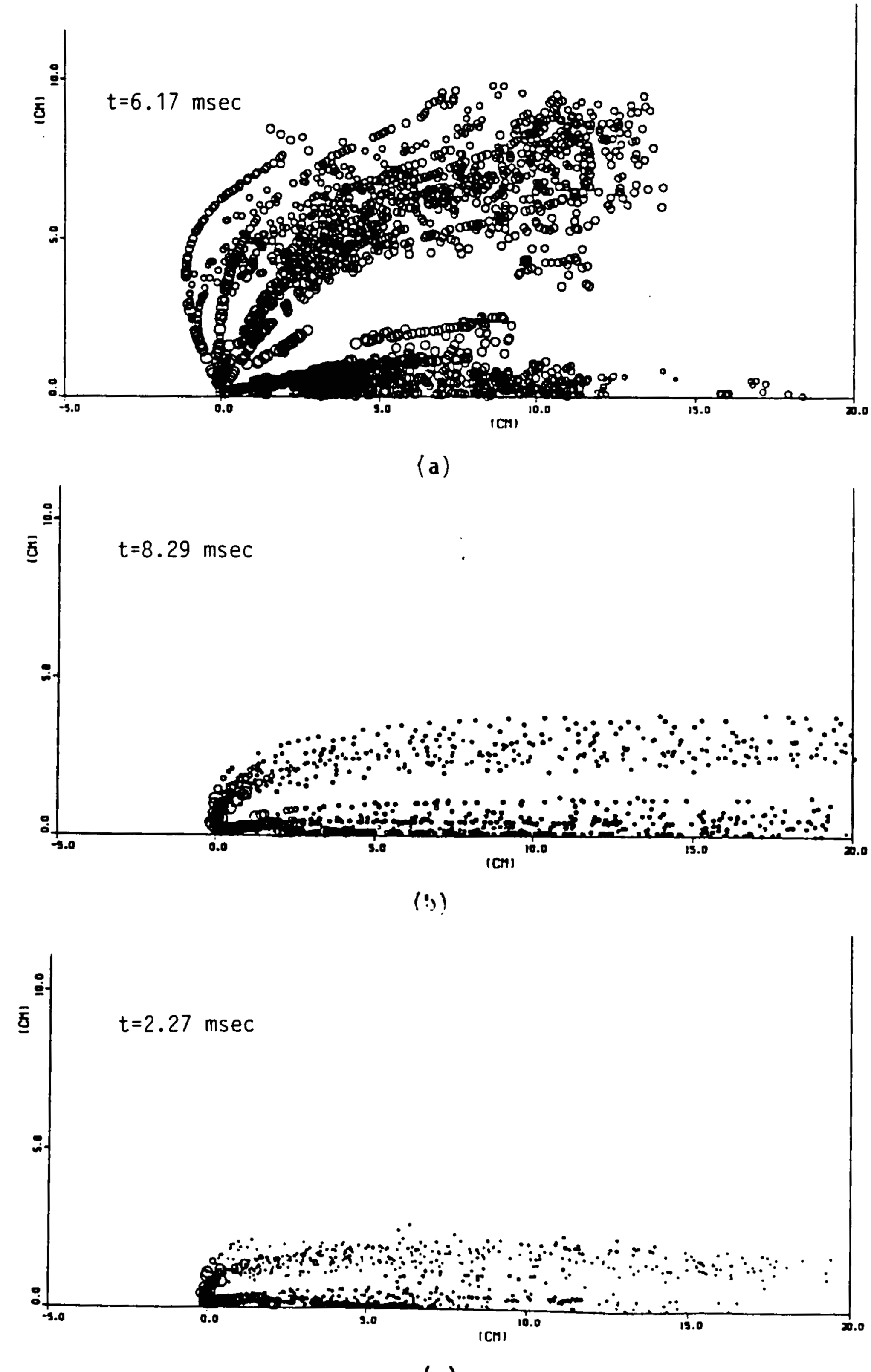

Fig. 5 Plots of droplet parcels for (a)case 3 (b)case 2 (c)case 4

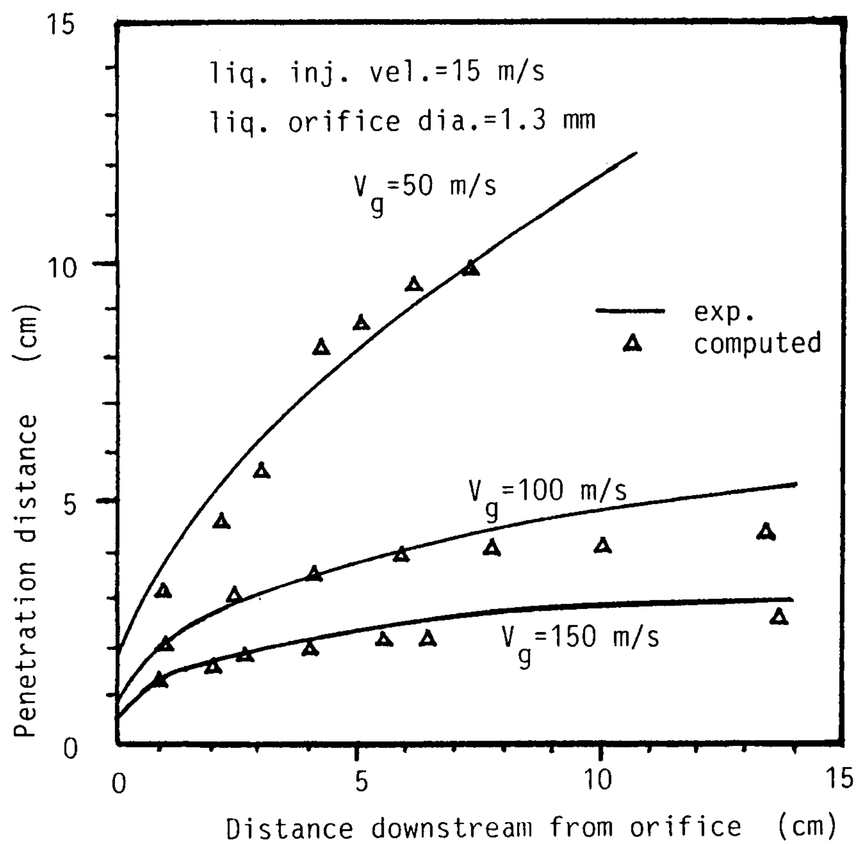

Fig. 1 Comparision of computed vs experimental drop penetration distances for different transverse gas velocities.

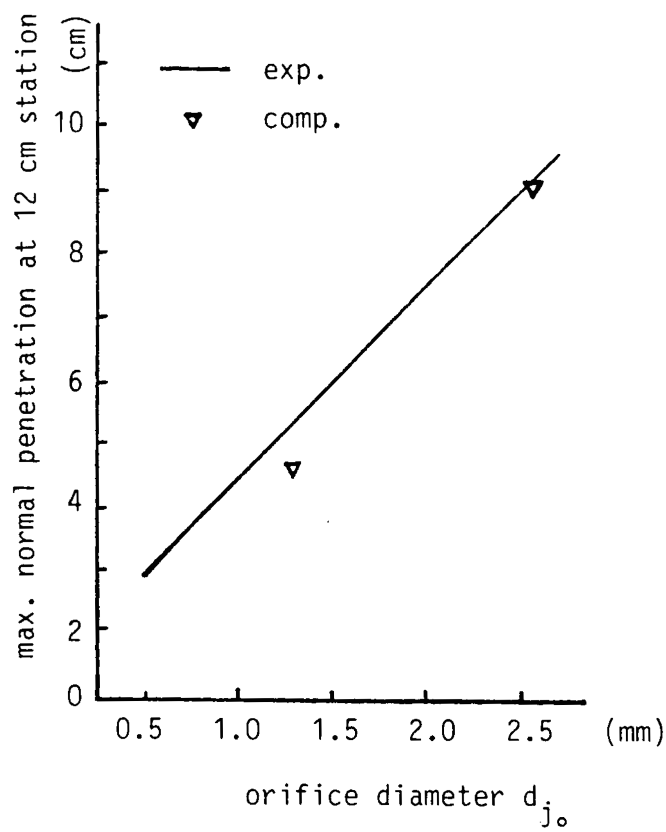

Fig. 2 Variation of penetration with orifice diameter; V_g=100 m/s, V_l=15 m/s.

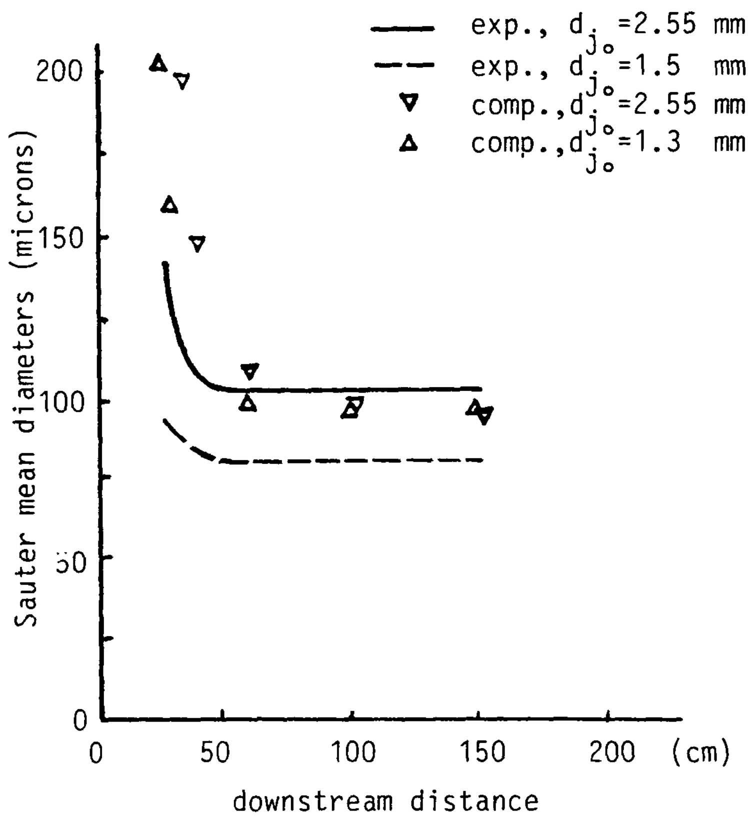

Fig. 3 Streamwise SMD profiles for various orifice diameters (d_{j_o}); V_g=100 m/s, V_l=15 m/s.

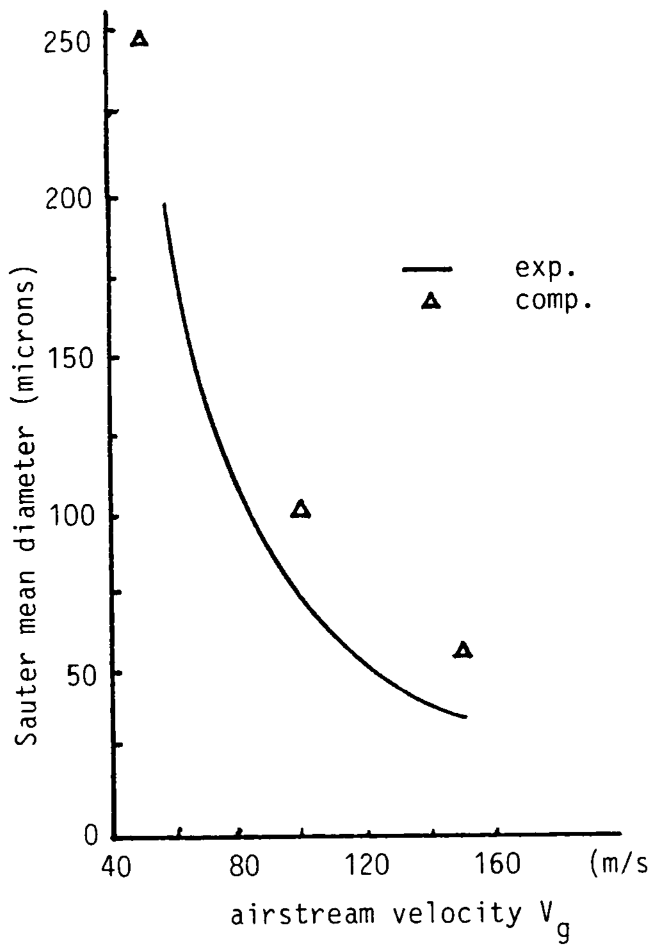

Fig. 4 Influence of airstream velocity on mean dropsize taken at 12 cm station; V_l=15 m/s, d_{j_o}=1.3 mm(comp), =1.5 mm(exp).

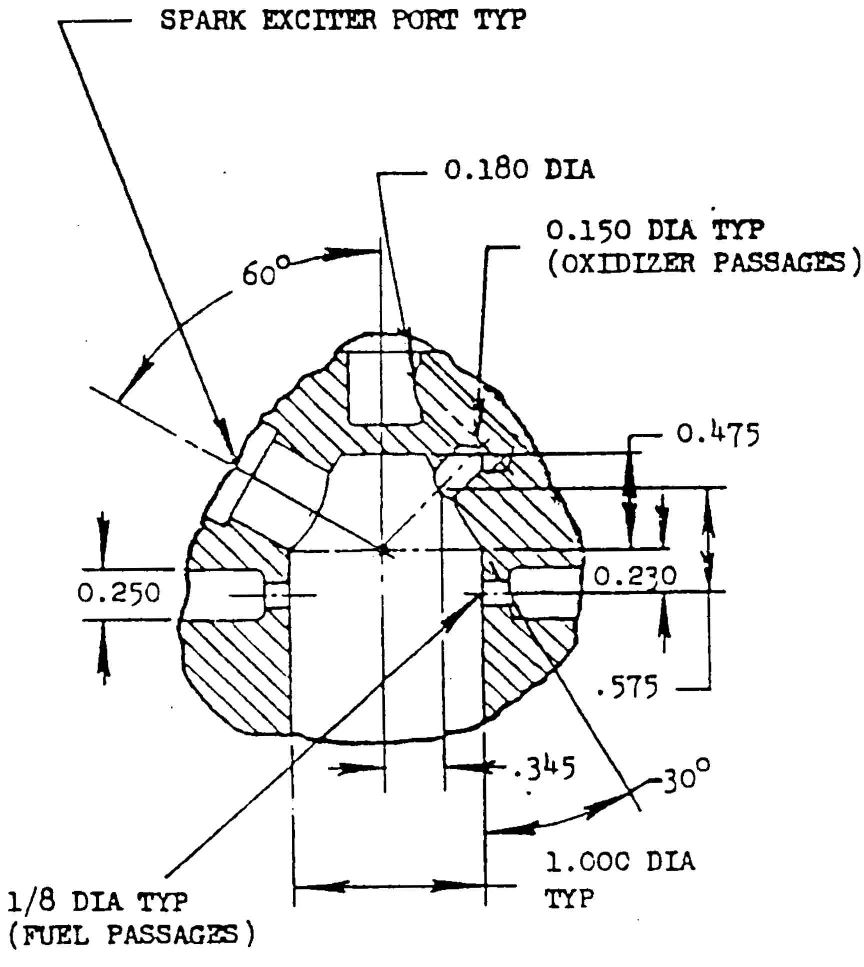

Fig. 1 Schematic of SSME Preburner ASI. (LOX ports are actually 90 deg. apart from spark plugs rather than being on same meridian plane as shown)

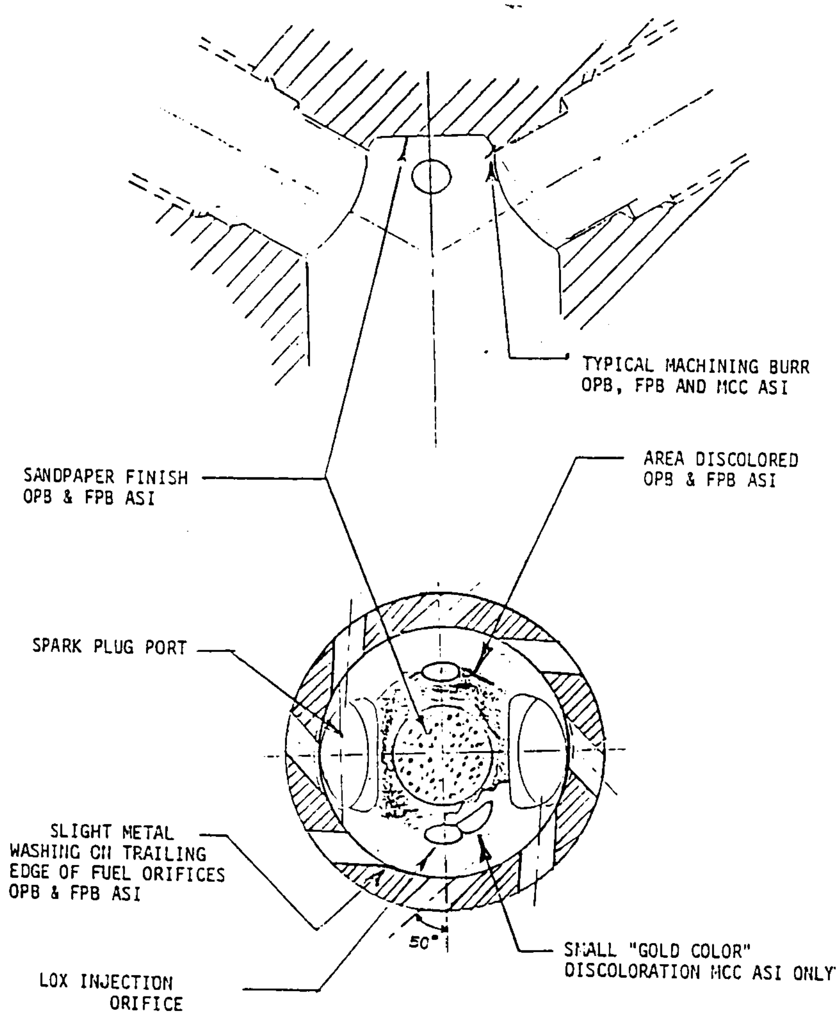

Fig. 2 Close-up Side and Top Views of ASI Dome Region

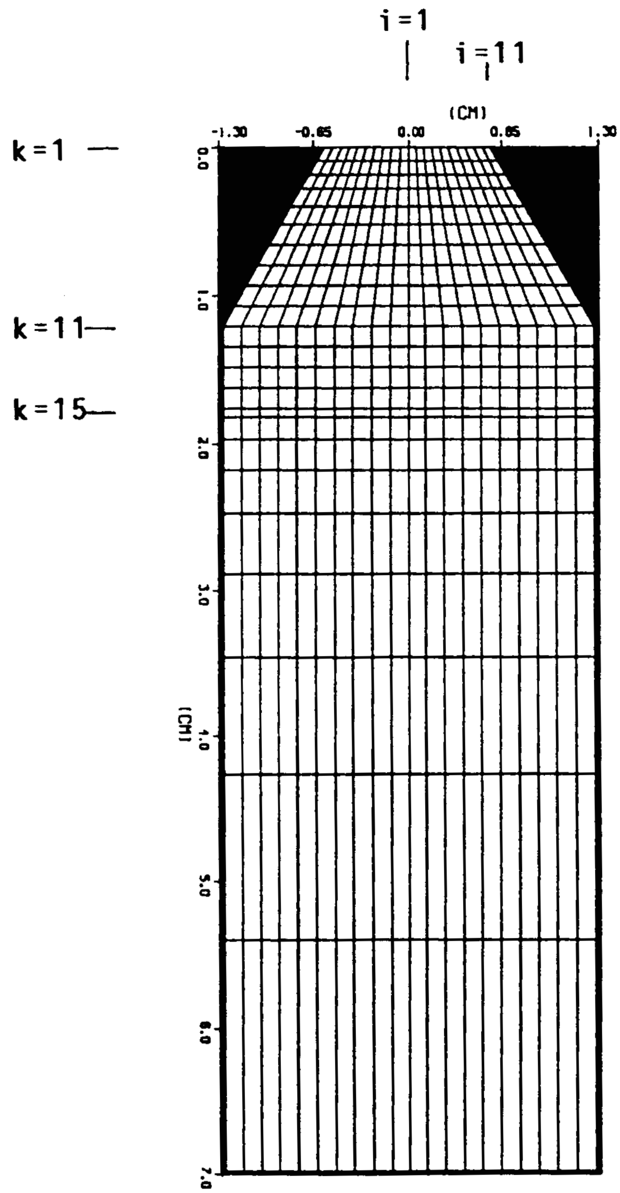

Fig. 3 Computational Grid (Partial) Across a J-plane (shown reflected across central axis to represent full chamber)

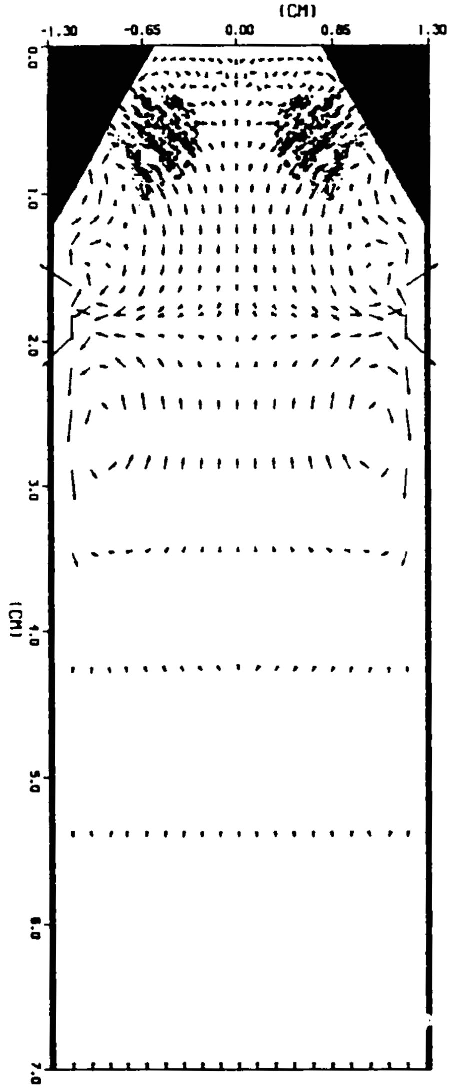

(a) j=7 plane

LOX port location

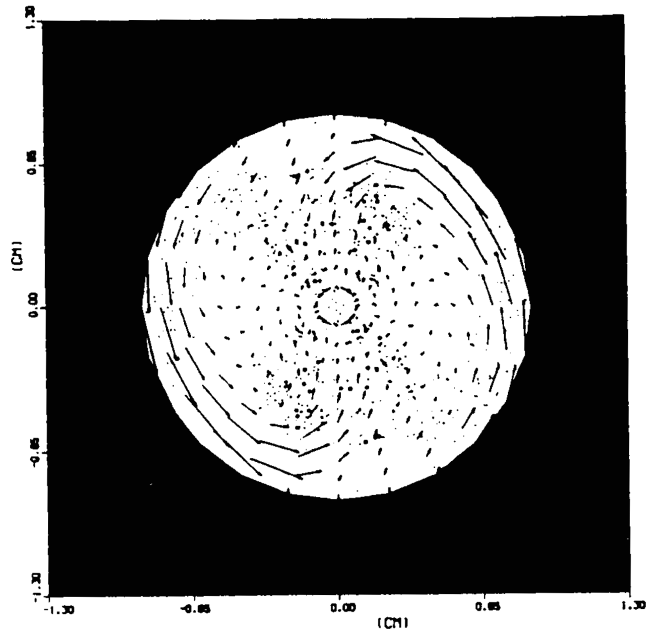

LOX port location

(b) k=6 plane

Fig. 4 Velocity Profiles In Vertical and Horizontal Cross Sectional Planes Before Ignition (t=.737 msec)

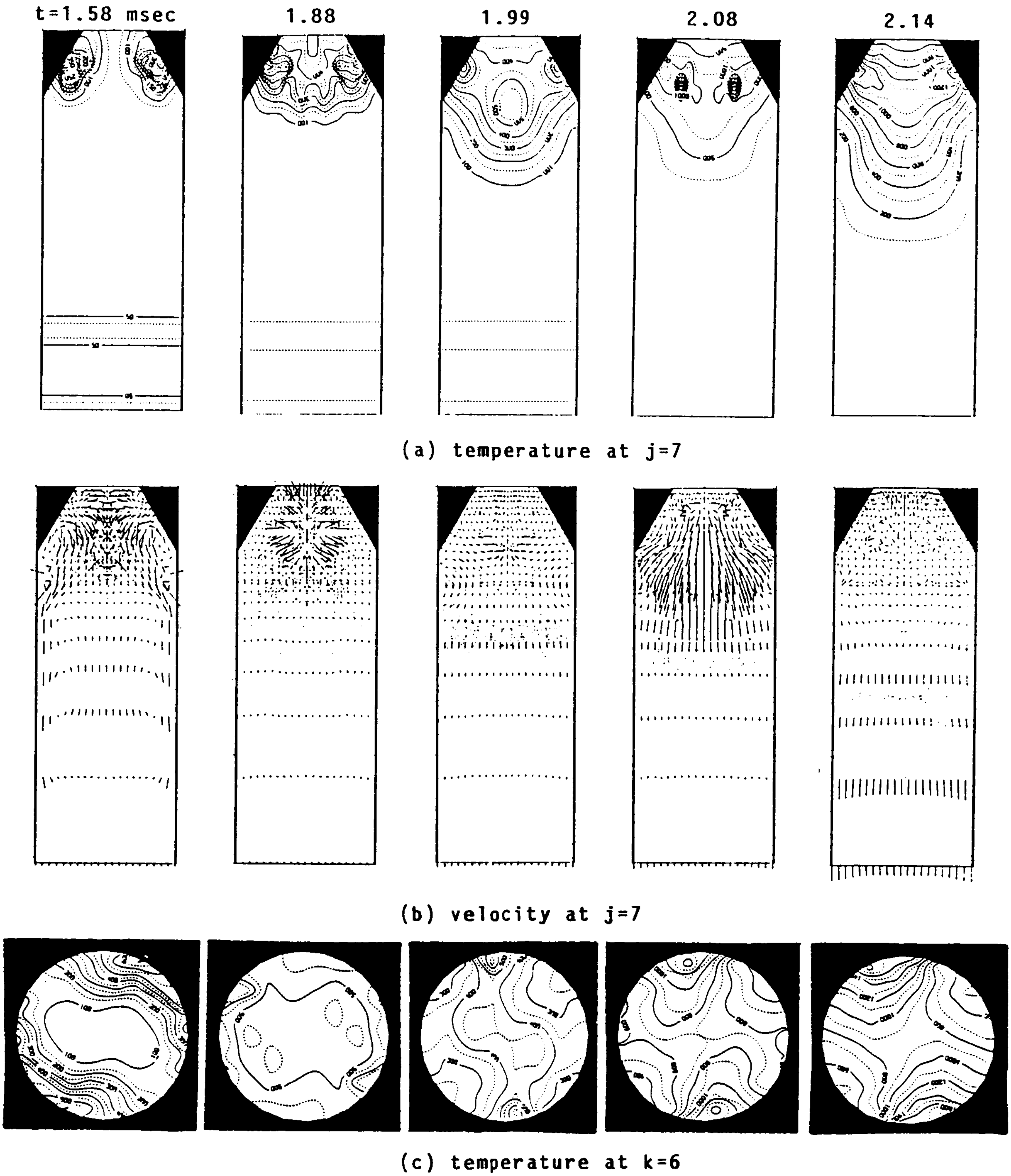

Fig. 5 Transient Temperature and Velocity Fields During and Right After Ignition by Spark Plugs

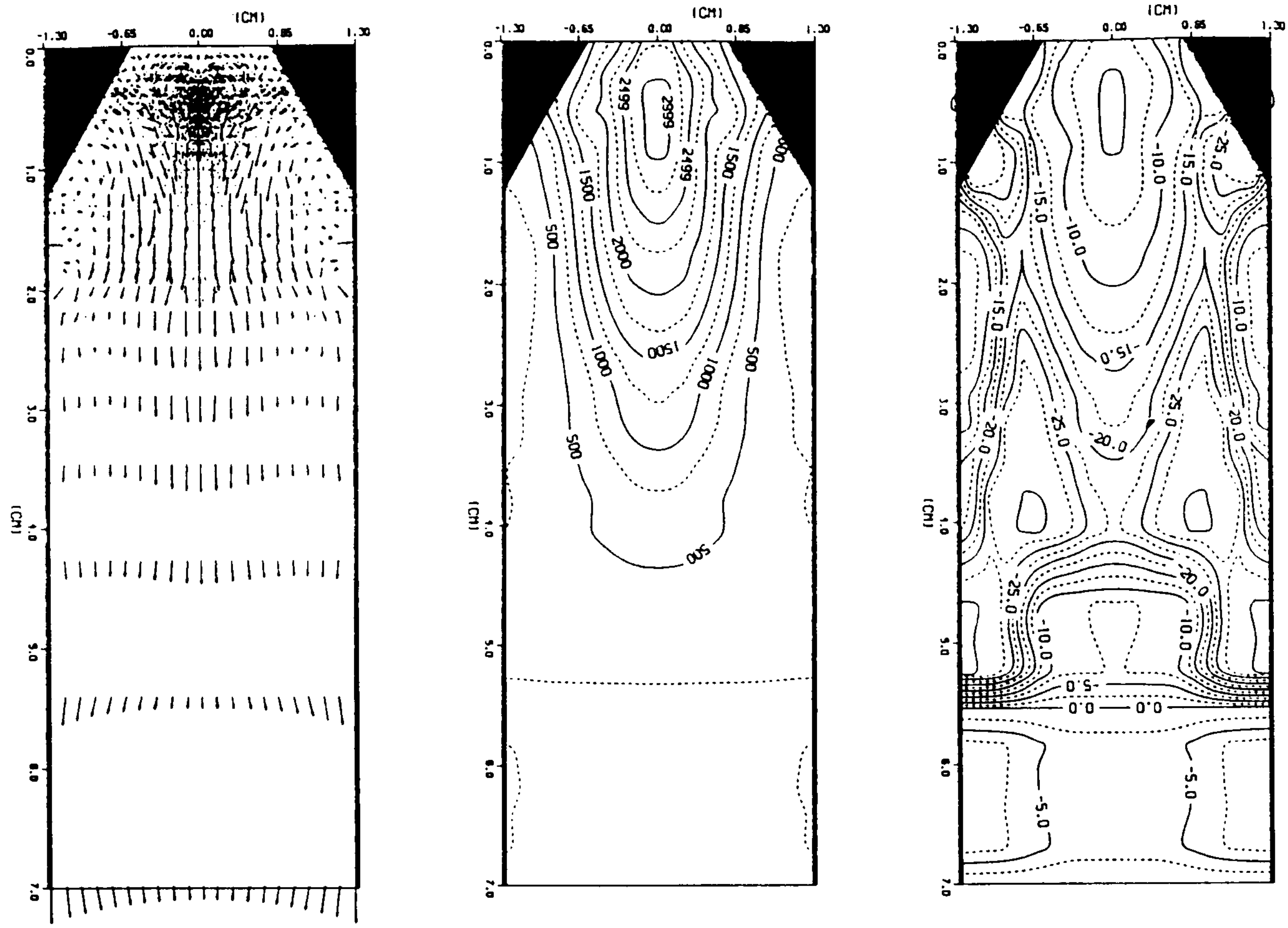

(a) velocity (b) temperature (c) log O_2 conc.

Fig. 6 Velocity, Temperature and Log O_2 Concentration Profiles Across j=7 Plane at Pseudo-steady State (t=4.10 msec)

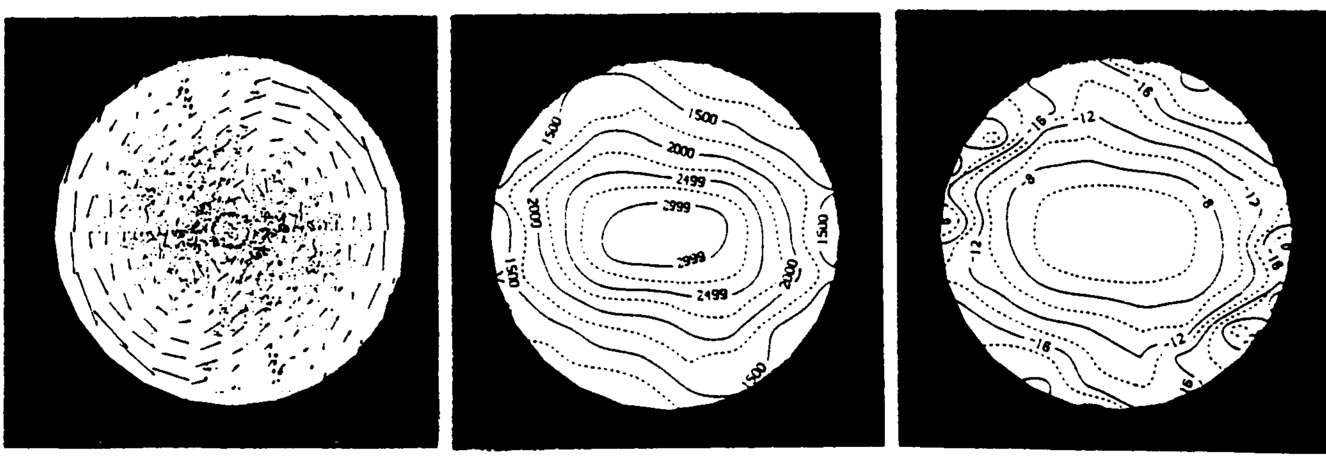

(a) velocity (b) temperature (c) log O_2 conc.

Fig. 7 Velocity, Temperature and Log O_2 Concentration Profiles Across k=6 Plane at Pseudo-steady State (t=4.10 msec)

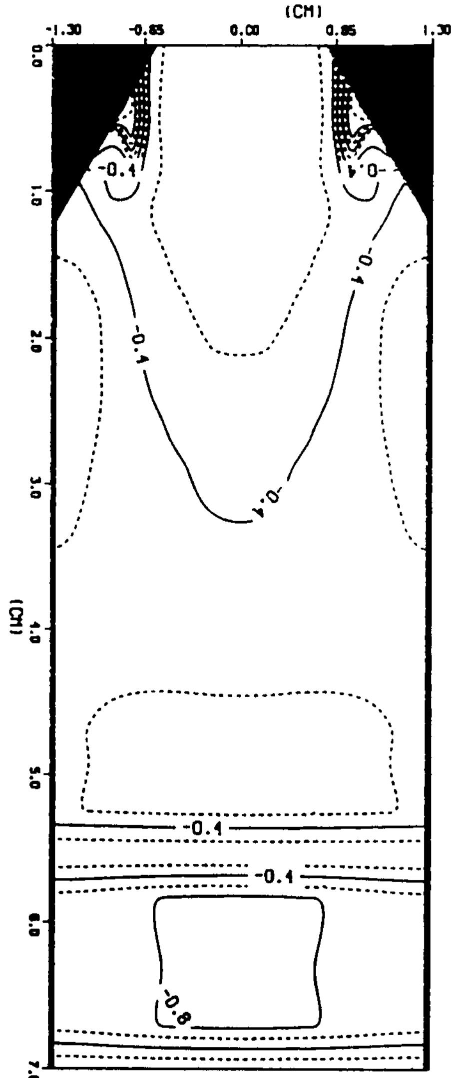

j = 7 plane

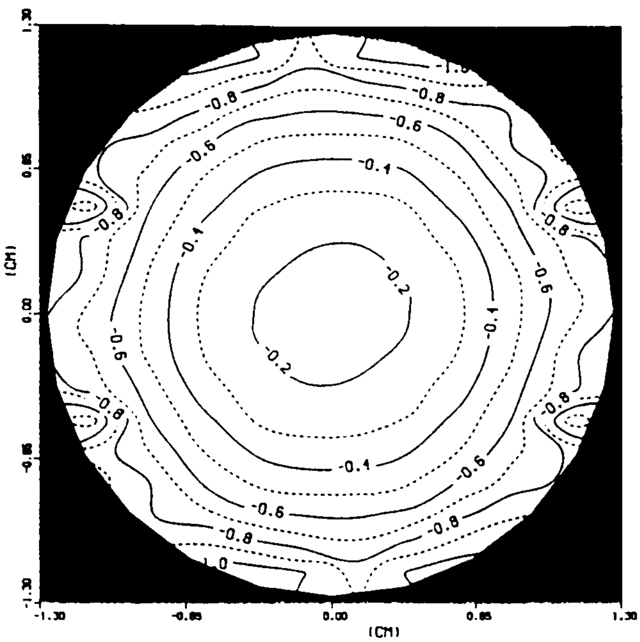

k = 15 plane

Fig. 8 Log H_2O Concentration Profiles at t=4.10 msec

SUMMARY OF OBSERVATIONS ON ASI

- HYDROGEN SWIRL DOMINATES COLD FLOWFIELD
- SUBSTANTIAL BLOCKAGE BY LOX JET AND SPRAY IMPLIES EFFECTIVELY TRANSVERSE SHEARING ATOMIZATION MODE
- SPARK ENERGY CAUSES VIOLENT MINI-EXPLOSIONS
- EVEN IN STEADY-STATE, INJECTED UNBURNED HYDROGEN FIRST SPIRALS UP TOWARD DOME, THEN DOWNWARD AFTER COMBUSTION. THUS WALL REMAINS COOL BELOW HYDROGEN PORTS

Rockwell International
Rocketdyne Division

CFD 92-030-001/D2/PYL

N92-32260

CFD MODELING OF TURBULENT FLOWS AROUND THE SSME MAIN INJECTOR ASSEMBLY USING POROSITY FORMULATION

Gary C. Cheng*, Y.S. Chen†, and Joseph H. Ruf‡

Abstract

Hot gas turbulent flow distributions around the main injector assembly of the Space Shuttle Main Engine (SSME) and LOX flow distributions through the LOX posts have great effect on the combustion phenomenon inside the main combustion chamber. An advanced computational fluid dynamics (CFD) analysis will help to provide more accurate and efficient characterization of this type of flow field. In order to design a CFD model to be an effective engineering analysis tool with good computational turn-around time (especially for 3-D flow problems) and still maintain good accuracy in describing the flow features, the concept of porosity is employed to describe the effects of blockage and drag force due to the presence of the LOX posts in the turbulent flow field around the main injector assembly of the SSME. A validated non-isotropic porosity model is developed and incorporated into an existing Navier-Stokes flow solver (FDNS). Volume and surface porosity parameters, which are based on the configurations of local LOX post clustering, will be introduced in to the governing equations, which can be written as

$$\frac{1}{J}\left(\nu_v \frac{\partial \rho q}{\partial t}\right) = -\frac{\partial \nu_i F_i}{\partial \xi_i} + \nu_v S_q + R_q$$

where J is the Jacobian, F_i is the sum of the convective flux and the viscous flux, ν_i is the surface porosity, ν_v is the volume porosity, S_q and R_q are the source and residual terms of the flow variable q, respectively. The drag force and the heat flux source due to the presence of LOX posts will be added to the residual term. 2-D numerical studies have been conducted to identify the drag coefficients of the flows both through tube banks and around the shielded posts with a wide range of Reynolds numbers. A verified model of the drag coefficients is incorporated into the FDNS flow solver. A 2-D flow study of the main injector assembly is performed to verify the proposed porosity model. A reasonable O/F ratio distribution was obtained, therefore, a 3-D CFD analysis is conducted with confidence. The 3-D CFD analysis of the SSME main injector assembly is divided into three parts, LOX dome, LOX post assembly torus, and hydrogen cavity. A 62 x 91 x 16 mesh system is constructed for the LOX dome, where a 37 x 91 x 25 grid system is employed for the torus region, and the hydrogen cavity is discretized into a 29 x 91 x 14 mesh system. The numerical study of the turbulent flow in the SSME Phase II+ power head is analyzed based on 104% power balance level, and the result will be presented in the coming CFD workshop meeting.

---

* SECA, Inc., 3313 Bob Wallace Ave., Suite 202, Huntsville, AL

† Engineering Sciences, Inc., 4920 Corporate Dr., Suite K, Huntsville, AL

‡ ED 32, NASA/Marshall Space Flight Center, Huntsville, AL

CFD MODELING OF TURBULENT FLOWS WITHIN SSME MAIN INJECTOR ASSEMBLY USING A POROSITY MODEL

By

Gary C. Cheng, SECA, Inc.

Y.S. Chen, ESI

AND

Joe Ruf
NASA/Marshall Space Flight Center

NASA Contract No. NAS8-38871

TENTH ANNUAL CFD WORKSHOP MEETING, APRIL, 1992

PRESENTATION OVERVIEW

- OBJECTIVE
- NUMERICAL APPROACH
- PROPOSED POROSITY MODEL
- 3-D POROSITY/CFD ANALYSIS OF PHASE II+ POWER HEAD
- CONCLUSIONS AND RECOMMENDATIONS

OBJECTIVE

- DEVELOPMENT OF ROBUST CFD METHODOLOGY FOR TURBULENT FLOWS IN THE ENGINE 0209
- VALIDATION OF A POROSITY MODEL FOR NAVIER-STOKES FLOW SOLVER
- PREDICTION OF LOCAL MASS FLOW RATE AND O/F RATIO DISTRIBUTIONS DOWNSTREAM OF THE PRIMARY FACE PLATE

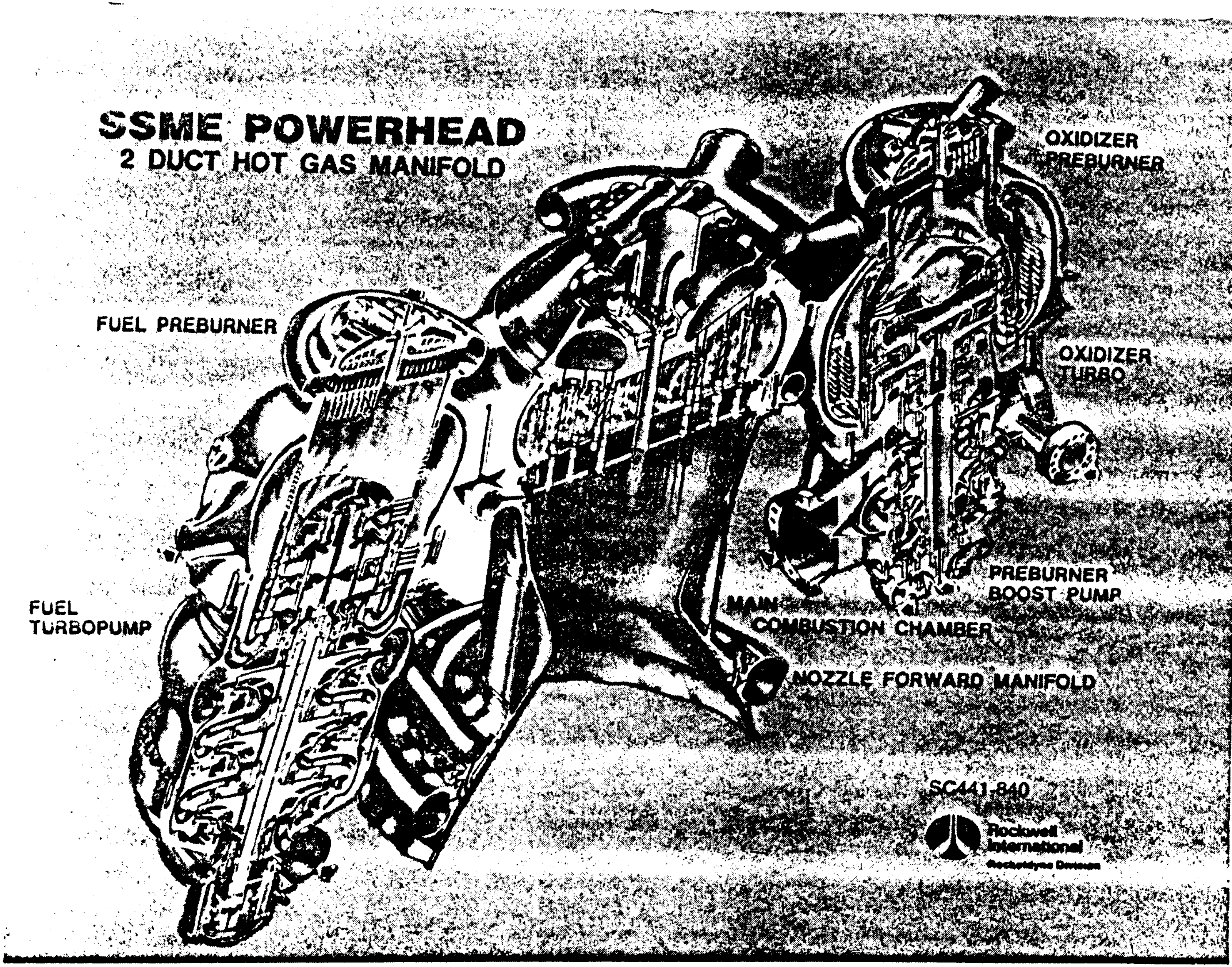

ORIGINAL PAGE IS
OF POOR QUALITY

NUMERICAL APPROACH

- FLOW AROUND LOX POST ELEMENTS IN SIMULATED AS FLOW THROUGH TUBE BANK

- MASS FLOW RATE THROUGH POST ELEMENTS AND THROUGH POROUS PLATES ARE CALCULATED BASED ON POROSITY MODEL

- BENCHMARK THE MODELS FOR POROUS MEDIA
  - Flow Through Tube Banks
  - Flow Through Shielded Posts With and Without Holes

- 3-D POROSITY MODEL/CFD ANALYSIS OF THREE COMPONENTS OF THE POWER HEAD (LOX DOME, LOX POST ASSEMBLY, HYDROGEN CAVITY)

PROPOSED POROSITY MODELS

- **DRAG COEFFICIENTS FOR FLOW THROUGH TUBE BANK**

  - NON-SHIELDED ELEMENTS

    - Re (Local Flow Reynolds no.) $< 4 \times 10^3$

      $$C_d = 0.417 \, \text{EXP}(4.932 \, Re^{-0.296})$$

    - $4 \times 10^3 < Re < 6 \times 10^4$

      $$C_d = 0.647 - 0.5 \times 10^{-6} \, Re$$

    - $6 \times 10^4 < Re < 10^6$

      $$C_d = 0.618 + 0.491 \times 10^{-6} \, Re - 6.303 \times 10^{-12} \, Re^2 + 10.694 \times 10^{-18} \, Re^3 - 5.2 \times 10^{-24} \, Re^4$$

    - $Re > 10^6$

      $$C_d = 0.2735$$

- SHIELDED ELEMENTS
  - With Holes: $C_d = 4.$
  - Without Hole: $C_d = 48.$

LOX DOME POROSITY MODEL (104% RPL)

K (Loss Coeff.) $\equiv \sqrt{\dfrac{\rho \, \Delta P}{\dot{m}^2}}$; $\Delta P = P_{exit} - P_{chamber}$; or $\Delta P = P_{exit} - P_{baffle}$

	$\dot{m}$ (lb/sec)	ΔP(psi)	K (ft^{-4})
Non-Baffle Elements	665.105	575.07	4.14×10^2
Baffle Elements	105.65	625.49	1.785×10^4
First Three Rows	56.154	575.07	5.809×10^4

- **LOX POST ASSEMBLY POROSITY MODEL (104% RPL)**

	Non-Baffle Elements			Baffle Elements
	Row #13	Row #12	Row #1 - #11	
K (in^{-4})	135	156	152	∞

- **HYDROGEN CAVITY POROSITY MODEL (104% RPL)**

	$\dot{m}$ (lb/sec)	ΔP (psi)	K (ft^{-4})
Primary Face Plate	6.77	251	3.578×10^4
Secondary Face Plate	3.41	98	5.506×10^4
Baffle Elements	15.25	301	8.467×10^3
Non-Baffle Elements	0	251	∞
BLC Holes	3.67	251	1.16×10^5

3-D POROSITY/CFD ANALYSIS OF PHASE II+ POWER HEAD

- **LOX DOME**
  - GRID SIZE: 62 x 91 x 16
  - INLET FLOW CONDITIONS
    - Static Pressure: 3670 psi
    - Static Temperature: 197 °R
    - Reynolds no.: $1.28 \times 10^{8}\ ft^{-1}$
    - Mass Flow Rate: 826.7 lb/sec
  - INCOMPRESSIBLE, SINGLE SPECIES

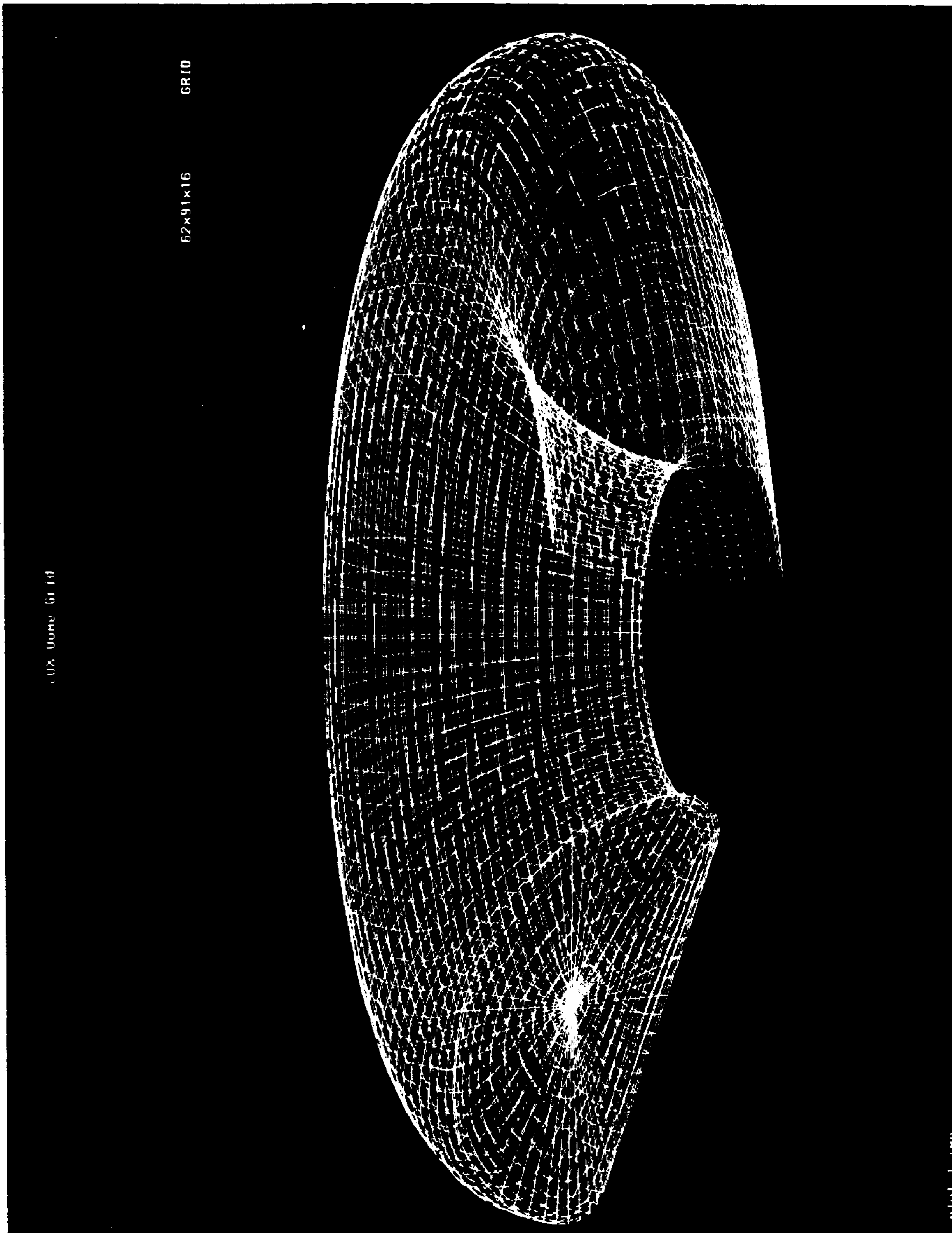
Dome Grid
62x91x16
GRID

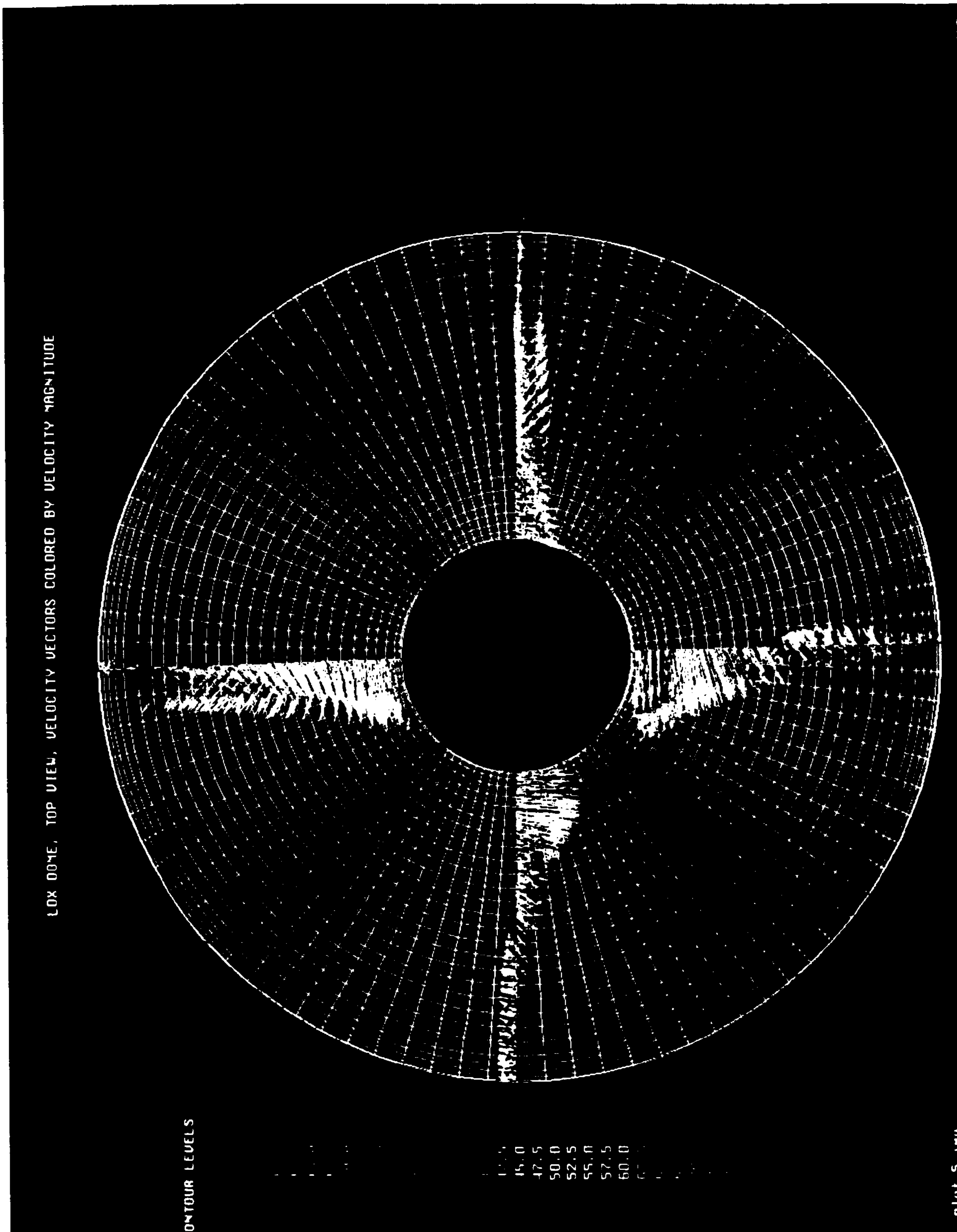
LOX DOME, TOP VIEW, VELOCITY VECTORS COLORED BY VELOCITY MAGNITUDE
CONTOUR LEVELS
47.5
50.0
52.5
55.0
57.5
60.0

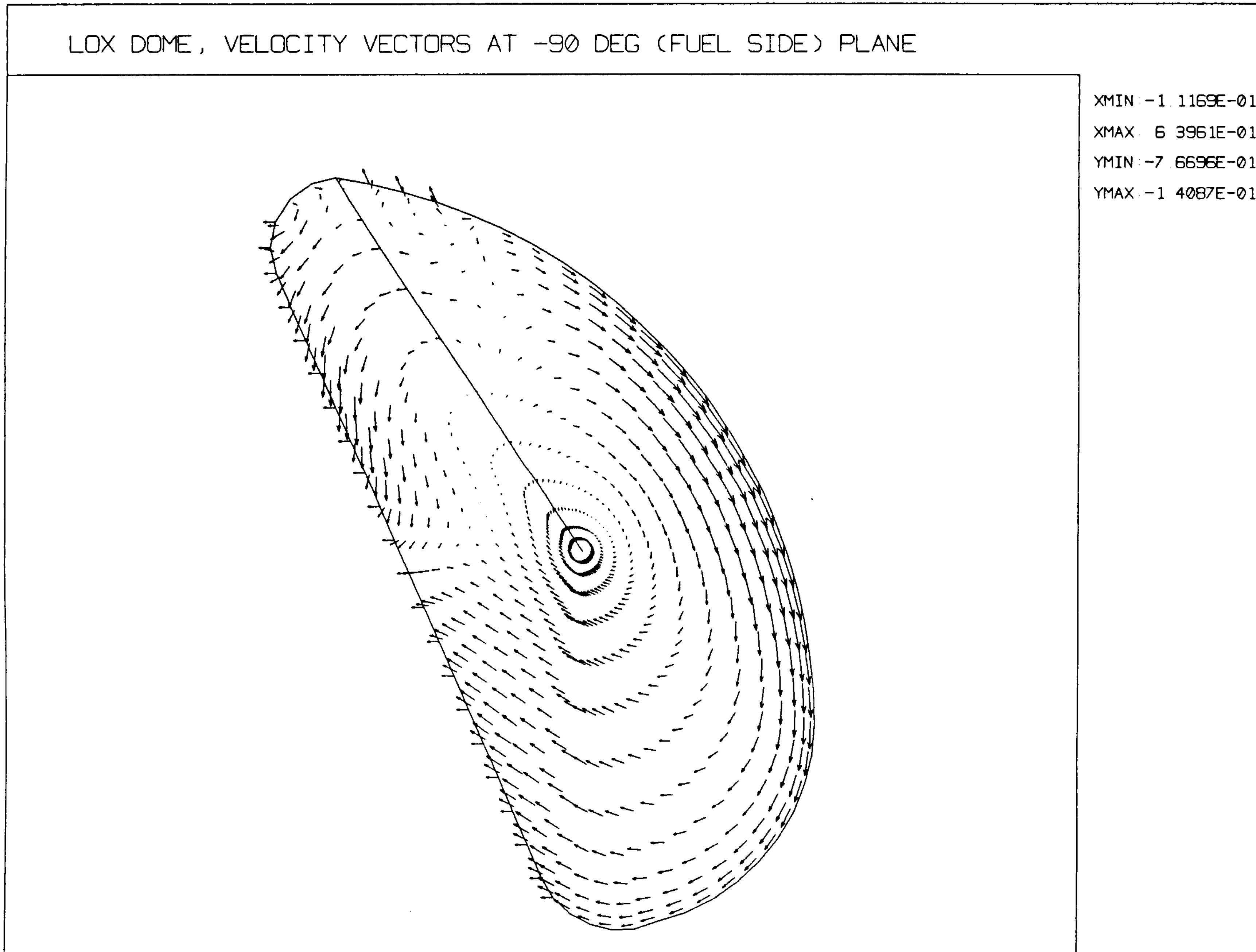
LOX DOME, VELOCITY VECTORS AT -90 DEG (FUEL SIDE) PLANE
XMIN -1.1169E-01
XMAX 6.3961E-01
YMIN -7.6696E-01
YMAX -1.4087E-01

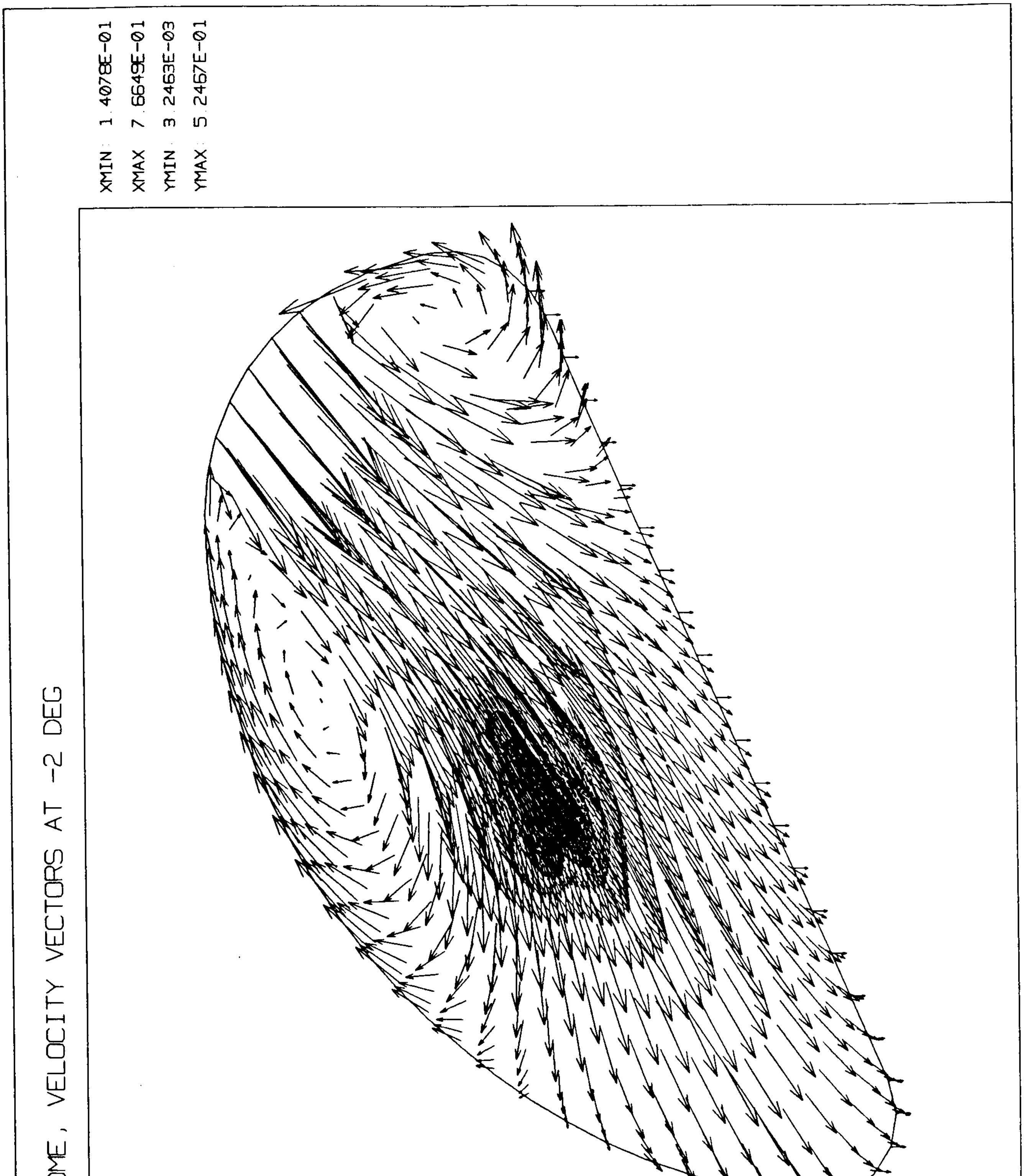
LOX DOME, VELOCITY VECTORS AT -2 DEG
XMIN: 1.4078E-01
XMAX: 7.6649E-01
YMIN: 3.2463E-03
YMAX: 5.2467E-01

LOX DOME, VELOCITY VECTORS AT 90 DEG (OXIDIZER SIDE) PLANE

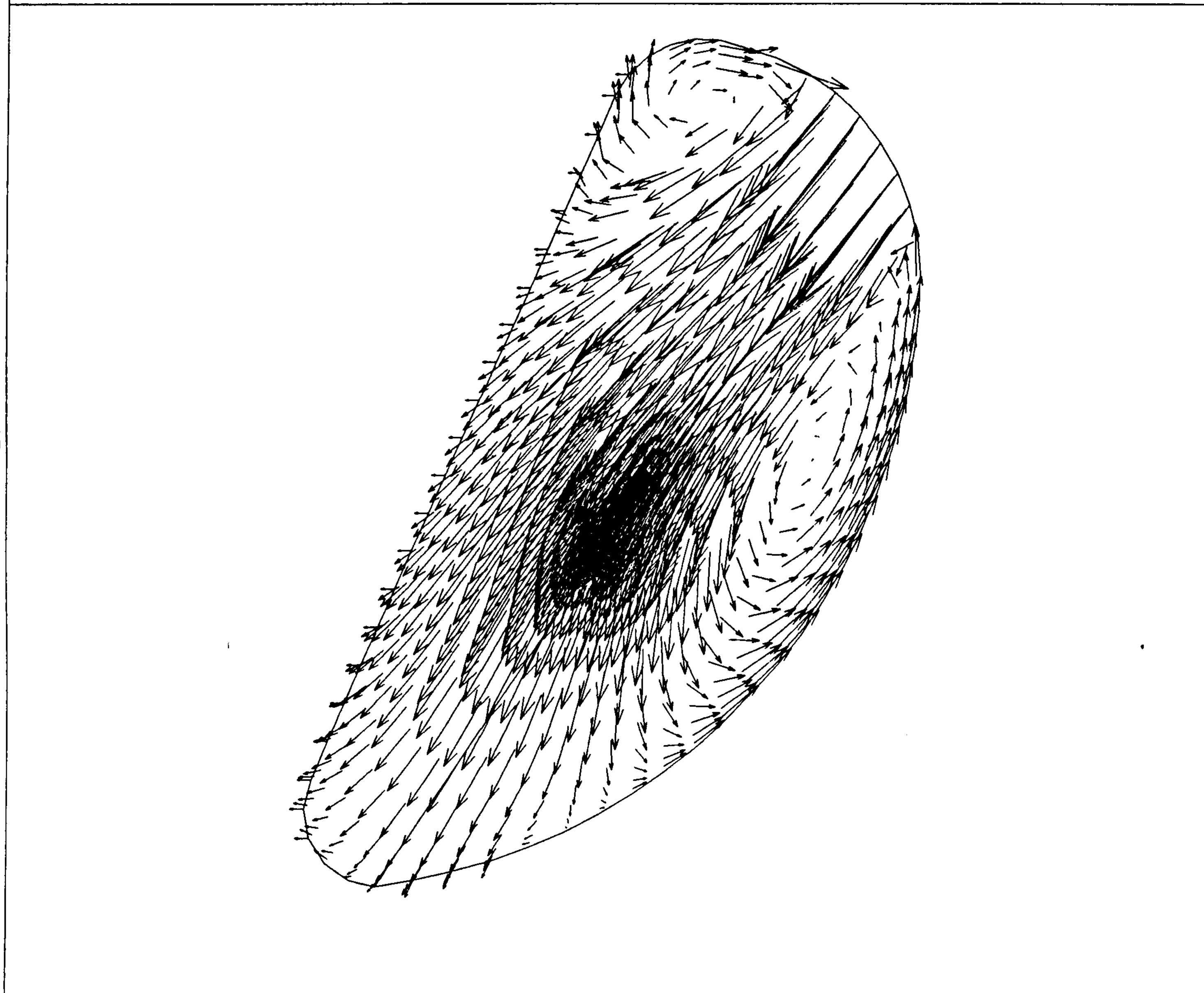

XMIN -1.1169E-01
XMAX 6.3961E-01
YMIN 1.4087E-01
YMAX 7.6696E-01

LOX DOME, VELOCITY VECTORS AT 178 DEG PLANE

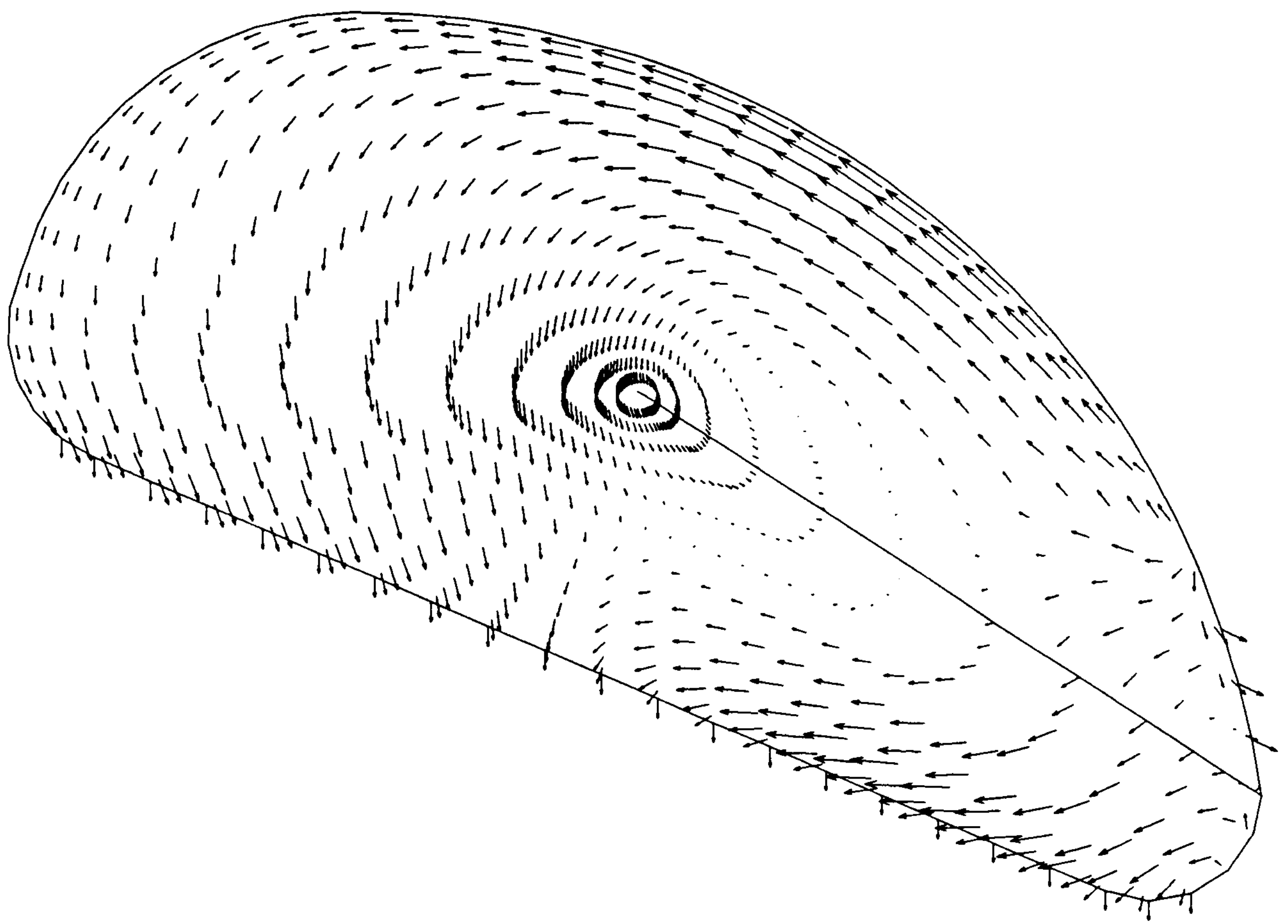

XMIN -7.6649E-01
XMAX -1.4078E-01
YMIN 3.2463E-03
YMAX 5.2467E-01

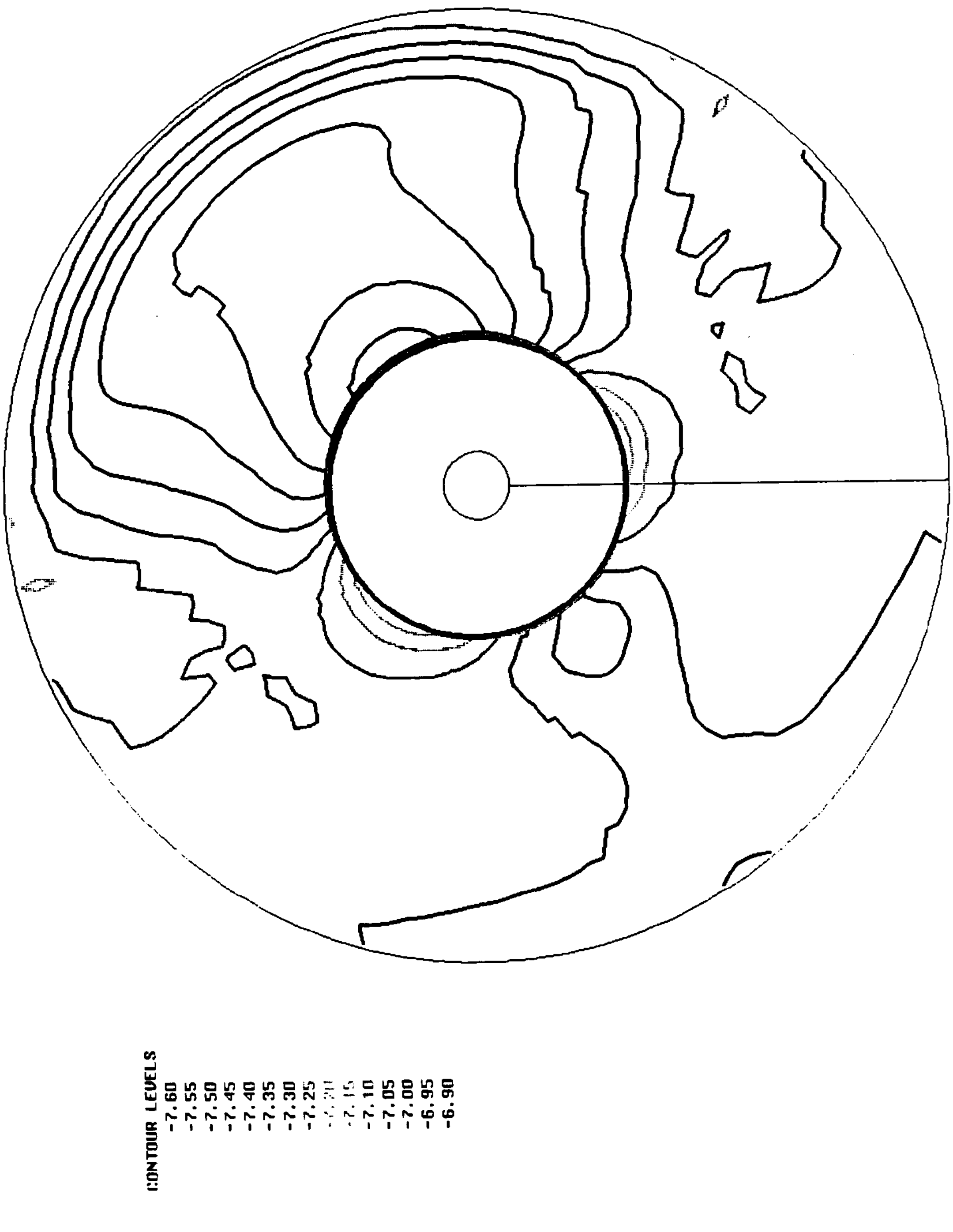

LOX Dome, Exit Flow Velocity Contours (ft/sec)

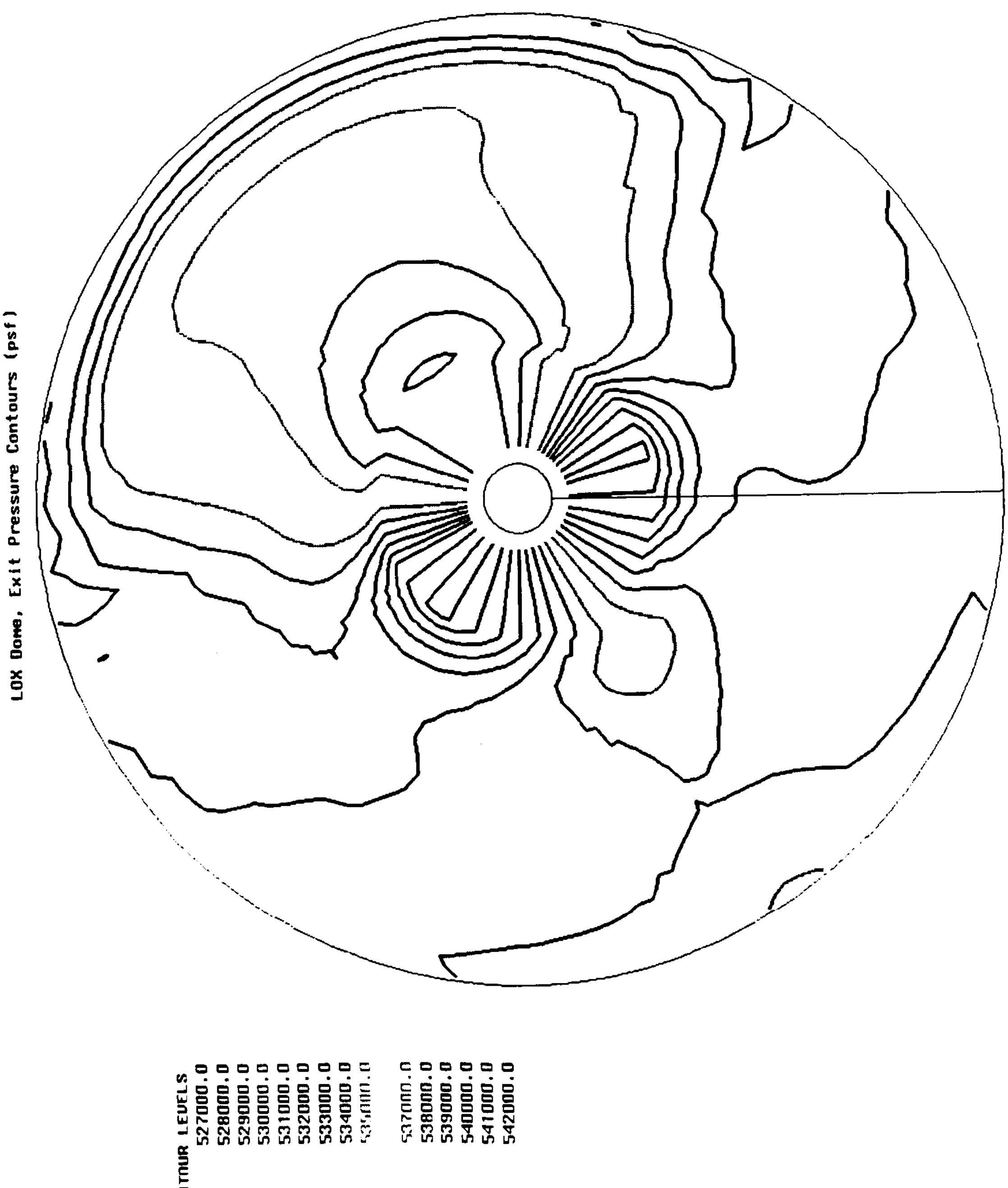

ORIGINAL PAGE IS
OF POOR QUALITY

- **MAIN INJECTOR ASSEMBLY WITH TRANSFER DUCTS**
  - THREE ZONES
    - Zone #1: 37 x 91 x 25 (Main Injector Assembly)
    - Zone #2: 10 x 21 x 17 (Fuel Transfer Duct)
    - Zone #3: 10 x 15 x 15 (Oxidizer Transfer Duct)
  - INLET FLOW CONDITIONS:
    - Fuel Side (Reference Conditions)

      Static Pressure: 3351 psi

      Static Temperature: 1666 ^{o}R

      Reynolds no.: 3.17 x 10^7 ft^{-1}

      Mass Flow Rate: 77.55 lb/sec (symmetrical)

      O/F Ratio: 0.8685

- Oxidizer Side

  Static Pressure: 3353 psi

  Static Temperature: 1254 °R

  Mass Flow Rate: 33.375 lb/sec (symmetrical)

  O/F Ratio: 0.599

  U/U_{ref}: 0.693

- INCOMPRESSIBLE, ISOTHERMAL, TWO SPECIES, NON-REACTING FLOW

Geometry of Hot Gas Injector Assembly

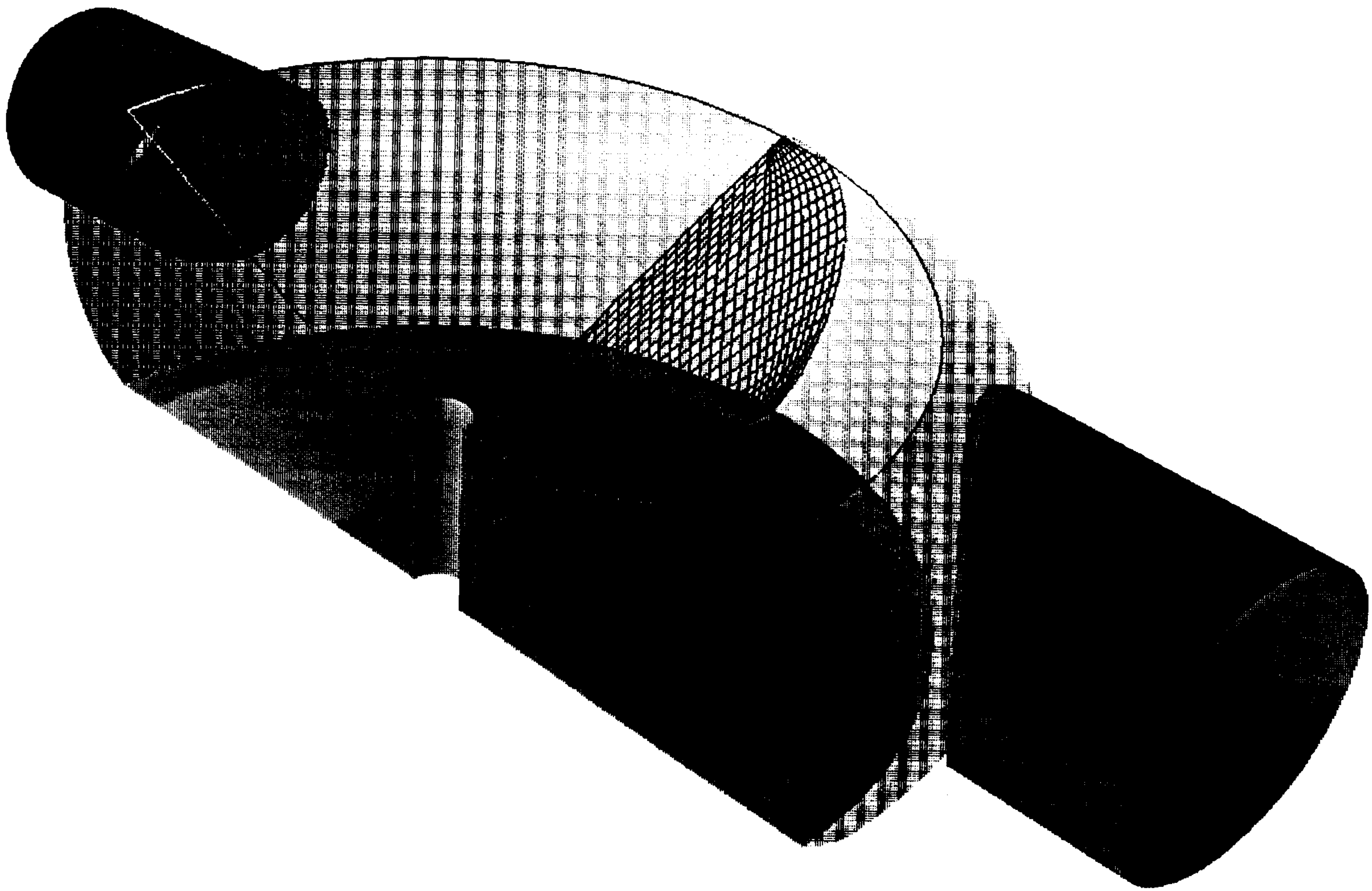

Geometry of Hot Gas Injector Assembly

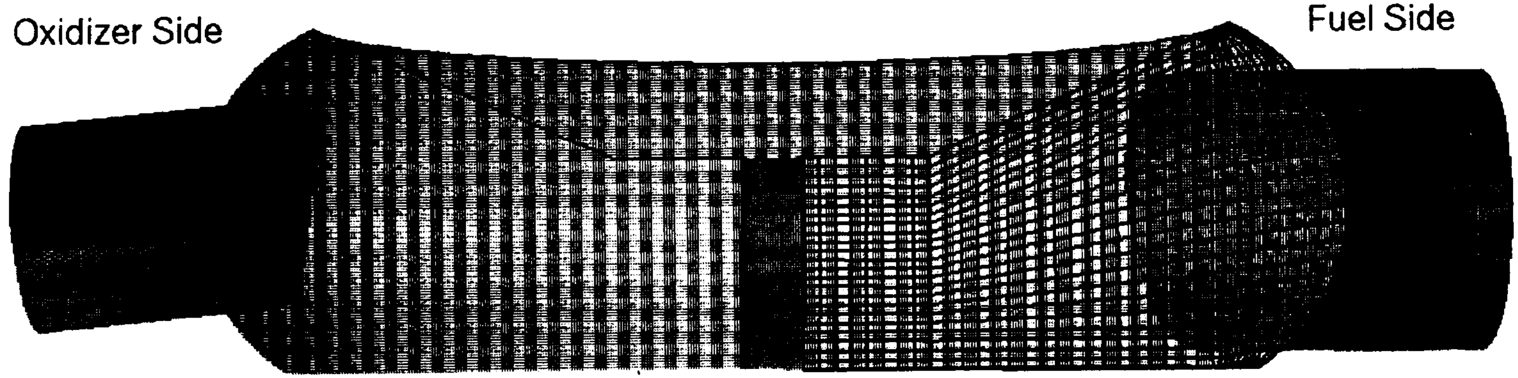

LOX POST ASSEMBLY TORUS, VELOCITY VECTORS AT SYMMETRY PLANE

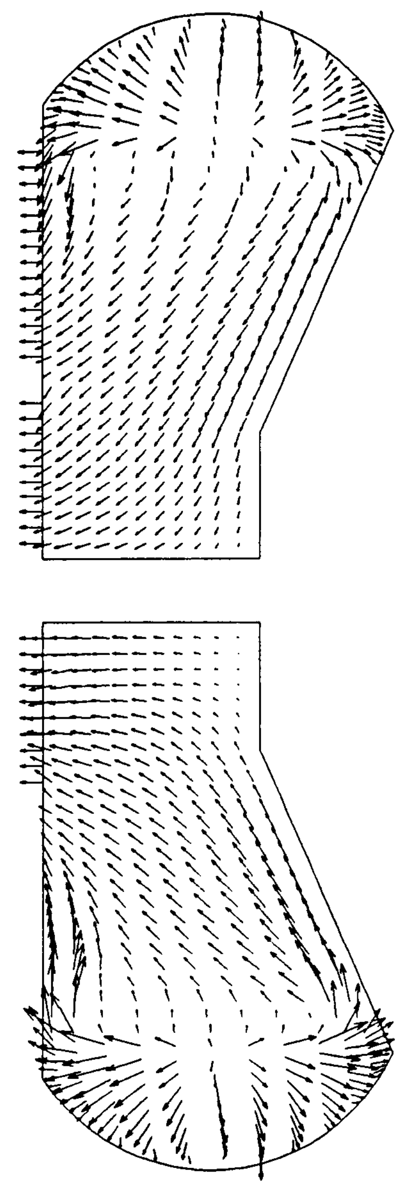

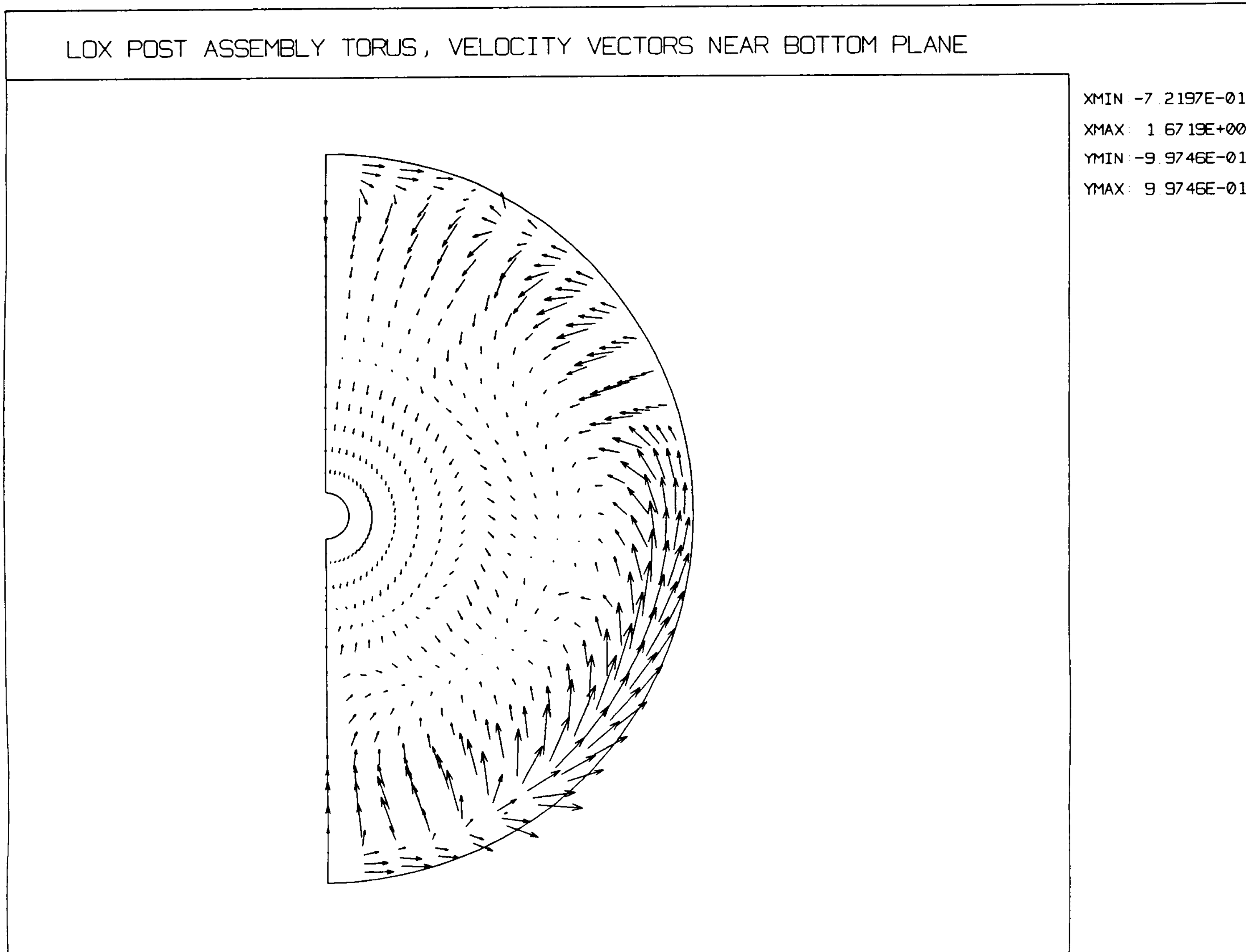
LOX POST ASSEMBLY TORUS, VELOCITY VECTORS NEAR BOTTOM PLANE
XMIN -7.2197E-01
XMAX 1.6719E+00
YMIN -9.9746E-01
YMAX 9.9746E-01

LOX POST ASSEMBLY TORUS, VELOCITY VECTORS NEAR MID PLANE

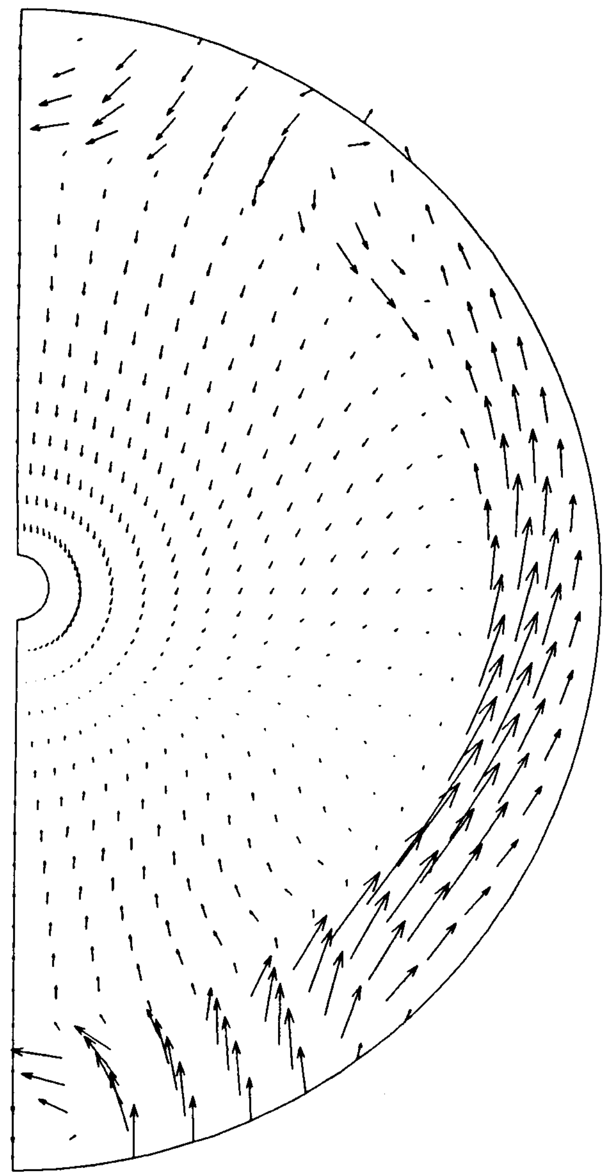

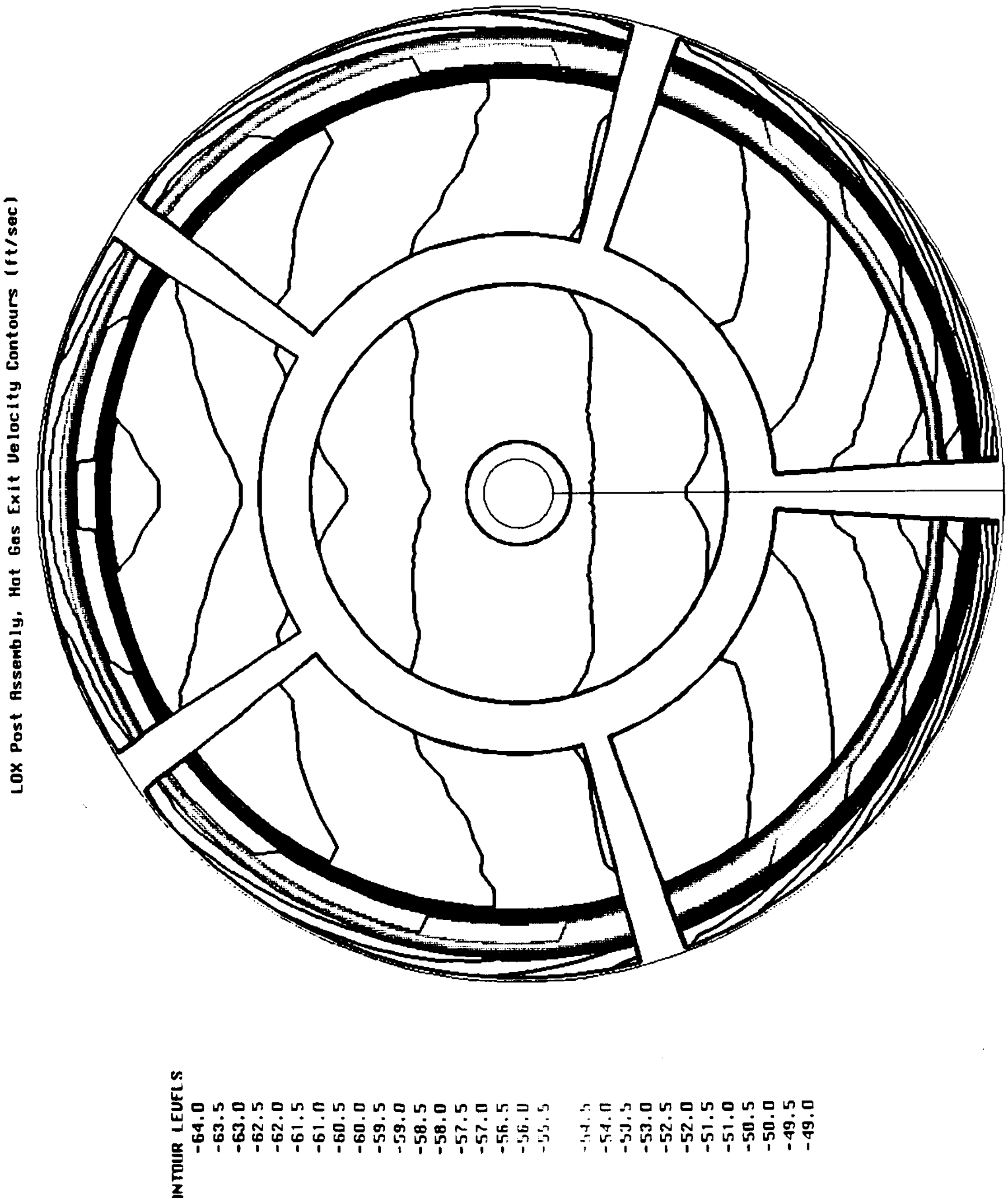

ORIGINAL PAGE IS
OF POOR QUALITY

LOX Post Assembly, Hot Gas Exit Pressure Contours (psf)

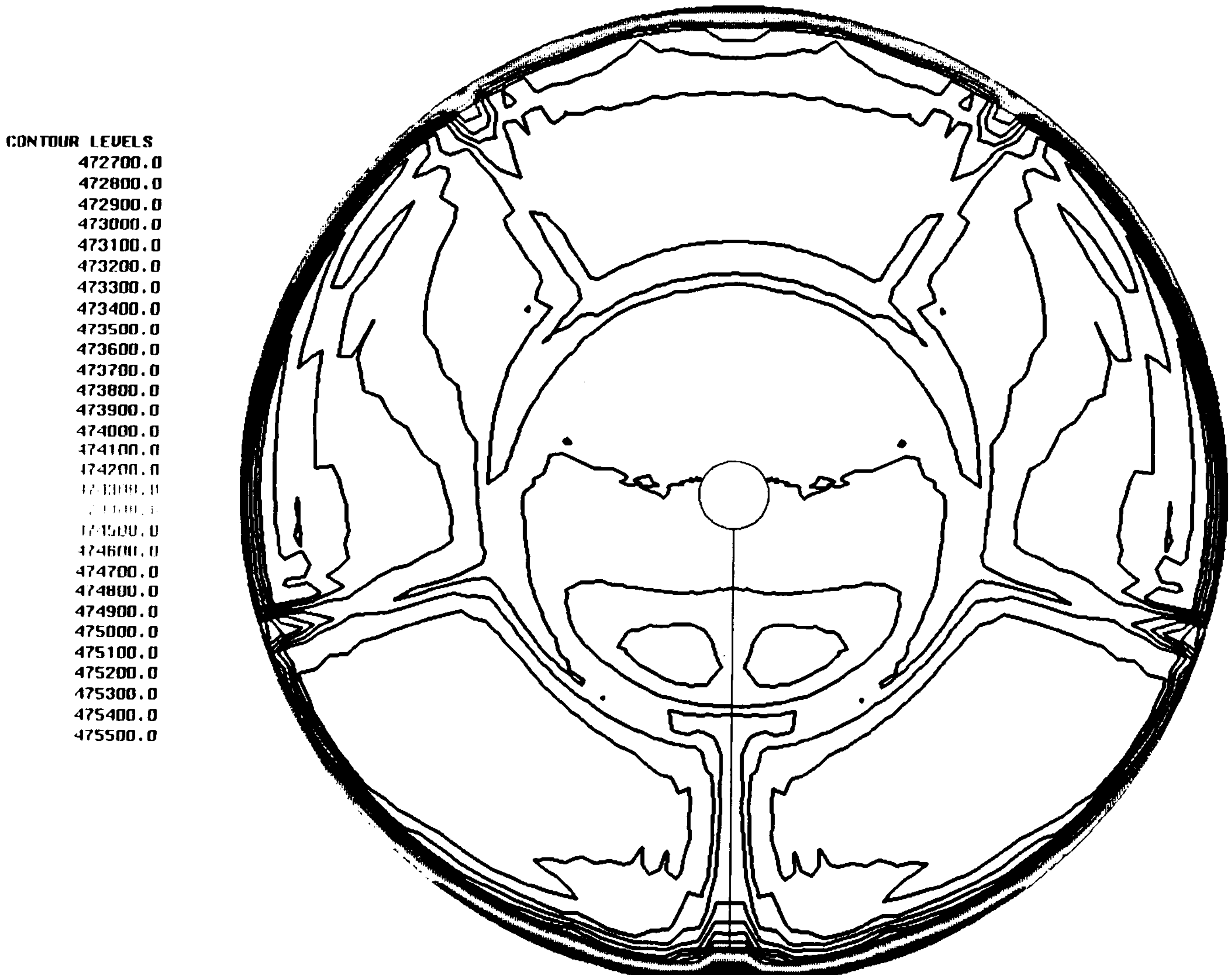

- **HYDROGEN CAVITY**
  - GRID SIZE: 29 x 91 x 14
  - INLET FLOW CONDITIONS
    - Static Pressure: 3395 psi
    - Static Temperature: 448.66 $^{\circ}R$
    - Reynolds no.: 2.52×10^{7} ft^{-1}
    - Mass Flow Rate: 14.55 lb/sec (symmetrical)
  - INCOMPRESSIBLE, SINGLE SPECIES

GRID SYSTEM OF THE HYDROGEN CAVITY (29 X 91 X 14)

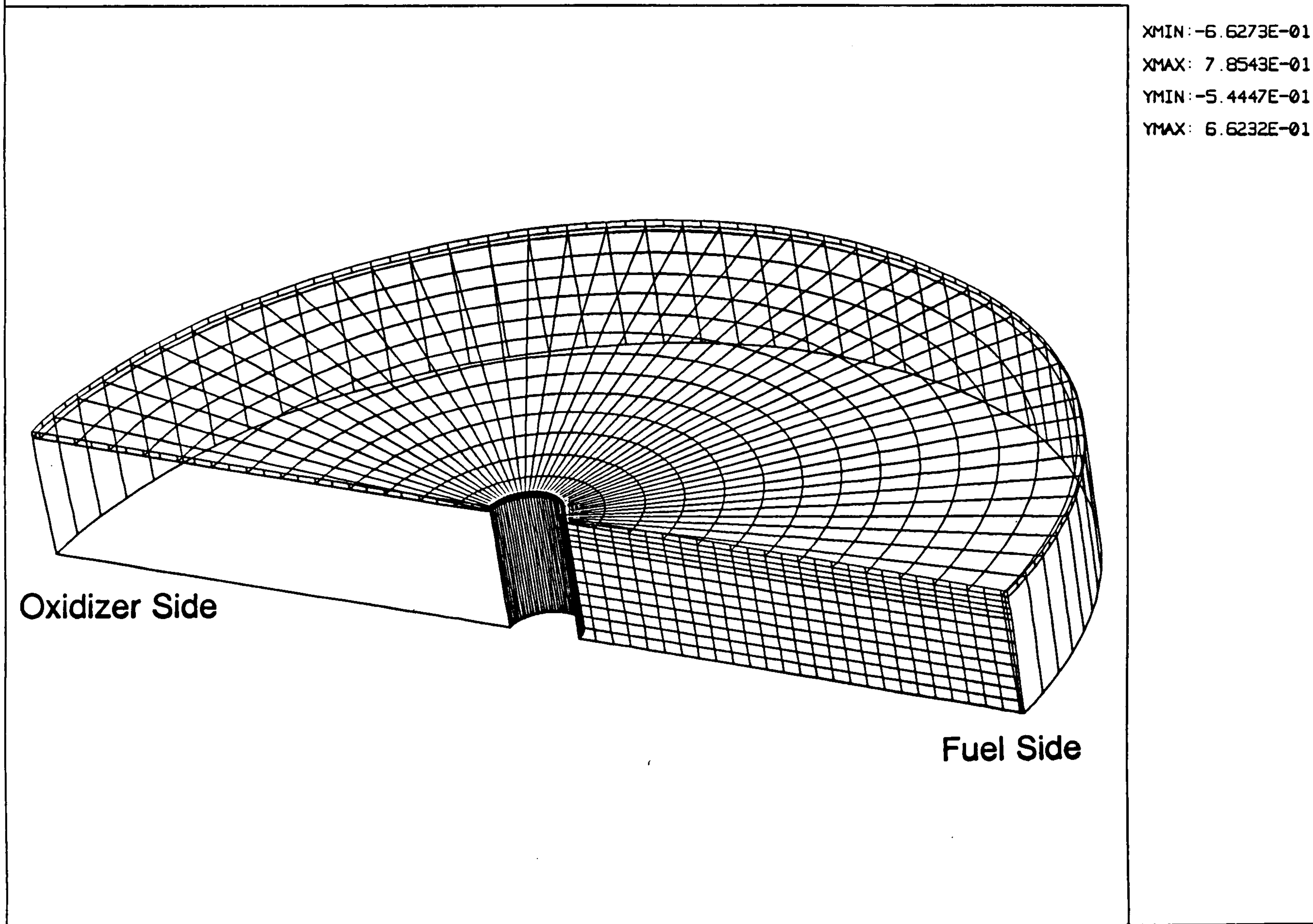

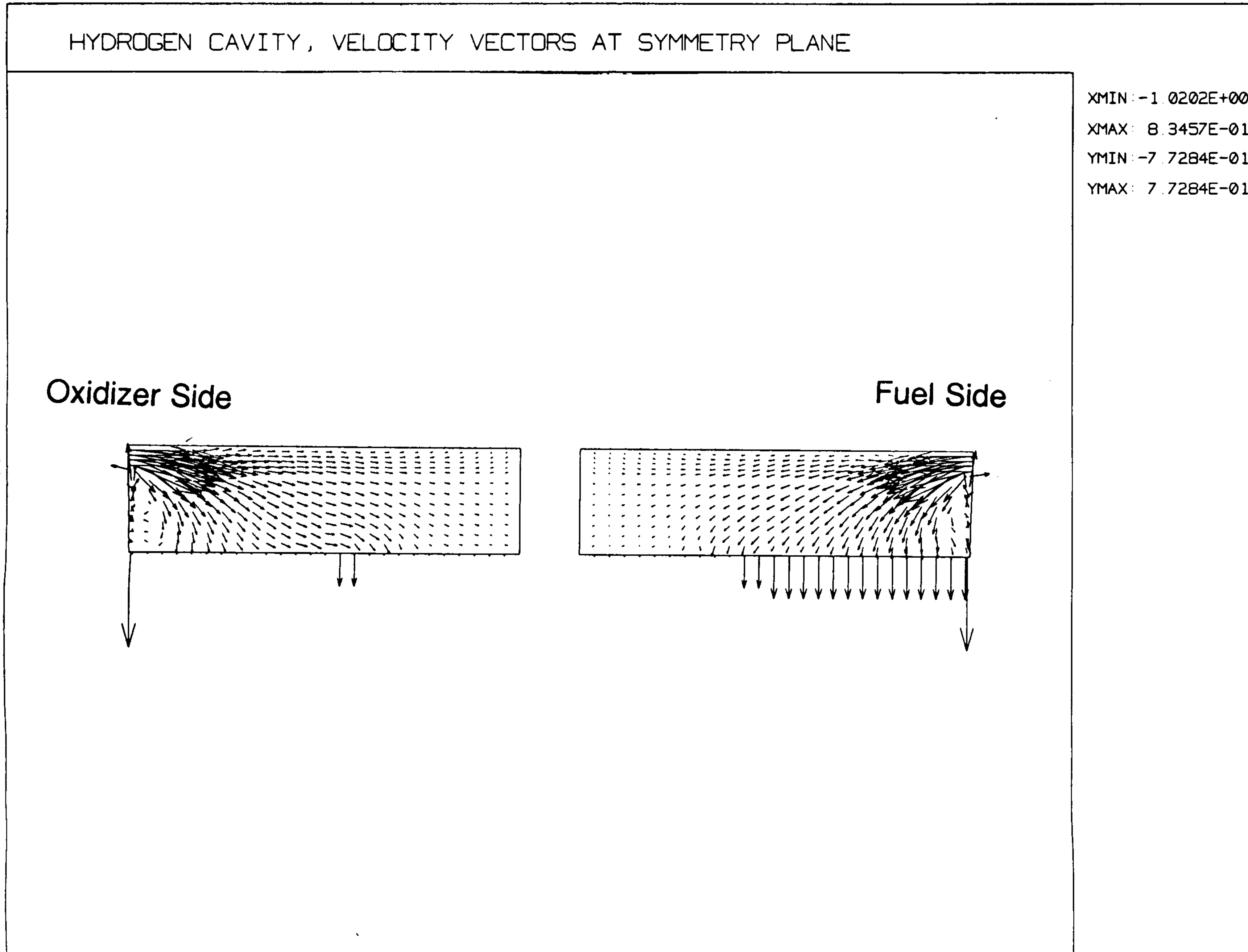
HYDROGEN CAVITY, VELOCITY VECTORS AT SYMMETRY PLANE
XMIN: -1.0202E+00
XMAX: 8.3457E-01
YMIN: -7.7284E-01
YMAX: 7.7284E-01
Oxidizer Side
Fuel Side

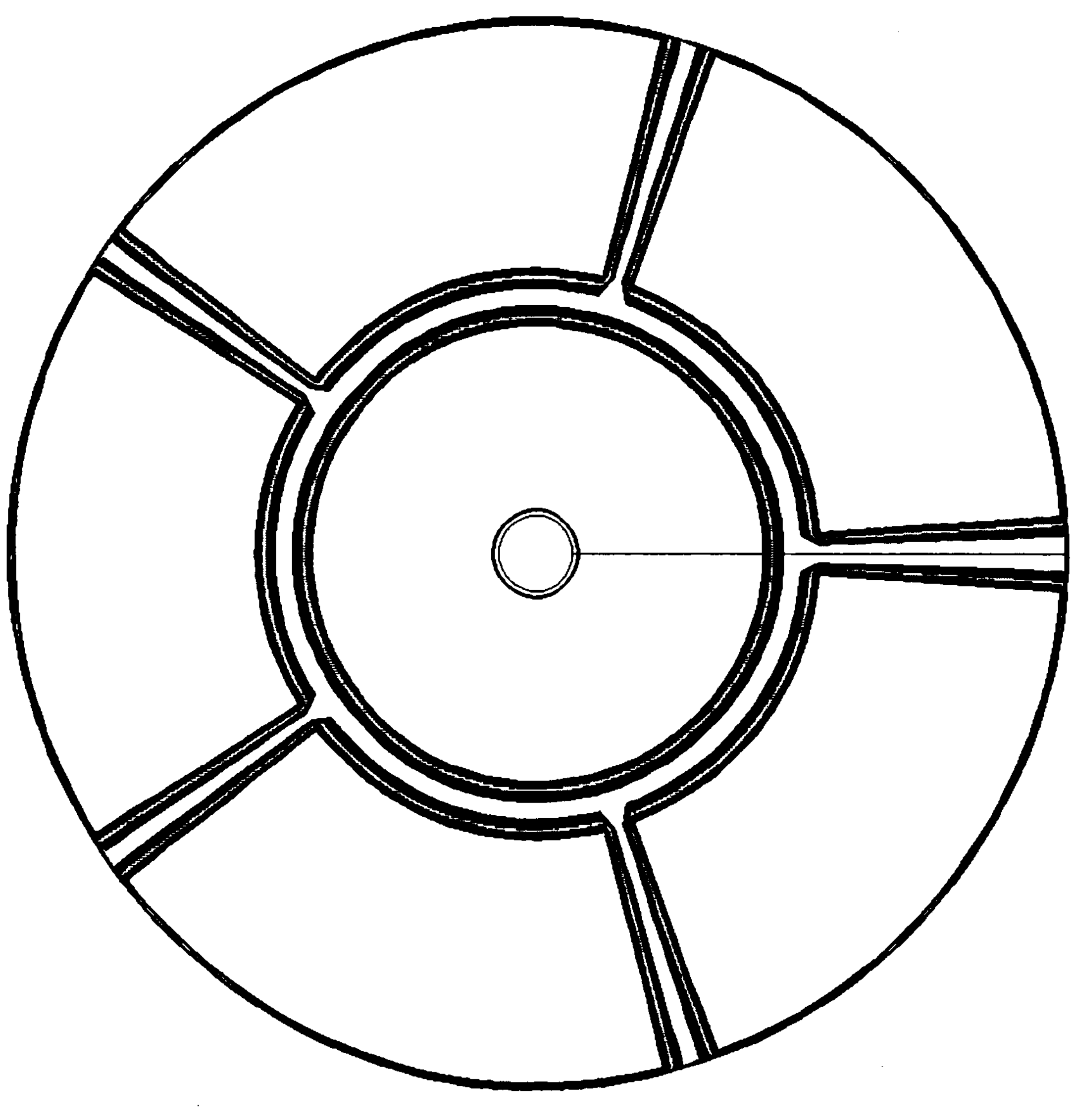
Hydrogen Cavity, Exit Flow Velocity Contours (ft/sec)
CONTOUR LEVELS
-61.0
-58.0
-55.0
-52.0
-49.0
-46.0
-43.0
-40.0
-37.0
-34.0
-31.0
-28.0
-22.0
-19.0
-16.0
-13.0
-10.0
-7.0
-4.0
-1.0

O/F Ratio Contours of the Main Injector Assembly (104% RPL)

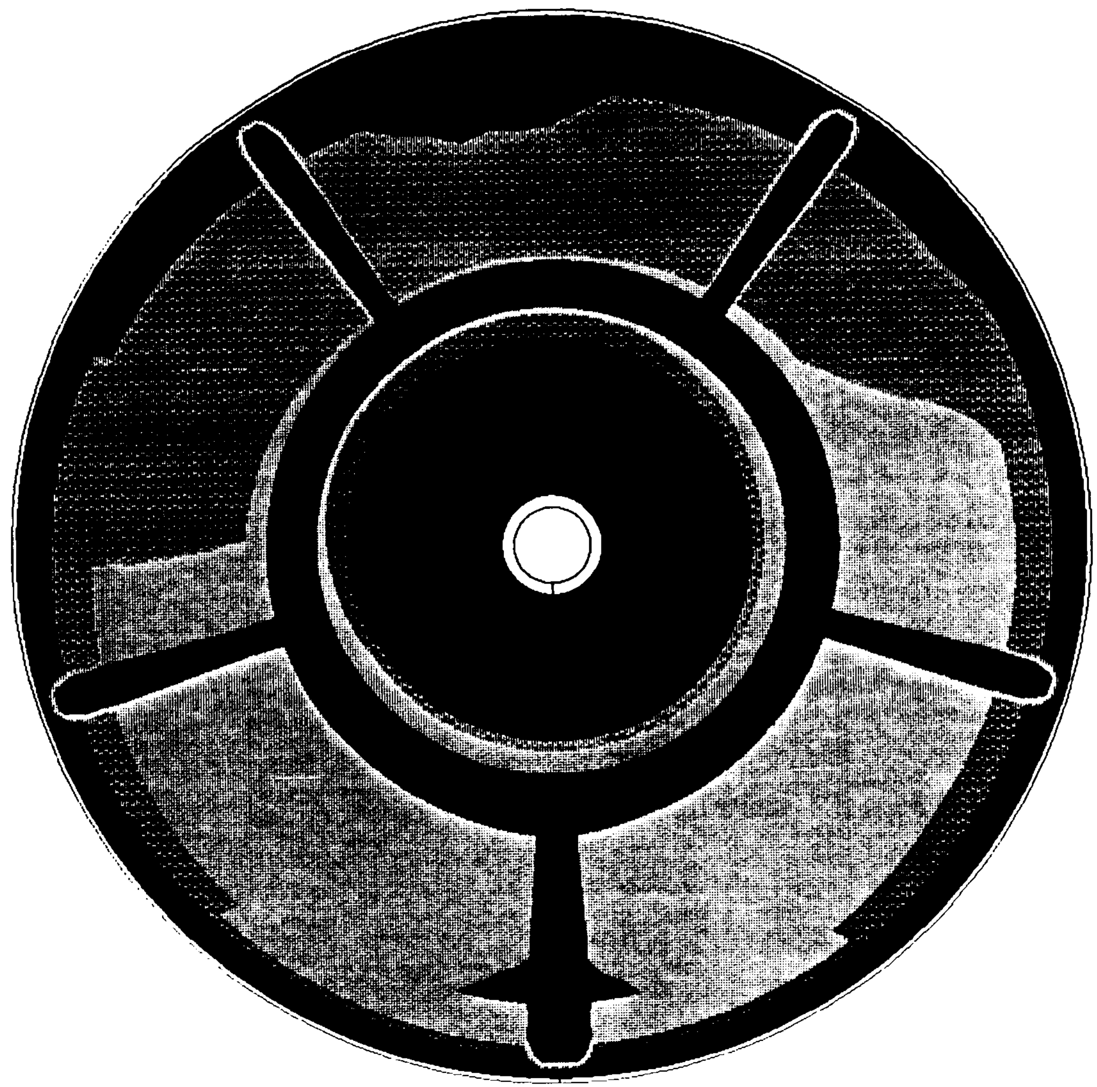

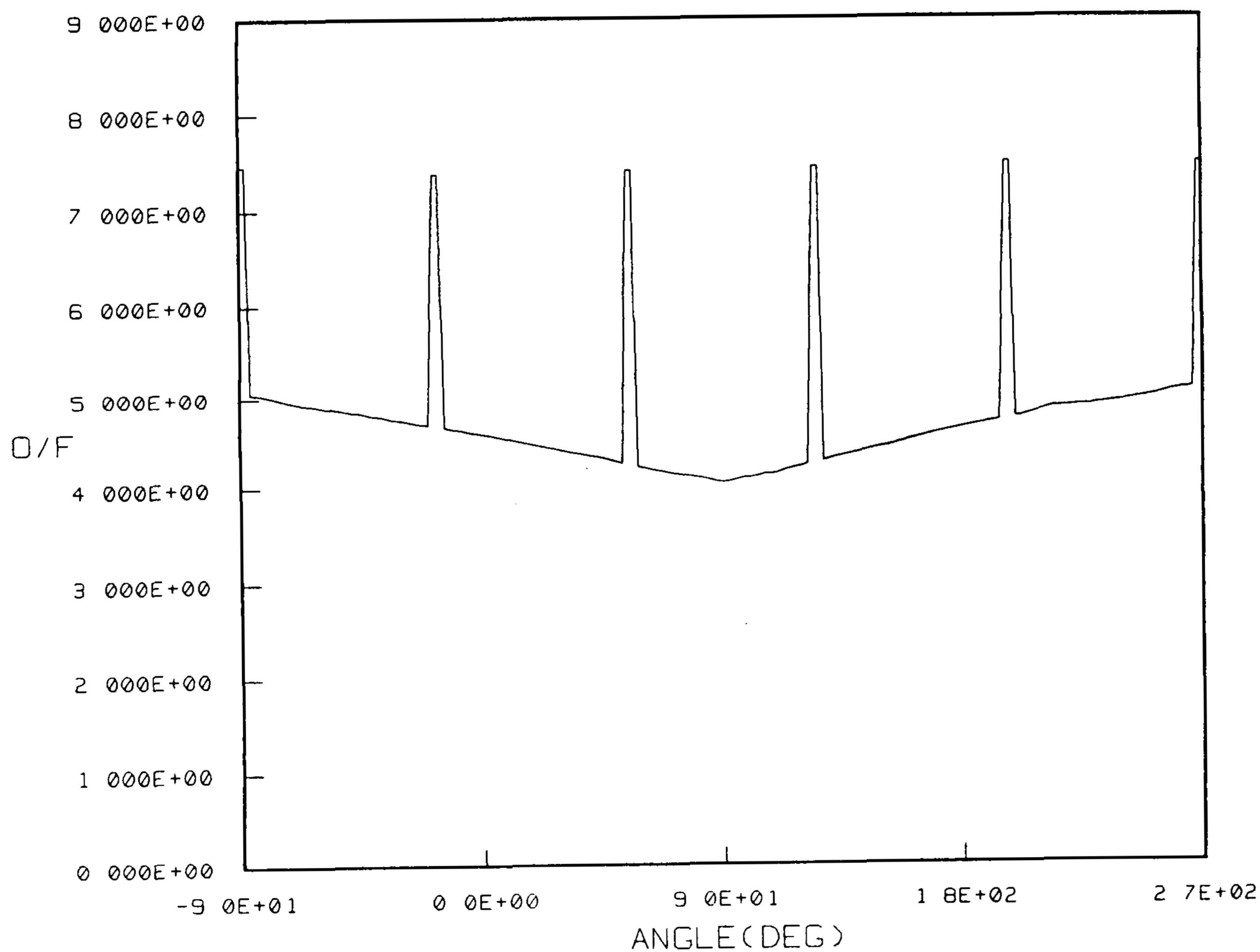

THE O/F RATIO DISTRIBUTION ALONG THE OUTER EDGE OF THE INJECTOR FACE (NO BLC COOLANT ADDED)

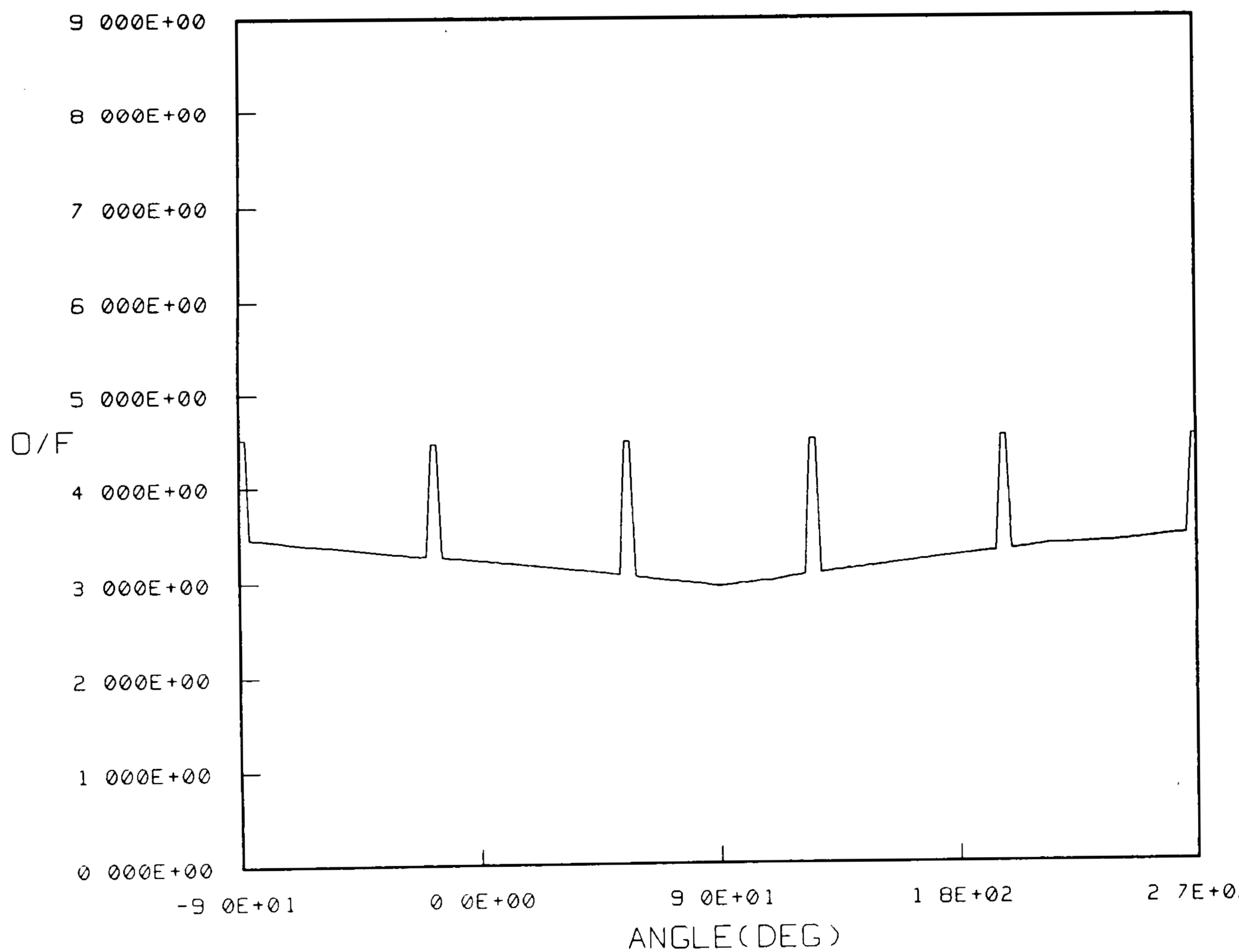

THE O/F RATIO DISTRIBUTION ALONG THE OUTER EDGE OF THE INJECTOR FACE (WITH BLC COOLANT ADDED)

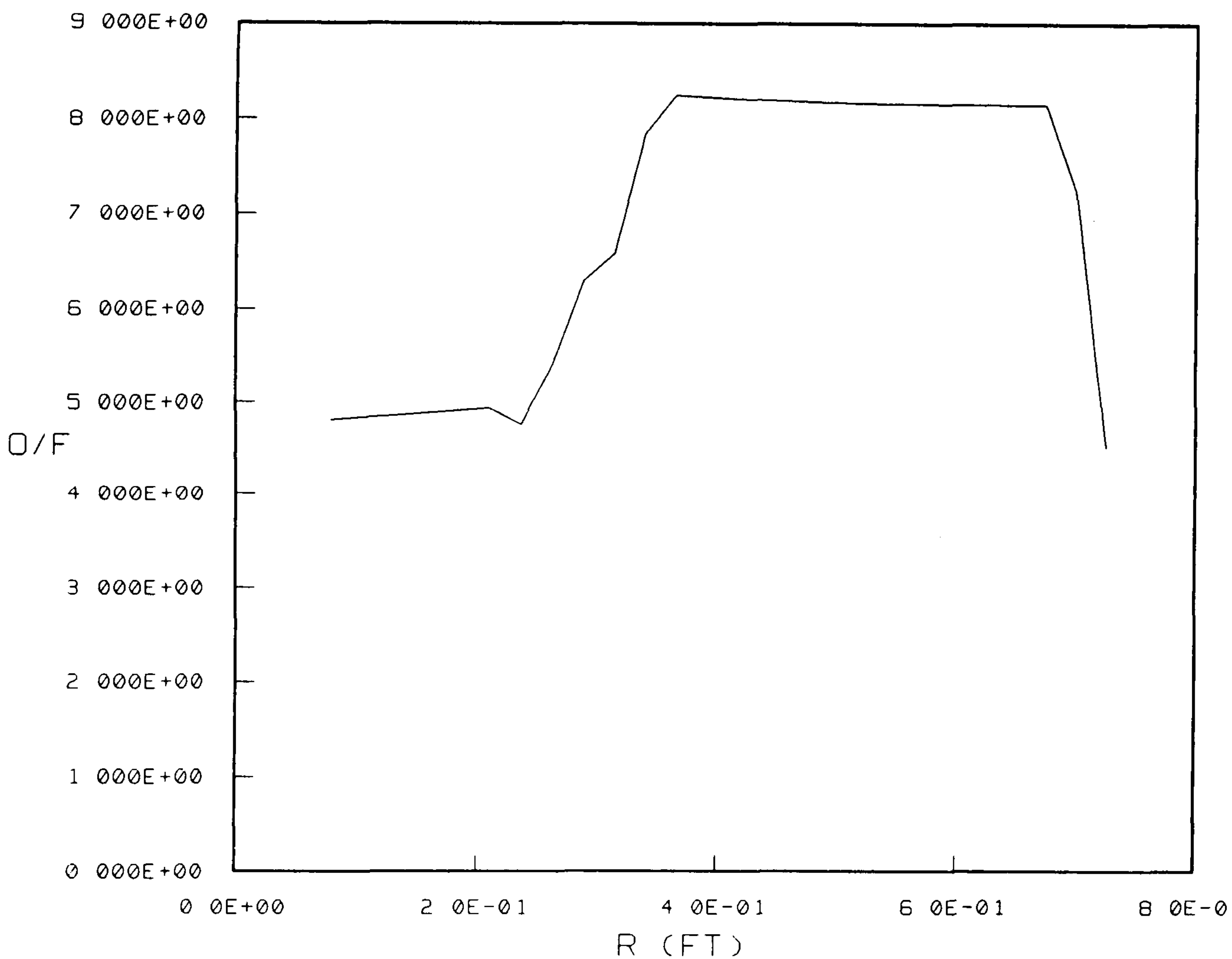

THE O/F RATIO DISTRIBUTION AT -90 DEG (FUEL SIDE) OF THE INJECTOR FACE (WITH BLC COOLANT ADDED)

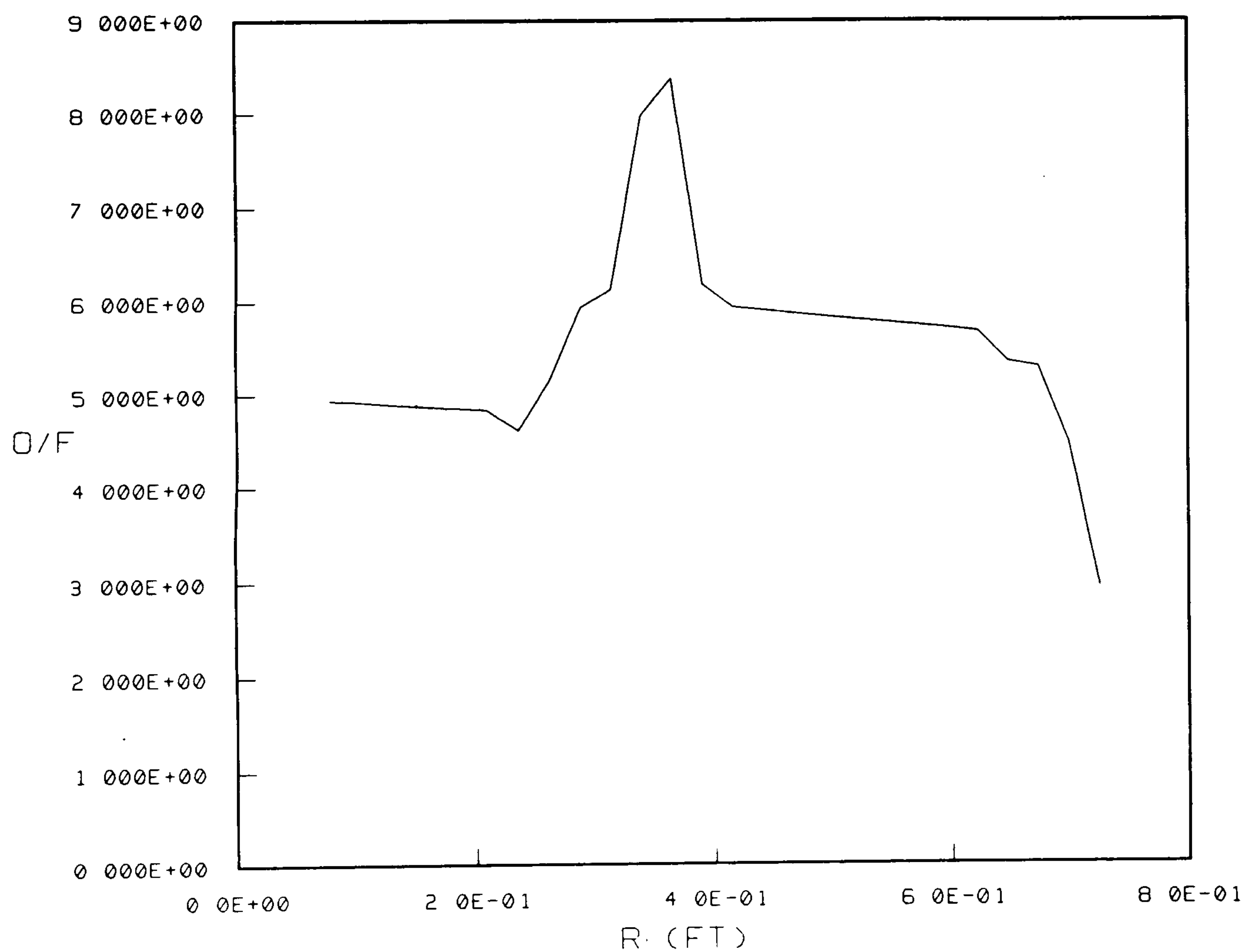

THE O/F RATIO DISTRIBUTION AT 90 DEG (OXIDIZER SIDE) OF THE INJECTOR FACE (WITH BLC COOLANT ADDED)

CONCLUSIONS AND RECOMMENDATIONS

- THE PREDICTED O/F RATIO IS CLOSE TO STOICHIOMETRIC AROUND BAFFLE ELEMENTS
- THE RESULTS OF THIS STUDY SHOULD BE USED TO PREDICT ENGINE PERFORMANCE AND HEAT LOADS
- LOCAL MASS FLOW RATE DISTRIBUTION IS DEPENDENT ON PRESSURE AND LOSS COEFFICIENT DISTRIBUTION
- THE 3-D POROSITY/CFD ANALYSIS OF THE POWER HEAD CAN BE IMPROVED BY
    - KNOWING THE DISTRIBUTION OF CHAMBER PRESSURE AND OF BAFFLE ELEMENT DISCHARGE PRESSURE
    - THE MEASUREMENT OF LOSS COEFFICIENTS FOR EACH COMPONENTS
    - USING PROPER INLET FLOW PROFILES TO THE LOX DOME

N92-32261

Computational Fluid Dynamics Analysis of SSME Phase II and Phase II+ Preburner Injector Element Hydrogen Flow Paths

Joseph H. Ruf

Computational Fluid Dynamics Branch

Marshall Space Flight Center, NASA

Phase II+ Space Shuttle Main Engine powerheads E0209 and E0215 degraded their Main Combustion Chamber (MCC) liners at a faster rate than is normal for phase II powerheads. One possible cause of the accelerated degradation was a reduction of coolant flow through the MCC. Hardware changes were made to the preburner fuel leg which may have reduced the resistance and, therefore, pulled some of the hydrogen from the MCC coolant leg.

The preburner injector element's hydrogen flow path changed significantly from the phase II to the II+ design. The hydrogen inlet area was reduced by 42 percent, the annulus length was shortened, and the geometry of the annulus convergence section changed. With the large reduction of inlet area, an increased resistance would normally be expected. However, a 10 percent decrease in fuel flow resistance was quoted for phase II+ preburner injector elements.

To resolve this discrepancy, a Computational Fluid Dynamics analysis was performed to determine hydrogen flow path resistances of the phase II+ fuel preburner injector elements relative to the phase II element. The analysis was performed for 104 percent RPL conditions. FDNS was implemented on axisymmetric grids with the hydrogen assumed incompressible. The analysis was performed in two steps. The first isolated the effect of the different inlet areas and the second modeled the entire injector element hydrogen flow path.

The isolated effect of the reduced inlet area was a 3. percent increased resistance for phase II+ elements. However, the entire flow path model showed no difference between phase II and II+ injector element resistances. Phase II+ annulus geometry changes compensated for the reduced inlet area such that there was no net effect on hydrogen flow path resistance.

Computational Fluid Dynamic Analysis of SSME Phase II and Phase II+ Preburner Injector Element Hydrogen Flow Paths

Joseph H. Ruf
Computational Fluid Dynamics Branch
Marshall Space Flight Center

George C. Marshall Space Flight Center
Structures and Dynamics Laboratory
Computational Fluid Dynamics Branch

NASA

Computational Fluid Dynamic Analysis of SSME Phase II and Phase II+ Preburner Injector Element Hydrogen Flow Paths

- OBJECTIVE
- BACKGROUND
- APPROACH
- RESULTS
- CONCLUSION

OBJECTIVE

- Analytically determine the hydrogen flow path resistance of the phase II+ preburner injector elements.

BACKGROUND

- A number engine hardware changes were made from phase II to II+ to improve the operating environment in the SSME.

- Hot fire testing of E0209 and E0215 phase II+ engines resulted in an increased rate of main combustion chamber (MCC) liner degradation.

- It was thought the phase II+ hardware changes altered the resistances in the fuel flow circuit such that the coolant flow to the MCC was reduced.

- One area of uncertainty was the resistance of the preburner injector elements. Phase II+ preburner injector element has a reduced hydrogen inlet area and a shorter hydrogen annulus.
  - Rocketdyne quoted a 10% decrease in hydrogen flow resistance for the phase II+ element with respect to phase II.

MAIN COMBUSTION CHAMBER

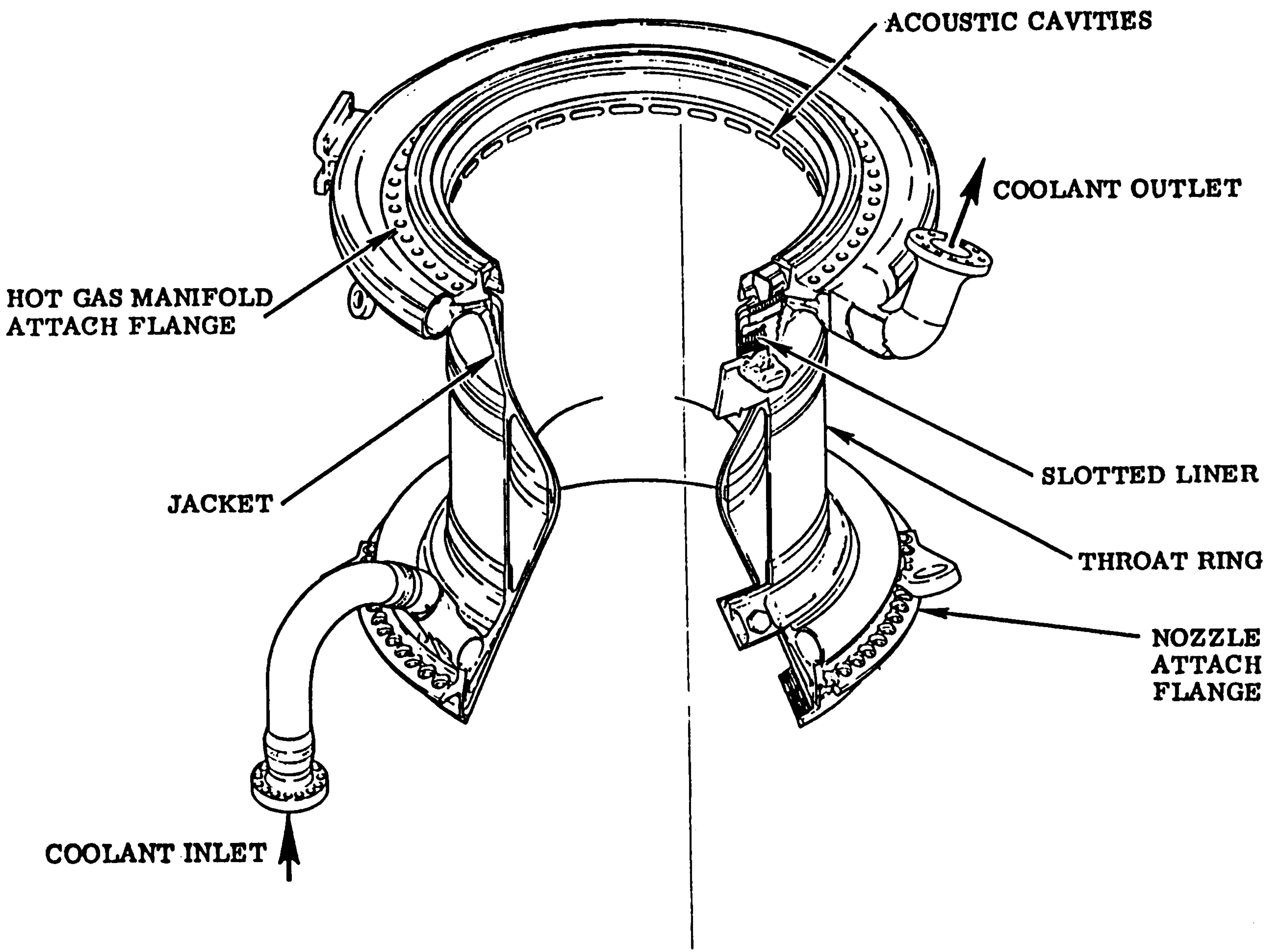

PHASE II+ INVESTIGATION

SIMPLIFIED RESISTANCE/FLOW MODEL SCHEMATIC:

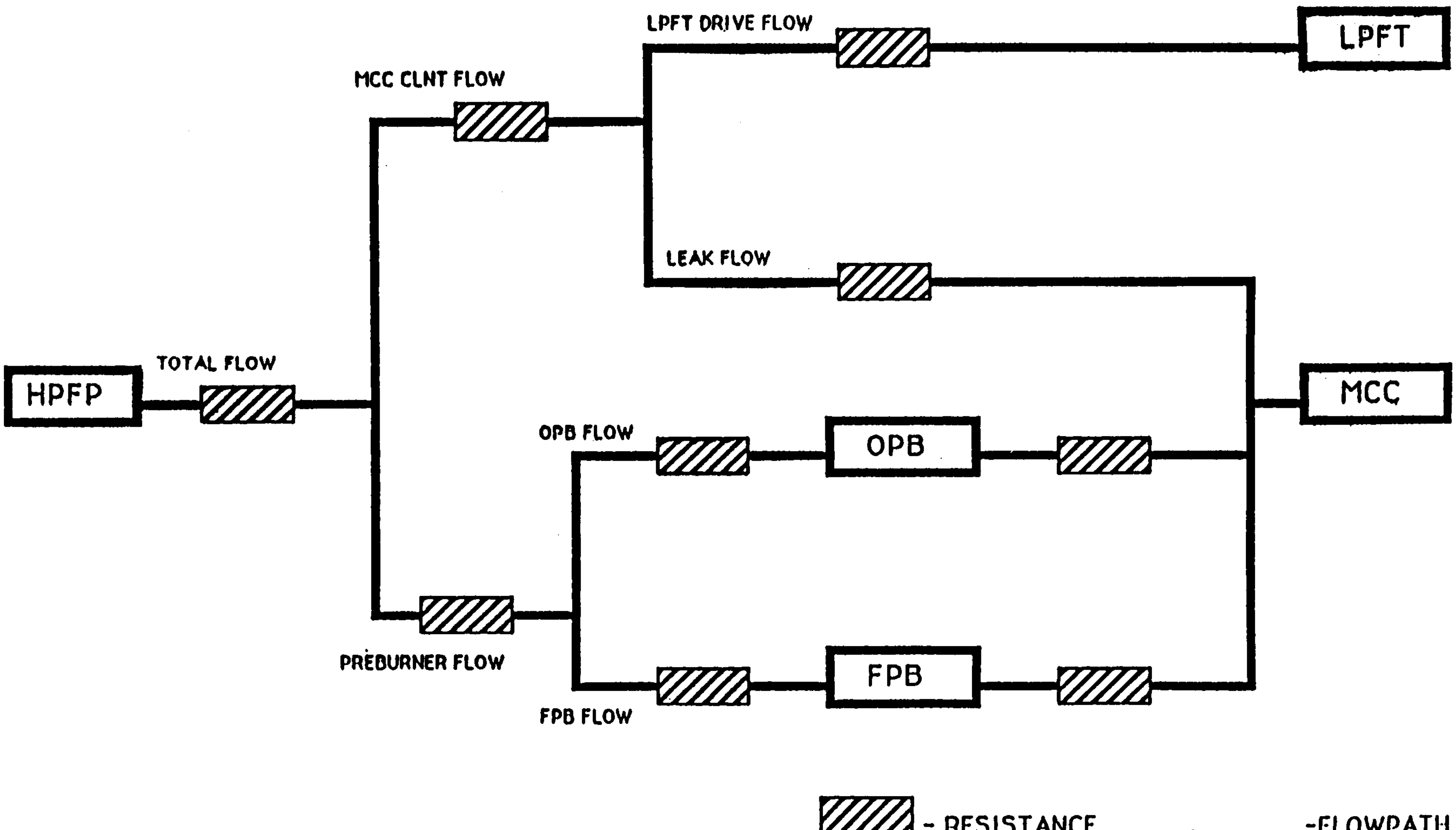

- PREBURNER INJECTOR ELEMENTS

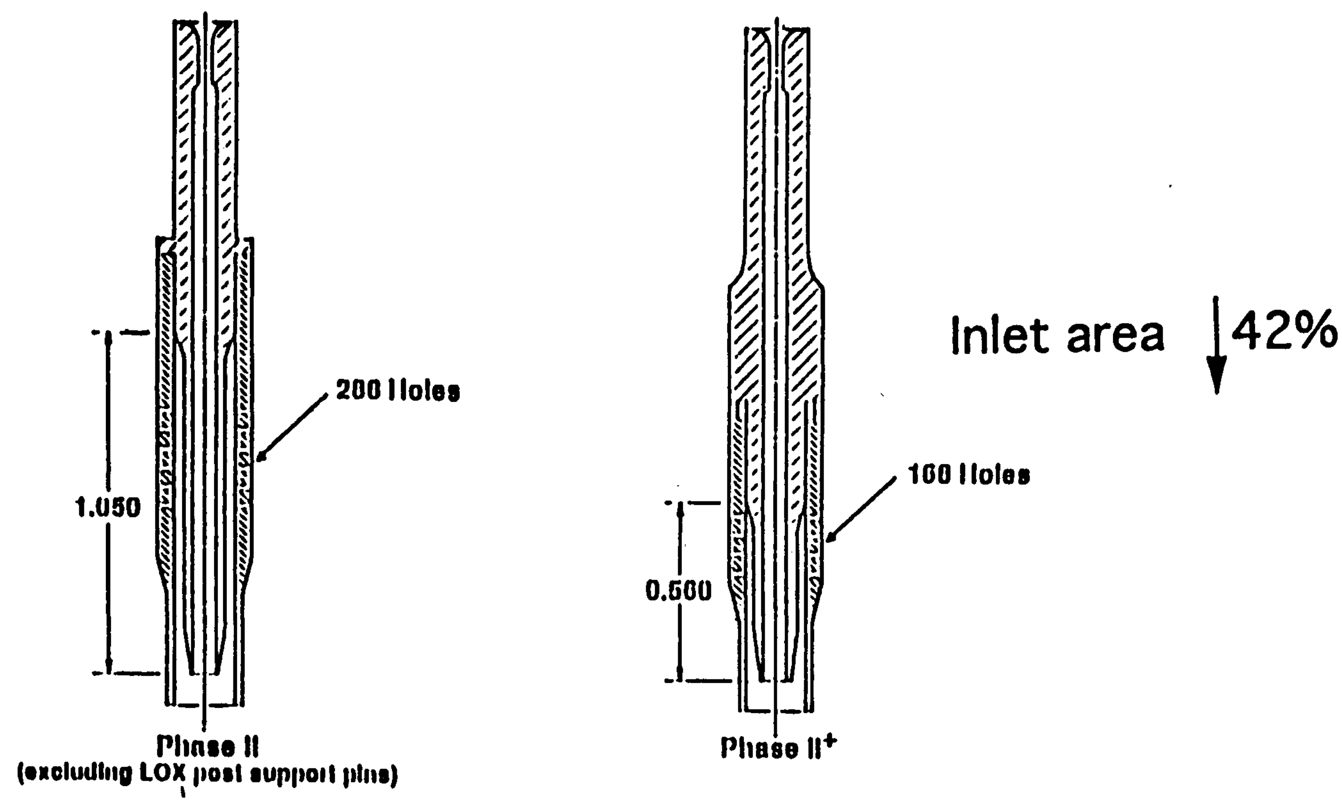

APPROACH

- Quantify the change in resistance/delta P with a comparative analysis of phase II and II+ elements.
  - phase II preburner injector element hydrogen flow delta P is 400 psi.

- Modeled the fuel preburner injector elements; oxidizer and fuel preburner injector elements are similar in both phase II and II+.

- Performed axisymetric CFD analysis (FDNS) of the hydrogen flow path of phase II and II+ elements at 104% RPL conditions
  - Assumptions:
    - o incompressible flow
    - o rows of inlet holes modeled as equivalent area circumferential channels
    - o LOX flow not modeled

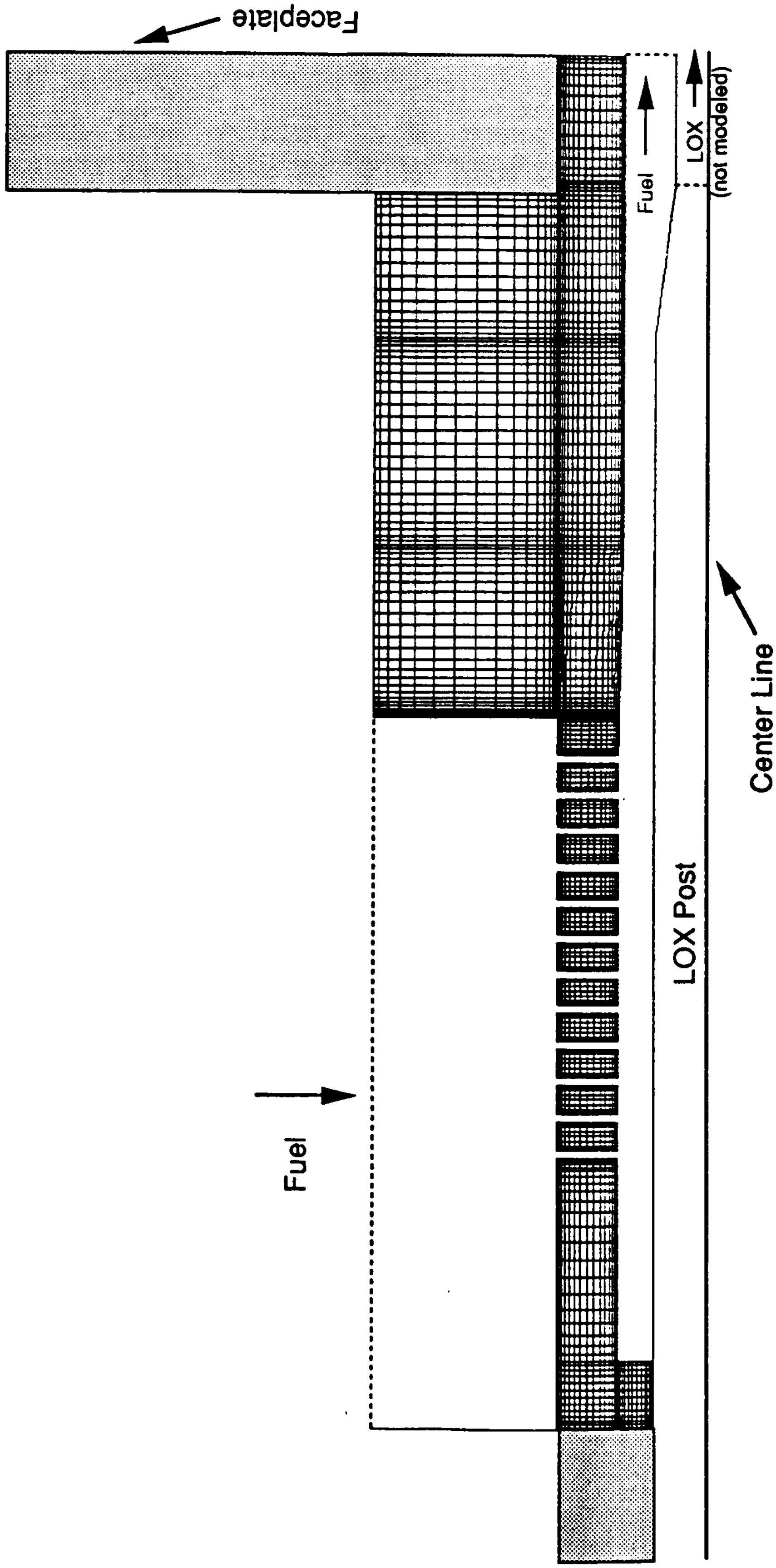
Faceplate
Fuel
LOX
(not modeled)
Center Line
LOX Post
Fuel

APPROACH, cont.

- Analysis done in two steps
  - quantify the effect of reduced inlet area
  - quantify effect of entire hydrogen flow path

- Specified mass flow rate and inlet pressure; resistance $\propto$ delta P.

- Performed grid independency study

Phase II

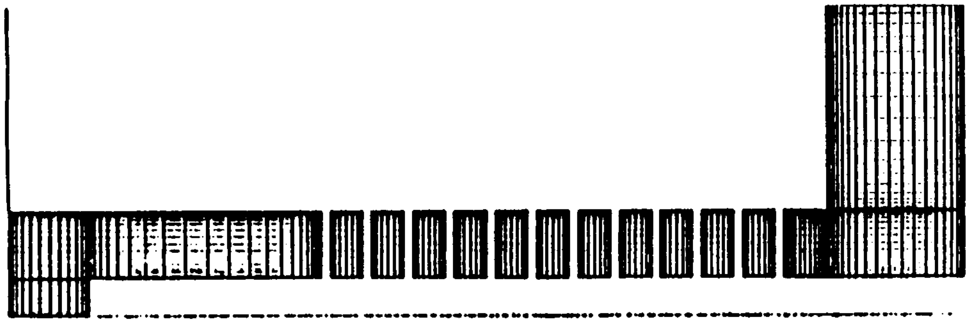

315x51 GRID

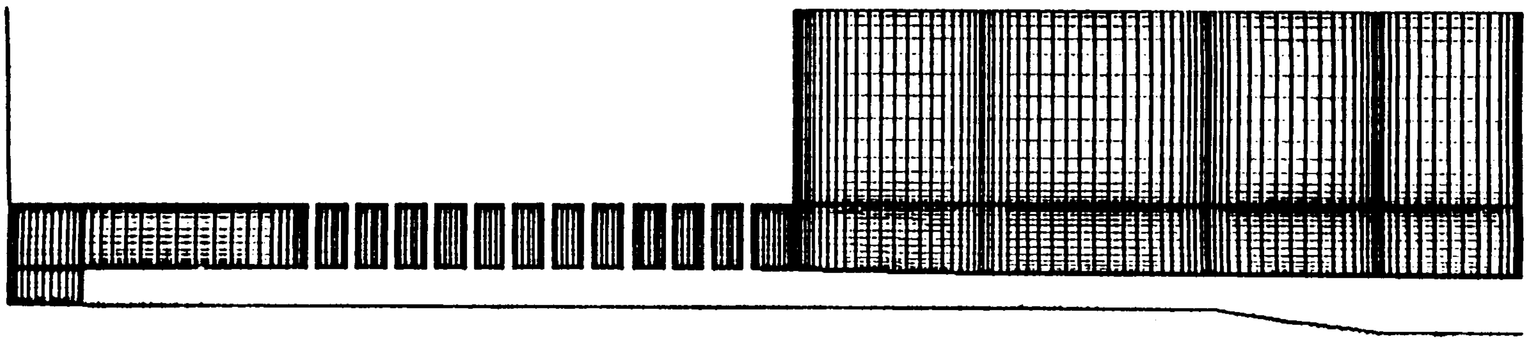

Phase II+

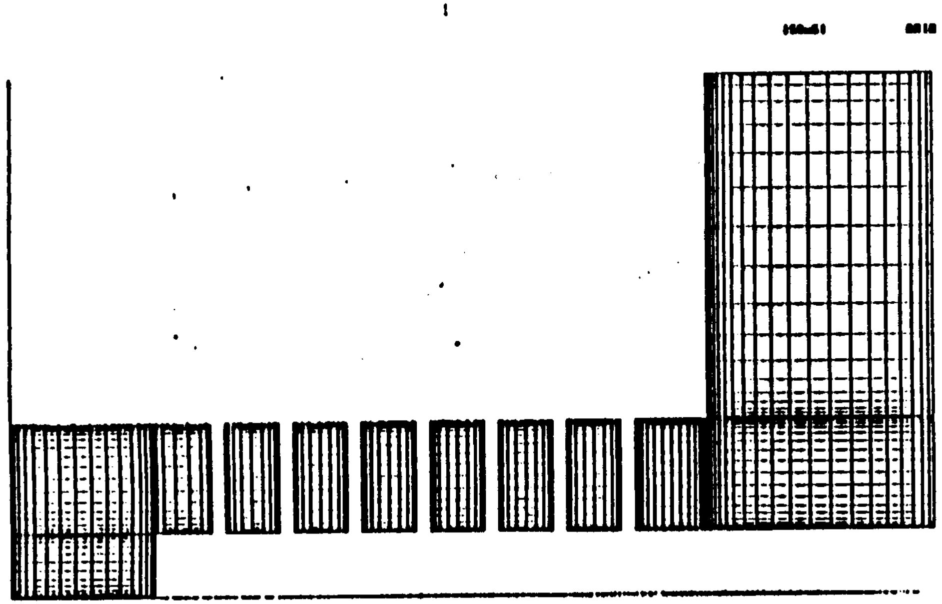

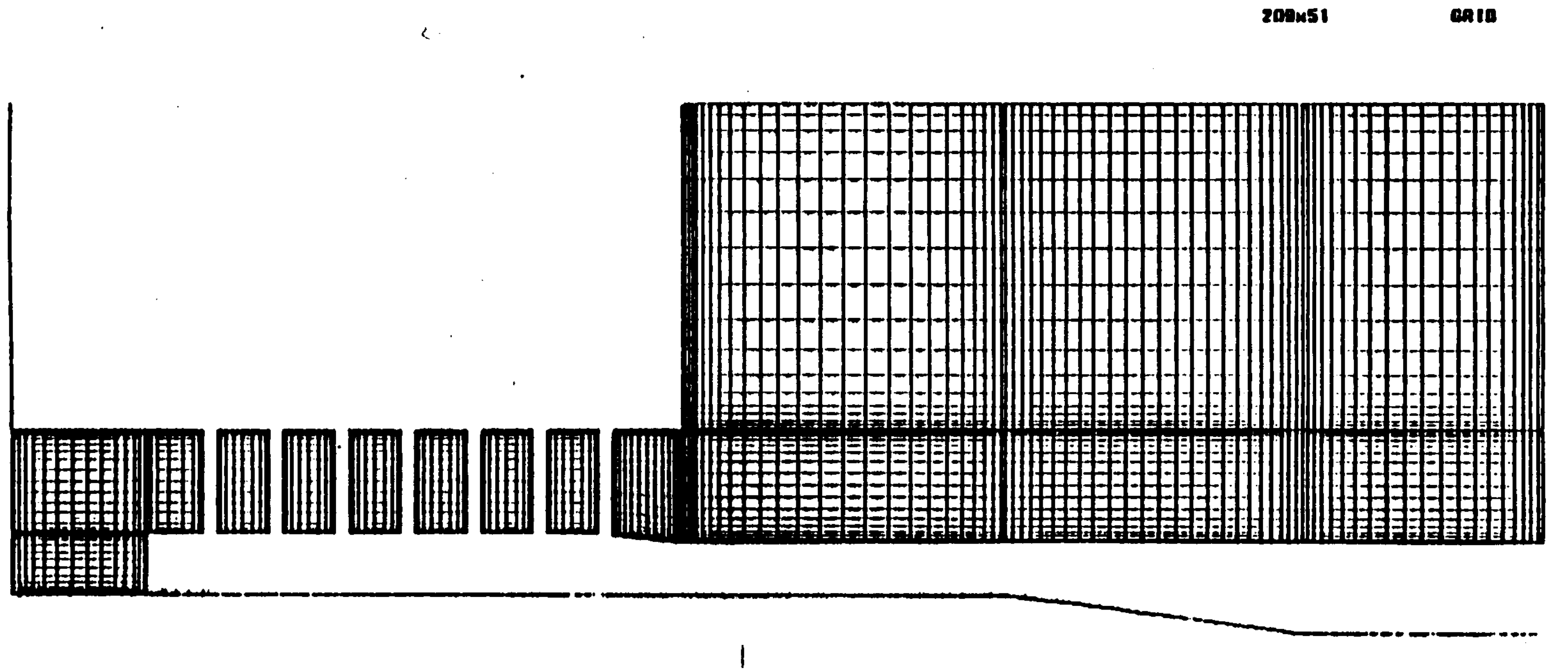

RESULTS

- Effect of inlet area
  - phase II delta P = 529 psi
  - phase II+ delta P = 545 psi — $\Delta = +3\%$
- Full hardware geometry
  - phase II delta P = 406 psi
  - phase II+ delta P = 405 psi — $\Delta = -0.25\%$
- Phase II calculated pressure drop matched well with accepted value (406 vs. 400 psi).
- Majority of the flow passes through the holes closest to the exit.

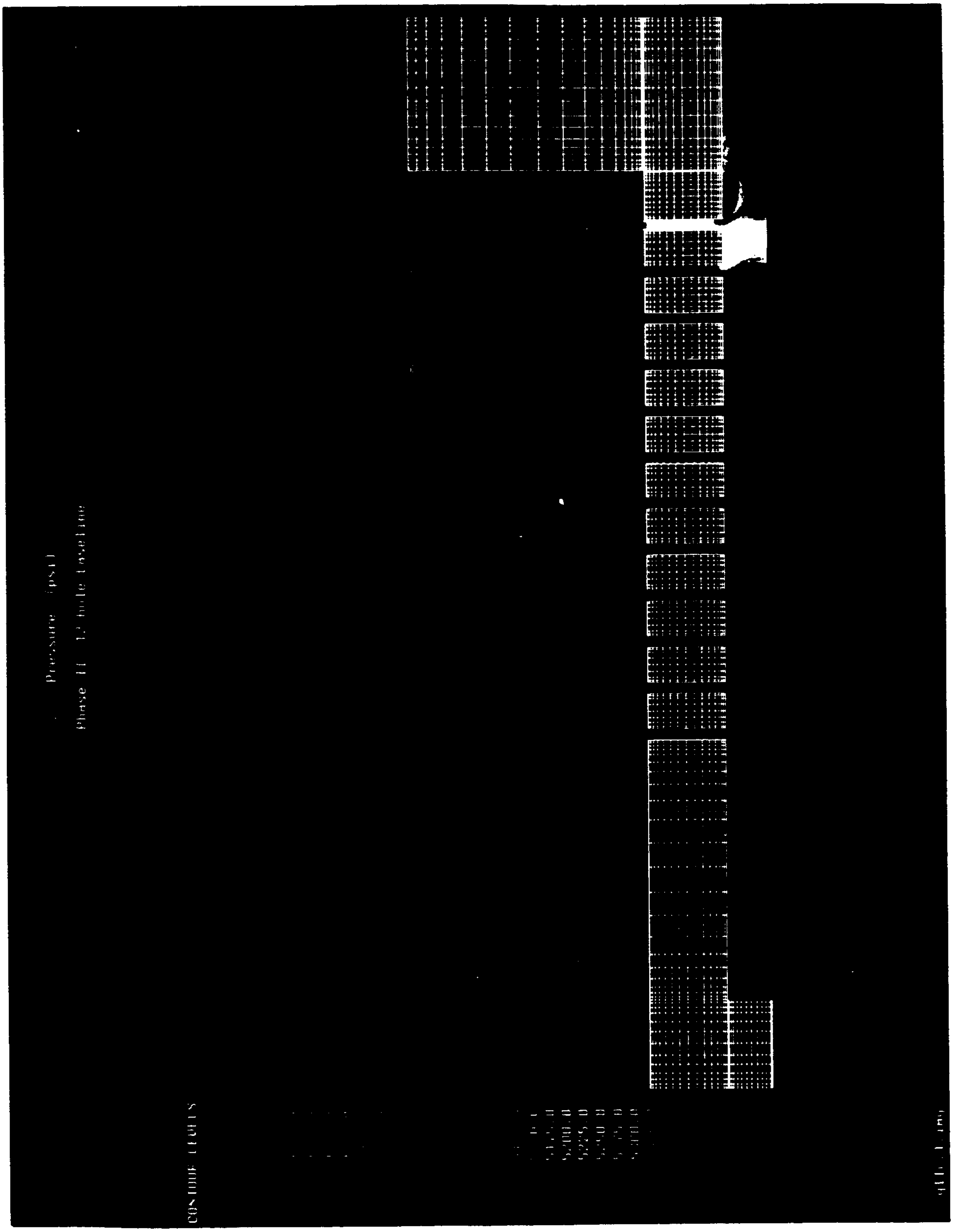
Pressure (psi)
CONTOUR LEVELS
5200.0
5225.0
5250.0

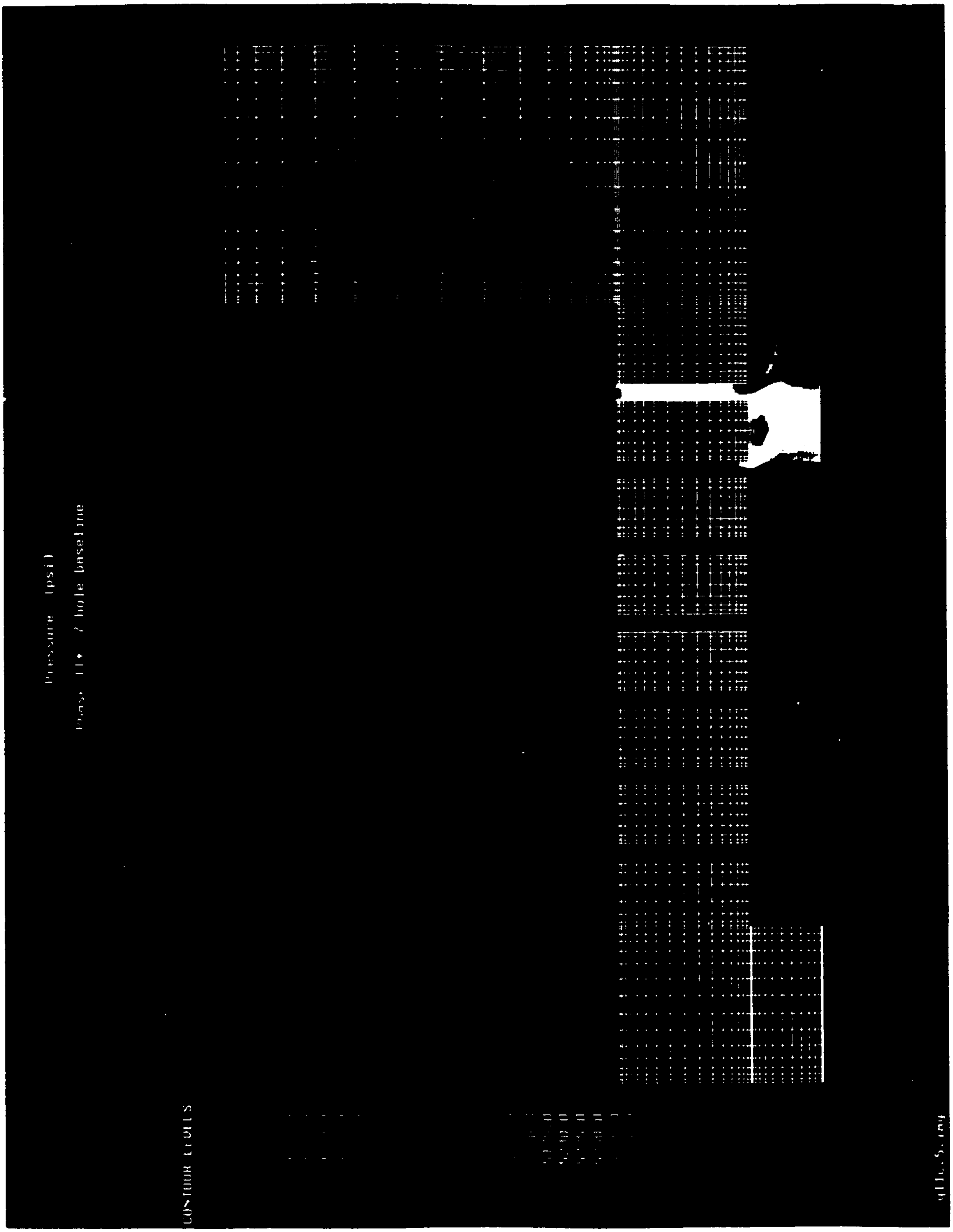

ORIGINAL PAGE IS
OF POOR QUALITY

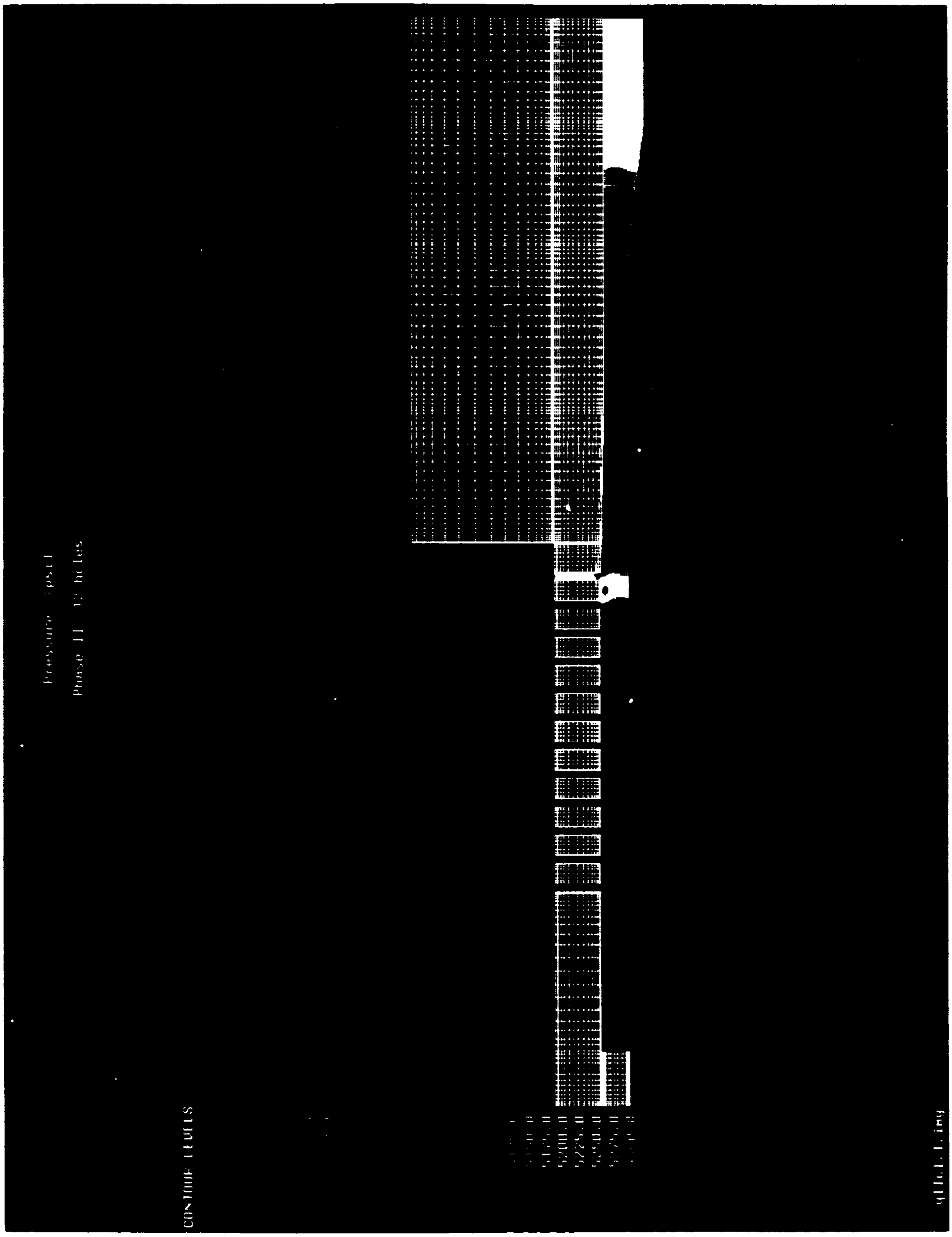
CONTOUR LEVELS

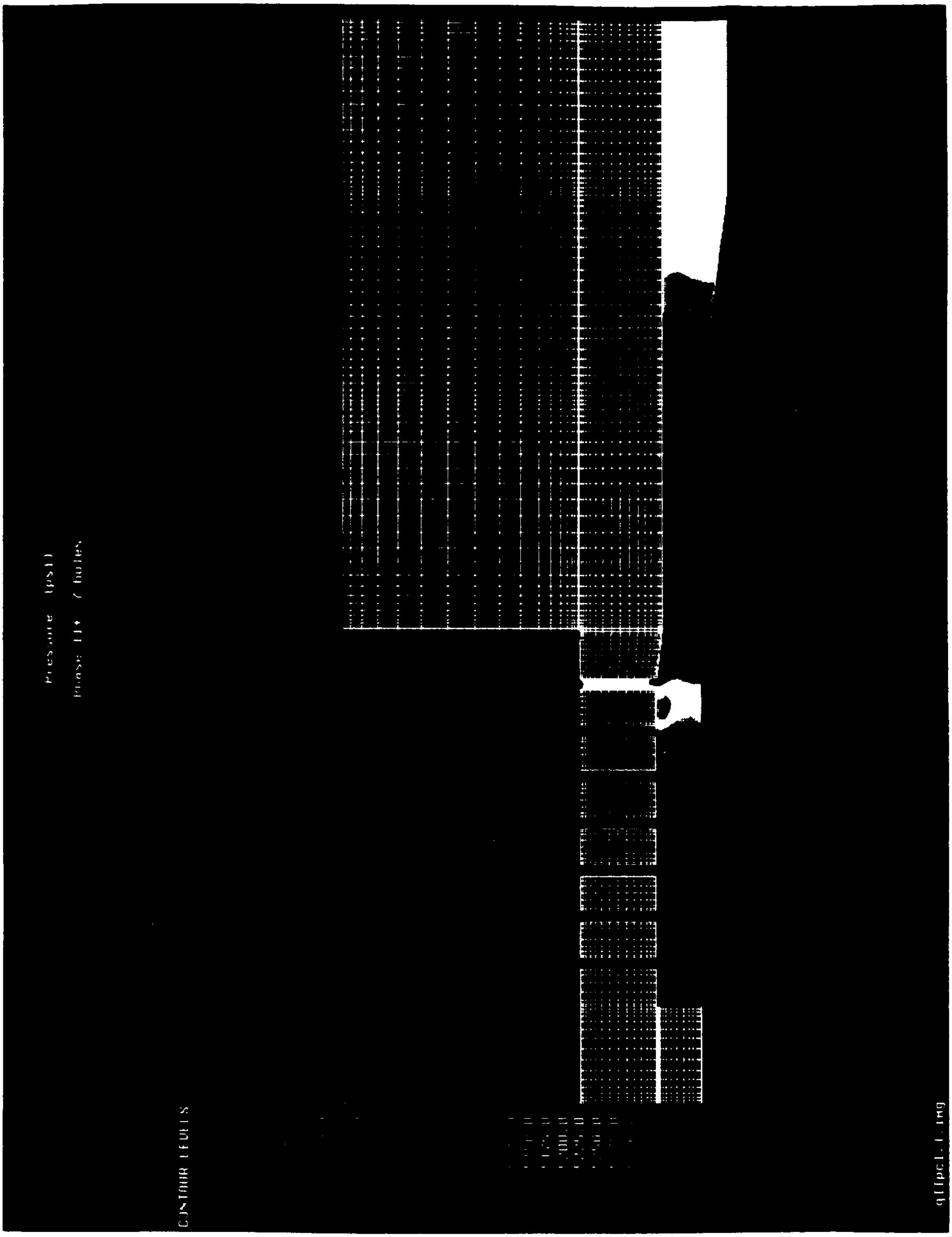
Pressure (psi)
Phase III + 7 holes
CONTOUR LEVELS

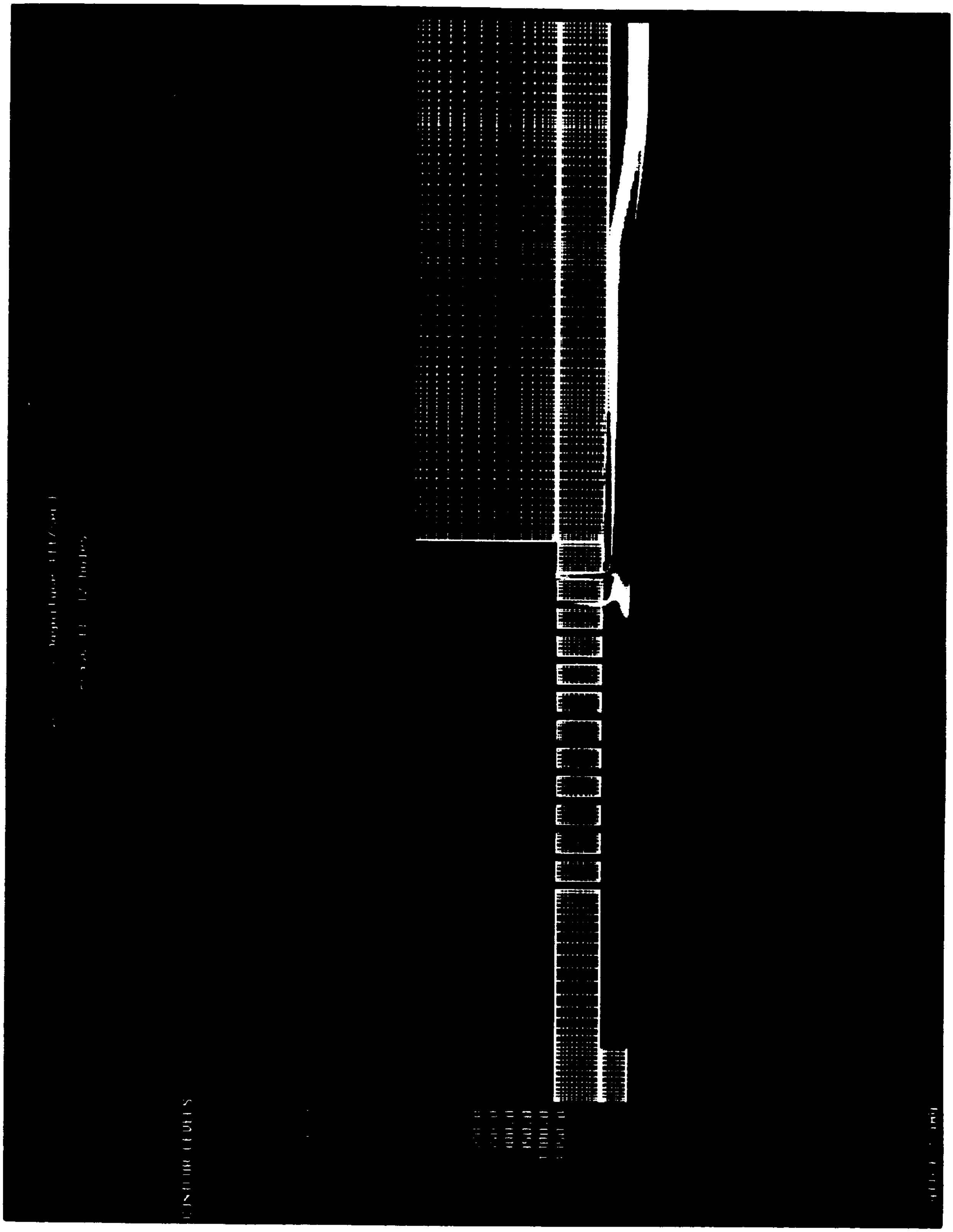

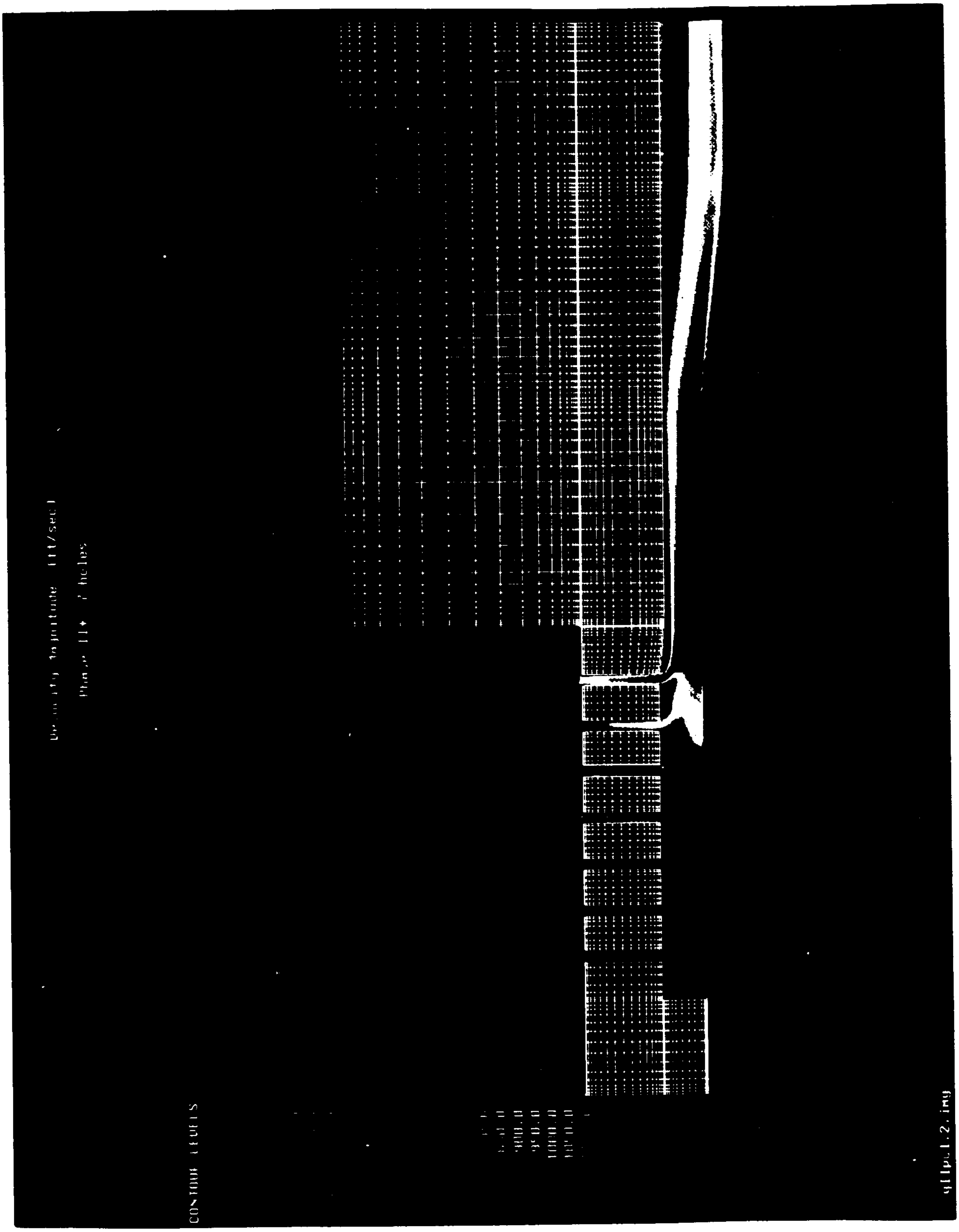
CONTOUR LEVELS

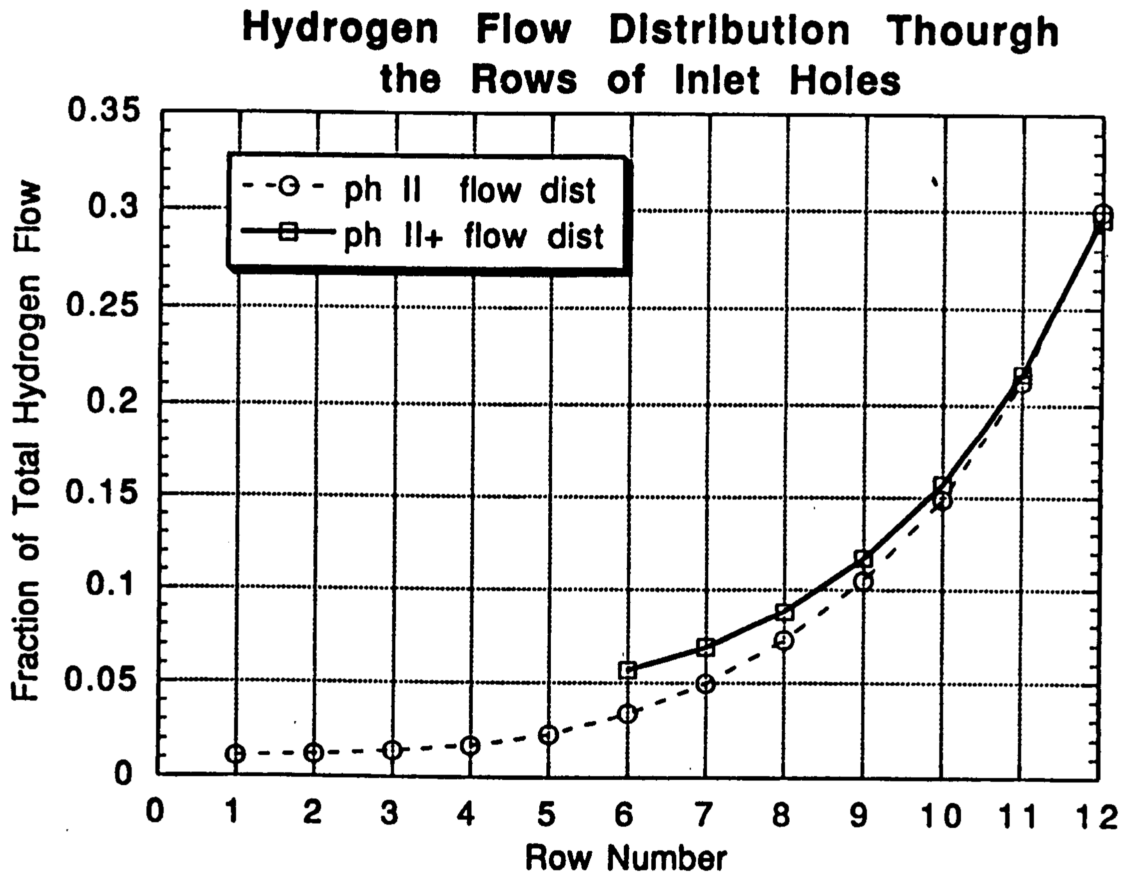
Hydrogen Flow Distribution Thourgh the Rows of Inlet Holes
- -o- ph II flow dist
—□— ph II+ flow dist
Fraction of Total Hydrogen Flow
0.35
0.3
0.25
0.2
0.15
0.1
0.05
0
0 1 2 3 4 5 6 7 8 9 10 11 12
Row Number

CONCLUSION

- No net effect of phase II+ hardware changes on preburner injector element hydrogen resistance/delta P.

N92-32262

STME HYDROGEN MIXER STUDY

Rob Blumenthal
Dongmoon Kim
George Bache'

ABSTRACT

The hydrogen mixer for the STME is used to mix cold hydrogen bypass flow with warm hydrogen coolant chamber gas, which is then fed to the injectors. It is very important to have a uniform fuel temperature at the injectors in order to minimize mixture ratio problems due to the fuel density variations. In addition, the fuel at the injector has certain total pressure requirements. In order to achieve these objectives, the hydrogen mixer must provide a thoroughly mixed fluid with a minimum pressure loss. The AEROVISC CFD code was used to analyze the STME hydrogen mixer, and proved to be an effective tool in optimizing the mixer design. AEROVISC, which solves the Reynolds Stress-Averaged Navier-Stokes equations in primitive variable form, was used to assess the effectiveness of different mixer designs. Through a parametric study of mixer design variables, an optimal design was selected which minimized mixed fuel temperature variation and fuel mixer pressure loss. The use of CFD in the design process of the STME hydrogen mixer was effective in achieving an optimal mixer design while reducing the amount of hardware testing.

GENCORP
AEROJET

Propulsion Division

STME HYDROGEN MIXER STUDY

TENTH ANNUAL WORKSHOP FOR CFD APPLICATIONS IN ROCKET PROPULSION

NASA MARSHALL SPACE FLIGHT CENTER

Robert F. Blumenthal
Dongmoon Kim
George Bache'

April 30, 1992

AEROJET

STME HYDROGEN MIXER PROVIDES UNIFORM TEMPERATURE HYDROGEN TO INJECTORS

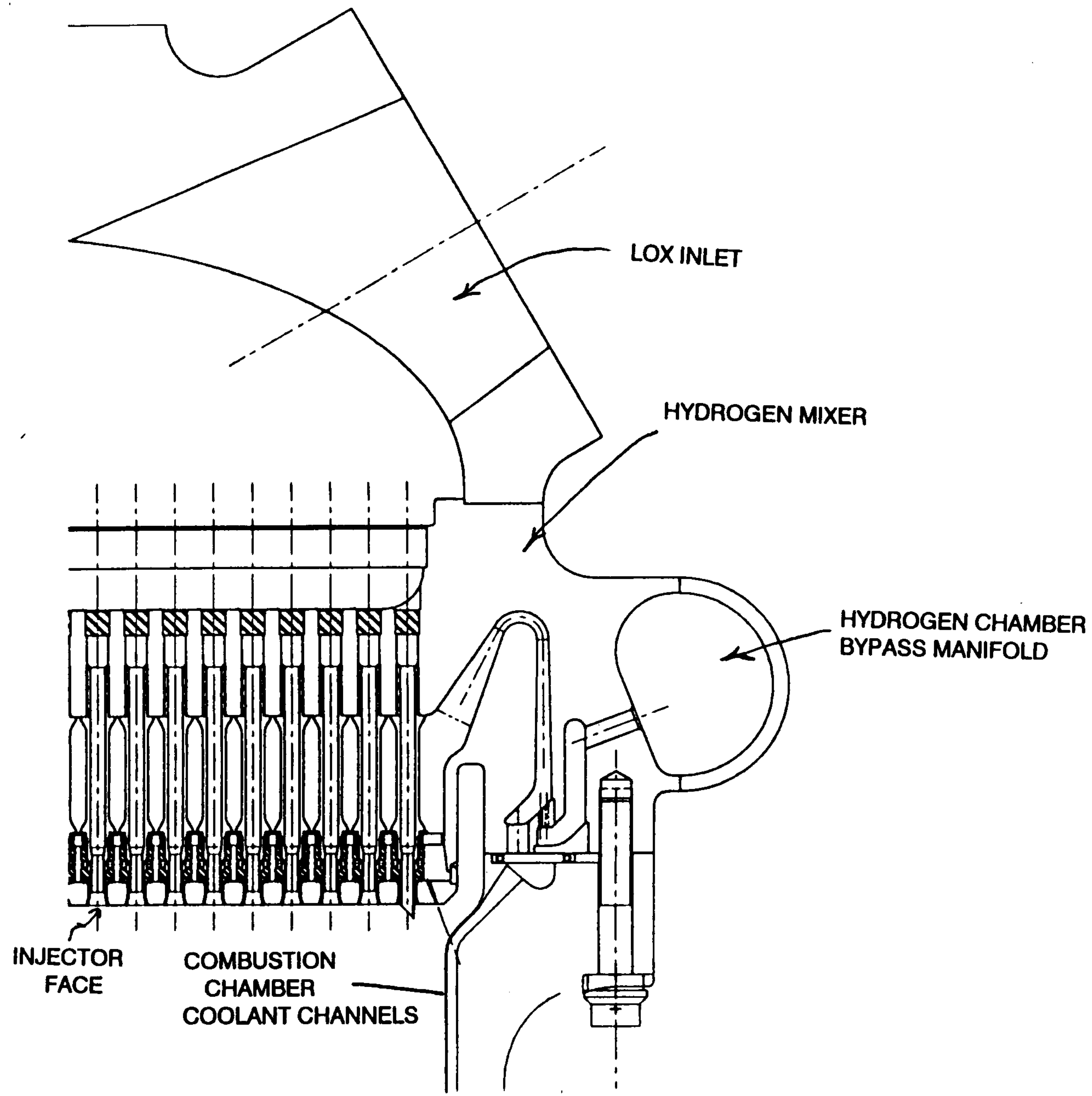

STME HYDROGEN MIXER

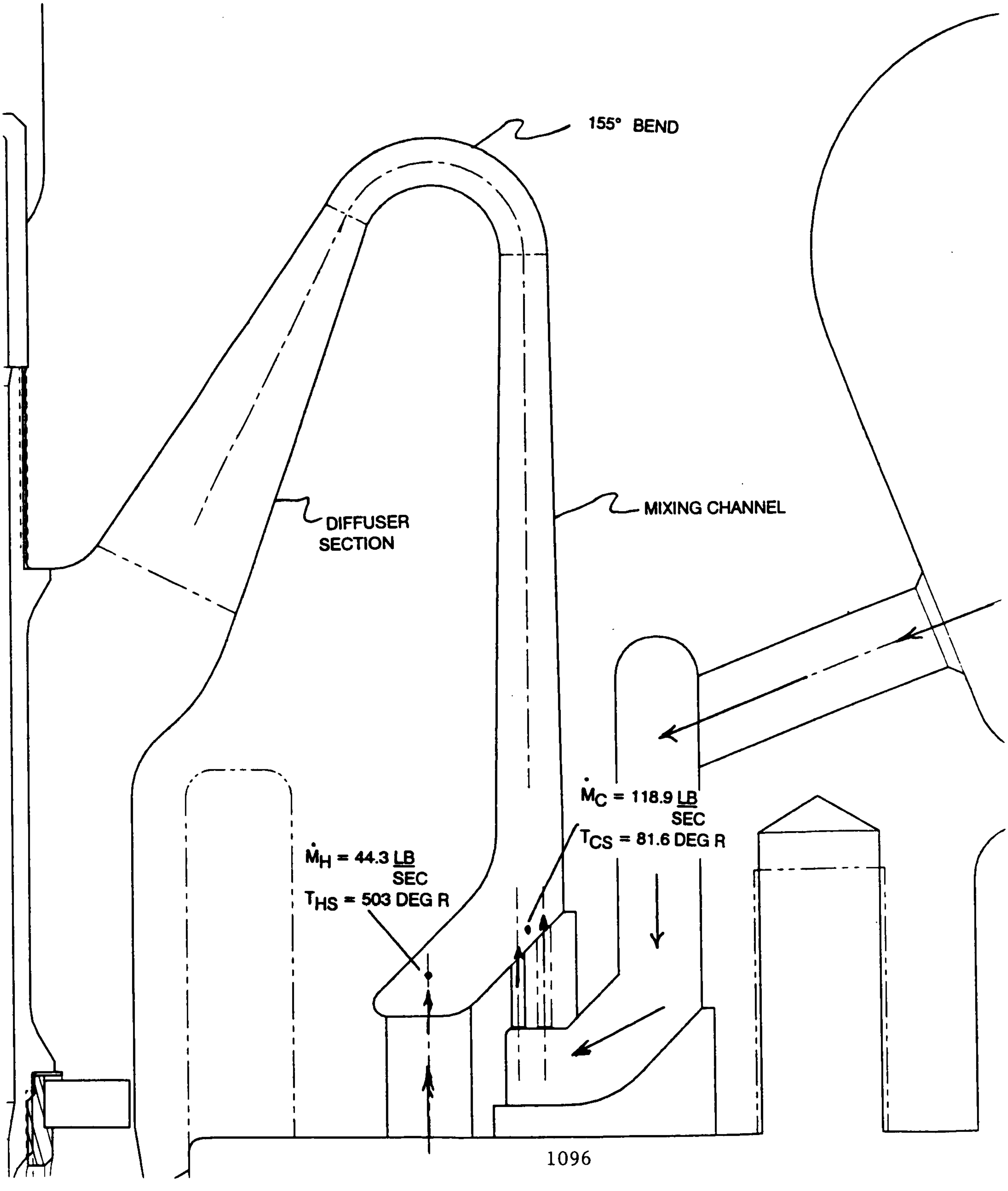

WHY IS MIXING IMPORTANT?

- Injector Elements All Designed With Identical Metering Orifice Areas and Equal ΔP Across Each Injector Element Which Therefore Require Uniform Hydrogen Density in Order to Have Equal H_2 Flow Rate to Each Element
- A Uniform Mixture Ratio Injector Core Delivers Highest ISP Performance
- Uniform H_2 Density (Mixture Ratio) Is Dependent on the Performance of the Hydrogen Mixer
- Uniform Temperature Implies Uniform Density

GENCORP AEROJET

MODELING ISSUES

Propulsion Division

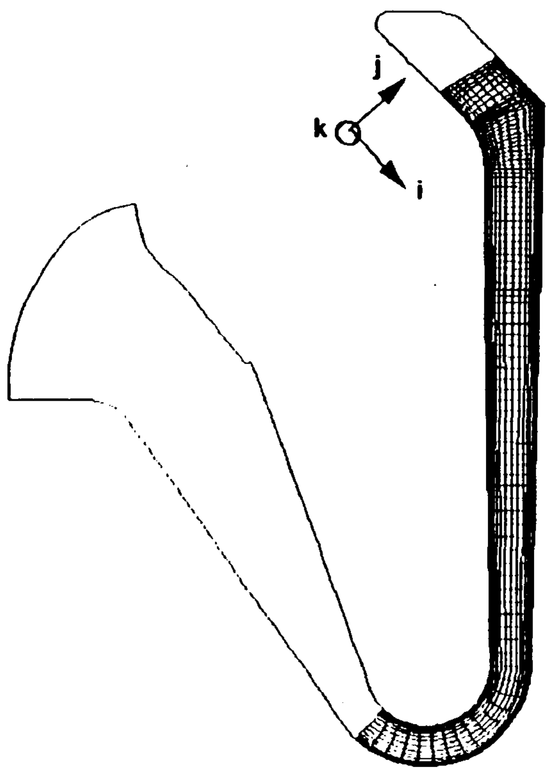

- DISCRETE COLD INLET HOLES
- HOT GAS INLET ASSUMES UNIFORM FLOW ACROSS PASSAGE
- 3-D WEDGE
- COMPRESSIBLE FLOW
- GAS PROPERTIES BASED ON MIXED TEMPERATURE
- STANDARD K-e TURBULENCE MODEL
- ADIABATIC WALLS
- EXIT PLANE AT BEGINNING OF DIFFUSER SECTION
- GRID SIZE 97 X 19 X 16

GenCorp Aerojet

Propulsion Division

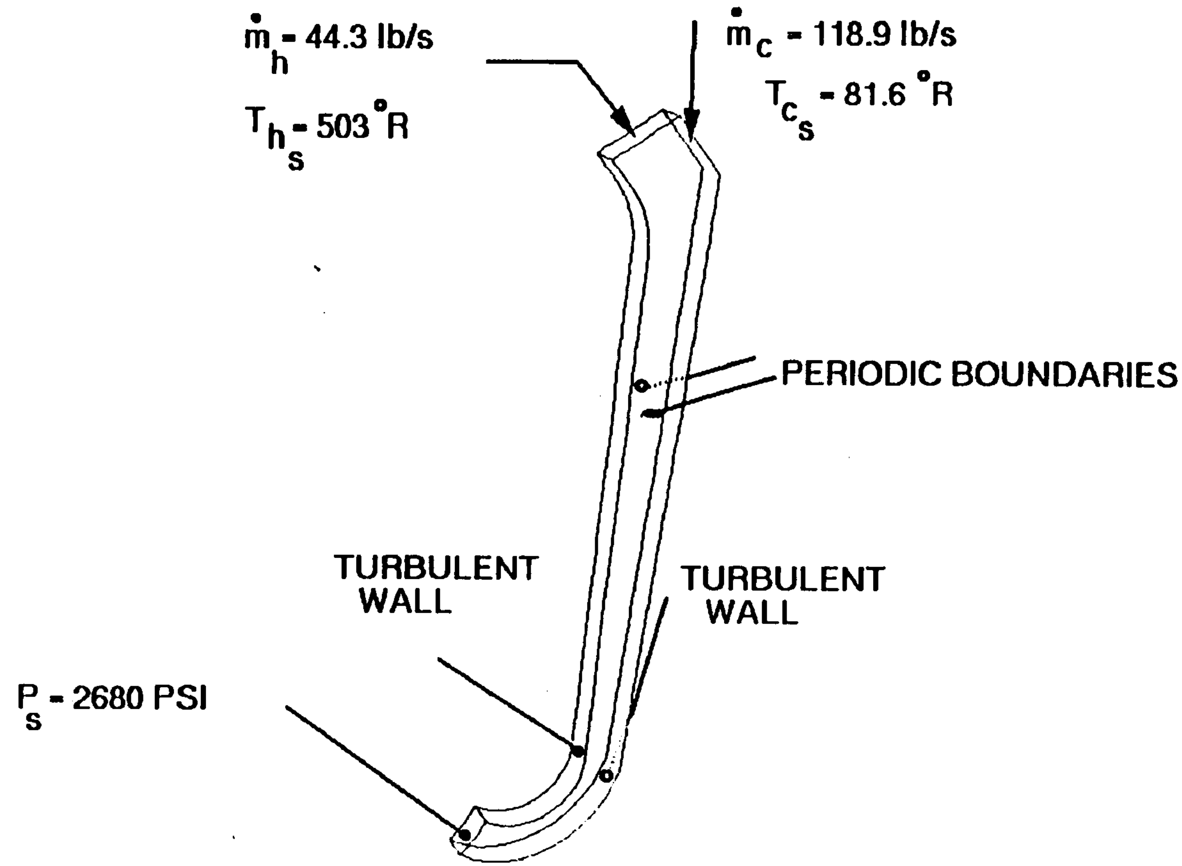

STME HYDROGEN MIXER

- Cold Hydrogen Inlet Hole Size Varied to Determine Effect on Mixing

N_{CNOM}	N_C	D_C [in]	A_{CTOT} [in^2]	Wedge Angle [Deg]
500	495	0.091	3.22	1.45
750	749	0.074	3.22	0.96
1000	1033	0.063	3.22	0.70

- Cold Hydrogen Inlet Holes Are Staggered With Respect to the Mixing Channel Centerline

GENCORP AEROJET

STATIC TEMPERATURE CORRESPONDING TO DIFFERENT L/Dh LOCATIONS

Propulsion Division

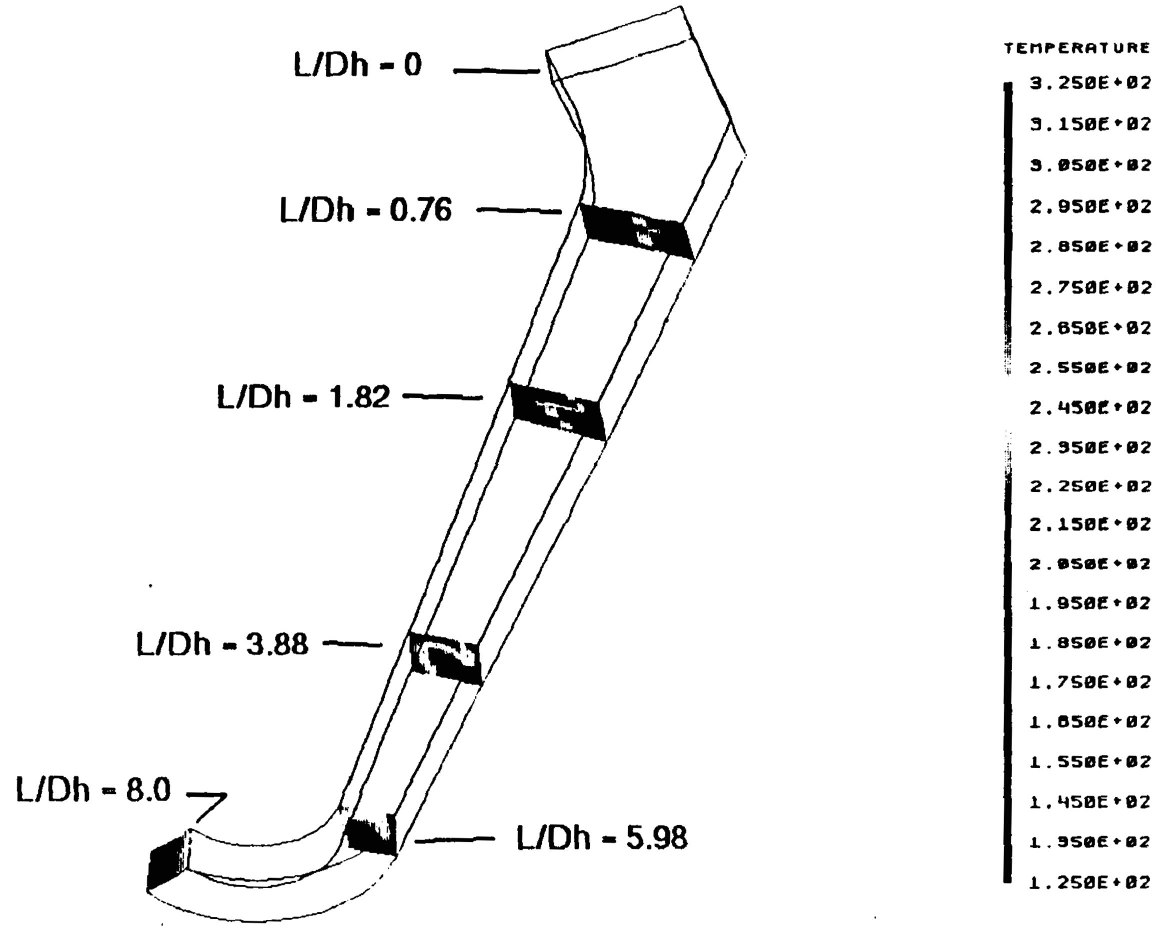

GENCORP AEROJET

Propulsion Division

TOTAL TEMPERATURE VARIATION INSIDE HYDROGEN MIXER

PLANE BETWEEN HOLES

PLANE THROUGH TOP HOLE

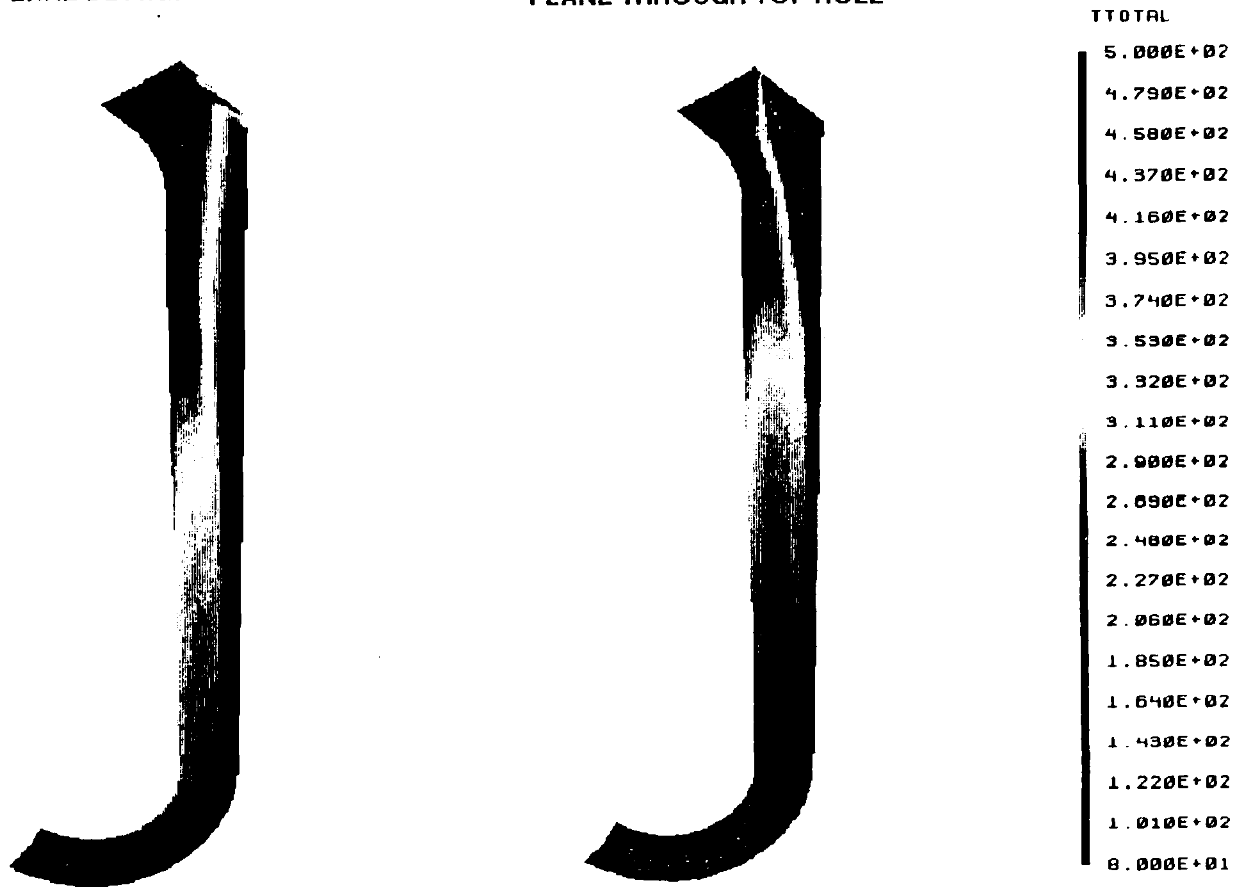

GENCORP AEROJET

Propulsion Division

NC - 750 HOLES

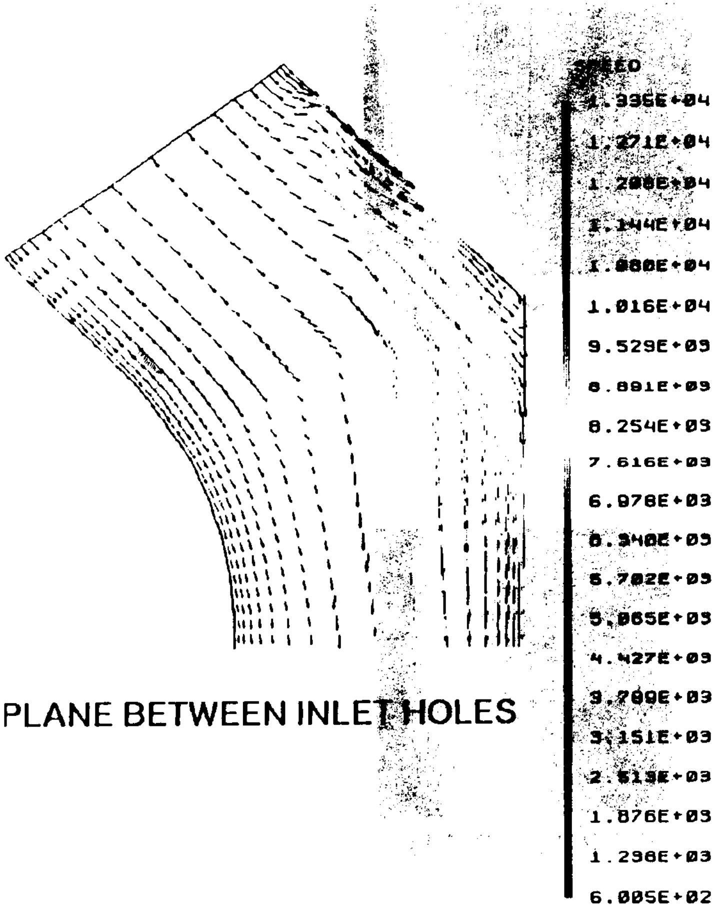

PLANE BETWEEN INLET HOLES

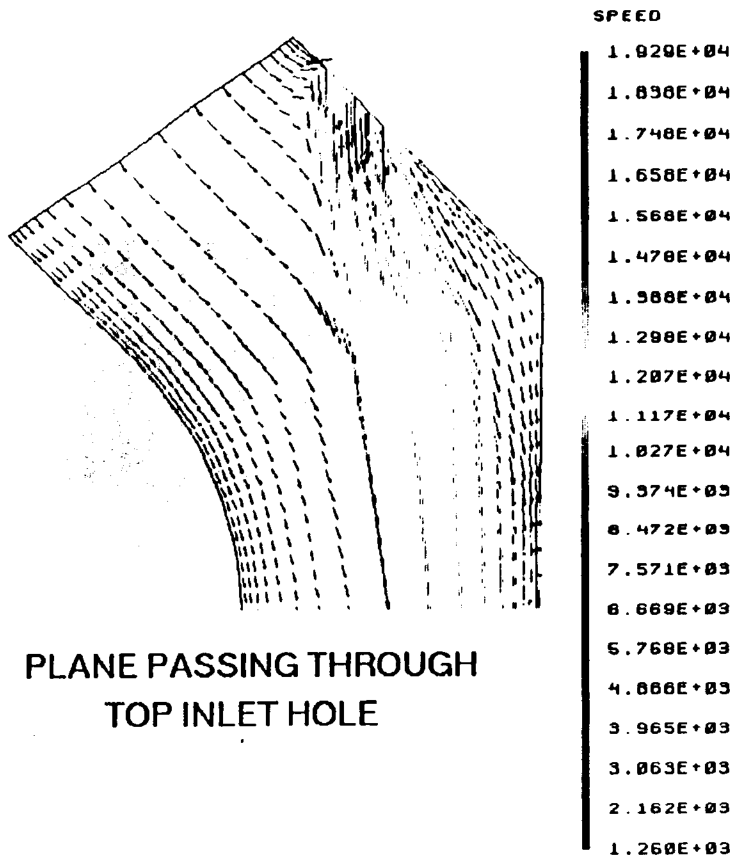

PLANE PASSING THROUGH TOP INLET HOLE

GENCORP AEROJET

Propulsion Division

EXIT PLANE TEMPERATURE DEPENDENT ON COLD HYDROGEN INLET HOLE SIZE

NC-500 HOLES

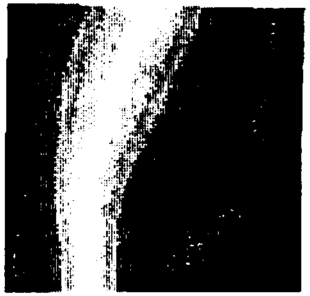

NC-750 HOLES

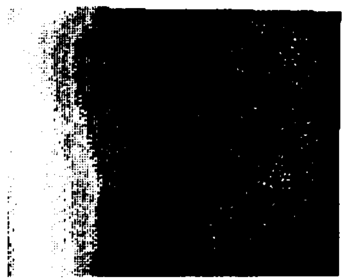

NC-1000 HOLES

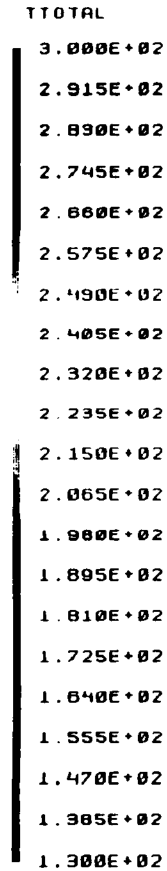

LOCATION OF L/Dh WITH RESPECT TO CFD MODEL

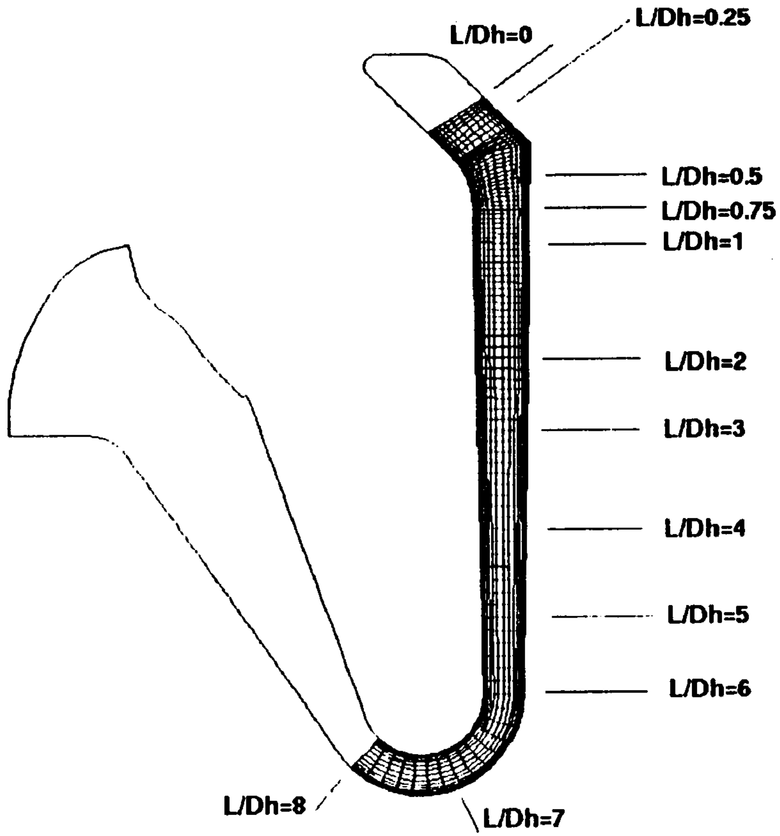

GENCORP AEROJET

Propulsion Division

TOTAL TEMPERATURE VARIATION VS. L/DH

NC=500, 750, 1000 HOLES

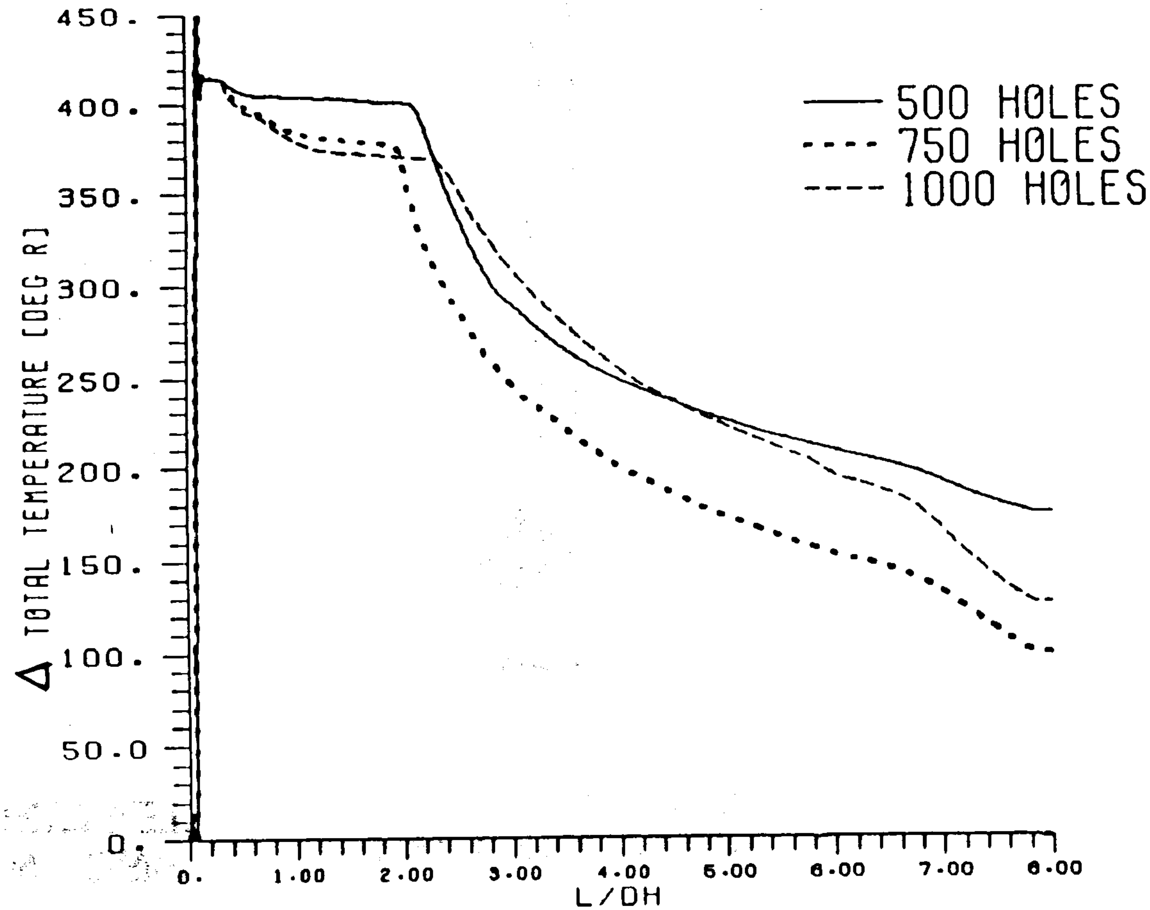

TOTAL PRESSURE VARIATION VS. L/DH

NC=500, 750, 1000 HOLES

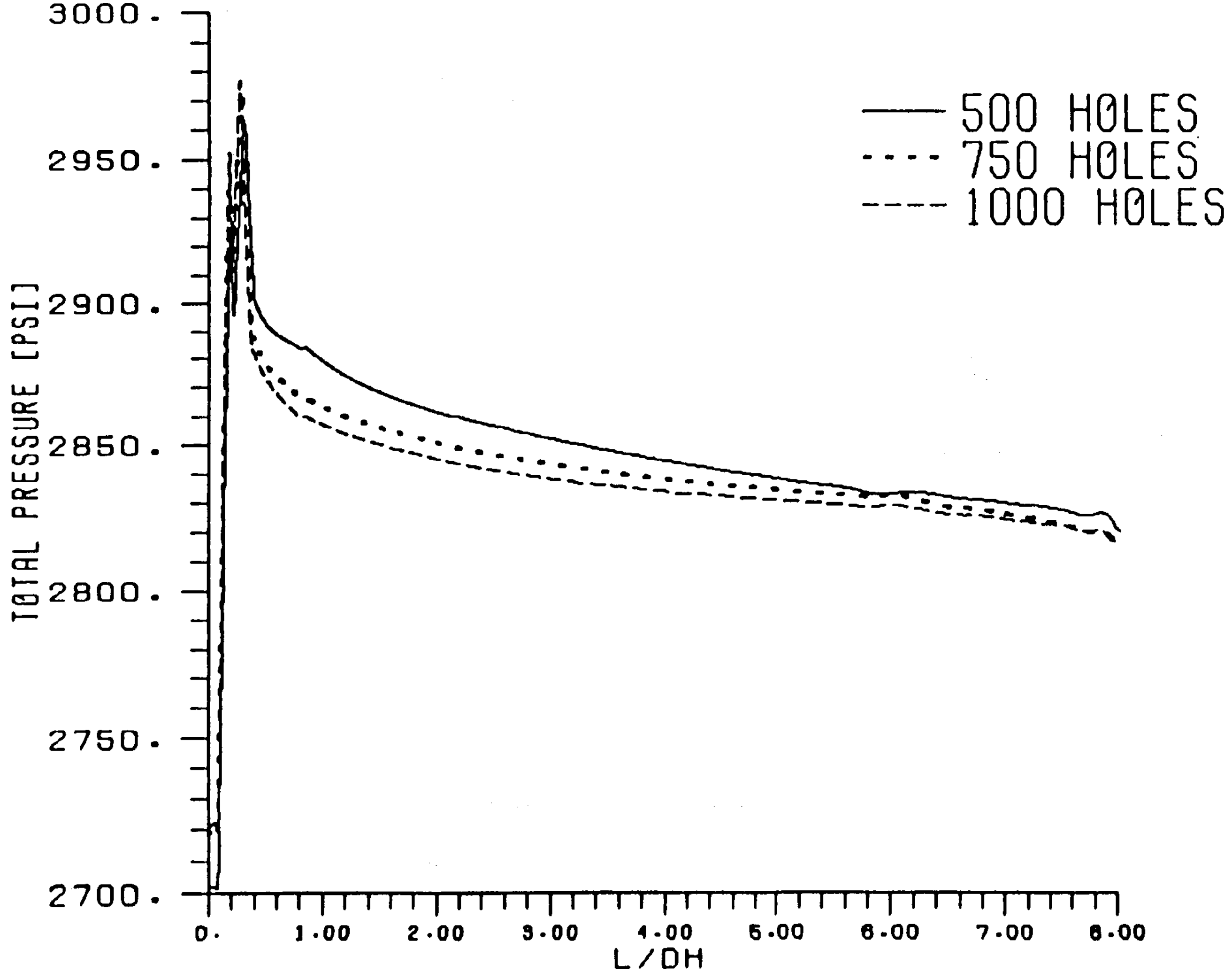

EXIT PLANE MASSFLOW VS. TOTAL TEMPERATURE

NC=500, 750, 1000 HOLES

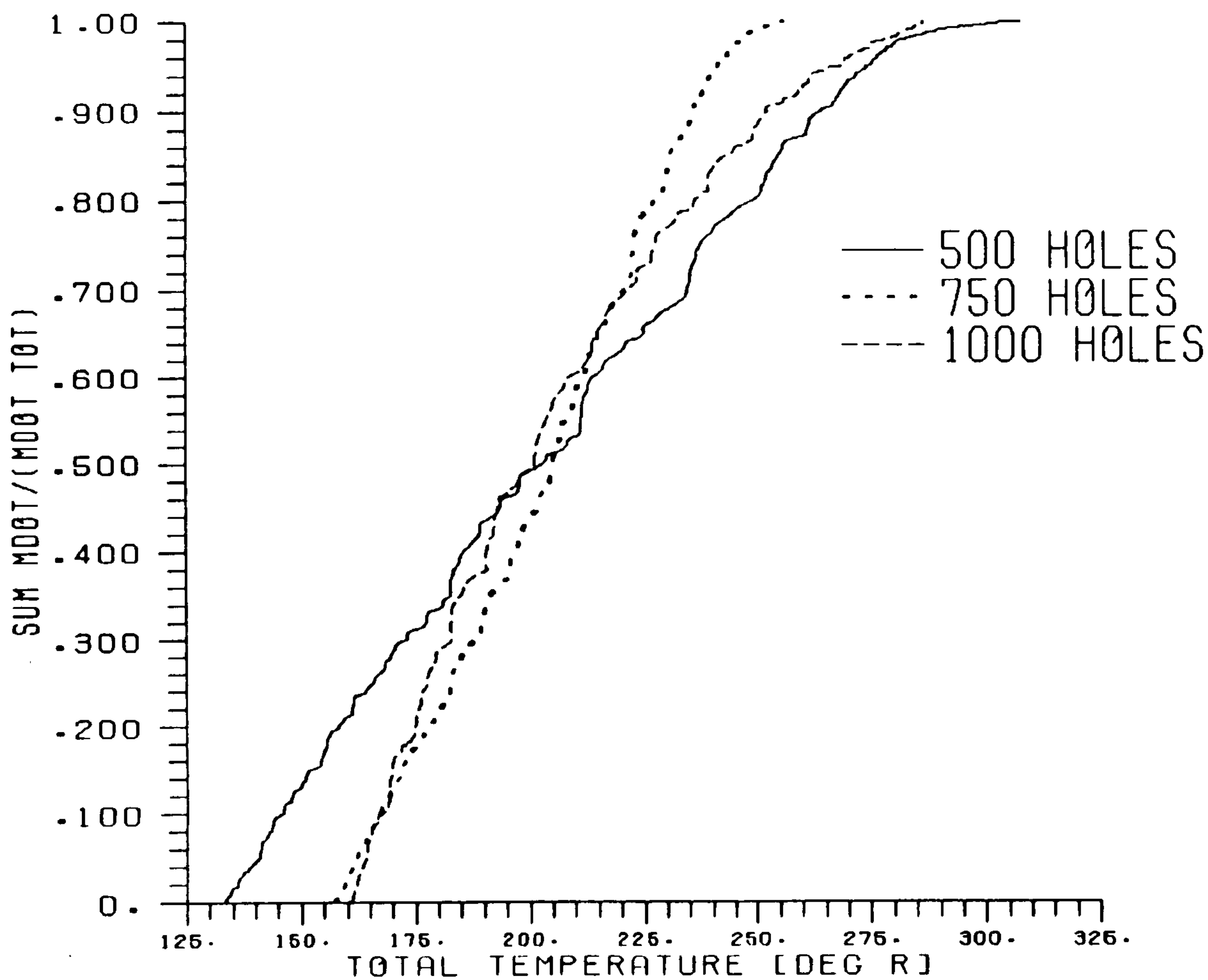

COLD HYDROGEN INLET HOLE SIZE RESULTS

N_C	T_{TAVE} [°R]	σ_T [°R]	ΔT_T [°R]	ΔP_T [Psi]
500	204.0	56.9	174.5	116.9
750	203.6	33.1	98.7	95.3
1000	205.5	44.2	126.2	93.3

T_{TAVE} = Mass-Averaged Value of Total Temperature at Exit Plane

ΔT_T = Total Temperature Range at Model Exit Plane

ΔP_T = Net Total Pressure Recovery (P_{TEXIT} - $P_{THINLET}$)

σ_T = Standard Deviation of Temperature at Exit Plane

COLD HYDROGEN INLET FLOW ANGLE WAS VARIED TO DETREMINE EFFECTS ON TOTAL TEMPERATURE AND PRESSURE

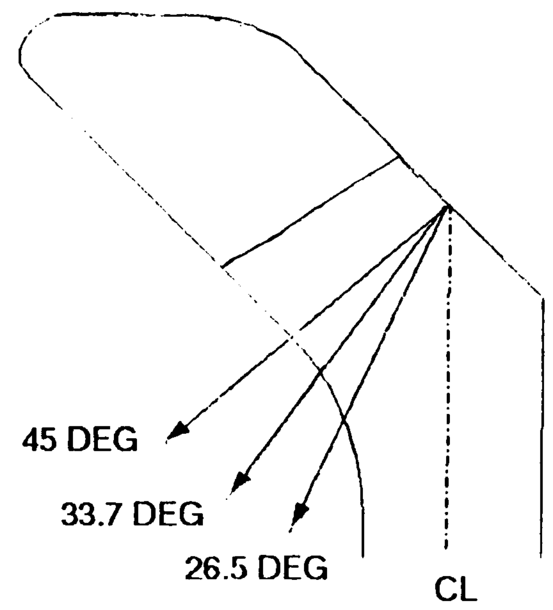

GENCORP AEROJET

EXIT PLANE TEMPERATURE DEPENDENT ON COLD HYDROGEN FLOW ANGLE

Propulsion Division

NC= 750 HOLES

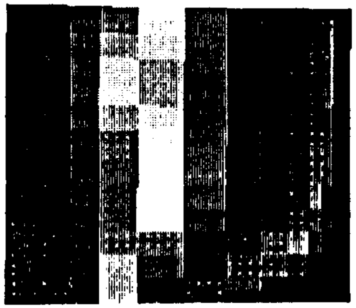

THETA=0 DEG

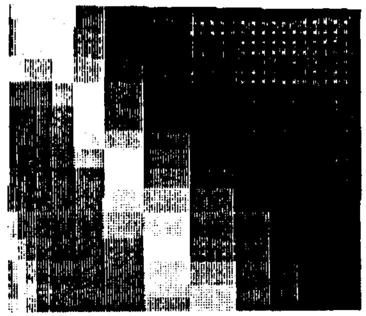

THETA=26.5 DEG

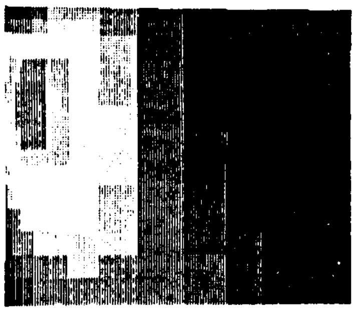

THETA=33.7 DEG

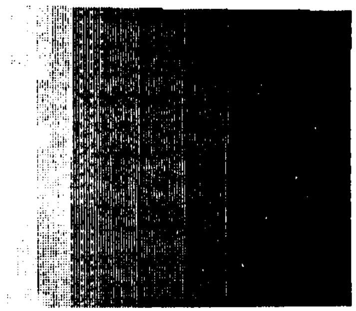

THETA=45 DEG

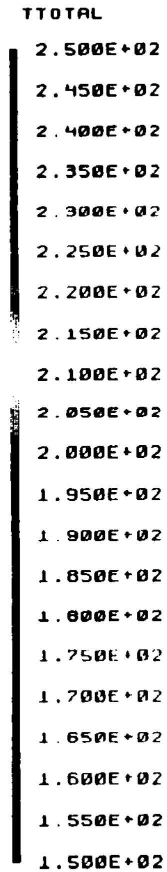

TOTAL PRESSURE VARIATION VS. L/DH

FLOW ANGLE=0, 26.5, 33.7, 45 DEG

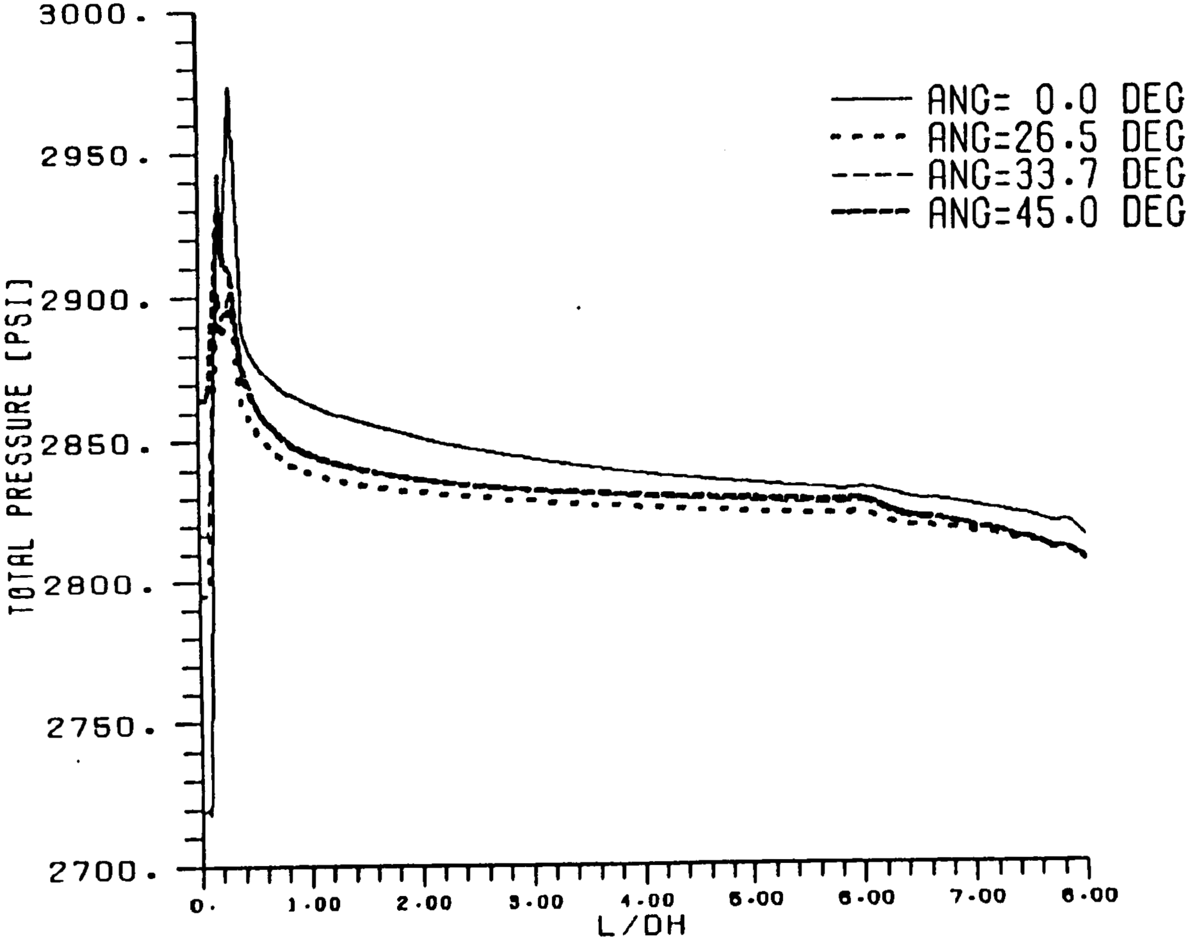

GENCORP
AEROJET

Propulsion Division

TOTAL TEMPERATURE VARIATION VS. L/DH

FLOW ANGLE=0, 26.5, 33.7, 45 DEG

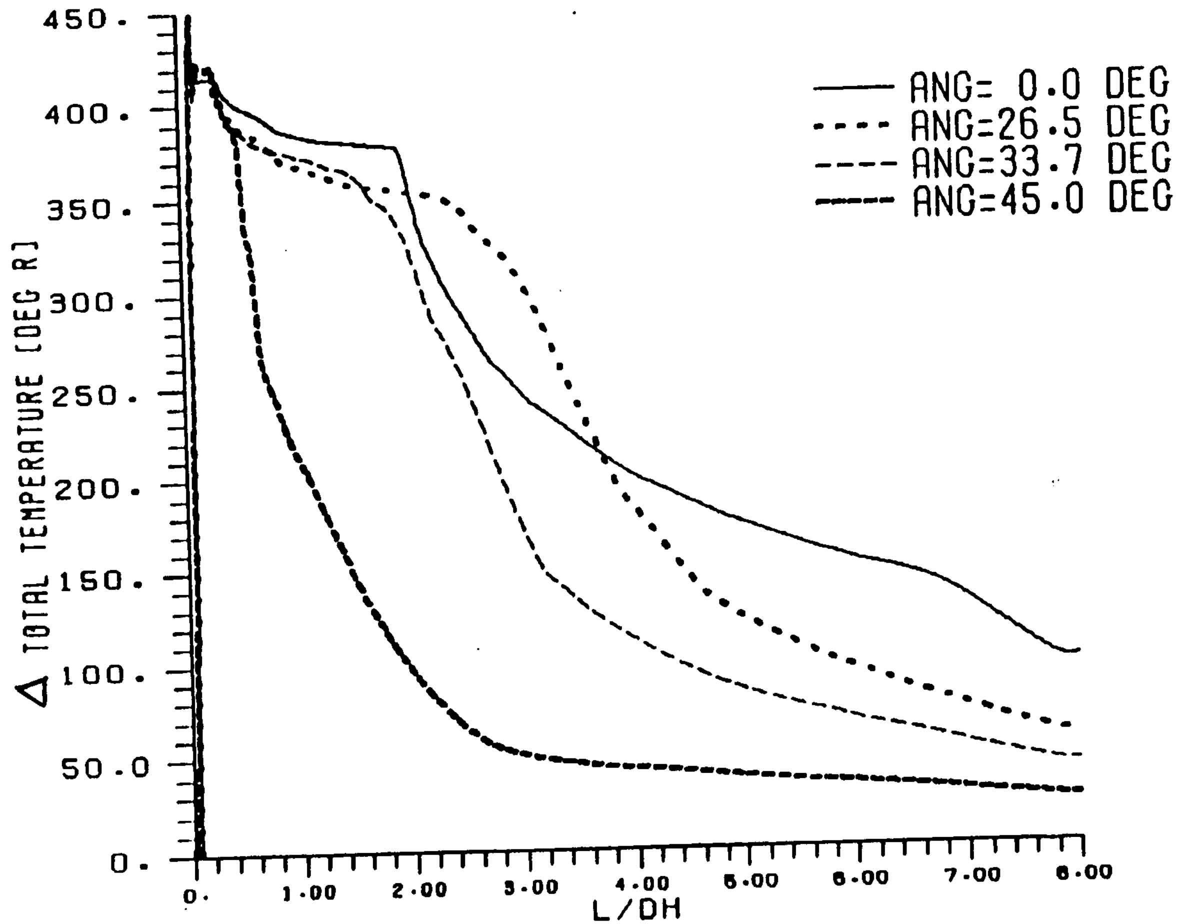

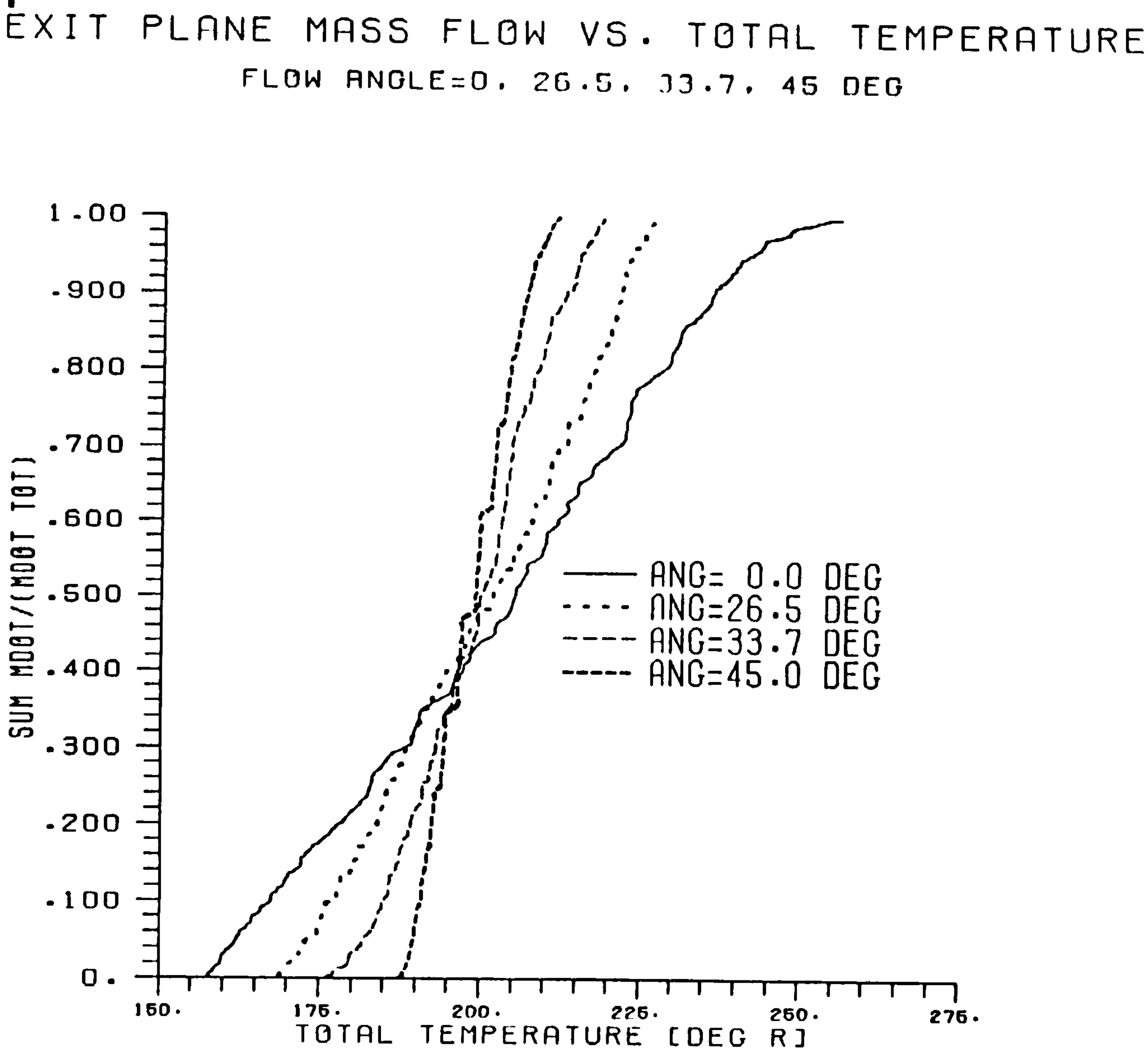
EXIT PLANE MASS FLOW VS. TOTAL TEMPERATURE
FLOW ANGLE=0, 26.5, 33.7, 45 DEG
SUM MDOT/(MDOT TOT)
1.00
.900
.800
.700
.600
.500
.400
.300
.200
.100
0.
150.
175.
200.
225.
250.
275.
TOTAL TEMPERATURE [DEG R]
ANG= 0.0 DEG
ANG=26.5 DEG
ANG=33.7 DEG
ANG=45.0 DEG

COLD HYDROGEN INLET FLOW ANGLE RESULTS

ANG [DEG]	T_{TAVE} [°R]	σ_T [°R]	ΔT_T [°R]	ΔP_T [Psi]
0	203.6	33.1	98.7	95.3
26.5	199.2	17.8	58.5	11.4
33.7	199.3	11.8	42.4	-9.5
45.0	198.8	8.1	24.3	-58.3

T_{TAVE} = Mass-Averaged Value of Total Temperature at Exit Plane

ΔT_T = Total Temperature Range at Model Exit Plane

ΔP_T = Net Total Pressure Recovery (P_{TEXIT} - $P_{THINLET}$)

Δ_T = Standard Deviation of Temperature at Exit Plane

FUTURE WORK

- Examine Other Configurations
  - Swirled Injection
  - Smaller Mixing Channel Area
  - Inline Cold Hydrogen Inlet Holes
  - Modifying Position of Cold Hydrogen Inlet Holes With Respect to the Mixing Channel Centerline
- Provide Design Requirements for Experimental Cold Flow Hardware
- Support Cold Flow Testing
- Analyze Cold Flow Data and Validate Aerovisc Predictive Capability
- Use Validated Model to Design Flight Mixer

N92-32263

AN EXPERIMENTAL STUDY OF THE FLUID MECHANICS ASSOCIATED WITH POROUS WALLS (AIAA 92-0769)

N. Ramachandran,
Universities Space Research Association,
J. Heaman,
A. Smith,
NASA Marshall Space Flight Center,
Huntsville, Al 35812

ABSTRACT

The fluid mechanics of air exiting from a porous material is investigated. The experiments are filter rating dependent, as porous walls with filter ratings differing by about three orders of magnitude are studied. The flow behavior is investigated for its spatial and temporal stability. The results from the investigation are related to jet behavior in at least one of the following categories: (1) Jet coalescence effects with increasing flow rate, (2) Jet field decay with increasing distance from the porous wall, (3) Jet field temporal turbulence characteristics and (4) Single jet turbulence characteristics. The measurements show that coalescence effects cause jet development and this development stage can be traced by measuring the pseudoturbulence (spatial velocity variations) at any flow rate. The pseudoturbulence variation with increasing mass flow reveals an initial increasing trend followed by a leveling trend, both of which are directly proportional to the filter rating. A critical velocity begins this leveling trend and represents the onset of fully developed jetting action in the flow field. A correlation is developed to predict the onset of fully developed jets in the flow emerging from a porous wall. The data further show, that the fully developed jet dimensions are independent of the filter rating, thus providing a length scale for this type of flow field (1 mm). Individual jet characteristics provide another unifying trend with similar velocity decay behavior with distance; however, the respective turbulence magnitudes show vast differences between jets from the same sample. Measurement of the flow decay with distance from the porous wall show that the higher spatial frequency components of the jet field dissipate faster than the low frequency components. Flow turbulence intensity measurements show an out of phase behavior with the velocity field and are generally found to increase as the distance from the wall is increased.

Solid Rocket Motor Air Flow Test Equipment

(PHASE I CONFIGURATION)

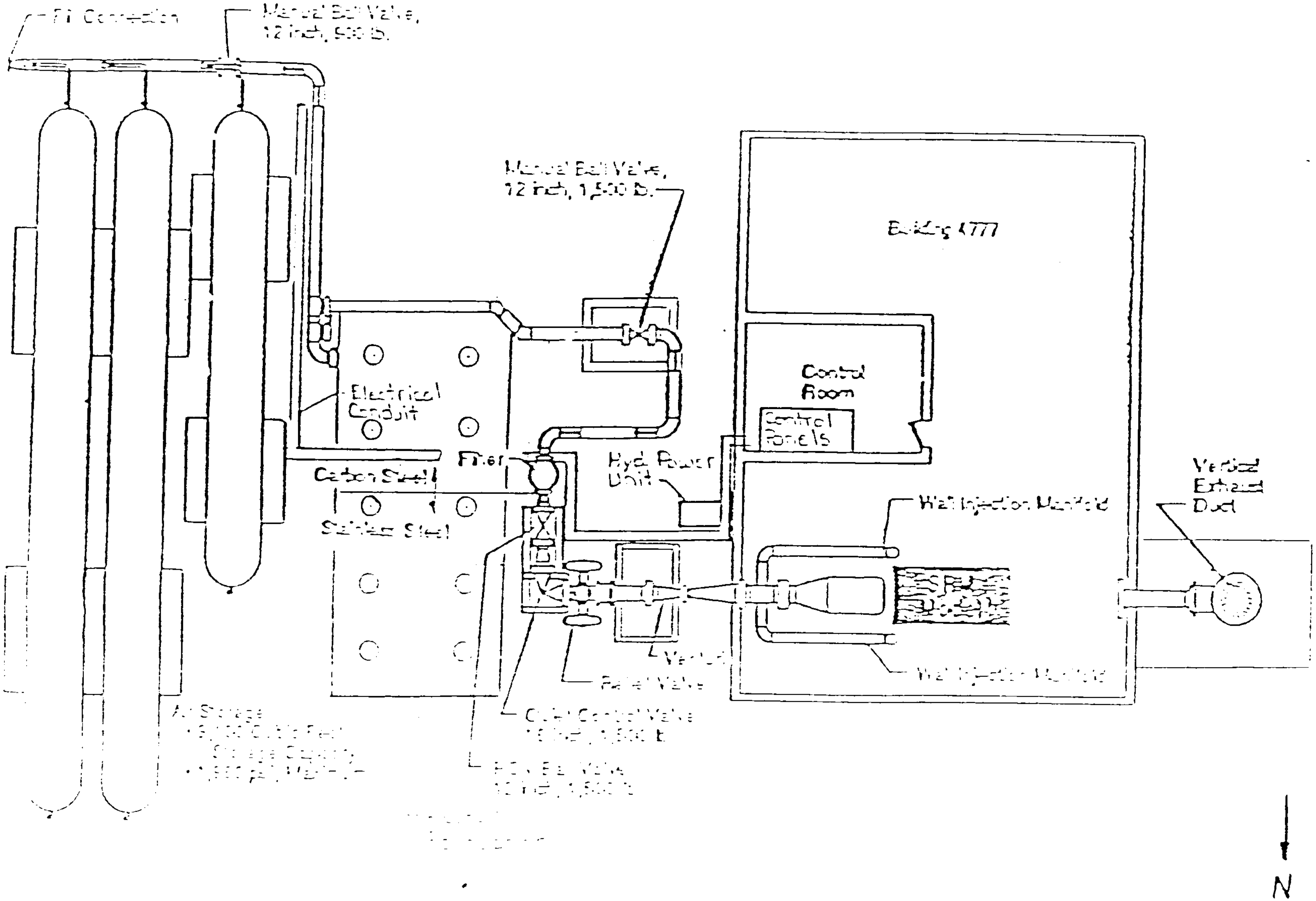

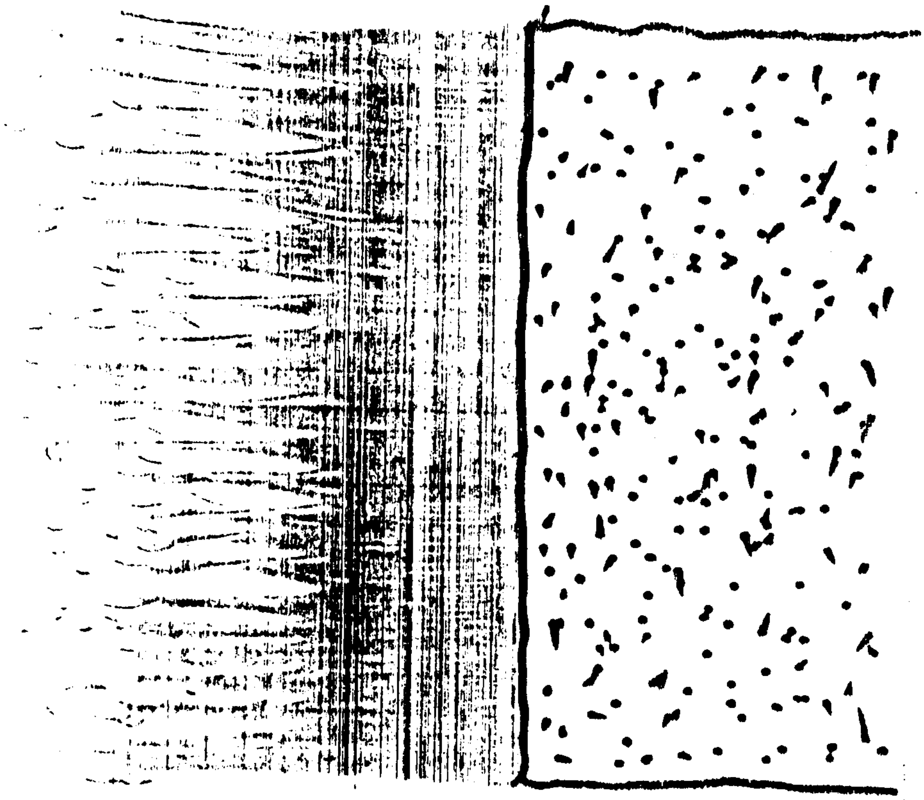


SIDE 2 50X 90-0841
200μm 20KV 85 115 S

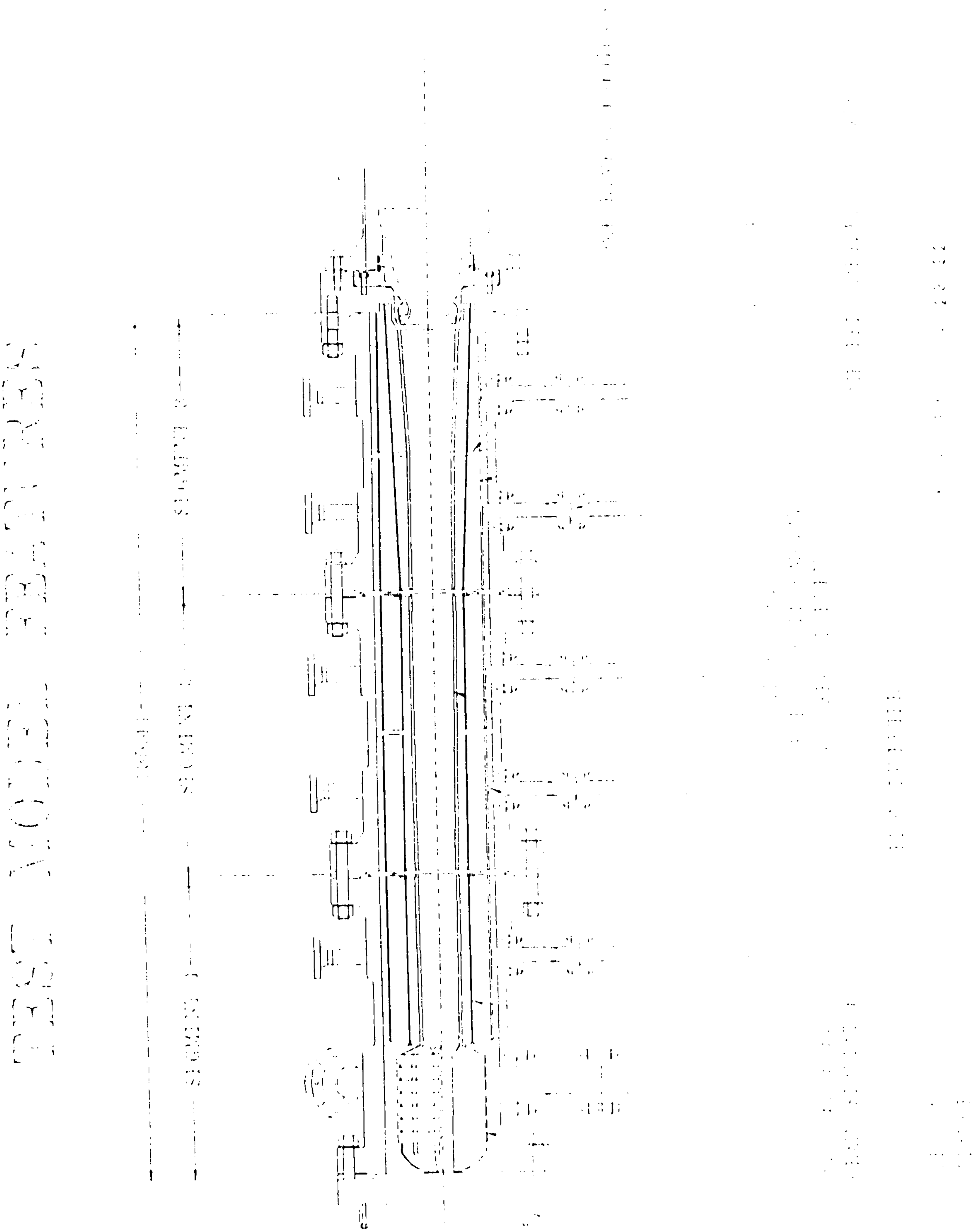

RELEVANT LITERATURE

REFERENCES

1. Dunlap, R., and Willoughby, P. G.: Cold Flow Study Test Report, United Technologies, Chemical Systems Division, 19[illegible].

2. MacPhail, D.: ARC R & M 1876, Aeronautical Research Council, England, 1939.

3. von Bohl, D.: Das Verhalten paralleler Luftstrahlen, Ingenieur Archiv, Vol. 11, 4, 1940, p 295.

4. Corrsin, S.: Investigation of the Behavior of Parallel Two-Dimensional Air Jets, ACR 2H24 NACA, 1944.

5. Morgan, P. G.: The Stability of Flow through Porous Screens, Journal of the Royal Aeronautical Society, Vol. 64, 1960, pp. 359-362.

6. Bradshaw, P.: The Effect of Wind-Tunnel Screens on Nominally Two-Dimensional Boundary Layers, Journal of Fluid Mechanics, Vol 22, 1965.

7. Schubauer, G. M.: Journal of the Aeronautical Sciences, V[illegible] 14 [illegible]47.

8. Pimenta, M., and Moffat, R.: Stability of Flow through P[illegible] Plates: Coalescent Jets Effect, AIAA Journal, Vol. 12, 10, 1974.

9. Traineau, J. C., Hervat, P., and Kuentzmann, P.: Cold-Flow Simulation of a Two-Dimensional Nozzleless Solid Rocket Motor, Presented at the AIAA/ASME/SAE/ASEE 22nd Joint Propulsion Conference, Huntsville, Alabama, AIAA-86-1447, June 16-18, 1986.

10. Labbe, J., and Hervat, P., Private communication.

11. Dunlap, R., et al.: Private Communication.

12. Tong, K., and Knight, C. J.: Flow around an Isolated Porous Tube with Nonuniform Wall Thickness, AIAA Journal, Vol. 17, No. 11, 1979, pp. 1262-1263.

13. Collins, R., E.: Flow of Fluids through Porous Materials, Reinhold Publishing Corp., NY, 1961.

14. Beddini, R. A.: Contribution to ERCI Fourth Quarterly Progress Report, NAS3-35679, 1991.

JETS

1. Interaction (coalescence)
2. size (filter rating dependent?)

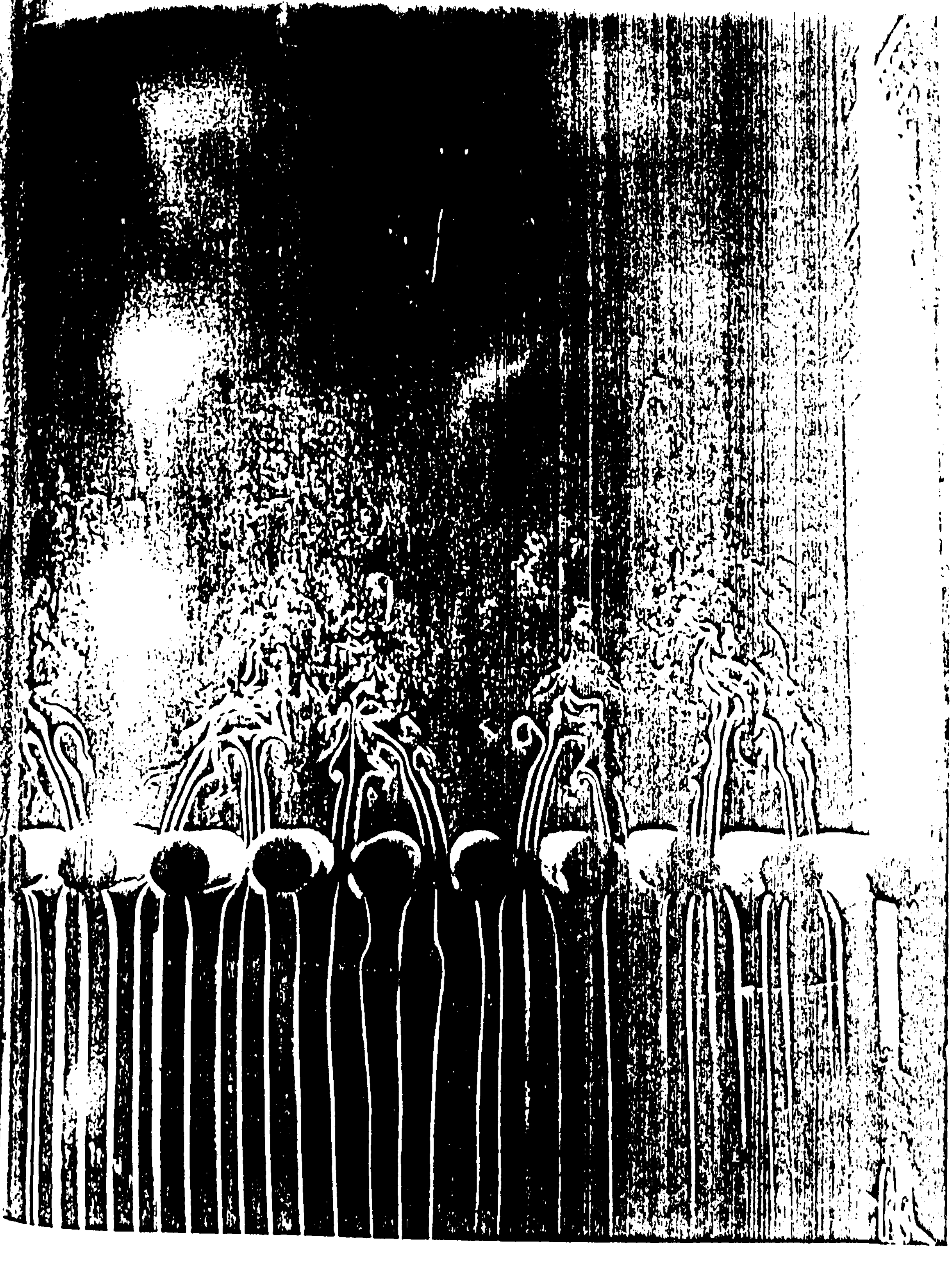

FIGURE 3 (plate 1). Unstable flow through a [illegible] with $Ud/\nu = 1500$. The large-scale pattern is steady in time.

BRADSHAW

Filter rating

$\neq$ pore size of material

$\neq$ particle size of material

ORGANIZATION: Experimental Branch, Aerophysics Division	MARSHALL SPACE FLIGHT CENTER	NAME: N. Ramachandran, A. Smith and J. Heaman
AIAA 30th Aerospace Sciences Meeting, Reno	An Experimental Study of the Fluid Mechanics Associated with Porous Walls	DATE: January 1992

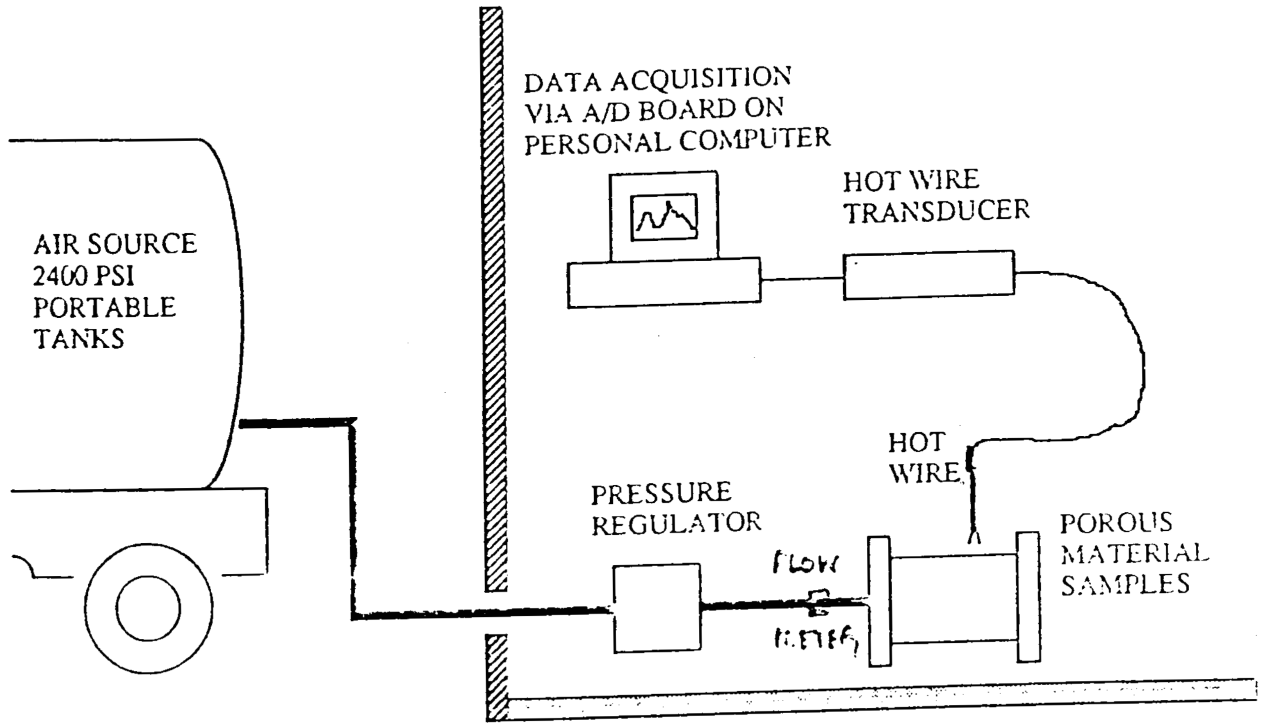

POROUS MATERIAL EXPERIMENTAL TEST EQUIPMENT
MARSHALL SPACE FLIGHT CENTER / EXPERIMENTAL BRANCH (ED35)
BUILDING 4777C

FILE NO.

ORGANIZATION	MARSHALL SPACE FLIGHT CENTER	NAME
Experimental Branch Aerophysics Division	An Experimental Study of the Fluid Mechanics Associated with Porous Walls	N. Ramachandran A. Smith and J. Heaman
AIAA 30th Aerospace Sciences Meeting, Reno		DATE: January 1992

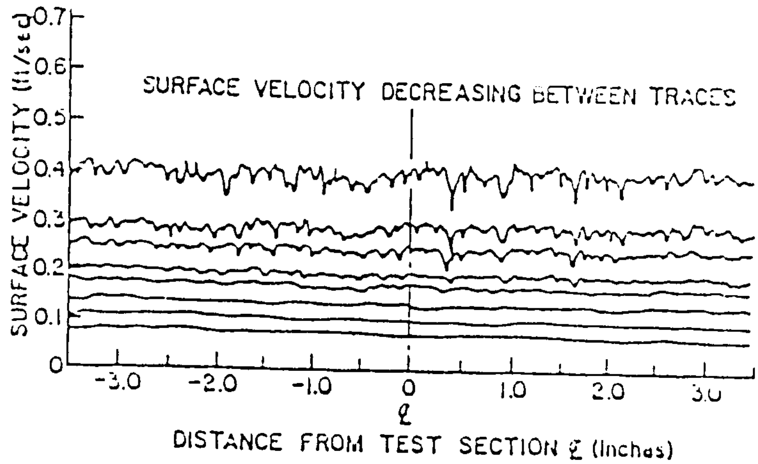

Fig. 1 Velocity distribution above roughness rig section.

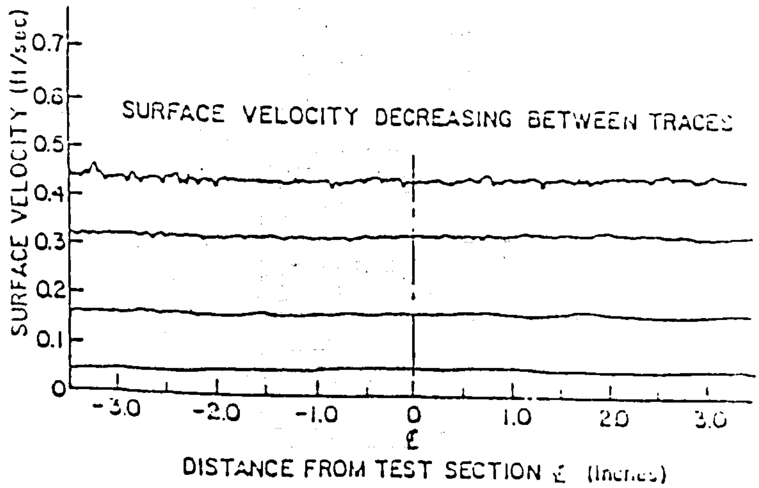

Fig. 2 Velocity distribution above smooth porous surface.

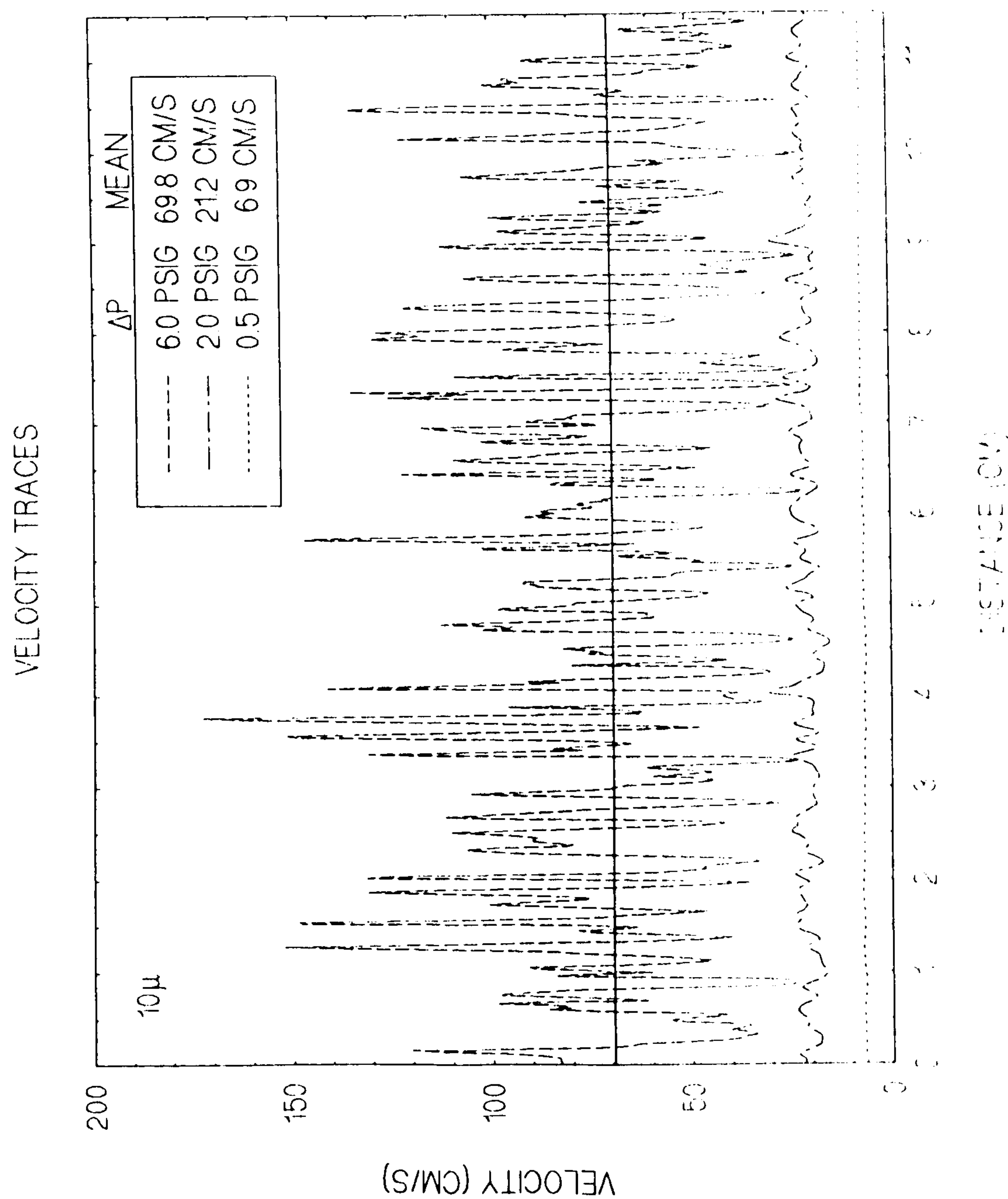

VELOCITY TRACES
ΔP MEAN
6.0 PSIG 69.8 CM/S
2.0 PSIG 212 CM/S
0.5 PSIG 69 CM/S
10μ
VELOCITY (CM/S)
200
150
100
50
0

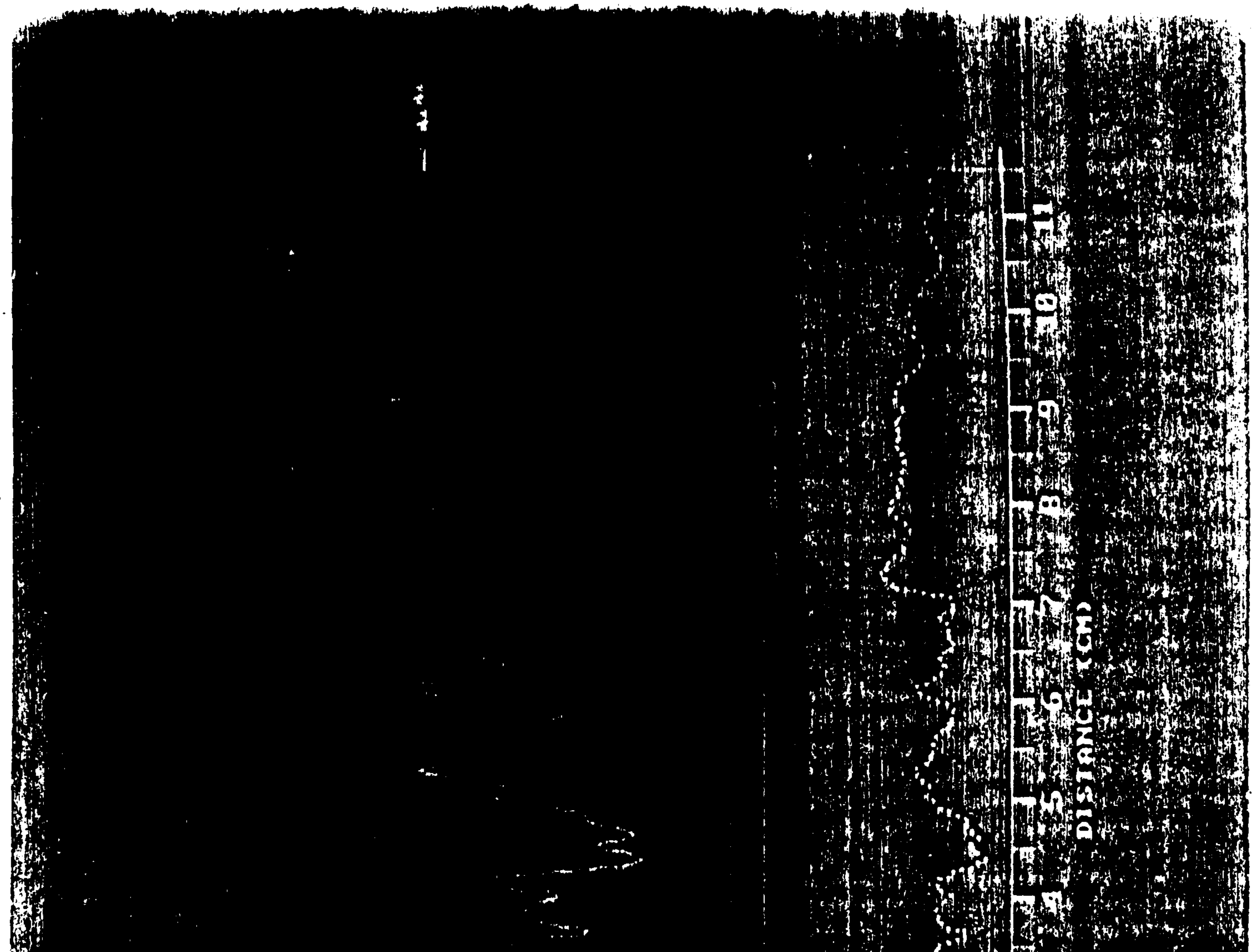
DISTANCE (CM)
0
1
2
3
4
5
6
7
8
9
10
11

Pseudoturbulence (PT I)

Velocity fluctuation levels on a length scale instead of a time scale.

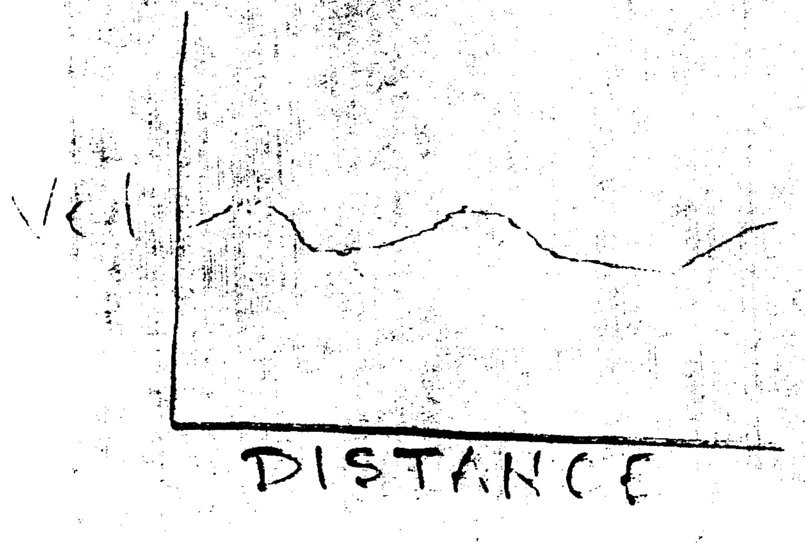

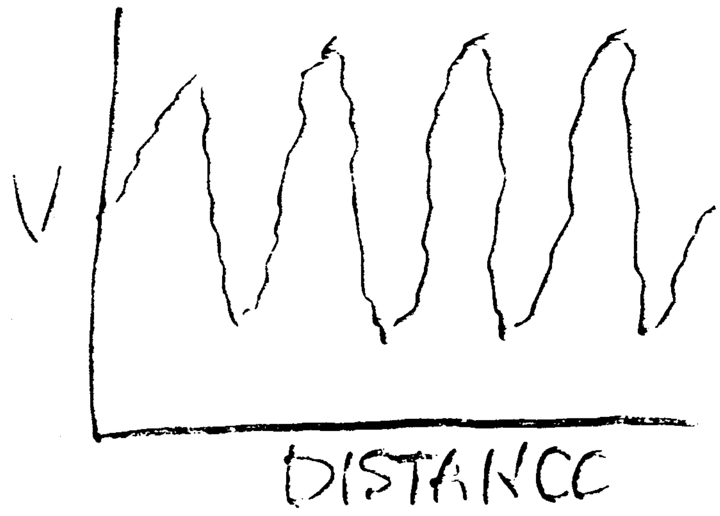

ENG'

PSEUDOTURBULENCE INTENSITY

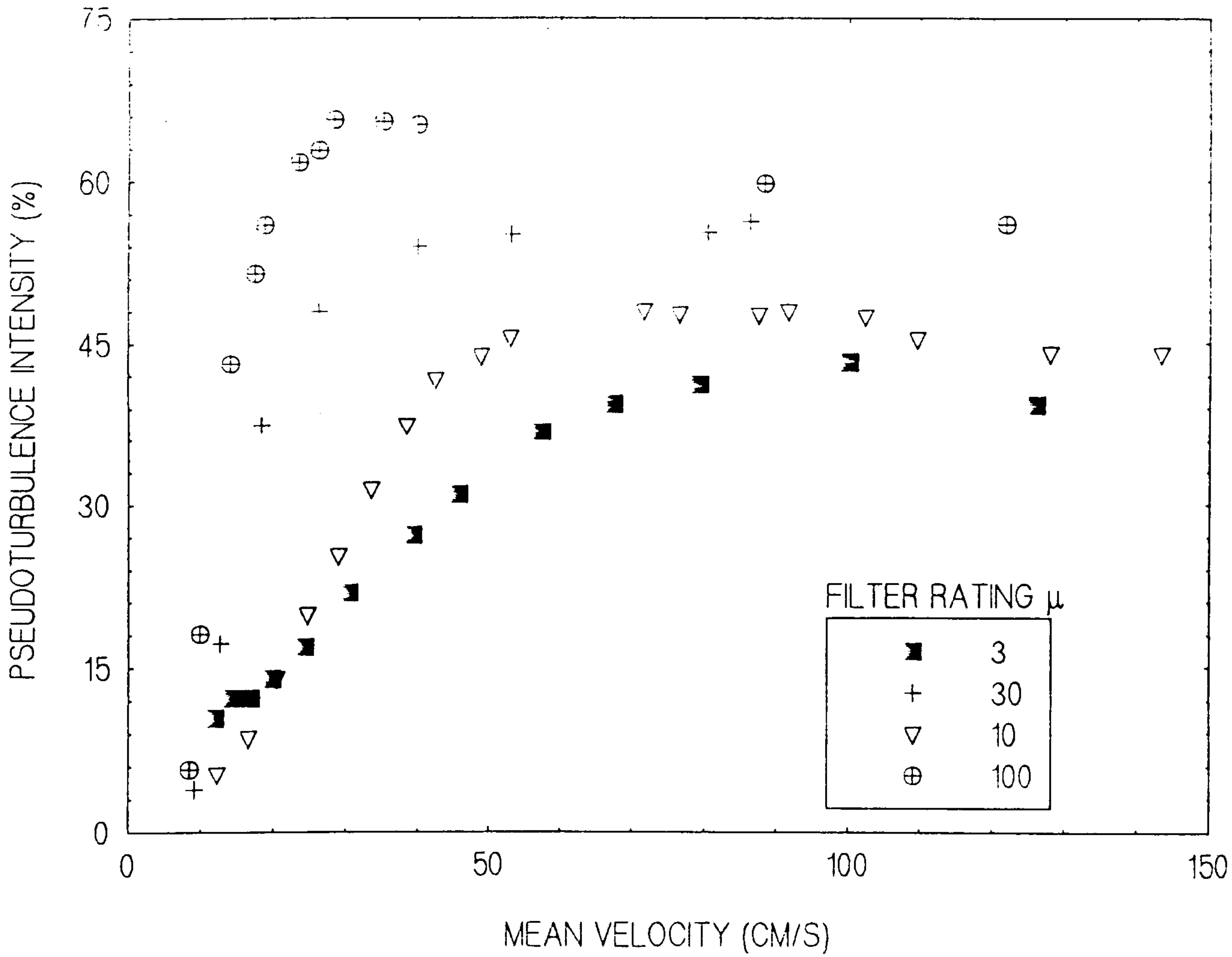

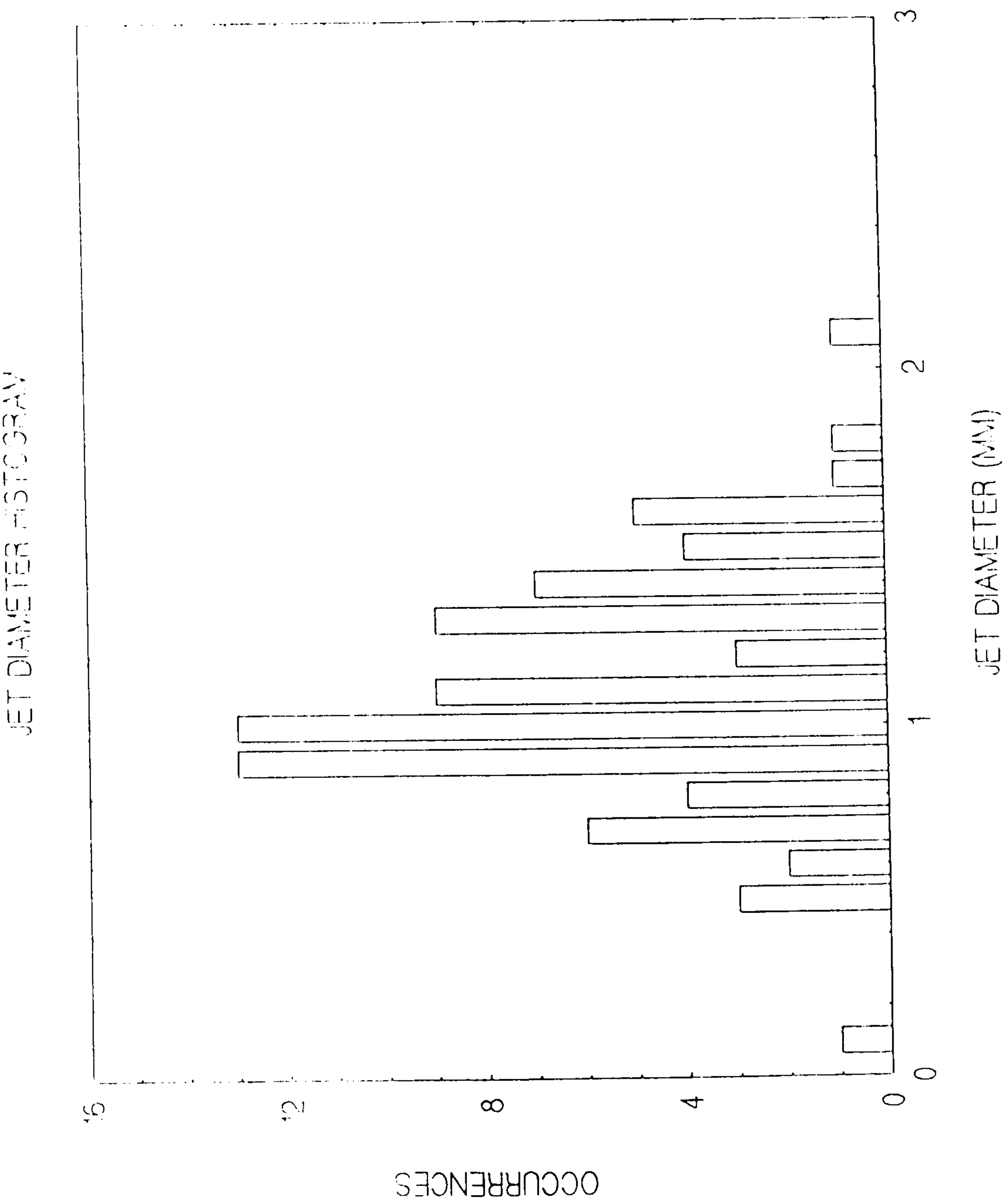
JET DIAMETER HISTOGRAM
JET DIAMETER (MM)
OCCURRENCES
0
1
2
3
0
4
8
12
16

ORGANIZATION: Experimental Branch, Aerophysics Division; AIAA 30th Aerospace Sciences Meeting, Reno	MARSHALL SPACE FLIGHT CENTER An Experimental Study of the Fluid Mechanics Associated with Porous Walls	NAME: N. Ramachandran, A. Smith and J. Heaman; DATE: January 1992

PSEUDOTURBULENCE (cont..)

Filter Rating μ	Porosity Φ	V_{CR} m/s	Re_{CR} $V_{CR}*D/\nu$	$Re_{CR}*\Phi^2$	$V_{CR}\Phi^2$
3	0.2838	0.78	49.09	3.95	0.0628
10	0.3445	0.53	33.35	3.96	0.0629
30	0.4173	0.399	25.11	4.37	0.0695
100	0.4760	0.284	17.87	4.08	0.0649

OTHER CATEGORIES OF RESULTS:

1. Jet field decay with distance from the surface.
2. Jet field turbulence characteristics.
3. Single jet turbulence characteristics.

N92-32264

"Experimental Studies of Characteristic Combustion-Driven Flows for CFD Validation"

R. J. Santoro, M. Moser, W. Anderson, S. Pal, H. Ryan and C. L. Merkle
Propulsion Engineering Research Center
The Pennsylvania State University
University Park, PA 16802

A series of rocket-related studies intended to develop a suitable data base for validation of CFD models of characteristic combustion-driven flows has been undertaken at the Propulsion Engineering Research Center at Penn State. Included are studies of coaxial and impinging jet injectors as well as chamber wall heat transfer effects. The objective of these studies is to provide fundamental understanding and benchmark quality data for phenomena important to rocket combustion under well-characterized conditions. Diagnostic techniques utilized in these studies emphasize determinations of velocity, temperature, spray and droplet characteristics and combustion zone distribution. Since laser diagnostic approaches are favored, the development of an optically accessible rocket chamber has been a high priority in the initial phase of the project. During the design phase for this chamber, the advice and input of the CFD modeling community were actively sought through presentations and written surveys. Based on this procedure, a suitable uni-element rocket chamber has been fabricated and is presently under preliminary testing. Results of these tests, as well as the survey findings leading to the chamber design, was presented.

In particular, laser-induced fluorescence imaging results for hydroxyl radicals have been obtained. These experiments were conducted using gaseous hydrogen/gaseous oxygen propellants in the optically accessible uni-element rocket chamber. Heat transfer studies demonstrated the effectiveness of the curtain window purge needed to protect the optical surfaces. These results also demonstrated the capability to determine wall heat transfer rates in the present rocket test chamber. Measurements indicated that heat transfer rates were approximately an order of magnitude smaller than observed in actual rocket chambers. If larger propellant flow rates are utilized, this difference should be further narrowed.

Related results from impinging jet studies under non-combusting conditions revealed several trends regarding drop size and liquid sheet breakup. The general experimental observation that breakup length increases with increasing jet velocity and decreasing impingement angle is in agreement with previous studies. However, this trend is opposite to predictions derived from linear stability-based analysis of liquid sheet atomization. However, drop size predictions for linear stability-based analysis reproduced the observed trend of decreasing drop size with increasing jet velocity and increasing impingement angle.

Experimental Studies of Characteristic Combustion-Driven Flows for CFD Validation

R. J. Santoro, M. Moser, W. Anderson,
S. Pal, H Ryan, and C. L. Merkle

The Propulsion Engineering Research Center
The Pennsylvania State University
University Park, PA 16802

Workshop for Computational Fluid Dynamic (CFD)
Applications in Rocket Propulsion

April 28-30, 1992

OUTLINE

- CFD Validation - Optically Accessible Rocket
- Heat Transfer Measurements
- Impinging Jet Studies
- Summary
- Future Work

CFD VALIDATION - OPTICALLY ACCESSIBLE ROCKET

M. Moser, S. Pal, R. Santoro, C. Merkle

OBJECTIVE

To Provide Benchmark-Quality Data for CFD Code Validation for Combustion-Driven Flows

Obtain Fundamental Data Under Realistic and Well Characterized Conditions

APPROACH

Emphasize Uni-element Coaxial Injectors

Obtain Fundamental Data Under Well Characterized and Realistic Conditions

- Pressure
- Combustion zone
- Mean Velocity
- Turbulence Intensity
- Species
- Droplet Size and Velocity

Employ Non-Intrusive Advanced Diagnostics

- Laser Induced Fluorescence
- Raman Spectroscopy
- Laser Velocimetry
- Flow Visualization
- Phase Doppler Particle Analyzer
- Polarization Ratio
- Raman Spectroscopy

Closely Integrate CFD Objectives Into Experimental Program

- Experiment Design
- Measured Quantities
- Boundary Condition Specification

SUMMARY OF SURVEY RESULTS

- **Square Geometry Is Acceptable**

  Initially Axisymmetric Approximation Suitable Eventually
  3-d Verification Required

- **Chamber Mach Number Need Not Be Matched to Actual Rocket Conditions**

- **Recirculation Effect In Uni-Element Chamber Can Be Accommodated If Suitable Measurements Are Available**

- **Measurements And Boundary Conditions - Nearly Everything Is Important**

  Typically All Parameters Rate 1 Or 2 On Scale Of 5

Responses From: MSFC
Aerojet
Rocketdyne
CFDRC

OPTICALLY ACCESSIBLE ROCKET

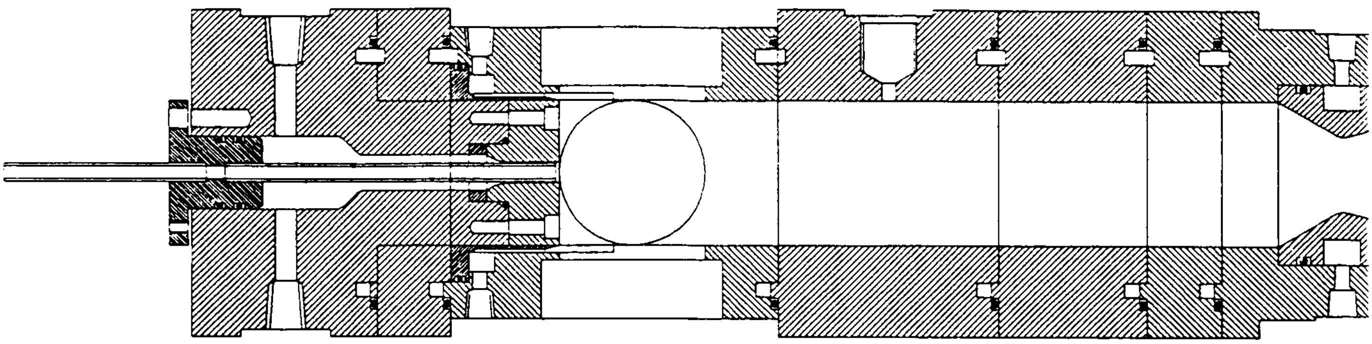

- Two Inch Square Cross-section
- Variable Length 6-12 Inches
- Two Inch Diameter Quartz Windows For Viewing
- Slot Windows For Laser Access
- Injector Design Is Modular

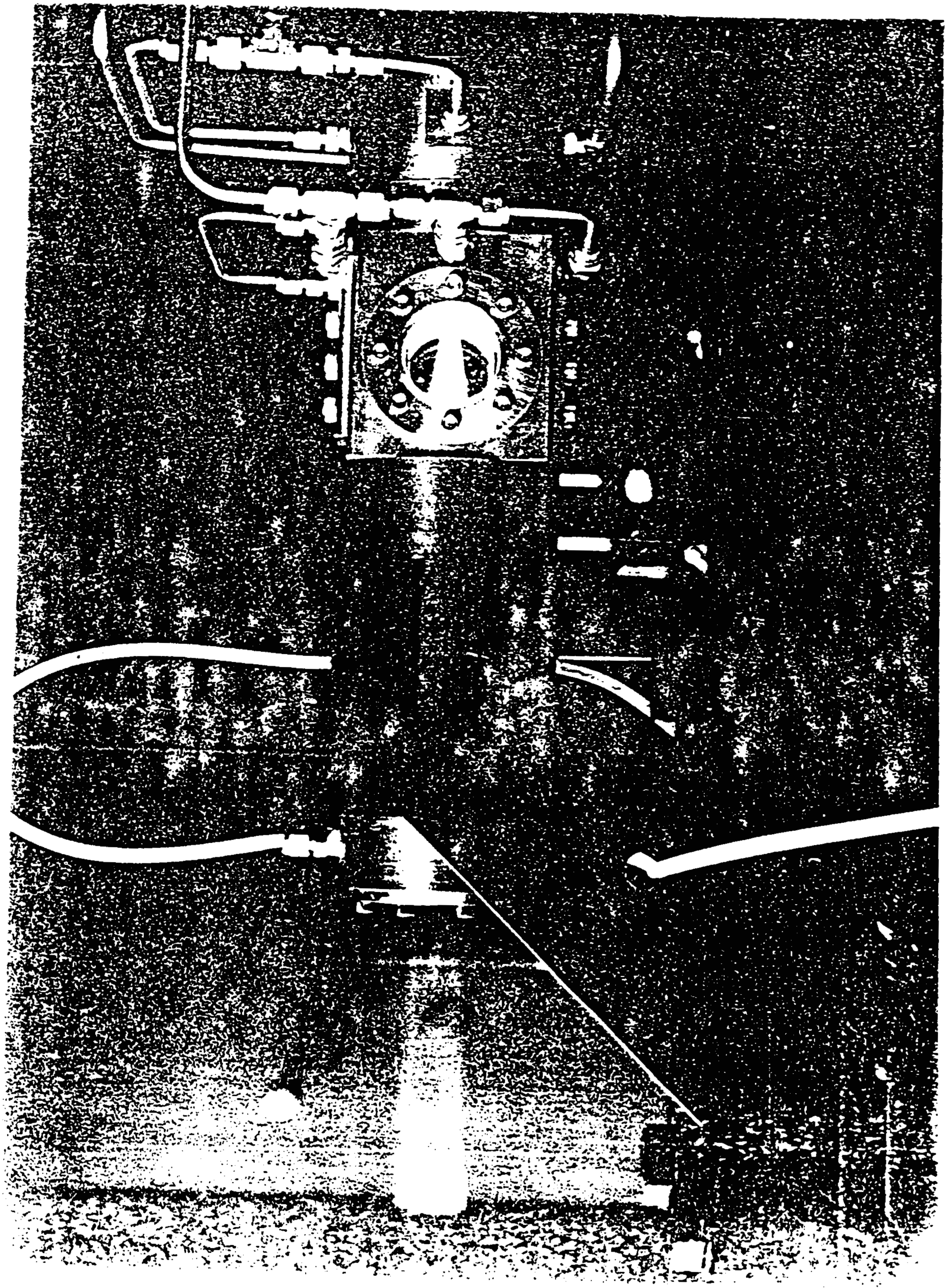

RESULTS

- **Rocket Chamber Has Been Checked Out To 400 psi Chamber Pressure**
- **Window Purges Effectiveness Tested With Heat Flux Gages**
- **Quartz Windows Tested To 200 psi For Four Second Firings**
- **Shadowgraph Photograph Obtained**
- **2-D Laser Induced Fluorescence Image Of OH Obtained**

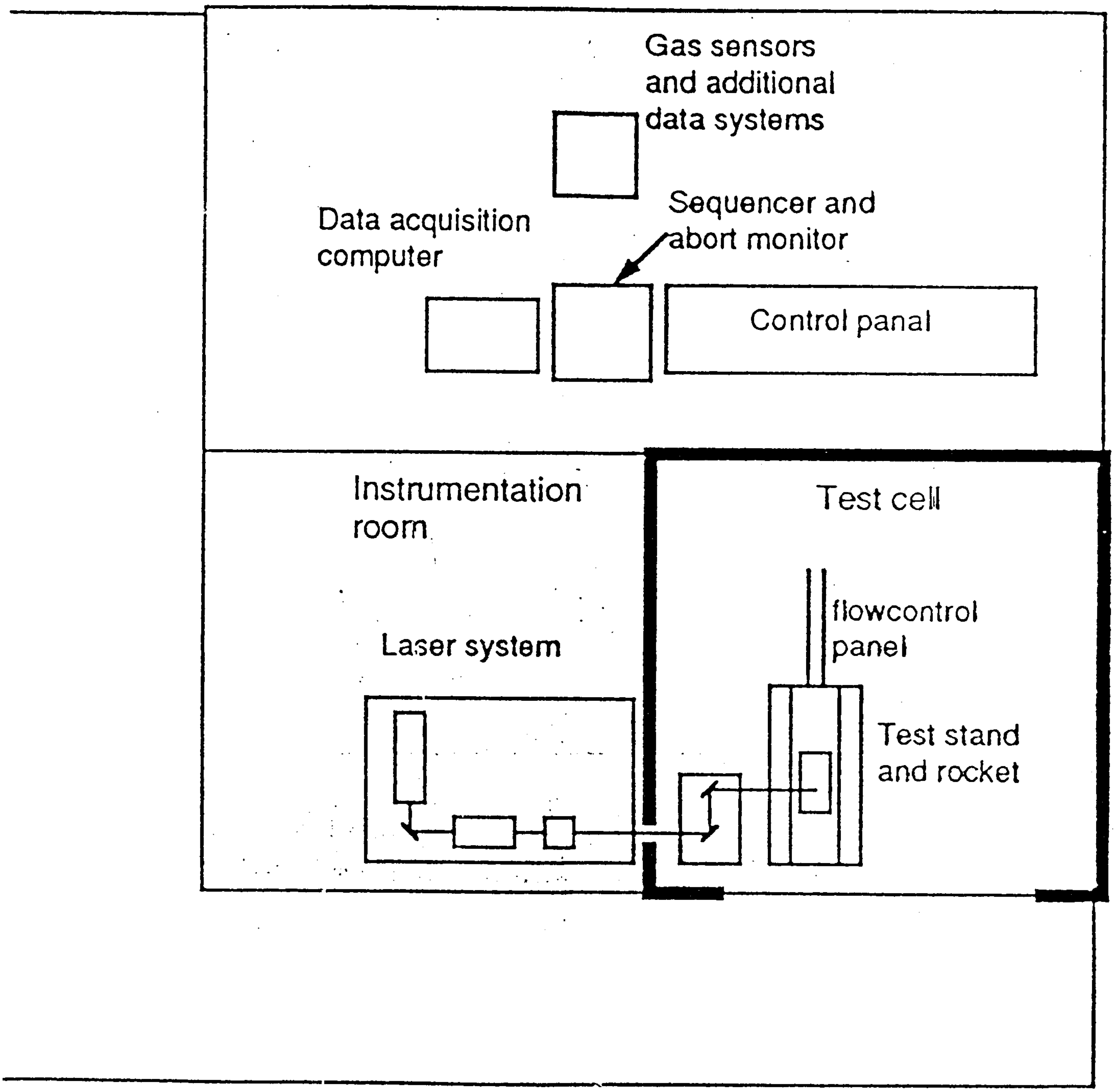
Gas sensors
and additional
data systems
Data acquisition
computer
Sequencer and
abort monitor
Control panal
Instrumentation
room
Test cell
flowcontrol
panel
Laser system
Test stand
and rocket

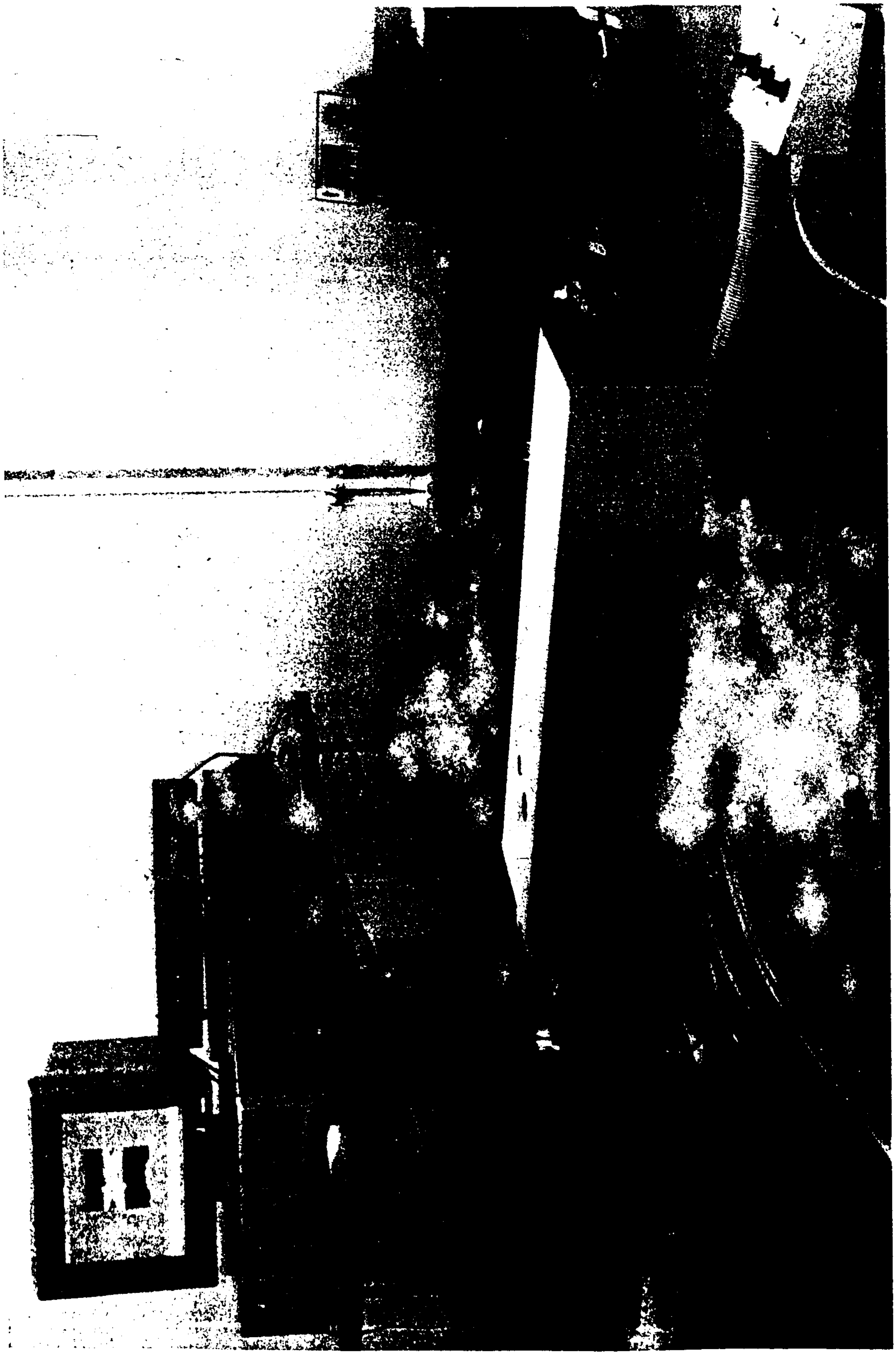

HEAT TRANSFER MEASUREMENTS

S. Pal, C. Merkle

Objective:

- Demonstrate Capability

- Test Effectiveness Of Window Purge

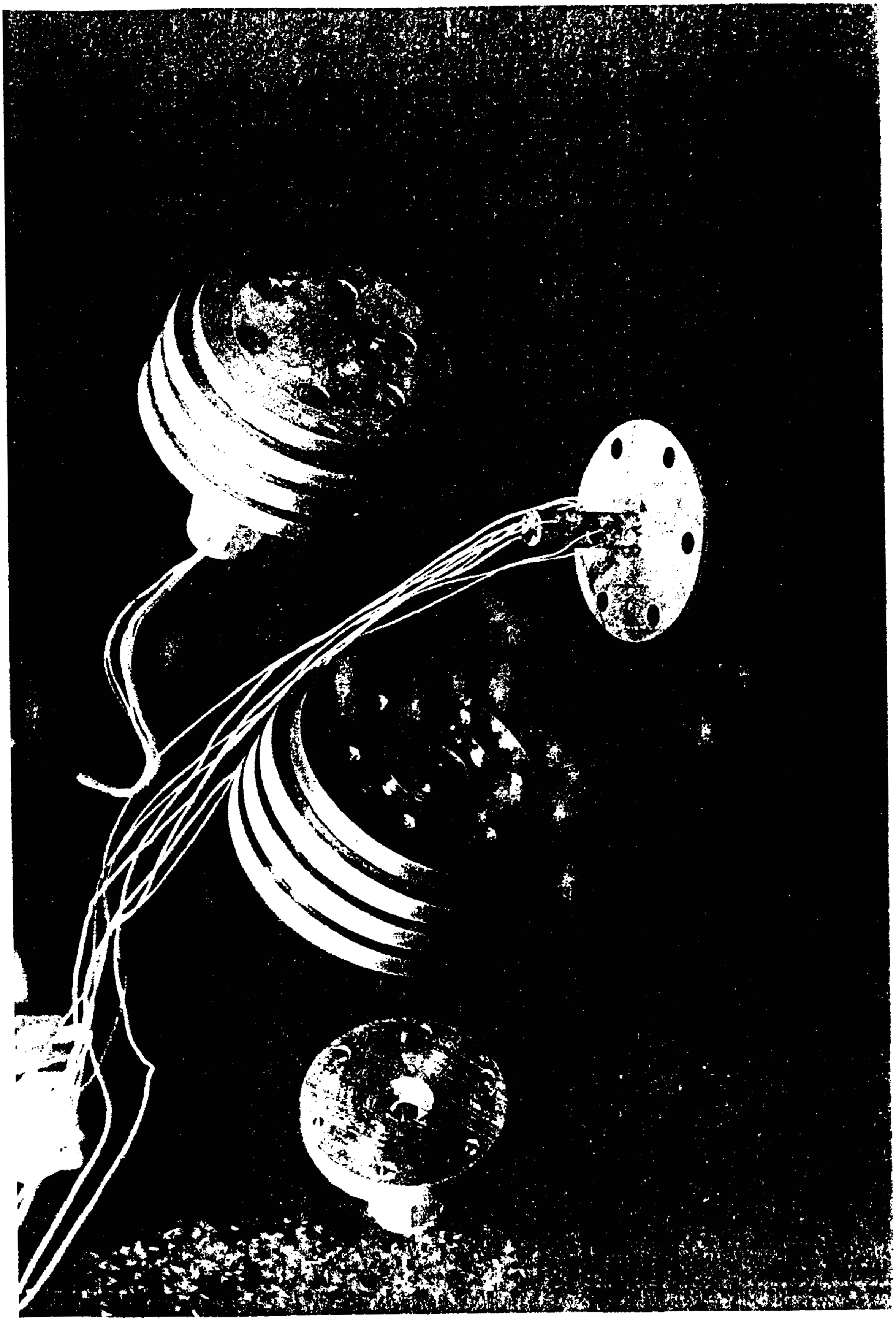

WINDOW PURGE COMPARISON

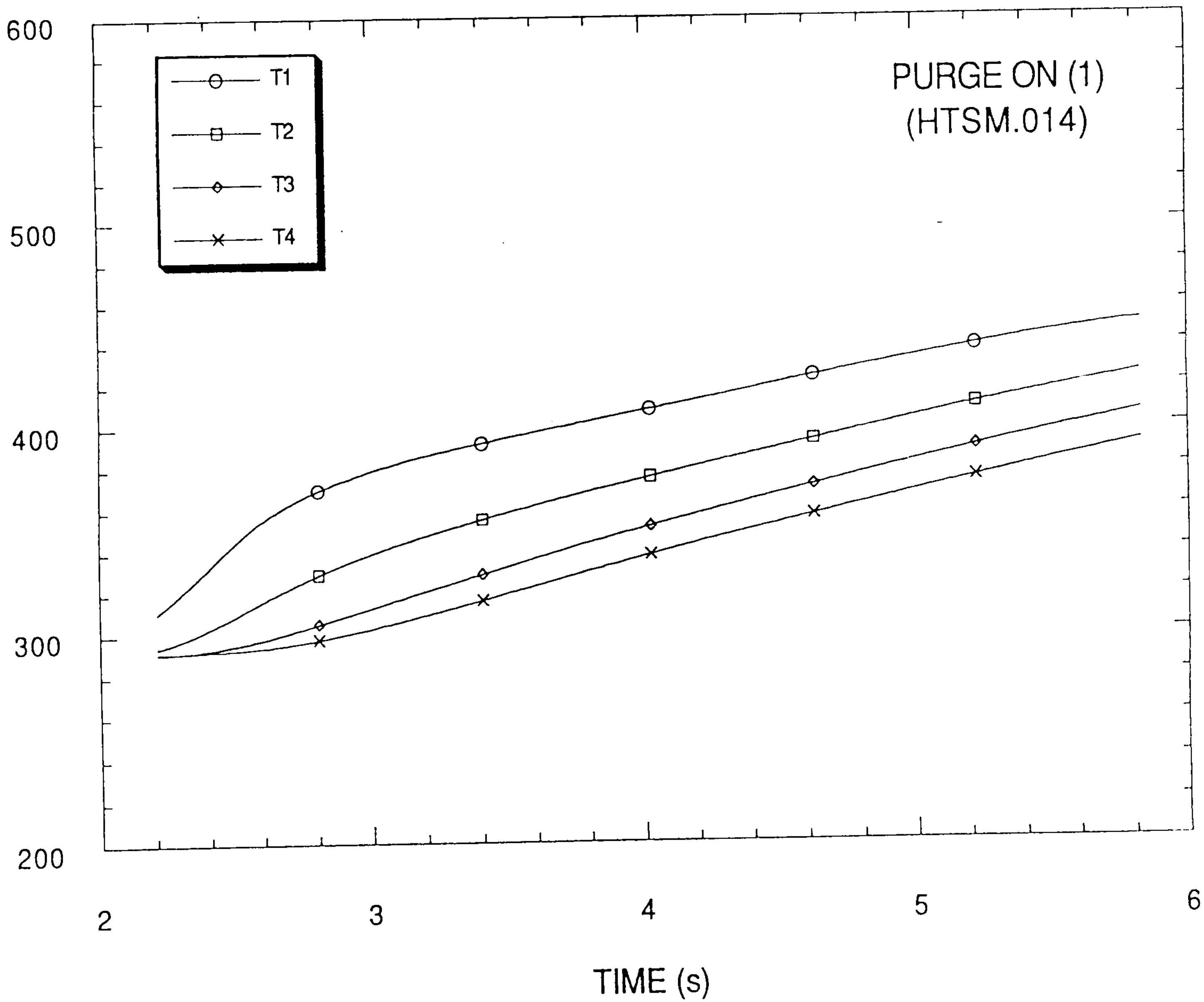

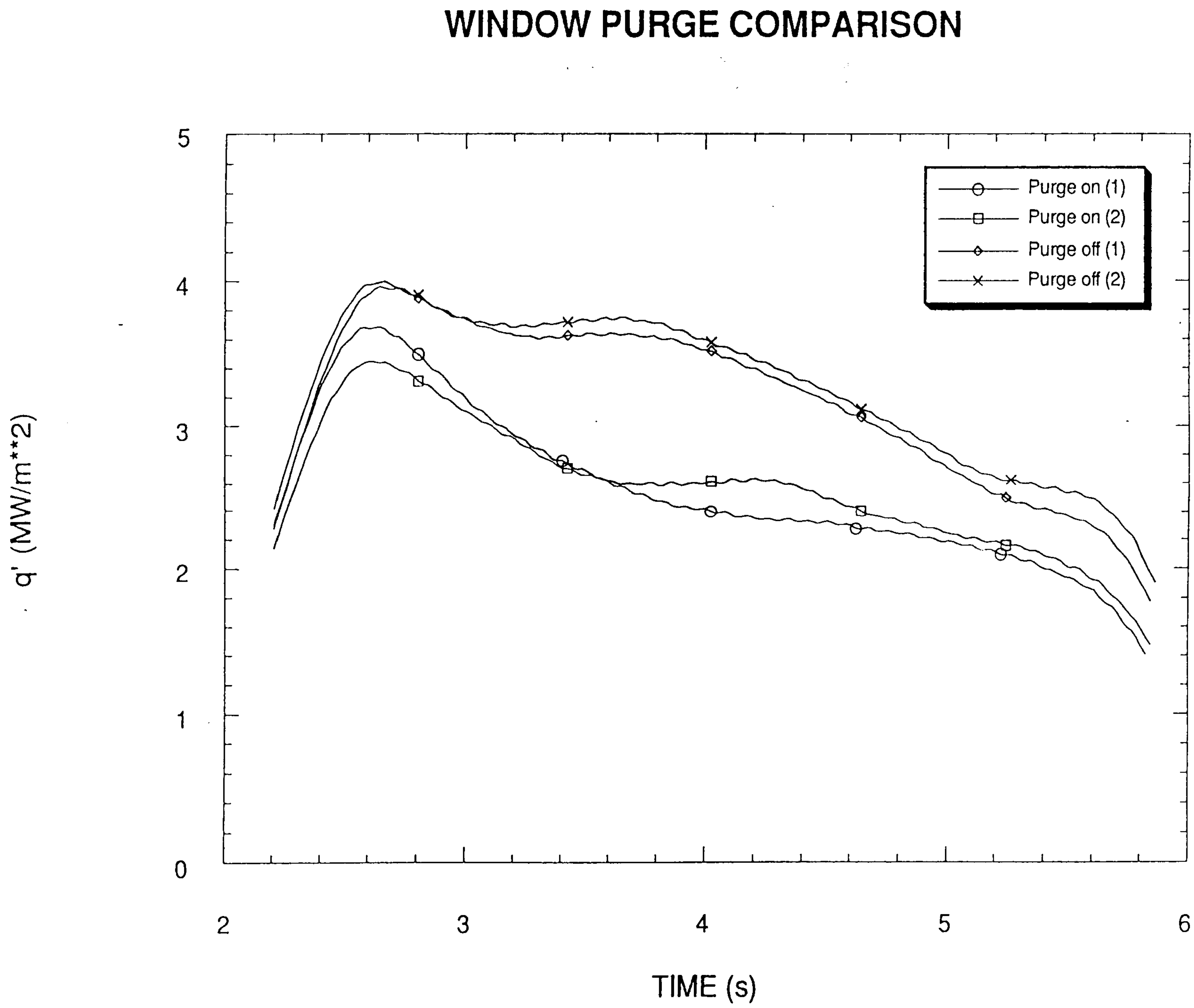

WINDOW PURGE COMPARISON
Purge on (1)
Purge on (2)
Purge off (1)
Purge off (2)
q' (MW/m**2)
TIME (s)
0
1
2
3
4
5
2
3
4
5
6

OBJECTIVES

- Characterize Spray Phenomena Associated With Impinging Jet Injectors
  - Breakup Length
  - Drop Size
  - Periodic Structures

- Investigate Sensitivity of Spray Characteristics to Geometric and Operational Parameters
  - Jet Velocity
  - Orifice Diameter
  - Impingement Angle
  - Pre-Impingement Length
  - Orifice Length

- Compare Experimental Results with Theoretical Models of Sheet Breakup and Drop Formation
  - Linear Growth of Surface Waves Due to Aerodynamic Forces

Impinging Jet Injector System

Impingement Effects
- Liquid Inertia
- Oscillations

Orifice Effects
- Vortex Shedding
- Cavitation
- Reattachment

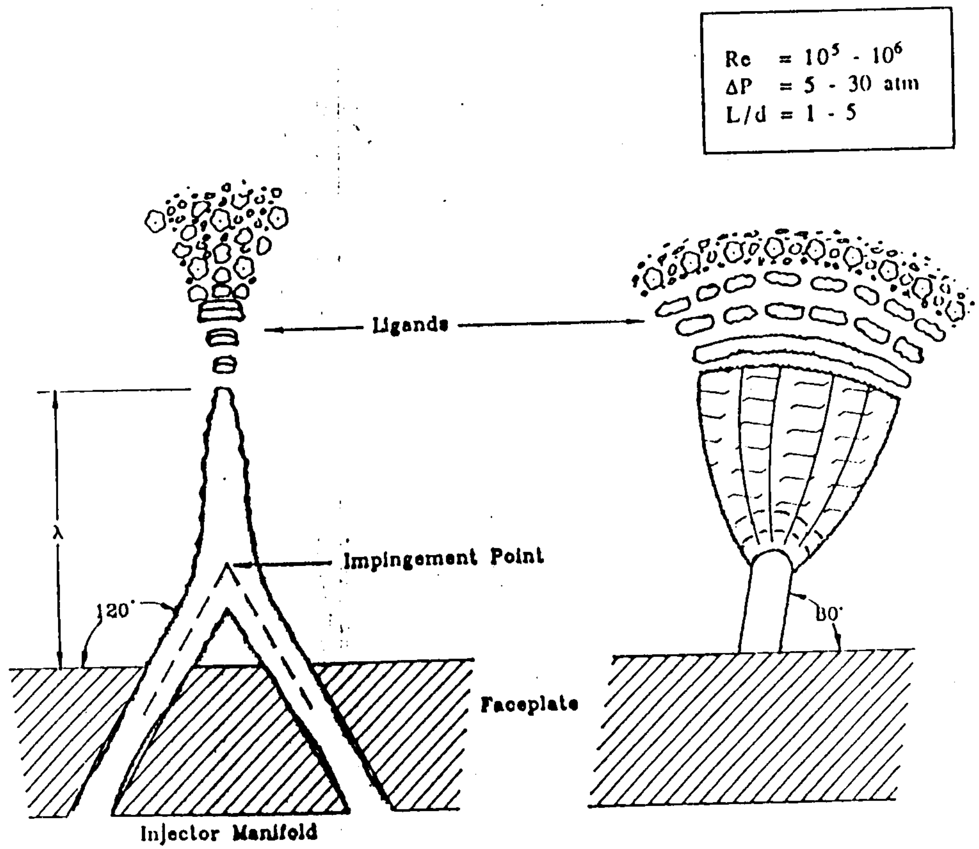

Upstream Effects
- Turbulence
- Flow Patterns

Ambient Phase Effects
- Pressure
- Friction
- Oscillations

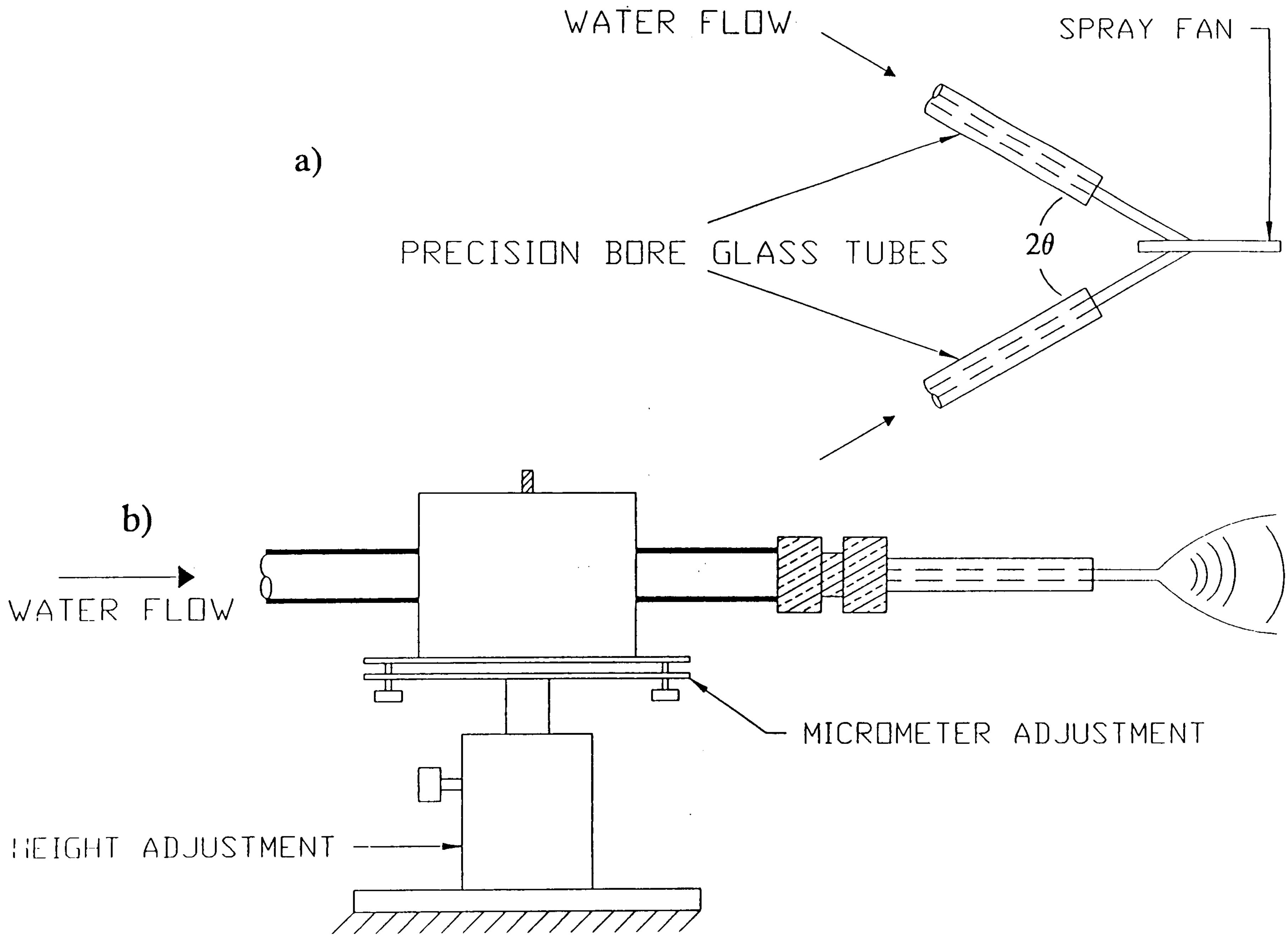
a)
WATER FLOW
SPRAY FAN
PRECISION BORE GLASS TUBES
2θ
b)
WATER FLOW
MICROMETER ADJUSTMENT
HEIGHT ADJUSTMENT

$U_j=6.4$ m/s

$2\theta=60°$

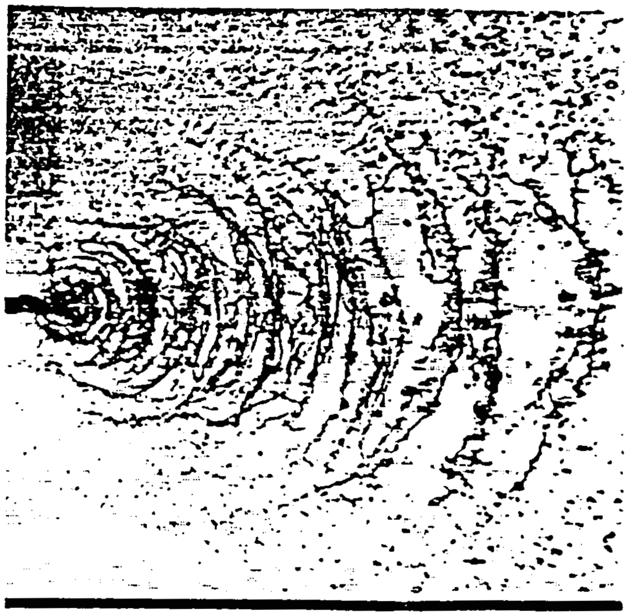

$U_j=18.5$ m/s

$2\theta=60°$

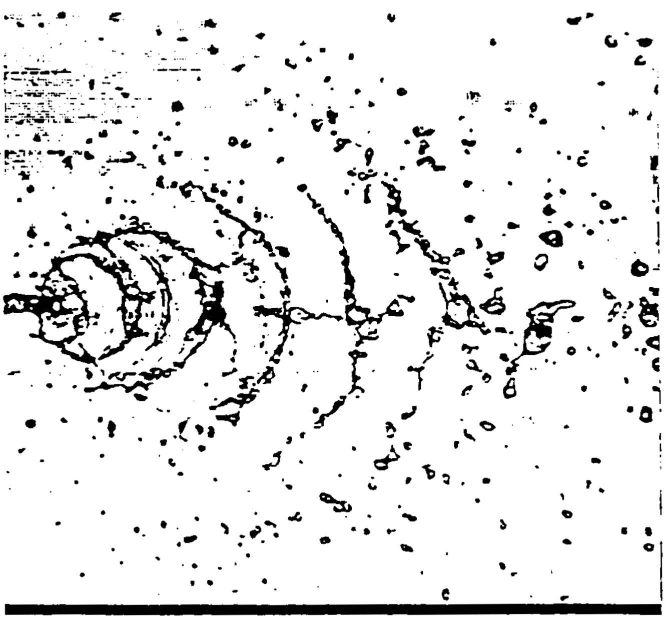

$U_j=6.4$ m/s

$2\theta=80°$

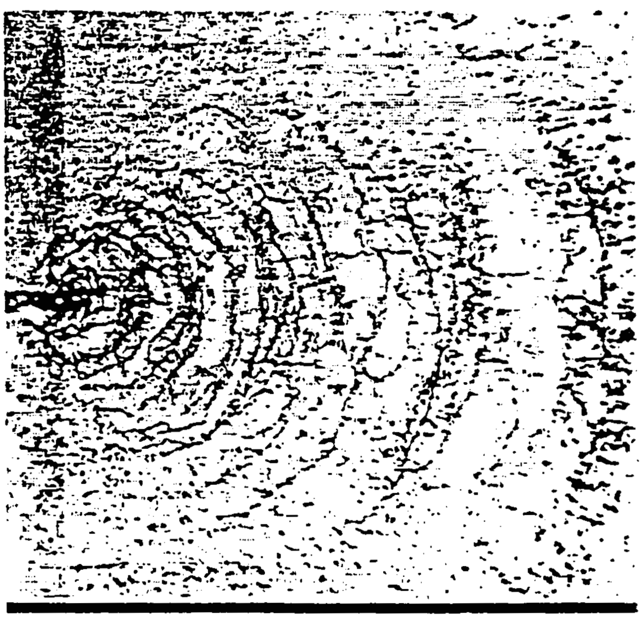

$U_j=18.5$ m/s

$2\theta=80°$

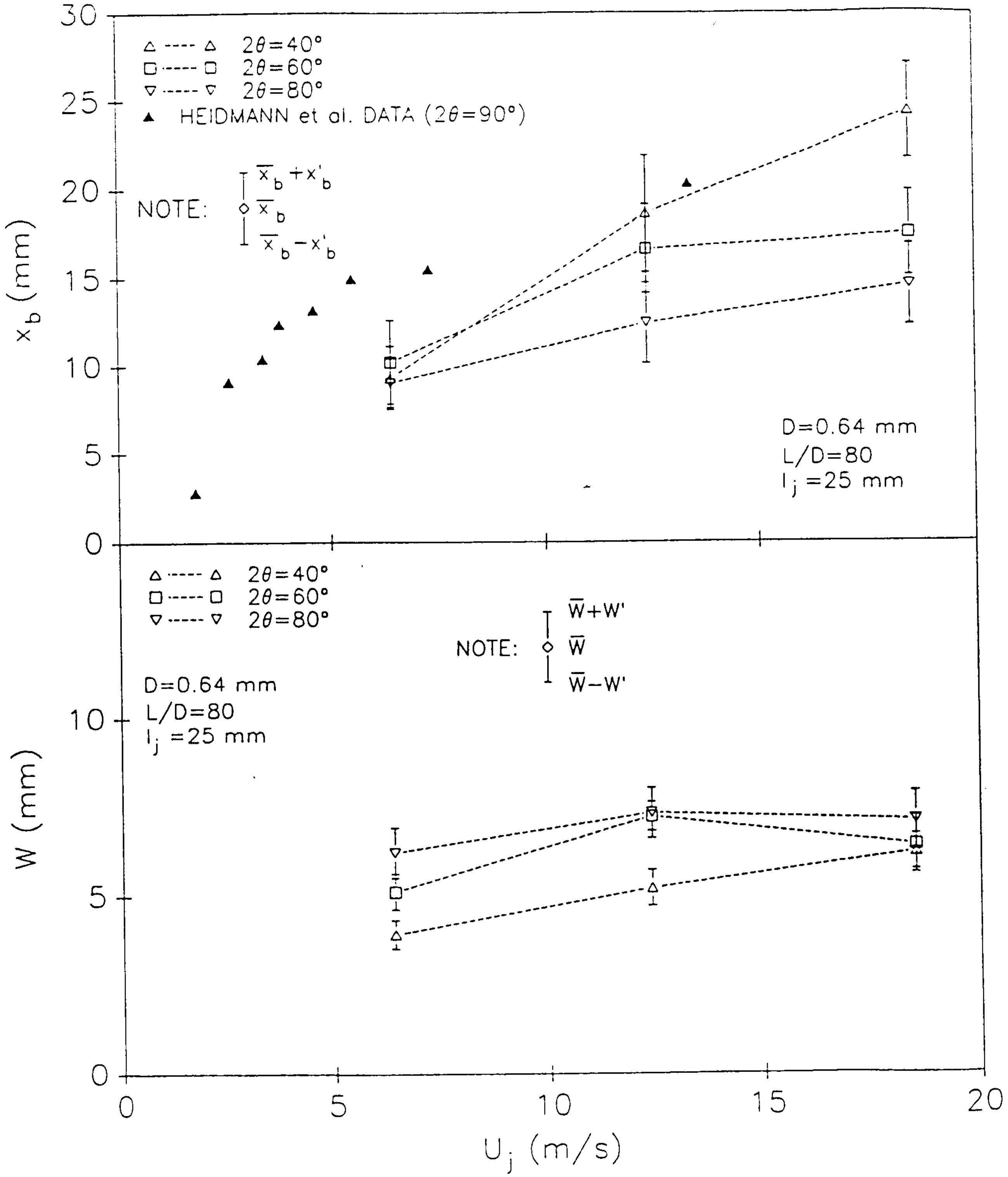

2θ=40°
2θ=60°
2θ=80°
HEIDMANN et al. DATA (2θ=90°)
NOTE:
x̄b + x'b
x̄b
x̄b − x'b
D=0.64 mm
L/D=80
lj =25 mm
xb (mm)
2θ=40°
2θ=60°
2θ=80°
NOTE:
W̄+W'
W̄
W̄−W'
D=0.64 mm
L/D=80
lj =25 mm
W (mm)
Uj (m/s)

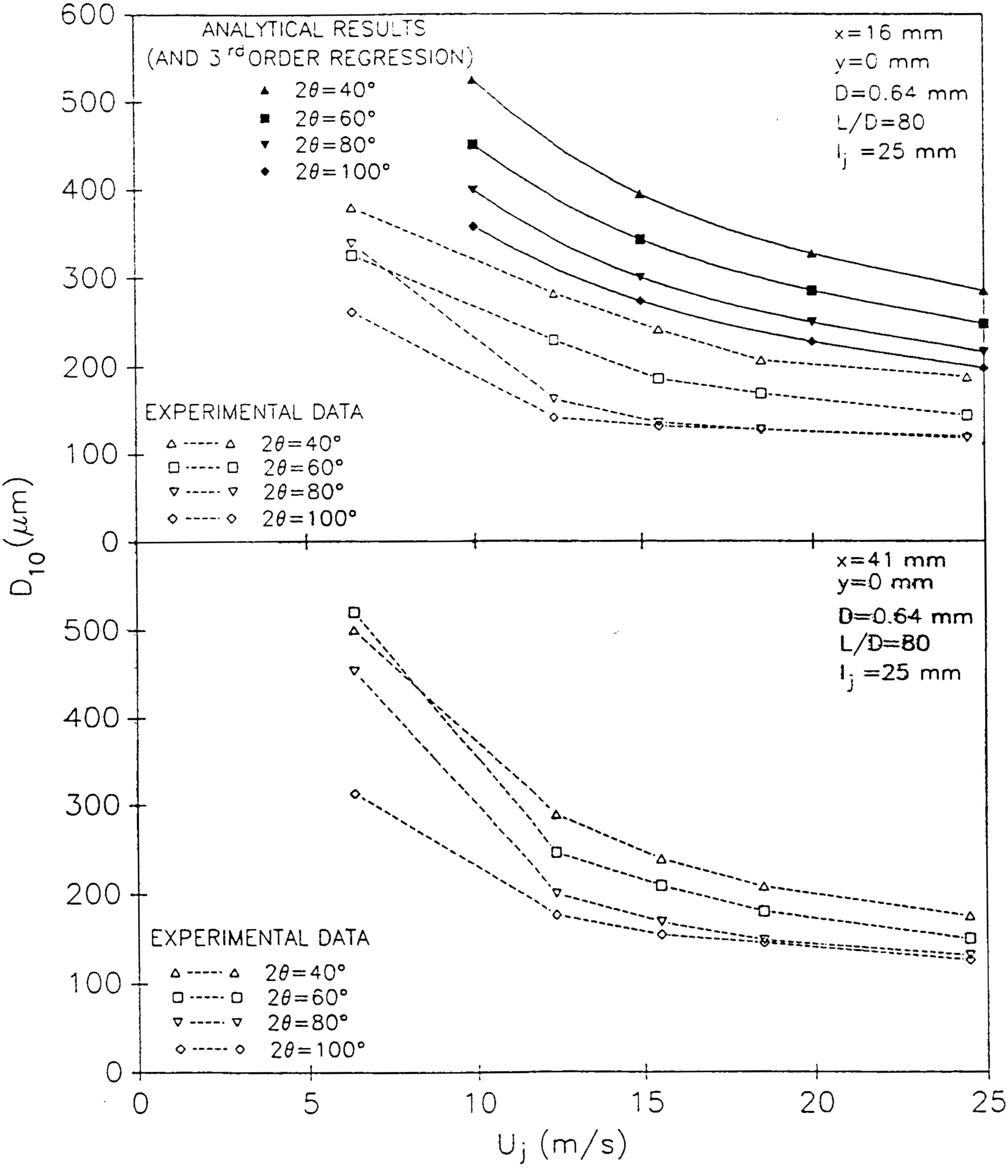
ANALYTICAL RESULTS
(AND 3 rd ORDER REGRESSION)
2θ=40°
2θ=60°
2θ=80°
2θ=100°
x=16 mm
y=0 mm
D=0.64 mm
L/D=80
l j =25 mm
EXPERIMENTAL DATA
2θ=40°
2θ=60°
2θ=80°
2θ=100°
x=41 mm
y=0 mm
D=0.64 mm
L/D=80
l j =25 mm
EXPERIMENTAL DATA
2θ=40°
2θ=60°
2θ=80°
2θ=100°
D10 (μm)
Uj (m/s)
0
100
200
300
400
500
600
0
5
10
15
20
25

SUMMARY

- Experimental Results Were Compared with Predictions From Linear Aerodynamic Instability Derived Model
    - Breakup Length Predictions Oppose Observed Trends
    - Drop Size Predictions Reproduce Observed Trend and Agree Within Factor of 2
- General Appearance Favors Impact Wave Breakup Mechanism
- Orifice L/D Has No Significant Effect on Spray Characteristics
- Pre-Impingement Length Has Measurable Effect on Breakup Length and Drop Size

SUMMARY

- Successful Firings of Optically Accessible Rocket Test Chamber Achieved

- Shadowgraph of Combustion Zone Obtained

- Preliminary Two-Dimensional OH Imaging Results Obtained

- Wall Heat Transfer Rate Measurement Capability Demonstrated

- Fundamental Studies of Impinging Sprays Are Elucidating Basic Atomization Mechanisms

FUTURE WORK

- Semi-Quantitative Measurement of Relative OH Concentration

- Velocimetry (initially single point measurements, eventually 2-D velocimetry measurements)

- Raman Spectroscopy

ACKNOWLEDGEMENTS

The CFD Validation Studies Are Supported By The Marshall Space Flight Center Under Contract NAS8-38862

the Impinging Jet Studies Are Supported by The Air Force Office Of Scientific Research Under Grant AFOSR-91-0336

N92-32265

TURBINE DISK CAVITY AERODYNAMICS AND HEAT TRANSFER

B. V. Johnson
W. A. Daniels
United Technologies Research Center
East Hartford, CT 06108

Experiments were conducted to define the nature of the aerodynamics and heat transfer for the flow within the disk cavities and blade attachments of a large-scale model, simulating the SSME turbopump drive turbines. These experiments of the aerodynamic driving mechanisms explored the following: (1) flow between the main gas path and the disk cavities, (2) coolant flow injected into the disk cavities, (3) coolant density, (4) leakage flows through the seal between blades, and (5) the role that each of these various flows has in determining the adiabatic recovery temperature at all of the critical locations within the cavities. The model and the test apparatus provide close geometrical and aerodynamic simulation of all the two-stage cavity flow regions for the SSME High Pressure Fuel Turbopump and the ability to simulate the sources and sinks for each cavity flow.

Carbon dioxide was used as a trace gas for constant density experiments or as the simulated "heavy gas" coolant. Gas samples were withdrawn at selected locations on the rotating and stationary surfaces in the fore and aft cavity and the interstage seal regions of the two stage system. The gas samples were used to determine the fraction of gas at a location which originates from each of three coolant injection locations or four gas path locations. Samples were also withdrawn at selected locations in the blade shank regions.

A parametric series of experiments was conducted with constant density fluids and an exploratory series of experiments was conducted with CO_2 as the simulated coolant. Experimental results showed (1) the variation of coolant distribution on the cavity and disk surfaces as a function of coolant flow ratio, (2) the effects on the coolant distribution for changes in the coolant inlet distributions, and (3) increased mixing of coolant with the ingested gas when a heavy gas (density ratio equal 1.5) was used as the coolant.

PRECEDING PAGE BLANK NOT FILMED

TURBINE DISK CAVITY AERODYNAMICS AND HEAT TRANSFER

Contract NAS8-37462

B.V. Johnson
W.A. Daniels

Tenth Workshop for Computational Fluid Dynamic Applications in Rocket Propulsion

April 30, 1992

UNITED TECHNOLOGIES RESEARCH CENTER

ACTUAL AND MODEL DISK/CAVITY SYSTEMS

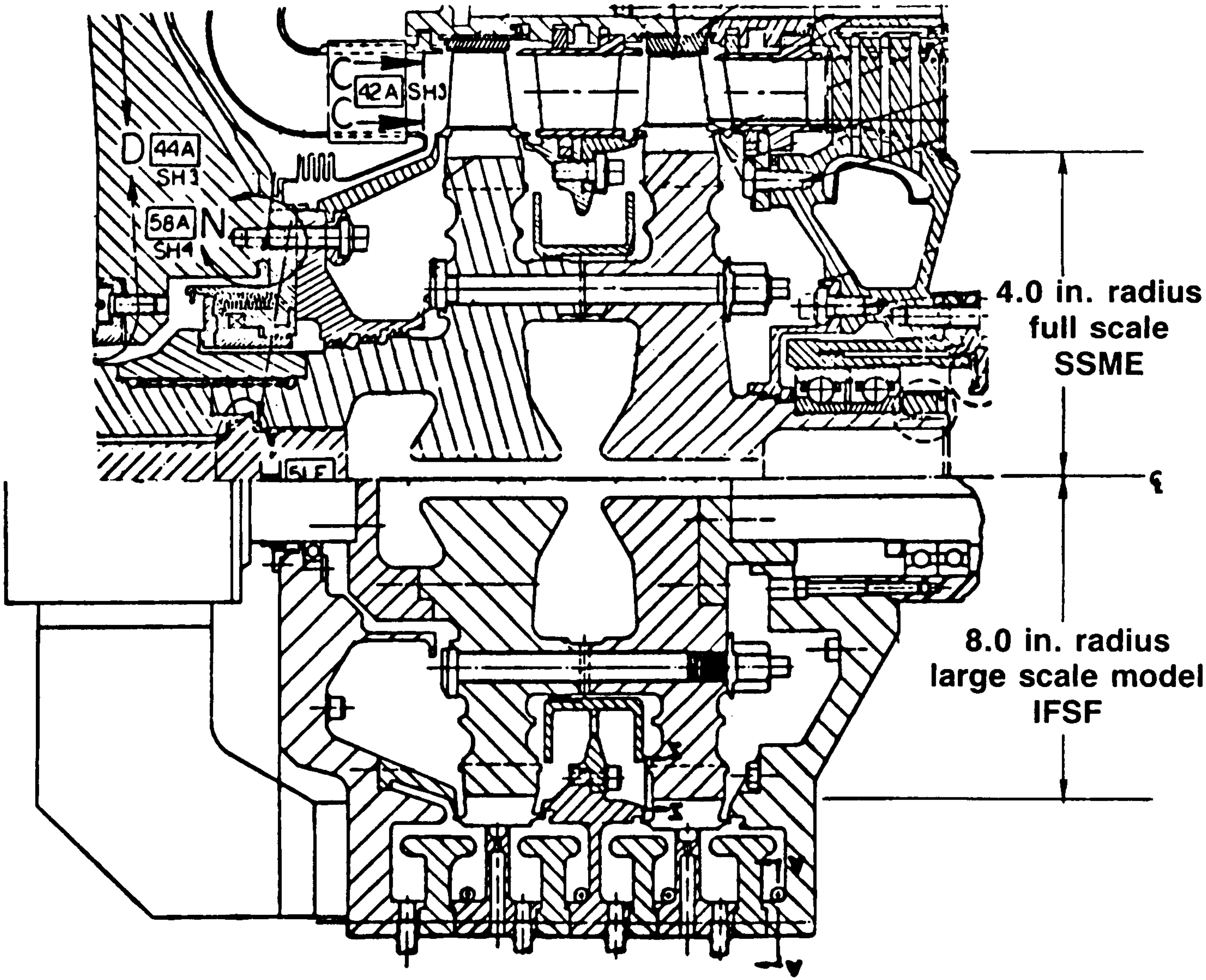

88-4-18-3

GAS SOURCES AND EXITS

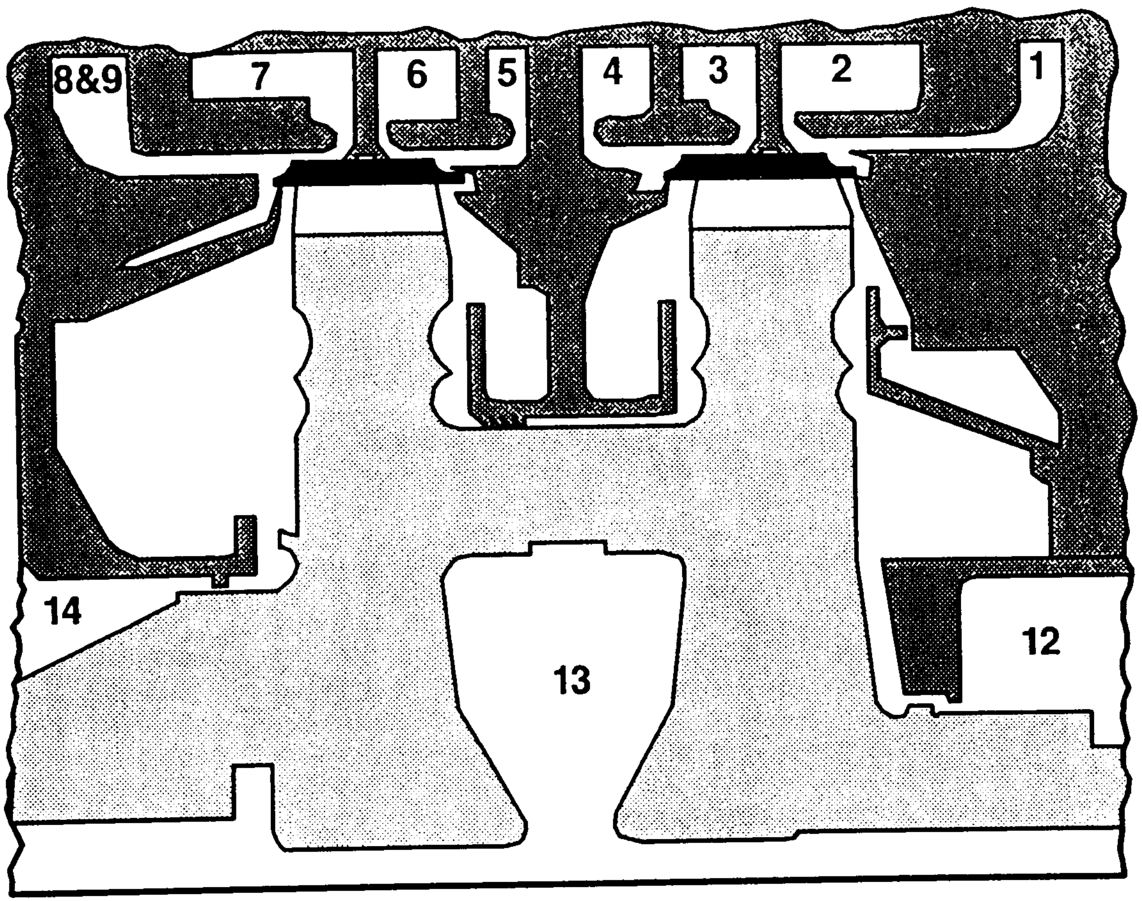

RB3278TX.008

MODEL INSTRUMENTATION

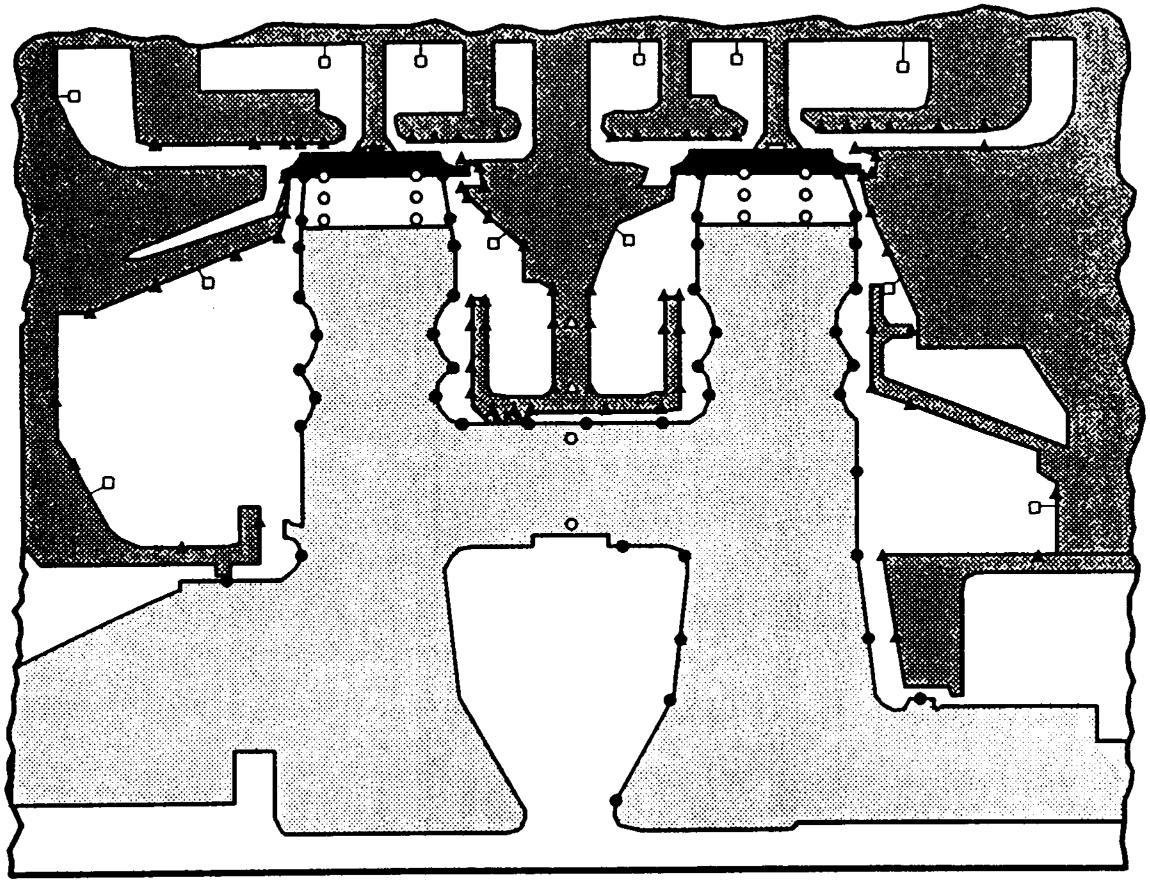

- □ Thermocouples
- ○ Pressure/CO_2 taps in passages
- ● Pressure/CO_2 taps on rotating components
- ▲ Pressure/CO_2 taps on stationary components

RB3278ETX.007

SSME TURBINE DISK CAVITY MODEL

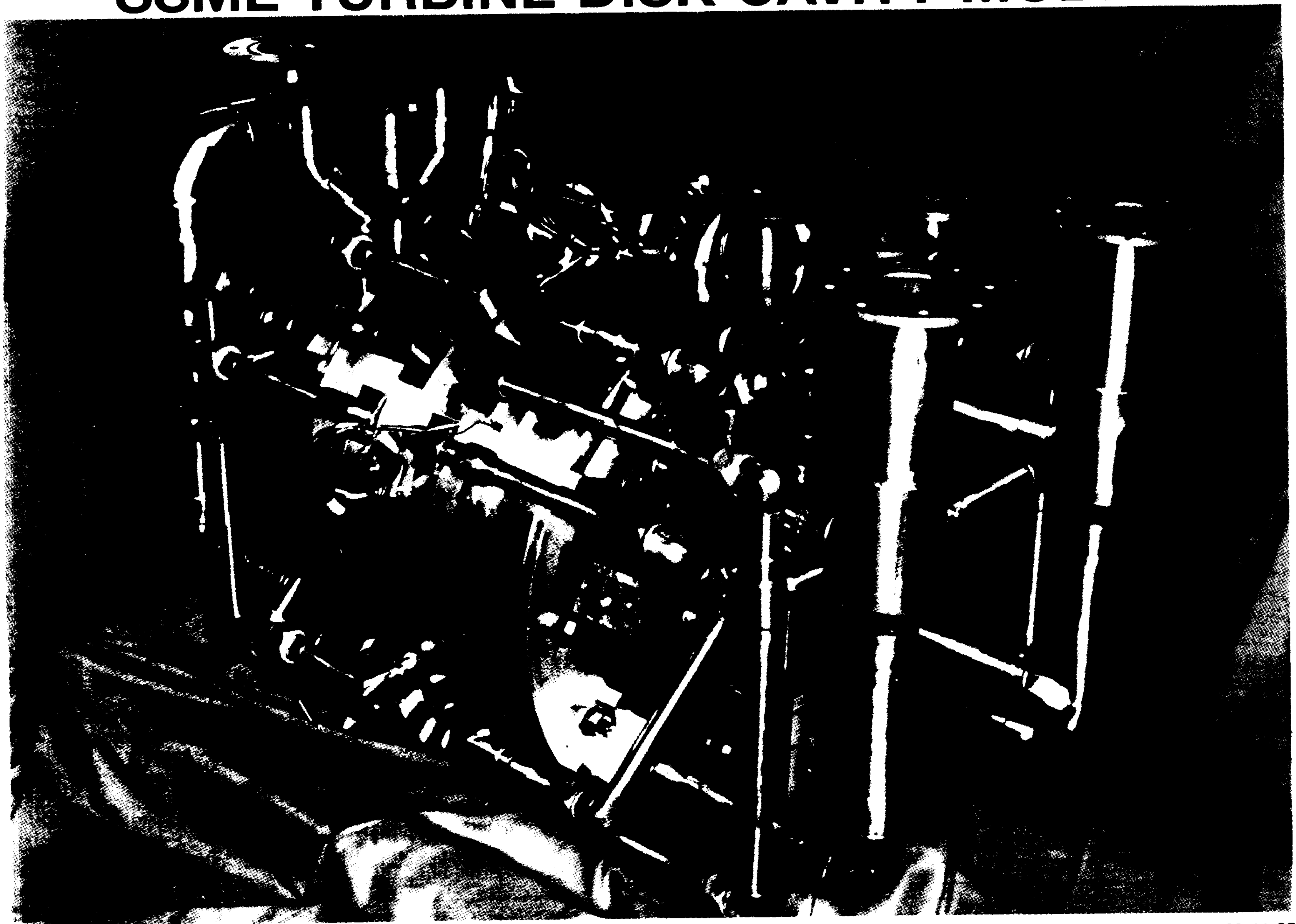

C89-414-B-2

89-11-25-1

MODEL IN INTERNAL FLOW FACILITY

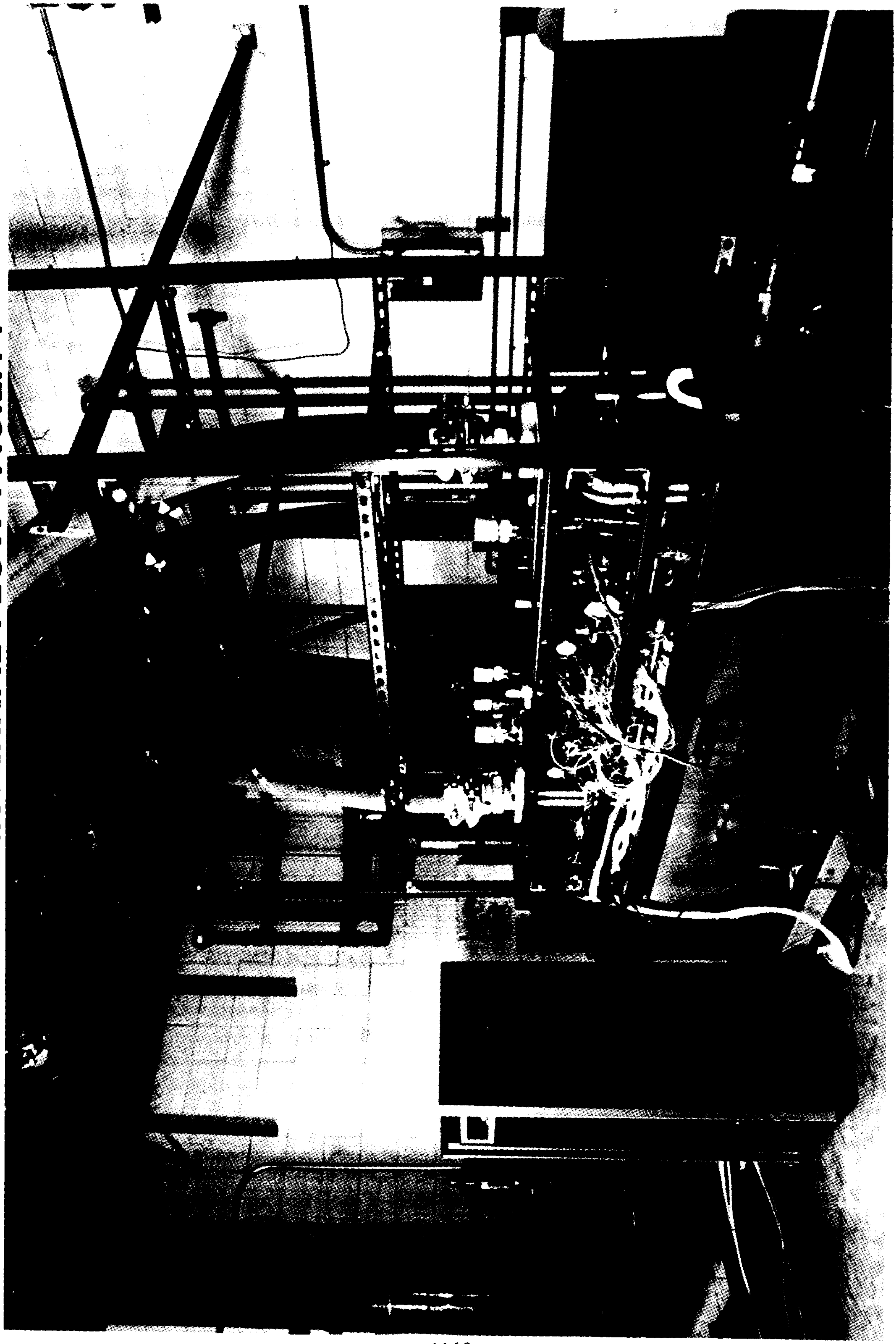

MODEL SEAL REGION AND GAS SOURCE/EXIT LOCATIONS

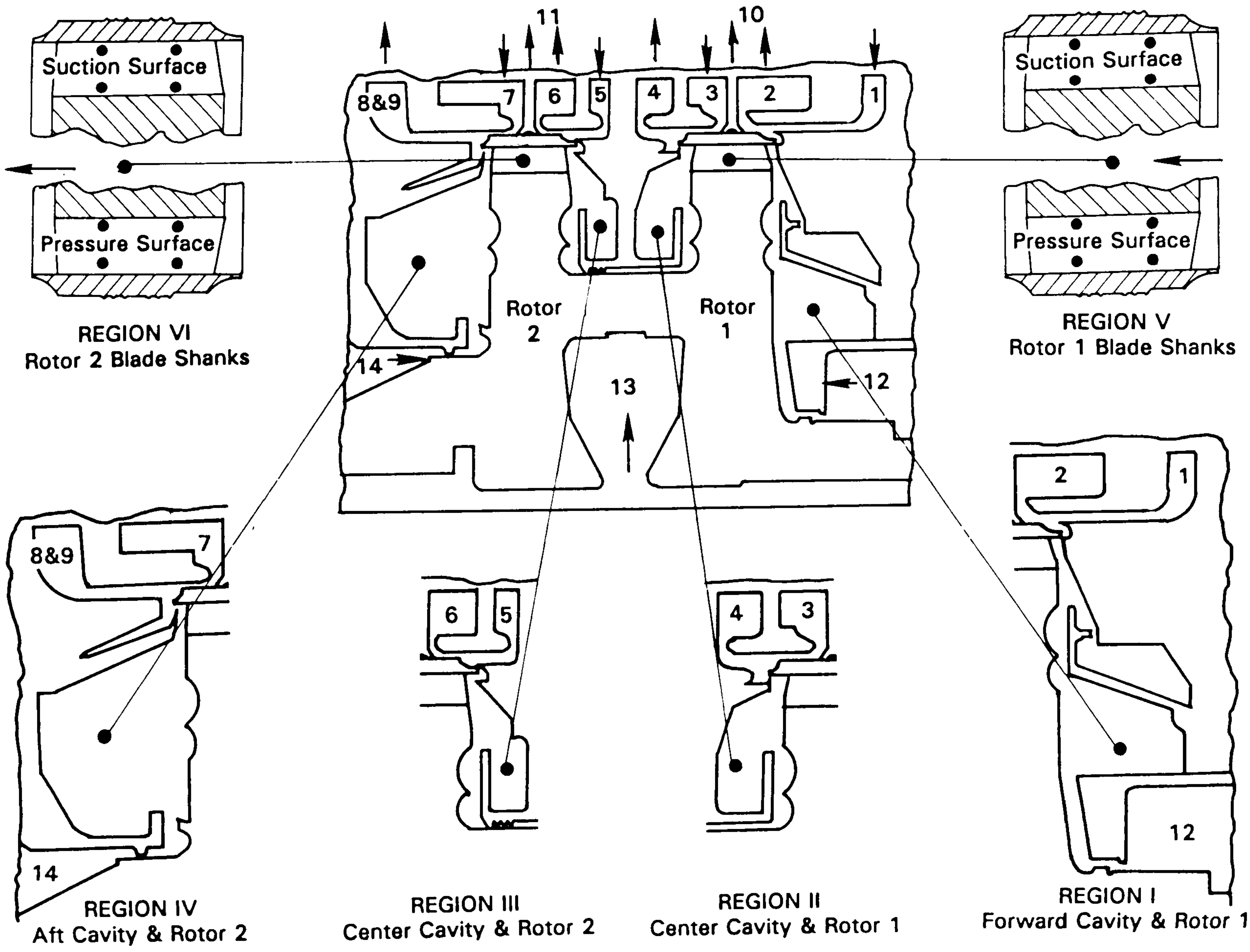

COOLANT CONCENTRATION ON ROTOR AND STATIONARY WALLS

Variables:
Radius
Coolant flow rate

Region IV: Aft Cavity & Rotor 2
Coolant: Air

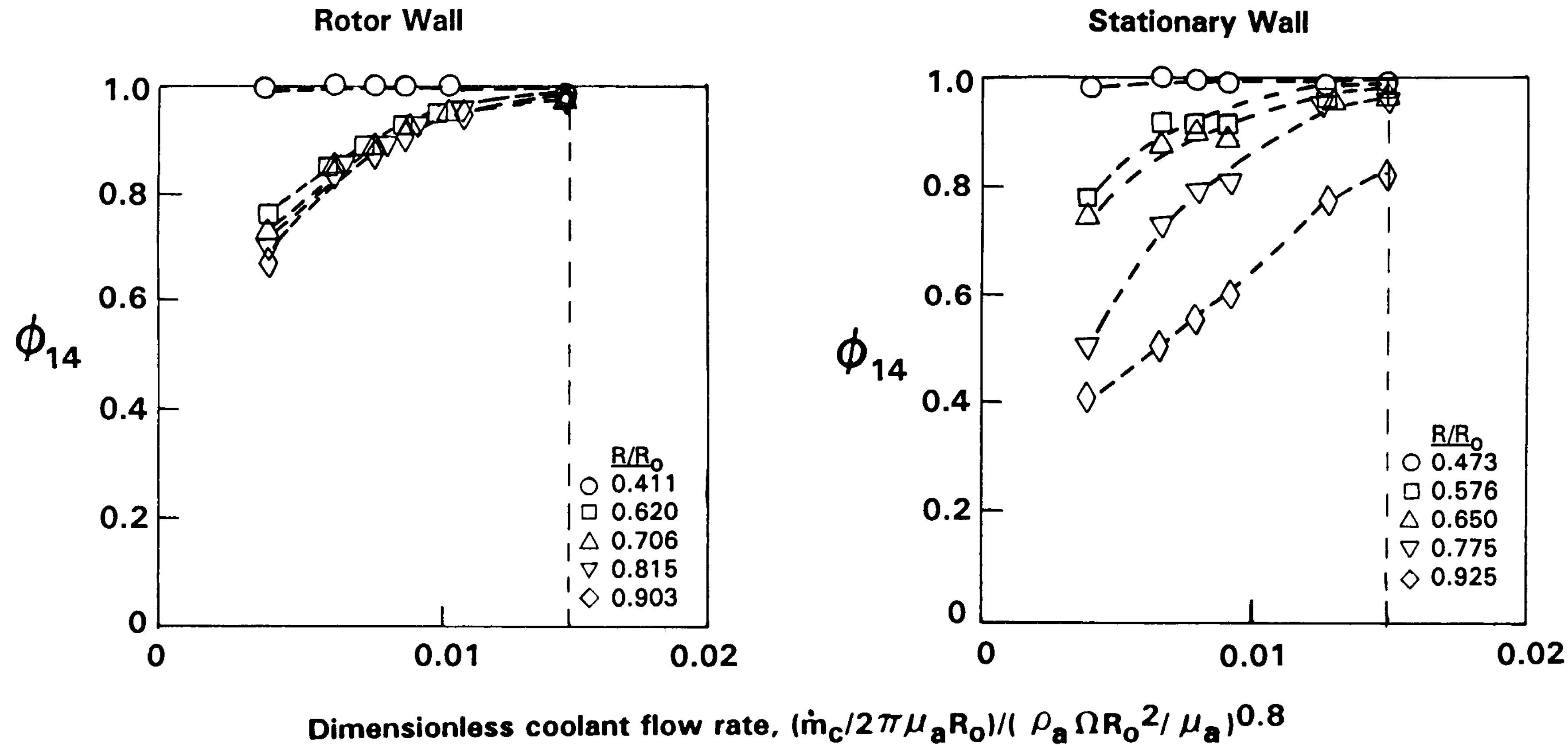

COOLANT CONCENTRATION ON ROTOR AND STATIONARY WALLS

Variables:
Radius
Coolant flow rate

Region IV: Aft Cavity & Rotor 2
Coolant: CO_2

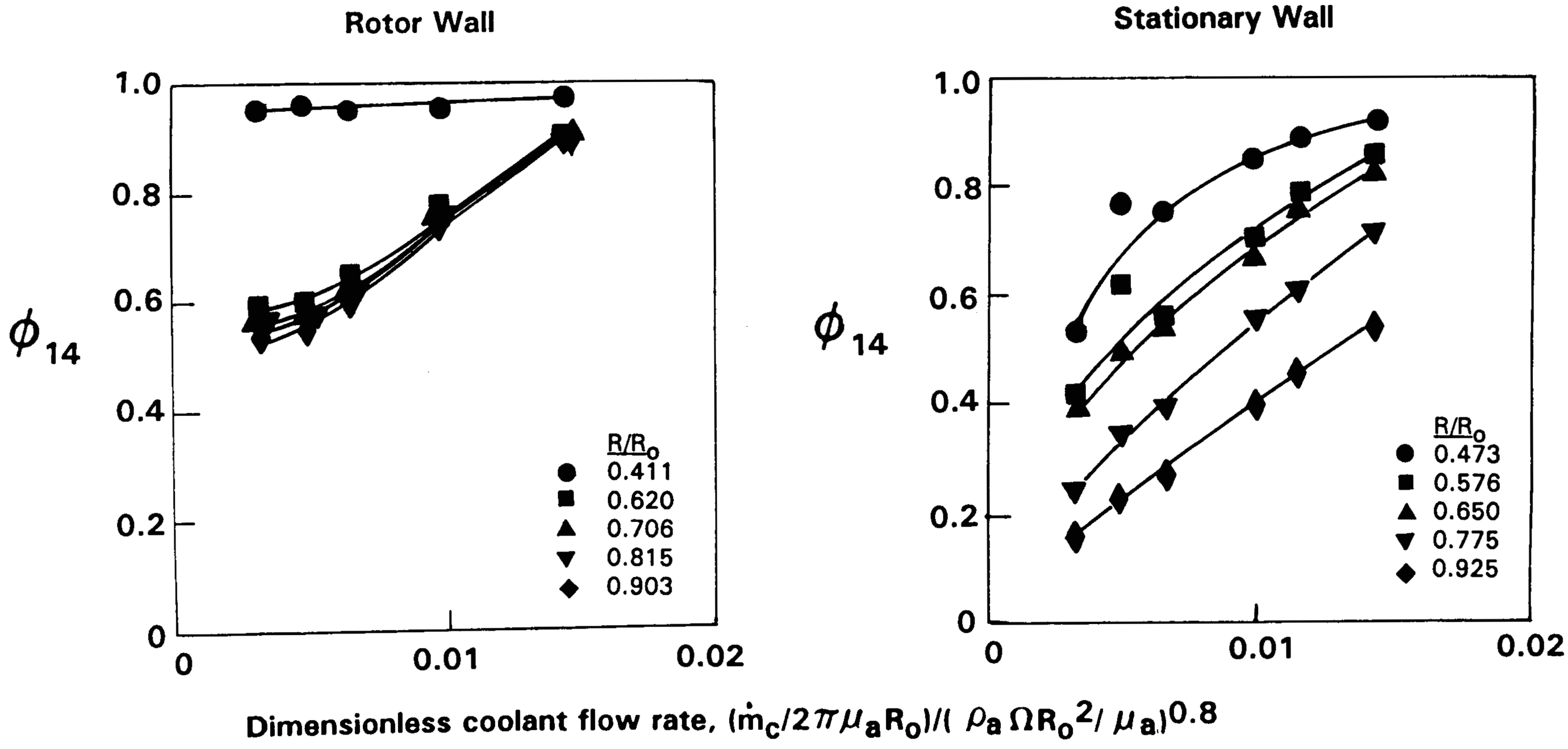

EFFECT OF COOLANT DENSITY ON DISTRIBUTION

Variables:
- Radius
- Coolant flow rate
- Coolant density

Region IV: Aft Cavity & Rotor 2

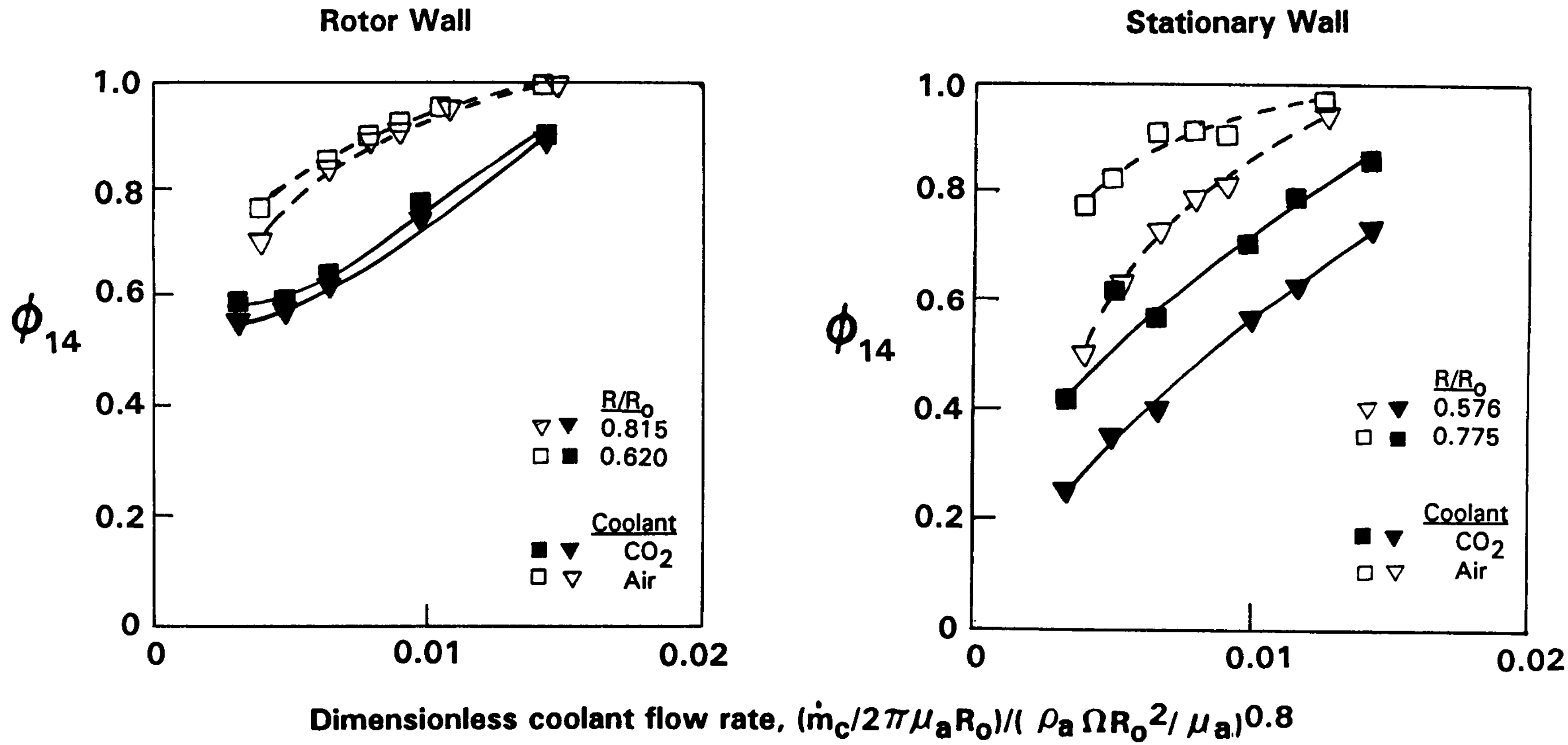

COOLANT DISTRIBUTION ON ROTOR

Region IV: Aft Cavity & Rotor 2
Coolant: Air

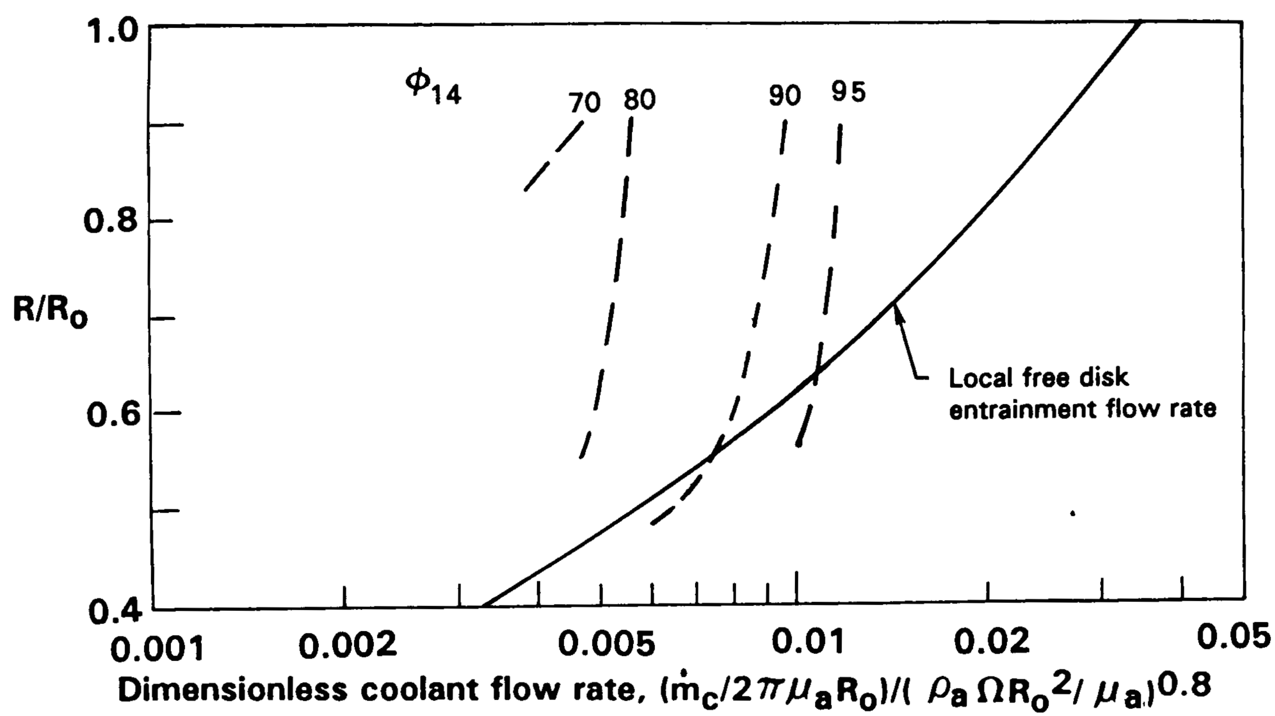

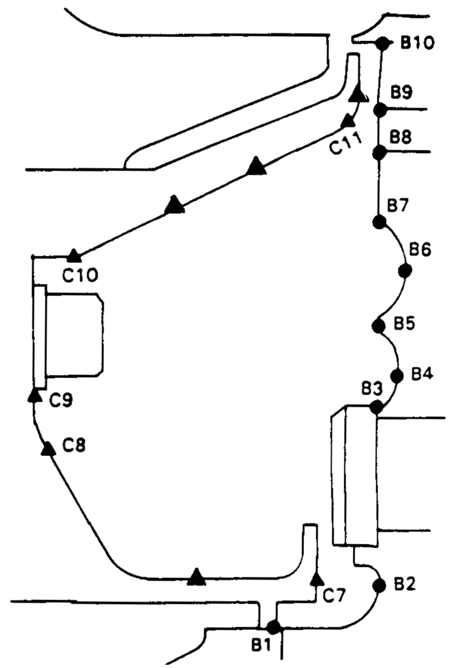

COOLANT DISTRIBUTION ON STATIONARY WALL

Region IV: Aft Cavity & Rotor 2
Coolant: Air

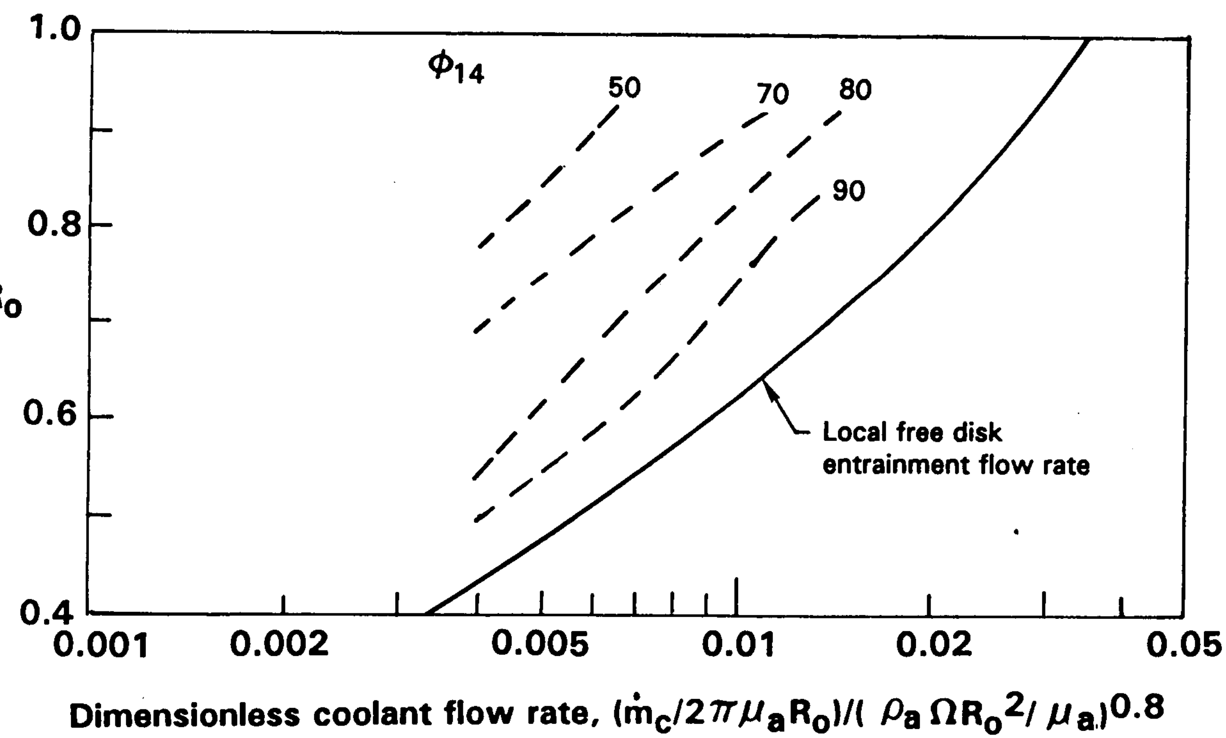

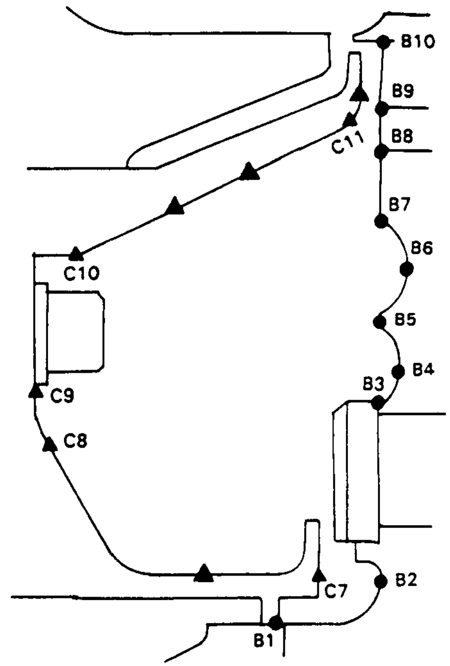

COOLANT DISTRIBUTION ON ROTOR

Region IV: Aft Cavity & Rotor 2
Coolant: CO_2

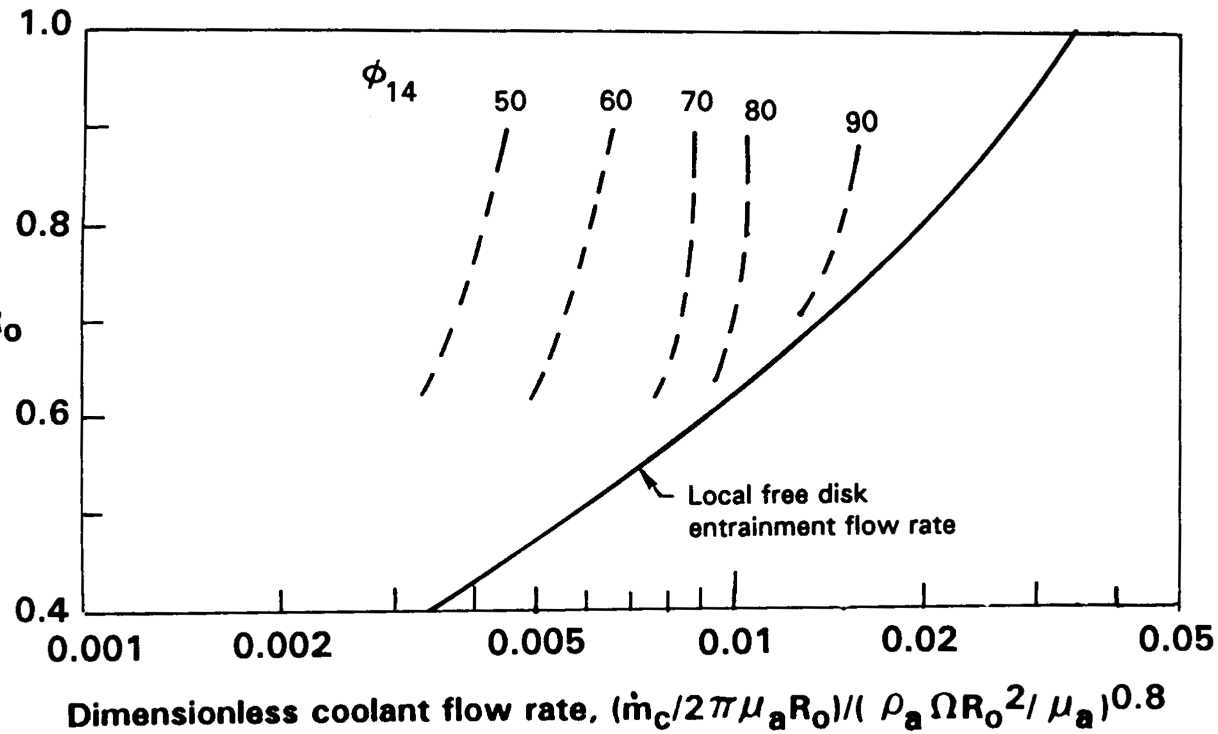

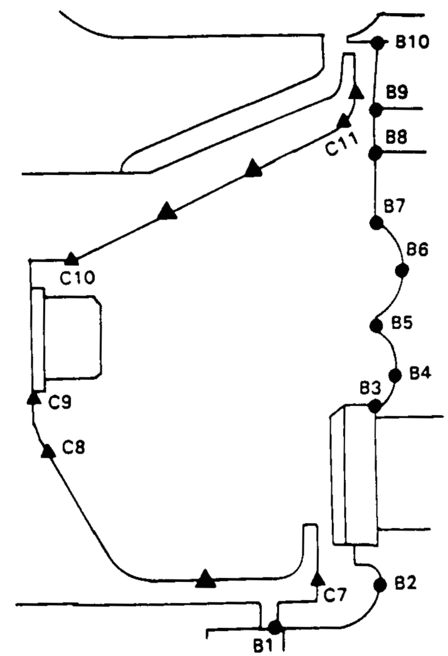

COOLANT DISTRIBUTION ON STATIONARY WALL

Region IV: Aft Cavity & Rotor 2
Coolant: CO_2

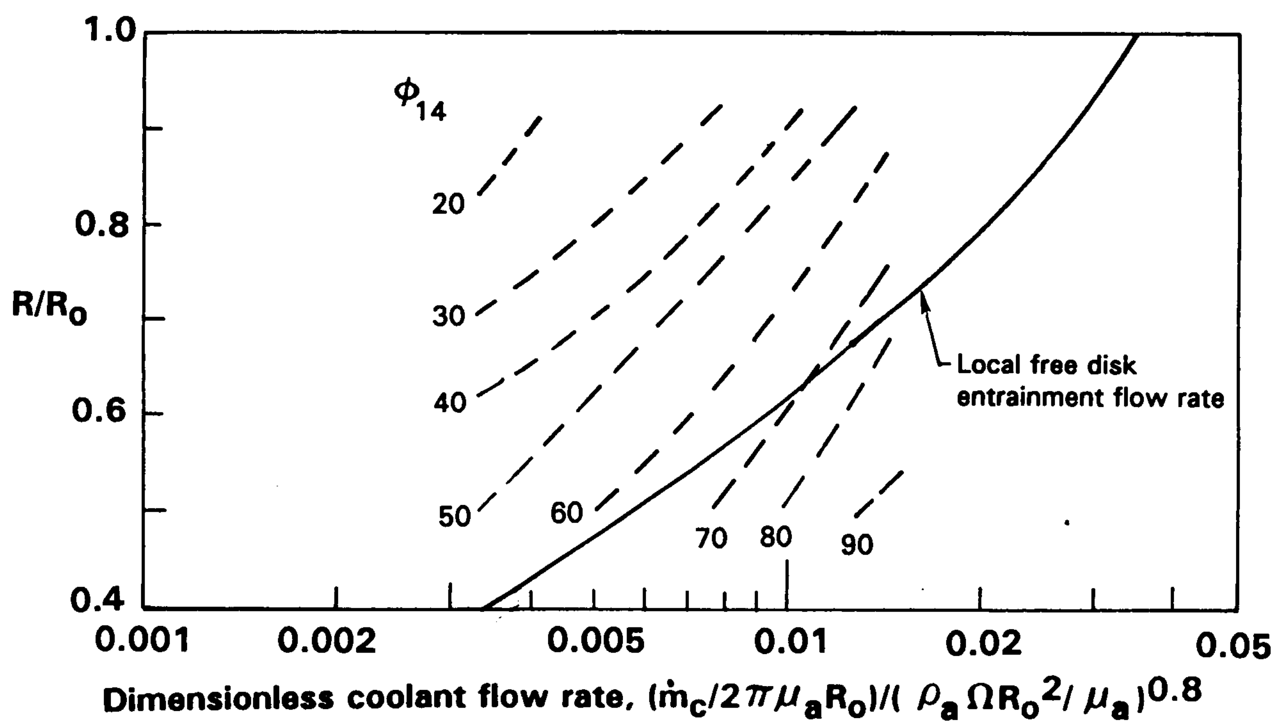

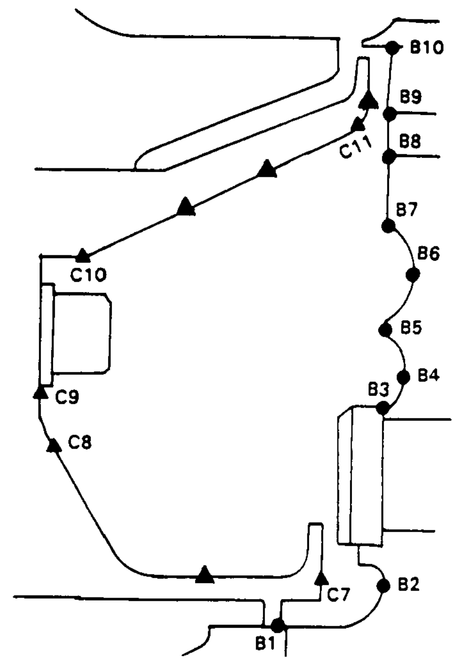

RESULTS/CONCLUSIONS

<u>Constant Density</u>

- Coolant flows approximately one-half free disk entrainment rate provide full purge of cavity (ϕ > 80% below blade shanks)

- Coolant concentration on rotor surface high (ϕ > 90%) for coolant flows 1/4 design flow rate

- Cavity walls have largest variation of ϕ with coolant flow rate

RESULTS/SPECULATION

<u>Variable Density</u> (Exploratory Experiments with CO_2)

- Density ratio has strong effect
  - Coolant concentration on rotor decreased from constant density results at comparable weight flow or volume flow rates.
  - Coolant concentration on aft cavity wall decrease significantly from constant density results at comparable flow rates.
- Decreased coolant concentration attributed to increased mixing and probable instability of rotating flow with higher gas densities at low radii.

N92-32266

A Numerical Study of Two-Dimensional Vortex Shedding From Rectangular Cylinders

A. H. Hadid, M. M. Sindir
CFD Technology Center
Rockwell International/Rocketdyne Division
Canoga Park., California
R. I. Issa
Department of Mineral Resources Engineering
Imperial College of Science
Technology and Medicine,
London, SW7, 2BP, England

An efficient time-marching, non iterative calculation method is used to analyze time-dependent flows around rectangular cylinders. The turbulent flow in the wake region of a square section cylinder is analyzed using an anisotropic k-ε model. Initiation and subsequent development of the vortex shedding phenomenon is naturally captured once a perturbation is introduced in the flow. Transient calculations using standard eddy-viscosity and an anisotropic k-ε models averaged over an integral number of cycles to get the fluctuating energy (organized and turbulent) are compared with experimental data. It is shown that the anisotropic k-ε model resolves the anisotropy of the Reynolds stresses and give mean energy distribution closer to the experiment than the standard k-e model.

A NUMERICAL STUDY OF TWO-DIMENSIONAL VORTEX SHEDDING FROM RECTANGULAR CYLINDERS

A. H. HADID AND M. M. SINDIR

ROCKWELL INTERNATIONAL/ROCKETDYNE DIVISION
CANOGA PARK, CA 91303

10TH WORKSHOP FOR CFD APPLICATIONS IN ROCKET PROPULSION

APRIL 28 - 30, 1992

Rockwell International
Rocketdyne Division

OVERVIEW

- AN EFFICIENT TIME-ACCURATE CALCULATIONAL METHOD IS USED TO PREDICT THE 2D TRANSIENT VORTEX SHEDDING MOTION BEHIND A SQUARE OBSTACLE
- THE SEPARATED TURBULENT FLOW BEHIND THE OBSTACLE IS MODELED USING AN ANISOTROPIC k-ε TURBULENCE MODEL
- COMPARISONS WITH EXPERIMENTAL RESULTS SHOW REASONABLE AGREEMENT AND RIGHT TRENDS

Rockwell International
Rocketdyne Division

INTRODUCTION

- VORTEX SHEDDING IS A PERIODIC UNSTEADY FLOW PHENOMENON OF PRACTICAL IMPORTANCE
- ATTEMPTS TO CALCULATE TWO-DIMENSIONAL VORTEX SHEDDING FLOW PAST SQUARE CYLINDERS WERE SUCCESSFUL AT LOW REYNOLDS NIMBERS WHERE FLOW IS LAMINAR AND THE PERIODIC FLUCTUATIONS ARE RESOLVED BY THE UNSTEADY N-S EQUATION
- AT HIGH REYNOLDS NUMBERS, TURBULENT FLUCTUATIONS ARE SUPERIMPOSED ON THE PERIODIC UNSTEADY MOTION WHICH MUST BE MODELED
- PREVIOUS ANALYSIS OF VORTEX SHEDDING FLOW AT HIGH REYNOLDS NUMBERS WERE NOT SUCCESSFUL DUE TO THE INADEQUACY OF THE STANDARD k-ε MODELS TO ACCOUNT FOR THE ANISOTROPY OF THE TURBULENT INTENSITIES

Rockwell International
Rocketdyne Division

INTRODUCTION (CONTD.)

- STANDARD k-ε MODELS TEND TO DAMP PERIODIC SHEDDING MOTION UNDERPREDICTING THE STROUHAL NUMBER
- FOR A SUCCESSFUL SIMULATION OF TRANSIENT TURBULENT FLOWS A RELIABLE TIME ACCURATE NUMERICAL PROCEDURE AND A GOOD TURBULENCE MODELS ARE NEEDED
- AN EFFICIENT NON-ITERATIVE TIME ACCURATE NUMERICAL SCHEME BASED ON THE "PISO" METHODOLOGY IS EMPLOYED TO ANALYZE THE TRANSIENT VORTEX SHEDDING FLOW
- TURBULENCE IS MODELLED BY USING THE ANISOTROPIC k-ε TURBULENCE MODEL

Rockwell International
Rocketdyne Division

"PISO" NUMERICAL PROCEDURE

- THE INCOMPRESSIBLE TIME-DEPENDENT N-S EQUATIONS ARE IMPLICITLY DISCRETIZED ON A NON-STAGGERED GRID USING THE FINITE-VOLUME METHODOLOGY

$$u_p = H_p(u) + D^u P_\xi + E^u P_\eta + C_p^u$$

$$v_p = H_p(v) + D^v P_\xi + E^v P_\eta + C_p^v$$

- A PRESSURE CORRECTION EQUATION IS ASSEMBLED UTILIZING THE CONTINUITY EQUATION

- AT EACH TIME STEP, THE VELOCITY FIELD IS UPDATED ACCORDING TO

$$u_p^{\lambda+2} = H_p(u^\lambda) + D^u P_\xi^{\lambda+2} + E^u P_\eta^{\lambda+1}$$

$$v_p^{\lambda+2} = H_p(v^\lambda) + D^v P_\xi^{\lambda+1} + E^v P_\eta^{\lambda+2}$$

WHERE λ REPRESENTS THE CORRECTOR STAGE LEVEL

Rockwell International
Rocketdyne Division

"PISO" NUMERICAL PROCEDURE (CONTD.)

- A MINIMUM OF TWO-CORRECTOR STAGES ARE NECESSARY FOR MANY PRACTICAL PURPOSES
- METHOD IS ESSENTIALLY NON-ITERATIVE WHERE THE SOLUTION PROCESS IS SPLIT INTO A SERIES OF STEPS WHEREBY OPERATINS ON PRESSURE ARE DECOUPLED FROM THOSE ON VELOCITY AT EACH TIME STEP IN A SERIES OF CORRECTOR STEPS

Rockwell International
Rocketdyne Division

MODEL EQUATIONS

- IN TRANSIENT PERIODIC FLOWS, THE INSTANTANEOUS VELOCITY (u_i) IS DECOMPOSED (TRIPLE DECOMPOSITION) INTO:

$$u_i = U_i + u'_i = \overline{u_i} + \tilde{u}_i + u'_i$$

WHERE, U_i IS THE PHASE AVERAGED VELOCITY

$$U_i\,(x_i,t) = \frac{1}{N}\sum_{n=0}^{N} u_i(x_i,t+nT)$$

$\overline{u_i}$ IS THE TIME MEAN VELOCITY COMPONENT

$\tilde{u}_i$ IS THE PERIODIC ORGANIZED FLUCTUATING COMPONENT

u'_i IS THE RANDOM TURBULENT FLUCTUATING COMPONENT

- PHASE AVERAGED MOMENTUM EQUATIONS

$$\frac{\partial U_i}{\partial t} + U_j\frac{\partial U_i}{\partial x_j} = -\frac{1}{\rho}\frac{\partial P}{\partial x_i} + \frac{\partial}{\partial x_j}\left(\nu\frac{\partial U_i}{\partial x_j} + R_{ij}\right)$$

WHERE $R_{ij} = -\langle \dot{u}_i \dot{u}_j \rangle$ IS THE PHASE-AVERAGED REYNOLDS STRESS TENSOR AND ν IS THE KINEMATIC VISCOSITY

Rockwell International
Rocketdyne Division

MODEL EQUATIONS (CONTD.)

STANDARD k-ε MODEL

- EDDY VISCOSITY CONCEPT

$$R_{ij} = -\frac{2}{3} k \delta_{ij} + \nu_t \left(\frac{\partial U_i}{\partial x_j} + \frac{\partial U_j}{\partial x_i}\right)$$

WHERE k IS THE PHASE AVERAGED TURBULENT KINETIC ENERGY
AND $\nu_t = C_\mu \frac{k^2}{\varepsilon}$, ε IS THE PHASE AVERAGED ENERGY DISSIPATION RATE

- k AND ε ARE DETERMINED FROM

$$\frac{\partial k}{\partial t} + U_i \frac{\partial k}{\partial x_i} = \frac{\partial}{\partial x_i}\left[\left(\nu + \frac{\nu_t}{\sigma_k}\right) \frac{\partial k}{\partial x_i} \right] + G - \varepsilon$$

$$\frac{\partial \varepsilon}{\partial t} + U_i \frac{\partial \varepsilon}{\partial x_i} = \frac{\partial}{\partial x_i}\left[\left(\nu + \frac{\nu_t}{\sigma_\varepsilon}\right) \frac{\partial \varepsilon}{\partial x_i} \right] + \frac{\varepsilon}{k} (C_1 G - C_2 \varepsilon)$$

WHERE $G = R_{ij} \frac{\partial U_i}{\partial x_j}$ IS THE TURBULENT GENERATION TERM

Rockwell International
Rocketdyne Division

MODEL EQUATIONS (CONTD.)

ANISOTROPIC k-ε MODEL

- NONLINEAR CORRECTIONS ARE ADDED TO IMPROVE THE EDDY-VISCOSITY REPRESENTATION ON THE REYNOLDS-STRESSES AS DEVELOPED BY YOSHIZAWA USING "TSDIA" AND BY SPEZIALE

$$R_{ij} = -\frac{2}{3} k \,\delta_{ij} + \nu_t \left(\frac{\partial U_i}{\partial x_j} + \frac{\partial U_j}{\partial x_i}\right) + \frac{1}{3}\left(\sum_{m=1}^{3} \tau_m S_{mkk}\right)\delta_{ij} - \sum_{m=1}^{3} \tau_m S_{mij}$$

WHERE $\tau_m = C_{\tau m} \frac{k^3}{\varepsilon^2}$

$$S1_{ij} = \frac{\partial U_i}{\partial x_k}\frac{\partial U_j}{\partial x_k}$$

$$S2_{ij} = \frac{1}{2}\left(\frac{\partial U_i}{\partial x_k}\frac{\partial U_k}{\partial x_j} + \frac{\partial U_j}{\partial x_k}\frac{\partial U_k}{\partial x_i}\right)$$

$$S3_{ij} = \frac{\partial U_k}{\partial x_i}\frac{\partial U_k}{\partial x_j}$$

$C_{\tau m}$ (m=1,2,3) ARE MODEL CONSTANTS

Rockwell International
Rocketdyne Division

C-6

MODEL EQUATIONS (CONTD.)

- NISIZIMA USED THIS MODEL TO STUDY FULLY DEVELOPED TURBULENT SQUARE DUCT FLOW WHERE DEVIATIONS OF THE REYNOLDS STRESSES FROM ITS ISOTROPIC EDDY-VISCOSITY PLAYS A CENTRAL ROLE

- YOSHIZAWA SHOWED FOR THE SIMPLE ASYMMETRIC CHANNEL FLOW BETWEEN A ROUGH AND A SMOOTH WALLS THE NONCOINCIDENCE OF THE LOCATION OF ZERO SHEAR AND MAXIMUM VELOCITY

- MYONG AND KASAGI USED THE MODEL FOR FULLY DEVELOPED TURBULENT CHANNEL FLOW WHITH $C_{\tau 1}$ AND $C_{\tau 2}$ OPTIMIZED TO REPRODUCE THE ANISOTROPY OF TURBULENT INTENSITIES

- IN THE PRESENT STUDY THE MODEL CONSTANTS $C_{\tau 1}$, $C_{\tau 2}$ AND $C_{\tau 3}$ WERE OPTIMIZED TO 0.01, 0.01 AND 0.001 RESPECTIVELY TO SATISFY THE REALIZABILITY CONSTRAIN

- WALL FUNCTIONS WERE USED TO BRIDGE THE NEAR OBSTACLE WALL REGION

Rockwell International
Rocketdyne Division

RESULTS AND DISCUSSIONS

- EXPERIMENTAL RESULTS OF DURAO ET AL. FOR TURBULENT FLOW AROUND A SQUARE CYLINDER MOUNTED IN A WATER CHANNEL AT RE=14000 WERE USED TO COMPARE WITH THE COMPUTATIONS

- IN THEIR MEASUREMENTS THEY USED SPECTRAL ANALYSIS AND DIGITAL FILTERING OF THE LDV DATA TO SEPARATE AND QUANTIFY THE TURBULENT AND NON TURBULENT PERIODIC MOTIONS

- THEY MEASURED THE INSTANTANEOUS VALUES OF THE VELOCITY COMPONENTS AND EVALUATED THE TIME MEAN VALUES OF THE STRESSES AND KINETIC ENERGY

- CALCULATIONS ARE PERFORMED FOR TURBULENT FLOW AROUND A SQUARE OBSTACLE (STEP HEIGHT H=20 mm) IN A DOMAIN EXTENDING ABOUT 16H DOWNSTREAM AND 2.5H UPSTREAM OF OBSTACLE

Rockwell International
Rocketdyne Division

RESULTS AND DISCUSSIONS (CONTD.)

- CALCULATIONS CAPTURED THE VORTEX SHEDDING PHENOMENON AFTER EXPLICITLY PERTURBING THE FLOW AT THE INLET
- COMPUTATIONAL DOMAIN WAS RESOLVED BY 75X40 CELLS WITH CLUSTERING AT THE OBSTACLE WALLS
- AN OPTIMIZED TIME STEP OF 0.001 sec. WAS CHOSEN IN THE CALCULATIONS

Rockwell International
Rocketdyne Division

NORMAL VELOCITY HISTORY AT CENTERLINE 5 STEP HEIGHTS DOWNSTREAM AT RE=14000

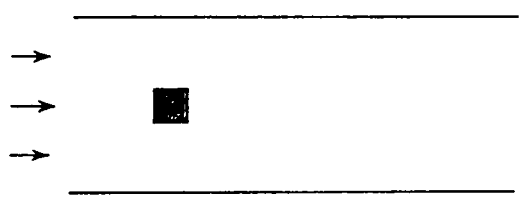

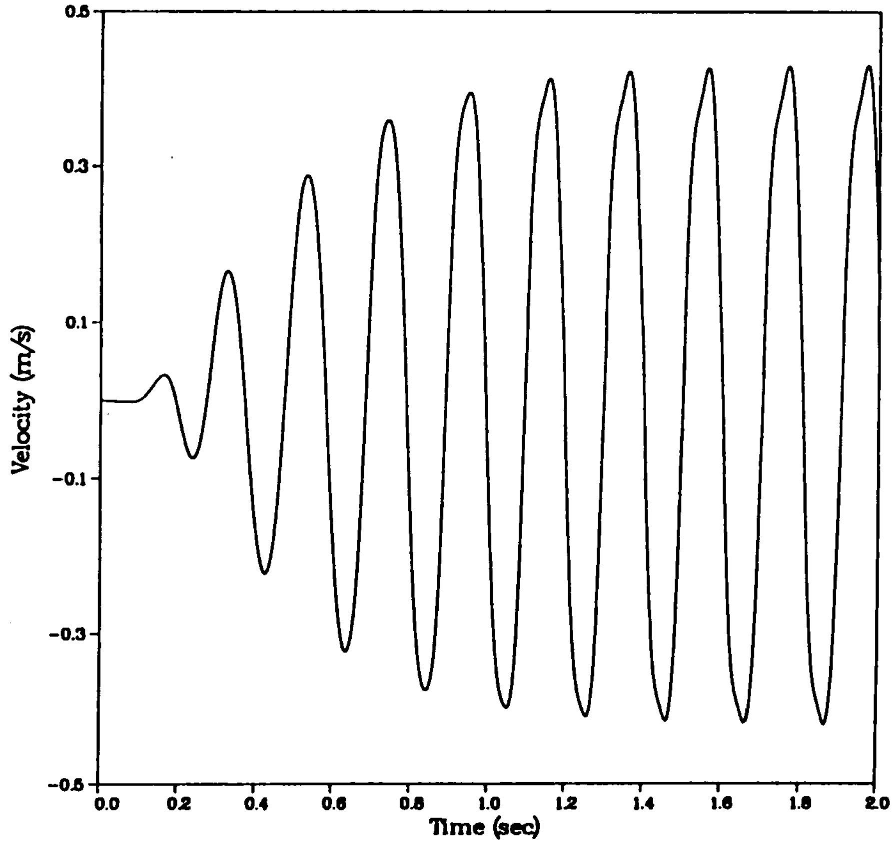

Rockwell International
Rocketdyne Division

POWER SPECTRUM OF THE NORMAL VELOCITY FLUCTUATIONS

- FIGURE CONFIRMS OSCILLATORY NATURE OF THE FLOW WITH A SINGLE PREDOMINANT FREQUENCY AT ABOUT 4.7 Hz IN AGREEMENT WITH EXPERIMENT

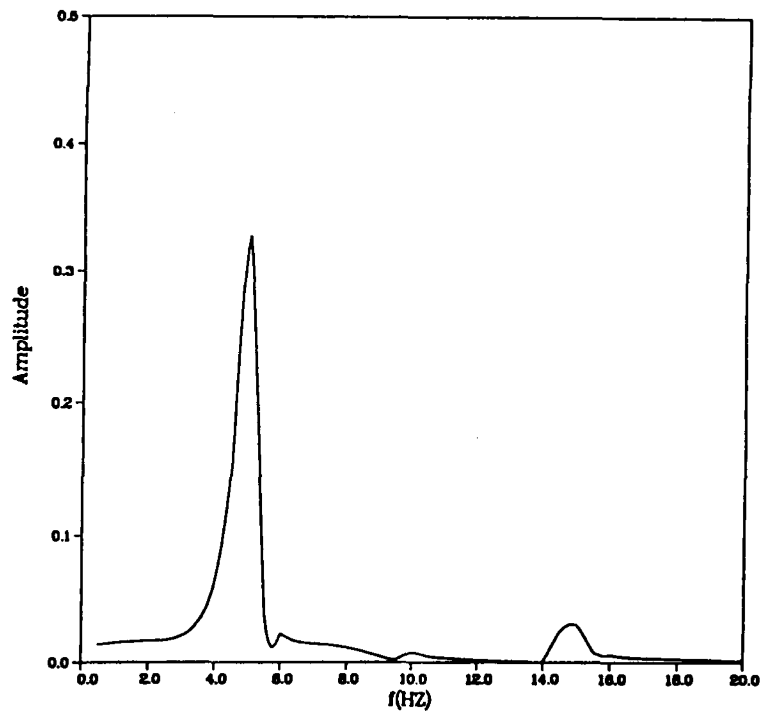

Rockwell International
Rocketdyne Division

STREAKLINE PLOT AT RE = 14000

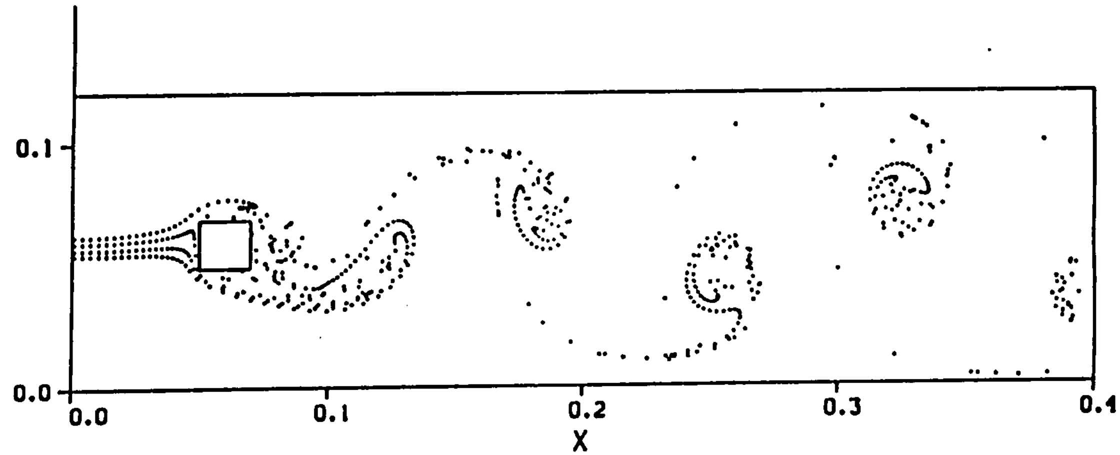

Rockwell International
Rocketdyne Division

RESULTS AND DISCUSSIONS (CONTD.)

- TO CALCULATE THE TIME-MEAN KINETIC ENERGY OF THE VELOCITY FLUCTUATIONS (ORGANIZED + TURBULENT), LET

$$\hat{u}_i = \tilde{u}_i + u'_i = u_i - \overline{U_i}$$

THE TIME-MEAN KINETIC ENERGY CAN BE WRITTEN AS;

$$\overline{E} = \frac{3}{4}\left(\overline{\hat{u}_1^2} + \overline{\hat{u}_2^2}\right)$$

WHERE $\overline{\hat{u}_i^2} = \overline{U_i^2} - \overline{U_i}^2 + \overline{u_i'^2} \quad (i=1,2)$

- THE FIRST TWO TERMS ON THE RIGHT HAND SIDE REPRESENT THE ORGANIZED PERIODIC ENERGY CONTRIBUTION
- THE LAST TERM REPRESENT THE TURBULENT ENERGY CONTRIBUTION

Rockwell International
Rocketdyne Division

MEAN AXIAL VELOCITY ALONG THE CENTERLINE

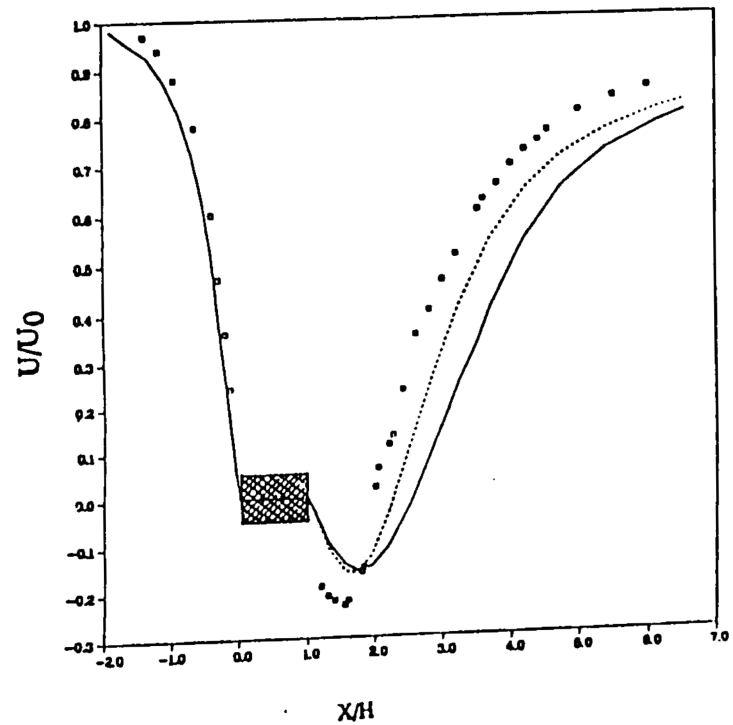

Centreline Distribution of Mean Axial Velocity

□ Durão et al. [8]

—— Standard k-ε Model

--- Anisotropic k-ε Model

Rockwell International
Rocketdyne Division

MEAN KINETIC ENERGY ALONG THE CENTERLINE

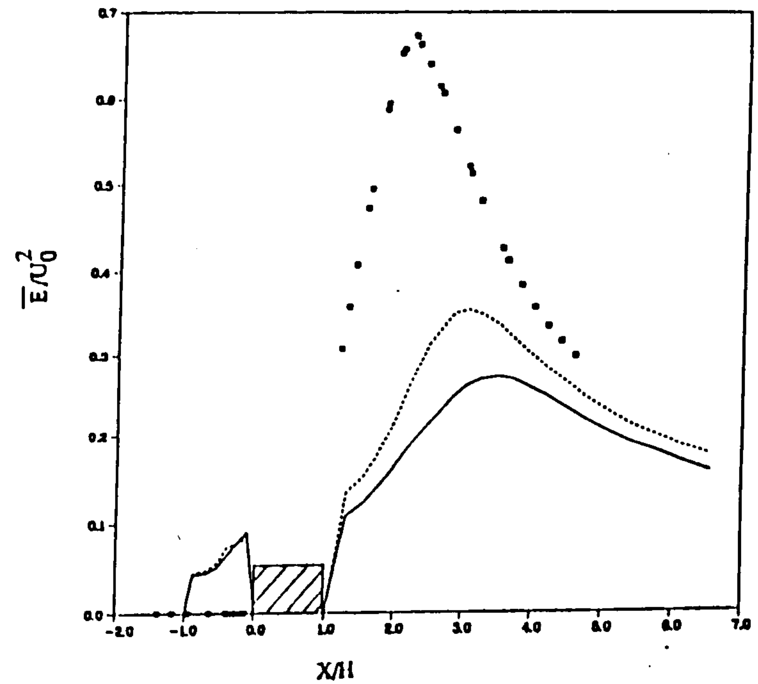

Time-Mean Kinetic Energy of the Velocity Fluctuations

□ Durão et al. [8]

— Standard k-ε Model

--- Anisotropic k-ε Model

Rockwell International
Rocketdyne Division

MEAN AXIAL VELOCITY ALONG THE CENTERLINE

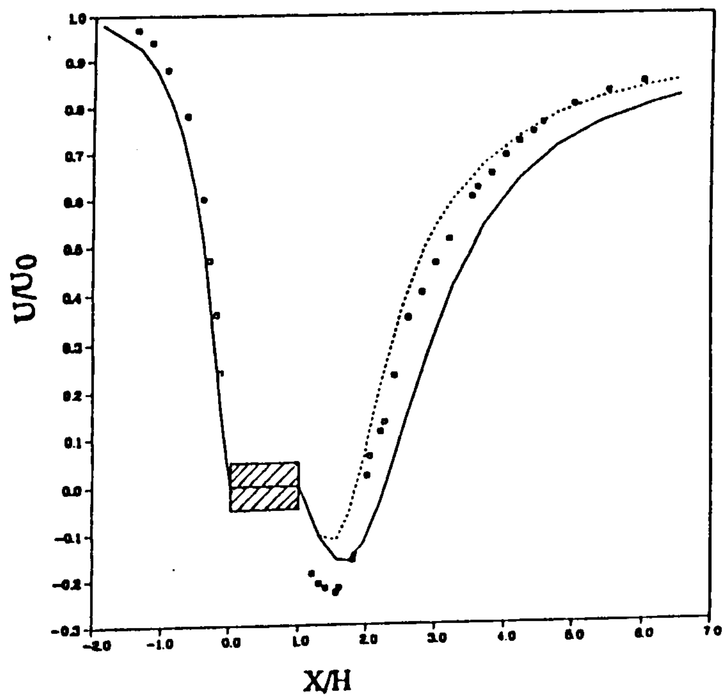

Centreline Distribution of Mean Axial Velocity
□ Durão et al. [8]
— Anisotroic k-ε Model
---Anisotropic k-ε Model With Zero Production of k Upstream of Obstacle

Rockwell International
Rocketdyne Division

MEAN KINETIC ENERGY ALONG THE CENTERLINE

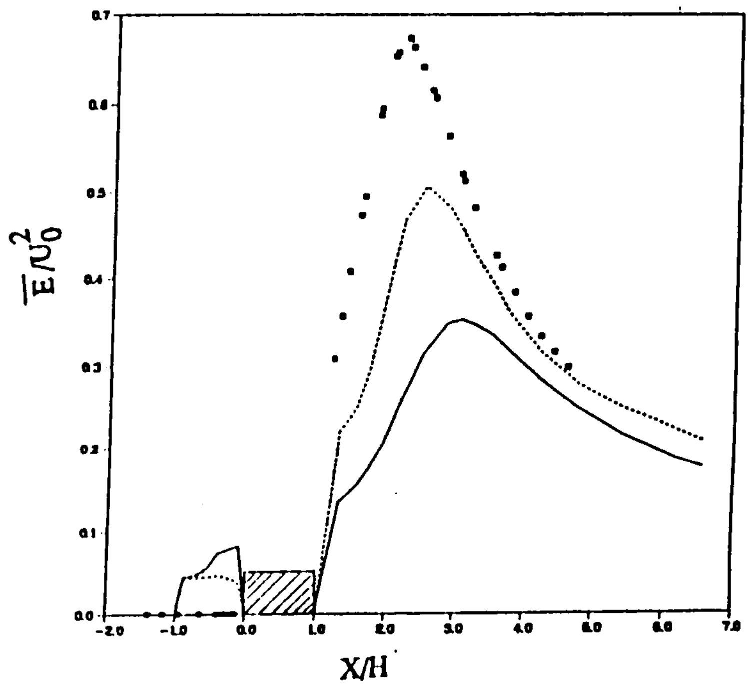

Time-Mean Kinetic Energy of the Velocity Fluctuations

▫ Durão et al. [8]

— Anisotroic k-ε Model

--- Anisotropic k-ε Model With Zero Production of k Upstream of Obstacle

Rockwell International
Rocketdyne Division

NORMAL STRESS CONTOURS

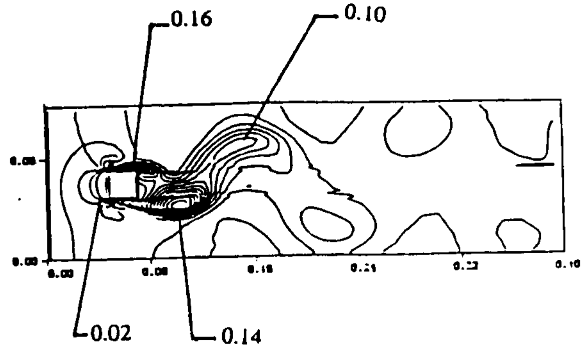

$\langle v'v' \rangle / U_0^2$ contours at T=3 sec., Using the Standard k-ε Model

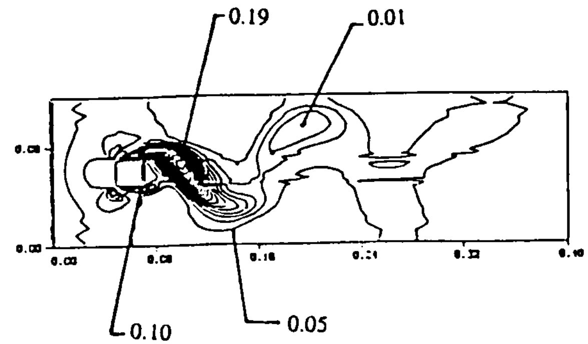

$\langle v'v' \rangle / U_0^2$ contours at T=3 sec., Using the Anisotropic k-ε Model

Rockwell International
Rocketdyne Division

DISCUSSION

- RESULTS OF MEAN KINETIC ENERGY SHOW THAT THE ANISOTROPIC k-ε MODEL PREDICTS A BETTER TREND THAN THE STANDARD ISOTROPIC MODEL

- THE IMPROVED TREND IS MANILY DUE TO AN INCREASE IN THE TURBULENT ENERGY CONTRIBUTION AS SHOWN FROM THE NORMAL STRESSES CONTOURS

- LENGTH OF RECIRCULATION ZONE BEHIND OBSTACLE AND THE LOCATION OF THE MAXIMUM FLUCTUATING ENERGY ARE IMPROVED USING THE ANISOTROPIC MODEL

Rockwell International
Rocketdyne Division

DISCUSSION (CONTD.)

- MEASUREMENTS INDICATE THAT IN FRONT OF OBSTACLE THE FLOW REMAINED VIRTUALLY LAMINAR WITH NEGLIGIBLE FLUCTUATIONS
- IN THE k-ε MODEL VELOCITY GRADIENTS ARE LARGE AT THE STAGNATION POINT PRODUCING EXCESSIVELY LARGE TURBULENT KINETIC ENERGY
- WHEN THIS UNREALISTIC PRODUCTION OF ENERGY IS SUPRESSED IN FRONT OF THE OBSTACLE, THE TURBULENT KINETIC ENERGY IS DECREASED EVERYWHERE
- HOWEVER, THE ENERGY OF THE PERIODIC FLUCTUATIONS IS INCREASED TO GIVE A NET INCREASE IN THE ENERGY OF THE TOTAL FLUCTUATIONS
- THERE STILL SEEMS TO BE SOME FINITE KINETIC ENERGY IN FRONT OF THE OBSTACLE WHICH CAN ONLY BE DUE TO THE PERIODIC FLUCTUATIONS WHICH IS NOT INDICATED IN THE EXPERIMENTAL RESULTS

Rockwell International
Rocketdyne Division

N92-32267

Submitted for the CFD Workshop -- 1992

A Status of the Turbine Technology Team Activities

Lisa W. Griffin

A Status of the activities of the Turbine Technology Team of the Consortium for Computational Fluid Dynamics (CFD) Application in Propulsion Technology is presented. The team consists of members from the government, industry, and universities. The goal of this team is to demonstrate the benefits to the turbine design process attainable through the application of CFD. This goal is to be achieved by enhancing and validating turbine design tools for improved loading and flowfield definition and loss prediction, and transferring the advanced technology to the turbine design process.

In order to demonstrate the advantages of using CFD early in the design phase, the Space Transportation Main Engine (STME) turbines for the National Launch System (NLS) were chosen on which to focus the team's efforts. The Turbine Team activities run parallel to the STME design work.

Work during the past year has centered on transferring technology obtained through the team's Generic Gas Generator Turbine Program (reported on in the 1990 workshop) to the STME LOX turbine design point. A preliminary baseline design was analyzed through CFD, and areas requiring refinement to eliminate local overspeeds and separations were found. An improved baseline design has been finalized. The team is currently comparing results from five team members (Aerojet, NASA/Ames Research Center, NASA/Lewis Research Center, Pratt & Whitney, and Scientific Research Associates). These solutions will be compared to data to be obtained in the Marshall Space Flight Center Turbine Airflow Facility. Interrogation of these solutions are also in progress to determine high loss locations and to provide guidance for developing and/or implementing concepts to control these losses.

National Aeronautics and
Space Administration

A Summary of the Activities of the NASA/MSFC Turbine Technology Team

LISA GRIFFIN
MAY 1, 1992

National Aeronautics and
Space Administration

A Summary of the Activities of the NASA/MSFC Turbine Technology Team

Overview

- Structure/Objectives
- Turbine Team Participants
- Program Overview
  - Code Development/Enhancement
  - Validation Experiments
  - Advanced Hardware Development
- Subsonic Turbine Development Program
  - Background
  - Gas Generator Oxidizer Turbine (GGOT)
- New Programs
  - Volute Development
  - Supersonic Turbine Development
- Summary

National Aeronautics and
Space Administration

A Summary of the Activities of the NASA/MSFC Turbine Technology Team

Structure/Objectives

The consortium for CFD application in propulsion technology

Objectives:
- Development/enhancement of CFD models and codes
- Validation of state-of-the-art CFD codes
- Application of CFD in design of advanced hardware concepts
- Verification testing of advanced hardware concepts

Turbine Team

Objectives:
- Coordinate/focus MSFC turbine technology activities
- Provide a forum for interaction/technology transfer
- Provide peer review for turbine technology activities

Pump Stage Team

Combustion Devices Team

National Aeronautics and
Space Administration

A Summary of the Activities of the NASA/MSFC Turbine Technology Team

Participants

- NASA Marshall Space Flight Center (MSFC)
- NASA Ames Research Center (ARC)
- NASA Lewis Research Center (LeRC)
- Aerojet
- Pratt and Whitney (P&W)
- Rocketdyne (RKDN)
- Calspan - University of Buffalo Research Center (CUBRC)
- Rotodata
- Scientific Research Associates (SRA)
- SECA
- United Technologies Research Center (UTRC)
- Carnegie Mellon University (CMU)
- Pennsylvania State University (PSU)
- The University of Alabama (UA)
- The University of Alabama in Huntsville (UAH)
- Virginia Polytechnic Institute (VPI)

National Aeronautics and Space Administration

A Summary of the Activities of the NASA/MSFC Turbine Technology Team

Program Overview

- Code Development/Enhancement
  - Rotor/Stator Interaction (NASA/ARC)
  - 3D Navier-Stokes Code for Volutes (NASA/LeRC)
  - Validation of 3D Unsteady Rotor/Stator Interaction Code ROTOR3 (P&W)
  - Enhancement and Validation of ROTOR3 for Supersonic Turbines (RKDN)
  - Turbulence Modeling (PSU)

- Validation Experiments
  - 3D Rotor Heat Transfer (UTRC)
  - Unsteady Interrow Aerodynamics (P&W)
  - SSME HPFTP Fuel Turbine
    - Baseline Aerodynamics (MSFC)
    - Baseline Unsteady Aerodynamics/Heat Transfer (CUBRC)
    - Smooth Blades (MSFC)
    - Circumferential Exit ΔP (MSFC)
    - ATD (MSFC)

National Aeronautics and
Space Administration

A Summary of the Activities of the NASA/MSFC Turbine Technology Team

Program Overview

- Advanced Hardware Development
  - Subsonic Turbine Development
  - Volute Development
  - Supersonic Turbine Development

National Aeronautics and Space Administration

A Summary of the Activities of the NASA/MSFC Turbine Technology Team

Subsonic Turbine Development Program Background

- Focused flow analysis tools on the STME fuel turbine design point resulting in Generic Gas Generator (G^3T) design
  - Advanced Turbine concept developed
    - Reduced parts
    - Increased efficiency
  - Analyses in overlapping regions with different codes showed consistent results
  - Axial gap selection modified
    - Improved efficiency (1 pt.)
    - Reduced blade loadings/stresses
- Design concept incorporated into STME LOX turbine
- Focused flow analysis tools on the STME LOX turbine design point resulting in Gas Generator Oxidizer Turbine (GGOT)

National Aeronautics and Space Administration

TURBINE FLOW ANALYSIS TECHNOLOGY

Background

Aerodynamic Design Approach

	Previous State -of - the-Art	G^3T Design
General Description	70/30 Work Split Nominal Annulus Height	50/50 Work Split Increased Annulus Height
Blade Turning	135°	160°
Fluid Acceleration	0.9	1.6
Max Blade Mach Number	1.32	0.87
Efficiency	Base	+10 percent
Airfoil Count	Base	-55 percent

BASELINE GGGT AERODYNAMIC DESIGN

Calculated Streamlines - Midspan

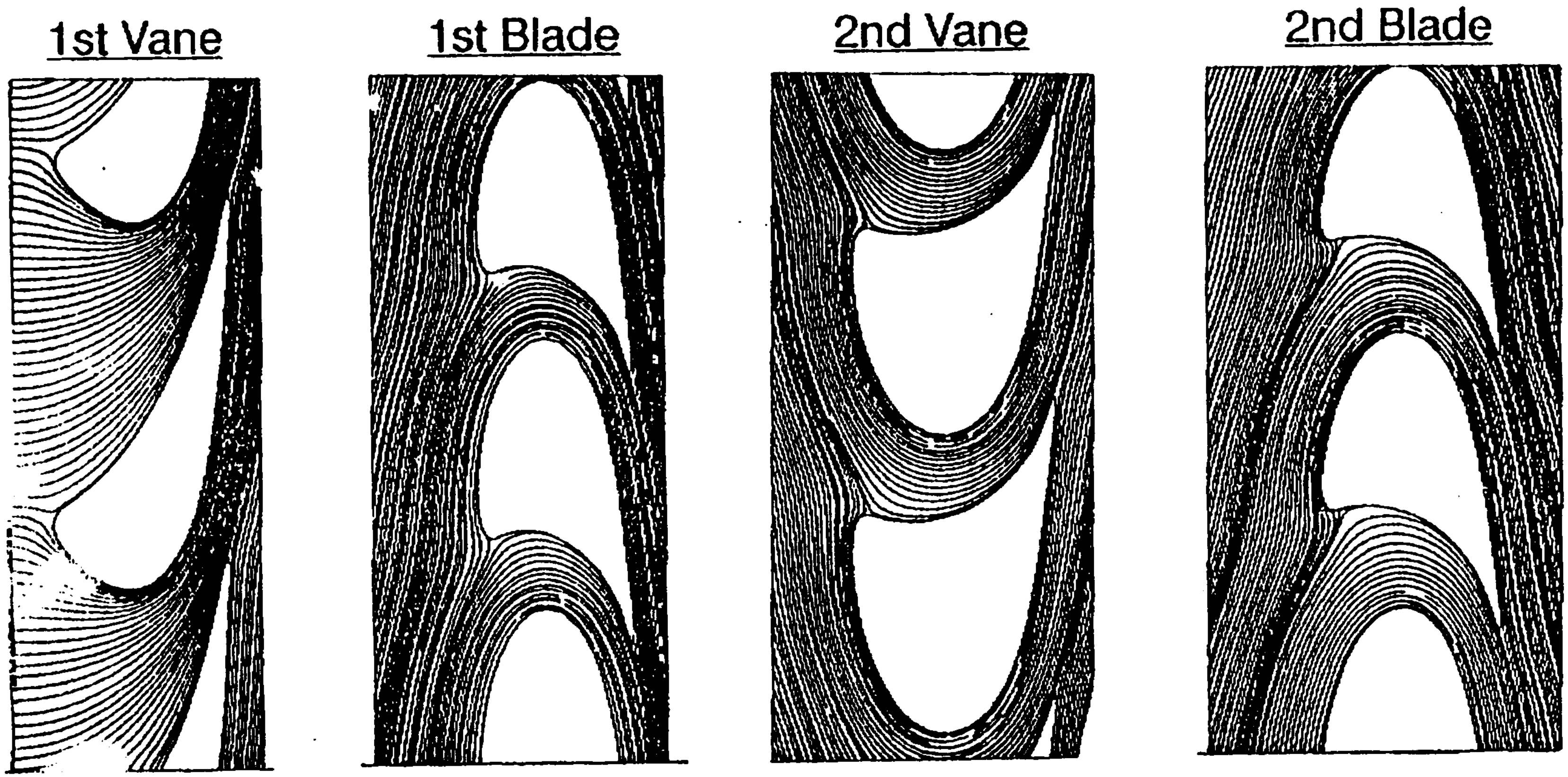

CONSORTIUM FOR CFD APPLICATION IN PROPULSION TECHNOLOGY

Turbine Stage Technology Team-Baseline GGGT aerodynamic analyses

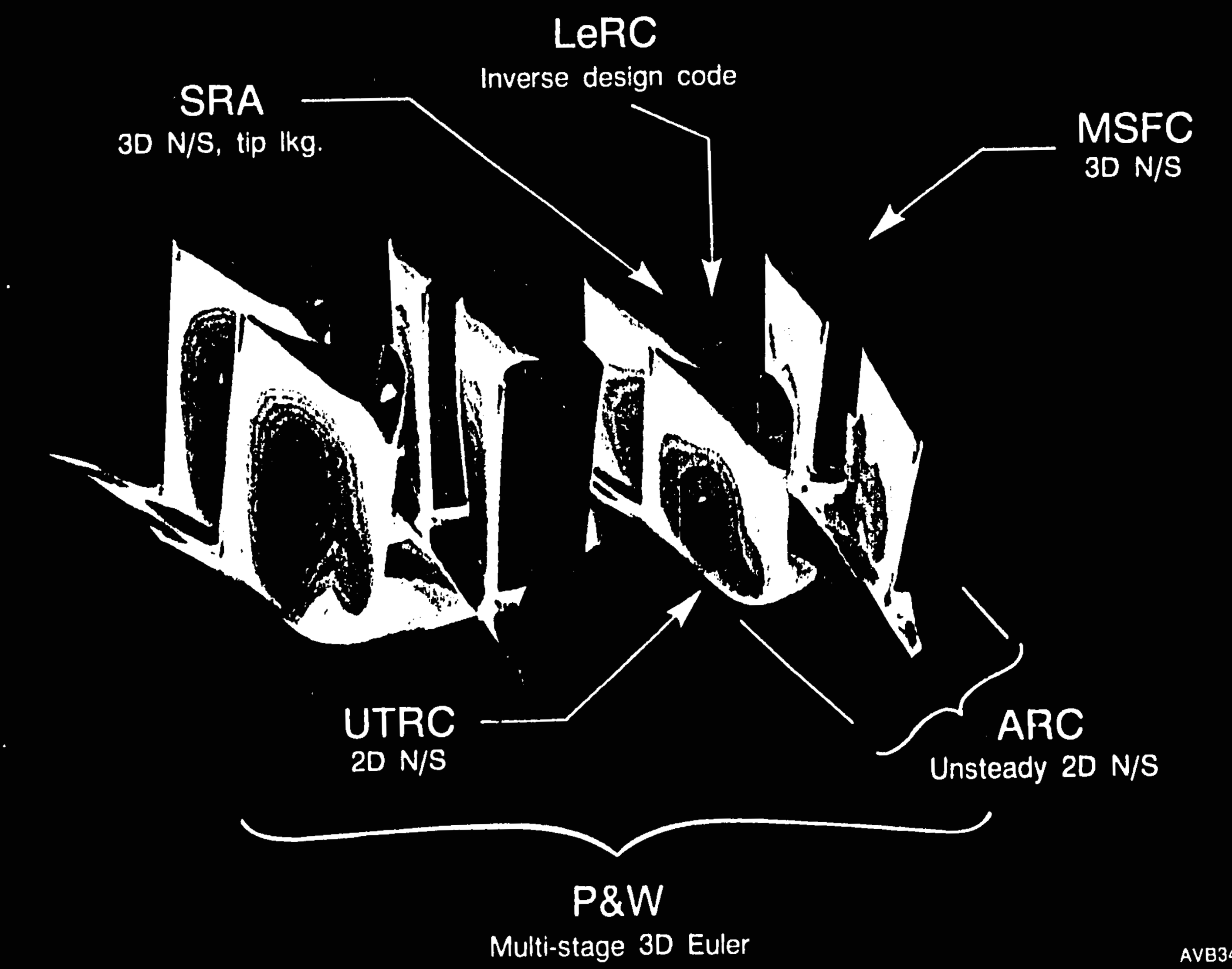

AVB344072 902711

ORIGINAL PAGE IS OF POOR QUALITY

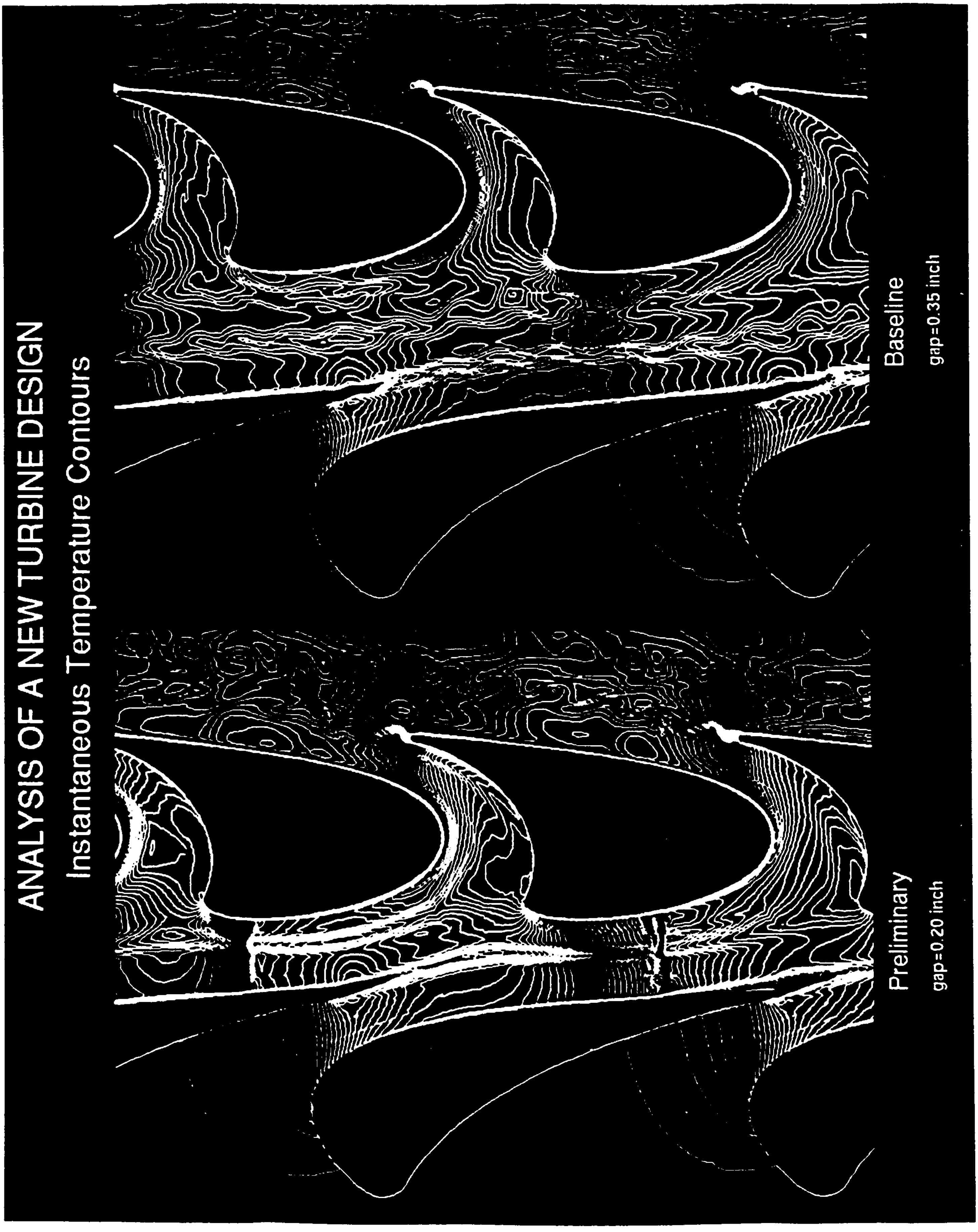

ANALYSIS OF A NEW TURBINE DESIGN
Instantaneous Temperature Contours
Preliminary
gap=0.20 inch
Baseline
gap=0.35 inch

National Aeronautics and Space Administration

A Summary of the Activities of the NASA/MSFC Turbine Technology Team

Subsonic Turbine Development Program GGOT

- Phase I Task Description
  - Development of preliminary baseline design (P&W)
  - Analyses of preliminary design (P&W, NASA/ARC, and NASA/LeRC)
  - Modification of preliminary design (P&W)
  - Analysis of modified design (P&W, NASA/ARC, NASA/LeRC, SRA, and Aerojet)
  - Development of final baseline design (P&W)
  - Comparisons of CFD solutions
  - Experimental evaluation of baseline design (MSFC)

- Phase II Task Description
  - Interrogate baseline results for regions of losses
  - Development of concepts to control losses
    - -- Parametric studies with CFD
  - Development of advanced design
  - Detailed analyses of advanced design
  - Experimental evaluation of advanced design

CONSORTIUM FOR CFD APPLICATION IN PROPULSION TECHNOLOGY

Turbine Technology Team - Baseline GGOT Aerodynamic Analyses

- **Pratt & Whitney** - *Steady 3D Euler*
- ARC - *Unsteady 2D Navier/Stokes*
- LeRC - *Steady 3D Navier/Stokes*

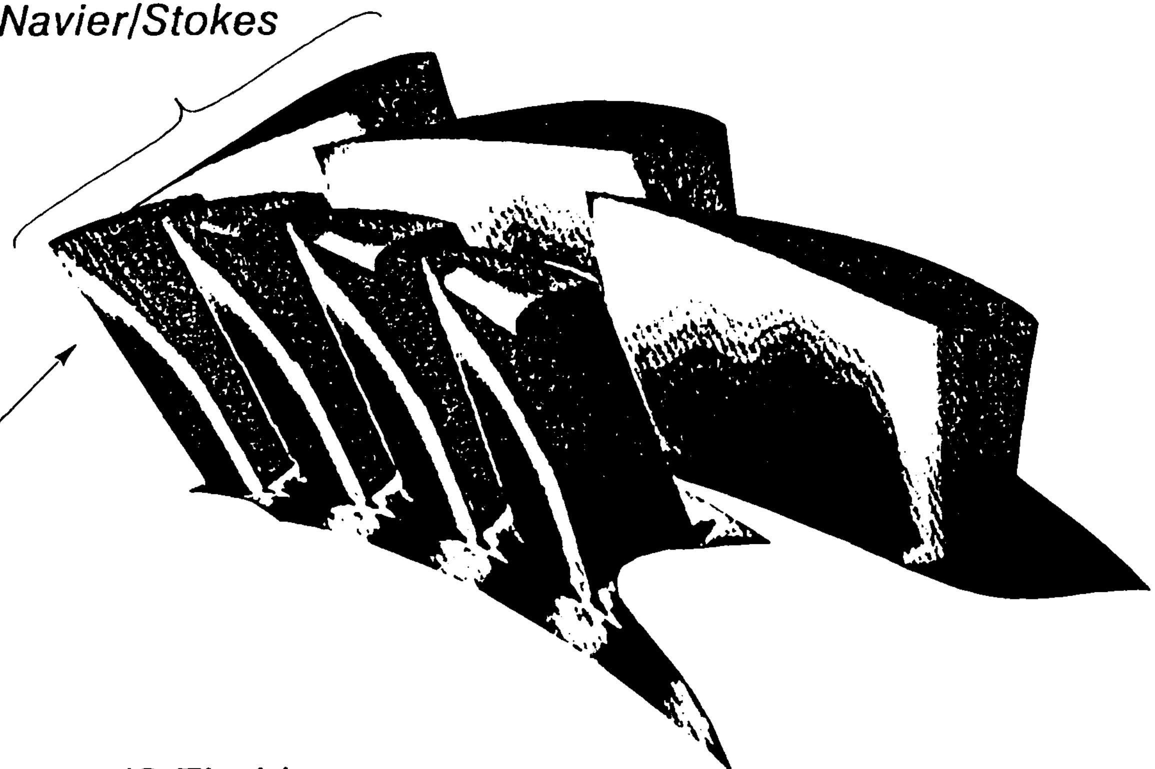

- SRA - *Steady 3D N/S,Tip Lkg*
- **Aerojet** - *Steady 3D N/S, Tip Lkg*

GAS GENERATOR OXIDIZER TURBINE (GGOT) DESIGN

Streaklines Downstream of Rotor

Preliminary

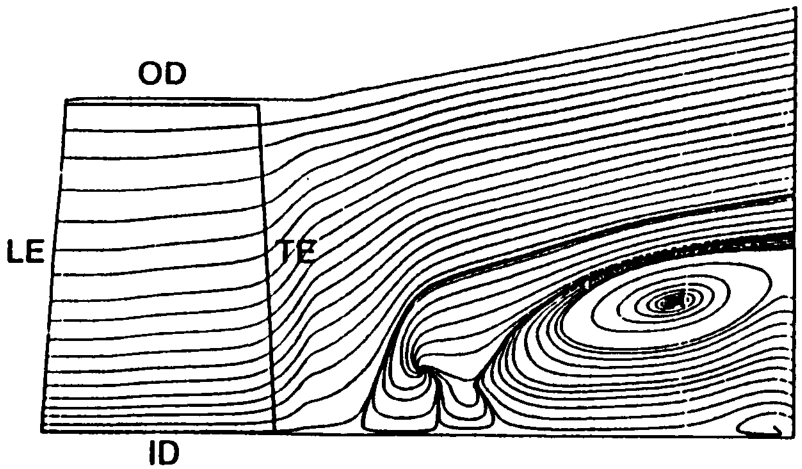

3D Flow Analysis Shows Separation
Downstream of Rotor

Baseline

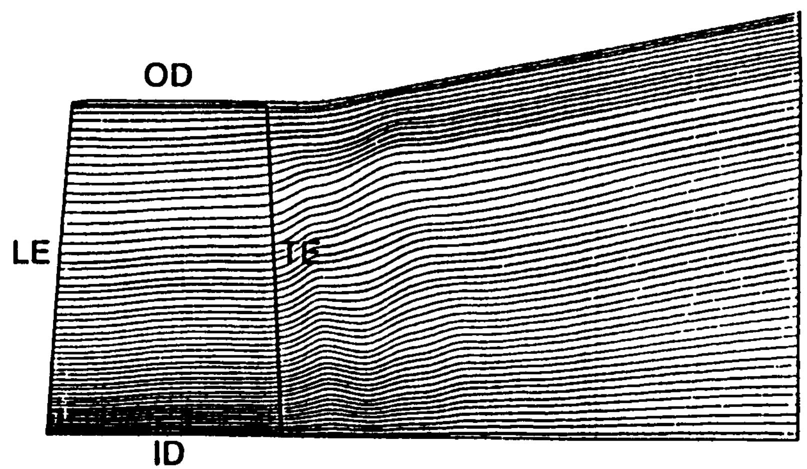

3D Flow Analysis Shows
Downstream Separation Eliminated

OXIDIZER TECHNOLOGY TURBINE BASELINE DESIGN

Concerns / Potential Weaknesses

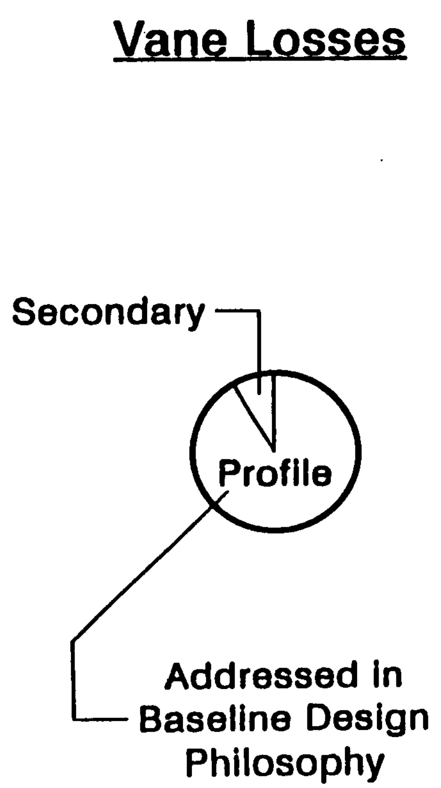

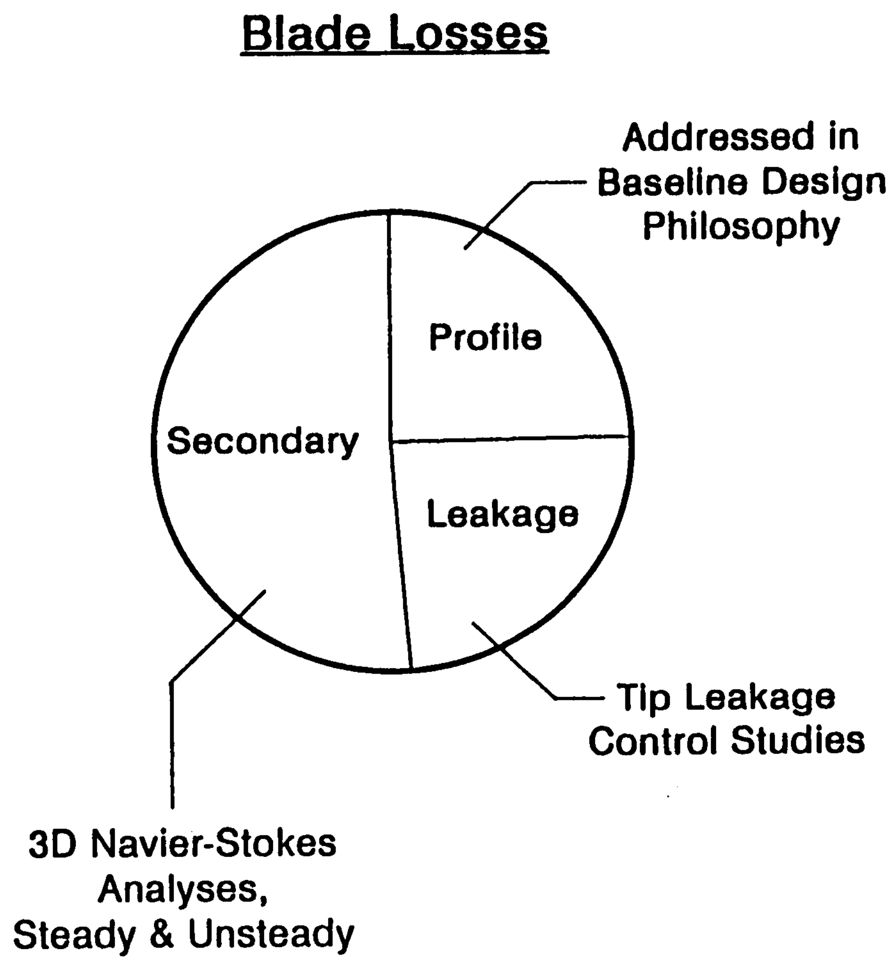

GGOT ROTOR - TIP LEAKAGE FLOW

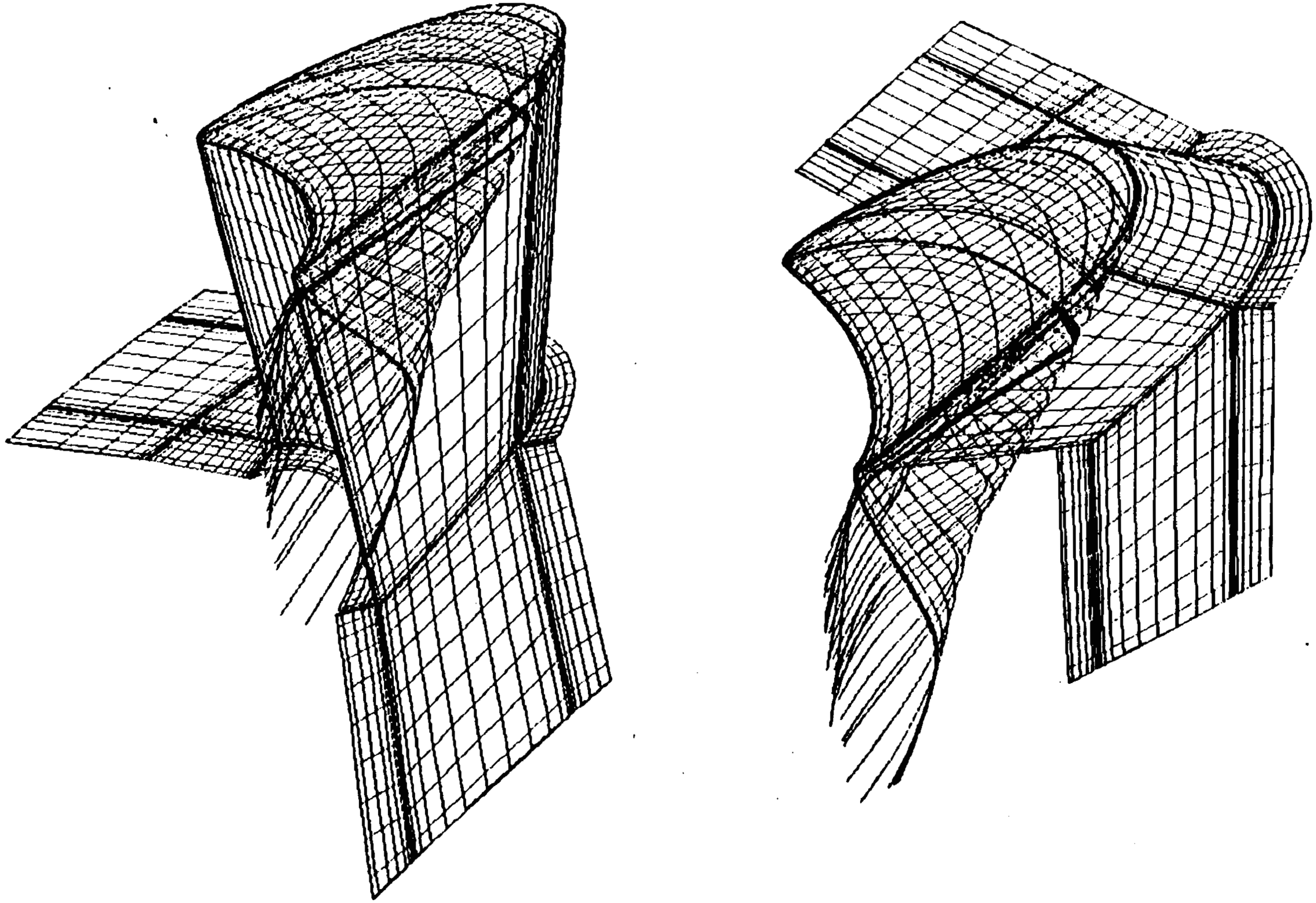

GGOT ROTOR - PRESSURE LOSS COEFFICIENT CONTOURS

15% AXIAL CHORD DOWNSTREAM OF ROTOR

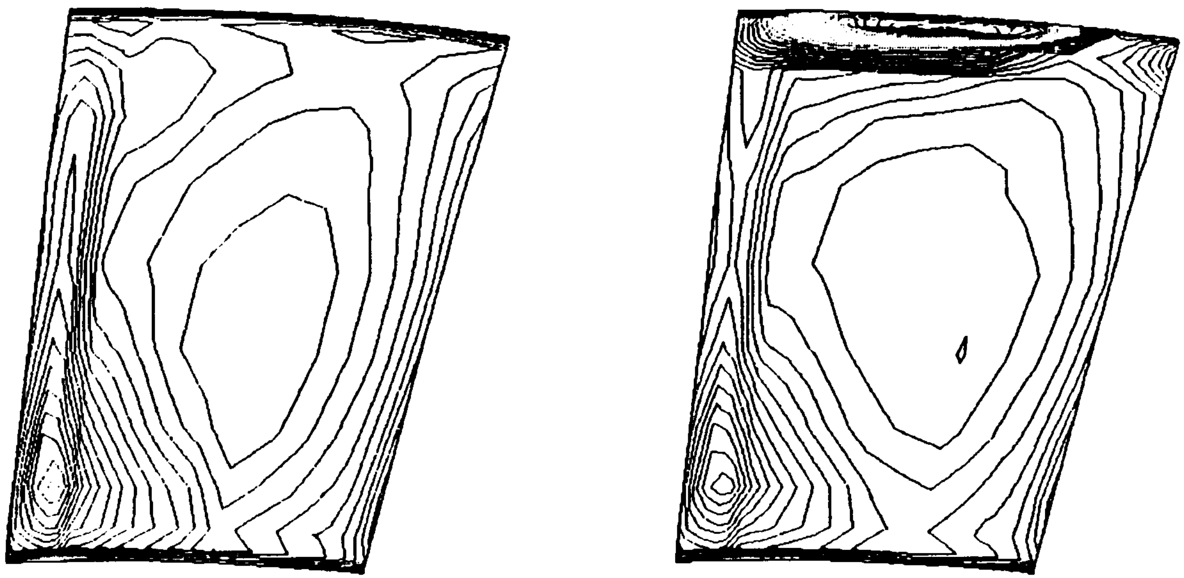

NO TIP LEAKAGE — **WITH TIP LEAKAGE**

Cpt

2.370E+00
2.264E+00
2.159E+00
2.053E+00
1.948E+00
1.842E+00
1.737E+00
1.631E+00
1.526E+00
1.420E+00
1.315E+00
1.209E+00
1.104E+00
9.985E-01
8.930E-01
7.875E-01
6.820E-01
5.765E-01
4.710E-01
3.655E-01
2.600E-01

$$Cpt = \frac{Pt_r\ (\text{max inlet}) - Pt_r}{1/2\ \rho_o V_o^2}$$

GGOT ROTOR - PRESSURE LOSS COEFFICIENT CONTOURS

99% AXIAL CHORD DOWNSTREAM OF ROTOR

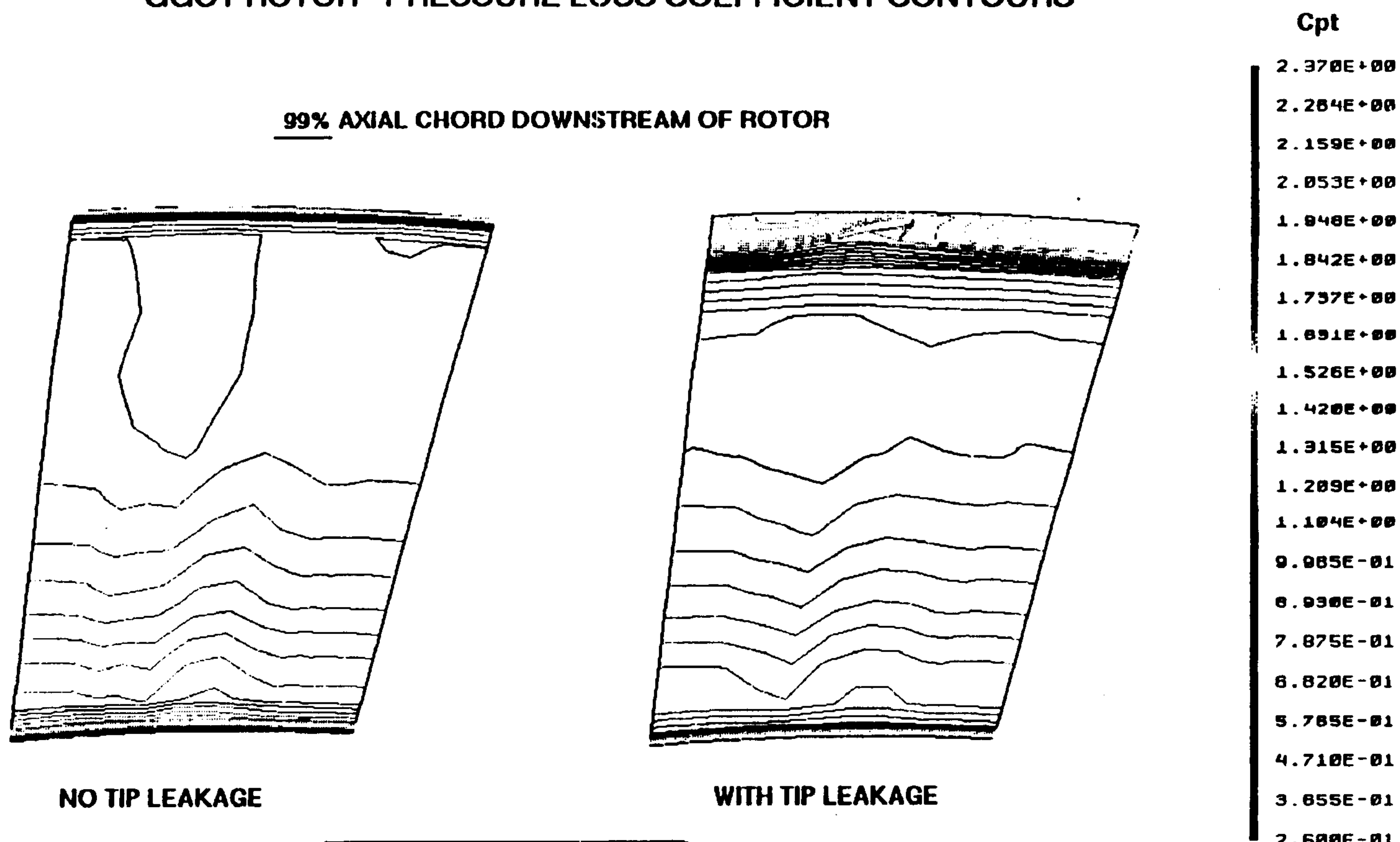

$$Cpt = \frac{Pt_r\ (\text{max inlet}) - Pt_r}{1/2\ \rho_o V_o^2}$$

NASA
National Aeronautics and Space Administration

A Summary of the Activities of the NASA/MSFC Turbine Technology Team

New Program - Volute Development

- Issues
  - Volutes traditionally designed using existing database and limited analysis
  - STME LOX turbine volutes out of experience base
    - High Mach number
    - High swirl (discharge diffuser/volute)
    - Vaneless diffuser design considered for cost and weight
  - Benchmark quality volute dataset non-existent

- Task Descriptions
  - Design of three baseline volutes with existing design methodology
  - Analysis of baseline volutes for design and off-design conditions
  - Experimental evaluation of baseline volutes on GGOT for code validation
  - Development of loss control and side load reduction concepts
    - Parametric studies with CFD
    - Detailed analysis of improved designs
    - Experimental evaluation of improved volutes on advanced concepts GGOT

NASA
National Aeronautics and
Space Administration

A Summary of the Activities of the NASA/MSFC Turbine Technology Team

New Program - Supersonic Turbine Development

- Issues
  - High losses and blade excitations found in supersonic turbines
    - Durability requirements require special attention paid to unsteady loadings and shock interactions
    - Low confidence in the understanding of unsteady loadings
  - Supersonic turbine database from a rotating environment virtually non-existent

- Task Descriptions
  - Design baseline turbine with design requirements consistent with STME fuel turbine
  - Analysis of baseline STME fuel turbine
  - Experimental evaluation of baseline design for design verification, code validation, and database expansion
  - Development of advanced concepts
    - Parametric studies of candidate concepts to control losses and interactions
    - Detailed analyses of advanced design
    - Experimental evaluation of advanced design

National Aeronautics and Space Administration

A Summary of the Activities of the NASA/MSFC Turbine Technology Team

Summary

- Team of government, industry, and university experts in place and focused on relevant turbine design and analysis issues
- Codes and models are being developed and enhanced to address complex flows in turbines
- Unique experimental data is being taken to provide information for thorough calibration/validation of turbine analysis tools
- Team activities have been coordinated and focused on demonstration of CFD tools for turbine design

N92-32268

A CRITICAL EVALUATION OF A THREE-DIMENSIONAL NAVIER-STOKES CFD AS A TOOL TO DESIGN SUPERSONIC TURBINE STAGES

C. HAH, O. KWON, AND M. SHOEMAKER
NASA LEWIS RESEARCH CENTER
21000 BROOKPARK ROAD, CLEVELAND, OHIO

Three-dimensional flow phenomena in a supersonic turbine blade row have been studied numerically to evaluate CFD as a tool to design supersonic turbine stages.

The details of the three-dimensional flow structure inside the supersonic turbine blade row and the overall aerodynamic performance at design and off-design conditions are analyzed and the results are compared between the experimental data and the numerical results.

A CRITICAL EVALUATION OF A THREE-DIMENSIONAL NAVIER-STOKES CFD AS A TOOL TO DESIGN SUPERSONIC TURBINE STAGES

C. HAH, O. KWON, AND M. SHOEMAKER
NASA LEWIS RESEARCH CENTER
21000 BROOKPARK ROAD, CLEVELAND, OHIO

SUPERSONIC TURBINE STAGE

COMMONLY USED IN SPACE ENGINES

DESIGN IS BASED ON 2-D METHOD

VERY LOW EFFICIENCY

FLOWS INSIDE SUPERSONIC TURBINE

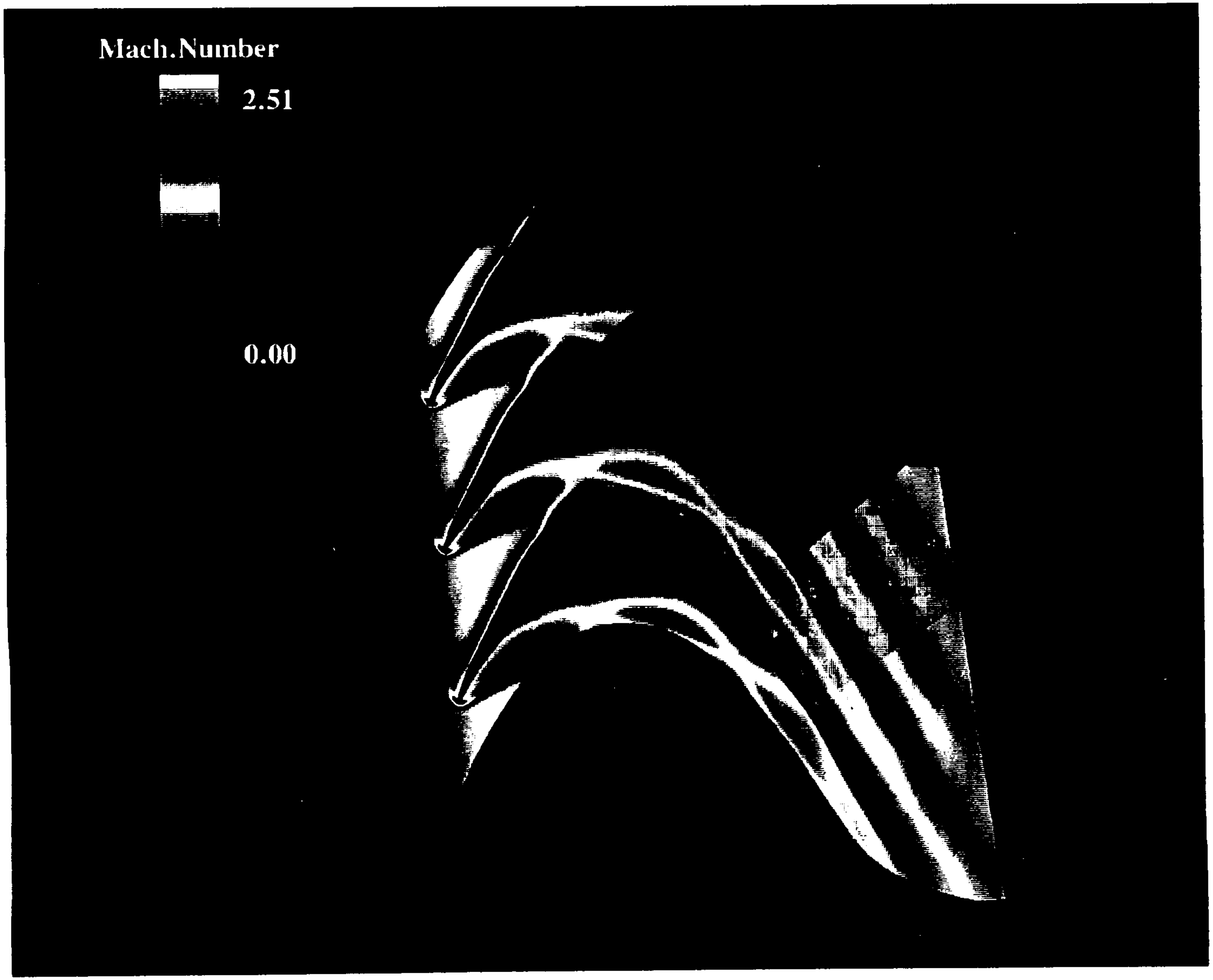

OBJECTIVES

UNDERSTAND DETAILED FLOW STRUCTURE

INVESTIGATE LOSS MECHANISM

DEVELOP 3-D DESIGN METHOD

FLOWS INSIDE SUPERSONIC TURBINE

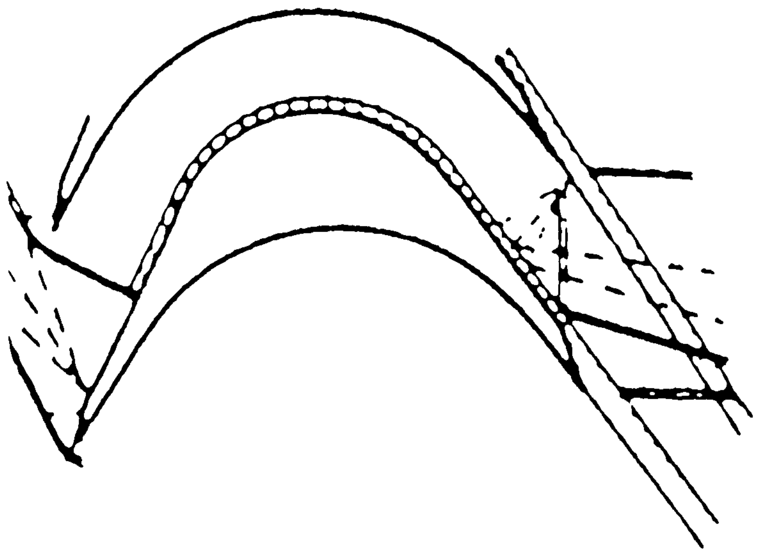

UNSTARTED FLOW

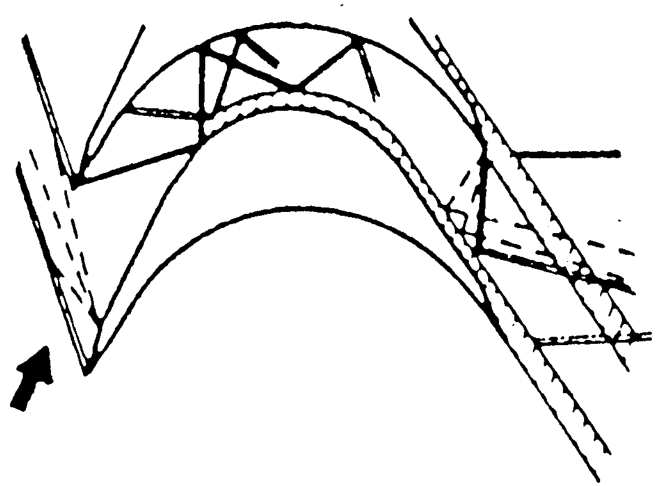

STARTED FLOW

OVERALL APPROACHES

APPLY 3-D NAVIER-STOKES CODE

VERIFY FOR STARTING MACH #, FLOW SEPARATION

EVALUATE CURRENT CAPABILITY

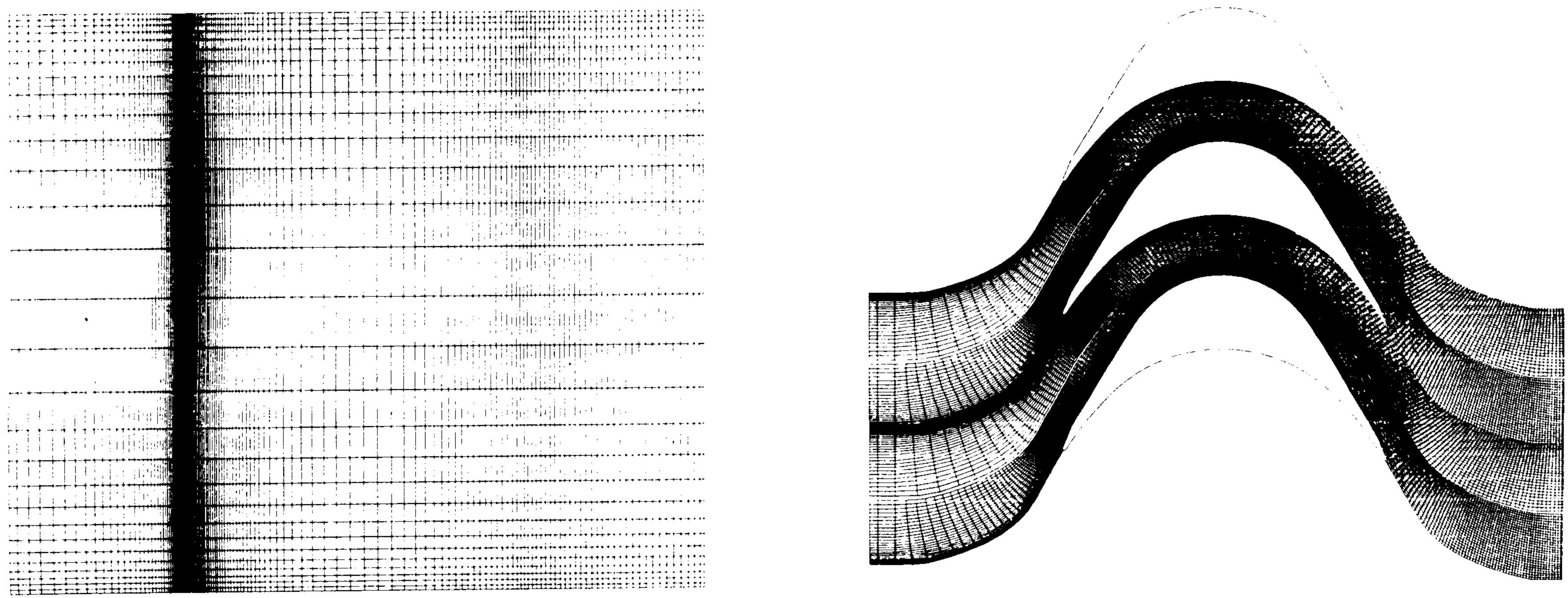

COMPUTATIONAL GRID

MEASURED

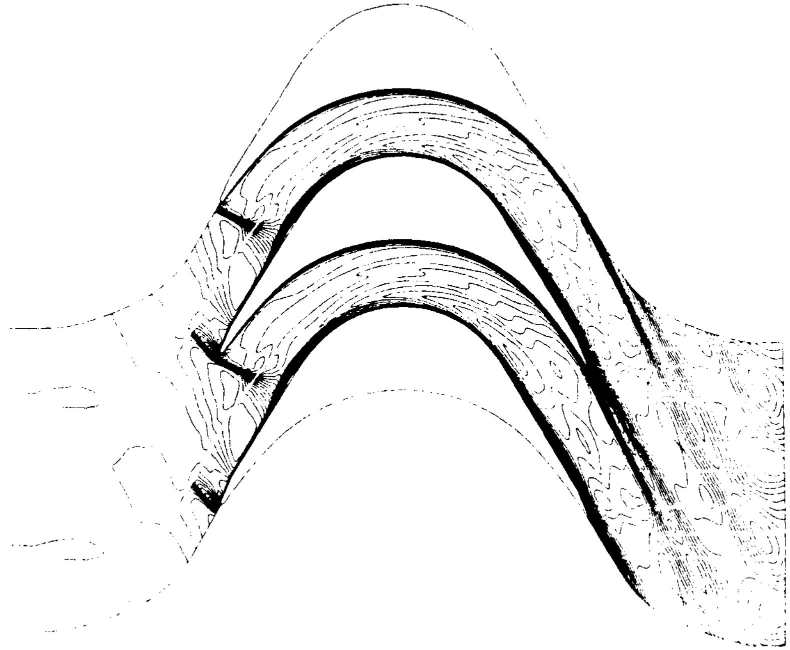

CALCULATED

COMPARISON FOR UNSTARTED FLOW

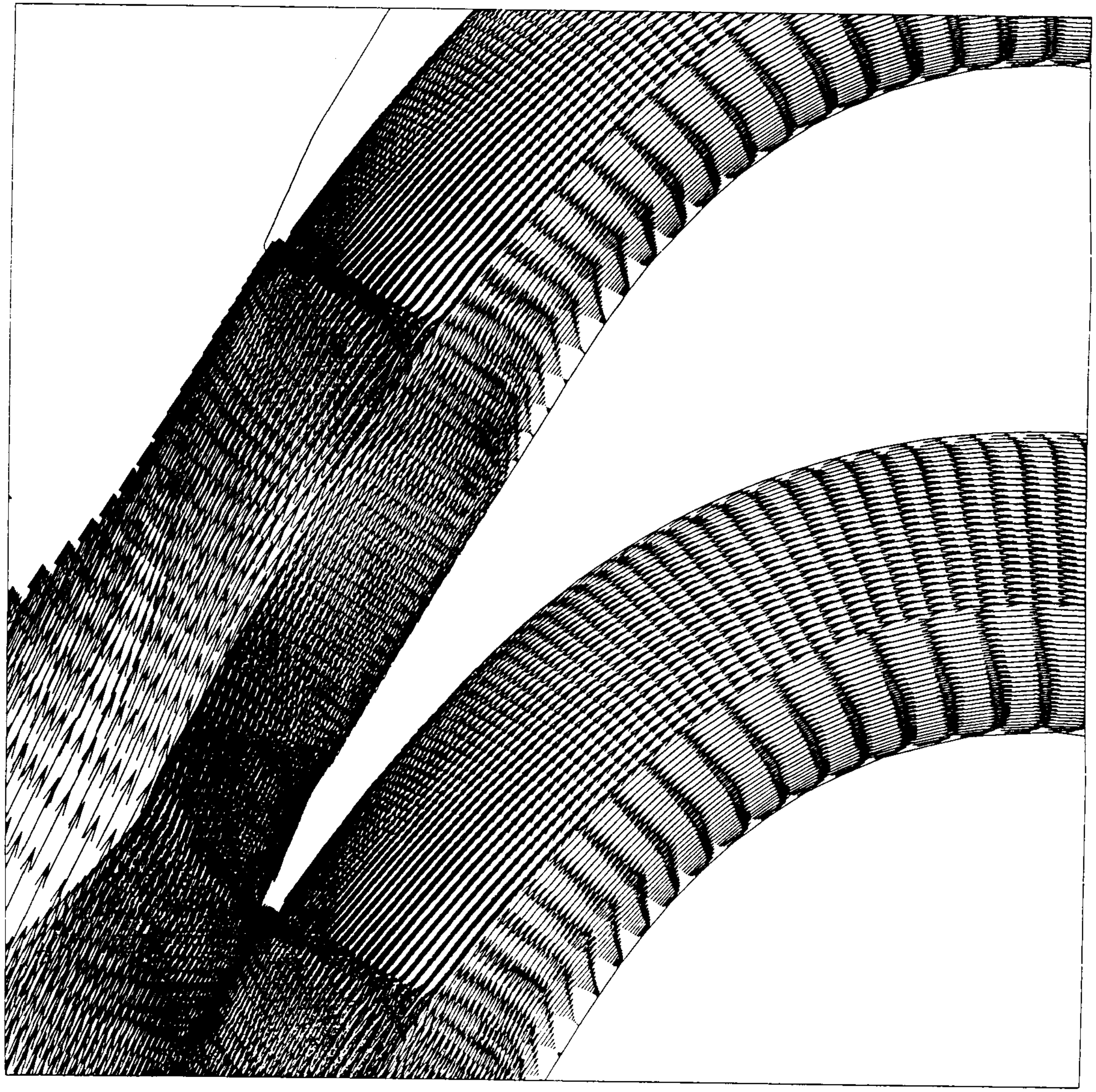

VELOCITY VECTORS FOR UNSTARTED FLOW

MEASURED

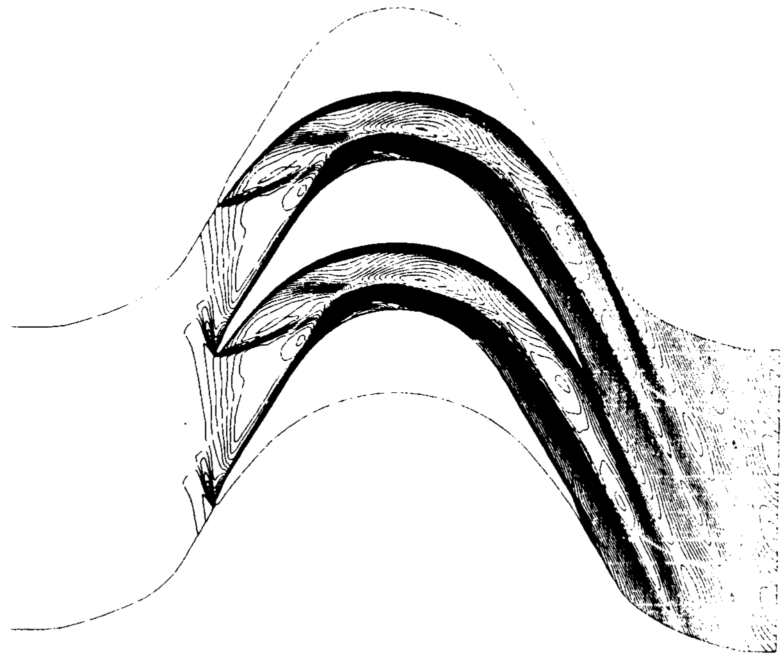

CALCULATED

COMPARISON FOR STARTED FLOW

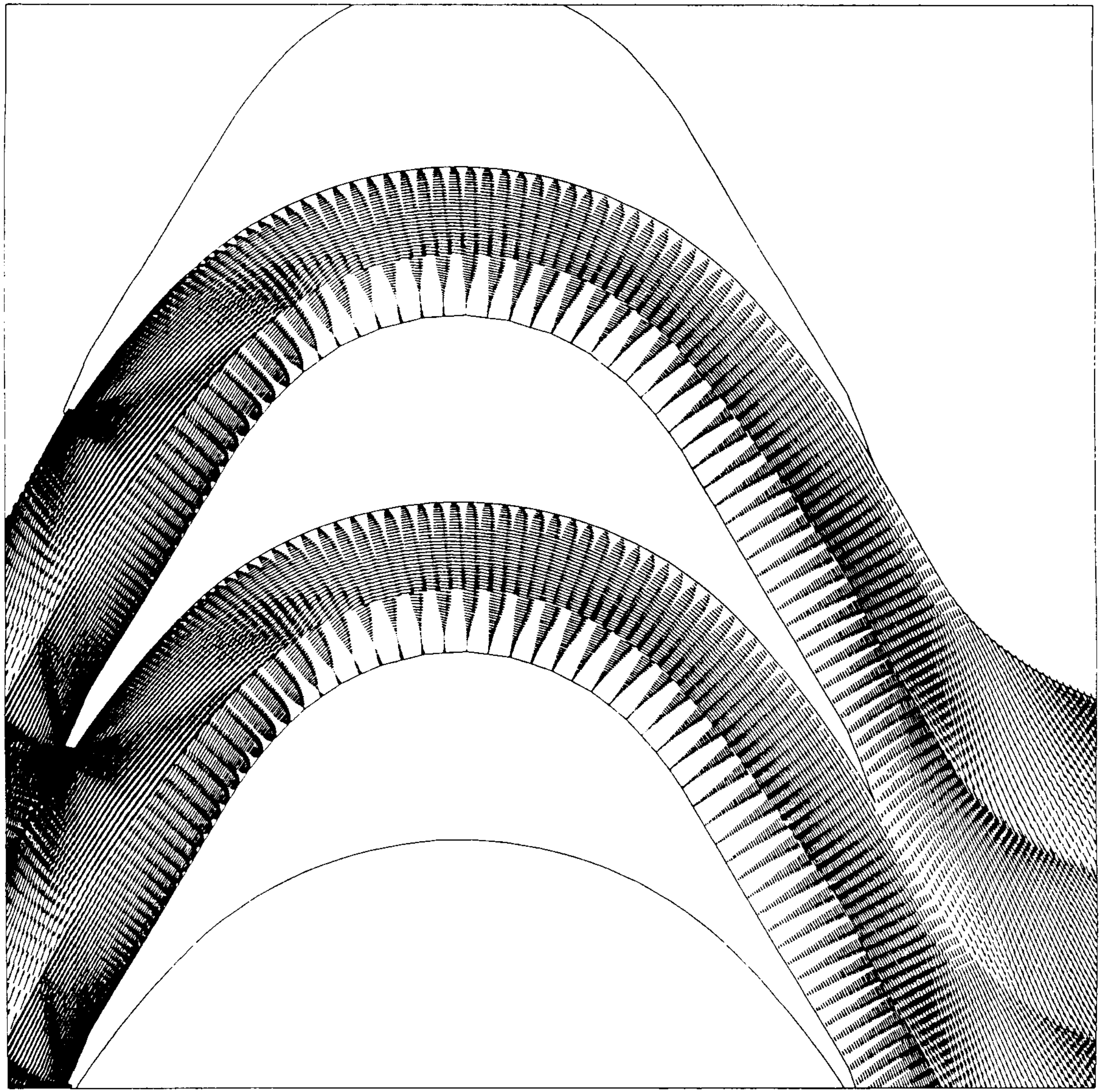

VELOCITY VECTORS FOR STARTED FLOW

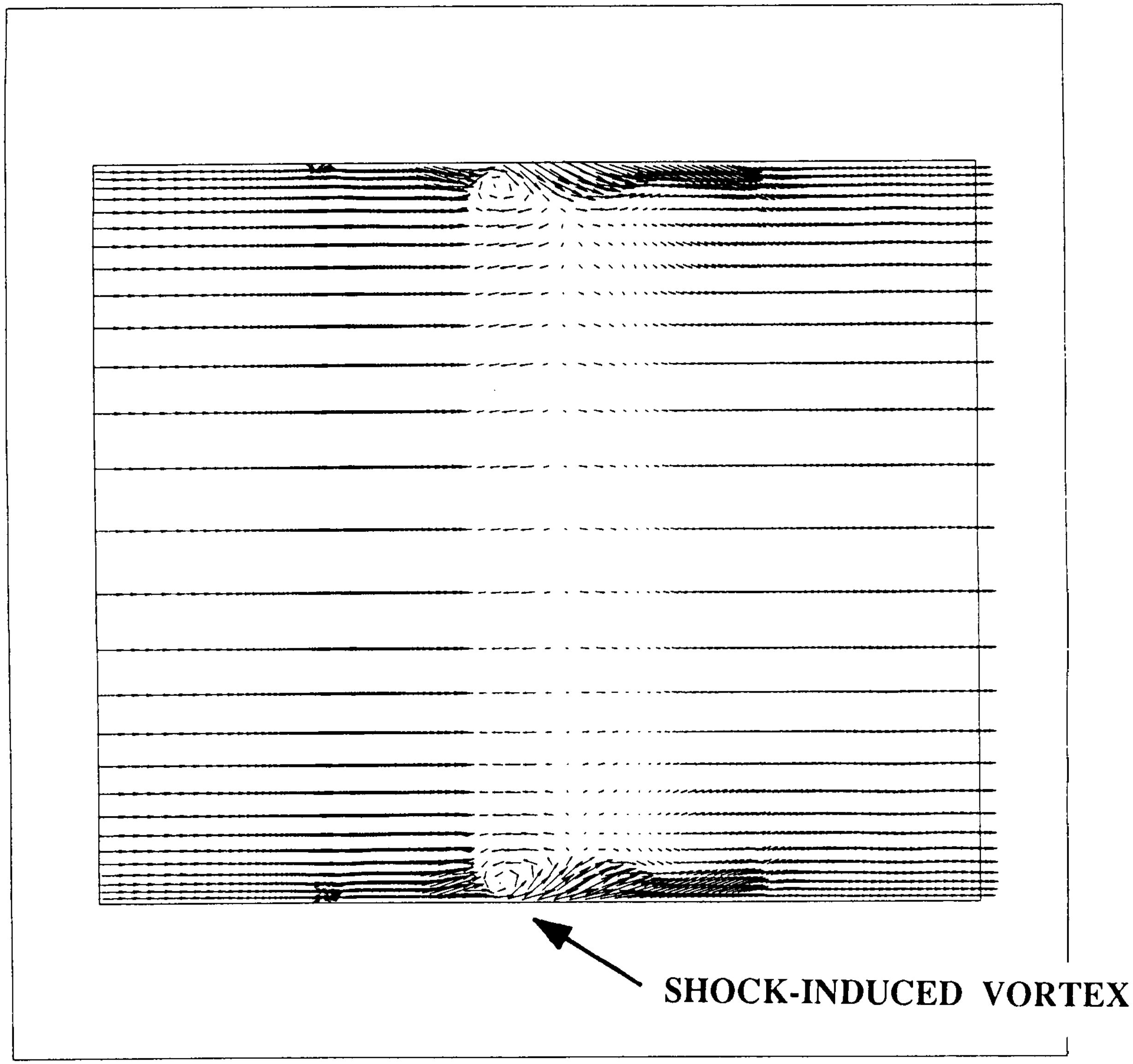

MERIDIONAL VELOCITY VECTORS

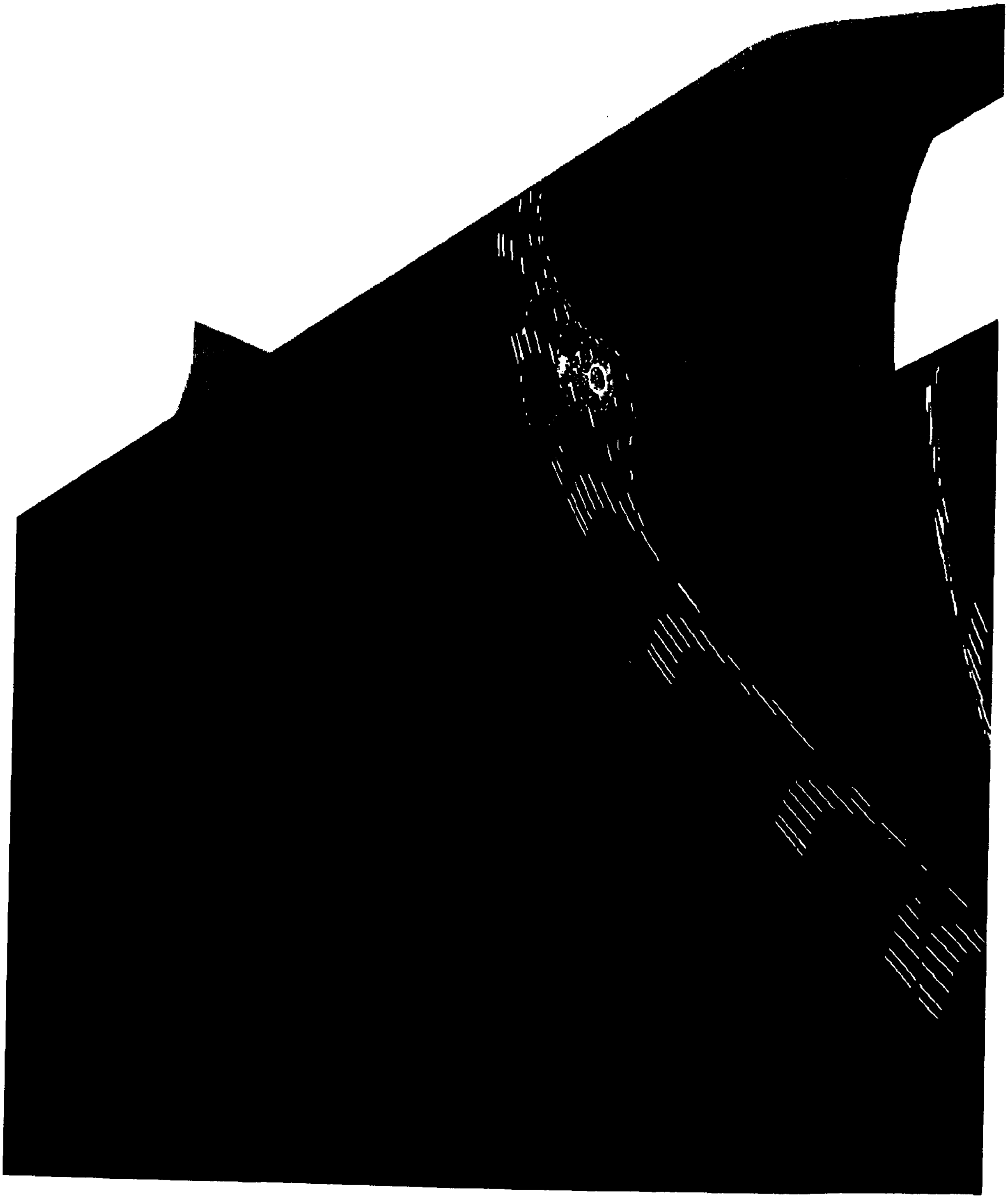

SHOCK-INDUCED VORTEX GENERATION

CONCLUSIONS

3-D VISCOUS CFD CAPTURES MOST FLOW STRUCTURE

CAN BE USED FOR DESIGN APPLICATION

NEEDS HIGH QUALITY DATA FOR VERIFICATION

N92-32269

NAVIER-STOKES ANALYSIS OF AN OXIDIZER TURBINE BLADE WITH TIP CLEARANCE†

Howard J. Gibeling
Jayant S. Sabnis*
Scientific Research Associates, Inc.
Glastonbury, CT

ABSTRACT

The Gas Generator Oxidizer Turbine (GGOT) Blade is being analyzed by various investigators under the NASA MSFC sponsored Turbine Stage Technology Team design effort. The present work concentrates on the tip clearance region flow and associated losses; however, flow details for the passage region are also obtained in the simulations. The present calculations simulate the rotor blade row in a rotating reference frame with the appropriate coriolis and centrifugal acceleration terms included in the momentum equations. The upstream computational boundary is located about one axial chord from the blade leading edge. The boundary conditions at this location have been determined by Pratt & Whitney using an Euler analysis without the vanes to obtain approximately the same flow profiles at the rotor as were obtained with the Euler stage analysis including the vanes. Inflow boundary layer profiles are then constructed assuming the skin friction coefficient at both the hub and the casing. The downstream computational boundary is located about one axial chord from the blade trailing edge, and the circumferentially averaged static pressure at this location was also obtained from the P&W Euler analysis.

Results have been obtained for the 3-D baseline GGOT geometry at the full scale design Reynolds number. Details of the clearance region flow behavior and blade pressure distributions have been computed. The spanwise variation in blade loading distributions are shown, and circumferentially averaged spanwise distributions of total pressure, total temperature, Mach number and flow angle are shown at several axial stations. The spanwise variation of relative total pressure loss shows a region of high loss in the region near the casing. Particle traces in the near tip region show vortical behavior of the fluid which passes through the clearance region and exits at the downstream edge of the gap. Future work will include collaboration with the P&W design team to identify design changes which may reduce clearance flow losses.

† Work supported under NASA MSFC Contract NAS8-38865.

* Currently at United Technologies Research Center, East Hartford, CT.

PRECEDING PAGE BLANK NOT FILMED

NAVIER-STOKES ANALYSIS OF OXIDIZER TURBINE BLADE (GGOT) WITH TIP LEAKAGE

WORKSHOP FOR CFD APPLICATIONS IN ROCKET PROPULSION

APRIL 30, 1992

HOWARD J. GIBELING
JAYANT S. SABNIS

SCIENTIFIC RESEARCH ASSOCIATES, INC.
GLASTONBURY, CT 06033

Scientific Research Associates

SUPPORTED BY

NASA MARSHALL SPACE FLIGHT CENTER

CONTRACT NAS8-38865

Scientific
Research
Associates

OBJECTIVE

APPLY CFD TECHNOLOGY TO ADVANCE TURBINE DESIGN FOR SPACE PROPULSION APPLICATIONS .

Scientific
Research
Associates

GGOT SIMULATION SUMMARY

UTILIZE SRA GMINT CODE

- GENERAL NON-RECTANGULAR BLOCK STRUCTURE
- SINGLE GRID
- FULL NAVIER-STOKES EQUATIONS
- NO-SLIP WALL BOUNDARY EQUATIONS WITH SUBLAYER RESOLUTION
- IMPLICIT LINEARIZED BLOCK SOLVER (ADI)

Scientific Research Associates

GGOT SIMULATION SUMMARY (Continued)

- GRID GENERATION
  - "FALSE CORNER" GRID STRUCTURE
  - 2-D ELLIPTIC GRIDS GENERATED WITH EAGLE

    100 x 160 POINTS IN CROSS-SECTIONAL PLANE
  - 3-D GRID CONSTRUCTION

    21 BLADE CROSS-SECTIONAL PLANES

    REDISTRIBUTION IN SPANWISE DIRECTION

      40 POINTS FROM HUB TO TIP

      25 POINTS IN CLEARANCE REGION

Scientific Research Associates

GGOT SIMULATION FLOW PARAMETERS

- SUPPLIED BY P&W DESIGN TEAM
- CIRCUMFERENTIALLY - AVERAGED SPANWISE DISTRIBUTIONS FROM EULER CODE
    - UPSTREAM AXIAL MASS FLUX
    - UPSTREAM TOTAL TEMPERATURE
    - UPSTREAM FLOW ANGLES
    - DOWNSTREAM STATIC PRESSURE
- HUB AND CASING ENDWALL BOUNDARY LAYER PROFILES CONSTRUCTED WITH ASSUMED $C_f = 0.002$

Scientific Research Associates

OXIDIZER TURBINE BASELINE DESIGN

FULL SCALE TURBINE FLOWPATH CLOSE-UP

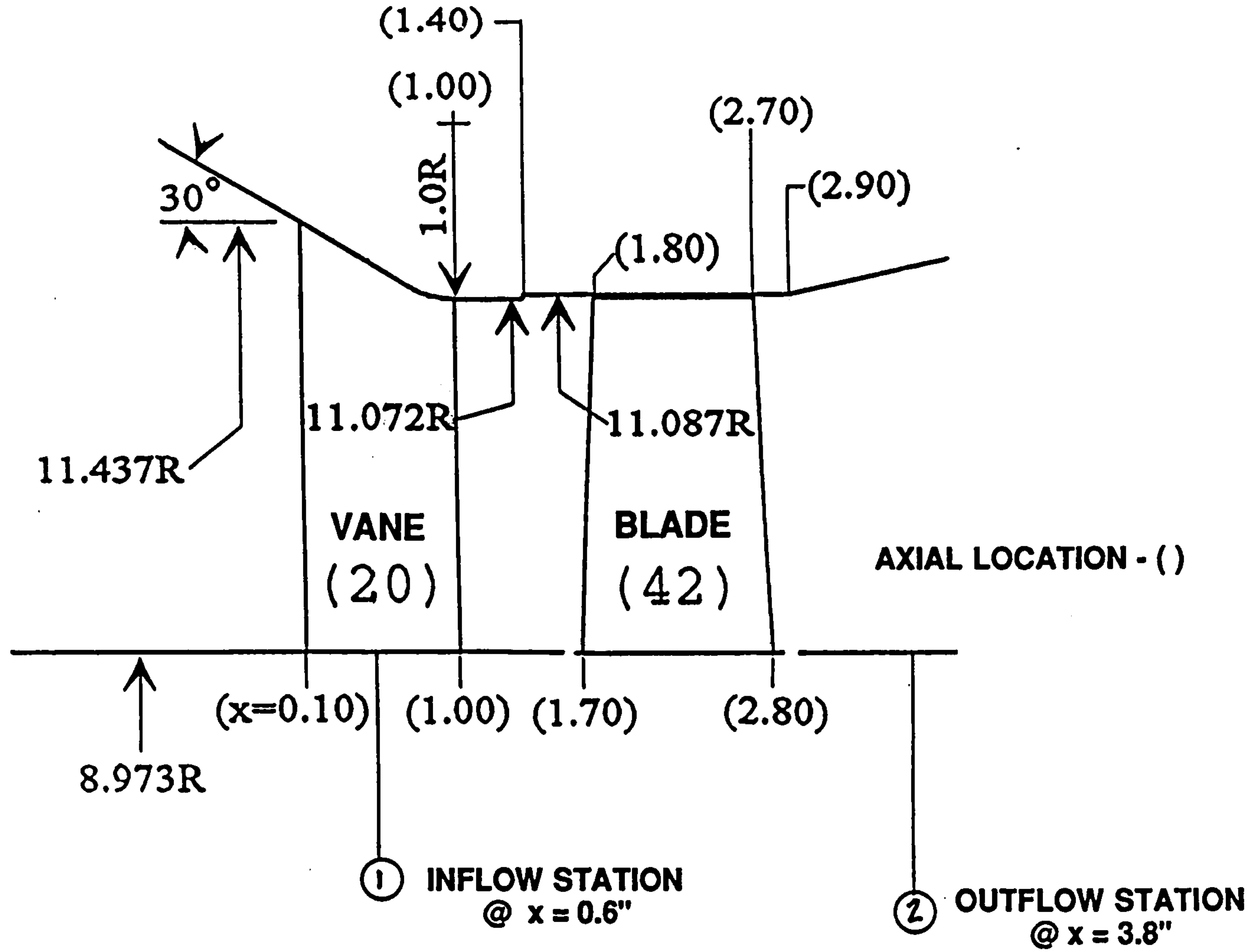

Scientific
Research
Associates

BASELINE GGOT HUB SECTION GRID
(100 x 60)

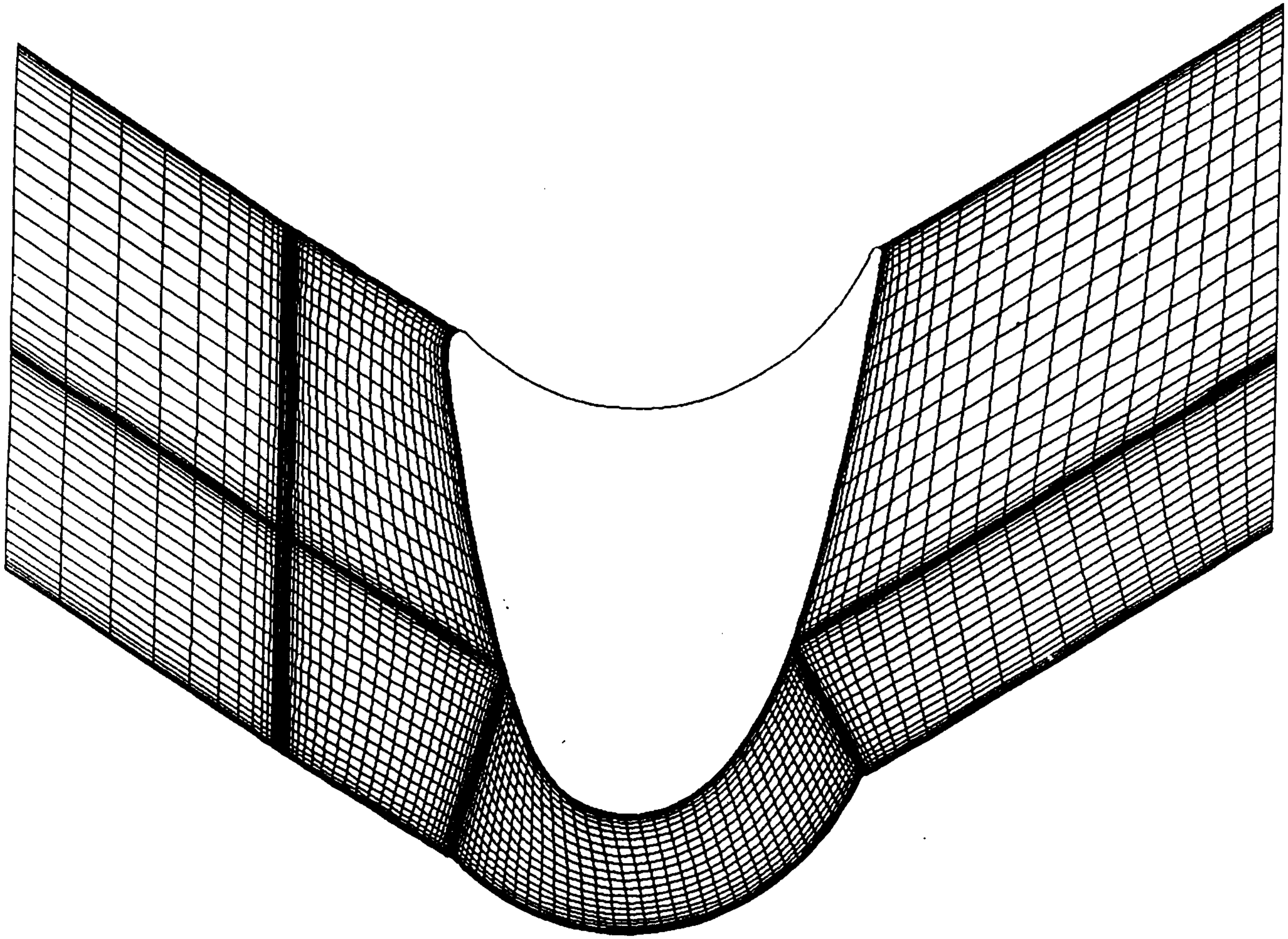

Scientific
Research
Associates

BASELINE GGOT MID-SPAN SECTION GRID
(100 x 60)

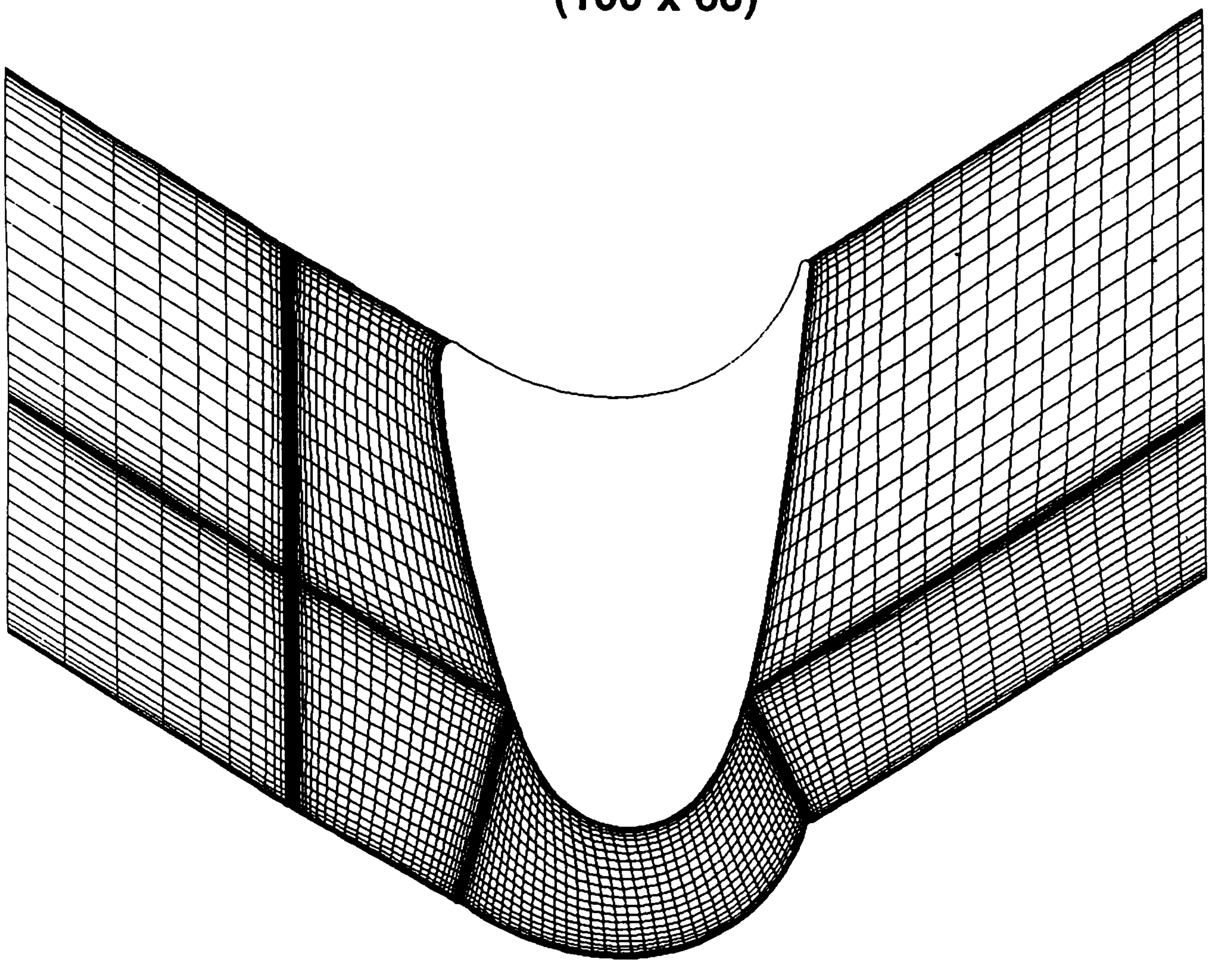

Scientific
Research
Associates

BASELINE GGOT TIP SECTION GRID
(100 x 60)

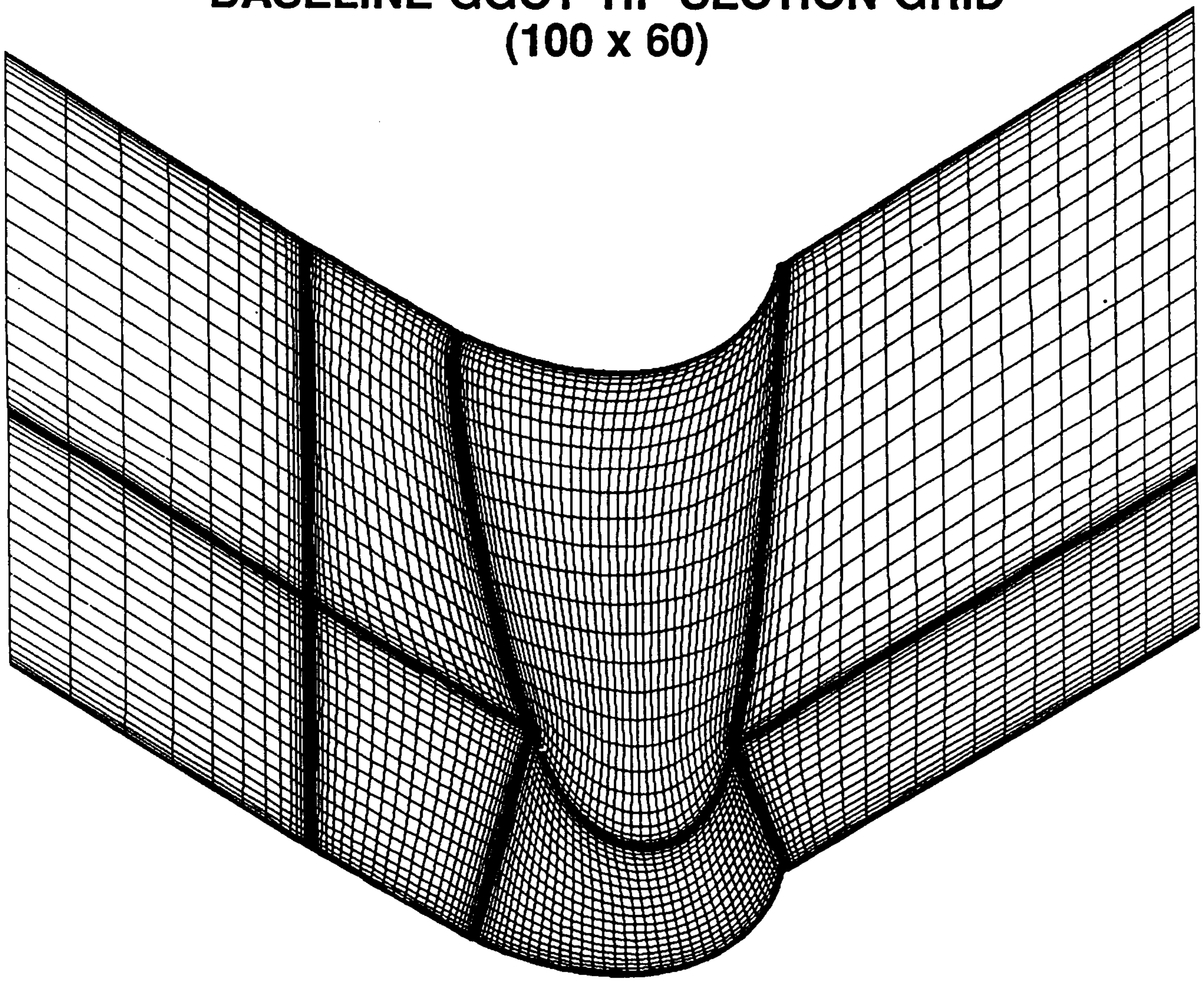

Scientific
Research
Associates

BASELINE GGOT 3-D GRID - HUB AND CASING SECTIONS

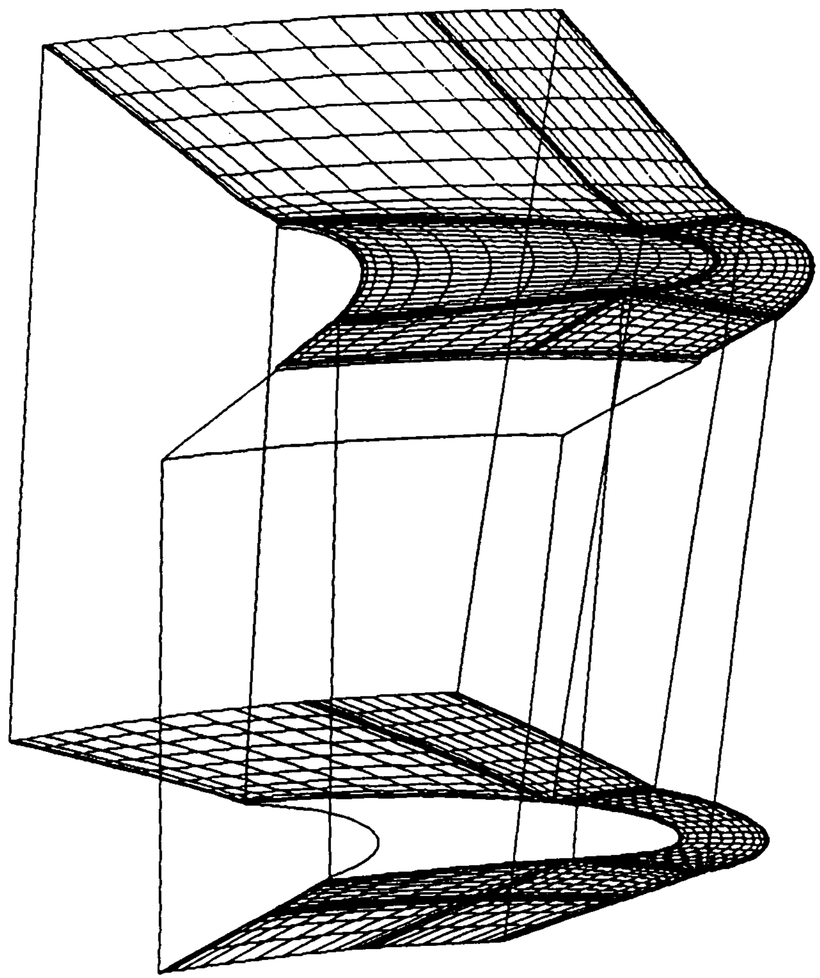

Scientific
Research
Associates

BASELINE GGOT WITH TIP CLEARANCE MACH NUMBER CONTOURS AT 9.2% SPAN

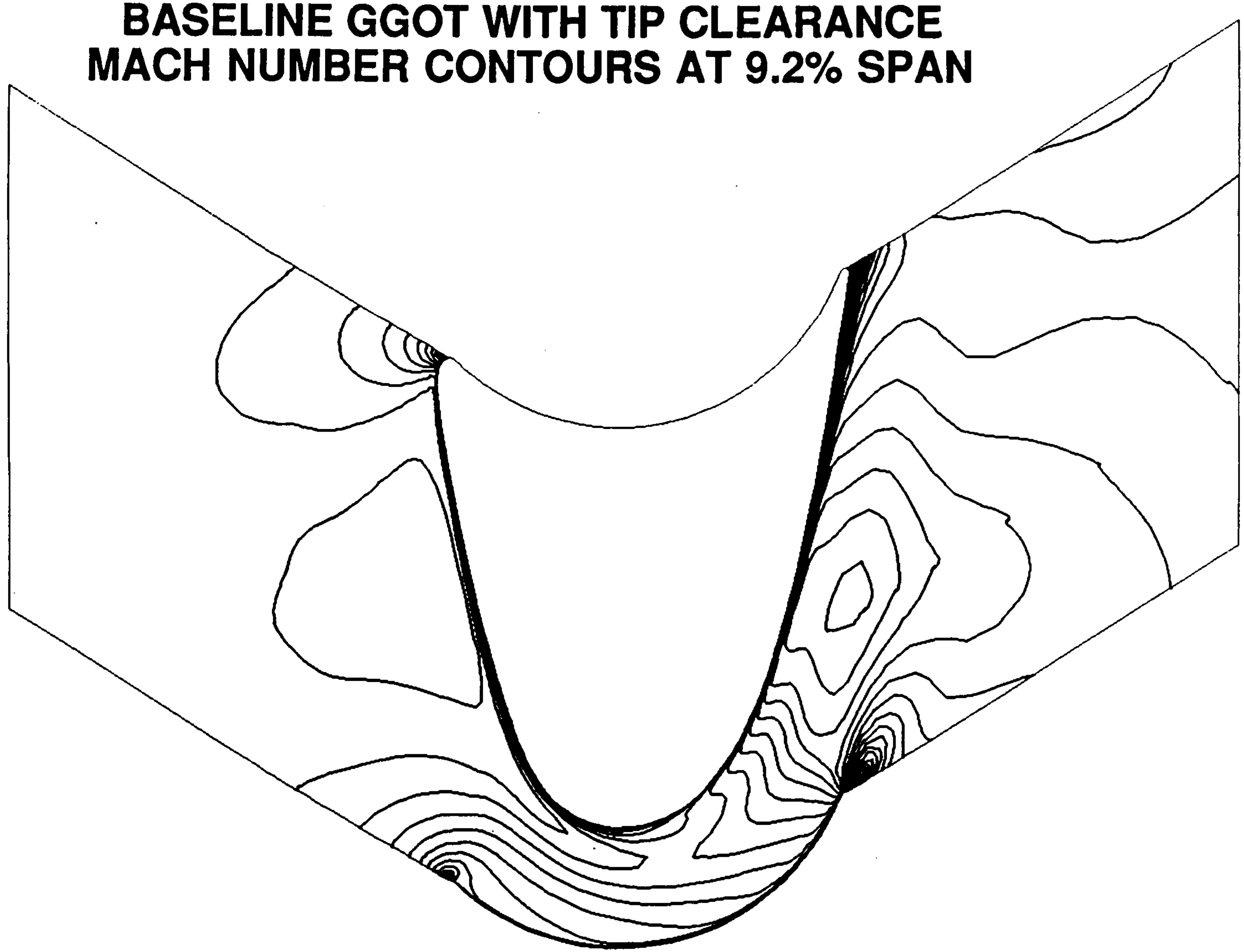

Scientific
Research
Associates

BASELINE GGOT WITH TIP CLEARANCE MACH NUMBER CONTOURS AT 53.5% SPAN

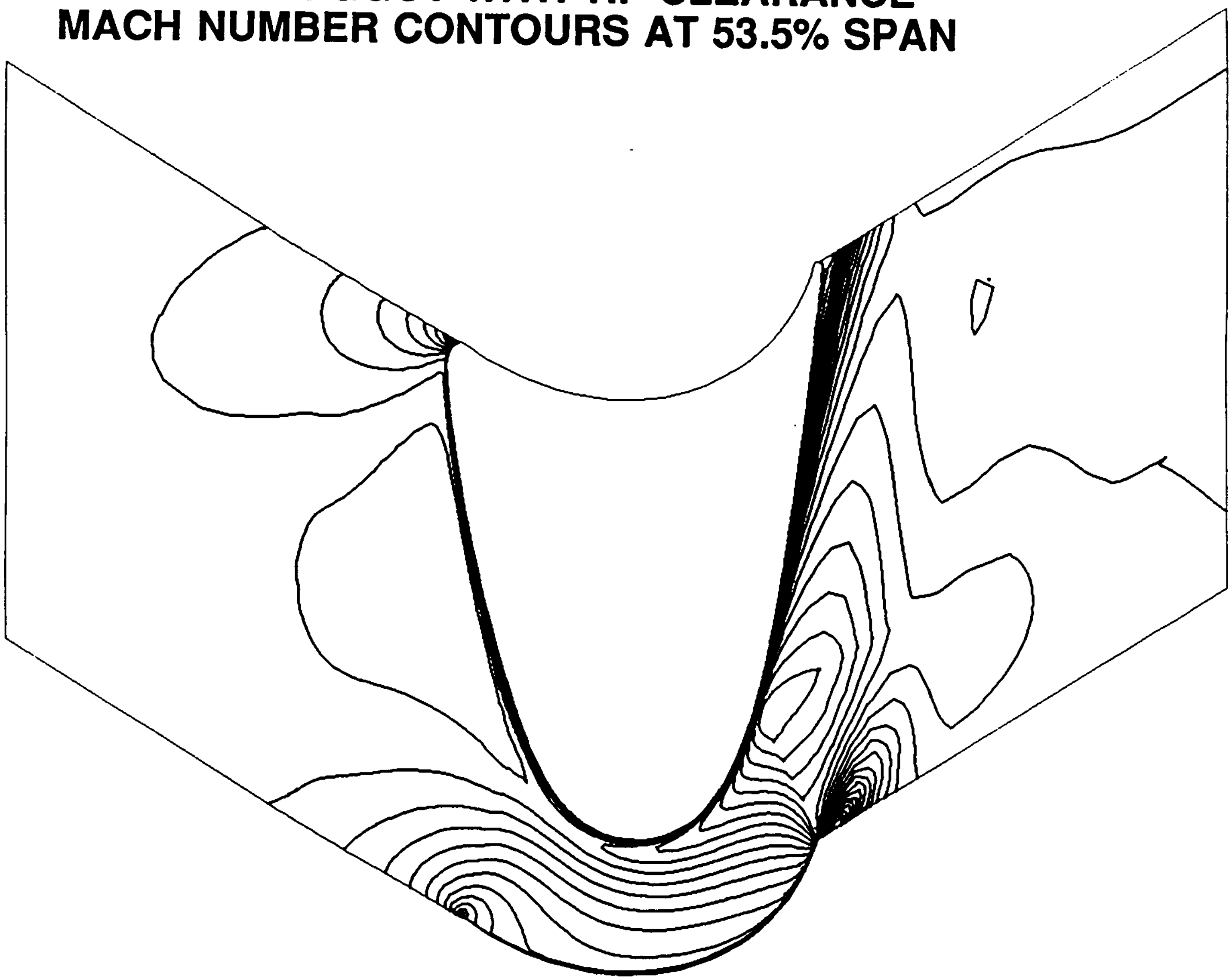

Scientific
Research
Associates

BASELINE GGOT WITH TIP CLEARANCE
MACH NUMBER CONTOURS AT 90% SPAN

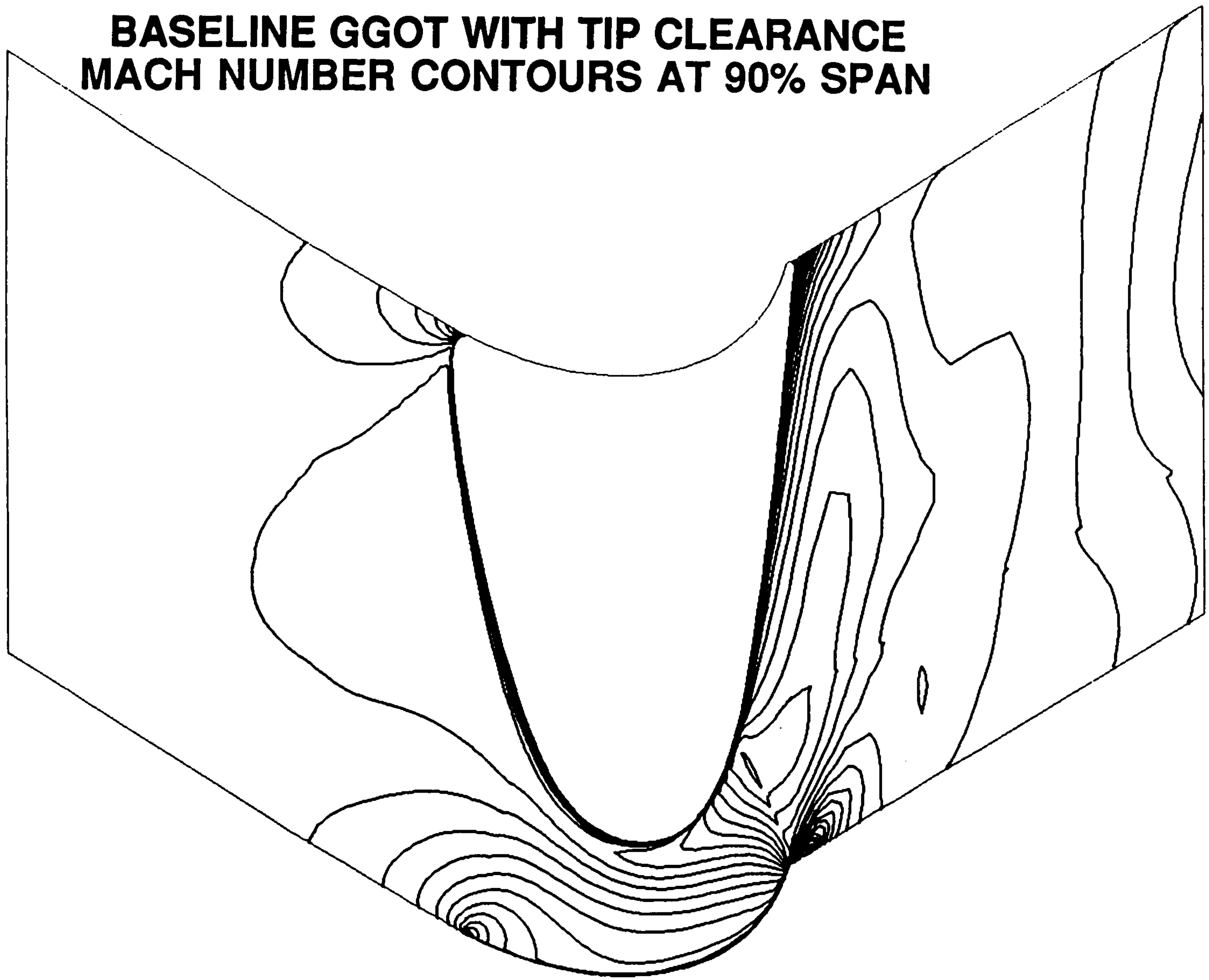

Scientific
Research
Associates

BASELINE GGOT WITH TIP CLEARANCE PRESSURE CONTOURS AT 9.2% SPAN

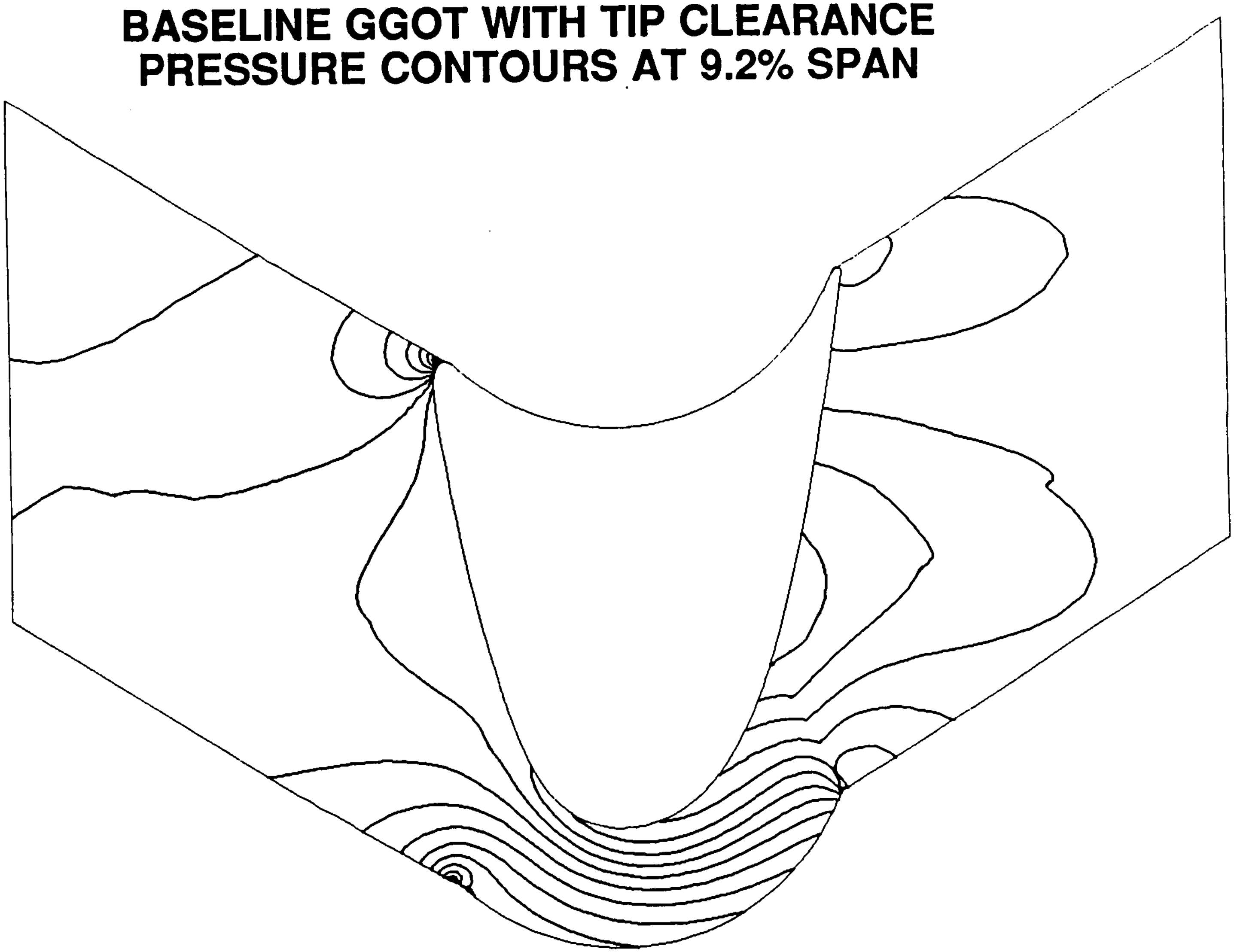

Scientific Research Associates

BASELINE GGOT WITH TIP CLEARANCE PRESSURE CONTOURS AT 53.5% SPAN

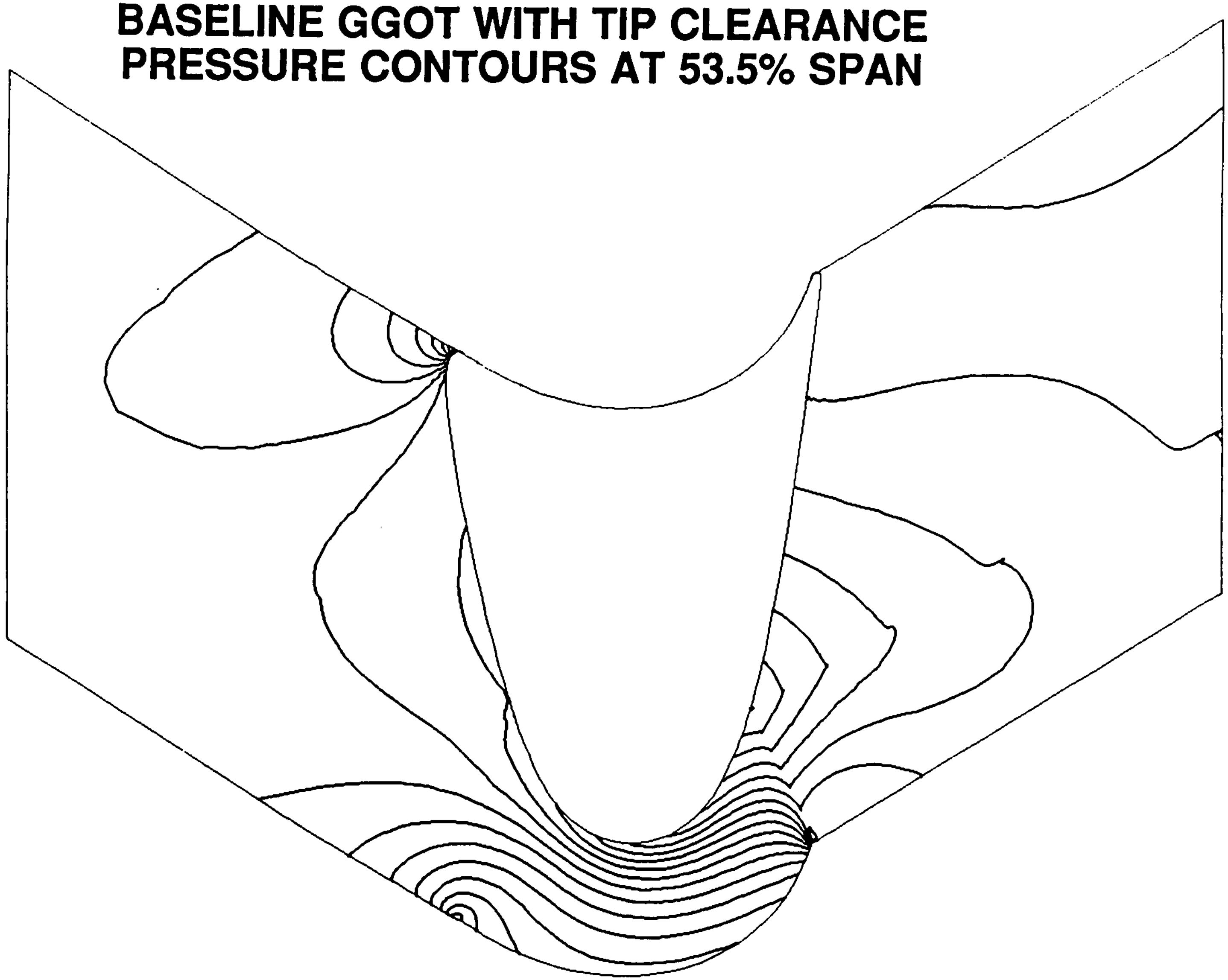

Scientific
Research
Associates

BASELINE GGOT WITH TIP CLEARANCE PRESSURE CONTOURS AT 90% SPAN

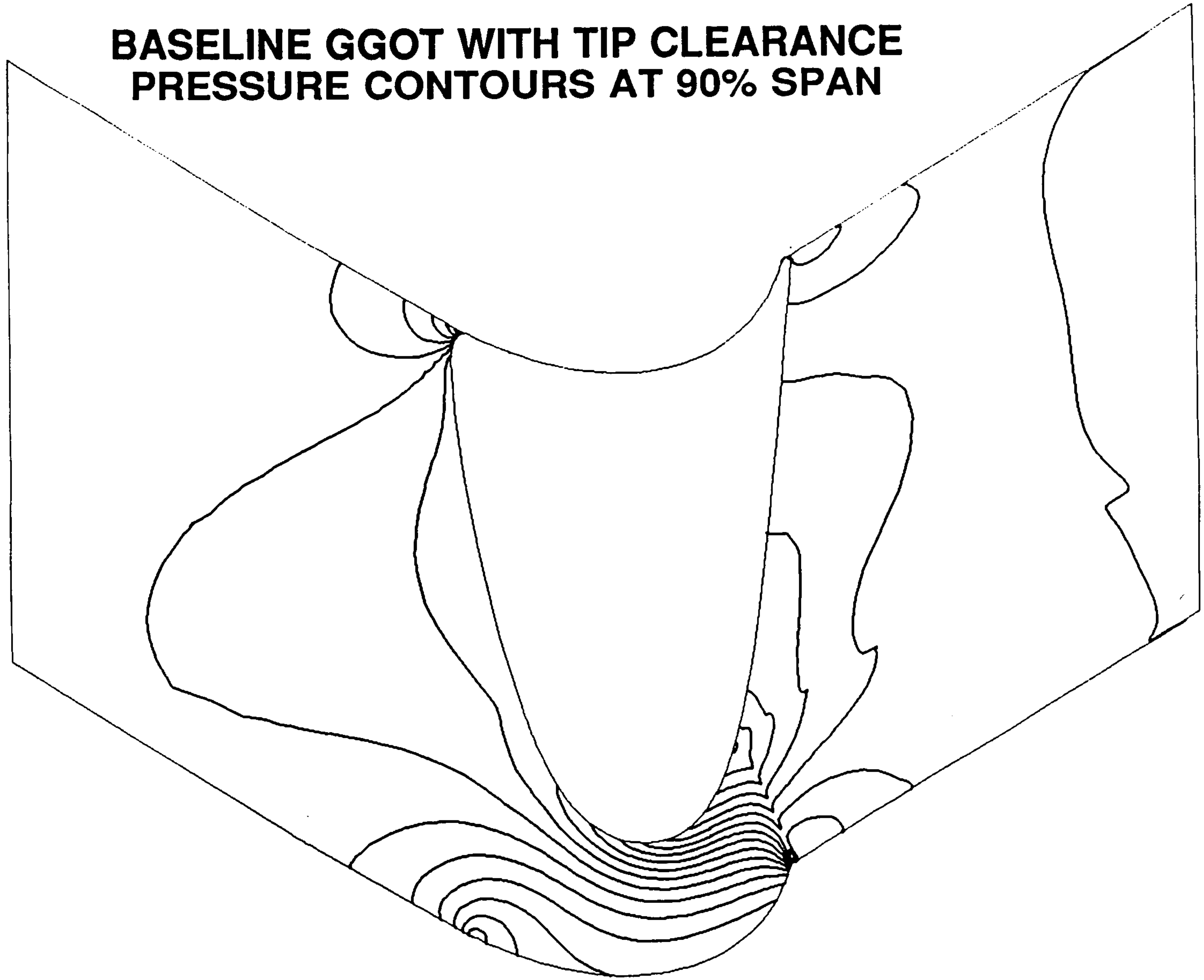

Scientific Research Associates

Baseline GGOT with Clearance
Blade Surface Pressure (9.2% span)

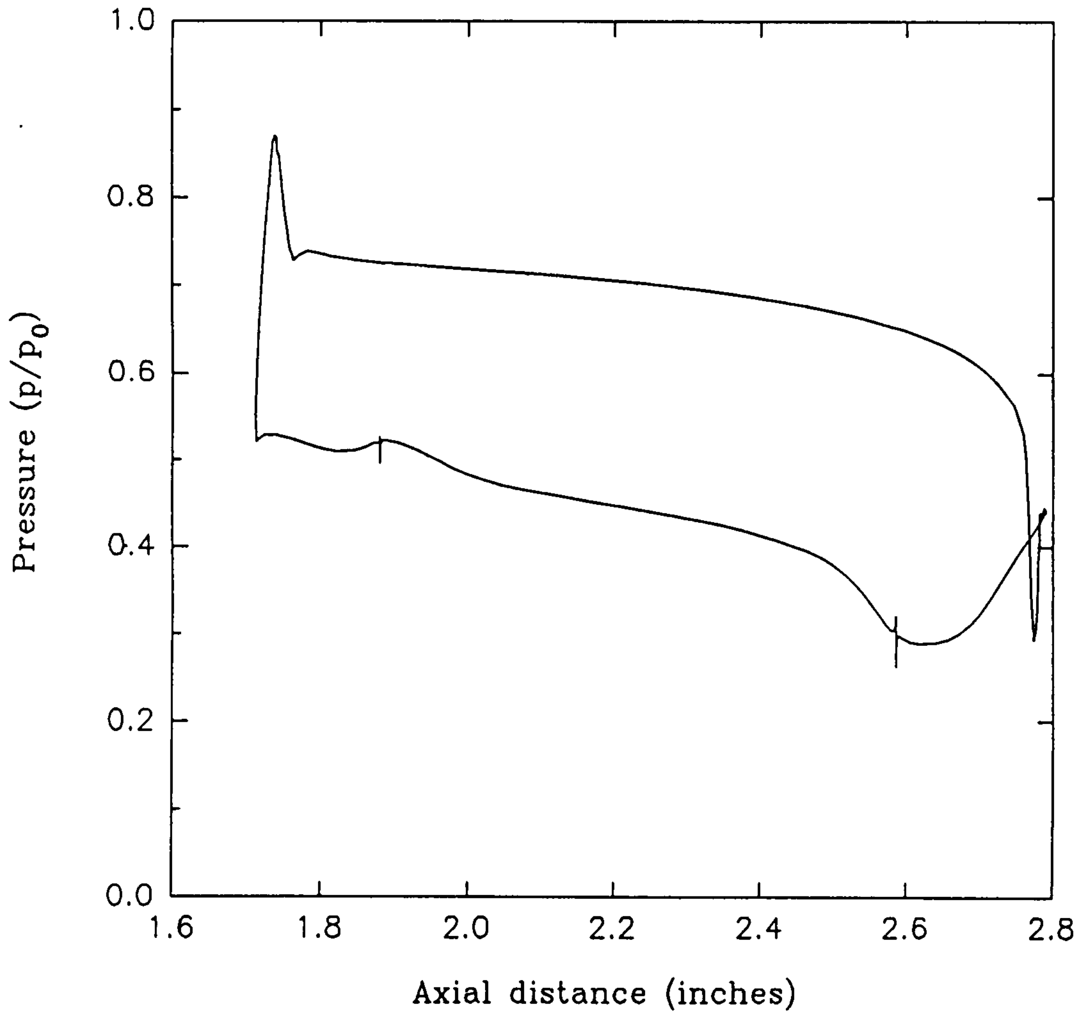

Scientific
Research
Associates

Baseline GGOT with Clearance
Blade Surface Pressure (53.5% span)

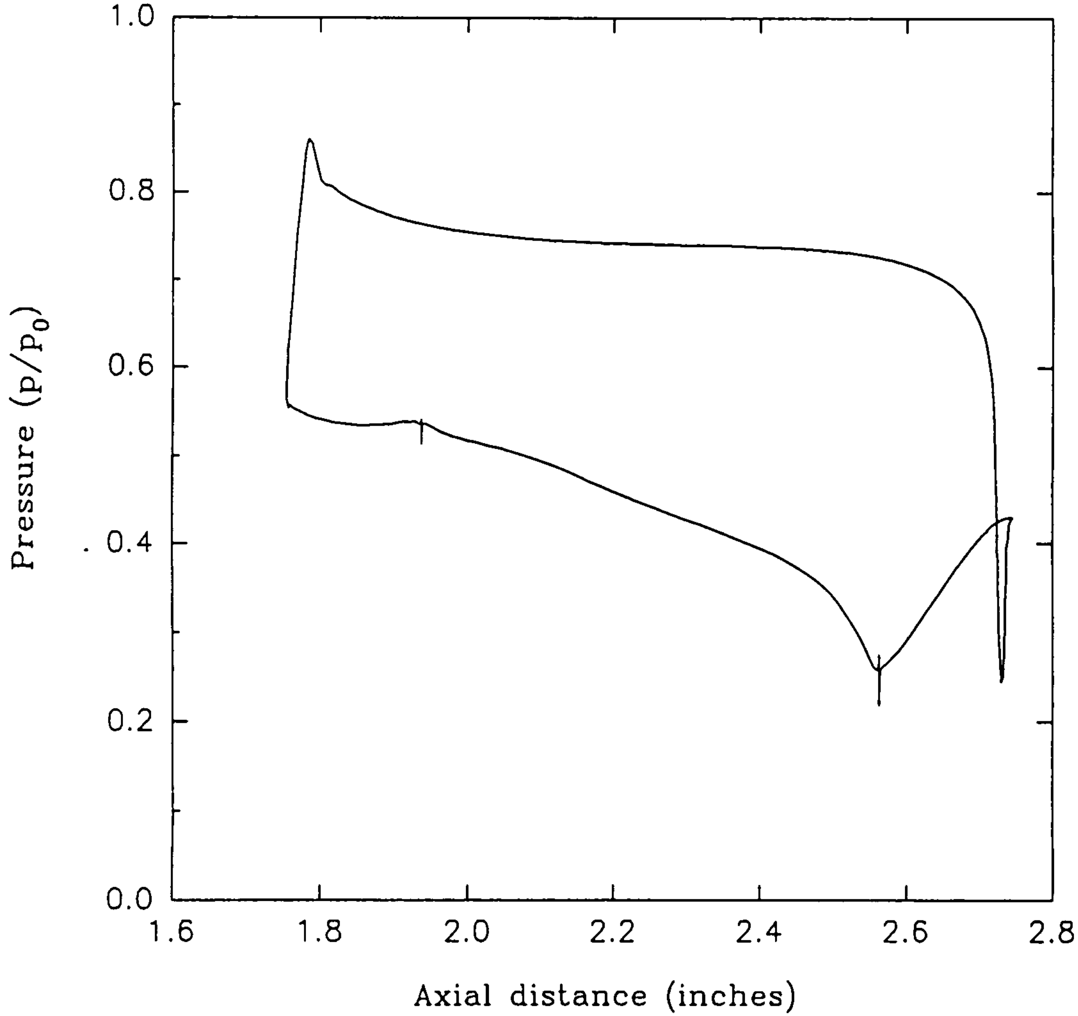

Scientific Research Associates

Baseline GGOT with Clearance
Blade Surface Pressure (90% span)

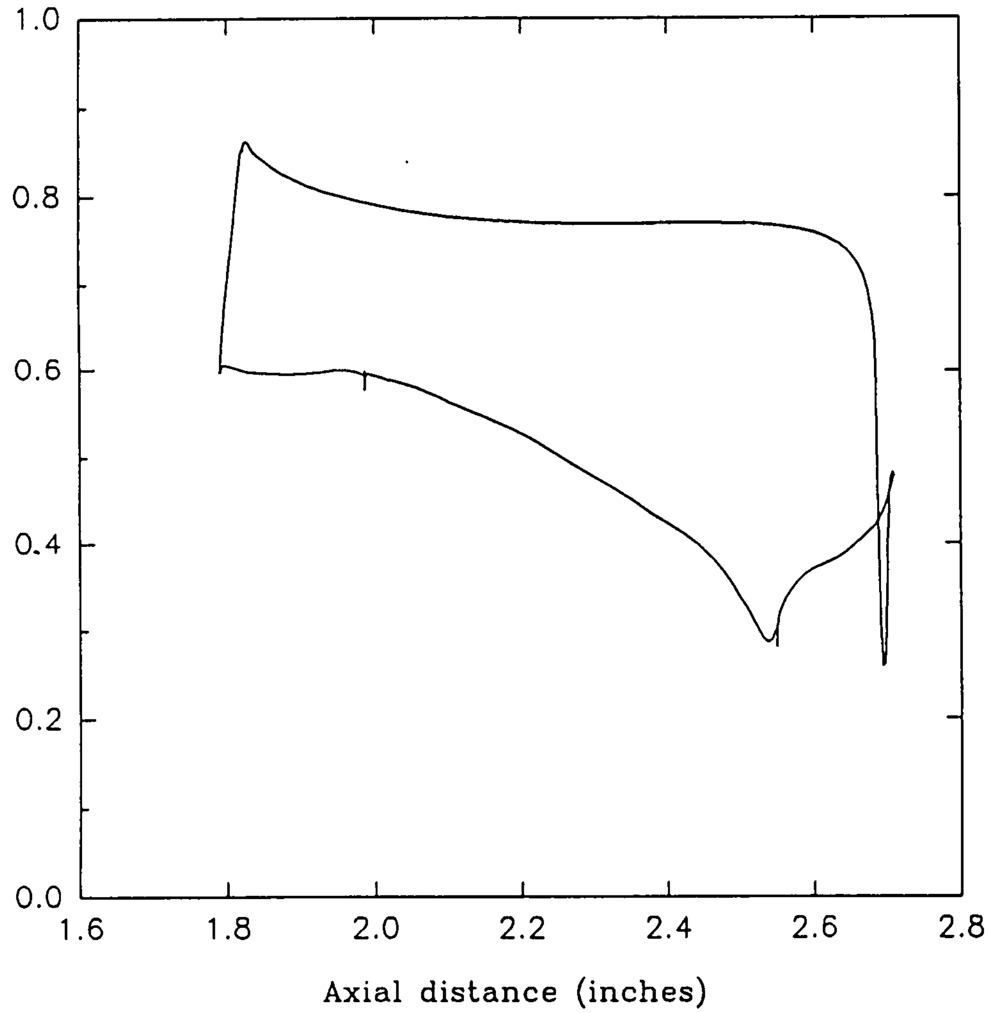

Scientific
Research
Associates

Circumferentially Averaged Variables
Total Pressure Loss Across Blade

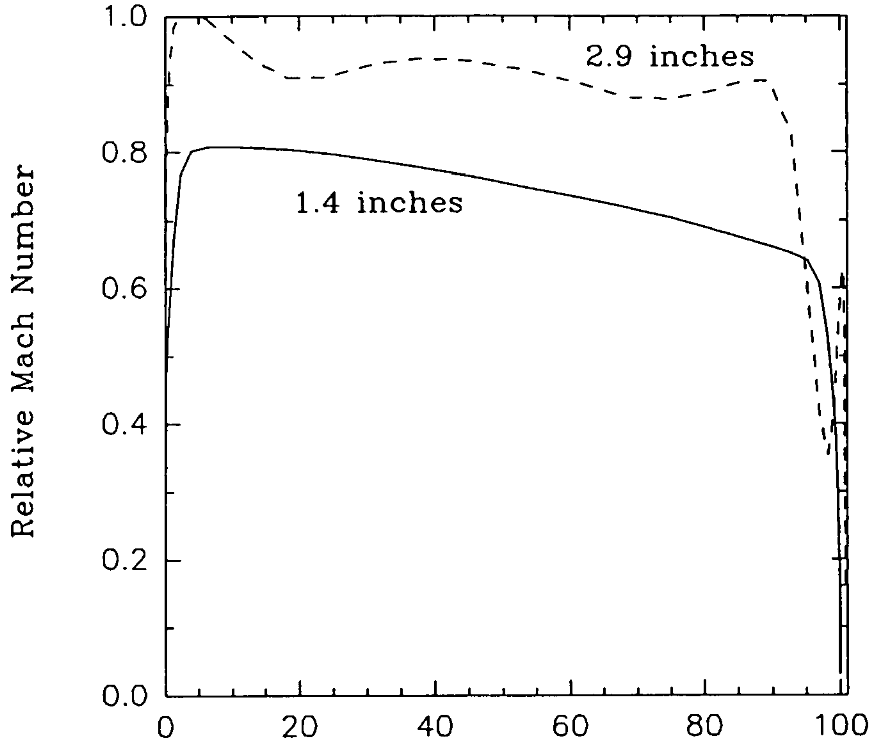

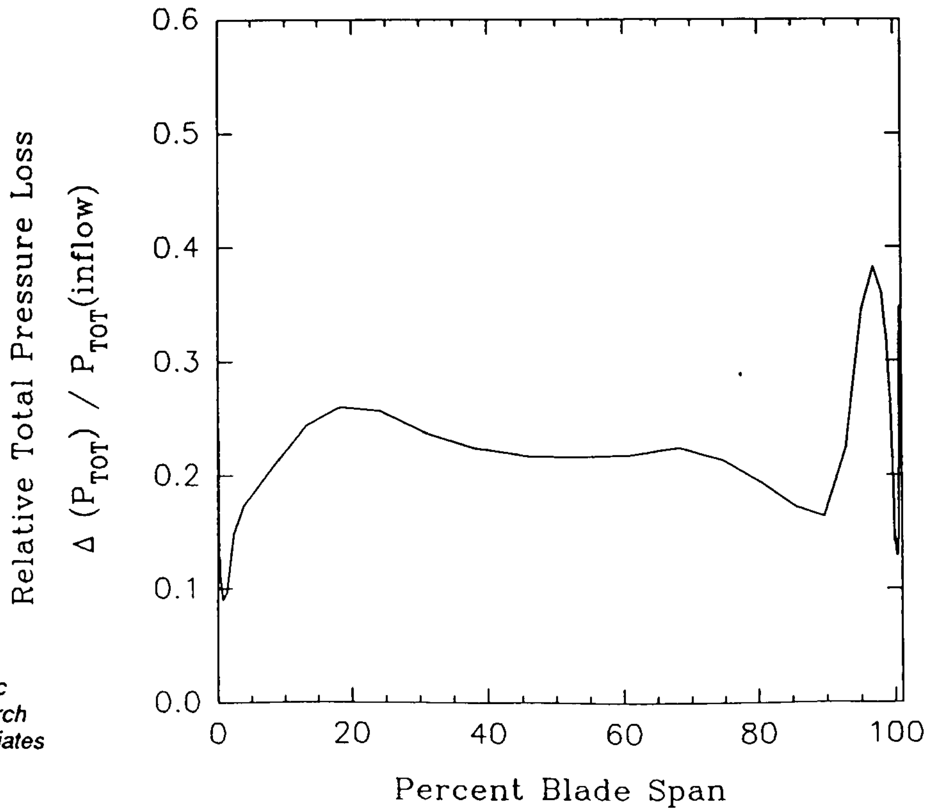

Scientific Research Associates

PARTICLES TRACES
BASELINE GGOT WITH TIP CLEARANCE
MID GAP STREAK LINES

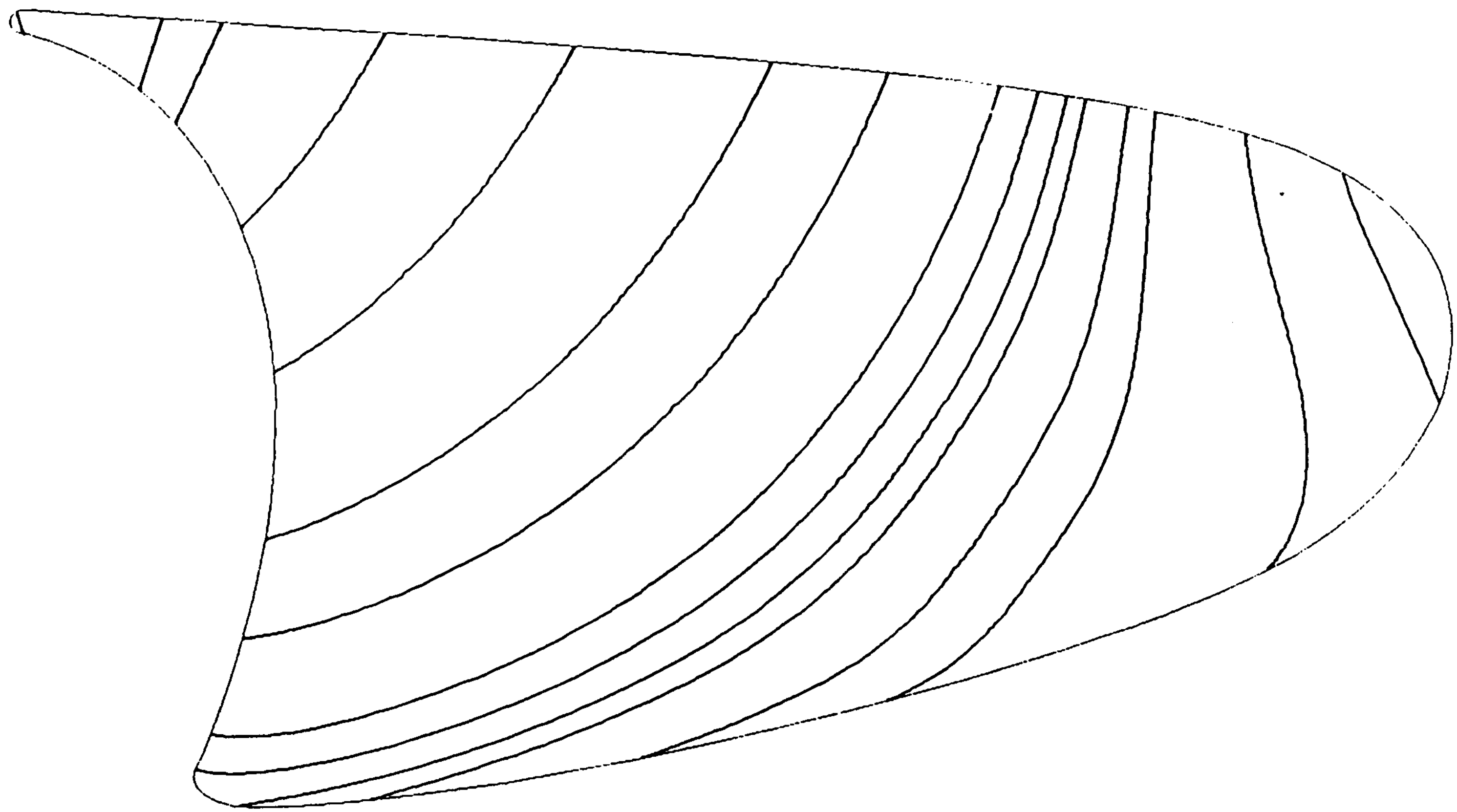

Scientific
Research
Associates

PARTICLES TRACES
BASELINE GGOT WITH TIP CLEARANCE
BLADE TIP STREAK LINES

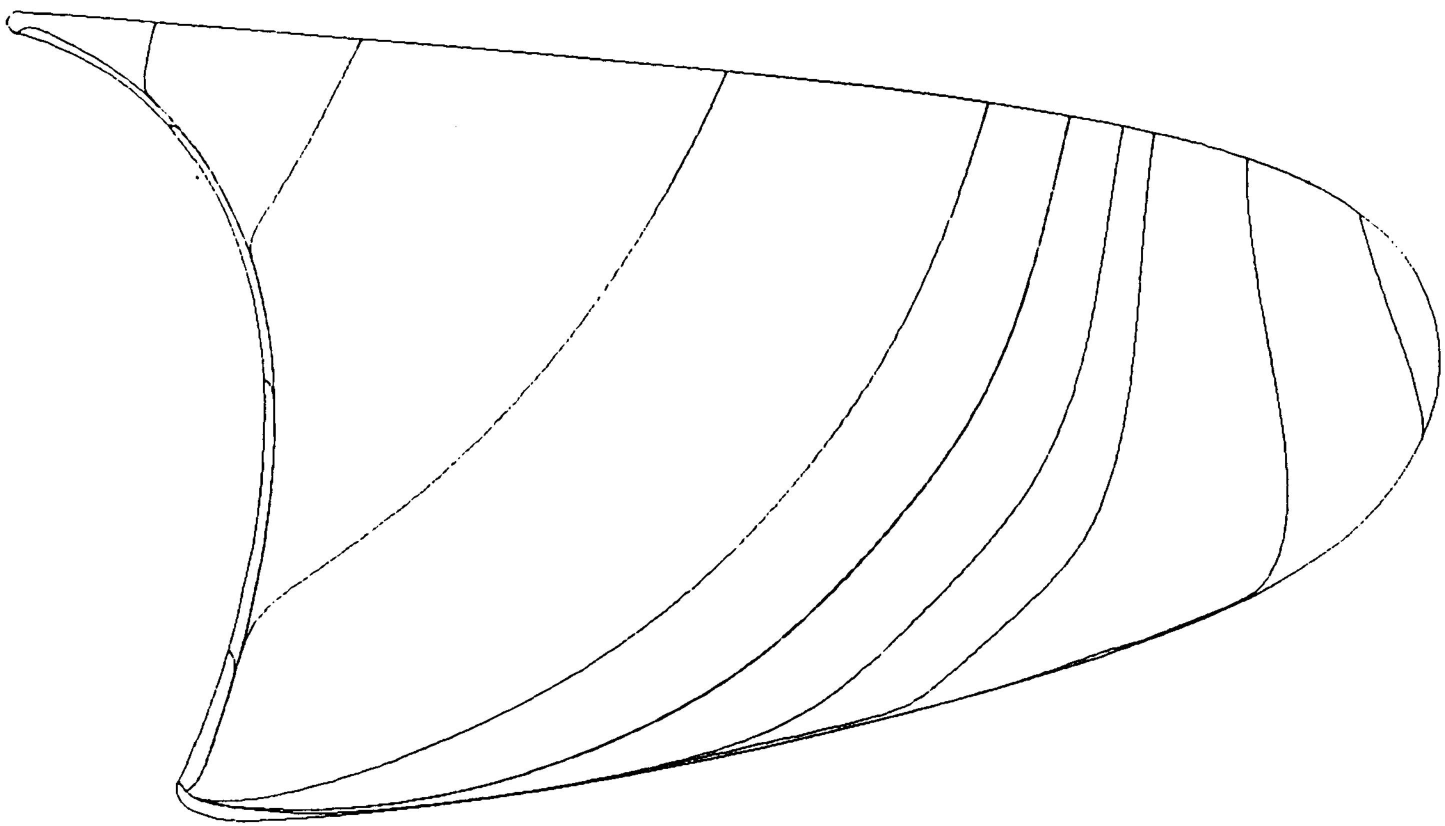

Scientific
Research
Associates

PARTICLE TRACES

BASELINE G6OT WITH TIP CLEARANCE

TRACES ORIGINATING AT 100% SPAN - INFLOW VIEW

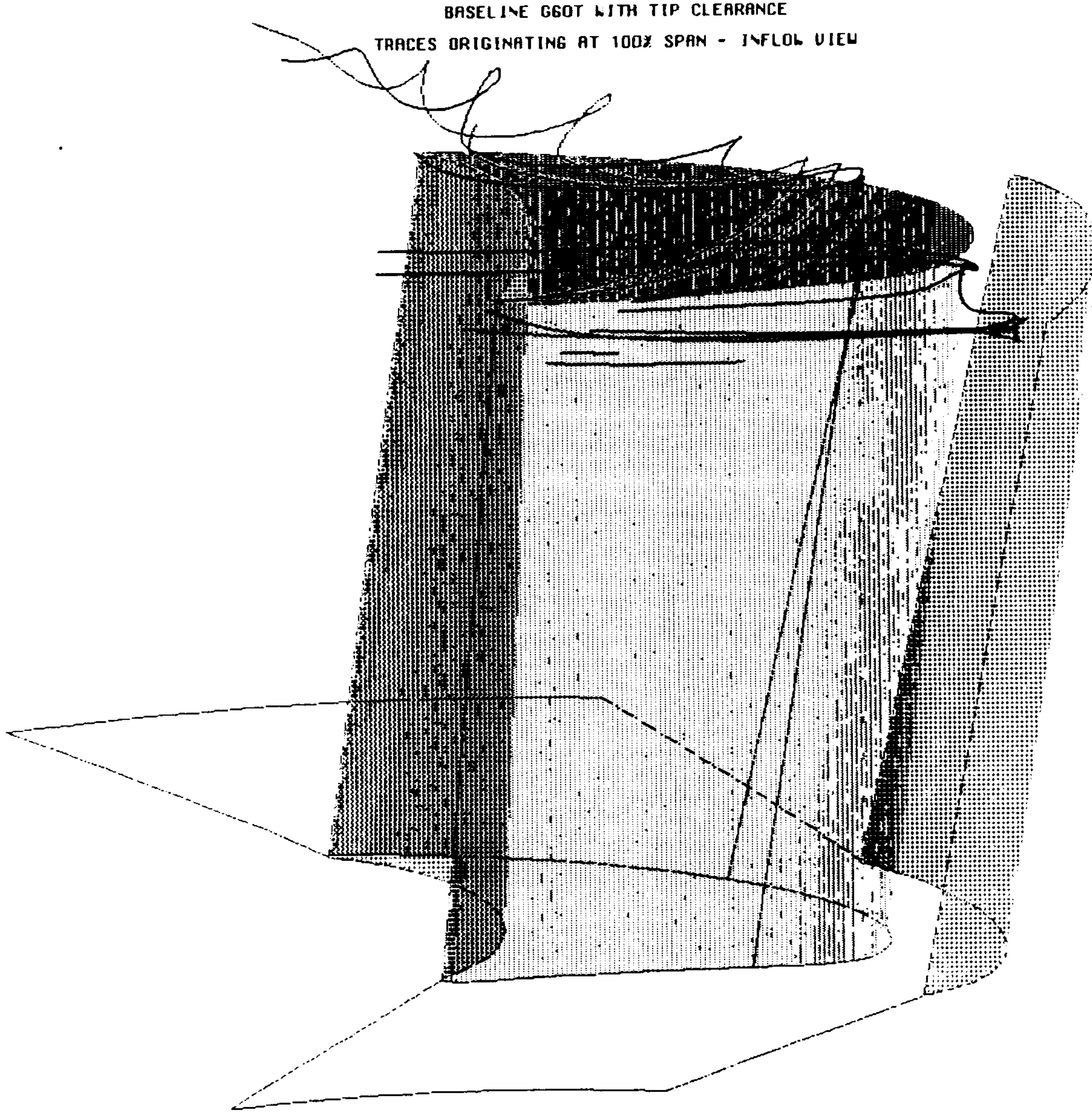

0.885	MACH
1.37 DEG	ALPHA
2.63x10**6	Re
1.46x10**3	TIME
100x160x40	GRID

Scientific
Research
Associates

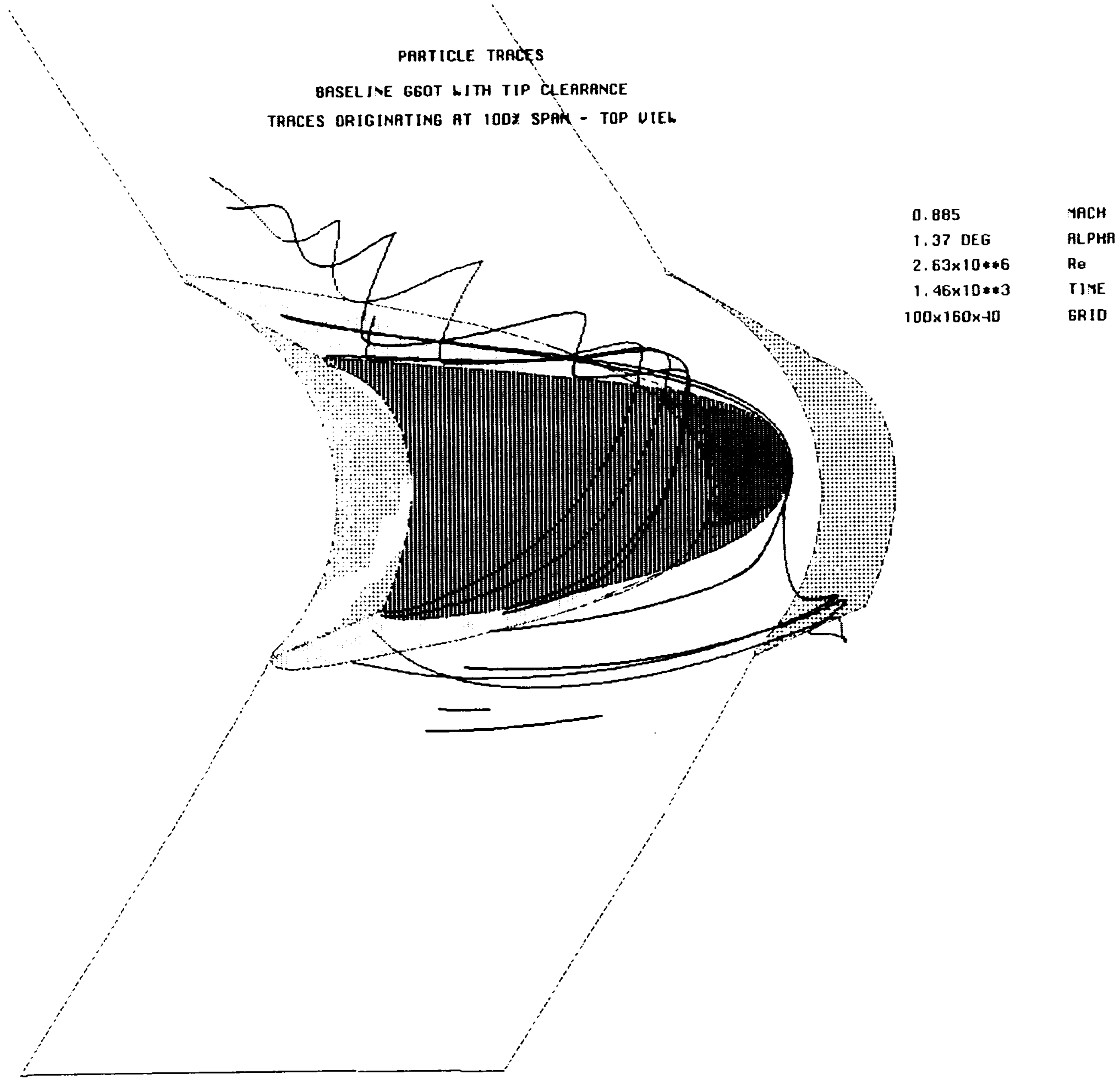

Scientific Research Associates

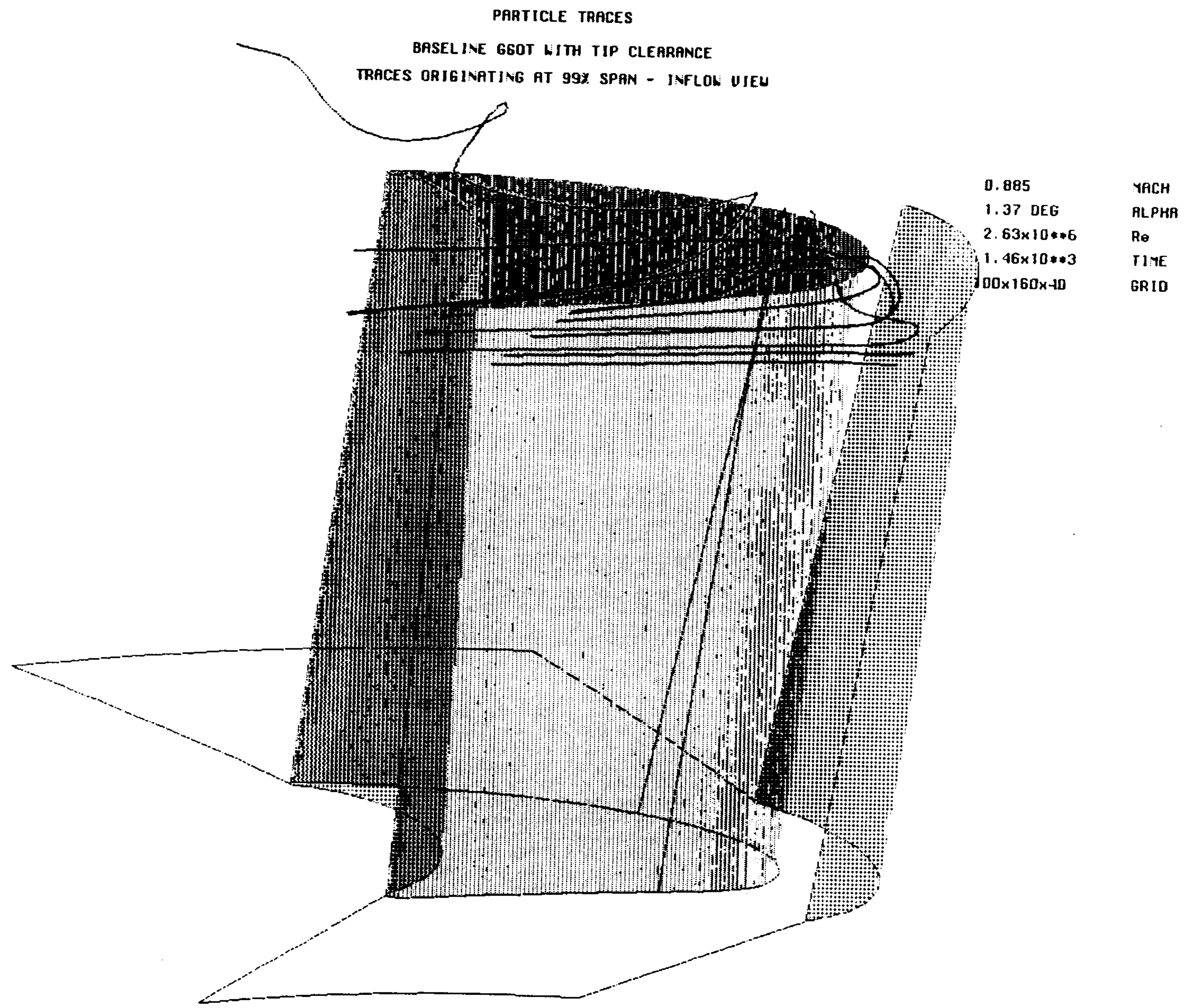
PARTICLE TRACES
BASELINE 660T WITH TIP CLEARANCE
TRACES ORIGINATING AT 99% SPAN - INFLOW VIEW
0.885 MACH
1.37 DEG ALPHA
2.63x10**6 Re
1.46x10**3 TIME
100x160x40 GRID
Scientific Research Associates

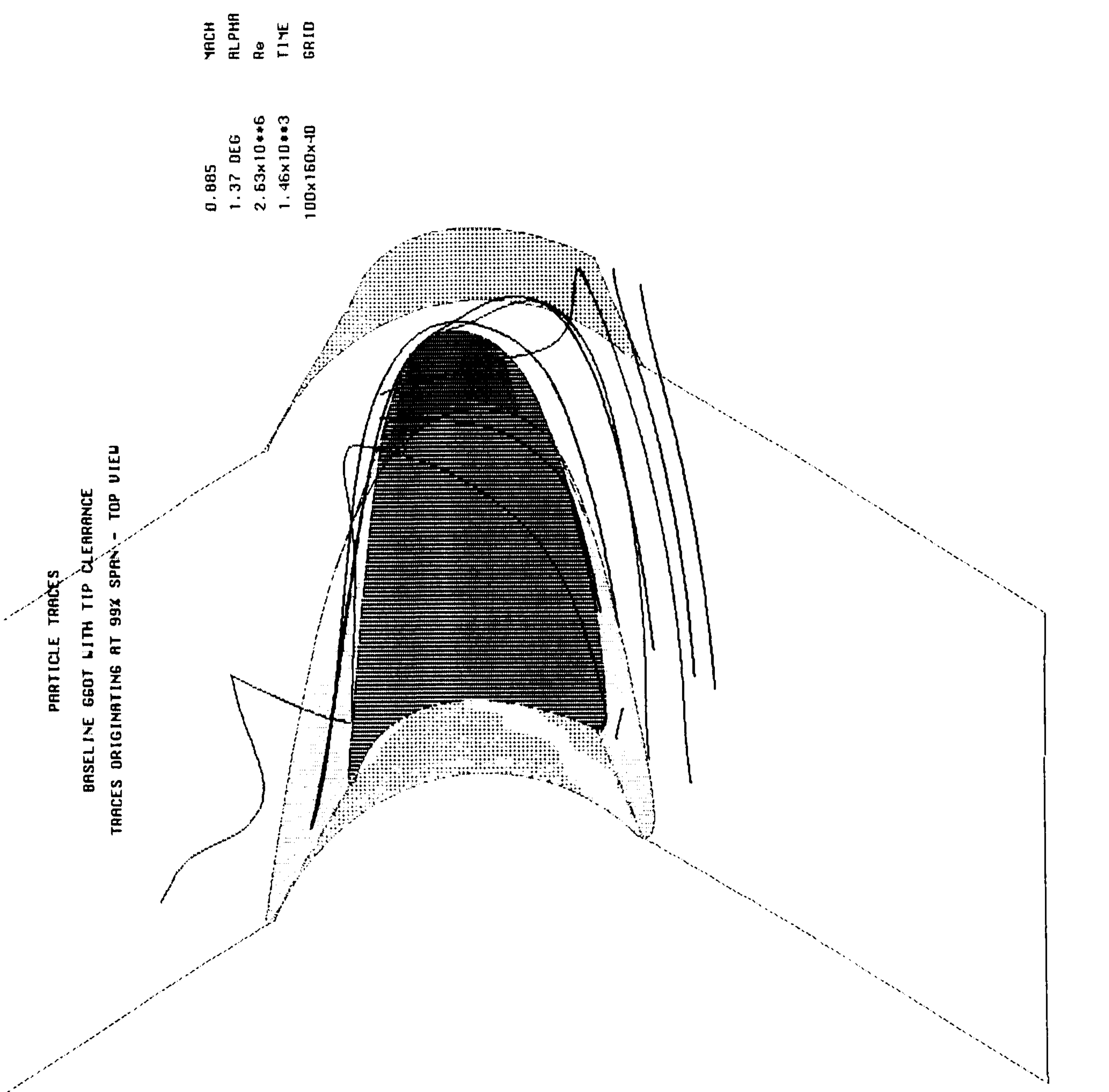

Scientific Research Associates

PARTICLE TRACES

BASELINE G60T WITH TIP CLEARANCE

TRACES ORIGINATING AT 90% SPAN - INFLOW VIEW

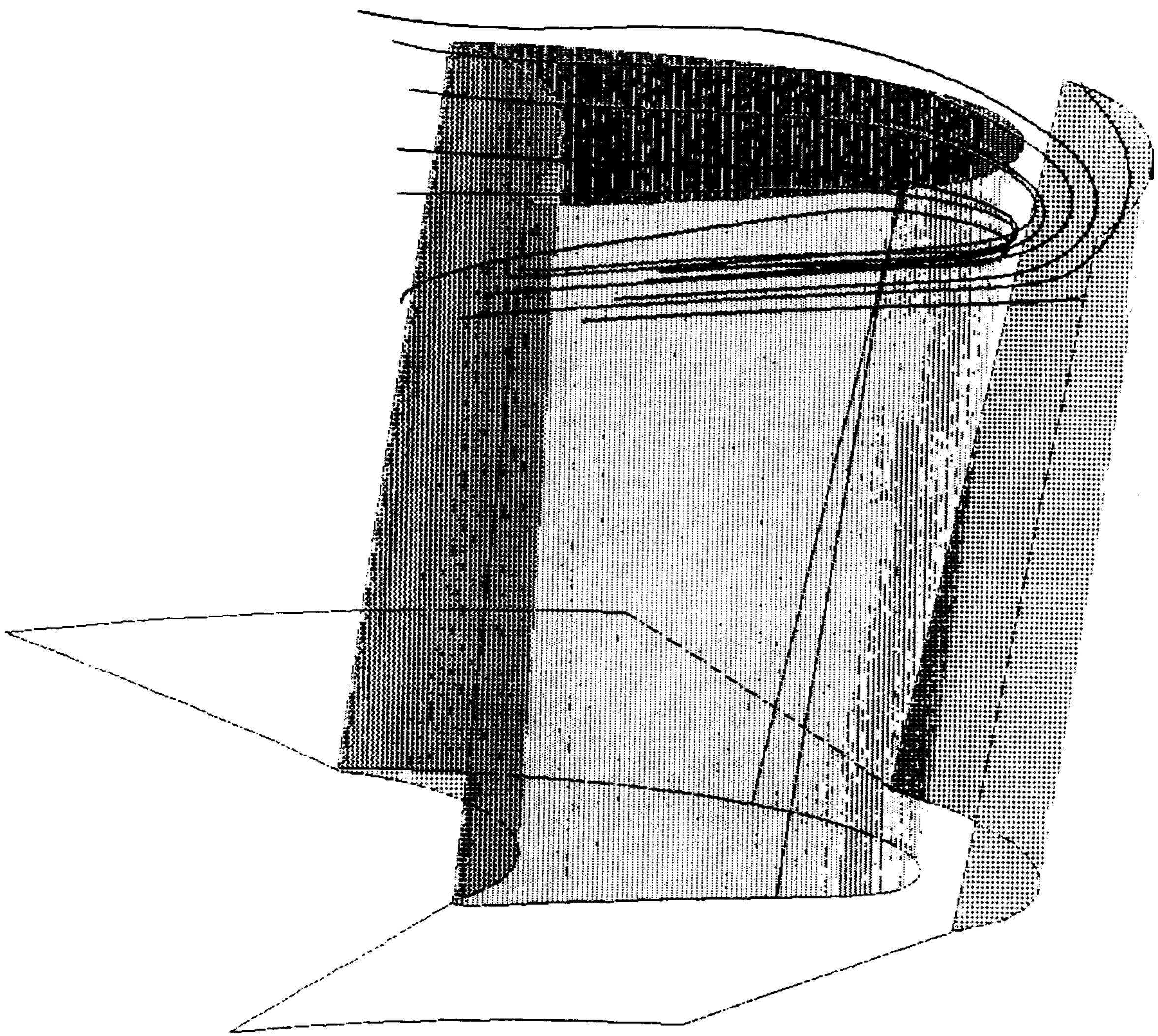

Scientific Research Associates

PARTICLE TRACES

BASELINE G6OT WITH TIP CLEARANCE

TRACES ORIGINATING AT 90% SPAN - TOP VIEW

0.885	MACH
1.37 DEG	ALPHA
2.63x10**6	Re
1.46x10**3	TIME
100x160x40	GRID

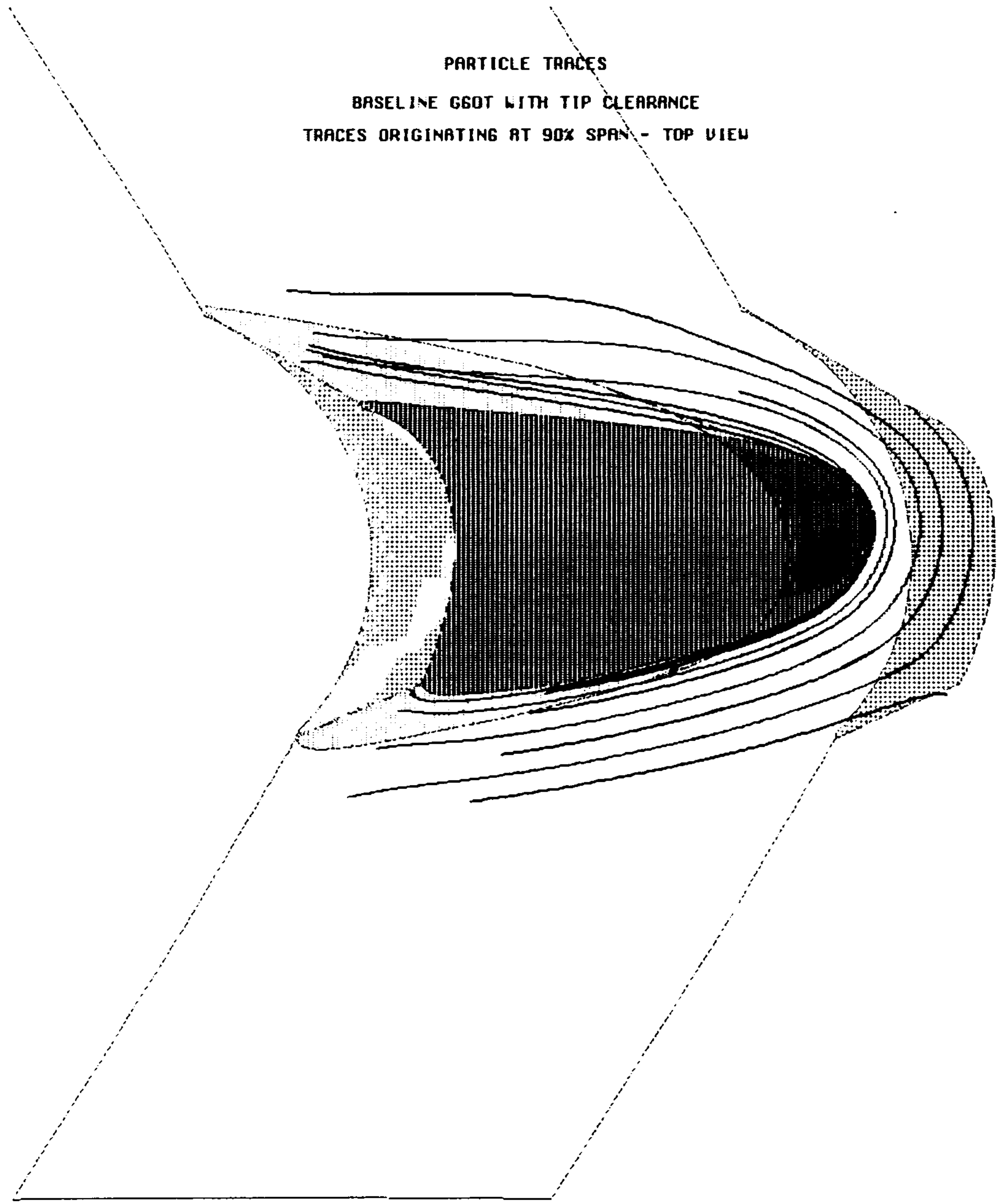

Scientific Research Associates

CONCLUSIONS AND FUTURE WORK

- CLEARANCE FLOW DETAILS PREDICTED
- BLADE PRESSURE DISTRIBUTIONS - BLOCKAGE EFFECTS
- SPANWISE VARIATION OF TOTAL PRESSURE LOSS
- FURTHER ANALYSIS OF DATA NECESSARY
    - TIP CLEARANCE FLOW BEHAVIOR
    - SECONDARY FLOW BEHAVIOR
- COORDINATION WITH PRATT AND WHITNEY DESIGN EFFORT

Scientific
Research
Associates

N92-32270

NUMERICAL SIMULATION OF TURBOMACHINERY FLOWS WITH ADVANCED TURBULENCE MODELS

B. Lakshminarayana, R. Kunz, J. Luo, S. Fan
The Pennsylvania State University

A three dimensional full Navier-Stokes (FNS) code is used to simulate complex turbomachinery flows. The code incorporates an explicit multistep scheme and solves a conservative form of the density averaged continuity, momentum and energy equations in body fitted coordinates. Rotation terms are included for the computation of rotor flows. A compressible low-Reynolds number form of the $k-\epsilon$ turbulence model, and a $q-\omega$ model and an algebraic Reynolds stress model have been incorporated in a fully coupled manner to approximate Reynolds stresses.

The code is used to predict viscous flow field in a backswept transonic centrifugal compressor for which laser two focus data is available. The tip clearance flow, and curvature and rotation induced secondary flows are captured to good accuracy. Solutions which incorporate Reynolds stress model show significant, though not dramatic, differences in predicted secondary flows, wall shear stress and performance parameters, when compared to the $k-\epsilon$ solution.

The code is also utilized to simulate the tip clearance flow in a cascade. An embedded H-grid topology was utilized to resolve the flow physics in the gap. The data and predictions were performed with and without tip clearance, endwall, wall motion. Additionally, both Euler and Navier-Stokes computations were performed. The results indicate that the Navier-Stokes code captures the flow physics accurately, including tip vortex strength, trajectory, loading and interaction of tip clearance flow with the secondary flow.

The code has also been used to predict the two dimensional viscous and thermal flow field in a transonic turbine nozzle with 75° turning, M_1 = 015, M_2 = 0.7 to 1.11, Re = 0.5 - 2 x 10^6, and T_o = 415°K. Good agreement is obtained for pressure distribution, wake and surface heat transfer.

The code has been extended to include unsteady Euler solution for predicting the unsteady flow through a cascade due to incoming wakes, simulating rotor-stator interaction. Unsteady characteristic boundary conditions are specified at inlet and exit. The predicted unsteady surface pressure distribution, unsteady lift and moment, pressure wave propagation in a flat plate due to an incoming gust compares well with the analytical theories and earlier computations. This code will be integrated with a boundary layer code to capture the unsteady viscous flow and heat transfer.

NUMERICAL SIMULATION OF TURBOMACHINERY FLOWS WITH ADVANCED TURBULENCE MODELS

B. Lakshminarayana, R. Kunz, J. Luo, S. Fan
The Pennsylvania State University

1. Introduction

2. Technique and Turbulence Models

3. Computation of Transonic Centrifugal Compressor Flow Field

4. Computation of Tip Clearance Flows in Cascades

5. Computation of Aerothermal Field in a Transonic Nozzle

6. Simulation of Rotor/Stator Interaction

7. Conclusions

GOVERNING EQUATIONS
(Cartesian)

$$\frac{\partial Q}{\partial t} = -\left(\frac{\partial E}{\partial x} + \frac{\partial F}{\partial y} + \frac{\partial G}{\partial z}\right) + \left(\frac{\partial E_v}{\partial x} + \frac{\partial F_v}{\partial y} + \frac{\partial G_v}{\partial z}\right) + S$$

$$Q = \begin{pmatrix} \rho \\ \rho u \\ \rho v \\ \rho w \\ \rho e_0 \\ \rho k \\ \rho \varepsilon \end{pmatrix}, E = \begin{pmatrix} \rho u \\ \rho uu + p \\ \rho uv \\ \rho uw \\ (\rho e_0 + p)u \\ \rho uk \\ \rho u\varepsilon \end{pmatrix}, F = \begin{pmatrix} \rho v \\ \rho uv \\ \rho vv + p \\ \rho vw \\ (\rho e_0 + p)v \\ \rho vk \\ \rho v\varepsilon \end{pmatrix}, G = \begin{pmatrix} \rho w \\ \rho uw \\ \rho vw \\ \rho ww + p \\ (\rho e_0 + p)w \\ \rho wk \\ \rho w\varepsilon \end{pmatrix},$$

$$E_v = \begin{pmatrix} 0 \\ \tau_{xx} \\ \tau_{xy} \\ \tau_{xz} \\ u\tau_{xx} + v\tau_{xy} + w\tau_{xz} - q_x \\ \left(\mu_l + \frac{\mu_l}{Pr_k}\right)\frac{\partial k}{\partial x} \\ \left(\mu_l + \frac{\mu_l}{Pr_\varepsilon}\right)\frac{\partial \varepsilon}{\partial x} \end{pmatrix}, F_v = \begin{pmatrix} 0 \\ \tau_{yx} \\ \tau_{yy} \\ \tau_{yz} \\ u\tau_{yx} + v\tau_{yy} + w\tau_{yz} - q_y \\ \left(\mu_l + \frac{\mu_l}{Pr_k}\right)\frac{\partial k}{\partial y} \\ \left(\mu_l + \frac{\mu_l}{Pr_\varepsilon}\right)\frac{\partial \varepsilon}{\partial y} \end{pmatrix}, G_v = \begin{pmatrix} 0 \\ \tau_{zx} \\ \tau_{zy} \\ \tau_{zz} \\ u\tau_{zx} + v\tau_{zy} + w\tau_{zz} - q_z \\ \left(\mu_l + \frac{\mu_l}{Pr_k}\right)\frac{\partial k}{\partial z} \\ \left(\mu_l + \frac{\mu_l}{Pr_\varepsilon}\right)\frac{\partial \varepsilon}{\partial z} \end{pmatrix}, S = \begin{pmatrix} 0 \\ 0 \\ \rho(\omega^2 y + 2\omega w) \\ \rho(\omega^2 z - 2\omega v) \\ 0 \\ P - \rho\varepsilon + \mathcal{D} \\ (C_1 P - C_2 \rho\varepsilon)\frac{\varepsilon}{k} + \mathcal{E} \end{pmatrix}$$

- Relative velocities, constant rotation rate about x axis, ω. Averaged quantities.
- Energy, $e_0 = \varepsilon + \frac{q^2}{2} - \frac{\omega^2 r^2}{2}$, rothalpy constant along streamlines for inviscid steady state.

Governing Equations - Turbulence Model

- **Density-averaged low-R_e number k-ε, conservative form :**

$$\frac{\partial \hat{Q}}{\partial t} + \left(\frac{\partial \hat{E}_c}{\partial \xi} + \frac{\partial \hat{F}_c}{\partial \eta}\right) = \left(\frac{\partial \hat{E}_v}{\partial \xi} + \frac{\partial \hat{F}_v}{\partial \eta}\right) + \hat{S}$$

$$\tilde{k} = \frac{\frac{1}{2}\overline{\rho u_i'' u_i''}}{\bar{\rho}}, \quad \tilde{\varepsilon} = \frac{\overline{\nu\rho \frac{\partial u_i''}{\partial x_j}\frac{\partial u_i''}{\partial x_j}}}{\bar{\rho}}, \quad \mu_t = \frac{C_\mu f_\mu \bar{\rho}\, \tilde{k}^2}{\tilde{\varepsilon}},$$

$$\hat{Q} = \frac{1}{J}\begin{pmatrix} \overline{\rho}\tilde{k} \\ \overline{\rho}\tilde{\varepsilon} \end{pmatrix}, \quad \hat{E}_c = \frac{1}{J}\begin{pmatrix} \overline{\rho}\tilde{k}\tilde{U} \\ \overline{\rho}\tilde{\varepsilon}\tilde{U} \end{pmatrix}, \quad \hat{F}_c = \frac{1}{J}\begin{pmatrix} \overline{\rho}\tilde{k}\tilde{V} \\ \overline{\rho}\tilde{\varepsilon}\tilde{V} \end{pmatrix}, \quad \hat{S} = \frac{1}{J}\begin{pmatrix} P - \overline{\rho}\tilde{\varepsilon} + \mathcal{D} \\ (C_1 f_1 P - C_2 f_2 \overline{\rho}\tilde{\varepsilon})\frac{\tilde{\varepsilon}}{\tilde{k}} + \mathcal{E} \end{pmatrix},$$

$$\hat{E}_v = \frac{1}{J}\begin{pmatrix} \left[\mu_l + \frac{\mu_t}{Pr_k}\right]\left[(\nabla\xi\cdot\nabla\xi)\frac{\partial\tilde{k}}{\partial\xi} + (\nabla\xi\cdot\nabla\eta)\frac{\partial\tilde{k}}{\partial\eta}\right] \\ \left[\mu_l + \frac{\mu_t}{Pr_\varepsilon}\right]\left[(\nabla\xi\cdot\nabla\xi)\frac{\partial\tilde{\varepsilon}}{\partial\xi} + (\nabla\xi\cdot\nabla\eta)\frac{\partial\tilde{\varepsilon}}{\partial\eta}\right] \end{pmatrix}, \quad \hat{F}_v = \frac{1}{J}\begin{pmatrix} \left[\mu_l + \frac{\mu_t}{Pr_k}\right]\left[(\nabla\eta\cdot\nabla\xi)\frac{\partial\tilde{k}}{\partial\xi} + (\nabla\eta\cdot\nabla\eta)\frac{\partial\tilde{k}}{\partial\eta}\right] \\ \left[\mu_l + \frac{\mu_t}{Pr_\varepsilon}\right]\left[(\nabla\eta\cdot\nabla\xi)\frac{\partial\tilde{\varepsilon}}{\partial\xi} + (\nabla\eta\cdot\nabla\eta)\frac{\partial\tilde{\varepsilon}}{\partial\eta}\right] \end{pmatrix}$$

Coakley's q-ω model

- $q=\sqrt{k}$, $\omega=\varepsilon/k$
- $\mu_t=c_\mu f_\mu \rho q^2/\omega$

  $c_\mu=0.09$

  $f_\mu=1-\exp(-\alpha R)$

  $\alpha=0.02$

  $R=\frac{qy}{\nu}$

- q-equation

$$\frac{\partial(\rho q)}{\partial t}+\frac{\partial(\rho q u_j)}{\partial x_j}=\frac{\partial}{\partial x_j}[(\mu+\mu_t/Pr_q)\frac{\partial q}{\partial x_j}]$$

$$+\frac{1}{2}(c_\mu f_\mu \frac{S}{\omega^2}-\frac{2}{3}\frac{f_\mu}{\omega}-1)\rho\omega q$$

$$S=(\frac{\partial u_i}{\partial x_j}+\frac{\partial u_j}{\partial x_i})\frac{\partial u_i}{\partial x_j}-\frac{2}{3}(\frac{\partial u_k}{\partial x_k})^2$$

$Pr_q=2.0$

- ω-equation

$$\frac{\partial(\rho\omega)}{\partial t}+\frac{\partial(\rho\omega u_j)}{\partial x_j}=\frac{\partial}{\partial x_j}[(\mu+\mu_t/Pr_\omega)\frac{\partial\omega}{\partial x_j}]$$

$$+[c_1(c_\mu\frac{S}{\omega^2}-\frac{2}{3}\frac{f_\mu}{\omega})-c_2]\rho\omega^2$$

$c_1 = 0.5f_\mu + 0.055$

$c_2 = 0.833$

$Pr_\omega = 2.0$

$Pr_t = 0.9$

The above equations are in Favre-averaged form

In the fully turbulent region [$Y^+ = 0(10^2)$], a compressible extension to the high Reynolds number form of the ARSM due to Galmes and Lakshminarayana (1984) is adopted:

$$-\overline{\rho u_i'' u_j''} = -\frac{2}{3}\delta_{ij}\rho k - \rho k T_{ij}$$

where

$$T_{ij} = \frac{R_{ij}(2-C_2)/2 + (P_{ij} - 2P\delta_{ij}/3)(1-C_2)}{P + \rho\epsilon(C_1-1)},$$

$$R_{ik} = -2\omega_p(e_{ipj}\overline{\rho u_k'' u_j''} - e_{kpj}\overline{\rho u_i'' u_j''})$$

$$P_{ij} = (-\overline{\rho u_i'' u_k''}\frac{\partial u_j}{\partial x_k} - \overline{\rho u_j'' u_k''}\frac{\partial u_i}{\partial x_k}),\ 2P = P_{ii}$$

where $C_1 = 1.5$, $C_2 = 0.6$.

In the fully turbulent region [$Y^+ = 0(10^2)$], a compressible extension to the high Reynolds number form of the ARSM due to Galmes and Lakshminarayana (1984) is adopted:

$$-\overline{\rho u_i'' u_j''} = -\frac{2}{3}\delta_{ij}\rho k - \rho k T_{ij}$$

where

$$T_{ij} = \frac{R_{ij}(2-C_2)/2 + (P_{ij} - 2P\delta_{ij}/3)(1-C_2)}{P + \rho\epsilon(C_1-1)},$$

$$R_{ik} = -2\omega_p(e_{ipj}\overline{\rho u_k'' u_j''} - e_{kpj}\overline{\rho u_i'' u_j''})$$

$$P_{ij} = (-\overline{\rho u_i'' u_k''}\frac{\partial u_j}{\partial x_k} - \overline{\rho u_j'' u_k''}\frac{\partial u_i}{\partial x_k}),\ 2P = P_{ii}$$

where $C_1 = 1.5$, $C_2 = 0.6$.

RKCC Code

.Explicit Multistage, Conservative, Compressible Formulation

.Generalized Coordinates; 2-D, 3-D, Unsteady; ----> Turbomachinery (Rotation Periodic B.C.)

.Coupled Compressible Low-Reynolds-Number K-ε Model, q-ω Model, ARSM Model

.FNS + Full Turbulent KE Production Term

.IRS for 2-D

.Finite Diff (Flux Evaluation = Cell Vertex Finite Volume)

.Characteristic B.C.'s, Embedded H Mesh, Tip Clearance Topologies for Turbomachinery Application

.Eigenvalue & Local Velocity Scaling of Artificial Dissipation

$\dot{m} = 4.0$ Kg/s
$M_{1REL} = 0.8$
$N = 22,363$ RPM
$P_{02}/P_{01} = 4$

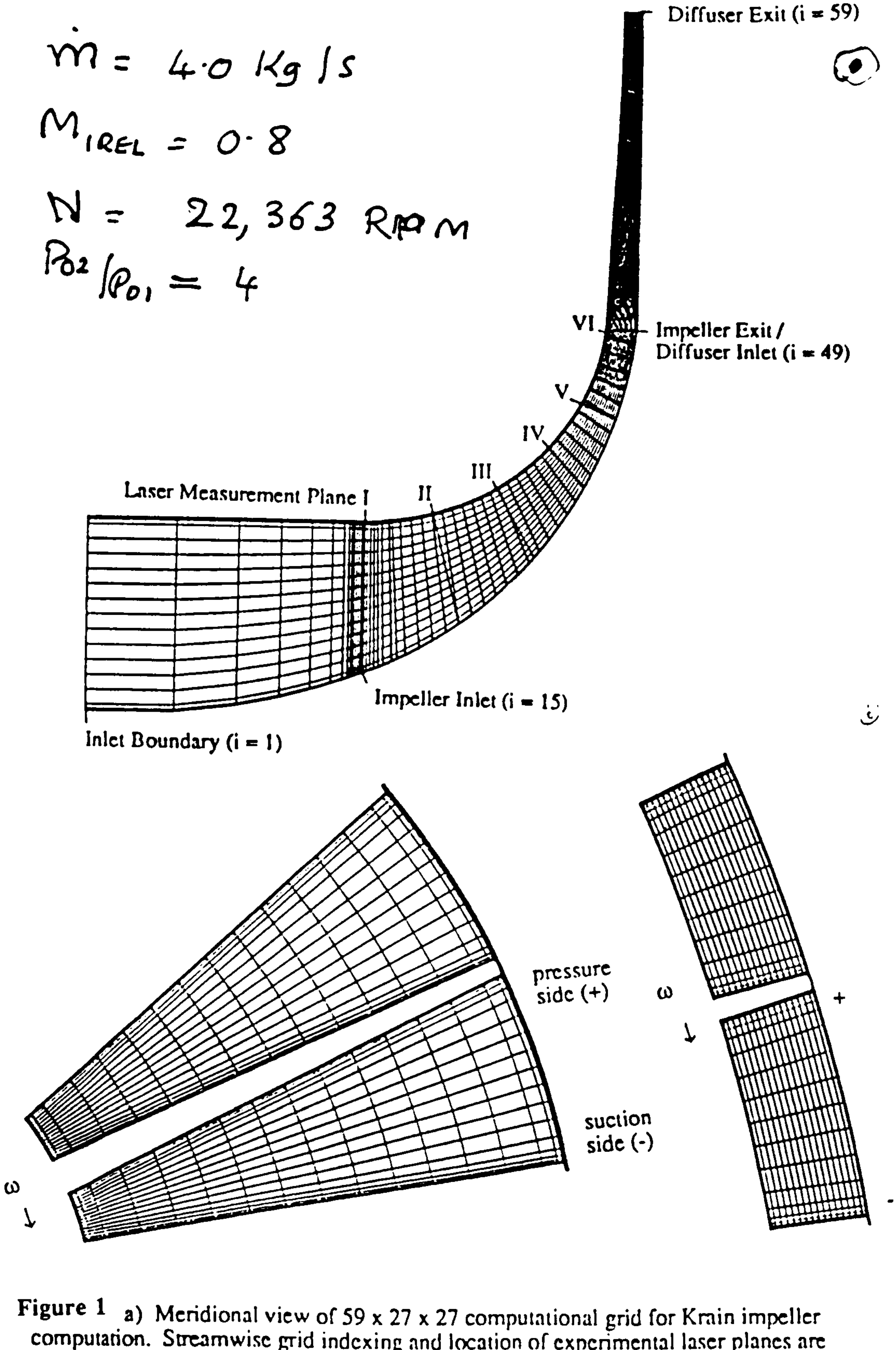

Figure 1 a) Meridional view of 59 x 27 x 27 computational grid for Krain impeller computation. Streamwise grid indexing and location of experimental laser planes are indicated for reference. b) Cross stream views of 59 x 27 x 27 computational grid for Krain impeller computation.

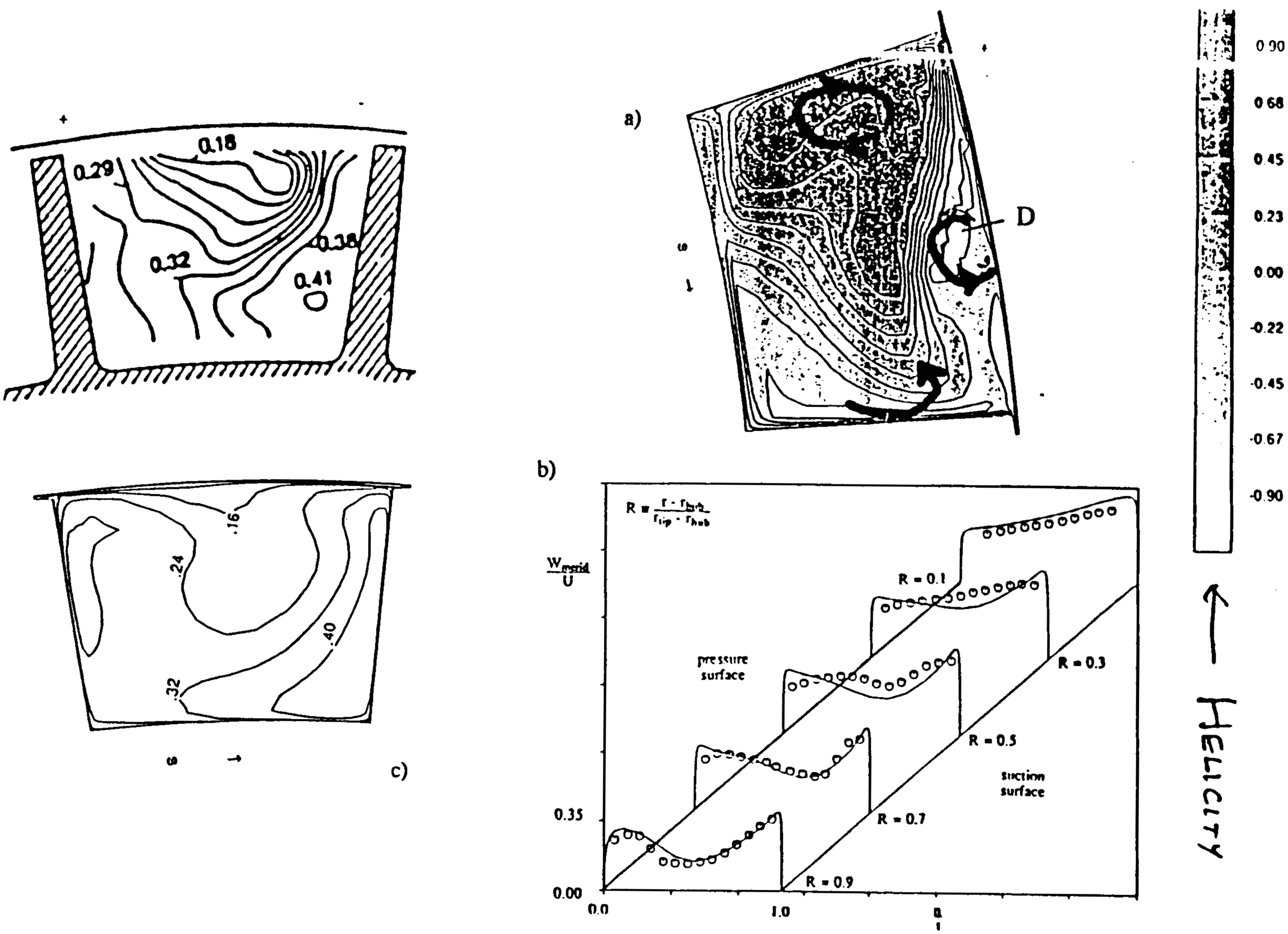

Figure 2. L2F data acquisition Plane IV: a) Computed normalized relative helicity contours. b) Meridional velocity profiles. Experimental measurements (symbols), computed values (solid line). c) Meridional velocity contours. Experimental contours (top), computed contours (bottom).

a)

b)

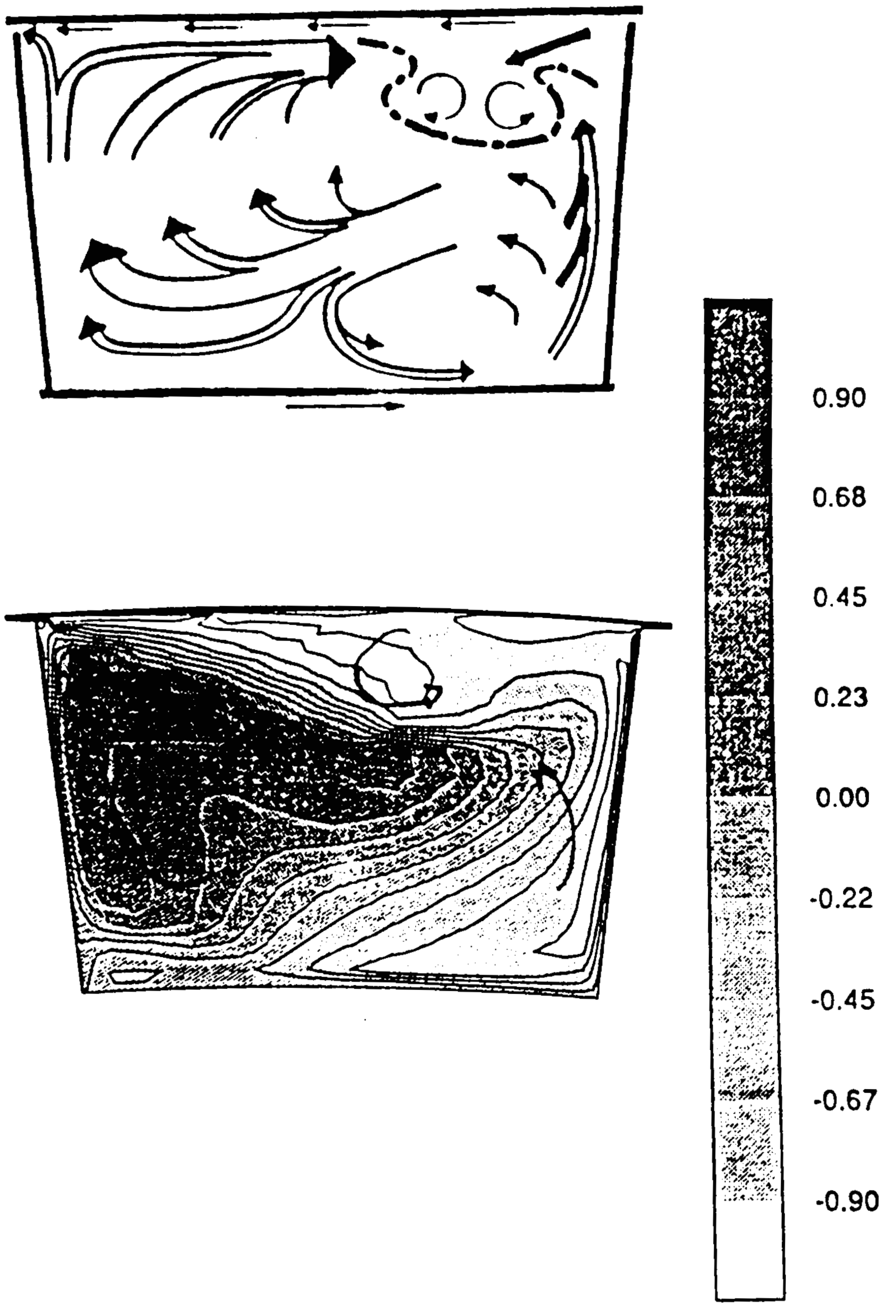

Figure 3 Qualitative representation of physical phenomena contributing to the formation of the wake flow region. a) Representative sketch adapted from Eckardt (1976) and b) computed normalized relative helicity at 68 % chord.

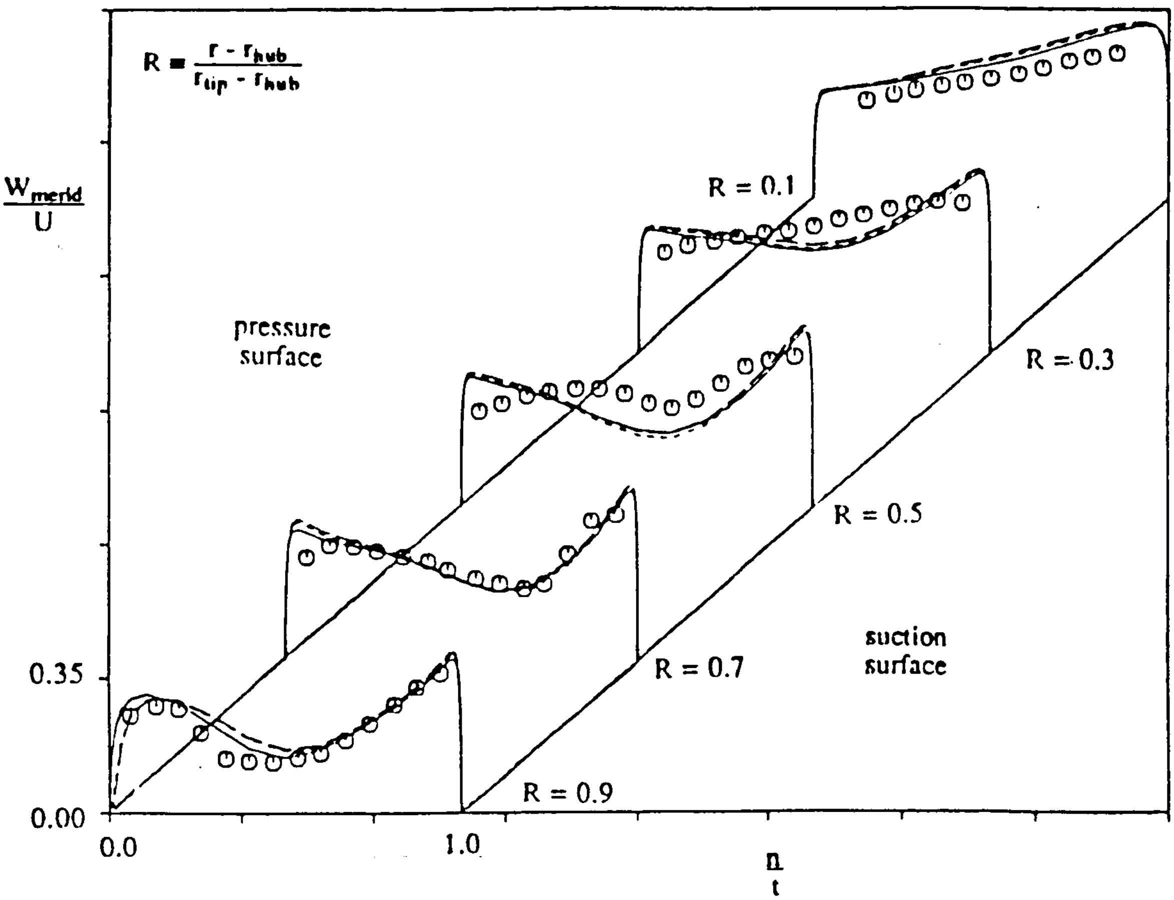

Figure 4 Meridional velocity profiles at L2F data acquisition Plane IV. Comparison of solutions using three turbulence models : low Reynolds number k-ε model (solid), k-ε/ARS model, $R_{ij} = 0$ (long dash), k-ε/ARS model, $R_{ij} \neq 0$ (short dash).

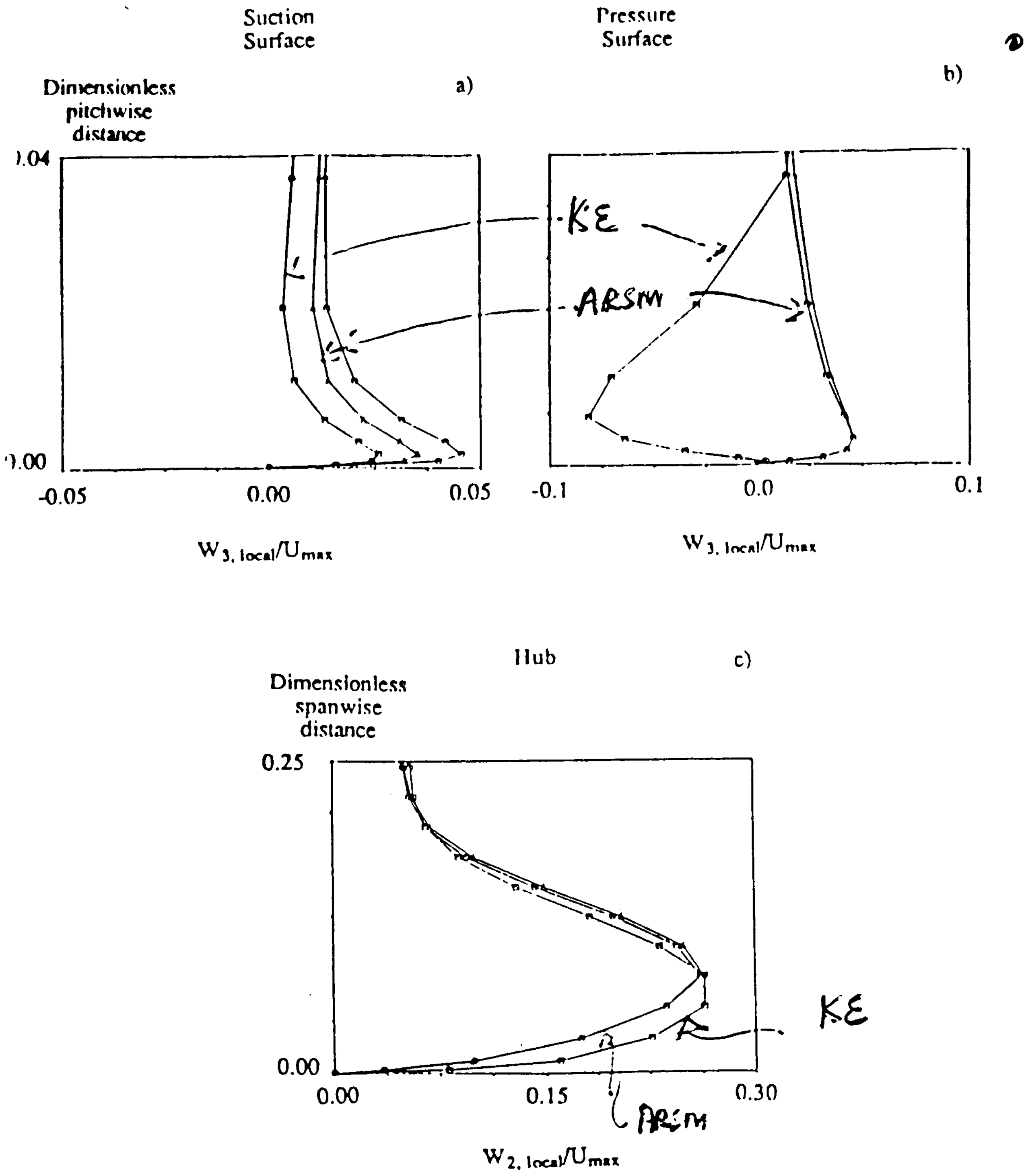

Figure 5 Near wall relative radial and crossflow velocity profiles at 90 % chord. a) midspan on suction surface, b) midspan on pressure surface, c) mid passage on hub. Comparison of solutions using three turbulence models : low Reynolds number k-ε model (square), k-ε/ARS model, $R_{ij} = 0$ (circle), k-ε/ARS model, $R_{ij} \neq 0$ (triangle). W_3 is the radial component (+ towards tip), W_2 is the relative circumferential component (+ towards pressure surface)

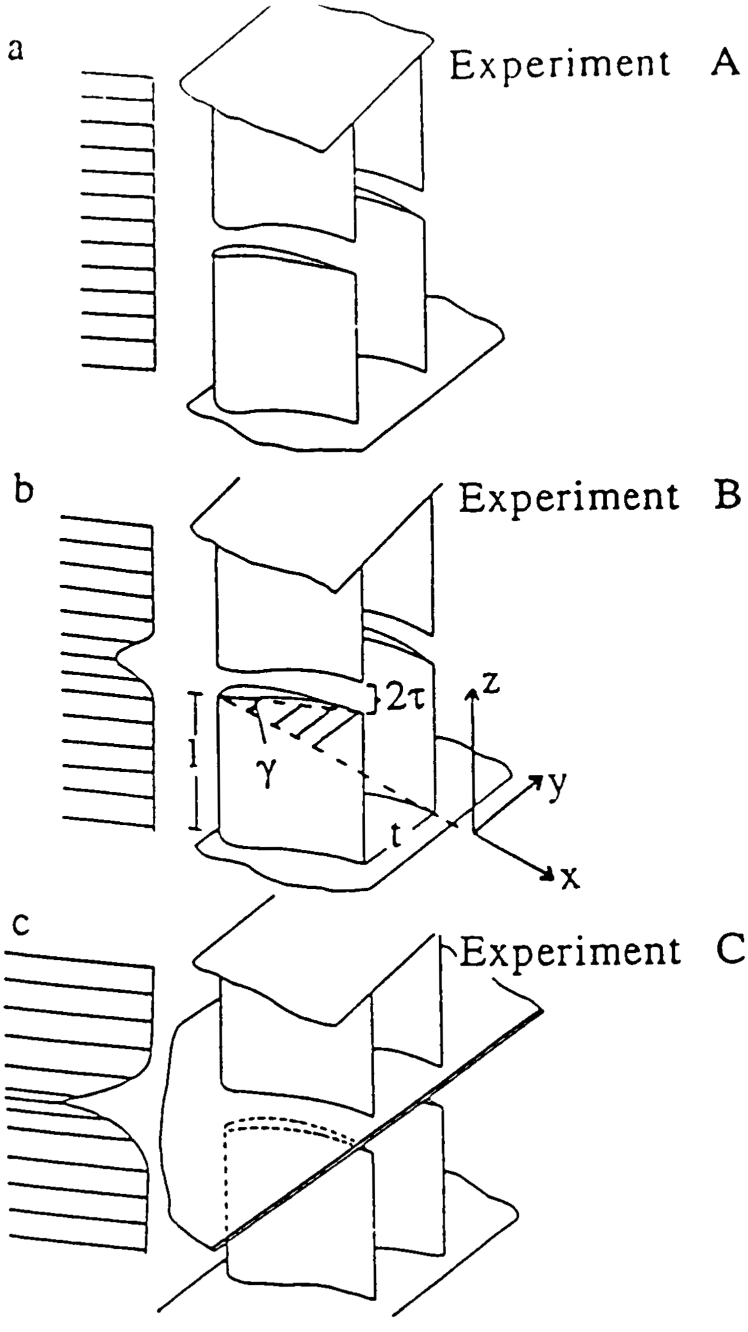

Figure 6 Schematic of experimental configurations. (Note: z = 0 is located .04 chord inboard of the cascade symmetry plane [k=nk]. For the cases with clearance, this corresponds to the blade tip [τ/c = .04])

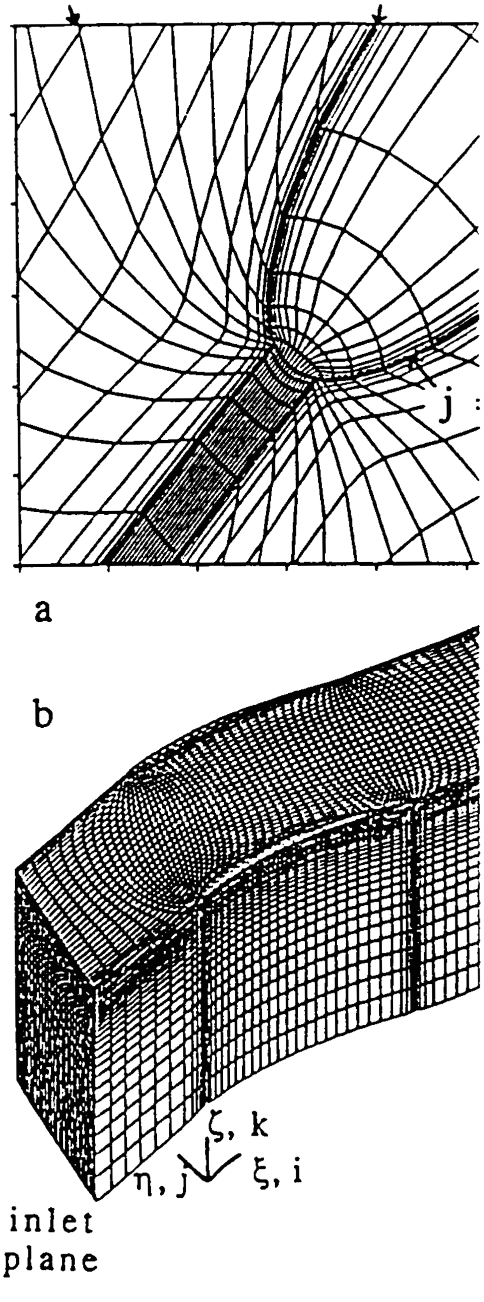

Figure 7. Views of computat nomenclature a) Detail of leading (three-dimensional grid.

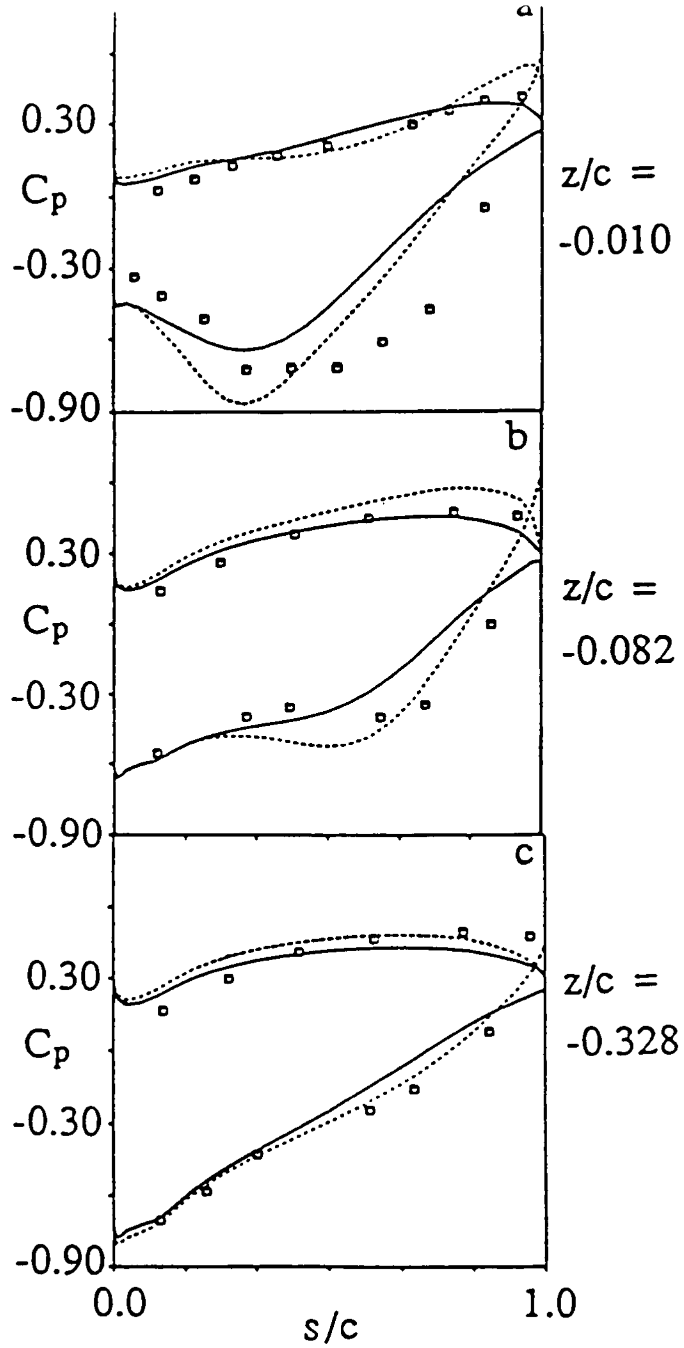

Figure 8. Comparison of computed and measured blade static pressure coefficient at three spanwise locations. Measured values (symbols), Navier-Stokes (solid line), Euler (short dash line).

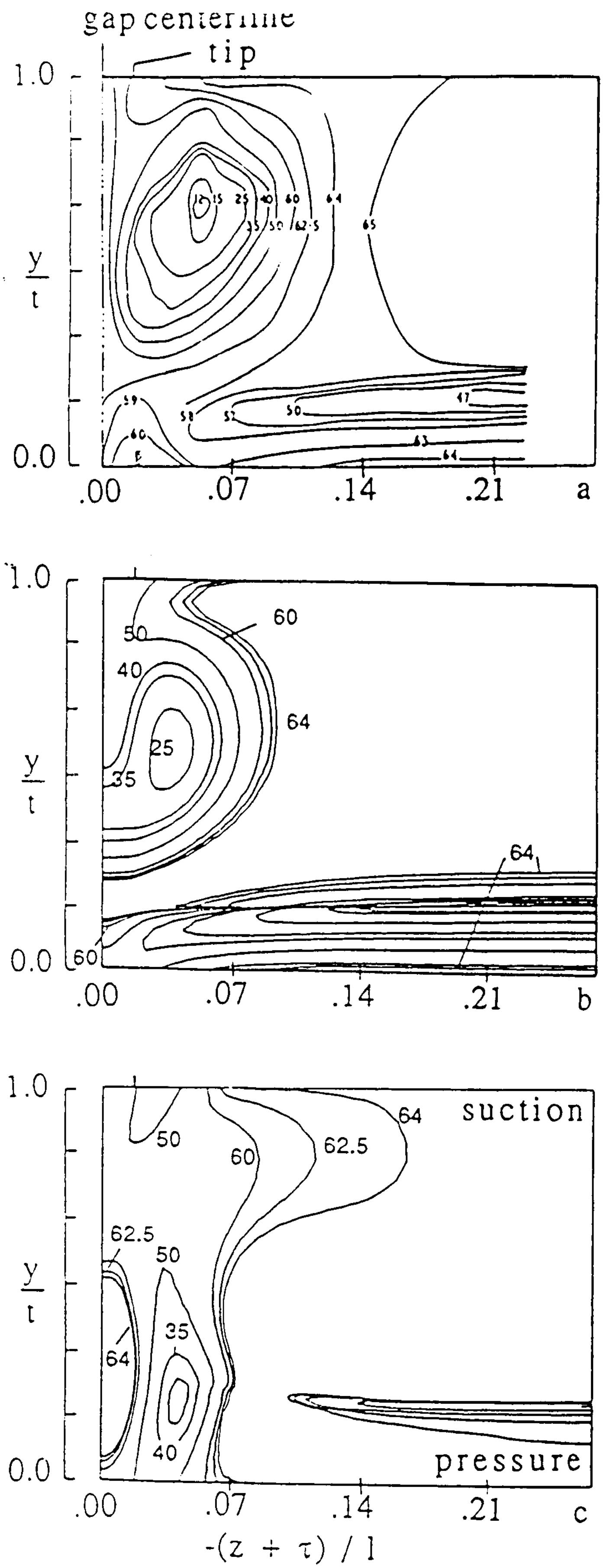

Figure 9 Contours of dynamic pressure ($\rho q^2/2$, in percent of inlet dynamic head) at outlet measurement plane. a) Experimental. b) Navier-Stokes. c) Euler.

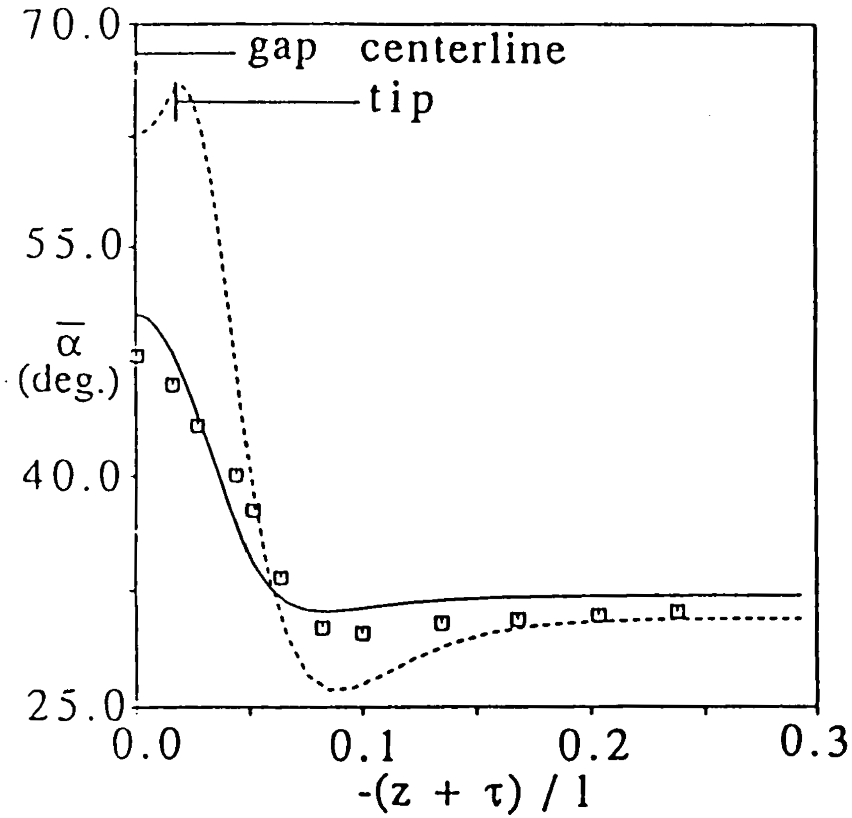

Figure 10 Comparison of computed and measured spanwise distribution of mass-weighted, pitchwise averaged outlet flow angle. Measured values (symbols), Navier-Stokes (solid line), Euler (short dash line).

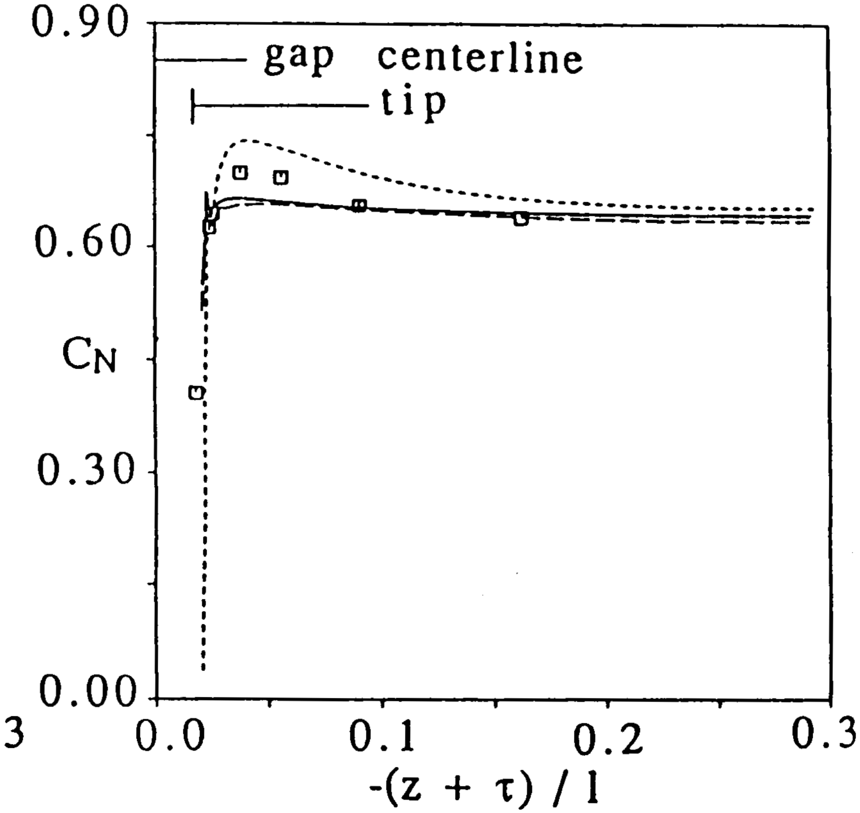

Figure 11 Comparison of computed and measured spanwise distribution of blade normal force coefficient. Measured values (symbols), Navier-Stokes, embedded H-grid (solid line), Navier-Stokes, "pinched" standard H-grid (long dash line), Euler (short dash line).

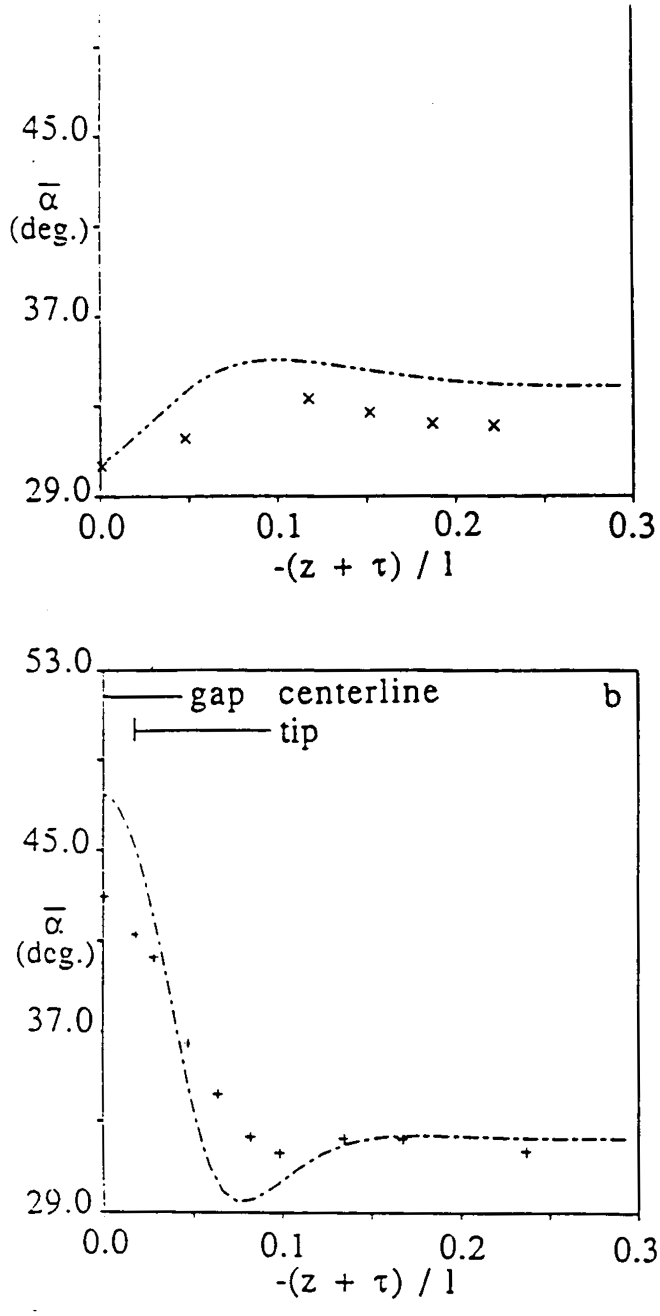

Figure 12 Comparison of computed and measured spanwise distribution of mass-weighted, pitchwise averaged outlet flow angle. Measured values (symbols), Navier-Stokes (line). a) Experiment B, τ/c = 0.00. b) Experiment B, τ/c = 0.04.

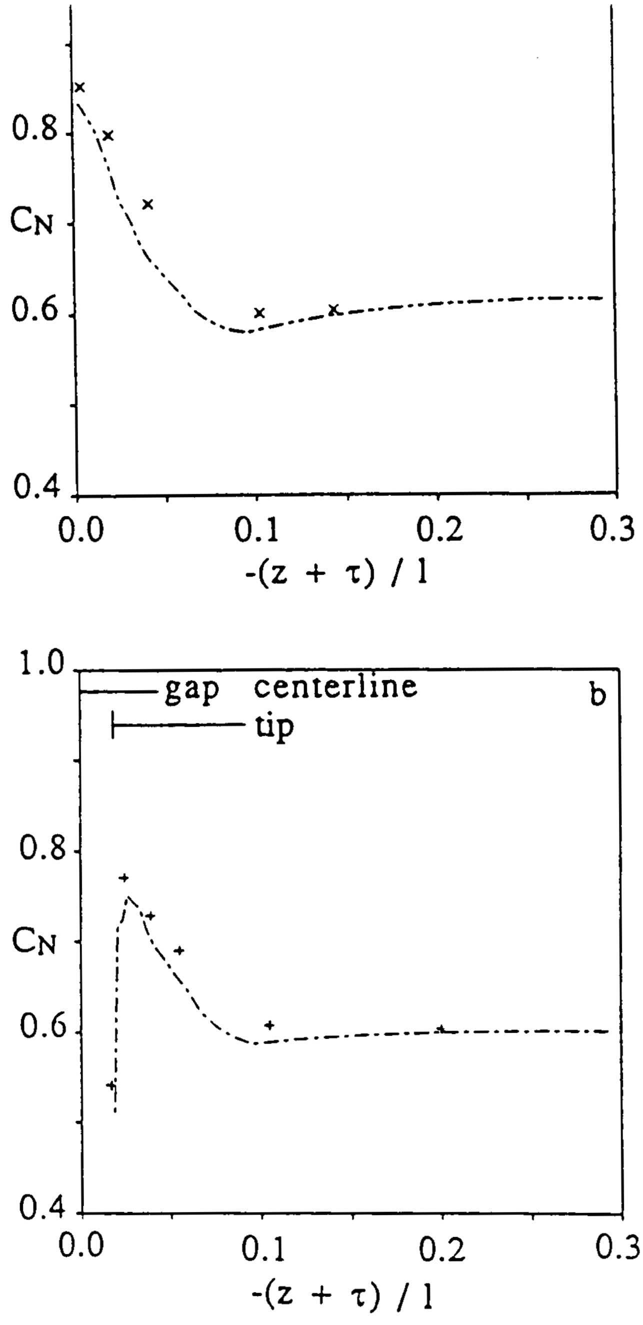

Figure 13 Comparison of computed and measured spanwise distribution of blade normal force coefficient. Measured values (symbols), Navier-Stokes (line). a) Experiment B, τ/c = 0.00. b) Experiment B, τ/c = 0.04.

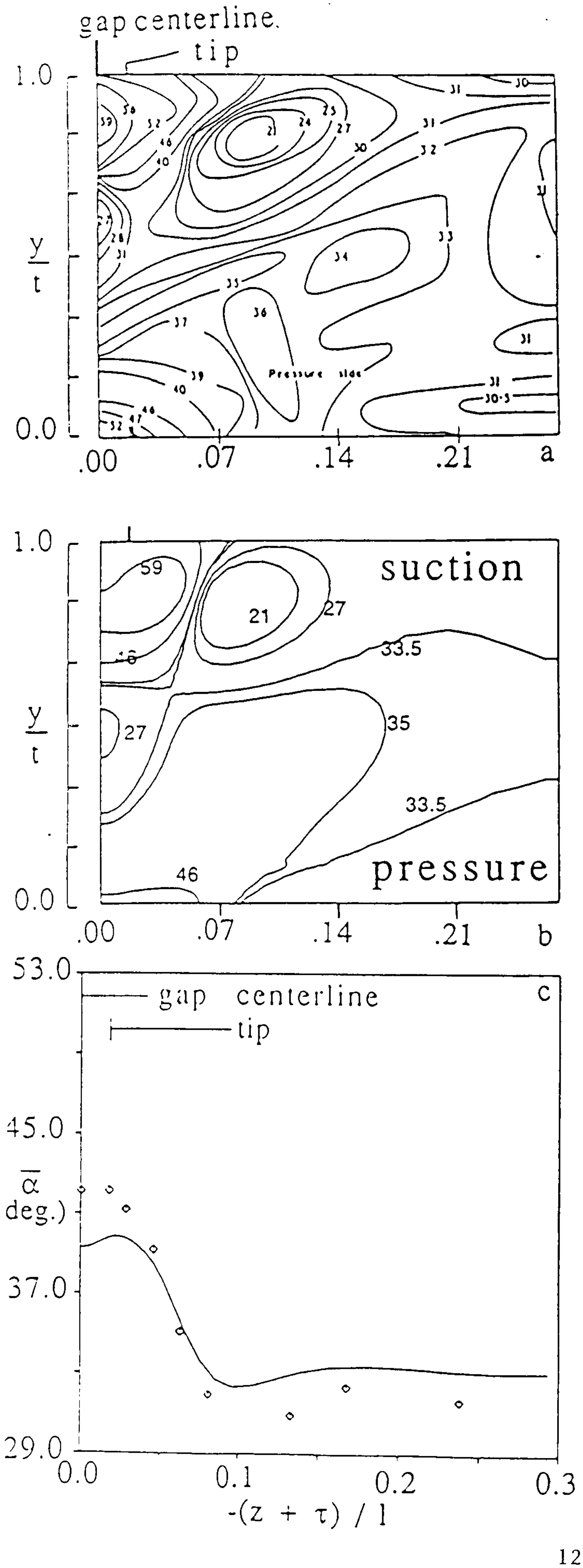

Figure 14 Contours of flow angle at outlet measurement plane for Experiment C, $\tau/c = 0.04$. a) Measured. b) Predicted. c) Comparison of computed and measured spanwise distribution of mass-weighted, pitchwise averaged outlet flow angle for Experiment C, $\tau/c = 0.04$. Measured values (symbols), Navier-Stokes (line).

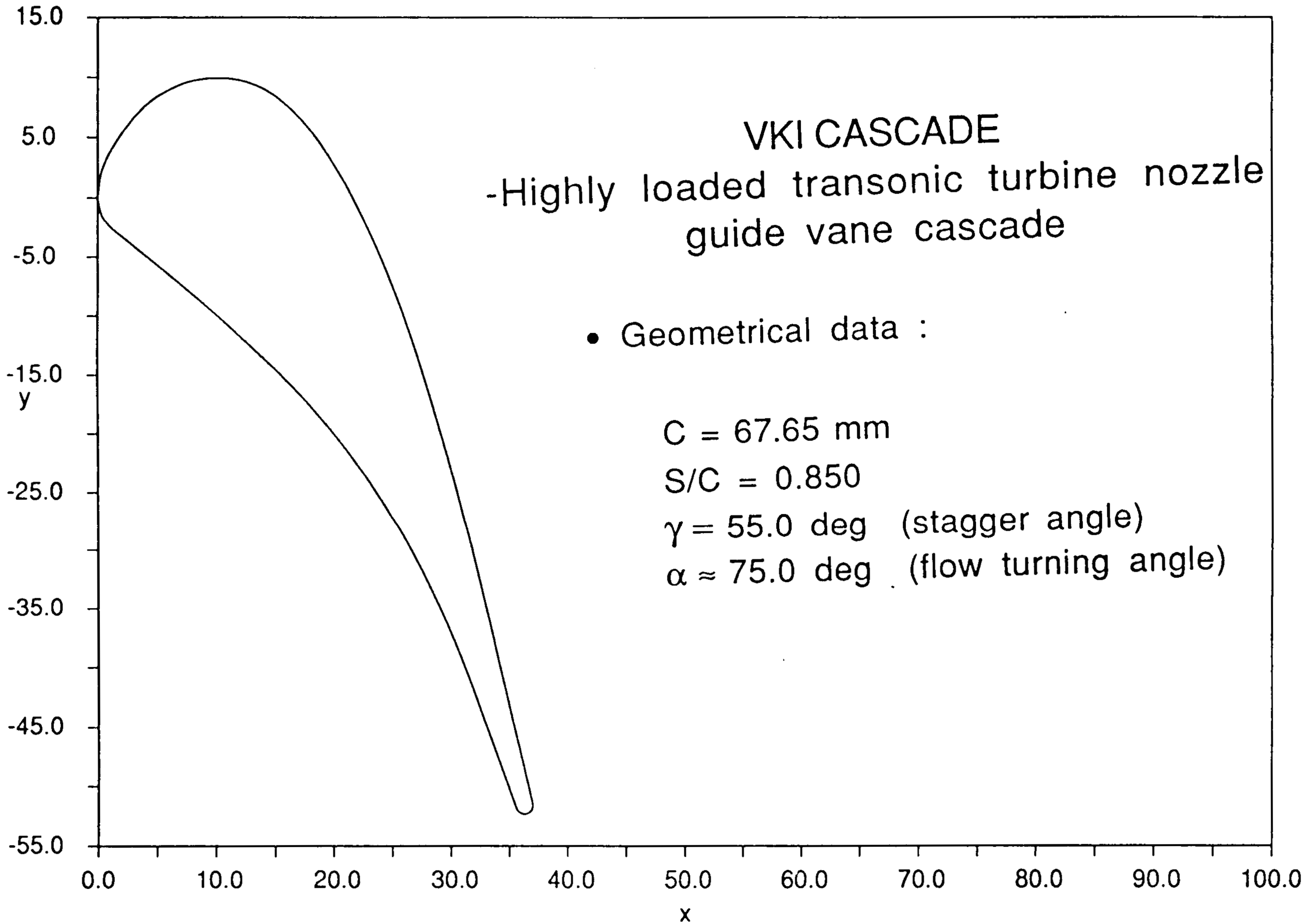
VKI CASCADE
-Highly loaded transonic turbine nozzle guide vane cascade
• Geometrical data :
C = 67.65 mm
S/C = 0.850
γ = 55.0 deg (stagger angle)
α ≈ 75.0 deg (flow turning angle)
15.0
5.0
-5.0
-15.0
y
-25.0
-35.0
-45.0
-55.0
0.0
10.0
20.0
30.0
40.0
50.0
60.0
70.0
80.0
90.0
100.0
x

Figure 15

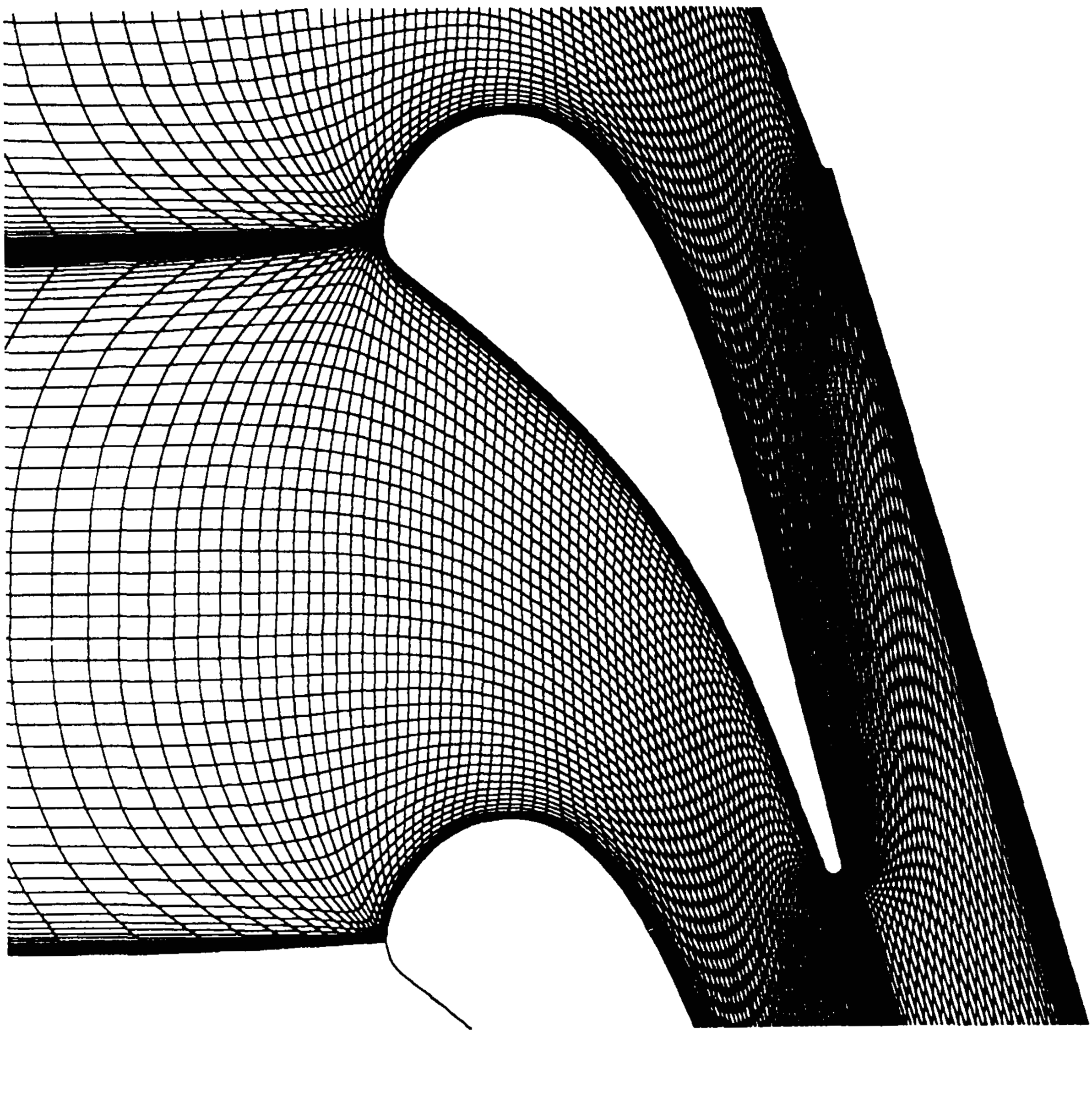

Figure 16 Computational grid system (129*61)

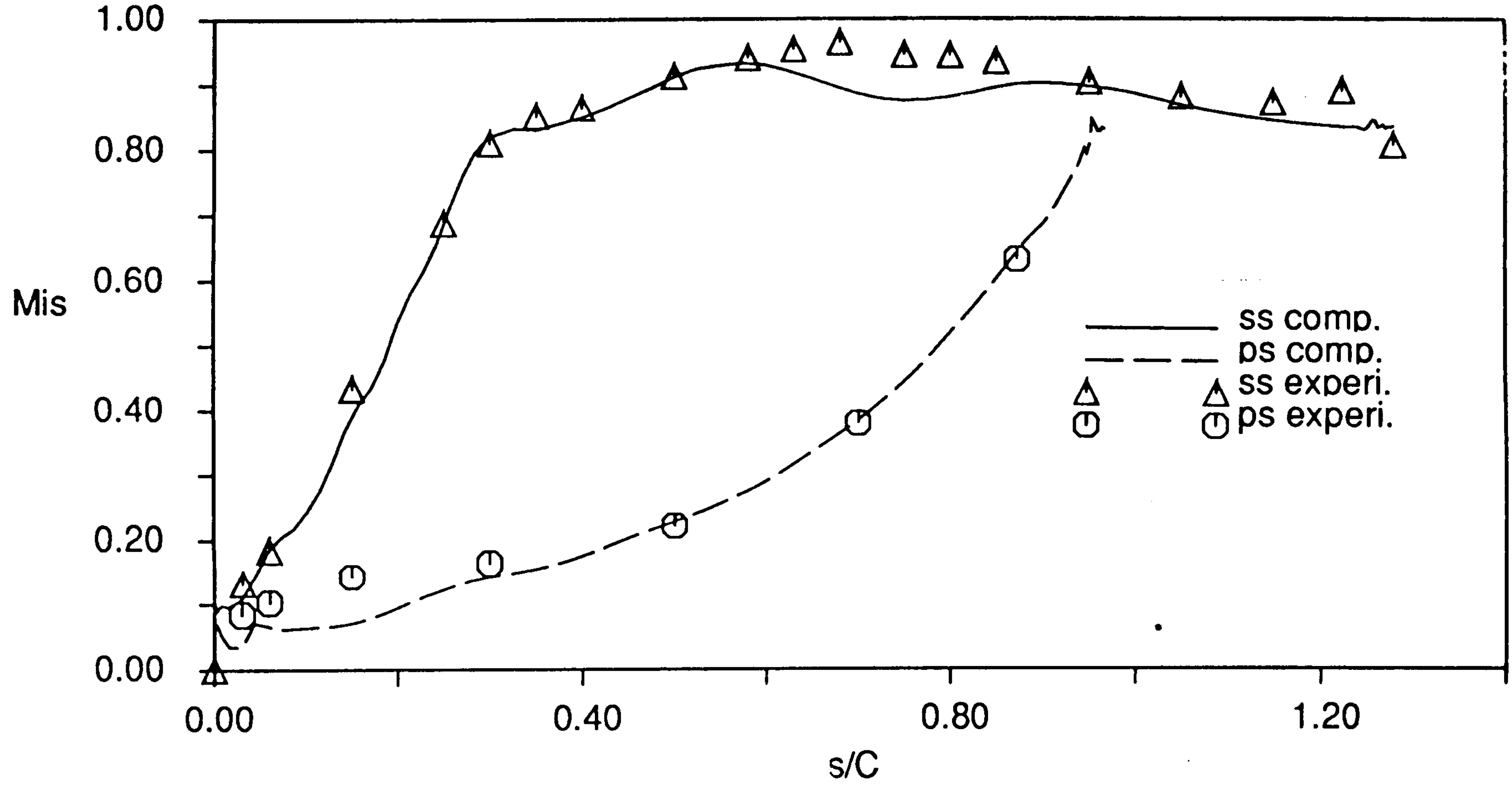

Figure 17 Blade isotropic Mach no. distribution (M_{2is}=0.84, P_{o1}=1.435 Bar, T_{o1}=412K, M_1=0.15, $Re_{,2} \approx$ 1000,000, Tu_∞=1%),

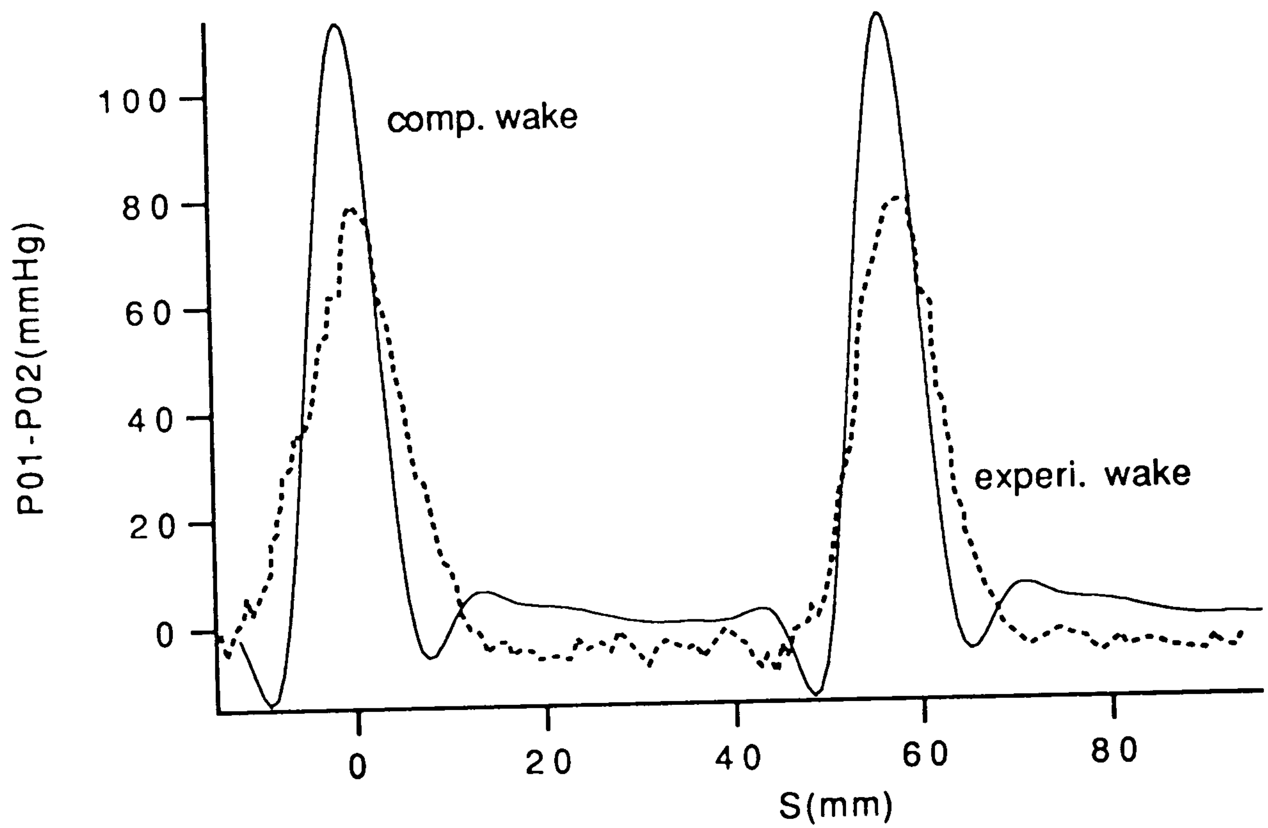

Figure 18 The computed and measured wakes for above case
(0.433 chord length downstream)

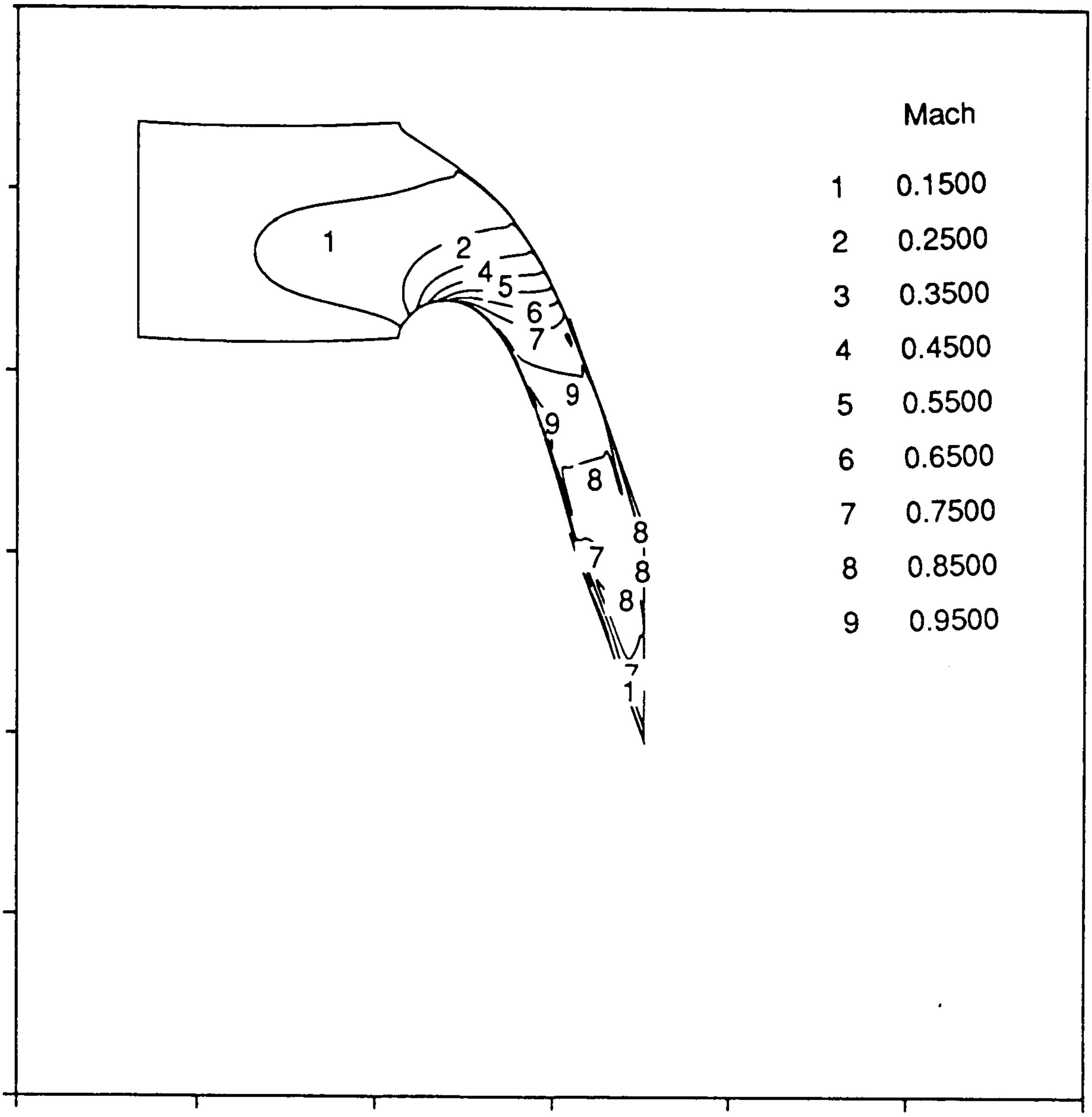

Figure 19 . Mach no. contour for above case

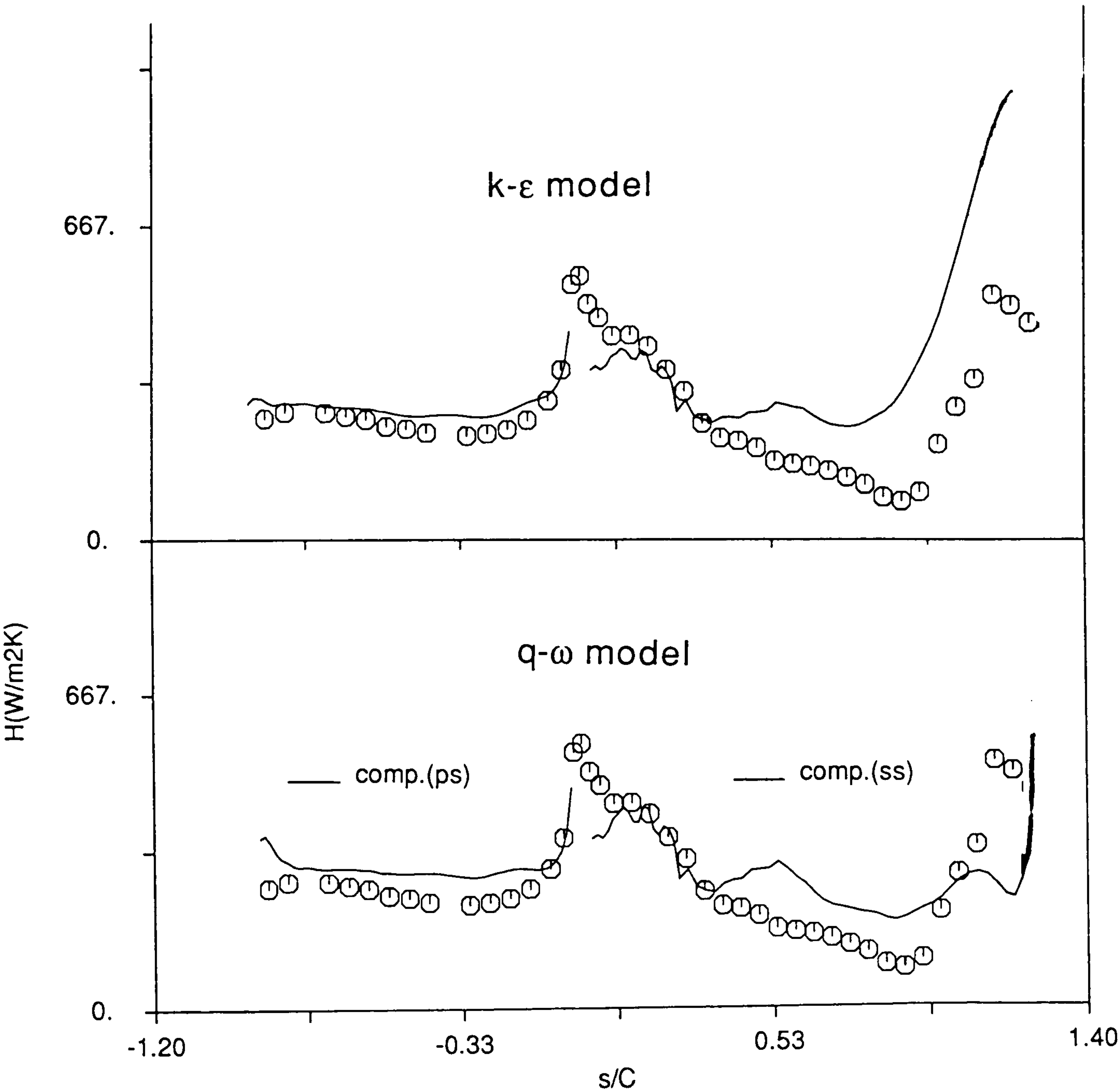

Figure 20 Blade heat transfer
(M_{2is}=0.93,P_{o1}=0.915 Bar, M_1 = 0.15
Tu_{∞}=1%,T_{o1}=403K, $Re_{,2} \approx$ 600,000)

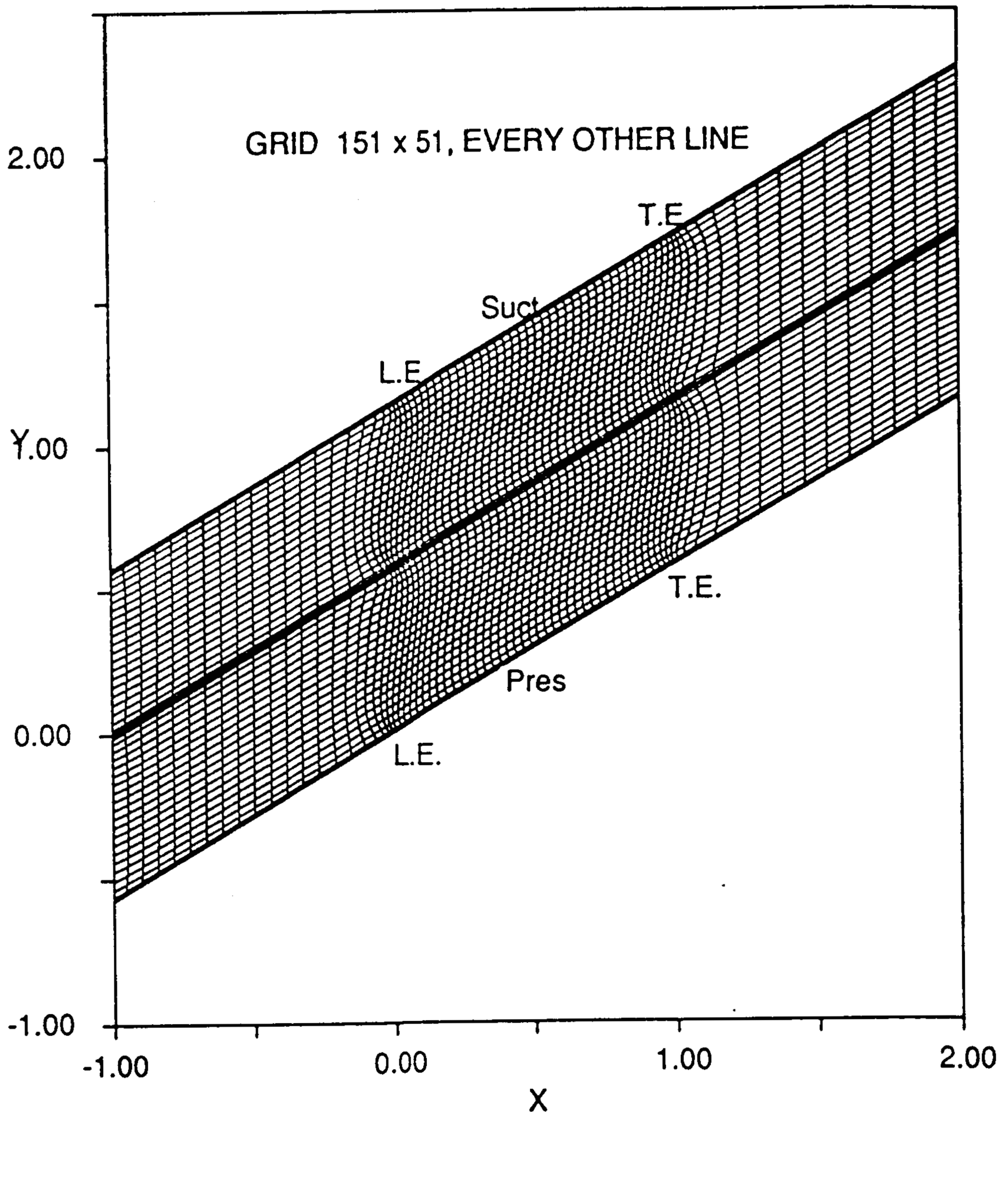

Figure 21 **Computation Grid for a Flat Plate Cascade**

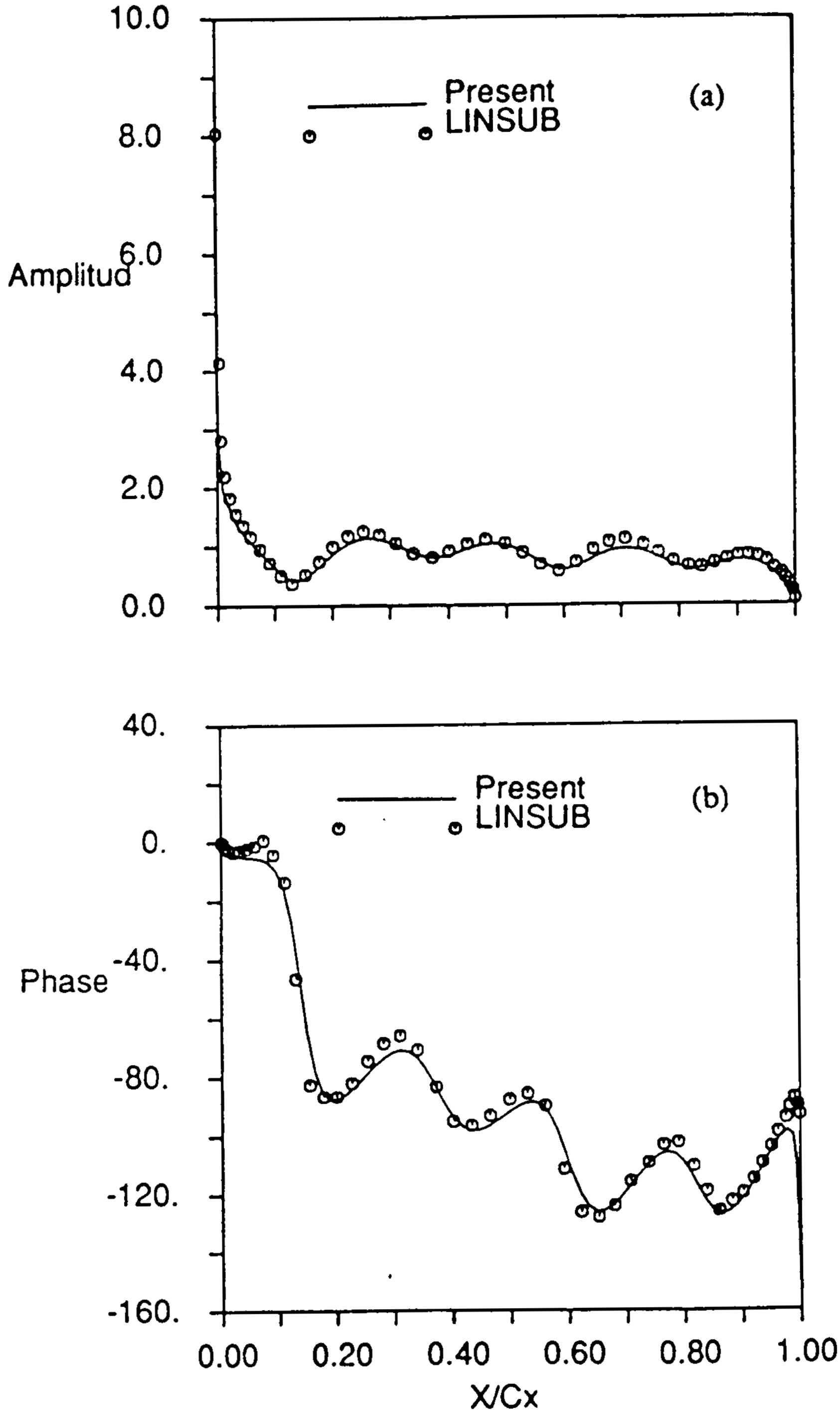

Figure 22 **Unsteady Blade Surface Pressure Jump a) Amplitude, b) Phase Angle**

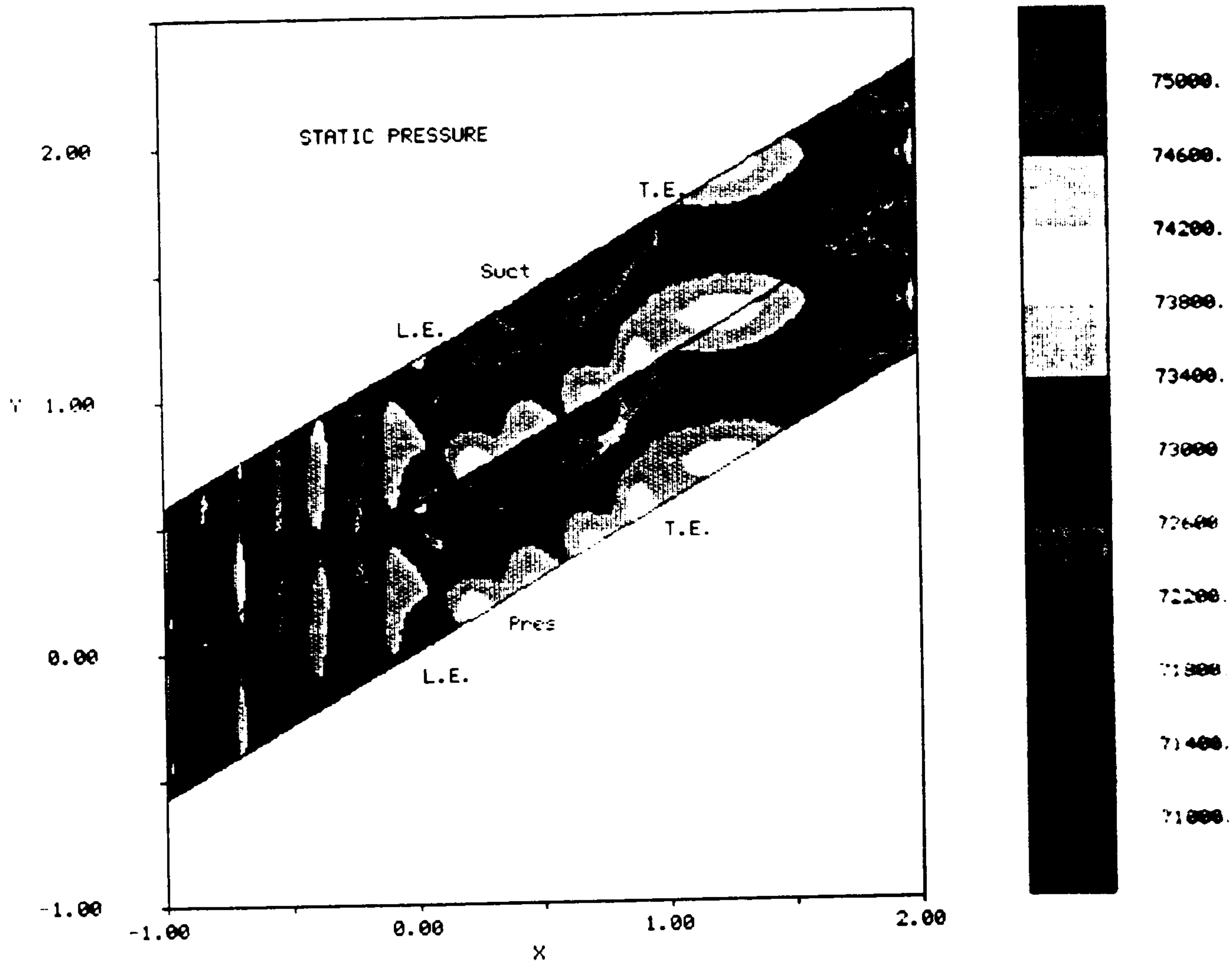

Figure 23 **Unsteady Blade Pressure for a Flat Plate Cascade (at zero steady incidence) with an Incoming Moving Wake (Runga-Kutta Explicit Technique, M=0.7)**

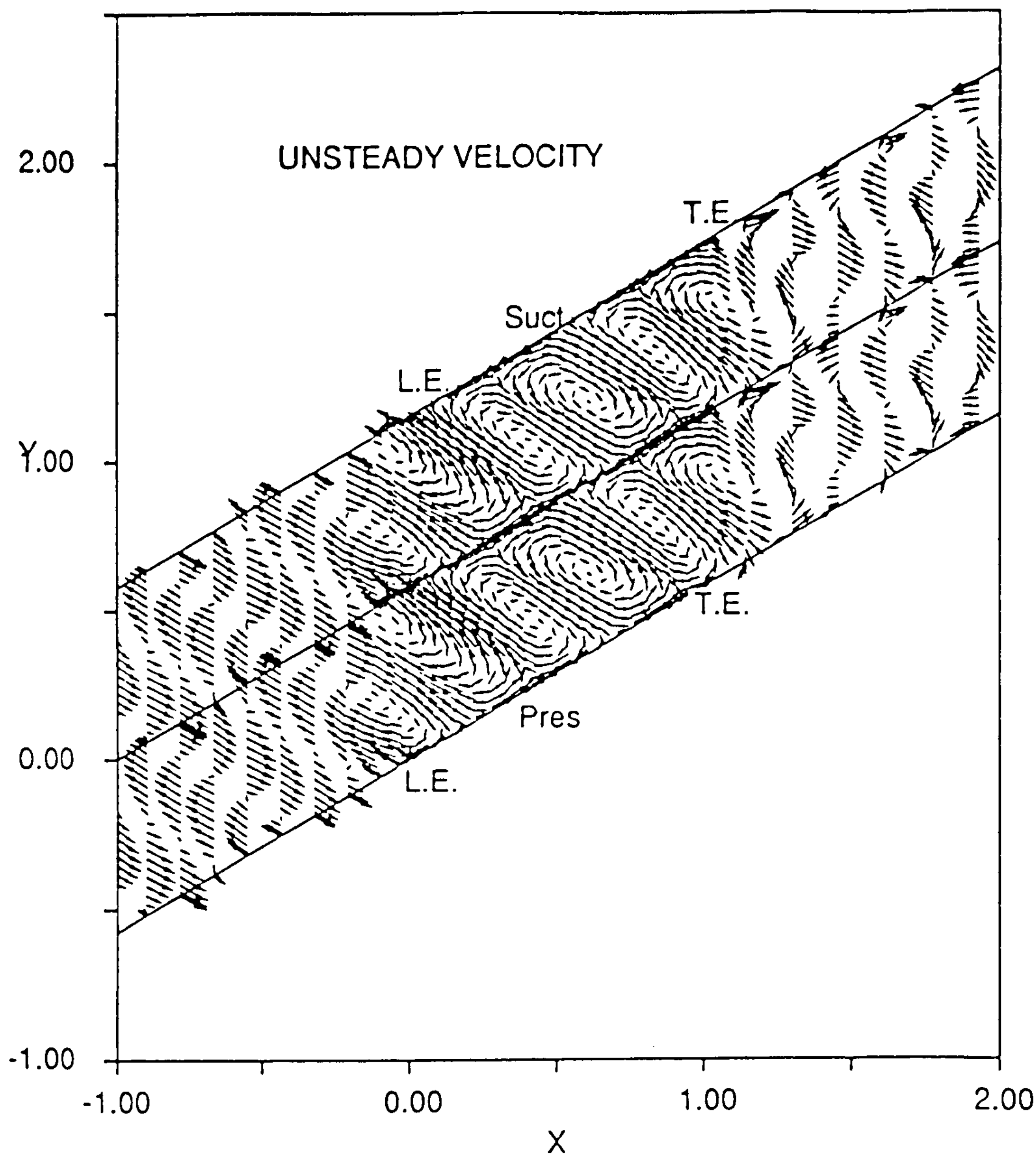

Figure 24 Vector plot of unsteady velocities (mean components is subtracted)

CONCLUSIONS
RKCC

- 3D CODE WITH K-ϵ/ARSM MODEL, GOOD ACCELERATION PROPERTIES AND OPTIMUM ARTIFICIAL DISSIPATION HAS BEEN CODED, VALIDATED AND USED EXTENSIVELY TO PREDICT VISCOUS FLOW FIELD IN SUPERSONIC CASCADE, SUBSONIC CASCADES, LOW SPEED COMPRESSOR, EVOLUTION OF TIP CLEARANCE FLOW, HIGH SPEED CENTRIFUGAL COMPRESSOR FLOW FIELD.

- 3D CODE IS PRESENTLY EXTENDED TO INCLUDE TIME ACCURATE SOLUTION ROTOR/STATOR INTERACTION EFFECTS.

- TURBULENCE MODEL SOURCE TERMS DO NOT AFFECT THE STABILITY OF THE NUMERICAL SCHEME - CONTRARY TO THAT GENERALLY PERCEIVED.

- IMPLICIT TREATMENT OF TURBULENCE SOURCE TERM DID NOT IMPROVE CONVERGENCE RATE.

- NO ADVANTAGE IS NUMERICALLY COUPLING THE GOVERNING EQUATION AND K-ϵ MODEL.

- NEAR WALL TURBULENCE PHYSICS AND THE EFFECT OF ROTATION AND COMPRESSIBILITY PREDICTED ACCURATELY.

•THE EFFECT OF ROTATION AND ENDWALL SECONDARY FLOW IN THE NEAR WAKE, AND EFFECT OF ROTATION ON 3D BLADE BOUNDARY LAYERS ARE CAPTURED ACCURATELY.

•THE SPANWISE DISTRIBUTION OF LOSSES IS PREDICTED WELL AWAY FROM THE ENDWALLS, BUT ONLY FAIR PREDICTION IS ACHIEVED IN THE ENDWALL REGION.

•STAGE PRESSURE RISE, MERIODIONAL VELOCITIES IN A CENTRIFUGAL COMPRESSOR IS PREDICTED TO ENGINEERING ACCURACY. THE CRITICAL ELEMENT IS GRID, FOLLOWED BY TURBULENCE MODELLING.

•THE "PINCHED" H GRID IS THE MOST APPROPRIATE GRID TO USE IN THE TIP CLEARANCE REGION.

•THE CODE ACCURATELY CAPTURES SHOCK WAVE/BOUNDARY LAYER INTERACTION IN A CASCADE, WITH THE EXCEPTION OF REFLECTED WAVES FROM THE SUCTION SURFACE; SHOCK LOSSES ARE PREDICTED WELL.

N92-32271

ABSTRACT

DEVELOPMENT OF A CFD CODE FOR INTERNAL FLOWS IN LIQUID FUILED ENGINES

SUBMITTED TO WORKSHOP FOR COMPUTATIONAL FLUID DYNAMIC APPLICATIONS IN ROCKET PROPULSION

To support the design efforts of engines in which liquid propellants are used, one is often required to analyze incompressible, two-dimensional or axisymmetric flows within ducts and cavities with rotating walls and complicated geometries. The steady-state solution is of interest in most cases.

This code is intended to provide a tool for efficient CFD analysis of such flow problems, taking advantage of the artificial compressibility concept and the Beam-Warming numerical scheme modified for second order accurate, implicit boundary conditions. These concepts ensure a stable, robust, and accurate algorithm due to the reduced speed of sound and the accuracy of the boundary conditions.

The code is dedicated only to two-dimensional or axisymmetric flows with or without swirl. Three-dimensional computation is excluded to increase efficiency and speed.

This paper briefly presents the theory of the code, as well as several benchmark applications with comparison to well known analytical solutions. In all these test cases, the code produced remarkably accurate results.

Youssef Dakhoul, Sverdrup Technology
620 Discovery Drive
Huntsville, AL 35806

DEVELOPMENT OF A CFD CODE FOR INTERNAL FLOWS IN LIQUID FUELED ENGINES

By

Youssef Dakhoul Sverdrup Technology

Presented to

The Tenth Workshop for CFD Applications in Rocket Propulsion
MSFC April 1992

Sverdrup

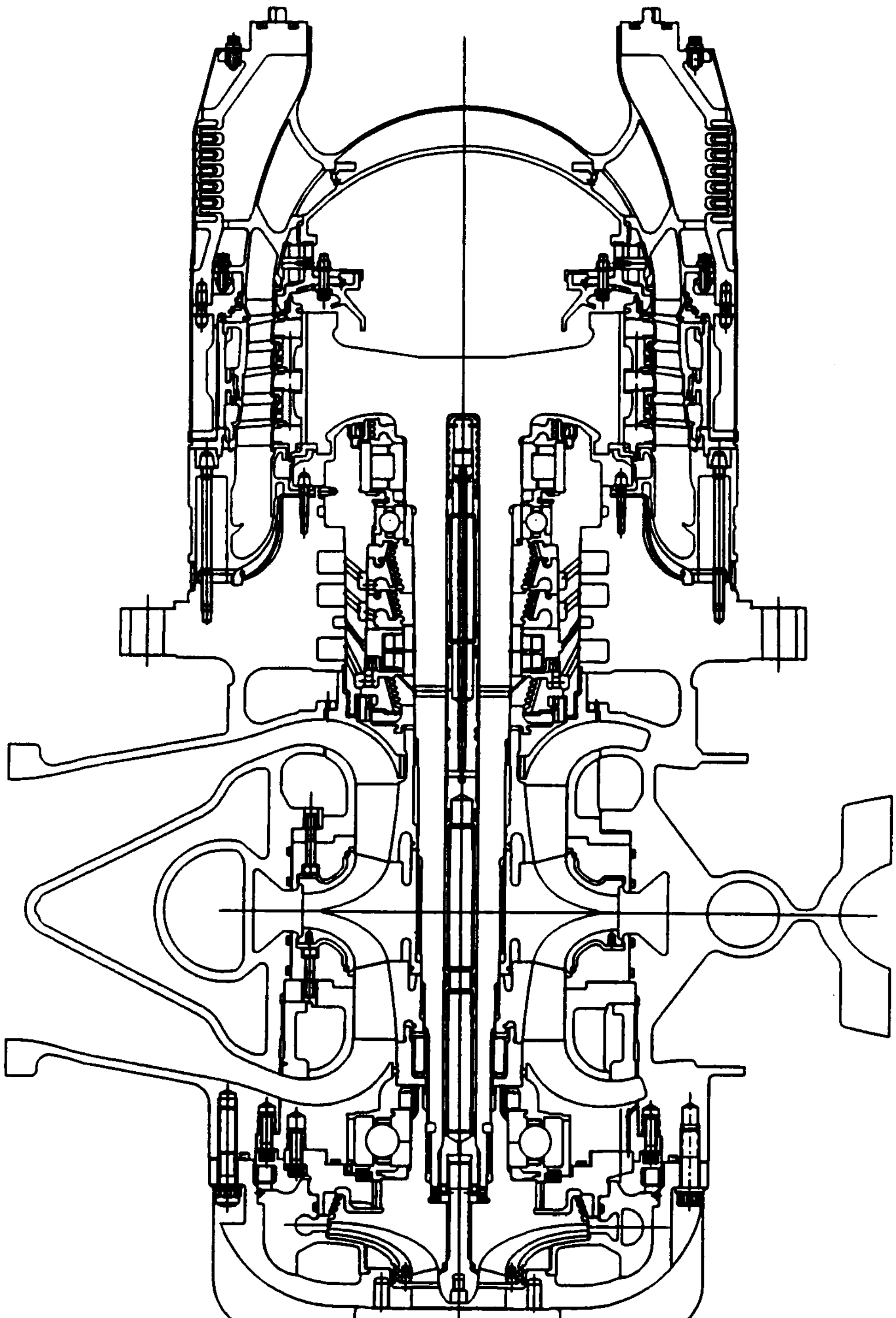

MOTIVATIONS

- CFD Analysis of cavity flows required to support design effort

- Desire to use the most recent and advanced methods

  Artificial compressibility   Reduces speed of sound   Improves stability

  Beam-Warming method   Stable   Robust

- Desire to develop a specific-purpose code with minimum overhead

  2D, Planer, Axisymmetric, with or without swirl, Incompressible

  No temperature computation   No chemistry

  No compressible flow   No 3D computation

Sverdrup

TECHNICAL OBJECTIVES

- Develop a CFD code for internal flows in liquid fueled engines
- Valid for 2D planer and axisymmetric flows with or without swirl
- Use the Artificial Compressibility Concept
- Use The Beam-Warming scheme with implicit boundary conditions
- Test the laminar capability of the code
- Add a suitable turbulence model
- Test the turbulent capability of the code

Sverdrup

Governing Equations

$$Q_t + E_x + F_y + \alpha H = 0$$

$$Q = \begin{bmatrix} p \\ u \\ v \\ w \end{bmatrix} \qquad E = \begin{bmatrix} \rho\beta u \\ uu + p/\rho - \nu(2u_x) \\ uv - \nu(u_y + v_x) \\ uw - \nu(w_x) \end{bmatrix}$$

$$F = \begin{bmatrix} \rho\beta v \\ uv - \nu(u_y + v_x) \\ vv + p/\rho - \nu(2v_y) \\ vw - \nu(w_y - w/y) \end{bmatrix} \qquad H = \frac{1}{y}\begin{bmatrix} \rho\beta v \\ uv - \nu(u_y + v_x) \\ vv - ww - \nu(2v_y - 2v/y) \\ 2vw - \nu(2w_y - 2w/y) \end{bmatrix}$$

Nondimensionalization

$$Q^*_{t^*} + E^*_{x^*} + F^*_{y^*} + \alpha H^* = 0$$

$$Q^* = \begin{bmatrix} p^* \\ u^* \\ v^* \\ w^* \end{bmatrix} \qquad E^* = \begin{bmatrix} \beta^* u^* \\ u^* u^* + p^* - \frac{\nu^*}{R_e}(2u^*_{x^*}) \\ u^* v^* - \frac{\nu^*}{R_e}(u^*_{y^*} + v^*_{x^*}) \\ u^* w^* - \frac{\nu^*}{R_e}(w^*_{x^*}) \end{bmatrix}$$

$$F^* = \begin{bmatrix} \beta^* v^* \\ u^* v^* - \frac{\nu^*}{R_e}(u^*_{y^*} + v^*_{x^*}) \\ v^* v^* + p^* - \frac{\nu^*}{R_e}(2v^*_{y^*}) \\ v^* w^* - \frac{\nu^*}{R_e}(w^*_{y^*} - w^*/y^*) \end{bmatrix} \qquad H^* = \frac{1}{y^*} \begin{bmatrix} \beta^* v^* \\ u^* v^* - \frac{\nu^*}{R_e}(u^*_{y^*} + v^*_{x^*}) \\ v^* v^* - w^* w^* - \frac{\nu^*}{R_e}(2v^*_{y^*} - 2v^*/y^*) \\ 2v^* w^* - \frac{\nu^*}{R_e}(2w^*_{y^*} - 2w^*/y^*) \end{bmatrix}$$

$$u^* = \frac{u}{v_{ref}} \qquad t^* = \frac{t}{t_{ref}} \qquad p^* = \frac{p}{\rho_{ref}\, v^2_{ref}} \qquad \beta^* = \frac{\beta}{v^2_{ref}} \qquad \nu^* = \frac{\nu}{\nu_{ref}} \qquad \rho^* = \frac{\rho}{\rho_{ref}} = 1$$

$\rho_{ref} = \rho =$ fluid density $\qquad t_{ref} = x_{ref} / v_{ref} \qquad R_e = x_{ref}\, v_{ref} / \nu_{ref}$

Sverdrup

Transformation

$$\mathcal{Q}_t + \mathcal{E}_\xi + \mathcal{F}_\eta + \alpha\mathcal{H} = 0$$

$$\mathcal{Q} = \frac{1}{J}\begin{bmatrix} p \\ u \\ v \\ w \end{bmatrix} \qquad \mathcal{E} = \frac{1}{J}\begin{bmatrix} \beta(\xi_x u + \xi_y v) \\ \xi_x(u^2 + p) + \xi_y uv - \frac{\nu}{R_e}(a_1 u_\xi + a_2 u_\eta + a_3 v_\xi + a_4 v_\eta) \\ \xi_x uv + \xi_y(v^2 + p) - \frac{\nu}{R_e}(a_5 u_\xi + a_6 u_\eta + a_7 v_\xi + a_8 v_\eta) \\ \xi_x uw + \xi_y vw - \frac{\nu}{R_e}(a_9 w_\xi + a_{10} w_\eta + a_{11} w) \end{bmatrix}$$

$$\mathcal{F} = \frac{1}{J}\begin{bmatrix} \beta(\eta_x u + \eta_y v) \\ \eta_x(u^2 + p) + \eta_y uv - \frac{\nu}{R_e}(b_1 u_\xi + b_2 u_\eta + b_3 v_\xi + b_4 v_\eta) \\ \eta_x uv + \eta_y(v^2 + p) - \frac{\nu}{R_e}(b_5 u_\xi + b_6 u_\eta + b_7 v_\xi + b_8 v_\eta) \\ \eta_x uw + \eta_y vw - \frac{\nu}{R_e}(b_9 w_\xi + b_{10} w_\eta + b_{11} w) \end{bmatrix}$$

$$\mathcal{H} = \frac{1}{J\,y}\begin{bmatrix} \beta v \\ uv - \frac{\nu}{R_e}(c_1 u_\xi + c_2 u_\eta + c_3 v_\xi + c_4 v_\eta) \\ v^2 - w^2 - \frac{\nu}{R_e}(c_5 v_\xi + c_6 v_\eta + c_7 v) \\ 2vw - \frac{\nu}{R_e}(c_5 w_\xi + c_6 w_\eta + c_7 w) \end{bmatrix}$$

Sverdrup

Flux Jacobians

$$Q_t + \mathcal{E}_\xi + \mathcal{F}_\eta + \alpha\mathcal{H} = 0$$

$$A = \frac{\partial \mathcal{E}}{\partial Q} = \begin{bmatrix} 0 & \xi_x\beta & \xi_y\beta & 0 \\ \xi_x & 2\xi_x u + \xi_y v - \frac{\nu}{JR_e}(a_1 J_\xi + a_2 J_\eta) & \xi_y u - \frac{\nu}{JR_e}(a_3 J_\xi + a_4 J_\eta) & 0 \\ \xi_y & \xi_x v - \frac{\nu}{JR_e}(a_5 J_\xi + a_6 J_\eta) & \xi_x u + 2\xi_y v - \frac{\nu}{JR_e}(a_7 J_\xi + a_8 J_\eta) & 0 \\ 0 & \xi_x w & \xi_y w & \xi_x u + \xi_y v - \frac{\nu}{JR_e}(a_9 J_\xi + a_{10} J_\eta + a_{11} J) \end{bmatrix}$$

$$B = \frac{\partial \mathcal{F}}{\partial Q} = \begin{bmatrix} 0 & \eta_x\beta & \eta_y\beta & 0 \\ \eta_x & 2\eta_x u + \eta_y v - \frac{\nu}{JR_e}(b_1 J_\xi + b_2 J_\eta) & \eta_y u - \frac{\nu}{JR_e}(b_3 J_\xi + b_4 J_\eta) & 0 \\ \eta_y & \eta_x v - \frac{\nu}{JR_e}(b_5 J_\xi + b_6 J_\eta) & \eta_x u + 2\eta_y v - \frac{\nu}{JR_e}(b_7 J_\xi + b_8 J_\eta) & 0 \\ 0 & \eta_x w & \eta_y w & \eta_x u + \eta_y v - \frac{\nu}{JR_e}(b_9 J_\xi + b_{10} J_\eta + b_{11} J) \end{bmatrix}$$

$$C = \frac{\partial \mathcal{H}}{\partial Q} = \frac{1}{y}\begin{bmatrix} 0 & 0 & \beta & 0 \\ 0 & v - \frac{\nu}{JR_e}(c_1 J_\xi + c_2 J_\eta) & u - \frac{\nu}{JR_e}(c_3 J_\xi + c_4 J_\eta) & 0 \\ 0 & 0 & 2v - \frac{\nu}{JR_e}(c_5 J_\xi + c_6 J_\eta + c_7 J) & -2w \\ 0 & 0 & 2w & 2v - \frac{\nu}{JR_e}(c_5 J_\xi + c_6 J_\eta + c_7 J) \end{bmatrix}$$

The Beam-Warming Method

$$\left[I + \Delta t\left(\frac{\partial}{\partial\xi}\mathcal{A}^n + \frac{\partial}{\partial\eta}\mathcal{B}^n + \alpha\mathcal{C}^n\right) - I\,\epsilon_{imp}^2\,J^{-1}\,(\delta_\xi^2 + \delta_\eta^2)\,J\right]\delta\mathcal{Q}^{n+1} =$$

$$\Delta\mathcal{Q}^n - \epsilon_{exp}^4\,J^{-1}\,(\delta_\xi^4 + \delta_\eta^4)\,J\,\mathcal{Q}^n$$

where I is the 4×4 unit matrix, and:

$$\delta\mathcal{Q}^{n+1} = \mathcal{Q}^{n+1} - \mathcal{Q}^n$$

$$\Delta\mathcal{Q}^n = -\Delta t\left[\mathcal{E}_\xi^n + \mathcal{F}_\eta^n + \alpha\,\mathcal{H}^n\right]$$

$$\delta_\xi^2 f = f_{i-1} - 2f_i + f_{i+1}$$

$$\delta_\xi^4 f = f_{i-2} - 4f_{i-1} + 6f_i - 4f_{i+1} + f_{i+2}$$

Sverdrup

The first step is:

$$\left[I + \Delta t \left(\frac{\partial}{\partial \xi} \mathcal{A}^n \right) - I\, \epsilon_{imp}^2\, J^{-1}\, \delta_\xi^2\, J \right] \delta \mathcal{Q}^* = \Delta \mathcal{Q}^n - \epsilon_{exp}^4\, J^{-1} \left(\delta_\xi^4 + \delta_\eta^4 \right) J\, \mathcal{Q}^n$$

which is solved for $\delta \mathcal{Q}^*$

and the second step is:

$$\left[I + \Delta t \left(\frac{\partial}{\partial \eta} \mathcal{B}^n + \alpha \mathcal{C}^n \right) - I\, \epsilon_{imp}^2\, J^{-1}\, \delta_\eta^2\, J \right] \delta \mathcal{Q}^{n+1} = \delta \mathcal{Q}^*$$

which is solved for $\delta \mathcal{Q}^{n+1}$ at all nodes.

Treatment of the Boundary Conditions

Writing the first step at each node from $i = 1$ to $i = imax$ (for a certain constant j) produces a set of equations that can be expressed in a block matrix form:

$$
\begin{bmatrix}
\bullet & \bullet & \circ & & & & & & & \\
\bullet & \bullet & \bullet & & & & & & & \\
 & \bullet & \bullet & \bullet & & & & & & \\
 & & \bullet & \bullet & \bullet & & & & & \\
 & & & & & \bullet & \bullet & \circ & & \\
 & & & & & & \bullet & \bullet & \bullet & \\
 & & & & & & & \bullet & \bullet & \bullet \\
 & & & & & & & \circ & \bullet & \bullet
\end{bmatrix}
\begin{bmatrix}
\delta Q_1^* \\ \delta Q_2^* \\ \delta Q_3^* \\ \\ \delta Q_i^* \\ \\ \\ \delta Q_{imax}^*
\end{bmatrix}
=
\begin{bmatrix}
d_1 \\ d_2 \\ d_3 \\ \\ d_i \\ \\ \\ d_{imax}
\end{bmatrix}
$$

Note that the existence of the 'o' matrices prevents the block matrix from being tridiagonal.

These 'o' matrices are associated with domain edges as well as east and west edges of blocked-out areas.

They appear because one-sided, second-order-accurate differencing was used at these edges.

To restore the tridiagonal nature of the block matrix, lag the third set of unknowns in the first set of equations, δQ_3^*, by one iteration. Now, the product o δQ_3^* can be subtracted from d_1 and the 'o' in the first row dissapears. Of course, similar treatment for the last row and for edges of blocked-out areas is required.

PIPE FLOW

GRID 81 × 31 NODES

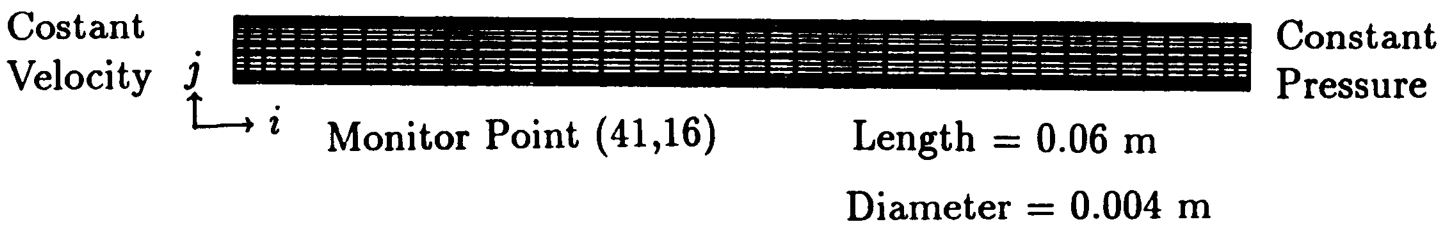

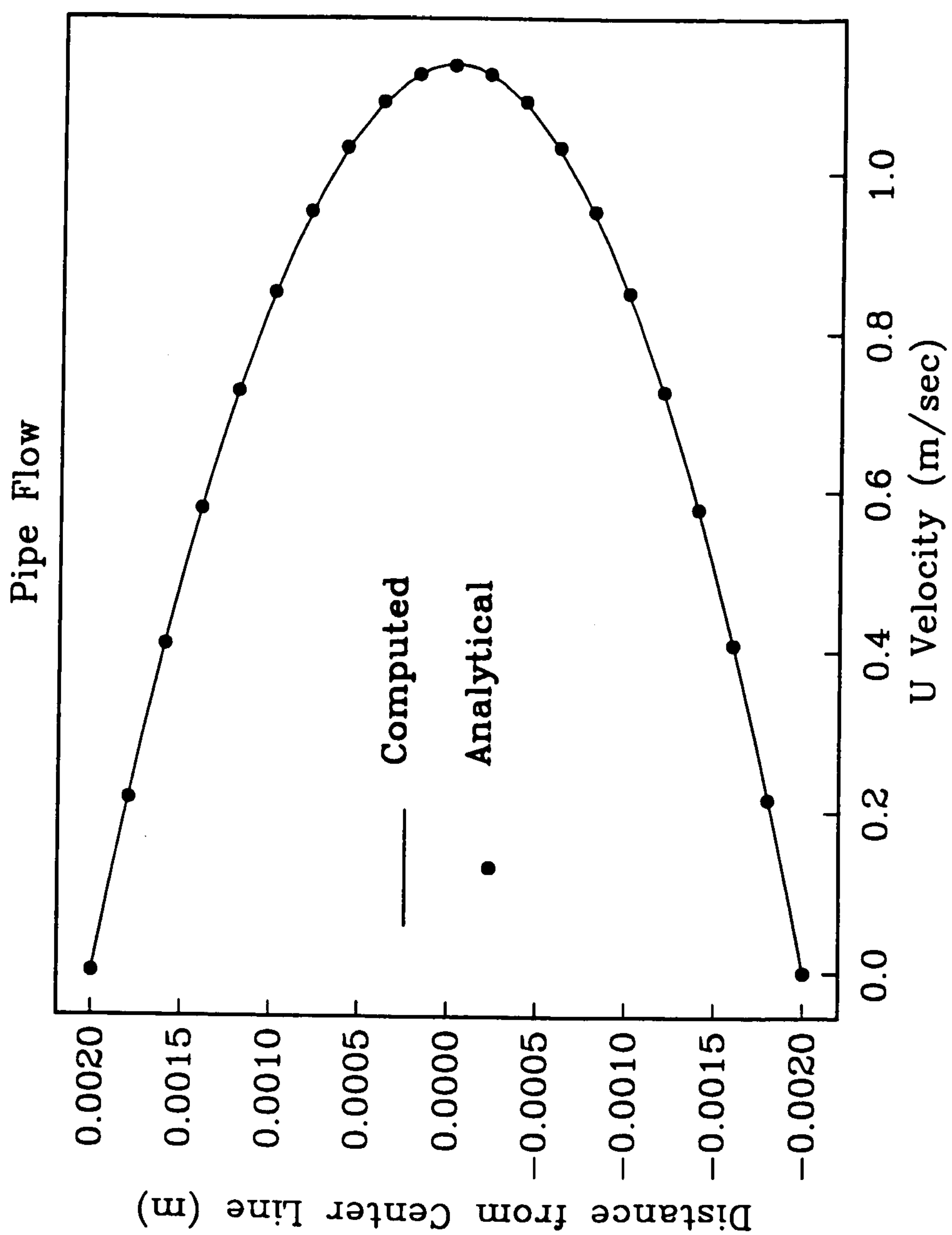
Pipe Flow
Computed
Analytical
U Velocity (m/sec)
0.0
0.2
0.4
0.6
0.8
1.0
Distance from Center Line (m)
0.0020
0.0015
0.0010
0.0005
0.0000
-0.0005
-0.0010
-0.0015
-0.0020

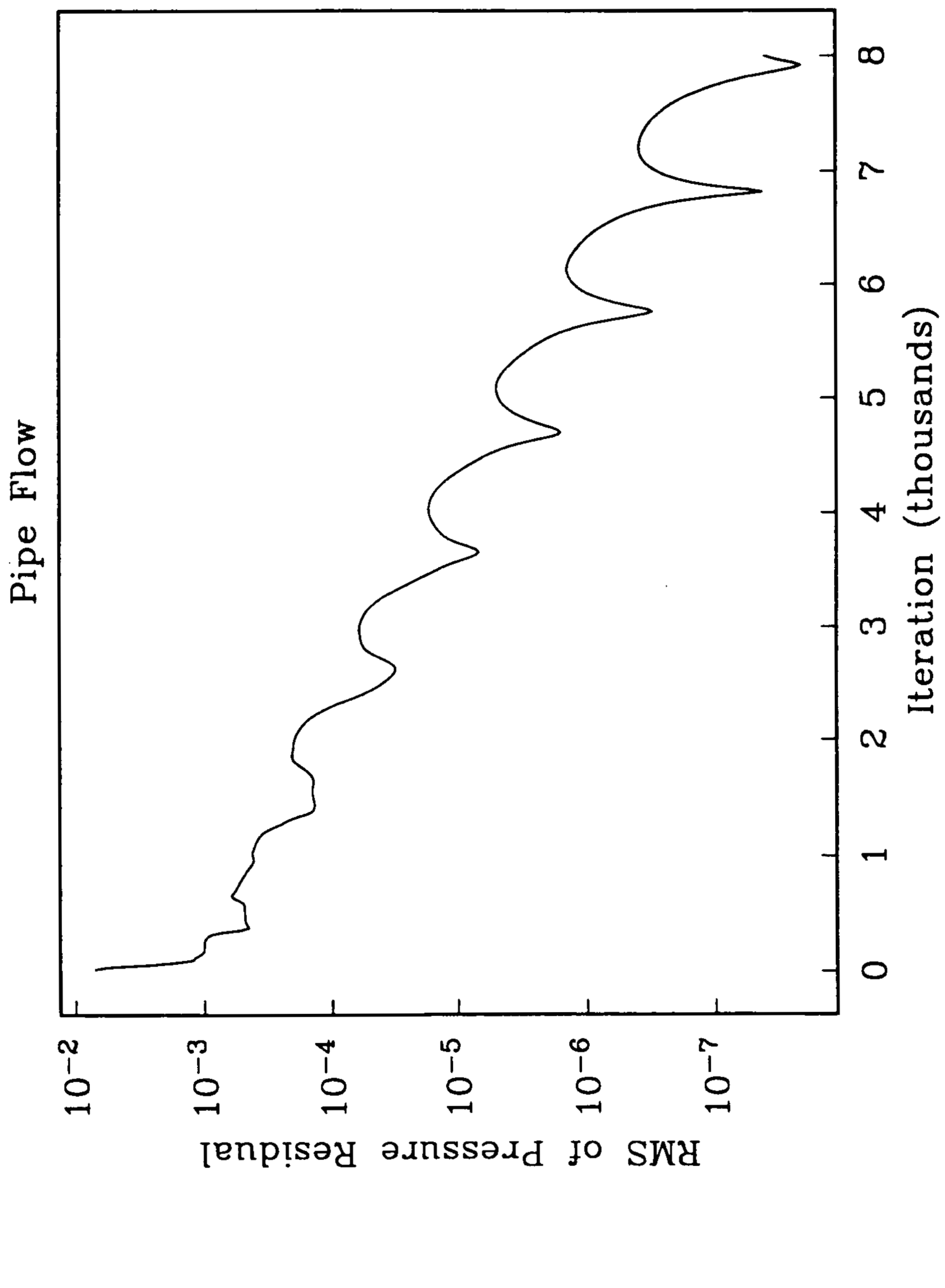

Pipe Flow
RMS of Pressure Residual
10^{-2}
10^{-3}
10^{-4}
10^{-5}
10^{-6}
10^{-7}
Iteration (thousands)
0
1
2
3
4
5
6
7
8

SLIDE BLOCK FLOW

GRID 111 × 21

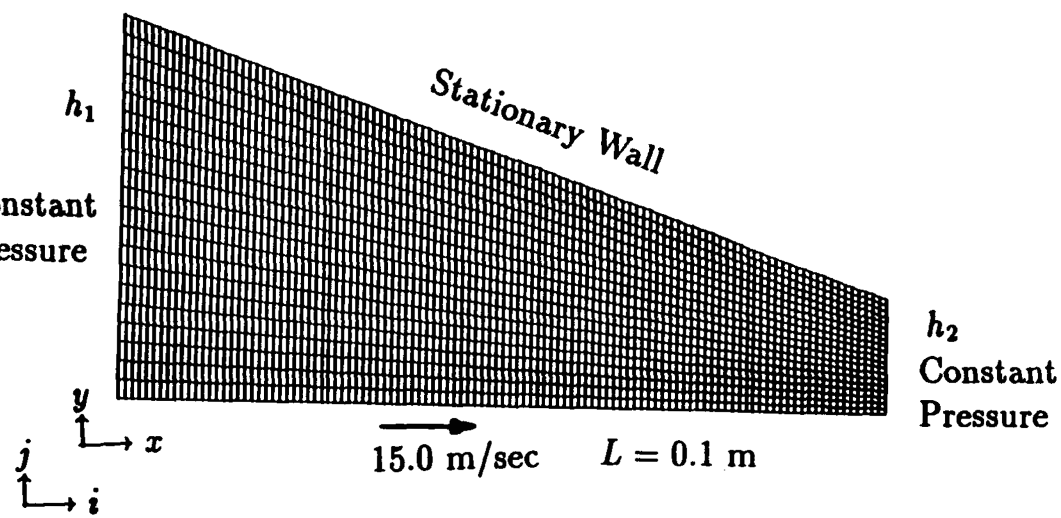

$h_1 = 3 \times 10^{-4}$ m

$h_2 = 9 \times 10^{-5}$ m

Monitor point (56,11)

Initial Pressure Field = 0.0

Initial Velocity Field = 0.0

SLIDE BLOCK FLOW
PRESSURE CONTOURS (Pascal)

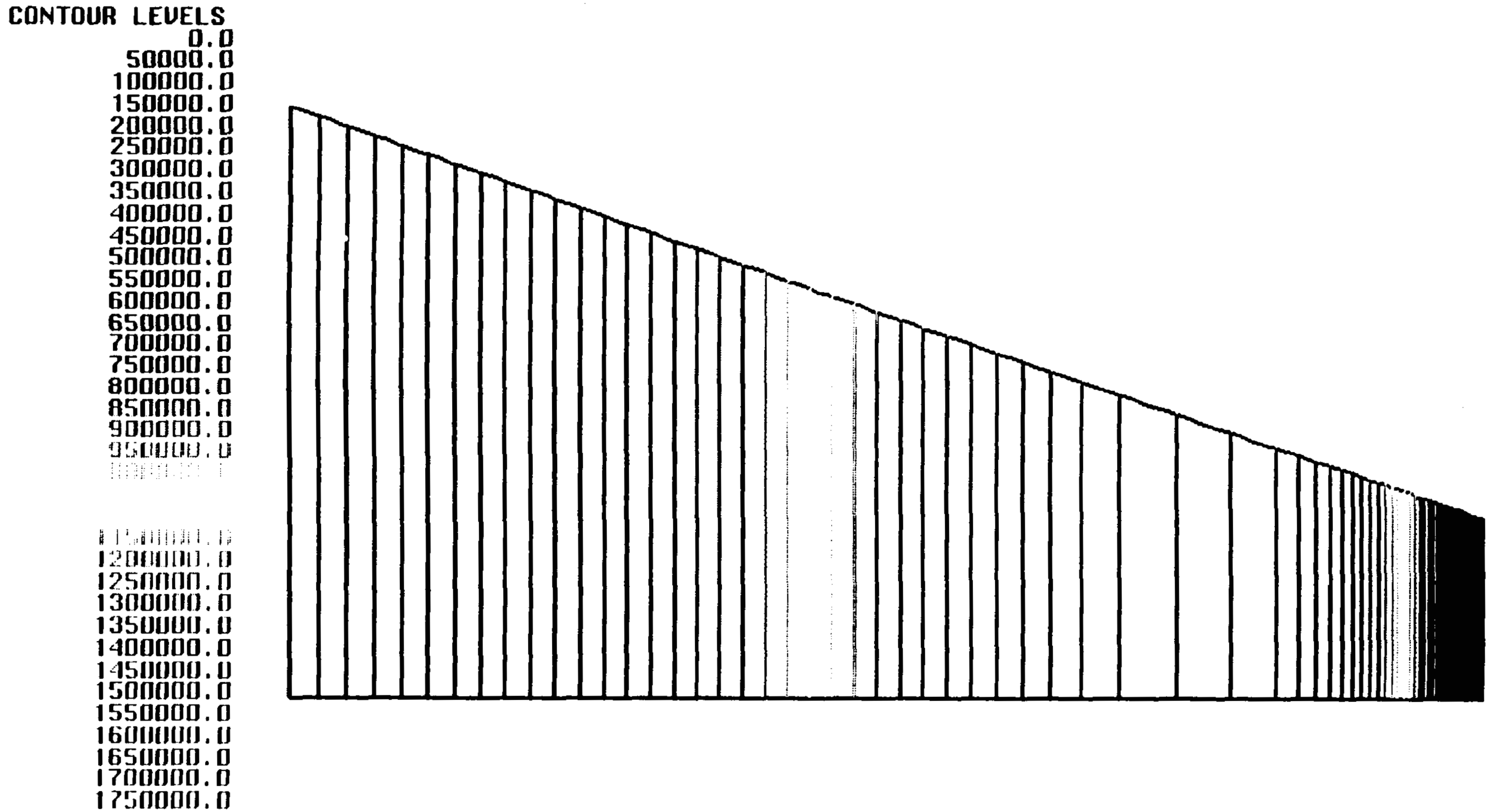

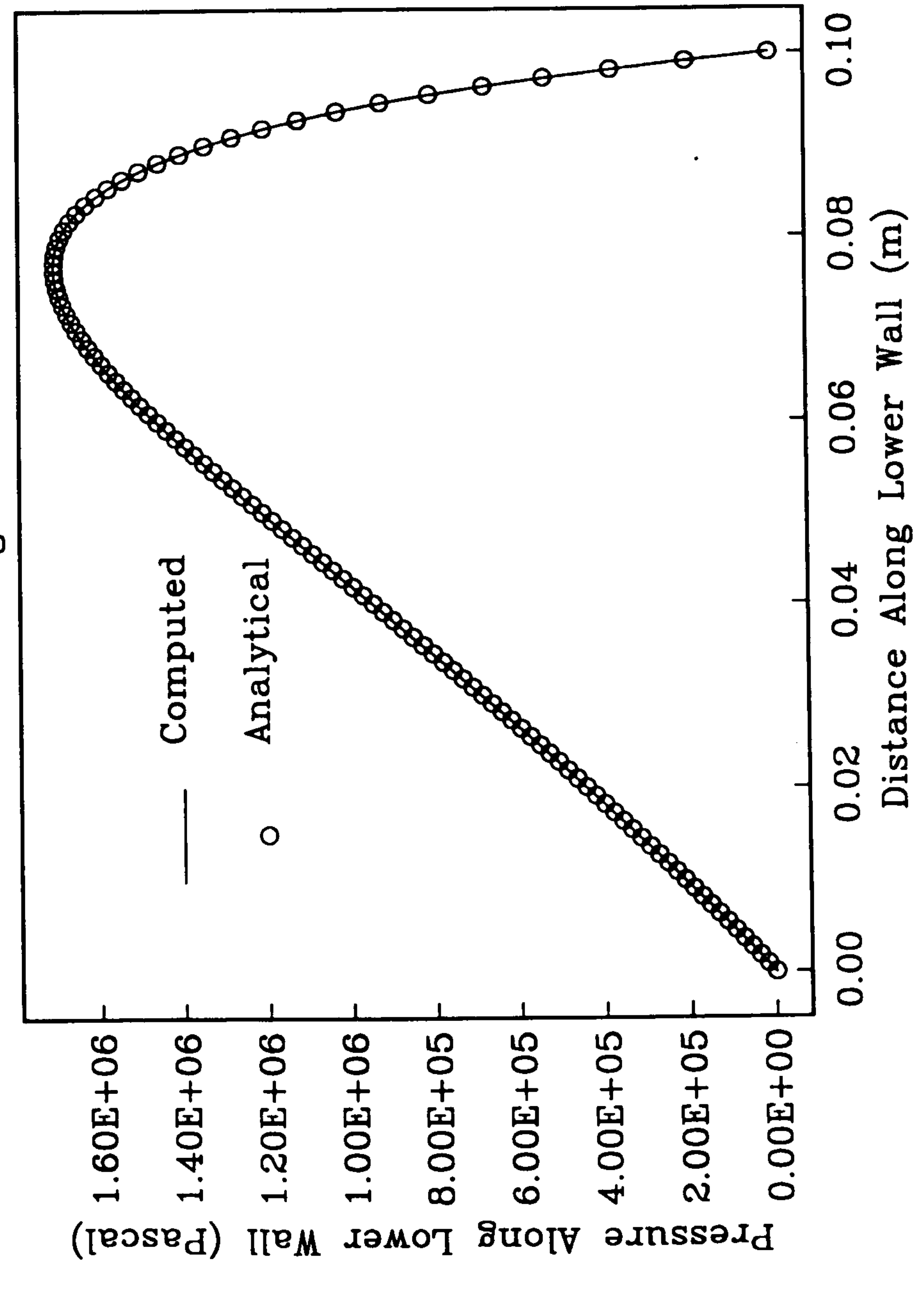

Wedge Flow
Computed
Analytical
Distance Along Lower Wall (m)
0.00
0.02
0.04
0.06
0.08
0.10
Pressure Along Lower Wall (Pascal)
0.00E+00
2.00E+05
4.00E+05
6.00E+05
8.00E+05
1.00E+06
1.20E+06
1.40E+06
1.60E+06

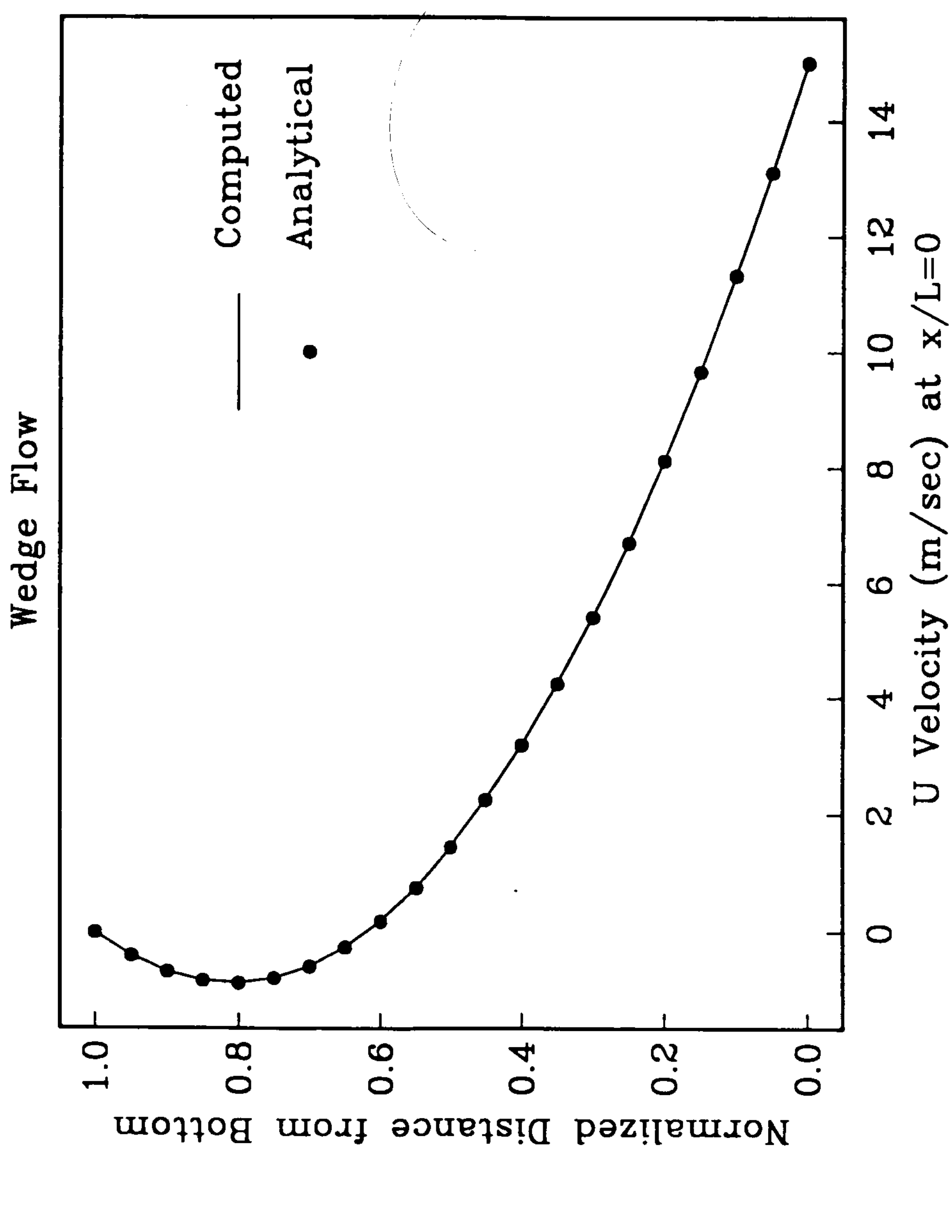
Wedge Flow
Computed
Analytical
U Velocity (m/sec) at x/L=0
Normalized Distance from Bottom
0
2
4
6
8
10
12
14
0.0
0.2
0.4
0.6
0.8
1.0

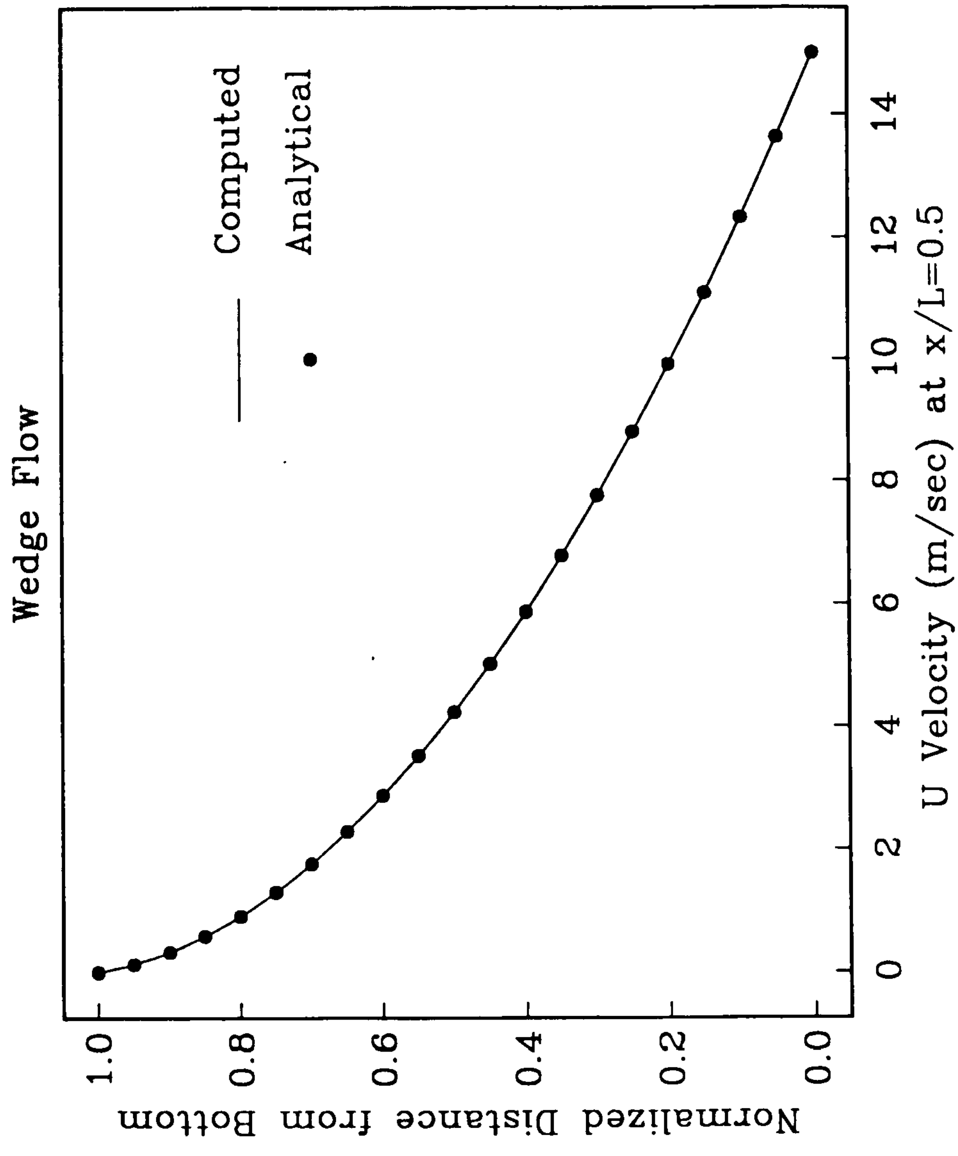

Wedge Flow
Computed
Analytical
U Velocity (m/sec) at x/L=0.5
Normalized Distance from Bottom
0
2
4
6
8
10
12
14
0.0
0.2
0.4
0.6
0.8
1.0

TWO CONCENTRIC CYLINDERS
GRID 61 x 21 NODES

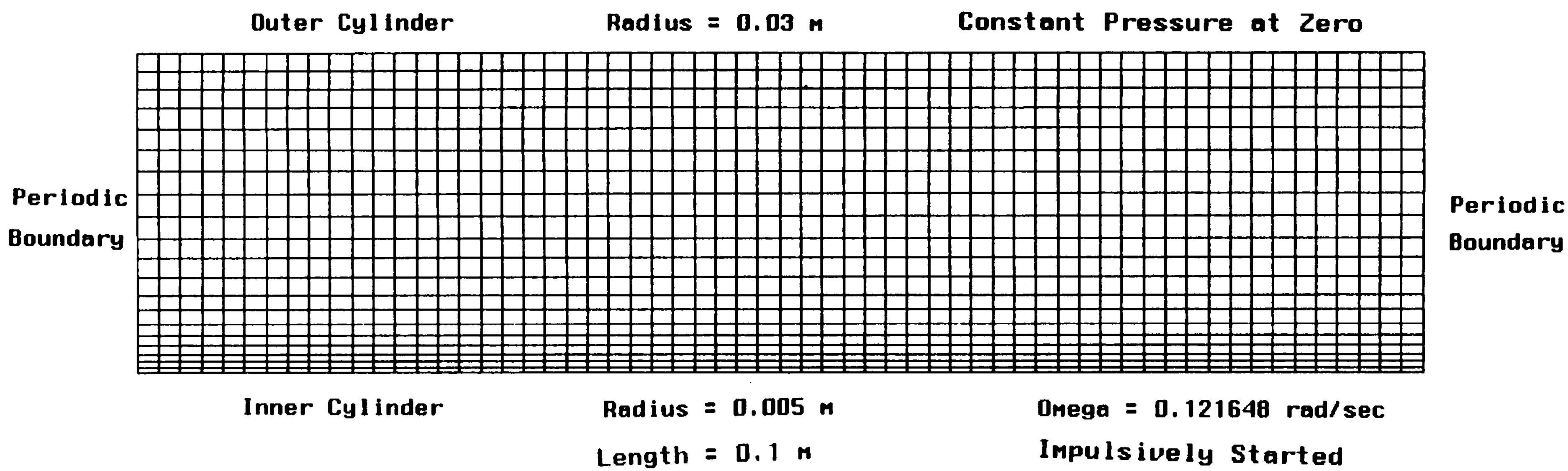

Initial Pressure Field = 0.0

Initial Velocity Field = 0.0

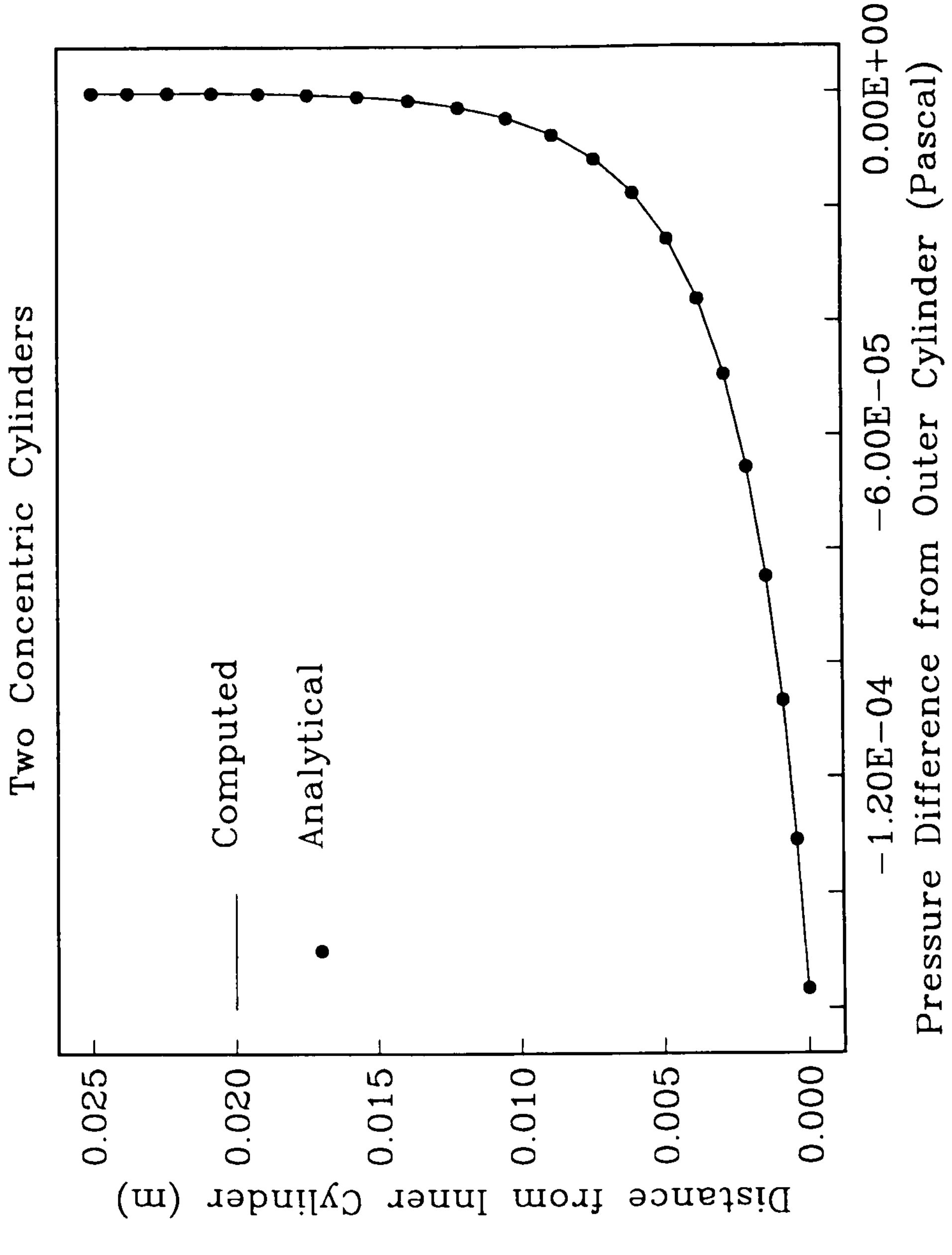
Two Concentric Cylinders
Computed
Analytical
Distance from Inner Cylinder (m)
0.000
0.005
0.010
0.015
0.020
0.025
Pressure Difference from Outer Cylinder (Pascal)
−1.20E−04
−6.00E−05
0.00E+00

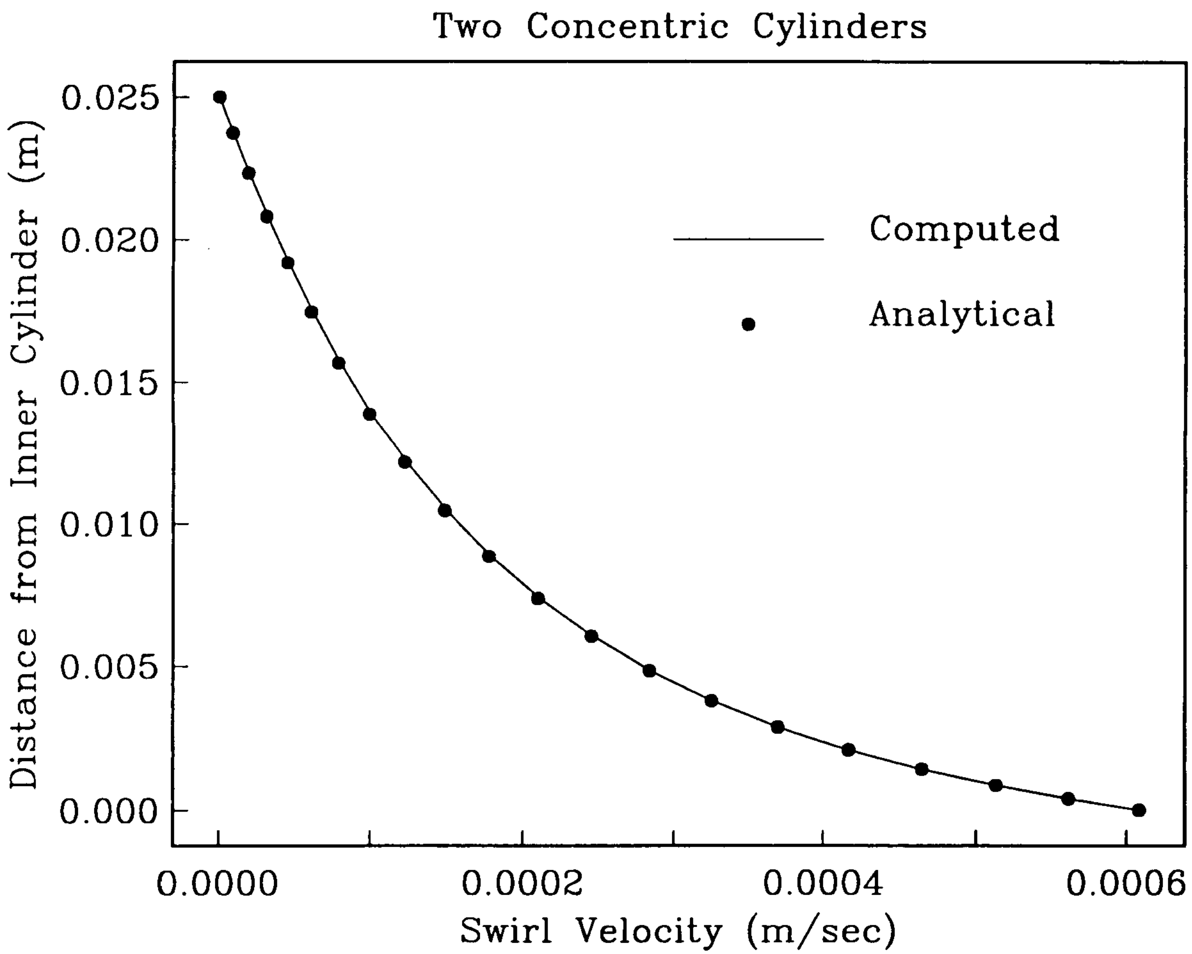
Two Concentric Cylinders
Computed
Analytical
Distance from Inner Cylinder (m)
0.025
0.020
0.015
0.010
0.005
0.000
0.0000
0.0002
0.0004
0.0006
Swirl Velocity (m/sec)

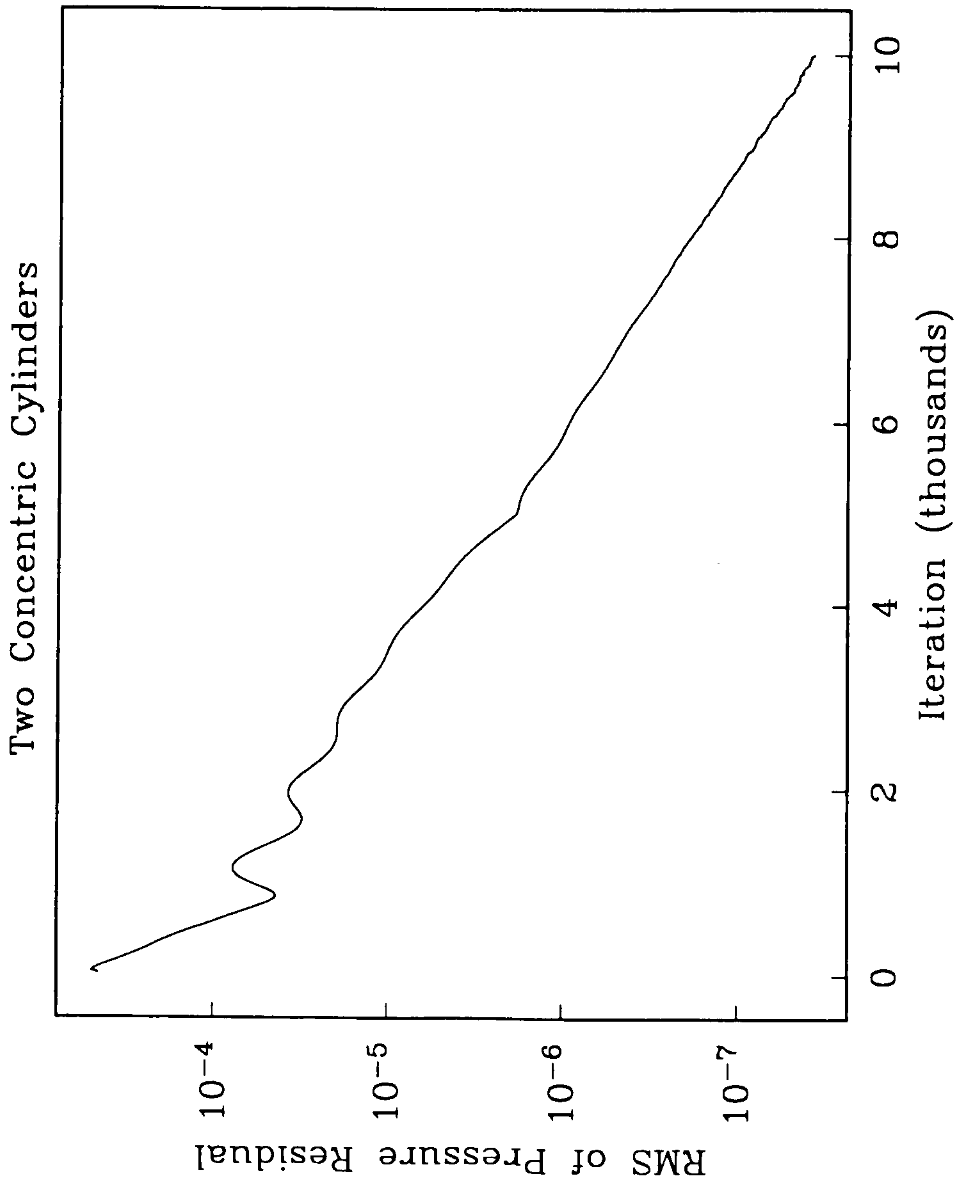

Two Concentric Cylinders
RMS of Pressure Residual
10^{-4}
10^{-5}
10^{-6}
10^{-7}
Iteration (thousands)
0
2
4
6
8
10

TAYLOR VORTICES
GRID 101 × 31 NODES

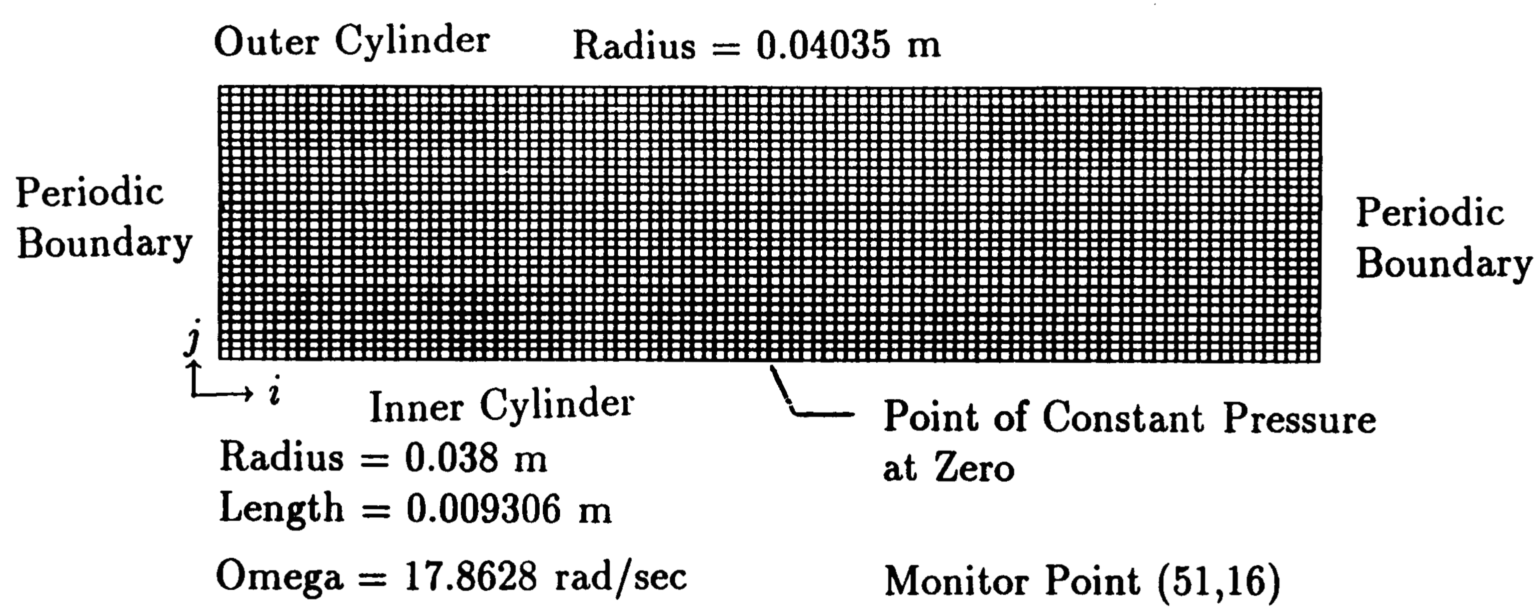

TAYLOR VORTICES

SWIRL VELOCITY CONTOURS (m/sec)

CONTOUR LEVELS
-.20000E-01
0.00000E+00
0.20000E-01
0.40000E-01
0.60000E-01
0.80000E-01
0.10000E+00
0.12000E+00
0.14000E+00
0.16000E+00
0.18000E+00
0.20000E+00
0.22000E+00
0.24000E+00
0.26000E+00
0.28000E+00
0.30000E+00
0.32000E+00
0.34000E+00
0.36000E+00
[illegible]
0.46000E+00
0.48000E+00
0.50000E+00
0.52000E+00
0.54000E+00
0.56000E+00
0.58000E+00
0.60000E+00
0.62000E+00
0.64000E+00
0.66000E+00
0.68000E+00

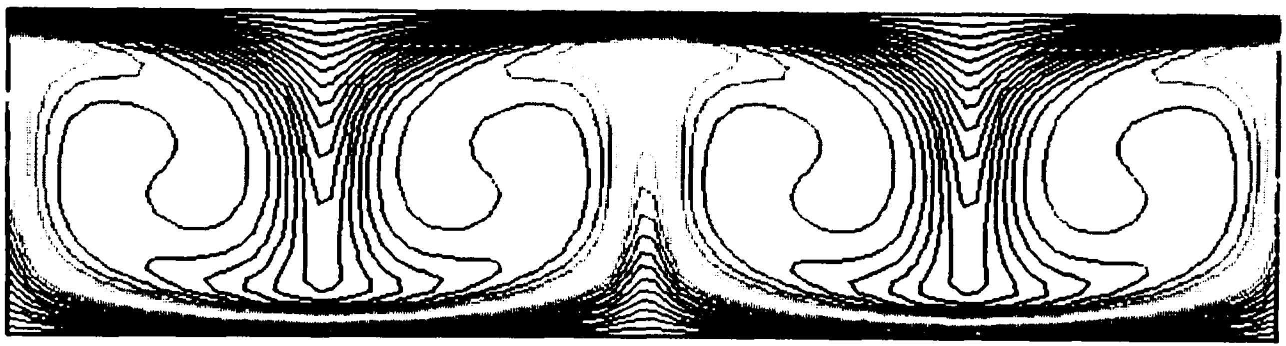

TAYLOR VORTICES
PRESSURE CONTOURS (Pascal)

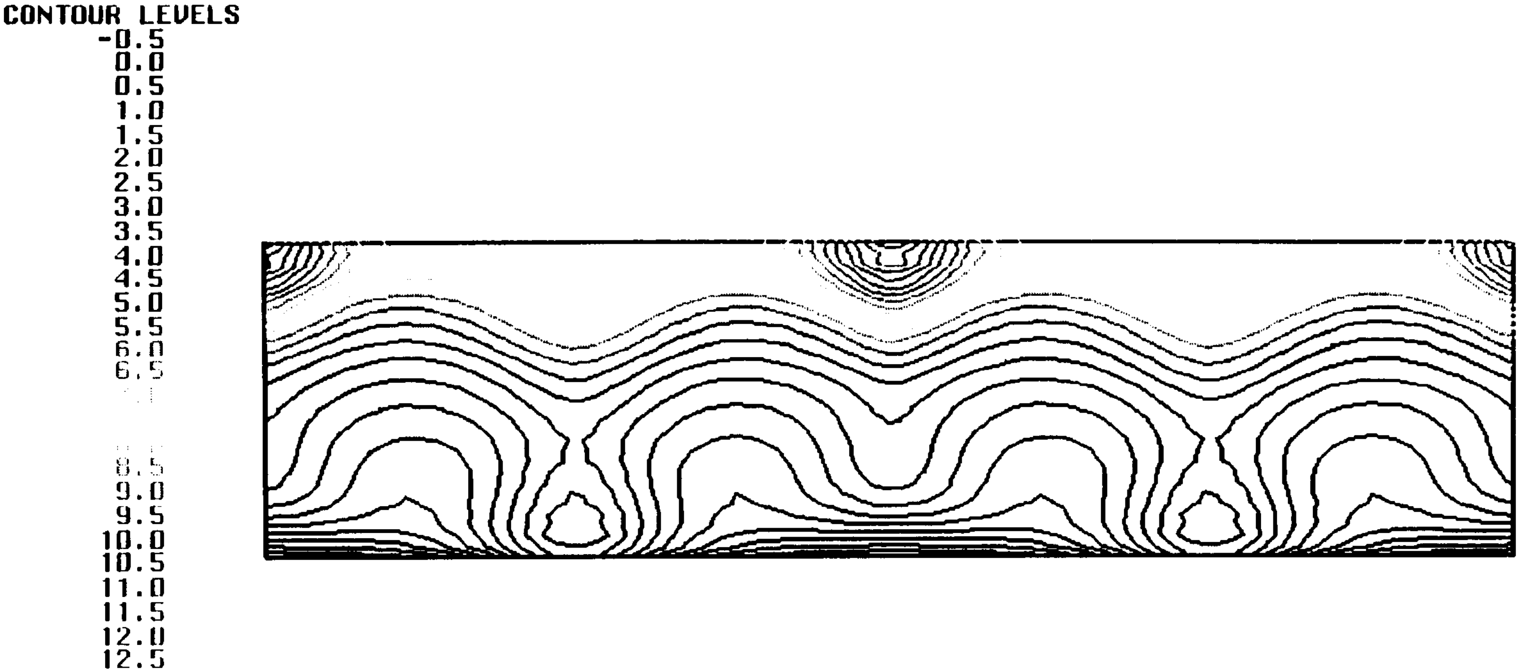

TAYLOR VORTICES
NORMALIZED STREAM FUNCTION

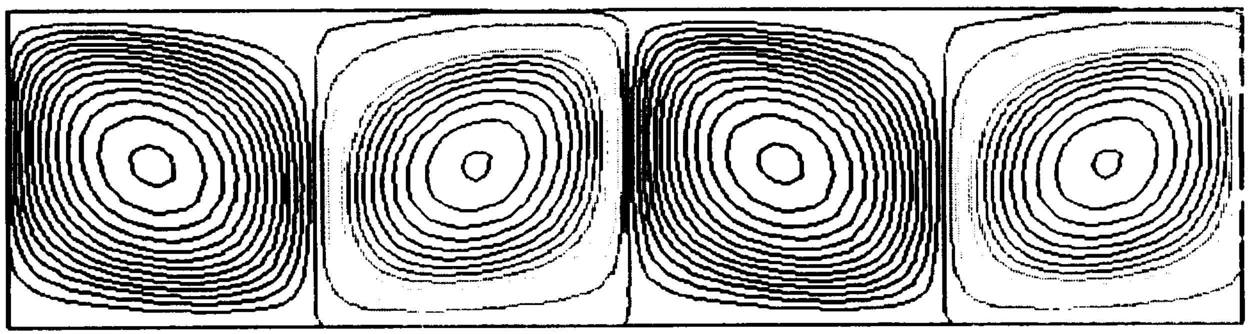

CONTOUR LEVELS
-.14000E-08
-.13000E-08
-.12000E-08
-.11000E-08
-.10000E-08
-.90000E-09
-.80000E-09
-.70000E-09
-.60000E-09
-.50000E-09
-.40000E-09
-.30000E-09
-.20000E-09
-.10000E-09
0.97145E-16
0.10000E-09
0.50000E-09
0.60000E-09
0.70000E-09
0.80000E-09
0.90000E-09
0.10000E-08
0.11000E-08
0.12000E-08
0.13000E-08
0.14000E-08

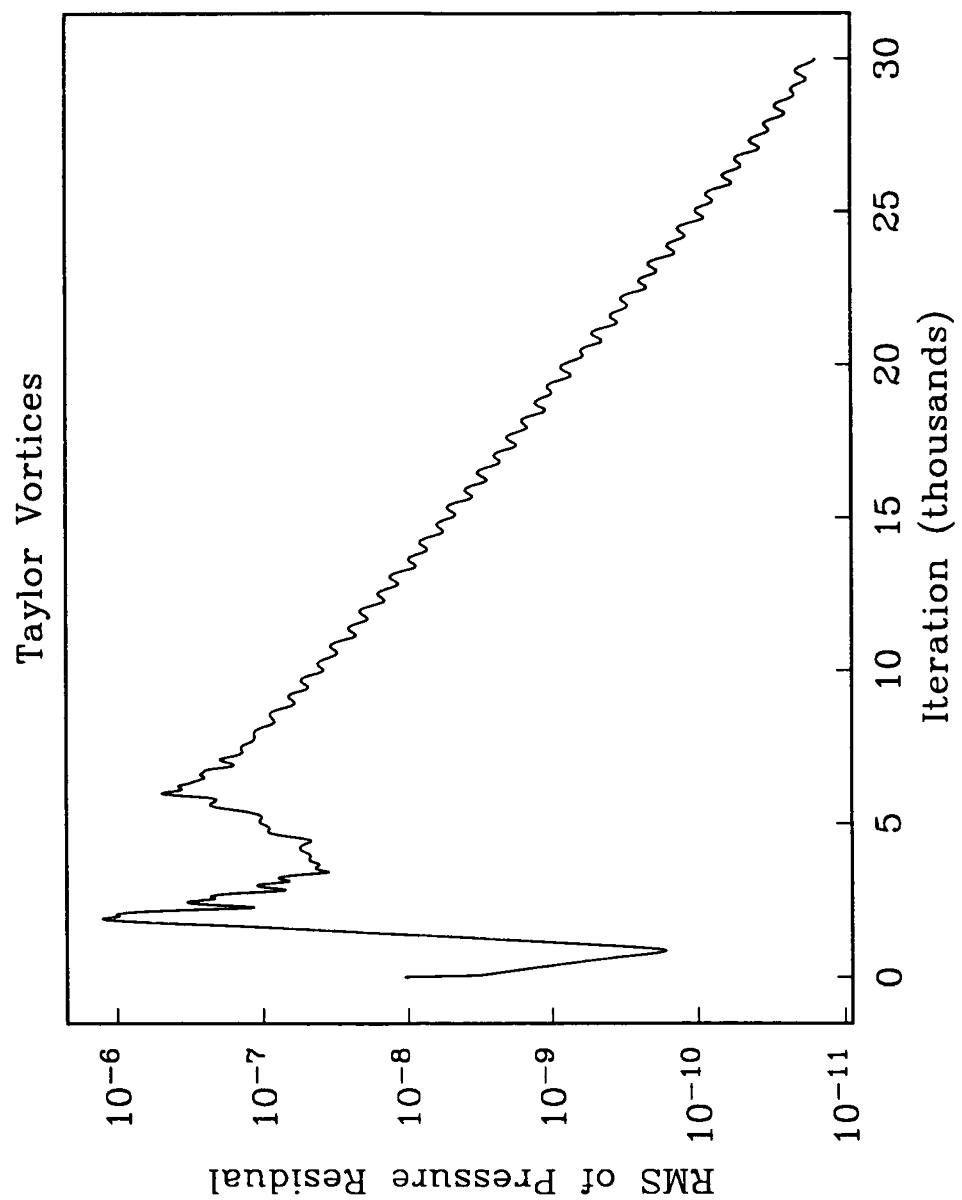
Taylor Vortices
RMS of Pressure Residual
Iteration (thousands)
10^{-6}
10^{-7}
10^{-8}
10^{-9}
10^{-10}
10^{-11}
0
5
10
15
20
25
30

DRIVEN CAVITY FLOW

GRID 51 × 51

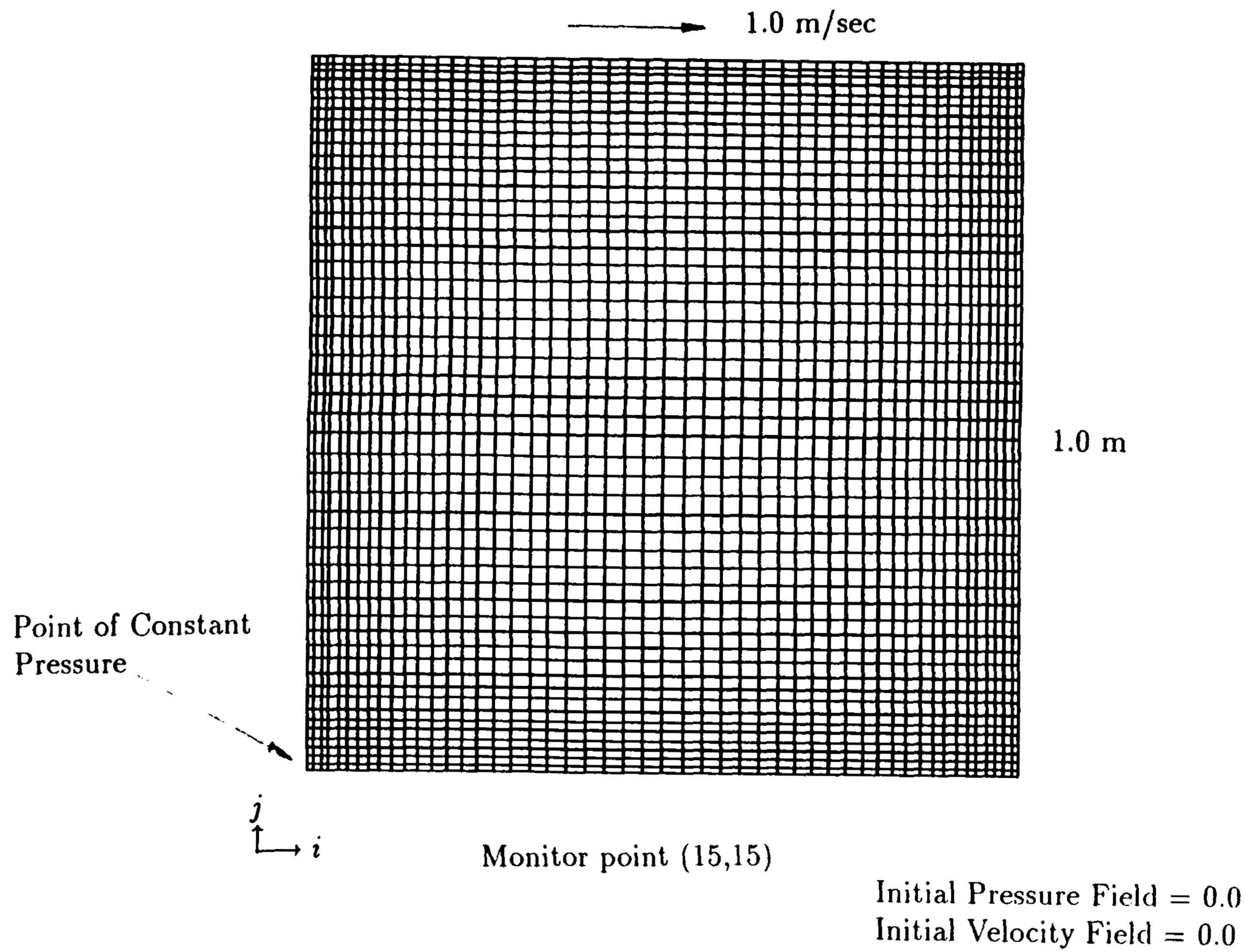

DRIVEN CAVITY FLOW

PARTICLE TRACES

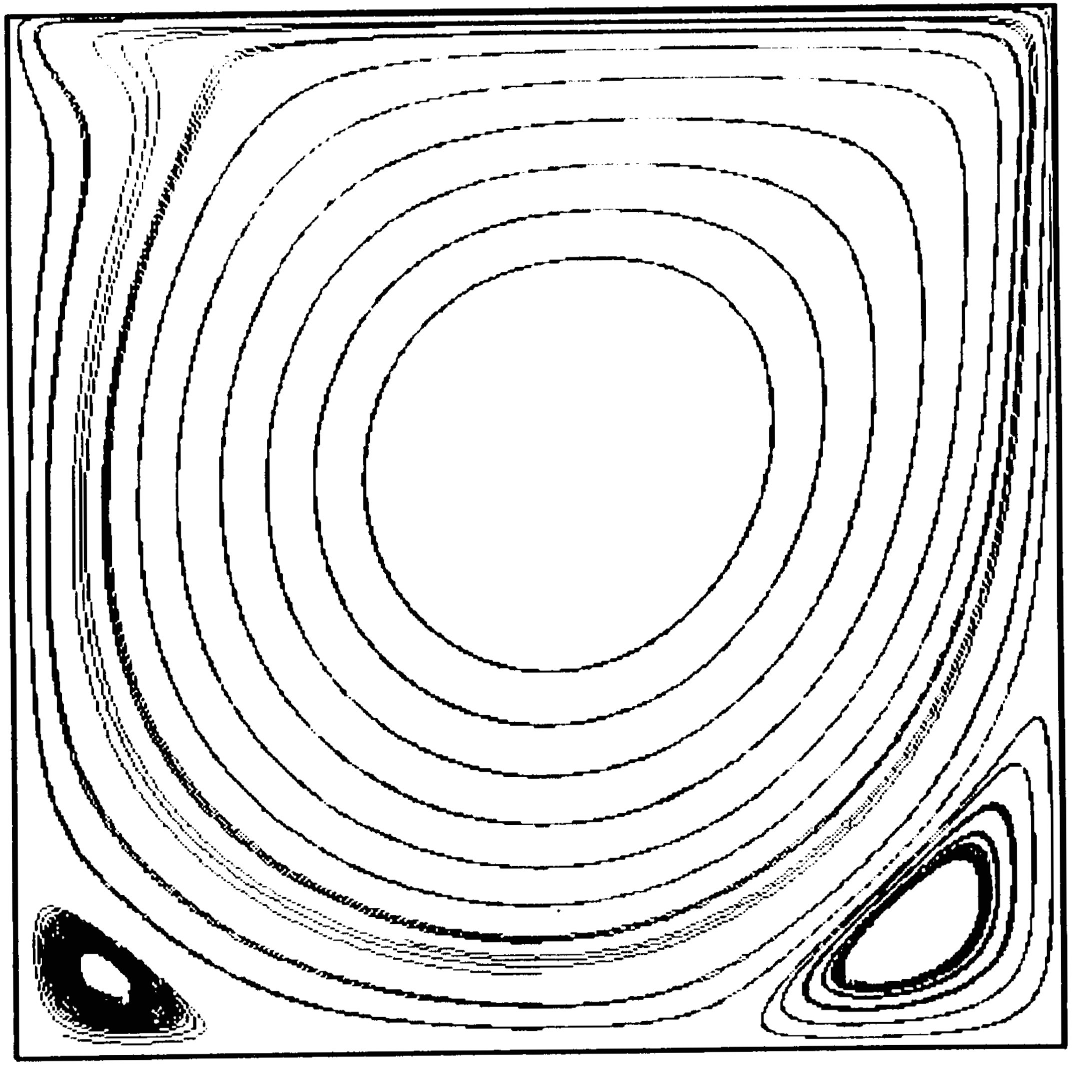

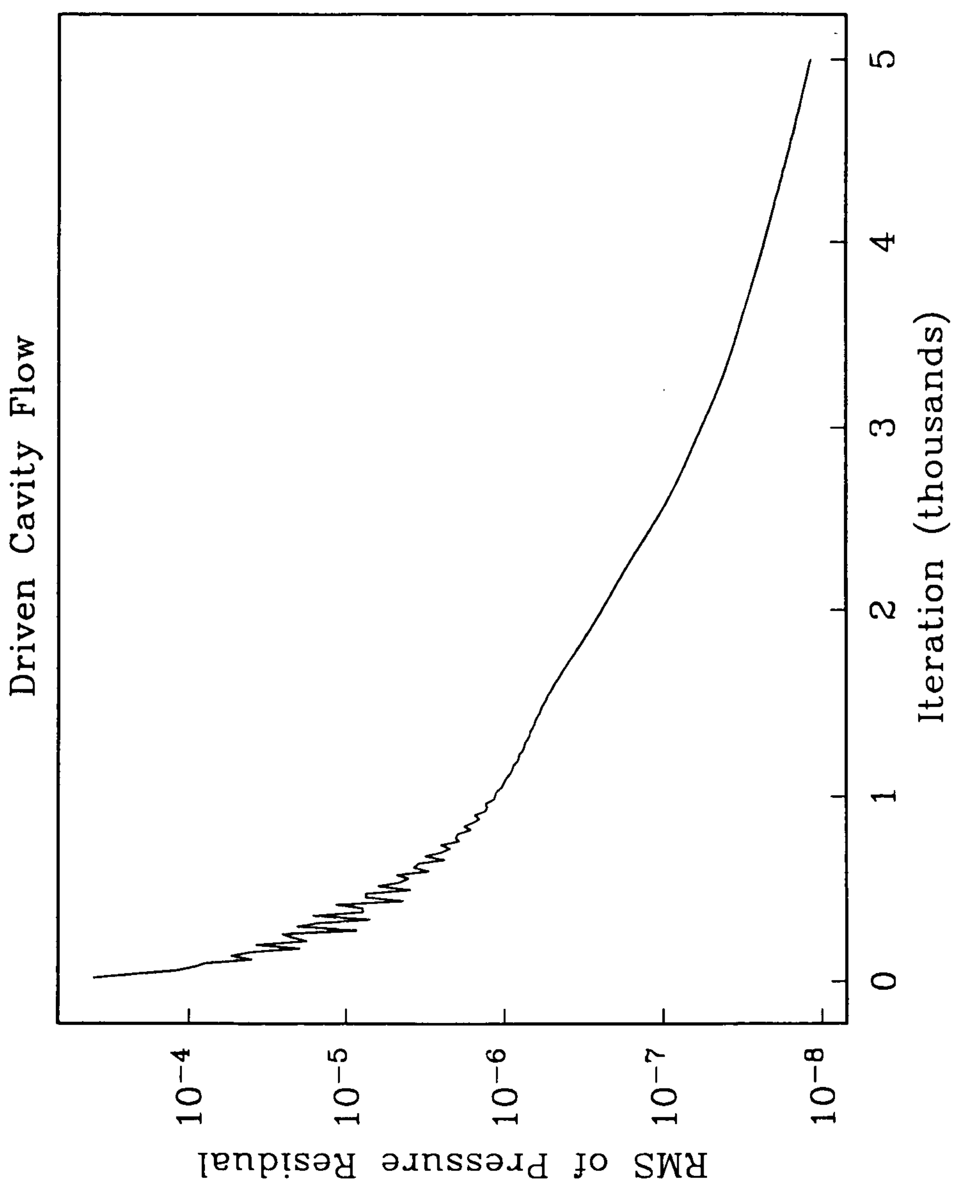
Driven Cavity Flow
RMS of Pressure Residual
10^{-4}
10^{-5}
10^{-6}
10^{-7}
10^{-8}
0
1
2
3
4
5
Iteration (thousands)

TWO ECCENTRIC CYLINDERS

GRID 81 × 31

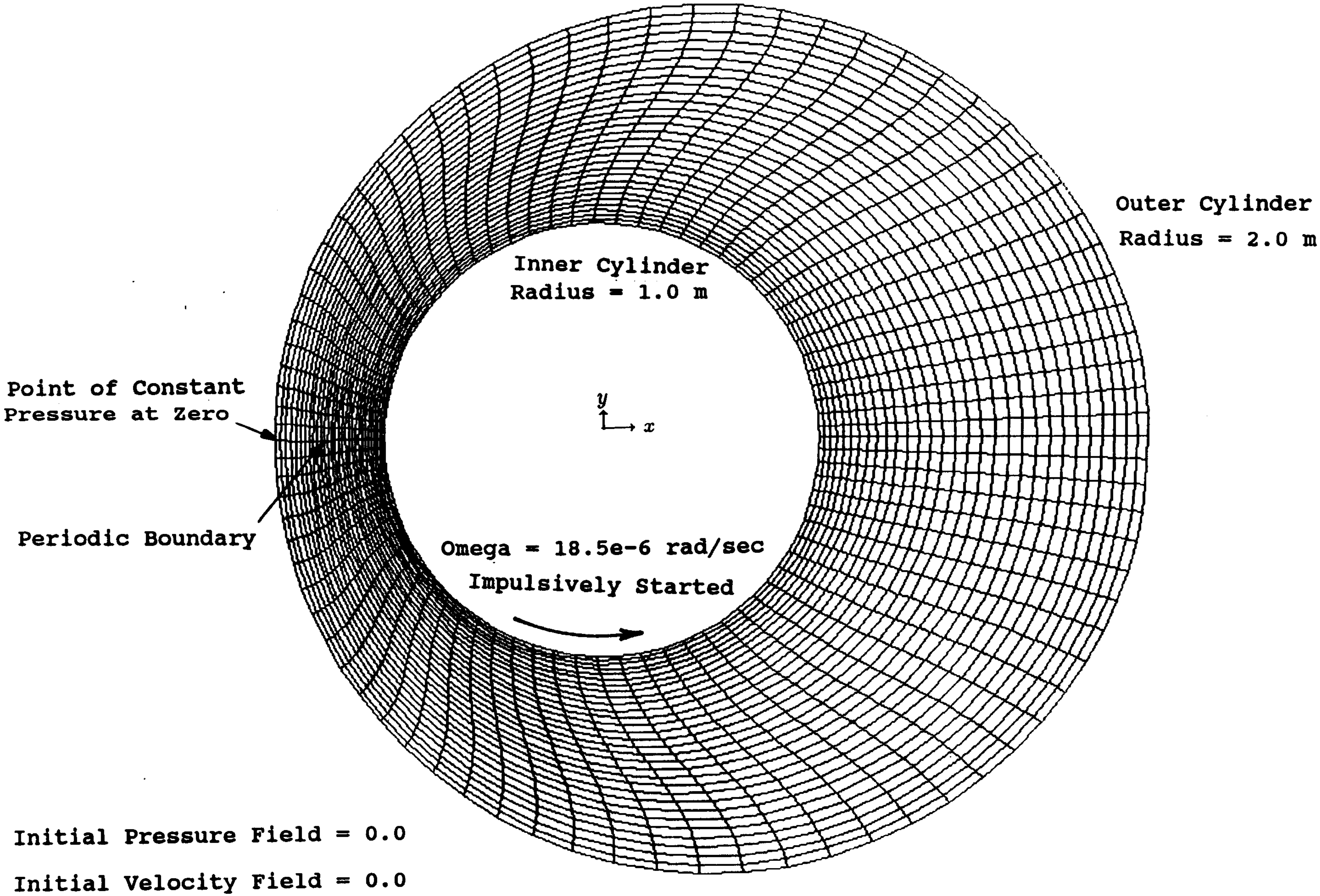

TWO ECCENTRIC CYLINDERS
VELOCITY MAGNITUDE CONTOURS (m/sec)

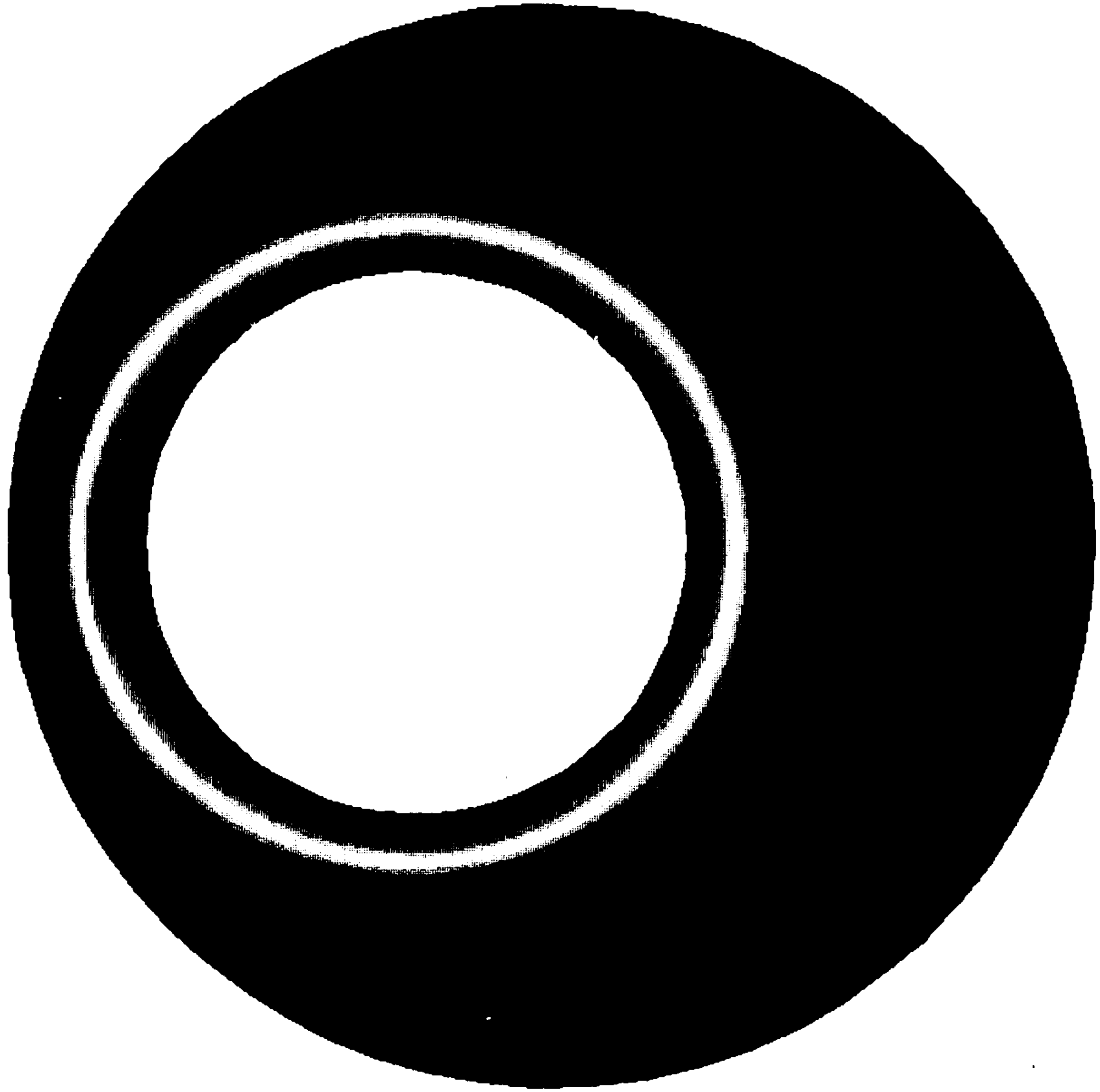

CONTOUR LEVELS
0.00000
0.00000
0.00000
0.00000
0.00000
0.00000
0.00000
0.00000
0.00000
0.00000
0.00001
0.00001
0.00001
0.00001
0.00001
0.00001
0.00001
0.00001
0.00001
0.00001
0.00001
[illegible]

[illegible]
0.00001
0.00001
0.00001
0.00001
0.00002
0.00002
0.00002
0.00002
0.00002
0.00002
0.00002
0.00002
0.00002

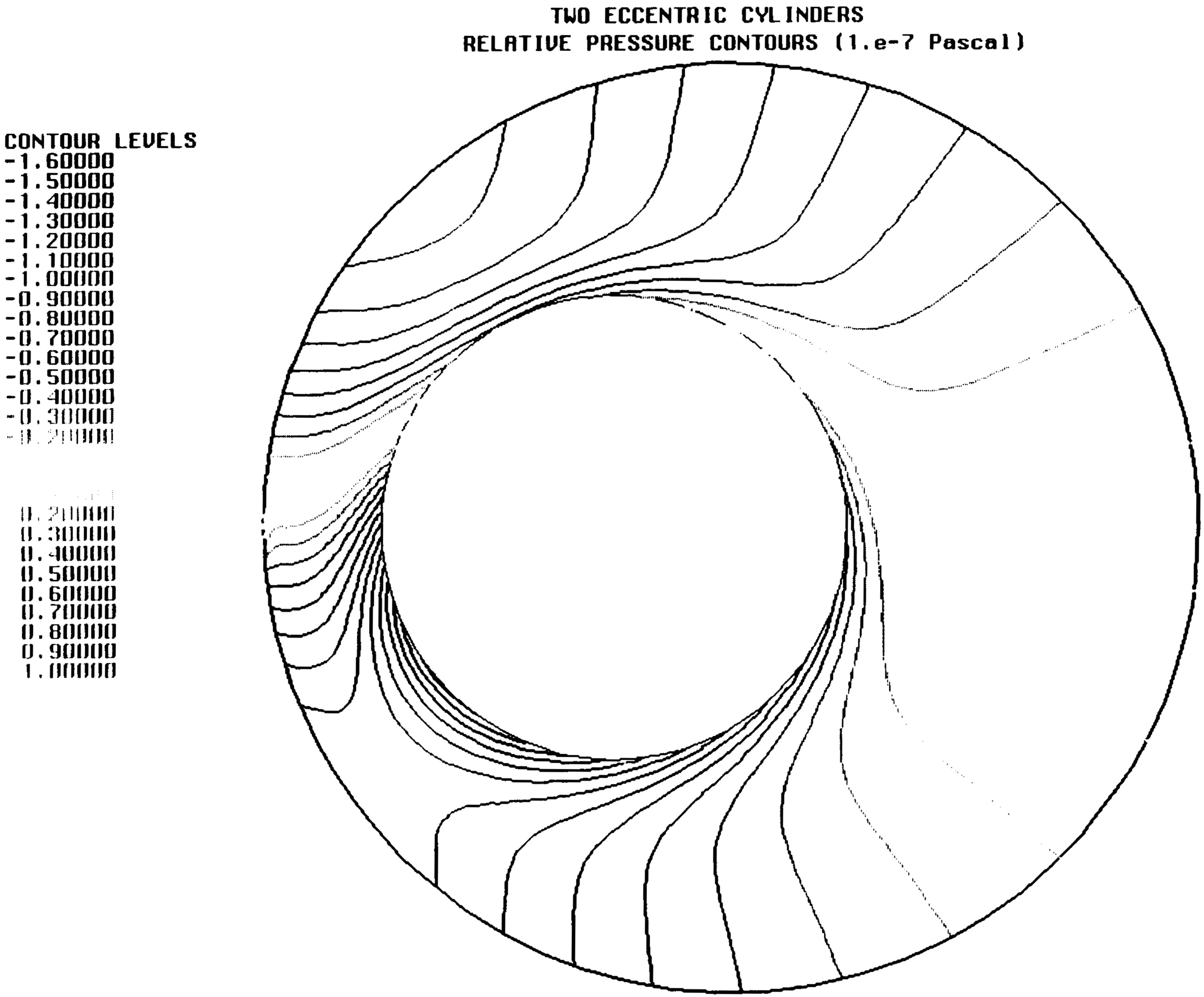
TWO ECCENTRIC CYLINDERS
RELATIVE PRESSURE CONTOURS (1.e-7 Pascal)
CONTOUR LEVELS
-1.60000
-1.50000
-1.40000
-1.30000
-1.20000
-1.10000
-1.00000
-0.90000
-0.80000
-0.70000
-0.60000
-0.50000
-0.40000
-0.30000
-0.20000
0.20000
0.30000
0.40000
0.50000
0.60000
0.70000
0.80000
0.90000
1.00000

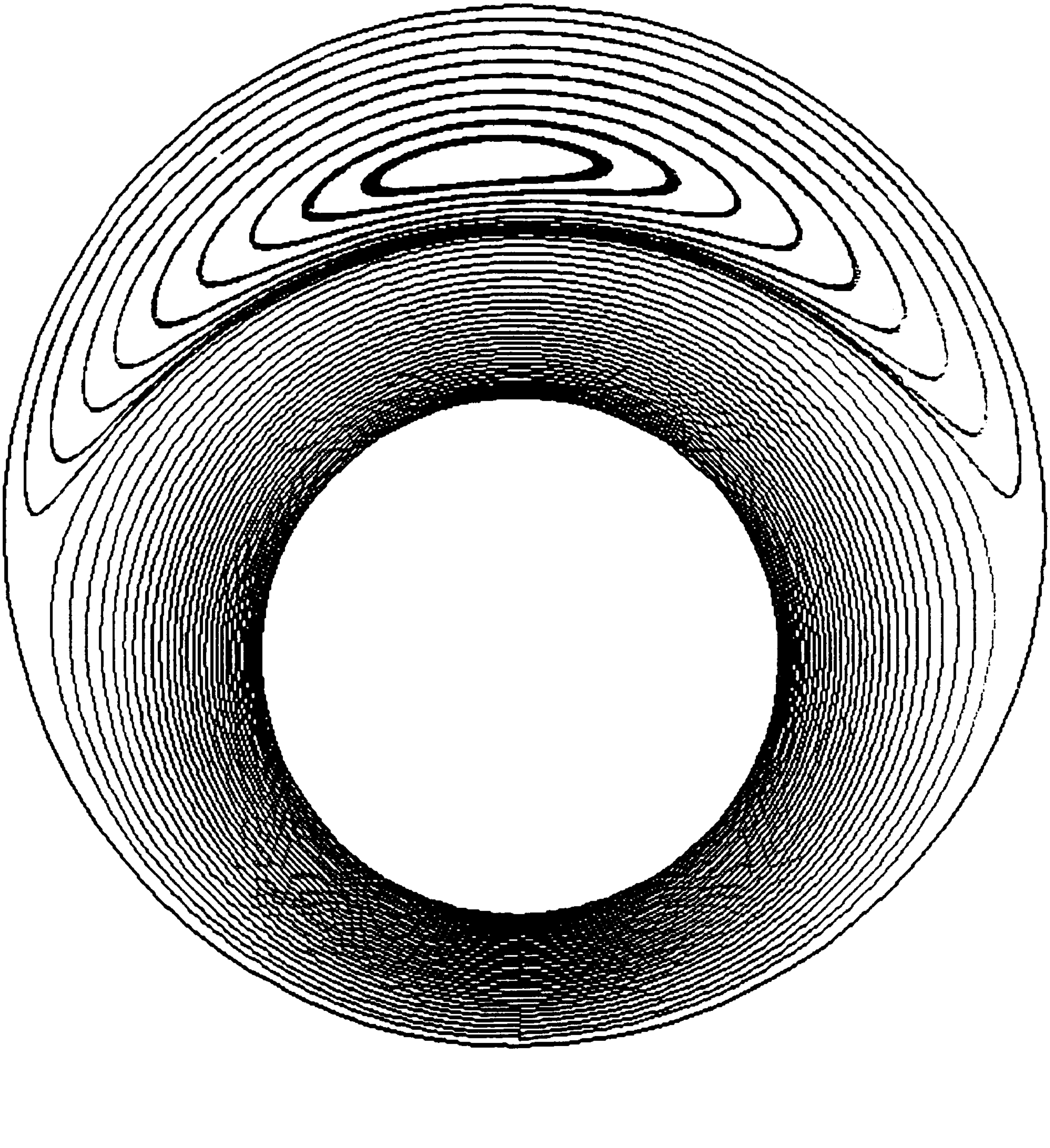

TWO ECCENTRIC CYLINDERS
PARTICLE TRACES

Preburner Pump Cavity

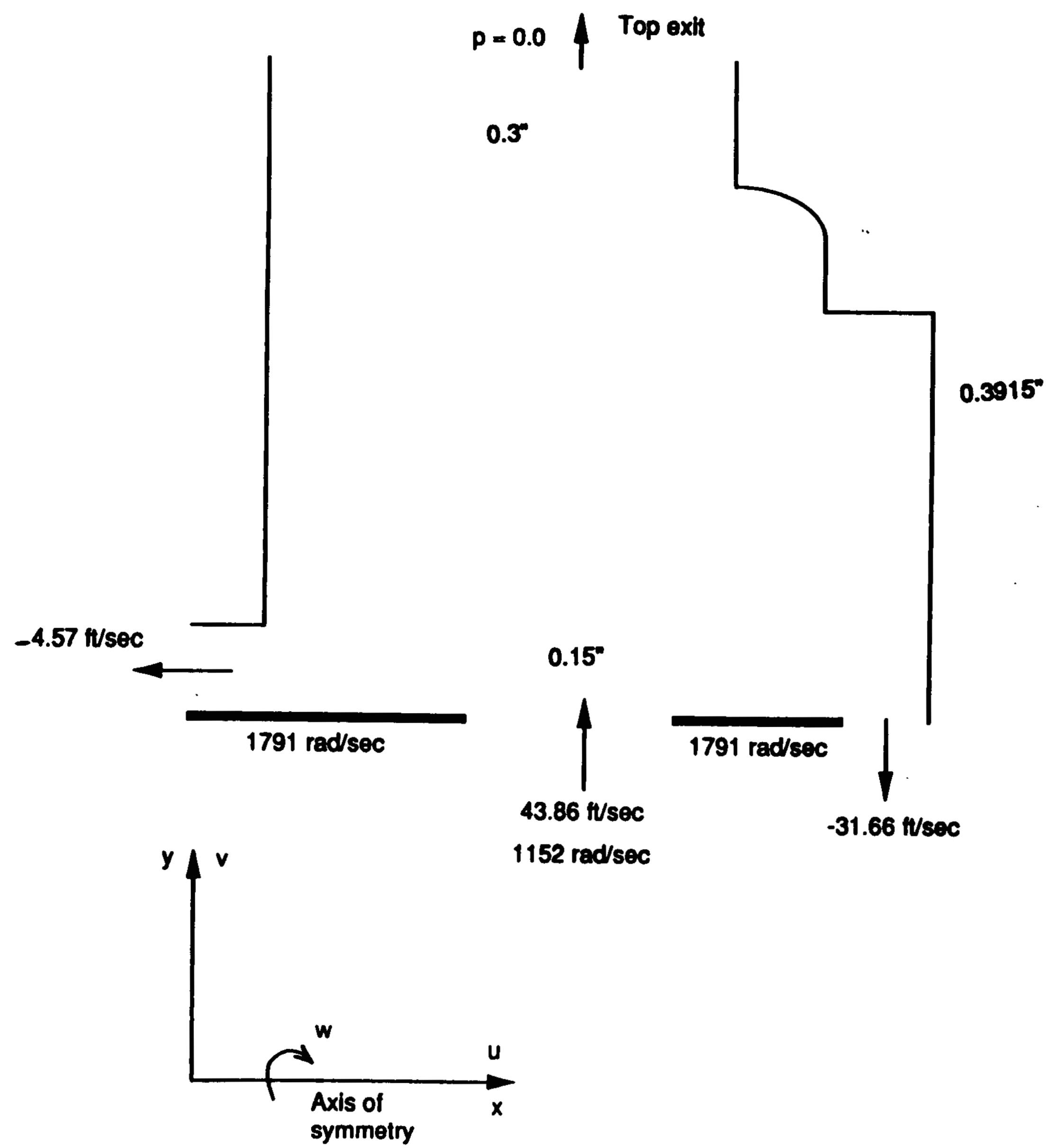

ATD PREBURNER DISCHARGE CAVITY
Grid 138 x 120

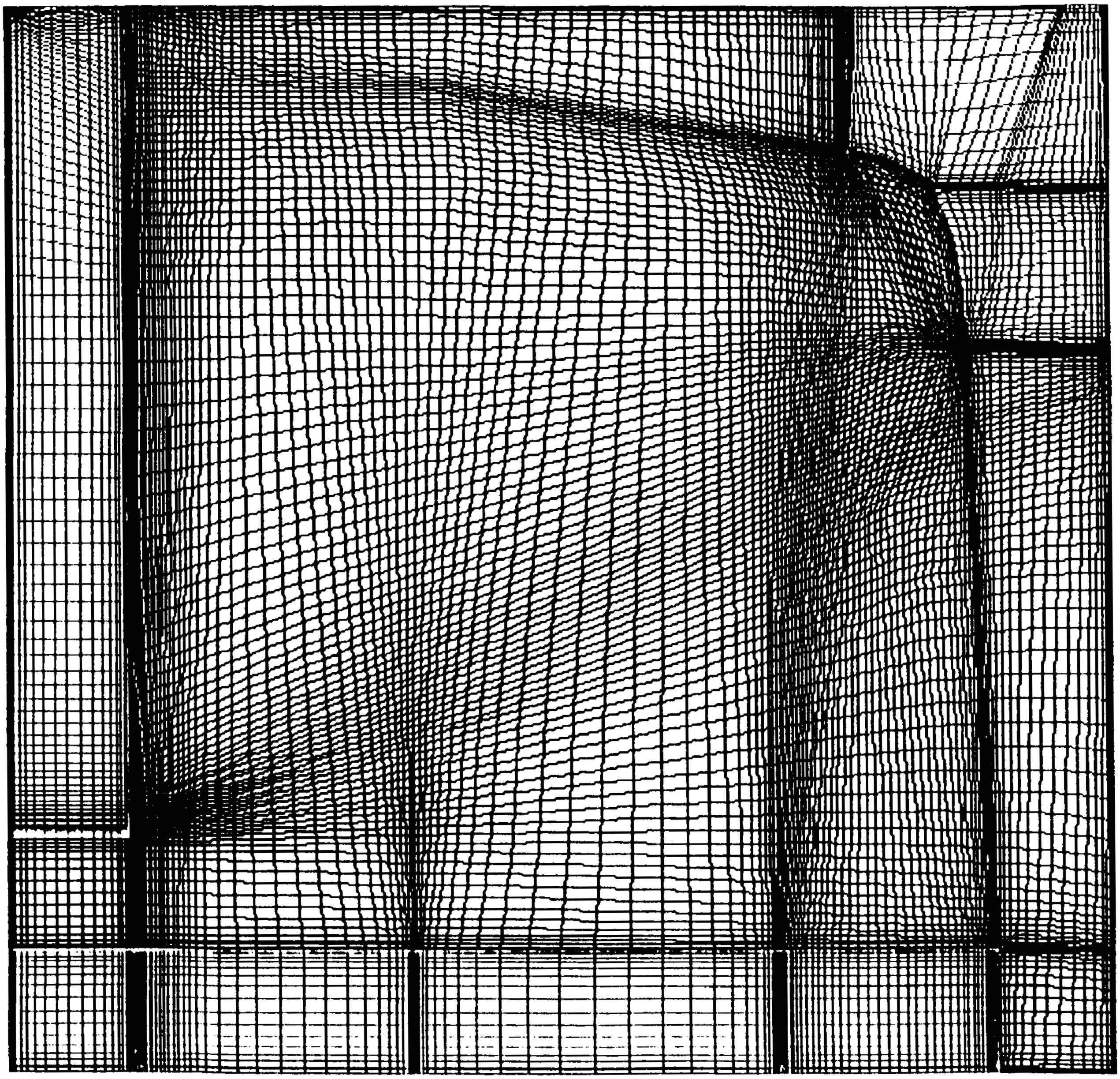

ATD PREBURNER DISCHARGE CAVITY

Relative Pressure Contours (psi)

CONTOUR LEVELS
-190.0
-180.0
-170.0
-160.0
-150.0
-140.0
-130.0
-120.0
-110.0
-100.0
-90.0
-80.0
-70.0

-40.0
-30.0
-20.0
-10.0
0.0
10.0
20.0
30.0

ATD PREBURNER DISCHARGE CAVITY
Swirl Velocity Contours (fps)

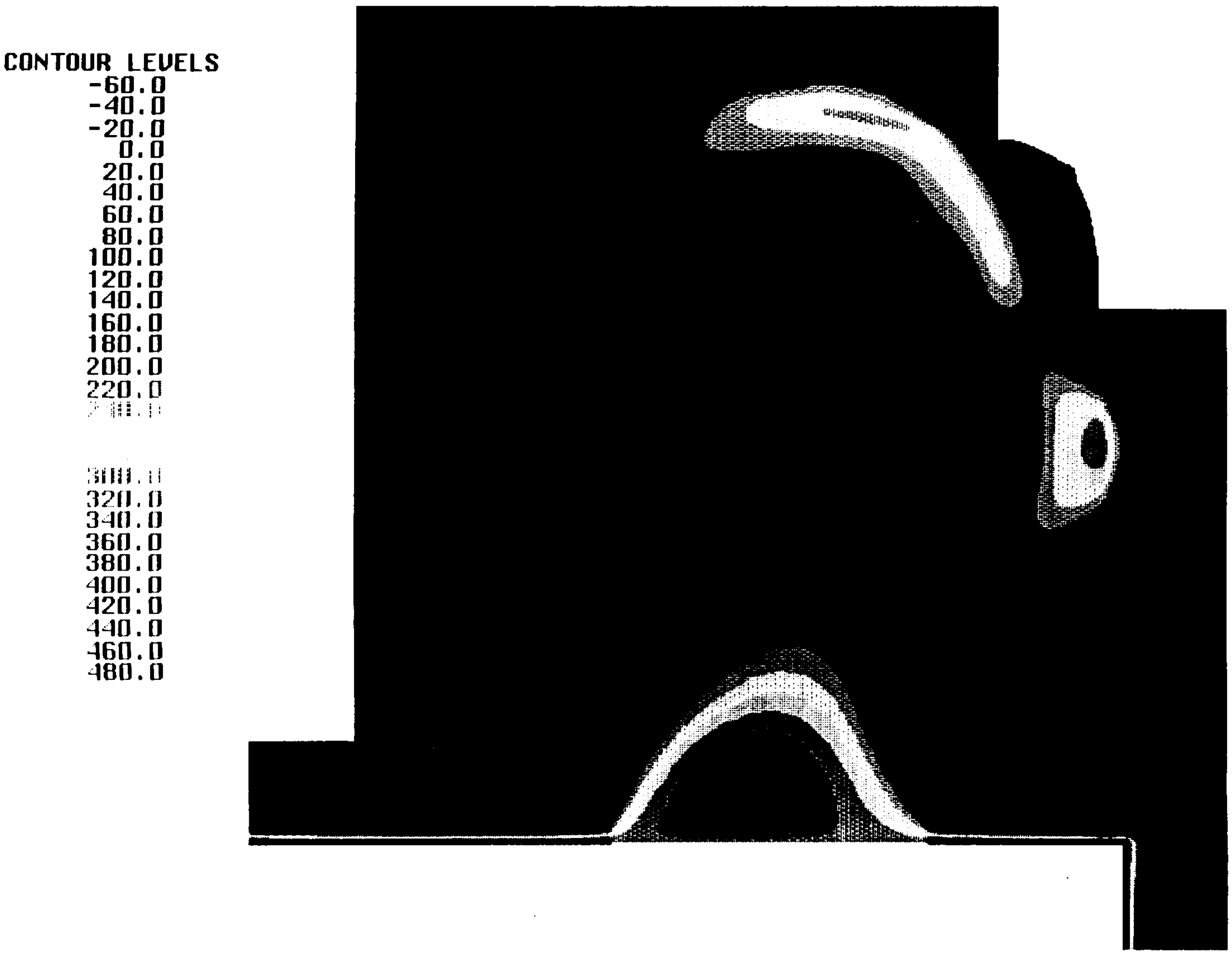

ATD PREBURNER PUMP CAVITY
Particle Traces

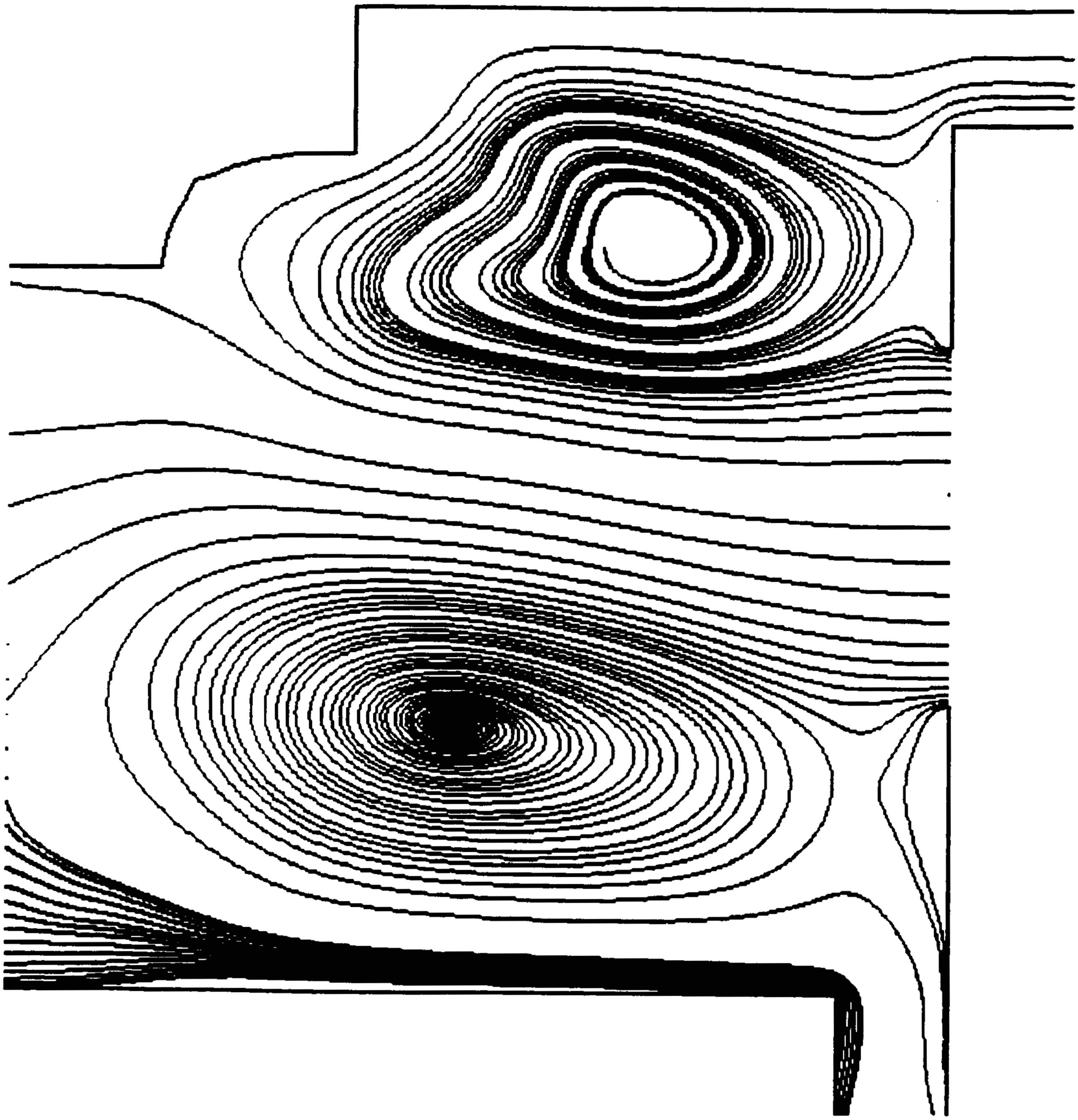

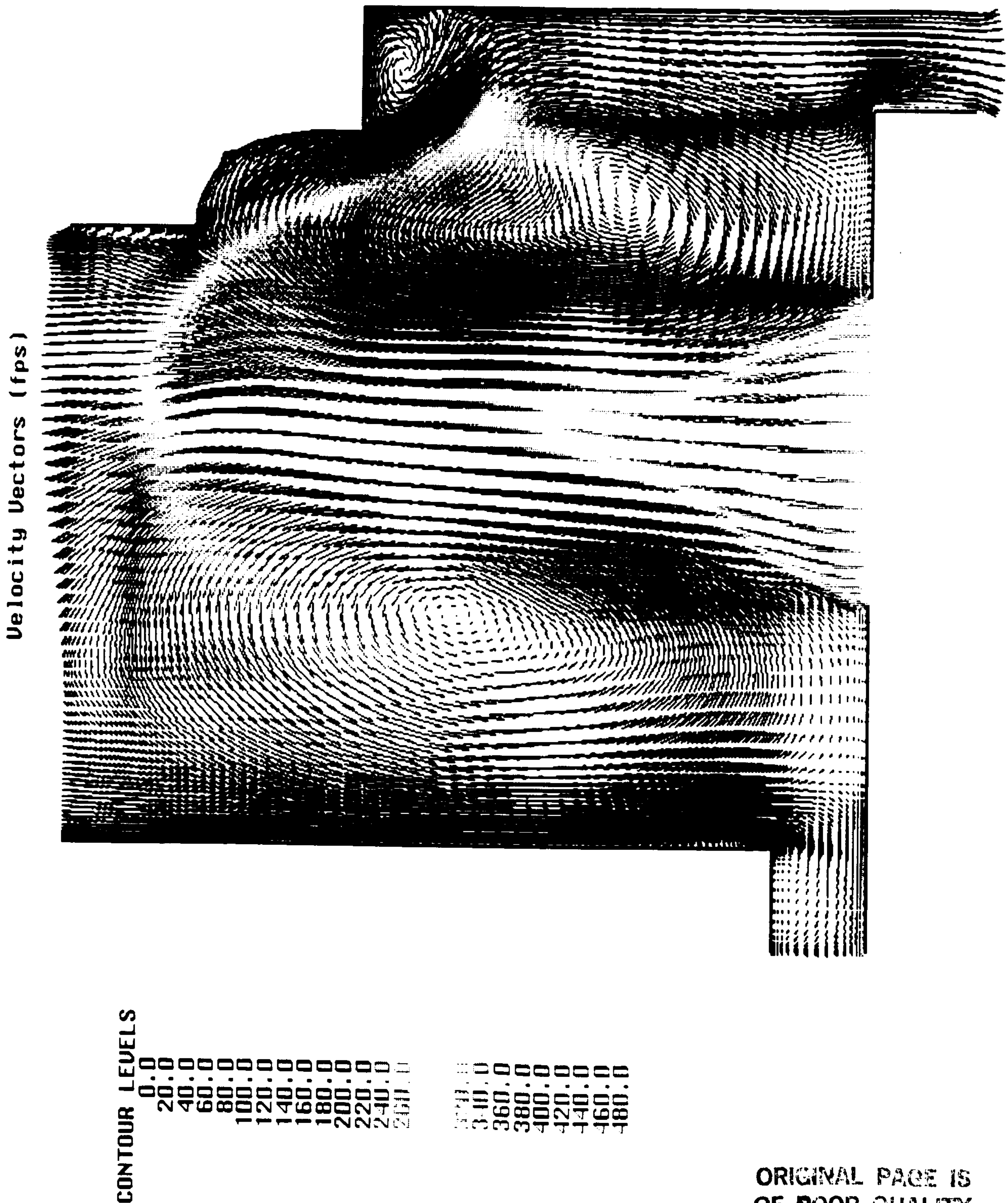

ORIGINAL PAGE IS
OF POOR QUALITY

N92-32272

Development of the KIVA-II CFD Code for Rocket Propulsion Applications

by Robert V. Shannon Jr.
and
Alvin L. Murray

Aerotherm Corporation
1500 Perimeter Parkway, Suite 225
Huntsville, AL 35806

Due to the existence of liquid, solid, and hybrid rocket motors a need exists for a fluid dynamics code which can solve for both the Navier-Stokes equations in multi-dimensions as well for liquid and solid particle motion within the gas flow domain. This type of CFD code must couple the gas and particle motion so that the effects of one upon the other can begin to be understood. Disciplines such as the evaluation of solid motor performance as well as nozzle erosion predictions for solid motors have a great need for the type of information that this type of computer code can provide. In addition, it is difficult to accurately simulate liquid motor combustion chamber flows without solving for the liquid oxidizer droplet motion, breakup, and evaporation coupled with the reacting gas flow.

The KIVA-II code, originally developed at Los Alamos National Laboratories to solve fluid dynamics problems in internal combustion engines, has been developed to solve rocket propulsion type flows. This work was supported by the NASA Solid Propulsion Integrity Program. The objective of the work performed was to develop this CFD code so that both liquid and solid particle motion could be simulated for arbitrary geometry and for high speed as well as low speed reacting flows.

Modification of the KIVA-II gas flow algorithm involved: incorporating independently specifiable supersonic and subsonic inflows and outflows, symmetric as well as periodic boundary conditions, the capability to use generalized single or multi-specie thermodynamic data and transport coefficients and allowing the user to specify arbitrary wall temperature/ heat flux distributions. Major modifications to the algorithms involving both convection and diffusion were successfully performed and results have been compared with some available experimental data on nozzle flows to verify these modifications.

Modification of the algorithms governing particle motion involved: incorporation of multi-specie particle types, generalized liquid property thermodynamic data, options which prevent or allow particle evaporation, a generalized particle injection algorithm, simulation of particle elastic or inelastic collisions with solid boundaries, periodic or symmetric particle boundary conditions at boundaries which are not inflow, outflow, or wall boundaries, and incorporation of a particle drag model which allows for both Reynolds and Mach number effects on particle drag coefficients.

This new CFD code has been shown to successfully solve rocket propulsion flows as well as rocket propulsion flows with entrained particles for several different rocket nozzles, submerged and otherwise. Verification of this new CFD code continues by comparing results to experimental data as well as to predictions of other CFD codes. This program is proving to be a valuable tool in the prediction of rocket propulsion flows.

Development of the KIVA-II CFD Code for Rocket Propulsion Applications

by

R.V. Shannon Jr.
and
A.L. Murray

Aerotherm Corporation
Huntsville, Alabama

Aerotherm Corporation
A Subsidiary of DynCorp

Original KIVA-II Code - General Information

- KIVA-II code originally issued in May 1989
- Approx. 14000 source lines including routines for plotting
- Authored by A.A. Amsden, P.J. O'Rourke, T.D. Butler
- Two-equation turbulence k-e model
- Kinetic and/or equilibrium chemical reaction modeling
- Stochastic particle technique for liquid sprays
- Initial and boundary conditions written specifically for IC engine calculations

Original KIVA-II Code - General Information

- Some boundary conditions inappropriate for high-speed flow problems
- Subsonic inflow boundary conditions not coupled with the overall pressure field solution
- Fuel spray was single component but modeling for droplet collisions and aerodynamic breakup was incorporated.

Aerotherm Corporation
A Subsidiary of DynCorp

KIVA-IIG Code - General Changes Gas Flows

- Approx. 30000 source lines not including routines for plotting
- Multiple inflow/outflows allowed
- Symmetric as well as periodic boundary conditions allowed
- Advection routines were recast in a form which directly computes the fluxes before using them
- Thermodynamic data input will allow for multiple species thermodynamic data. Alternatively, an equilibrium gas mixture can be modeled by a single Mollier table.
- Species transport property data is independently specified allowing for fewer points in regions where these quantities do not vary much. Viscosity, specific heats, and conductivity may all vary with pressure as well as temperature.

KIVA-IIG Code - General Changes Gas Flows

- Multiple wall types may be specified allowing the user to have a wall temperature distribution in his/her flowfield calculation.
- Conjugate Residual Method used for calculating the pressure and temperature fields now includes boundary condition specifications.

Aerotherm Corporation
A Subsidiary of DynCorp

KIVA-IIG Code - General Changes Parcel Motion

- Multiple particle species available
- Generalized liquid property thermodynamic data
- Option to prevent or allow particle evaporation for each particle type
- Generalized particle injection algorithm which makes each simulated injector independent of all other injectors as far as injector characteristics
- Simulation of particle elastic or inelastic collisions with solid boundaries
- Periodic or symmetric particle boundary conditions at fluid boundaries
- 3 different particle drag models available

JPL Nozzle Test Case

- Chamber temperature 1100 Kelvin
- Chamber pressure $4.9(10)^6$ dynes/cm^2 = 4.8 atm
- Air was modeled by a single Mollier table representing thermodynamic data for equilibrium air.

Aerotherm Corporation
A Subsidiary of DynCorp

PLANAR NOZZLE GRID

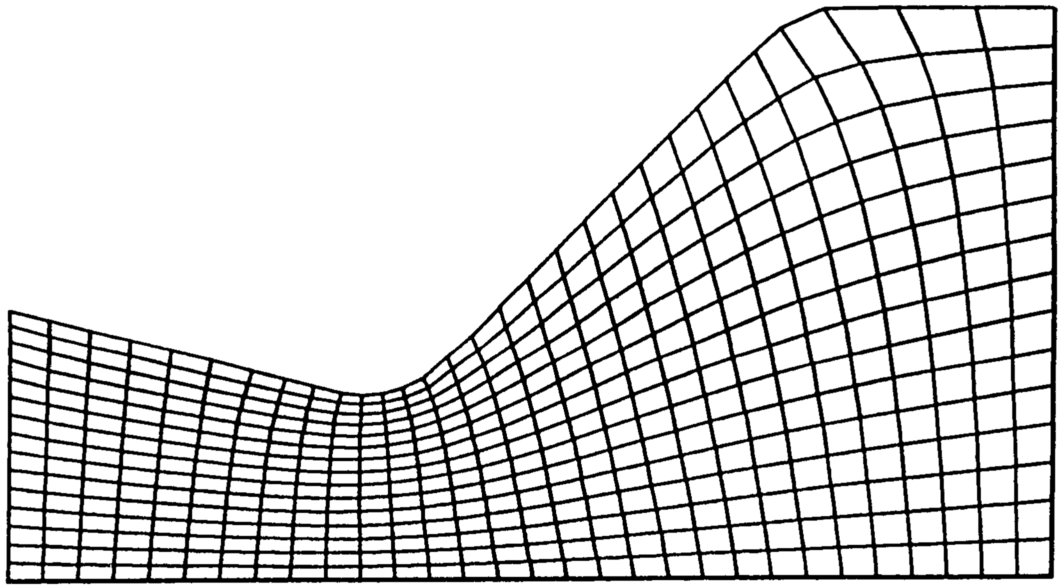

Aerotherm Corporation
A Subsidiary of DynCorp

VELOCITY VECTORS FOR PLANAR NOZZLE

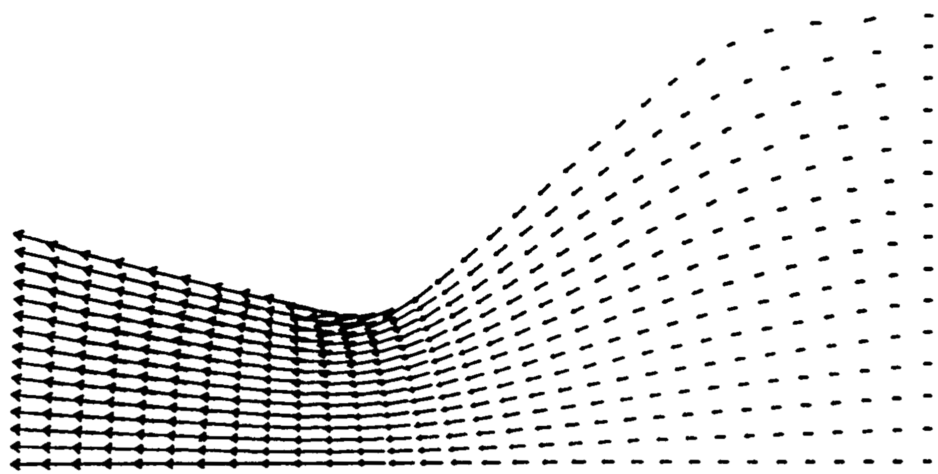

Aerotherm Corporation
A Subsidiary of DynCorp

PLANAR NOZZLE PRESSURE CONTOURS

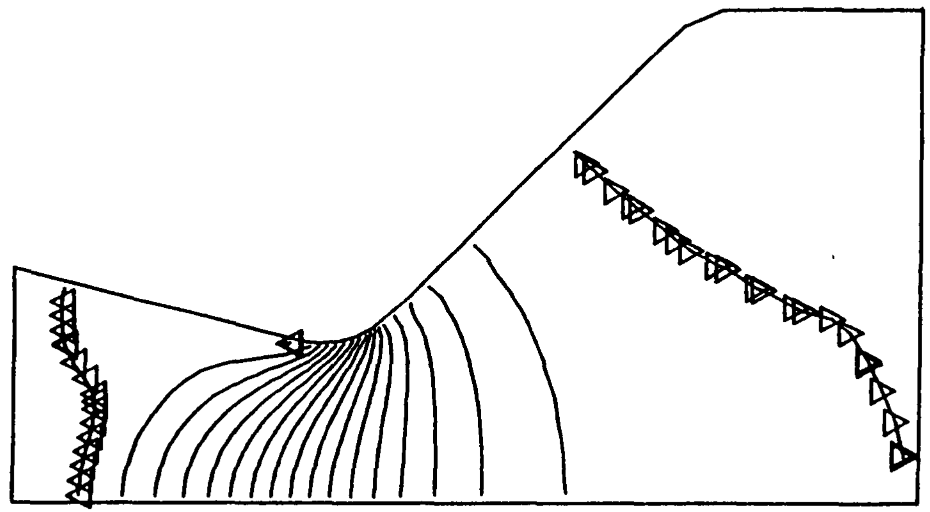

Aerotherm Corporation
A Subsidiary of DynCorp

PLANAR NOZZLE TEMPERATURE CONTOURS

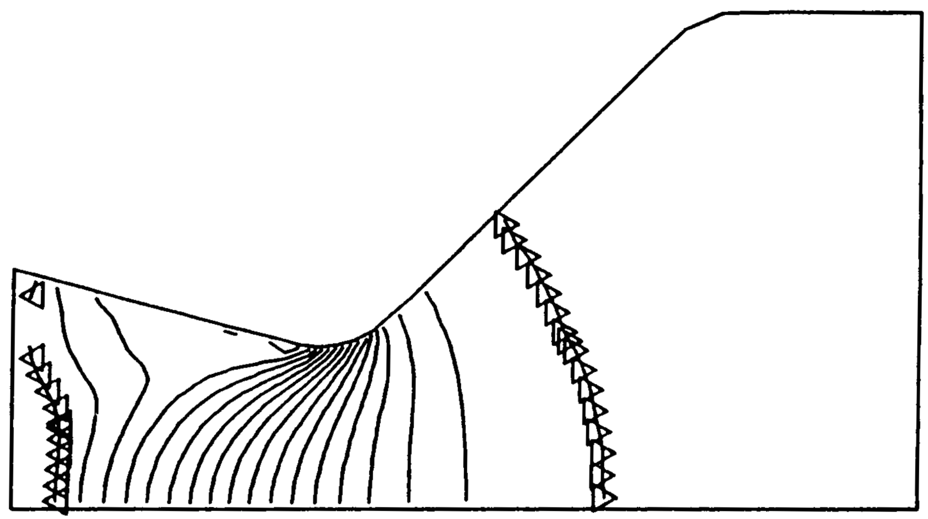

Aerotherm Corporation
A Subsidiary of DynCorp

PLANAR NOZZLE MACH NUMBER CONTOURS

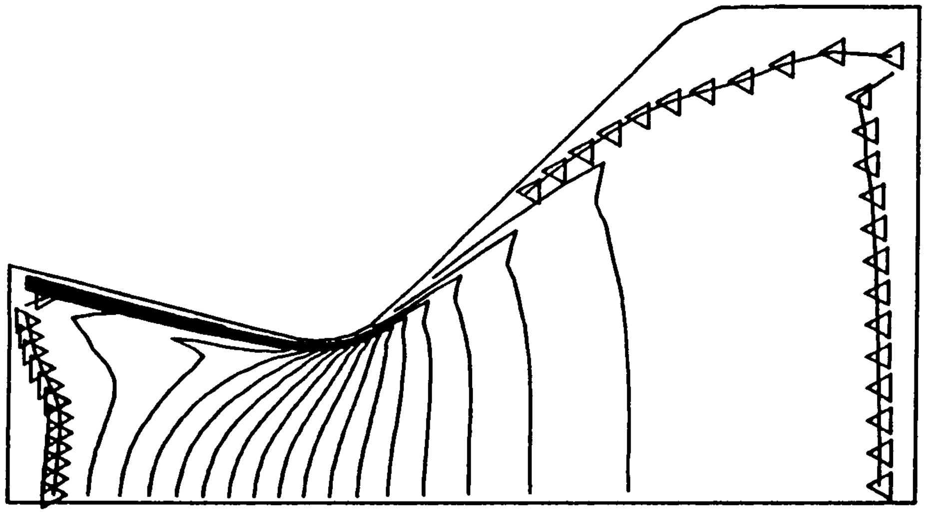

Aerotherm Corporation
A Subsidiary of DynCorp

Two Inch Motor Test Case

- Chamber temperature 3564 Kelvin
- Chamber pressure $5.9(10)^7$ dynes/cm^2 = 58 atm
- The gas mixture of many species was modeled by a single Mollier table representing thermodynamic data for the equilibrium mixture.
- Nozzle geometry is unusual.

TWO INCH MOTOR NOZZLE TEST CASE

FLOW ANALYSIS GRID

CALCULATED VELOCITY VECTORS

Aerotherm Corporation
A Subsidiary of DynCorp

TWO INCH MOTOR NOZZLE TEST CASE

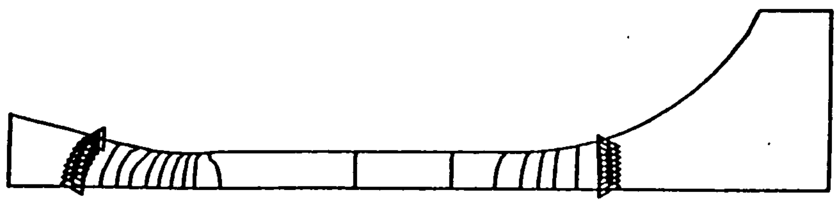

▷ QMAX = 5.64E+07 dynes/cm^2
◁ QMIN = 5.64E+06 dynes/cm^2
DQ = 2.98E+06 dynes/cm^2

CALCULATED PRESSURES

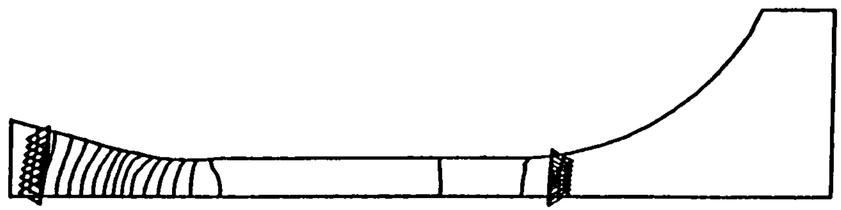

▷ QMAX = 3493 °K
◁ QMIN = 2254 °K
DQ 73 °K

CALCULATED TEMPERATURES

Aerotherm Corporation
A Subsidiary of DynCorp

TWO INCH MOTOR NOZZLE TEST CASE

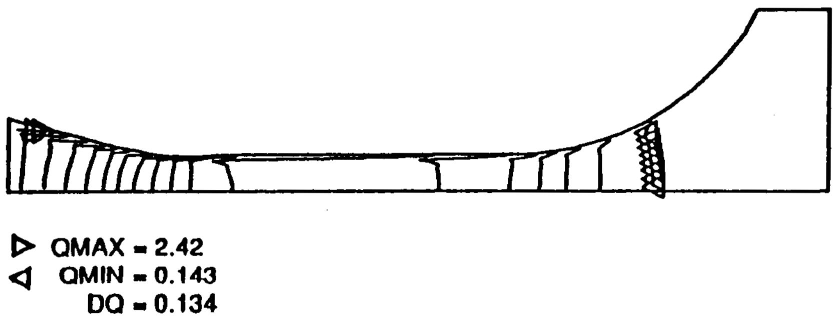

CALCULATED MACH CONTOURS

Aerotherm Corporation
A Subsidiary of DynCorp

MNASA Motor Test Nozzle Flowfield Analysis

- Chamber temperature 3564 Kelvin
- Chamber pressure $5.1(10)^7$ dynes/cm^2 = 50 atm
- The gas mixture of many species was modeled by a single Mollier table representing thermodynamic data for the equilibrium mixture.
- 10 micron particles "injected" into the flowfield. Injected particle density was 3.94 grams/cm^3.
- Crowe-Hermsen modified drag model used.
- Gas-particle momentum and energy coupled

Aerotherm Corporation
A Subsidiary of DynCorp

MNASA MOTOR TEST CONFIGURATION

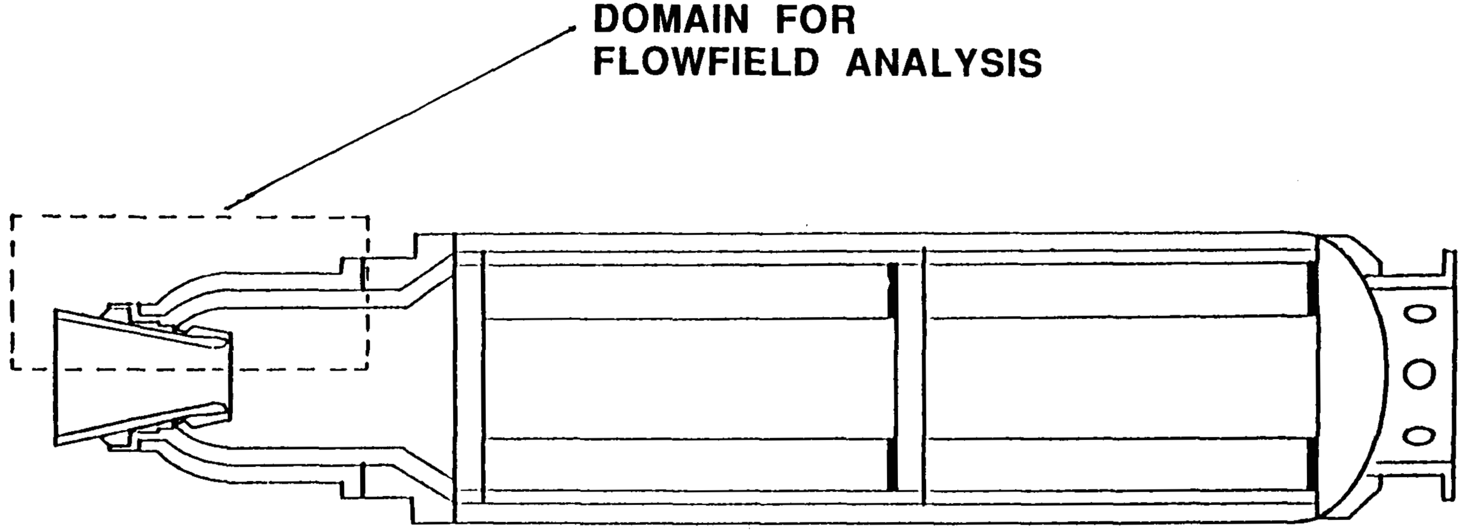

Reference Thiokol Report TWR-60115

Aerotherm Corporation
A Subsidiary of DynCorp

KIVA - IIG FLOWFIELD GRID

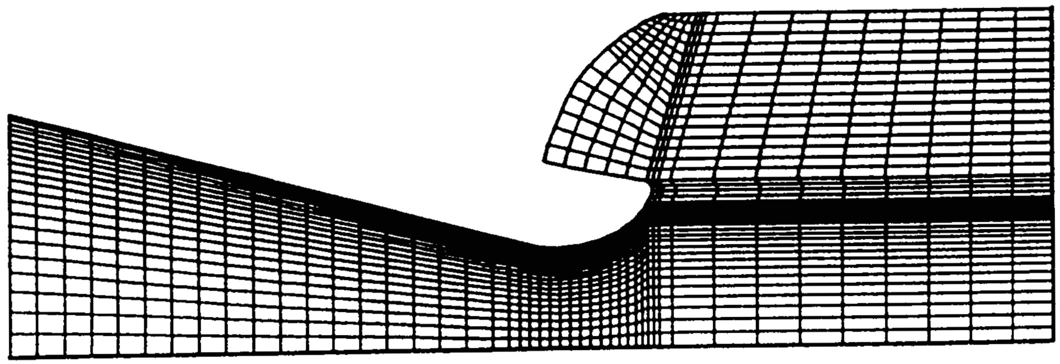

Aerotherm Corporation
A Subsidiary of DynCorp

MNASA MOTOR NOZZLE VELOCITY VECTORS

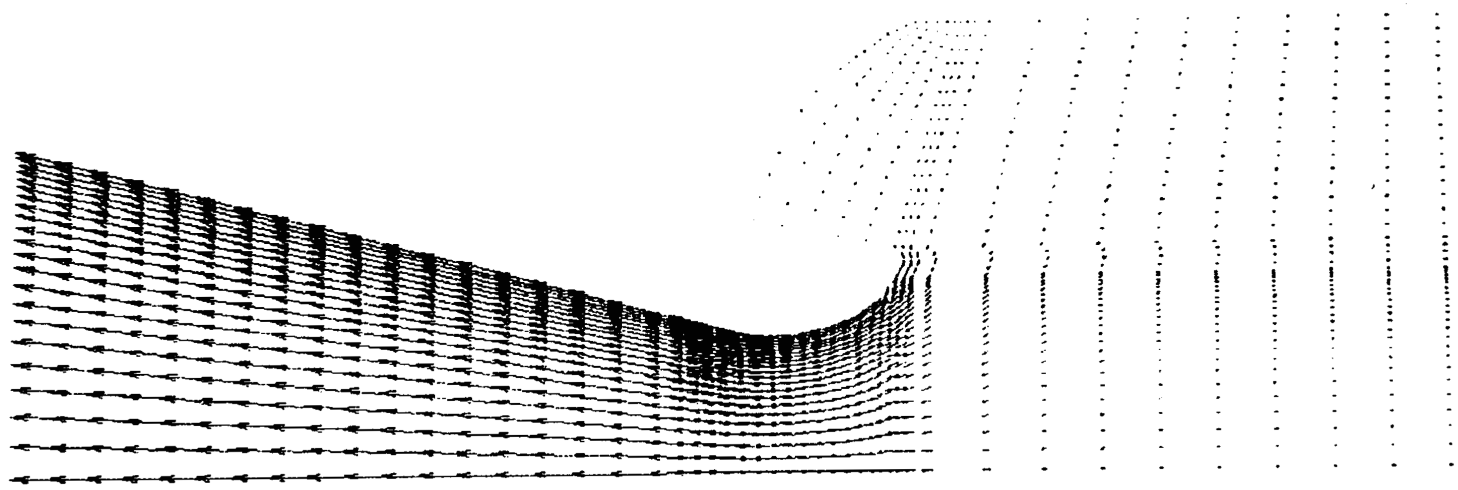

Aerotherm Corporation
A Subsidiary of DynCorp

MNASA MOTOR PRESSURE FIELD

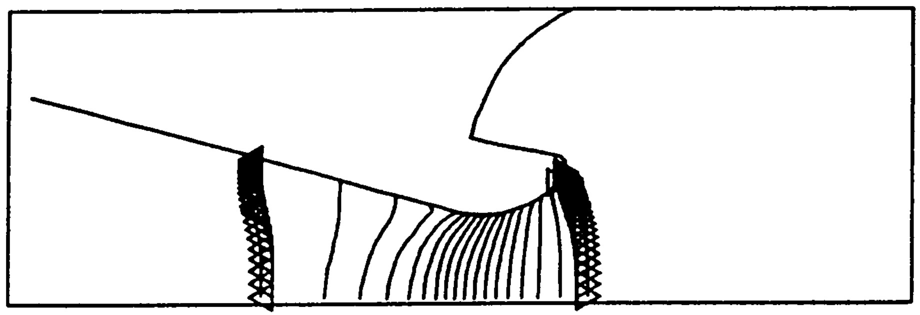

Aerotherm Corporation
A Subsidiary of DynCorp

MNASA MOTOR TEMPERATURE FIELD

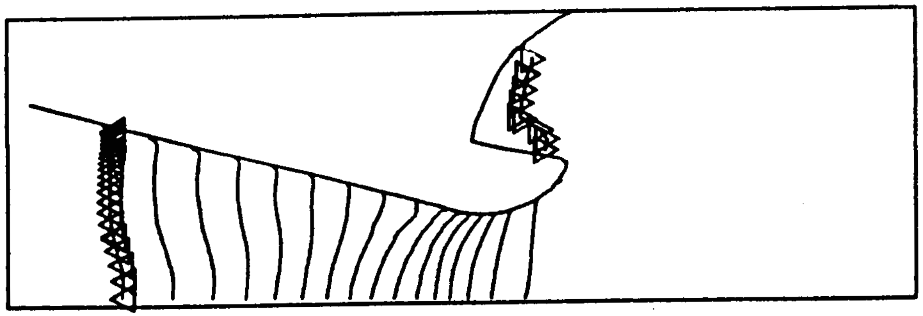

Aerotherm Corporation
A Subsidiary of DynCorp

MNASA MOTOR MACH NUMBER CONTOURS

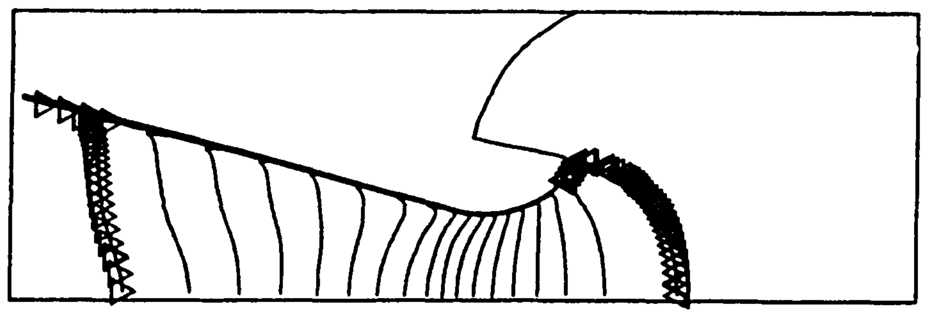

Aerotherm Corporation
A Subsidiary of DynCorp

PARCEL VELOCITY CHRONOLOGY

T = $7.5(10)^{-5}$ sec

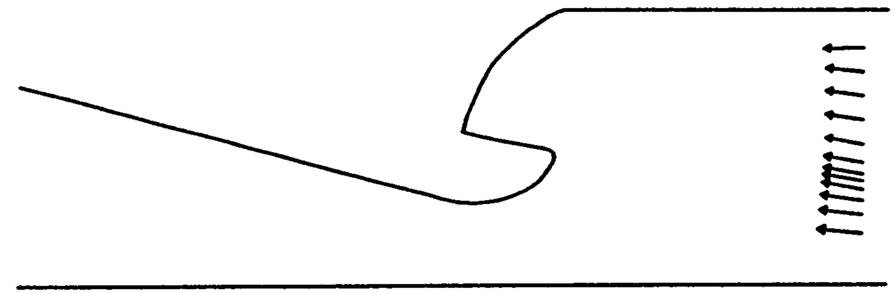

T = $2.8(10)^{-3}$ sec

T = $4.0(10)^{-3}$ sec

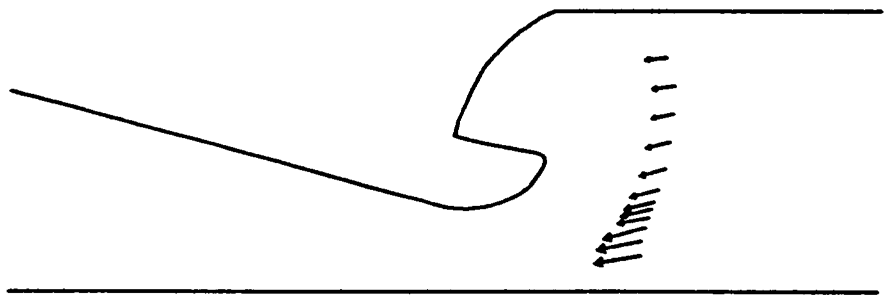

Aerotherm Corporation
A Subsidiary of DynCorp

PARCEL VELOCITY CHRONOLOGY

T = $4.4(10)^{-3}$ sec

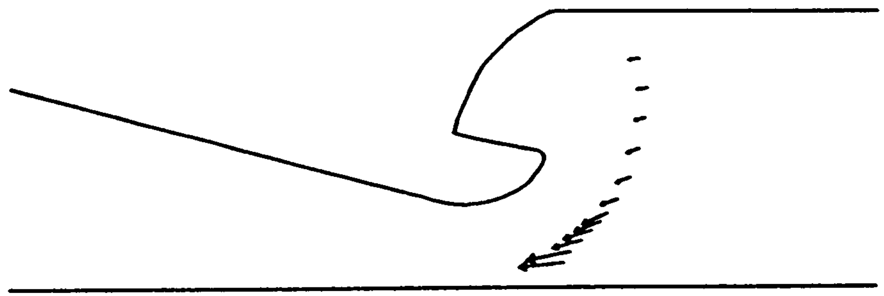

T = $4.7(10)^{-3}$ sec

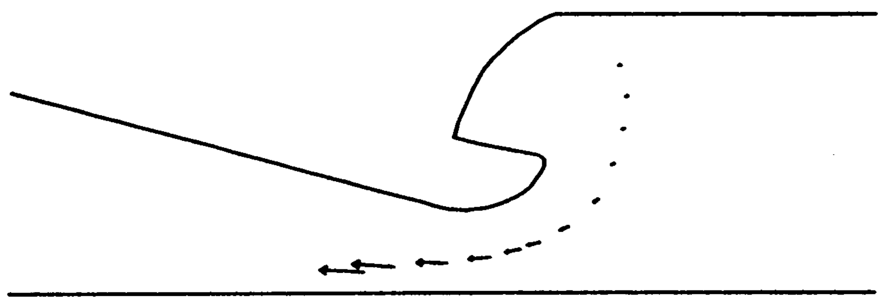

T = $4.8(10)^{-3}$ sec

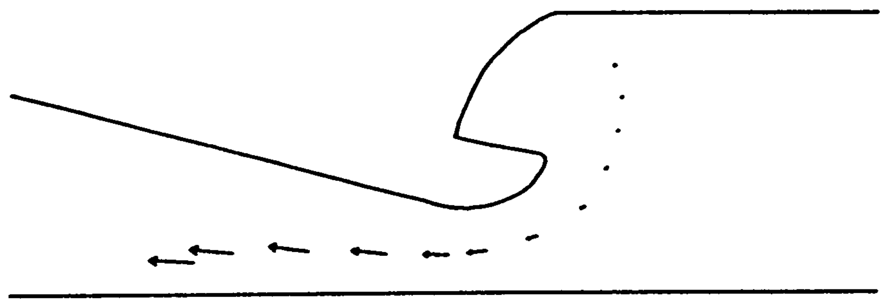

Aerotherm Corporation
A Subsidiary of DynCorp

PARCEL VELOCITY CHRONOLOGY

$T = 4.9(10)^{-3}$ sec

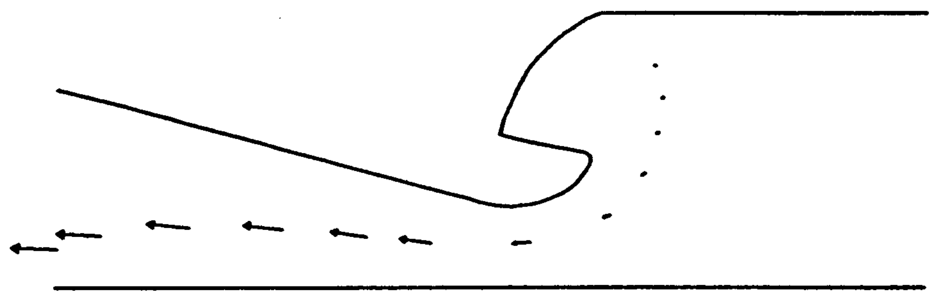

$T = 5.1(10)^{-3}$ sec

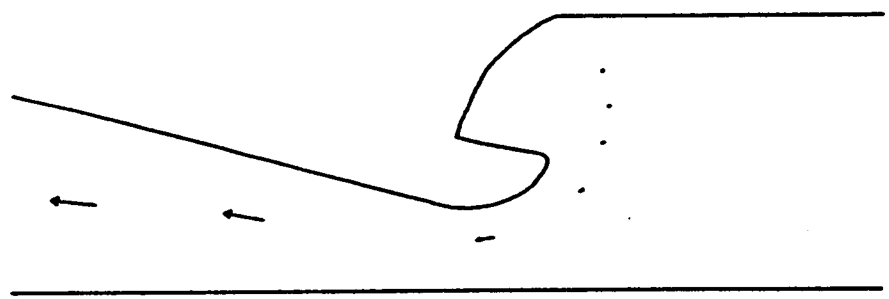

$T = 5.3(10)^{-3}$ sec

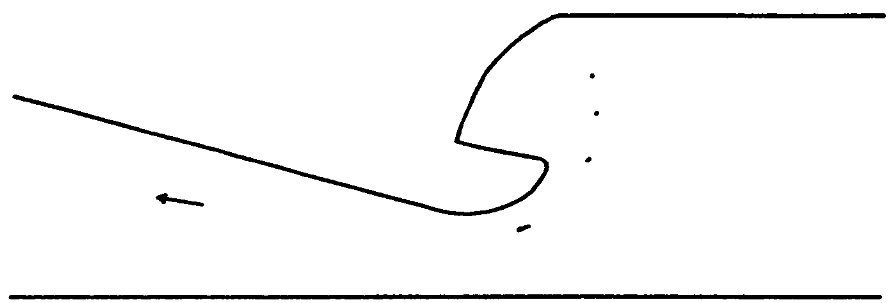

Aerotherm Corporation
A Subsidiary of DynCorp

PARCEL VELOCITY CHRONOLOGY

$T = 5.7(10)^{-3}$ sec

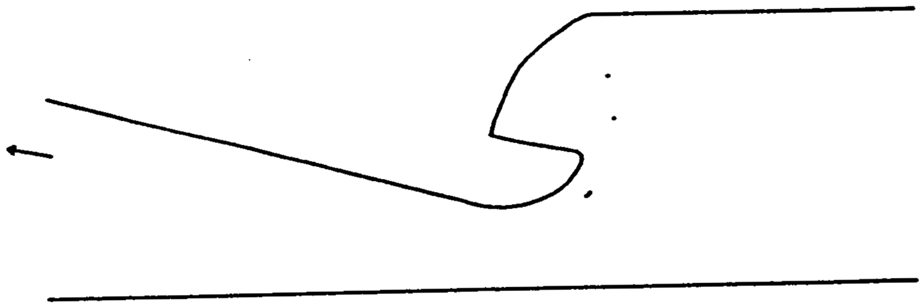

$T = 5.72(10)^{-3}$ sec

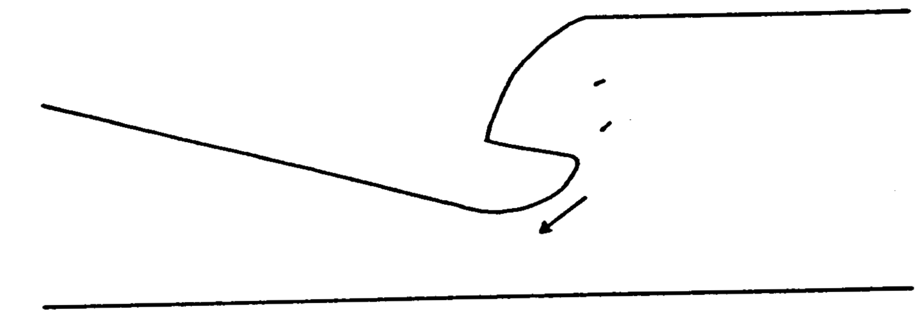

$T = 5.73(10)^{-3}$ sec

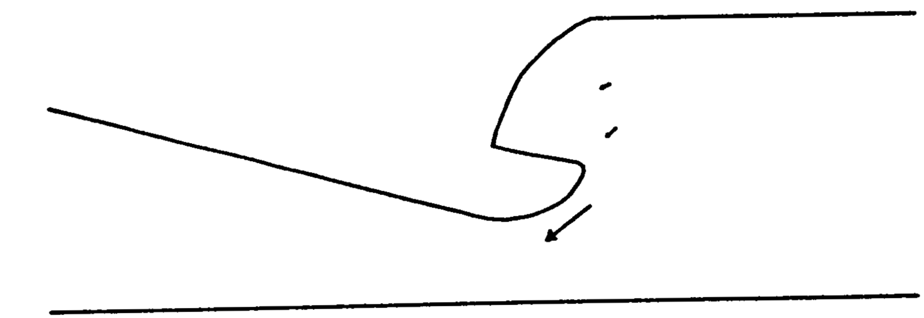

Aerotherm Corporation
A Subsidiary of DynCorp

MNASA MOTOR 10 MICRON PARTICLE TREJECTORIES

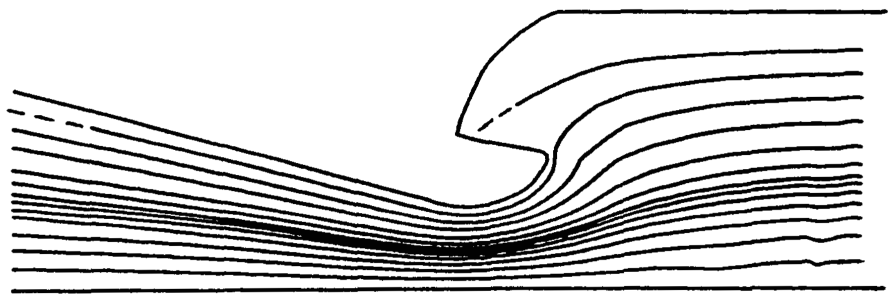

Aerotherm Corporation
A Subsidiary of DynCorp

Summary

- A new finite volume 2D/3D Navier-Stokes CFD code has been developed by using the KIVA-II code as the starting point.
- Demonstration of this new code has been shown with promising results and verification with experimental data will continue.
- Particle motion has been verified for low particle Reynolds numbers and demonstrated for typical solid rocket motor flowfields.

Aerotherm Corporation
A Subsidiary of DynCorp

N92-32273

A Computational Design System for Rapid CFD Analysis

E.P. Ascoli, S.L. Barson, M.E. DeCroix, and M.M. Sindir
CFD Technology Center
Rockwell International, Rocketdyne Division
Canoga Park, California

Effective application of computational fluid dynamics (CFD) in the engineering environment requires that key design and analysis tools be integrated to the greatest extent possible. A computational design system (CDS) is described in which these tools are integrated in a modular fashion. This CDS ties together four key areas of computational analysis; description of geometry, grid generation, computational codes, and postprocessing. Common input and output formats and necessary translators are established to facilitate data transfer between the four key areas and to enhance system modularity. Advances made in three key areas are described.

Significant progress has been made toward integration of geometry definition systems with CFD grid generation tools. Geometric data have successfully been passed from the Catia CAD and Patran CAE systems to the Rockwell Automated Grid Generation System (RAGGS). The IGES standard was employed in each case. The CFD Pump Consortium impeller geometry is used to illustrate that a reasonable level of integration is achievable for complex geometries.

While many CFD grid generators are available in the public domain, their capabilities vary widely. An effort is underway to systematically review available codes, identify those most applicable, and integrate them into the CDS described. Seven grid generation codes are currently being reviewed according to previously defined evaluation criteria described herein.

Postprocessing tools are being developed, reviewed, and integrated into the CDS as well. Engineering data extraction tools are being developed to be completely consistent with existing code methodologies and to remain completely modular. Tools for data visualization have advanced noticeably over the last few years. These are being reviewed and integrated into the CDS.

Integration of improved CFD analysis tools through integration with the Rocketdyne CDS has made a significant positive impact in the use of CFD for engineering design problems. Complex geometries are now analyzed on a frequent basis and with far greater ease.

a-8

A COMPUTATIONAL DESIGN SYSTEM FOR RAPID CFD ANALYSIS

E.P. Ascoli, S.L. Barson, M.E. DeCroix, and M.M. Sindir
Rockwell International, Rocketdyne Division

Workshop for Computational Fluid Dynamic
Applications in Rocket Propulsion

April 28-30, 1992
NASA Marshall Space Flight Center

Rockwell International
Rocketdyne Division

CFD 92-030-013/D2/SLB

INTEGRATION OF CFD TOOLS NEEDED FOR EFFICIENT APPLICATION IN ENGINEERING ENVIRONMENT

- **APPLICATION OF CFD IN ENGINEERING CYCLE REQUIRES:**
  - INTEGRATION WITH EXISTING TOOLS AND PROCEDURES
  - USE FOR MULTIPLE LEVELS OF ANALYSIS
    - RAPID TURNAROUND PARAMETRICS
    - FINAL DETAIL DESIGN ANALYSIS

- **PAST EMPHASIS ON FLOW SOLVER DEVELOPMENT OUTPACED THAT OF "PERIPHERAL" TOOLS**
  - PRE- AND POST-PROCESSING CAN TAKE MORE THAN 50% OF TOTAL CYCLE TIME
  - TOOL INTERFACES OFTEN POOR OR COMPLETELY LACKING

Rockwell International
Rocketdyne Division

CFD 92-030-014/D2/SLB

COMPUTATIONAL DESIGN SYSTEM INTEGRATES ANALYTICAL TOOLS FOR EFFICIENT USE

- **TIES TOGETHER FOUR KEY AREAS OF COMPUTATIONAL ANALYSIS**
  - GEOMETRIC DESCRIPTION - MATHEMATICAL REPRESENTATION OF HARDWARE GEOMETRY
  - GRID GENERATION - DISCRETIZATION OF FLOW DOMAIN
  - COMPUTATIONAL CODES - ANALYTICAL SOLUTION
  - POST-PROCESSING - REDUCTION, ORGANIZATION, AND PRESENTATION OF ANALYTICAL DATA
- **ESTABLISHES COMMON INPUT/OUTPUT FORMATS AND NECESSARY TRANSLATORS**
- **MODULAR APPROACH ALLOWS USE OF MOST APPROPRIATE TOOL FOR EACH APPLICATION**

Rockwell International
Rocketdyne Division

CFD 92-030-015/D2/SLB

ROCKETDYNE ADVANCED COMPUTATIONAL ENGINEERING SYSTEM (RACES)

GEOMETRY / SURFACE DEFINITION
- **EXISTING CAD SYSTEMS** (e.g. CATIA)
- **CAE SYSTEMS** (e.g. PATRAN)
- **USER-DEFINED** (e.g. ALGEBRAIC)

GRID GENERATION OPTIONS
(SURFACE AND VOLUME GRIDS)
- **INTEGRATED** (e.g. PATRAN)
- **SEPARATE** (e.g. RAGGS)

COMPUTATIONAL CODES
- **ALL EXISTING MAJOR RD CODES**
- **ADD OTHERS AS NEEDED**

POST-PROCESSING
- **ENGINEERING DATA REDUCTION**
- **DATA VISUALIZATION**
- **DATABASE OF CFD SOLUTIONS**

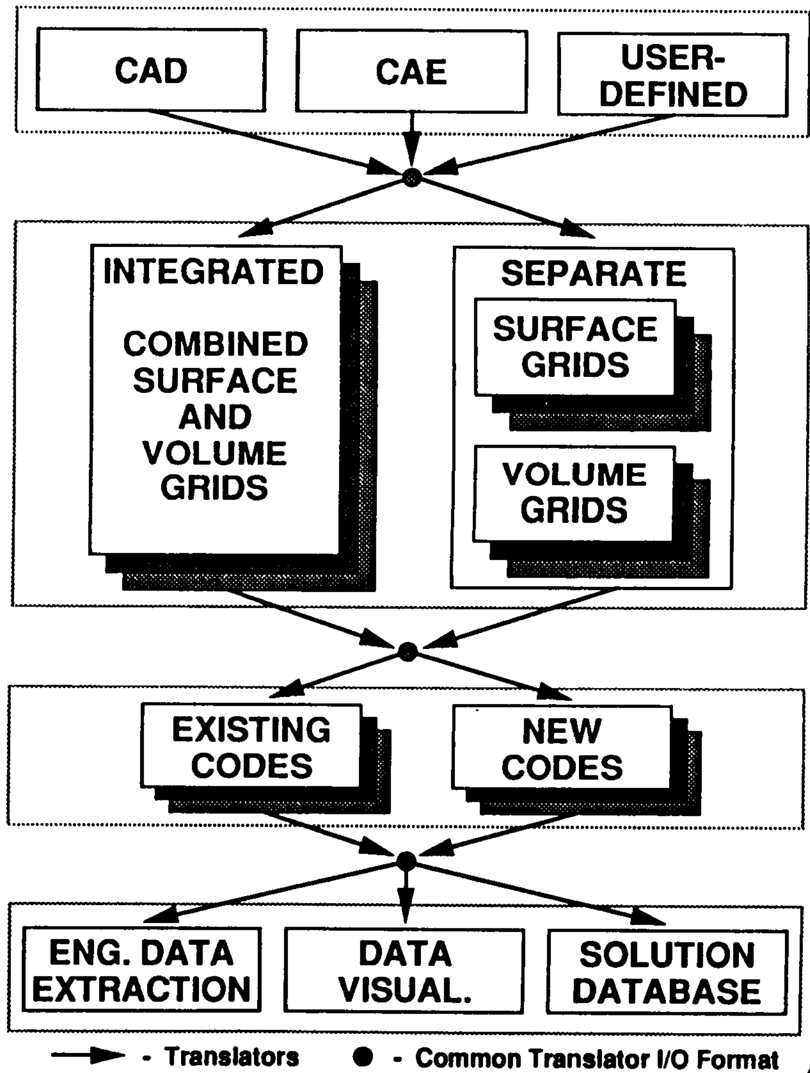

CFD 92-030-016/D2/SLB

Rockwell International
Rocketdyne Division

ADVANCES MADE TOWARD IMPROVED AND UNIFIED SET OF CFD TOOLS

- INTEGRATION OF GEOMETRY DEFINITION SYSTEMS WITH GRID GENERATORS
- SYSTEMATIC REVIEW AND INTEGRATION OF AVAILABLE GRID GENERATION TOOLS
- DEVELOPMENT AND INTEGRATION OF NEW POSTPROCESSORS

Rockwell International
Rocketdyne Division

CFD 92-030-017/D2/SLB

CAD / CAE INTERFACES ESTABLISHED

- **IGES INTERFACE IDENTIFIED AS PREFERRED STANDARD**
  - INDUSTRY STANDARD
  - SUPPORTED BY MOST CAD AND CAE SOFTWARE
- **CATIA (CAD) GEOMETRY FILES PASSED TO ROCKWELL AUTOMATED GRID GENERATION (RAGGS) CODE**
  - COMPLEX GEOMETRY - CONSORTIUM IMPELLER
  - TRANSLATOR UPGRADES REQUIRED
- **PATRAN (CAE) GEOMETRY FILES PASSED TO RAGGS**
  - SEVERAL CASES RANGING FROM SIMPLE TO COMPLEX
  - EASY GEOMETRY CREATION METHOD
- **TRANSLATOR CHARACTERIZATION AND VALIDATION REQUIRED**

Rockwell International
Rocketdyne Division

CFD 92-030-018/D2/SLB

CATIA IMPELLER GEOMETRY PASSED TO RAGGS

3-D CFD GRID GENERATED

CATIA ⟶ IGES ⟶ RAGGS

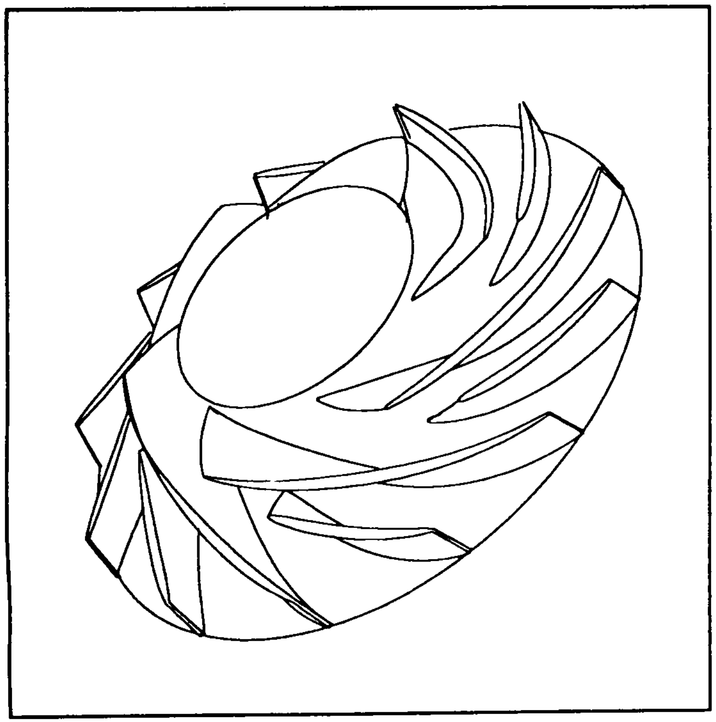

Rockwell International
Rocketdyne Division

CFD 92-030-019/D2/SLB

GRID GENERATORS REVIEWED

- **BACKGROUND**
  - MANY GRID GENERATION CODES CURRENTLY AVAILABLE
  - DIFFERENT APPROACHES AND CODE FEATURES
  - NEED EXISTS TO CONDUCT SYSTEMATIC REVIEW OF GRID GENERATION CODES CURRENTLY AVAILABLE
- **OBJECTIVE**
  - IDENTIFY MOST APPROPRIATE CODE(S)
  - INTEGRATE WITH RACES
- **APPROACH**
  - DEVELOP EVALUATION CRITERIA / SCORING GUIDELINES
  - IDENTIFY CANDIDATE CODES
  - THREE PHASES TO FINAL SELECTION
    - PRE-SCREEN
    - PRELIMINARY EVALUATION
    - FINAL EVALUATION

Rockwell International
Rocketdyne Division

CFD 92-030-020/D2/SLB

SEVEN GRID GENERATION CODES REVIEWED

• ICEM (CDC)	• EXTENSIVE CAD CAPABILITY • THIRD PARTY SOURCE
• IGB (NASA LEWIS)	• TEMPLATE TYPE FOR TURBINE BLADES • NOT A GENERAL PURPOSE CODE
• EAGLEVIEW (MSU)	• EAGLE BASED GRID GENERATION • NEW INTERACTIVE INTERFACE
• GENIE (MSU)	• FIRST GENERATION INTERACTIVE CODE • BEST SUITED FOR 2-D AND LIMITED 3-D
• GRIDGEN (GENERAL DYNAMICS)	• INTERACTIVE GENERAL PURPOSE CODE • HIGHLY RATED IN INDUSTRY
• PATRAN (PDA ENGINEERING)	• LIMITED AS CFD GRID GENERATOR • THIRD PARTY SOURCE
• RAGGS (ROCKWELL, NAA)	• INTERACTIVE GENERAL PURPOSE CODE • DEVELOPING PRODUCT

Rockwell International
Rocketdyne Division

CFD 92-030-021/D2/SLB

EVALUATION CRITERIA ESTABLISHED

FIVE MAIN CATEGORIES

- **GEOMETRY DEFINITION**
  - INTERFACES (INPUT AND OUTPUT)
  - CREATION CAPABILITY
  - SURFACE ACCURACY
    - AS TRANSLATED TO GG
    - AS CREATED IN GG
- **SURFACE AND VOLUME GRID CAPABILITIES**
  - ACCURACY WITH SURFACE DEFINITION
  - METHODOLOGIES AVAILABLE (e.g., ALGEBRAIC, ELLIPTIC, HYPERBOLIC)
- **GRID TYPES SUPPORTED**
  - MULTIZONE
  - PERIODIC
  - H-, C-, O-TYPES
  - FAN (DEGENERATE)

Rockwell International
Rocketdyne Division

CFD 92-030-022/D2/SLB

EVALUATION CRITERIA (CONT'D)

- **GRID CONTROL**
  - CLUSTERING OPTIONS
  - LOCAL REFINEMENT
  - ORTHOGONALITY
  - SMOOTHNESS
- **USABILITY**
  - TIME TO LEARN
  - SPEED(TOTAL CYCLE TIME)
  - MODIFY EXISTING GRID
  - SCRIPTING / TEMPLATE CAPABILITY
  - GRID DIAGNOSTICS
  - ERROR HANDLING
  - SIZE LIMITATIONS
  - DOCUMENTATION AND SUPPORT
- **OTHERS**
  - AVAILABILITY (SOURCE CODE, THIRD PARTY)
  - PORTABILITY
  - COST

Rockwell International
Rocketdyne Division

CFD 92-030-023/D2/SLB

DEVELOPMENT AND INTEGRATION OF POSTPROCESSORS

- **POSTPROCESSING MUST ACCOUNT FOR**
  - VARIOUS FLOW SOLVER METHODOLOGIES
  - ENGINEERING DATA EXTRACTION
  - DATA VISUALIZATION

- **OBJECTIVE: PROVIDE / DEVELOP CONSISTENT SET OF POSTPROCESSING TOOLS**

- **APPROACH**
  - DEVELOP GENERAL ENGINEERING DATA EXTRACTION CAPABILITY
  - REVIEW, SELECT, AND INTEGRATE DATA VISUALIZATION CODES

Rockwell International
Rocketdyne Division

CFD 92-030-024/D2/SLB

MODULAR ENGINEERING DATA EXTRACTION

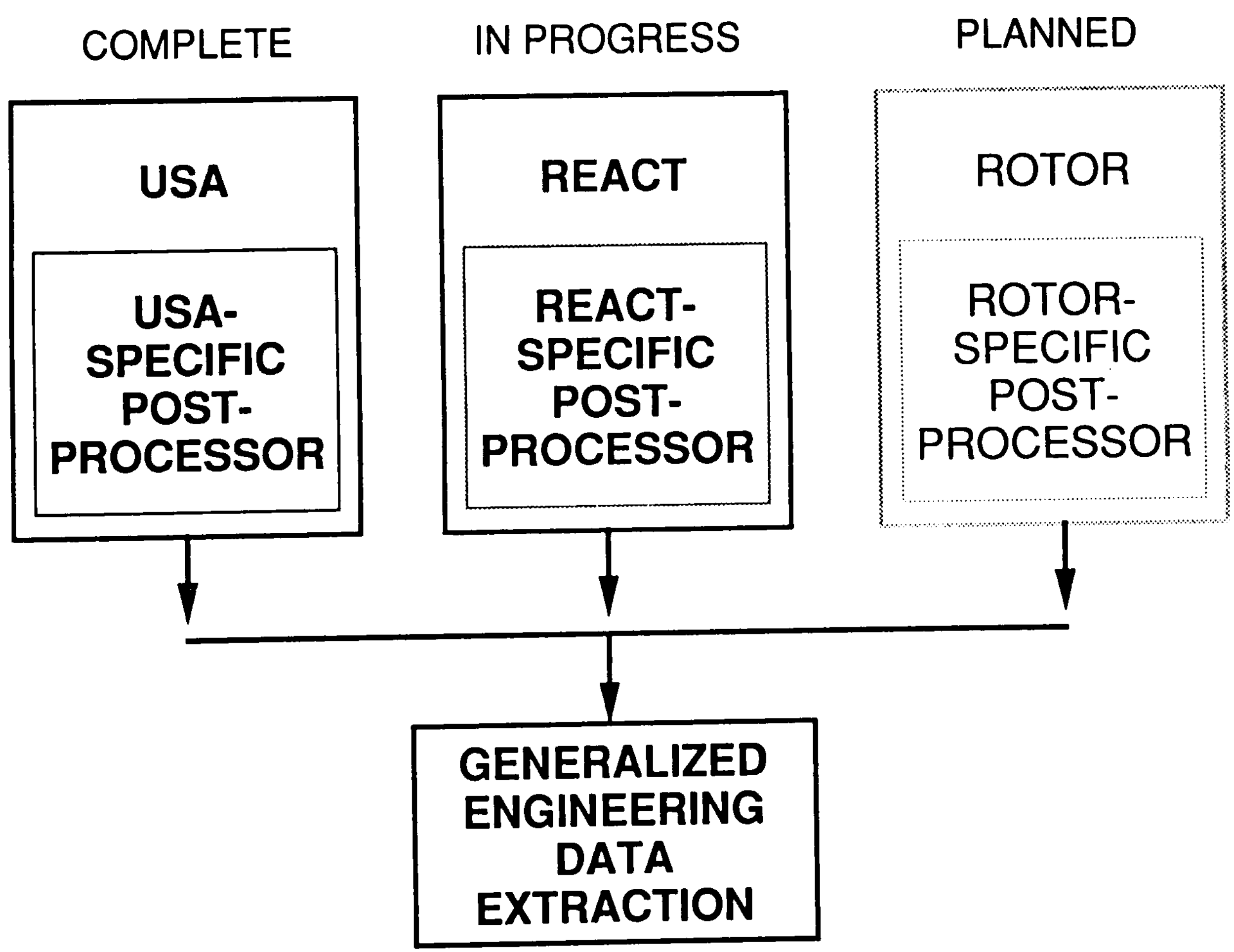

Rockwell International
Rocketdyne Division

CFD 92-030-025/D2/SLB

DATA VISUALIZATION

- **OBSERVATIONS**
  - SIGNIFICANT ADVANCES OVER RECENT YEARS
  - NUMEROUS CODES AVAILABLE
  - TRUE ENGINEERING TOOLS THAT AID IN UNDERSTANDING COMPLEX SOLUTIONS

- **ONGOING REVIEW OF AVAILABLE CODES**

- **FAST (NASA AMES) IS PRIMARY VISUALIZATION TOOL**
  - ATTRACTIVE USER INTERFACE
  - PLOT3D STANDARDS PLUS MANY ENHANCEMENTS
  - CURRENTLY IN BETA RELEASE (2.0)
  - BETA RELEASE (3.0) DUE FOR NEAR TERM RELEASE

Rockwell International
Rocketdyne Division

CFD 92-030-026/D2/SLB

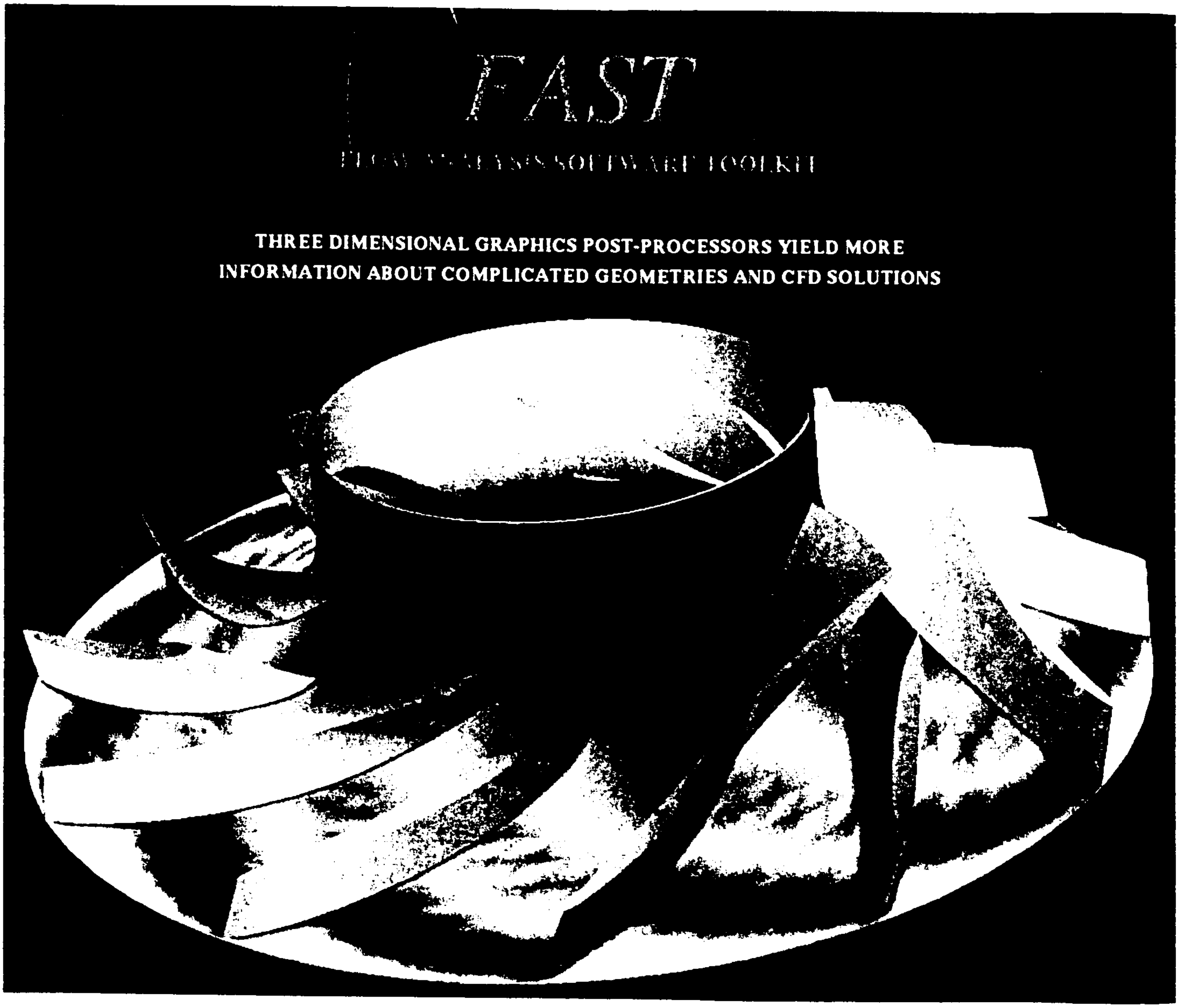
FAST
THREE DIMENSIONAL GRAPHICS POST-PROCESSORS YIELD MORE
INFORMATION ABOUT COMPLICATED GEOMETRIES AND CFD SOLUTIONS

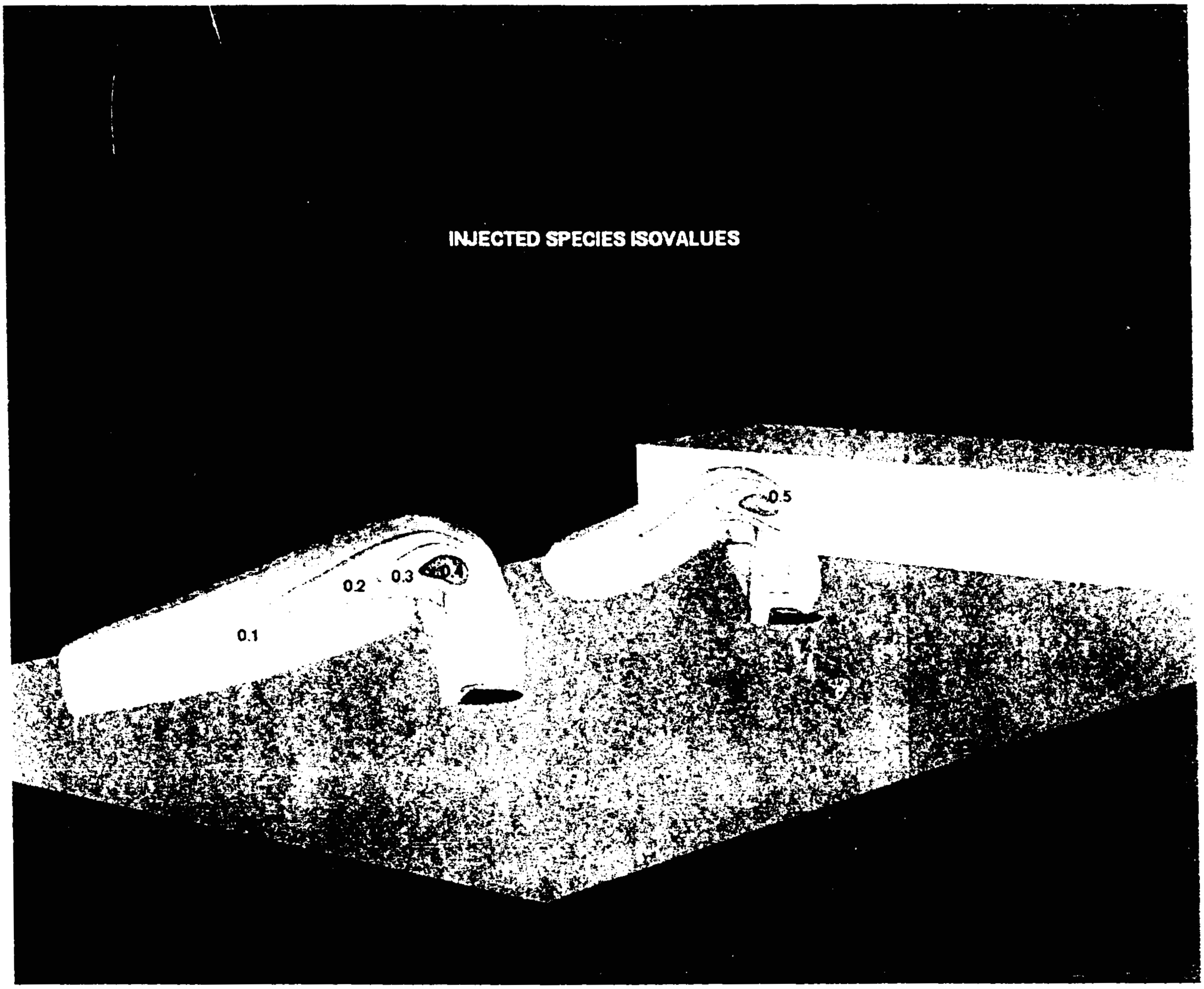
INJECTED SPECIES ISOVALUES
0.1
0.2
0.3
0.4
0.5

COMPUTATIONAL DESIGN SYSTEM SIGNIFICANTLY ENHANCES CFD ANALYSIS CAPABILITY

- **GOOD PROGRESS IN INITIAL PHASE**
  - BASIC CAPABILITY IN PLACE
  - IMMEDIATE POSITIVE IMPACT
- **FURTHER INTEGRATION EFFORTS REQUIRED**
  - GEOMETRY INTERFACES
  - INTERNAL TRANSLATORS
  - INTERDISCIPLINARY TRANSLATORS
- **EXTENDED DATABASE CAPABILITY ESSENTIAL**
  - DATA STORAGE, ORGANIZATION, AND RETRIEVAL
  - SIMPLIFY TRANSLATOR ISSUES

Rockwell International
Rocketdyne Division

CFD 92-030-029/D2/SLB

OPTIMUM DESIGN OF NINETY DEGREE BENDS

Vijay Modi
Department of Mechanical Engineering
Columbia University

Abstract

An algorithm for the optimum design of an internal flow component to obtain the maximum pressure rise is presented. Maximum pressure rise in a duct with simultaneous turning and diffusion is shown to be related the control of flow separation on the passage walls. Such a flow is usually associated with downstream conditions that are desirable in turbomachinery and propulsion applications to ensure low loss and stable performance. The algorithm requires the solution of an "adjoint" problem in addition to the "direct" equations governing the flow in a body, which in the present analysis are assumed to be the laminar Navier-Stokes equations. Earlier studies have usually addressed such problems for the case of inviscid and/or irrotational flow. These assumptions may not be valid in flows that undergo sharp turning resulting in strong secondary flows and possibly separating and recirculating regions. The theoretical framework and computational algorithms presented in this study are for the steady Navier-Stokes equations.

A novel procedure is developed for the numerical solution of the adjoint equations. This procedure is coupled with a direct solver in a design iteration loop, that provides a new shape with a higher pressure rise. This procedure is first validated for the design of optimum plane diffusers in two-dimensional flow. The direct Navier-Stokes and the "adjoint" equations are solved using a finite volume formulation for spatial discretization in an artificial compressibility framework. The discretized equations are integrated using explicit Runge-Kutta time steps to obtain steady-state solutions. It is found that the computational work required to solve the "adjoint" problem is of the same order as that required to solve the direct problem. It is also found that the procedure converges within about ten iterations, and in addition, the number of design iterations are not sensitive to the grid used for the calculations. This is a significant computational advantage over heuristic design procedures based on point by point sensitivity analysis where the work increases with the refinement of the grid.

A simplified version of the above approach is then utilized to design ninety degree diffusing bends. The bend inlet is square with intermediate and exit cross-sections constrained to be rectangular. The location of bend walls is then determined in order to obtain the maximum pressure rise through the bend. Calculations were carried out for a mean radius ratio at inlet of 2.5 and Reynolds numbers varying from 100 to 500. While at this stage laminar flow is assumed it is shown that a similar approach can be conceived for turbulent flows.

OPTIMUM DESIGN OF NINETY DEGREE BENDS

Vijay Modi, Assistant Professor

Hayri Cabuk, Post Doctoral Research Associate

Jian-Chun Huan, Graduate Student

Richard Quadracci, Graduate Student

Department of Mechanical Engineering,

Columbia University,

New York, New York 10027

MOTIVATION

How to shape internal flow passages

Combined turning and diffusing flow

Maximize pressure rise

Can not assume inviscid or 2-D flow

OBJECTIVES

Develop theoretical framework – laminar 3-D

Develop Navier-Stokes and Adjoint solvers

Validate Navier-Stokes solver
(Laminar 90 degree bend, Taylor et al. 1982)

Validate Optimization Approach on
2-D straight diffusers

Apply to the design of ninety degree bends

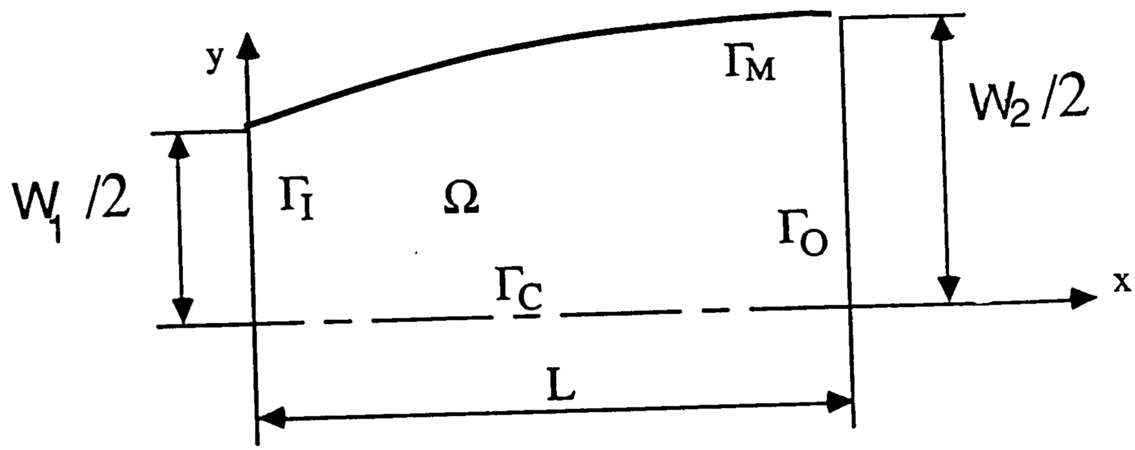

$$u_{i,i} = 0$$

$$u_j u_{i,j} = -p^*_{,i} + \nu u_{i,jj} \quad , \quad p^* = p/\rho$$

 # No slip BC on Γ_M

 # Dirichlet BC for u_i at Γ_I and Γ_O

$$J(\Gamma_M) = \int_{\Gamma_I} p^* u_i n_i ds + \int_{\Gamma_O} p^* u_i n_i ds$$

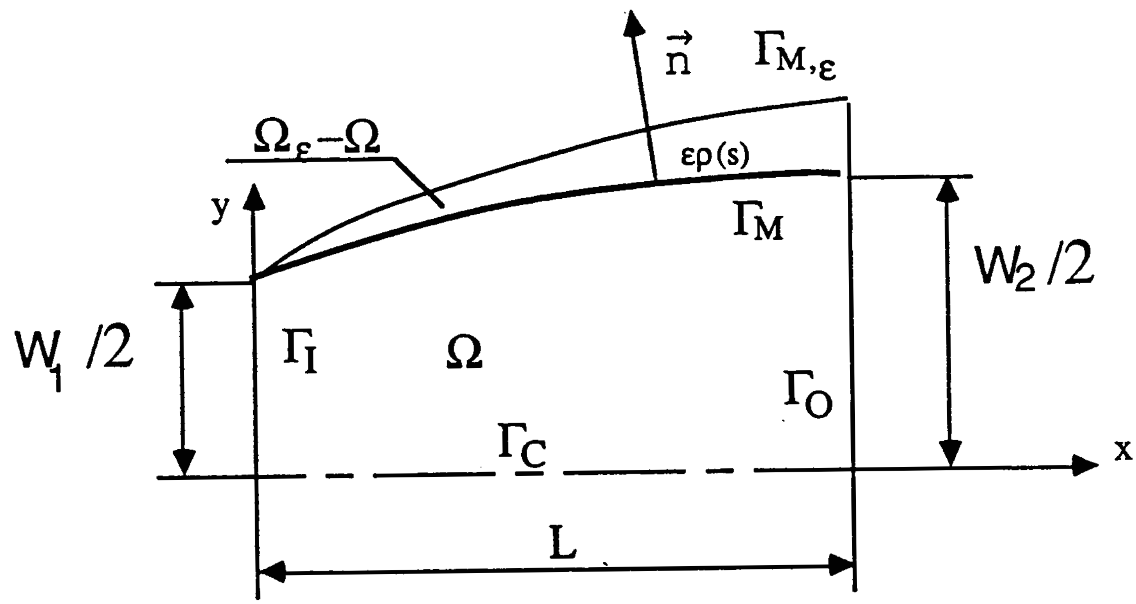

$$[u_i^\varepsilon, p^\varepsilon] \equiv \text{ Solution to NS in } \Omega_\varepsilon$$

$$u_i^\varepsilon = u_i + \epsilon\phi_i$$

$$p^\varepsilon = p^* + \epsilon\pi$$

$$\phi_{i,i} = 0$$

$$u_j\phi_{i,j} + \phi_j u_{i,j} = -\pi_{,i} + \nu\phi_{i,jj}$$

$$\phi_i = 0 \qquad \text{on } (\Gamma - \Gamma_M)$$

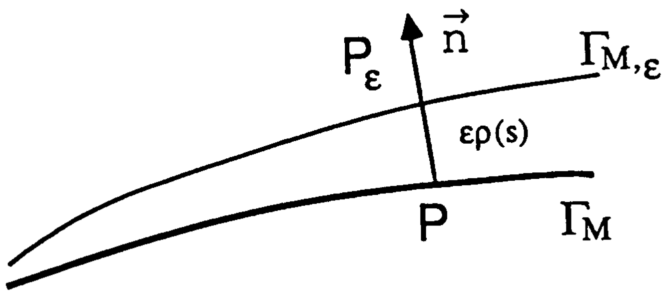

$$
\begin{aligned}
u_i^\varepsilon]_{P_\varepsilon} &= u_i^\varepsilon]_P + \epsilon\rho\left(\frac{\partial u_i^\varepsilon}{\partial n}\right)_P + O(\epsilon^2) \\
&= u_i]_P + \epsilon\phi_i]_P + \epsilon\rho\left(\frac{\partial u_i}{\partial n}\right)_P + O(\epsilon^2)
\end{aligned}
$$

$$
\phi_i = -\rho\left(\frac{\partial u_i}{\partial n}\right) \qquad \text{on } \Gamma_M .
$$

$$J(\Gamma_{M_\epsilon}) - J(\Gamma_M) = \epsilon \delta J + O(\epsilon^2)$$

$$\delta J = \int_{\Gamma_I} \pi u_i n_i ds + \int_{\Gamma_O} \pi u_i n_i ds$$

$$\begin{aligned} z_{i,i} &= 0 && \text{in } \Omega \\ \nu z_{i,jj} + u_j(z_{i,j} + z_{j,i}) - r_{,i} &= 0 && \text{in } \Omega \\ z_i &= u_i && \text{on } \Gamma \end{aligned}$$

$$\delta J = \nu \int_{\Gamma_M} \rho(s) \left(\frac{\partial u_i}{\partial n} \right) \left(\frac{\partial z_i}{\partial n} \right) ds$$

$$\rho(s) = \omega(s) \left(\frac{\partial u_i}{\partial n} \right) \left(\frac{\partial z_i}{\partial n} \right)$$

Our "Adjoint" equation:

$$\nu z_{i,jj} + u_j(z_{i,j} + z_{j,i}) - r_{,i} = 0 \qquad \text{in } \Omega$$

$$w_i = \frac{1}{2}(z_i - u_i)$$

$$q = \frac{1}{2}\left(r - p^* + (1/2)u_j^2 - 2u_j w_j\right)$$

Pironneau's "Adjoint" equation:

$$w_{i,i} = 0 \qquad \text{in } \Omega$$

$$\nu w_{i,jj} + u_j w_{i,j} + \underline{\underline{w_j u_{j,i}}} - q_{,i} = \underline{\underline{-u_j u_{i,j}}} \qquad \text{in } \Omega$$

$$w_i = 0 \qquad \text{on } \Gamma$$

$$\delta J = \nu \int_{\Gamma_M} \rho(s) \left(\frac{\partial u_i}{\partial n}\right) \left(\frac{\partial u_i}{\partial n} + 2\frac{\partial w_i}{\partial n}\right) ds$$

$$\frac{dw}{dt} = w(\text{const}) + \cdots$$

NAVIER-STOKES SOLVER

$$p_t = -\beta^2 u_{i,i}$$

$$u_{i,t} + u_j u_{i,j} = -p_{,i} + \nu u_{i,jj}$$

a) Artificial Compressibility

b) Runge-Kutta Time Integration

c) Finite Volume Discretization

d) Artificial Dissipation

e) Local Time Stepping

e) Implicit Residual Smoothing

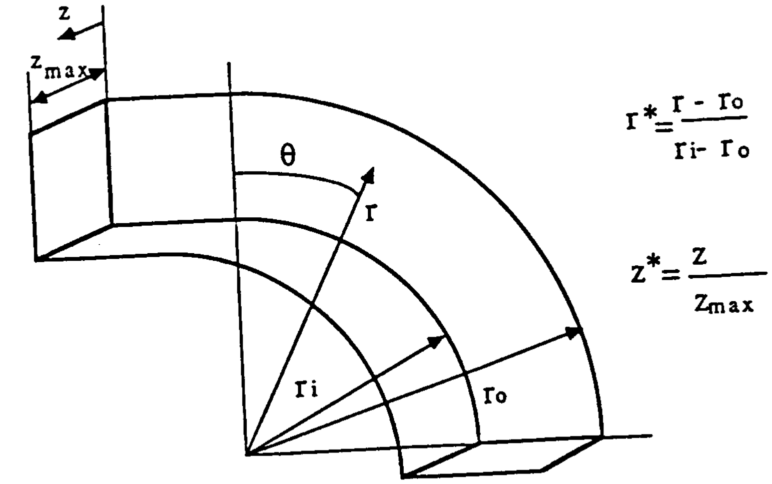

Figure 4: Geometry of a circular bend with square cross section.

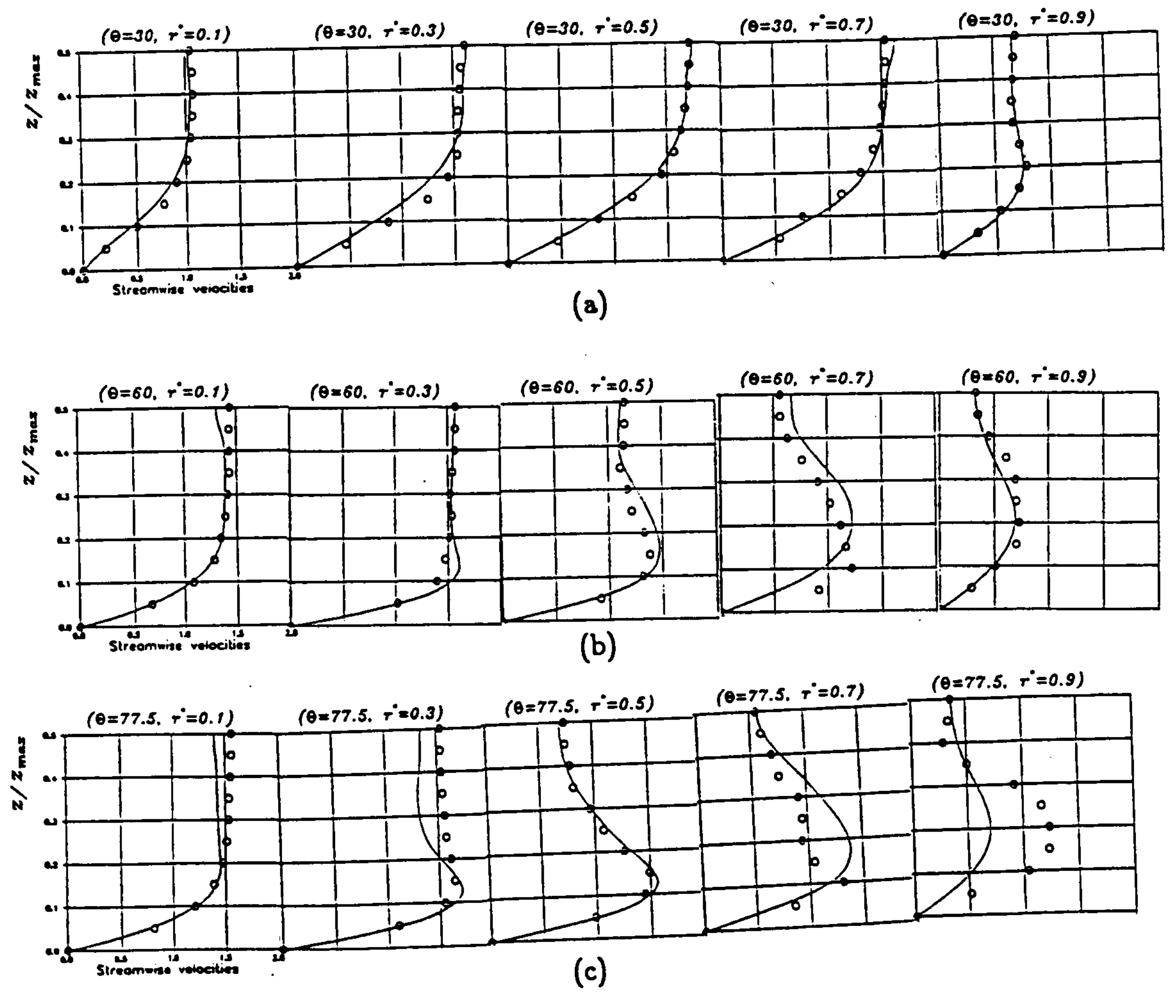

Figure 5: Streamwise velocities in a bend: a) $\Theta = 30$ degrees, b) $\Theta = 60$ degrees, c) $\Theta = 77.5$ degrees.

ADJOINT EQUATION SOLVER

$$r_t^* = -\beta^2 z_{i,i}$$

$$z_{i,t} = \nu z_{i,jj} + u_j(z_{i,j} + z_{j,i}) - \frac{1}{2}(z_k z_k)_{,i} - r^*_{,i}$$

MESH GENERATION

Thompson et al.

$$x_{\xi\xi} + x_{\eta\eta} = 0$$

$$y_{\xi\xi} + y_{\eta\eta} = 0$$

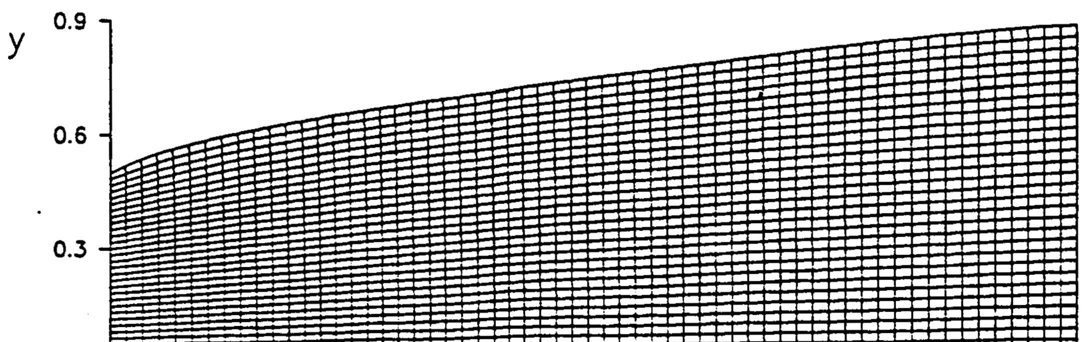

Boundary Conditions

No-slip bc on the walls

Zero normal derivatives at exit

Streamwise velocity component is specified at entrance

Zero normal derivatives for remaining velocities at entrance

Typical bc's at symettry planes

Zero second derivatives for pressure (a computational bc)

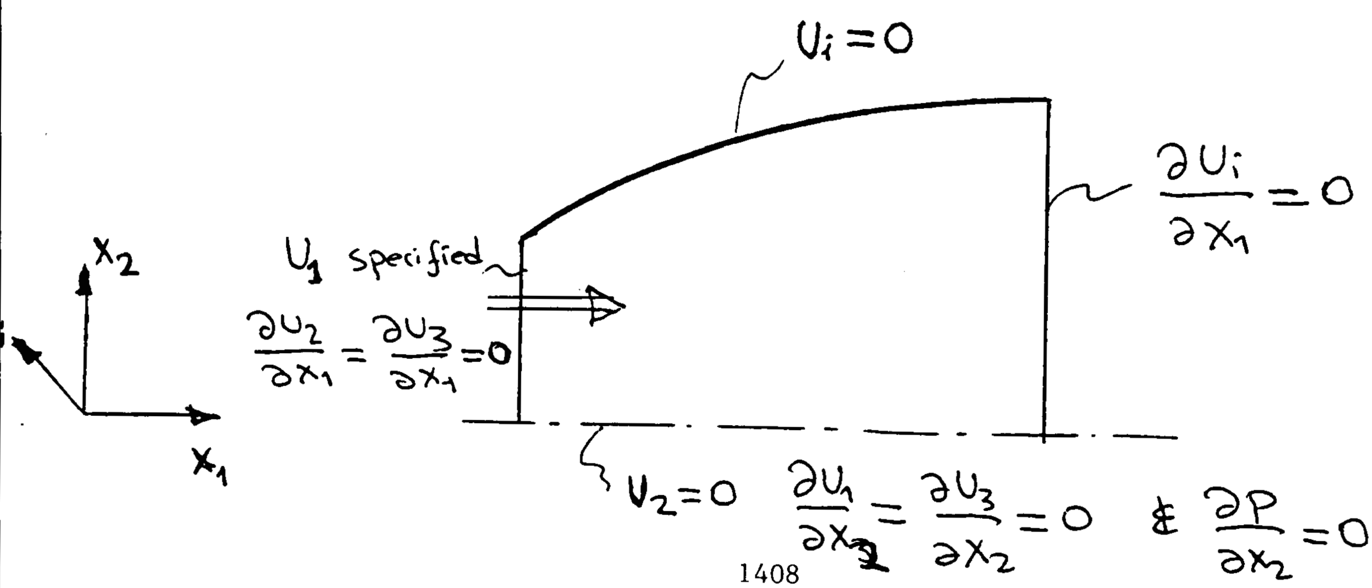

Diffuser Profile History

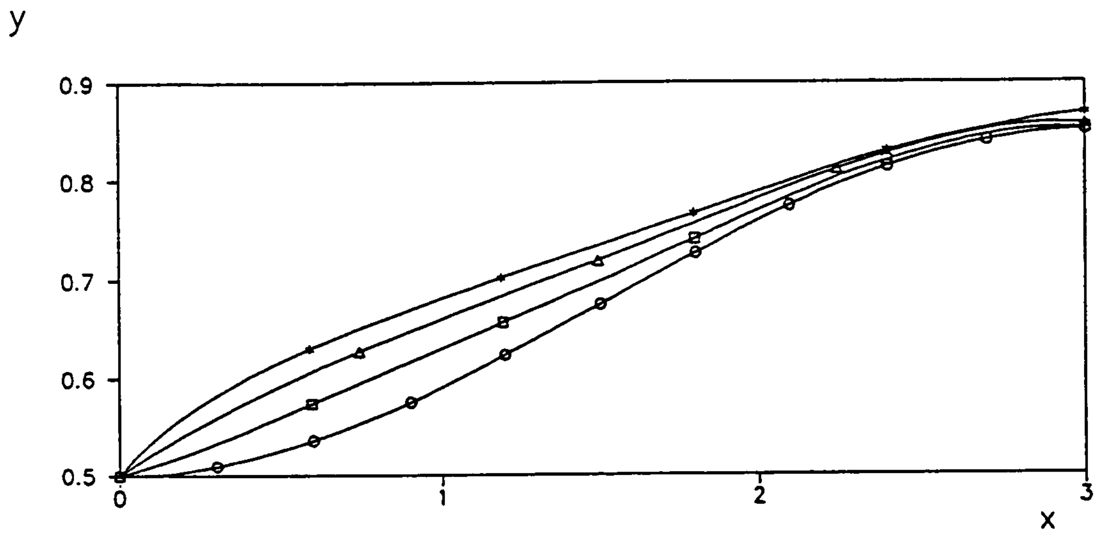

Re=200, 61 by 31 grid

○ : N=1

⊓ : N=2

△ : N=5

∗ : N=10

Skin Friction History

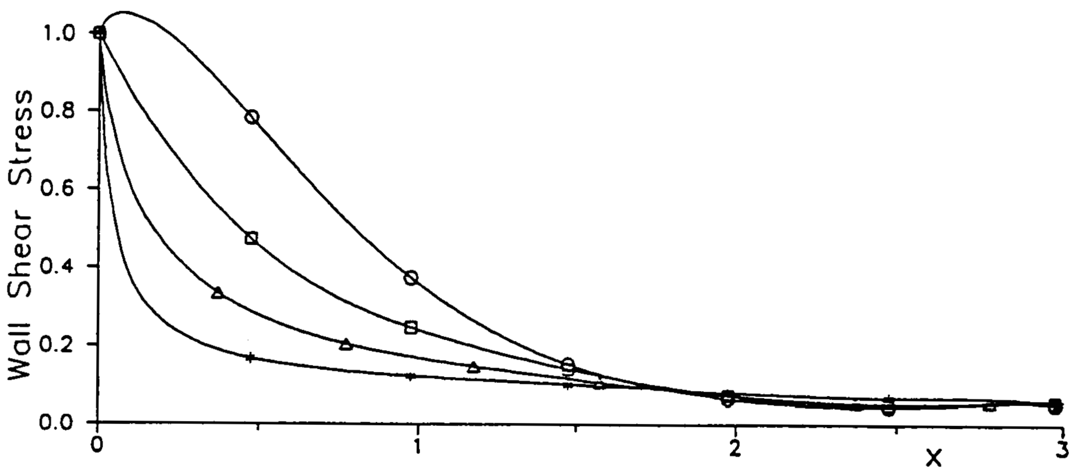

Re=200, 61 by 31 grid

○ : N=1

□ : N=2

△ : N=5

*** : N=10**

Pressure Rise History

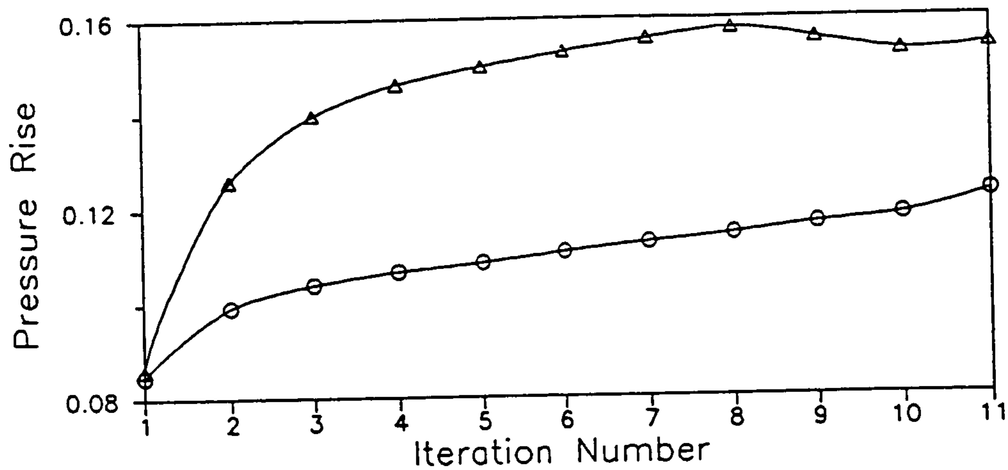

Re=200, 61 by 31 grid

○ : Area-averaged pressure rise

△ : Flow-averaged pressure rise

$$C_p \equiv \frac{\text{Actual Pressure Rise}}{\text{Ideal Pressure Rise}}$$

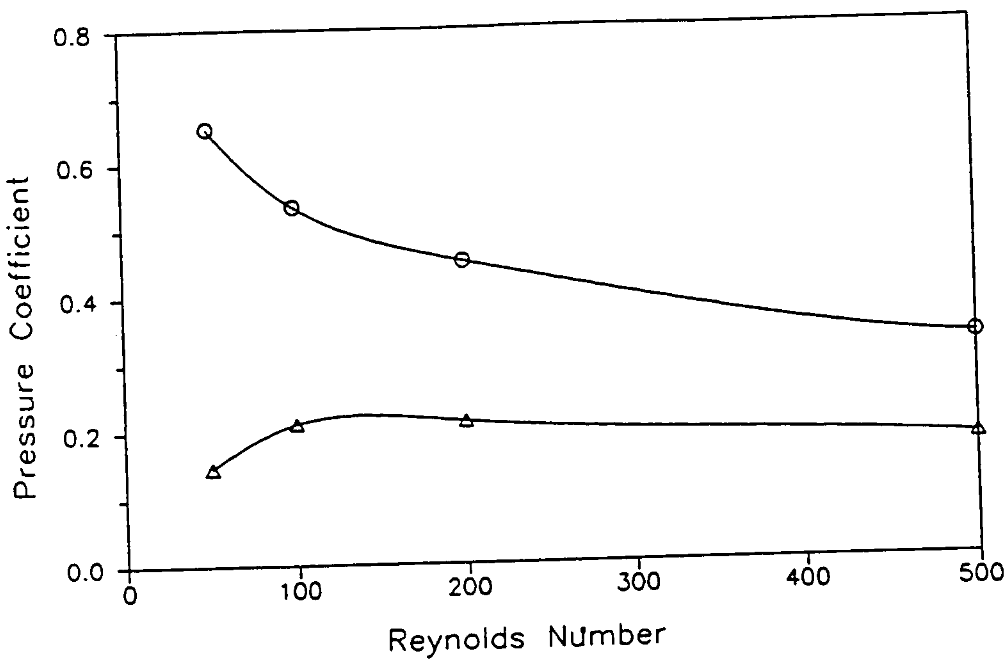

○ : **Optimal diffusers**

△ : **Straight diverging diffusers**

Separating Initial Profile

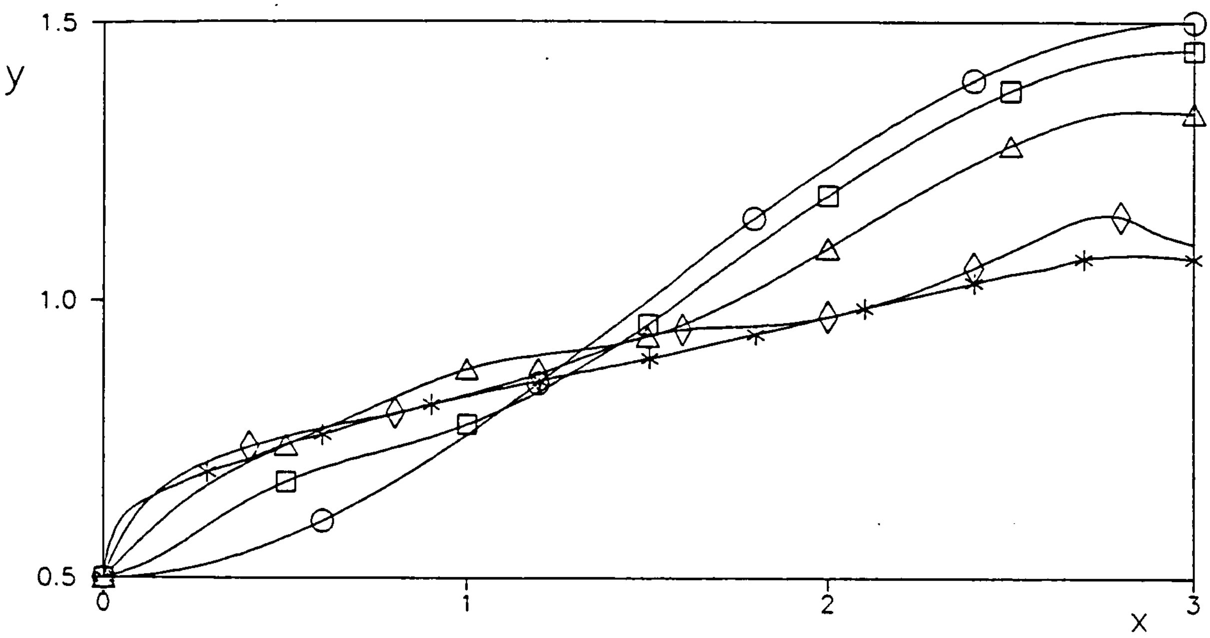

Re=100, 31 by 11 grid

○ : **N=1**

□ : **N=2**

△ : **N=3**

◇ : **N=4**

∗ : **N=11**

Grid Study

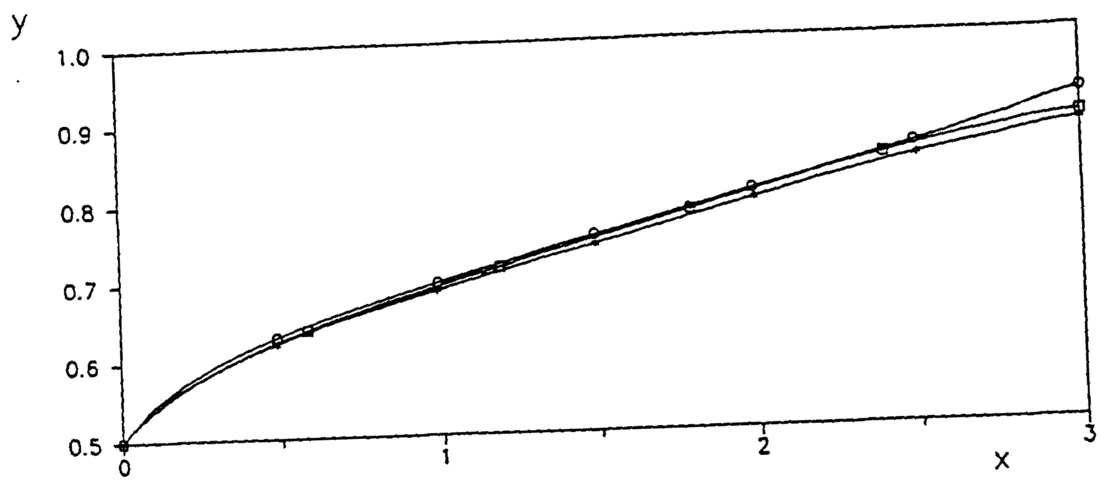

Re=200

○ : 31 by 16

□ : 61 by 31

*** : 121 by 61**

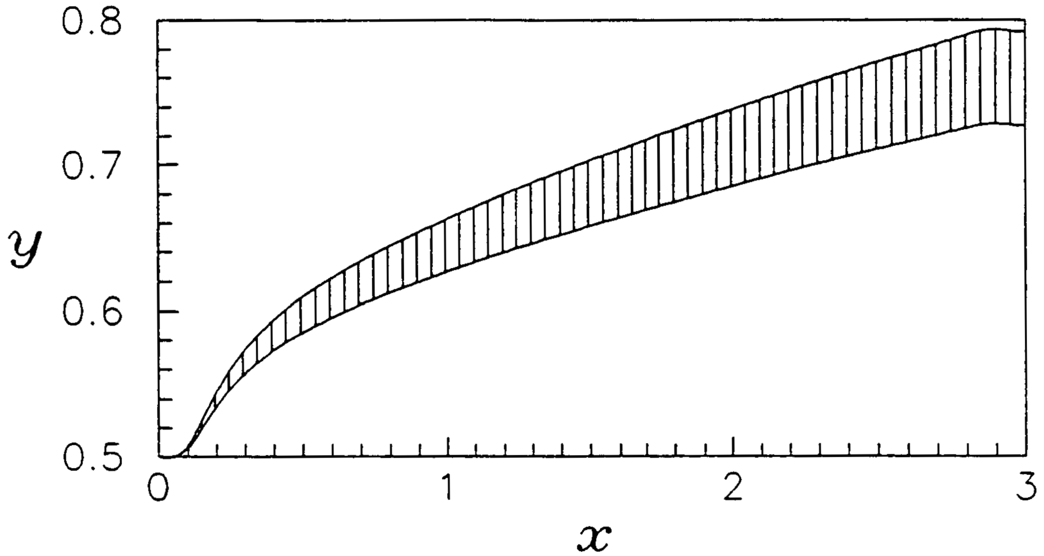

The error in the location of the optimal diffuser profile corresponding to a 2 percent error in the total pressure rise. The optimum shape lies between the high and low y−values shown in the graph ($Re=500$, grid size is 61 by 21, and $L/W_1=3$).

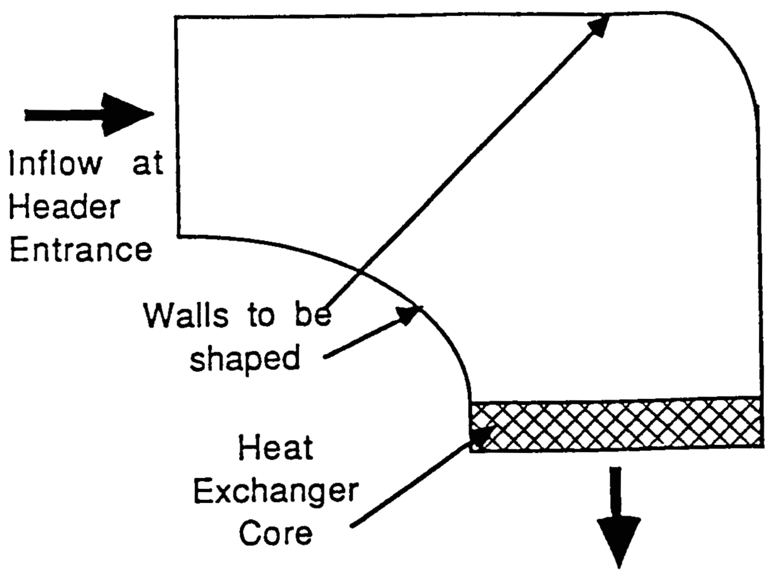

Sketch of the inlet header

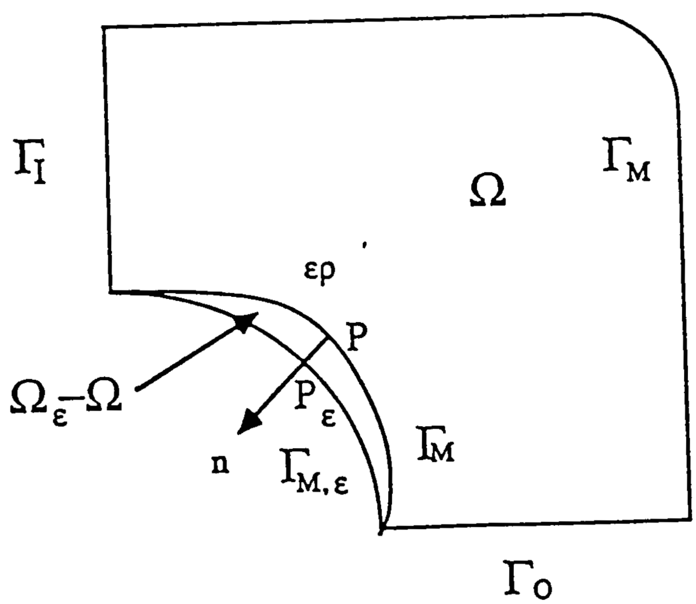

Figure 3: A representative section of a three-dimensional diffuser. Flow enters at upstream boundary Γ_I and exits at downstream boundary Γ_O. The walls to be shaped are Γ_M.

ISSUES

\# Geometry Constraints

In general: Move walls by $\epsilon\rho(s)$ along the normal direction, everywhere

New shape may not satisfy

- specified mean passage location
- specified cross-sectional shape
- overall system geometry

\# Present Work

- No correction on side walls ($z = 0$, $z = z_{\max}$)
- Apply mid-plane ($z = z_{\max}/2$) correction to all z locations
- Hence all cross-sections are rectangular

\# Laminar flow results ($Re < 500$)

Governing Equations:

$$u_{i,i} = 0$$

$$u_j u_{i,j} = -p_{,i} + \nu u_{i,jj}$$

Design Objective:

Maximize Static Pressure Rise

$$J = \int_{\Gamma_I} p \, ds + \int_{\Gamma_O} p \, ds$$

Cabuk and Modi, 1990

$$\left(\frac{\partial u}{\partial n}\right)_{\text{wall}} = 0$$

$$\left(\frac{\partial u}{\partial n}\right)_{\text{wall}} = \epsilon$$

DESIGN ALGORITHM

1: Choose an initial shape.

2: Generate the computational grid.

3: Solve the N-S equations.

4: Compute shear stress on the walls.

5: Compare wall shear stress to target distribution and determine the amount of boundary movement $\rho(s)$.

6: Update the shape.

7: Go to step (2)

$$\rho(s) = \omega(s)\left[\left(\frac{\partial u}{\partial n}\right)_{\text{wall}} - \left(\frac{\partial u}{\partial n}\right)_{\text{target}}\right]$$

Iteration History (Re=200)

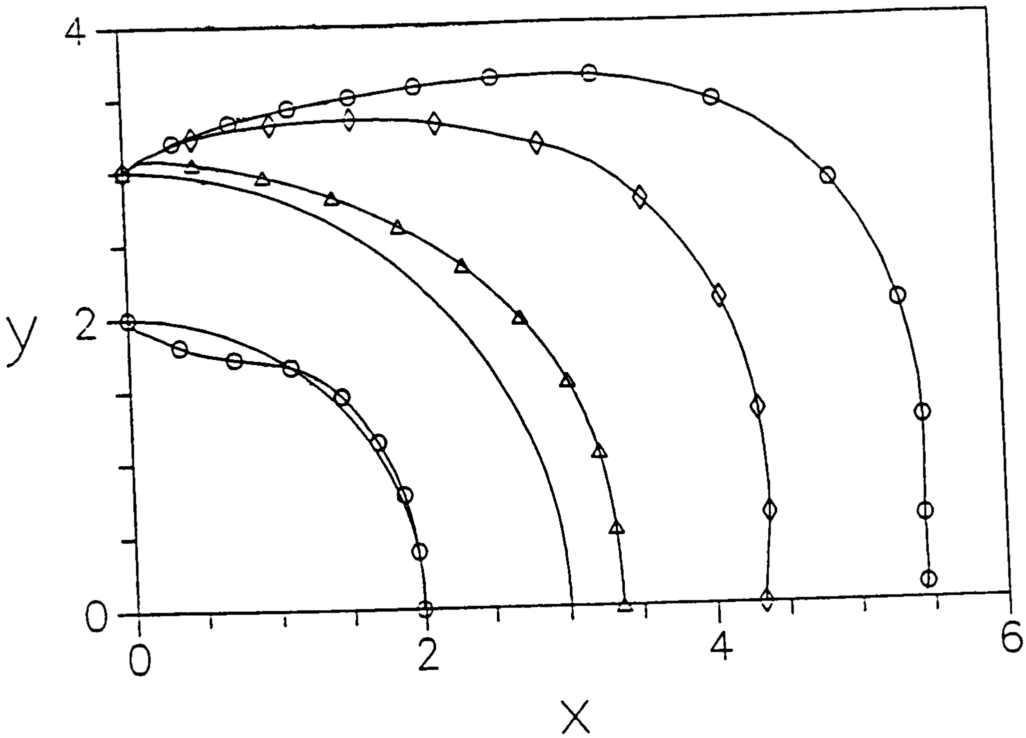

Dashed Curve : N=1

○ : N=8

△ : N=2

◇ : N=5

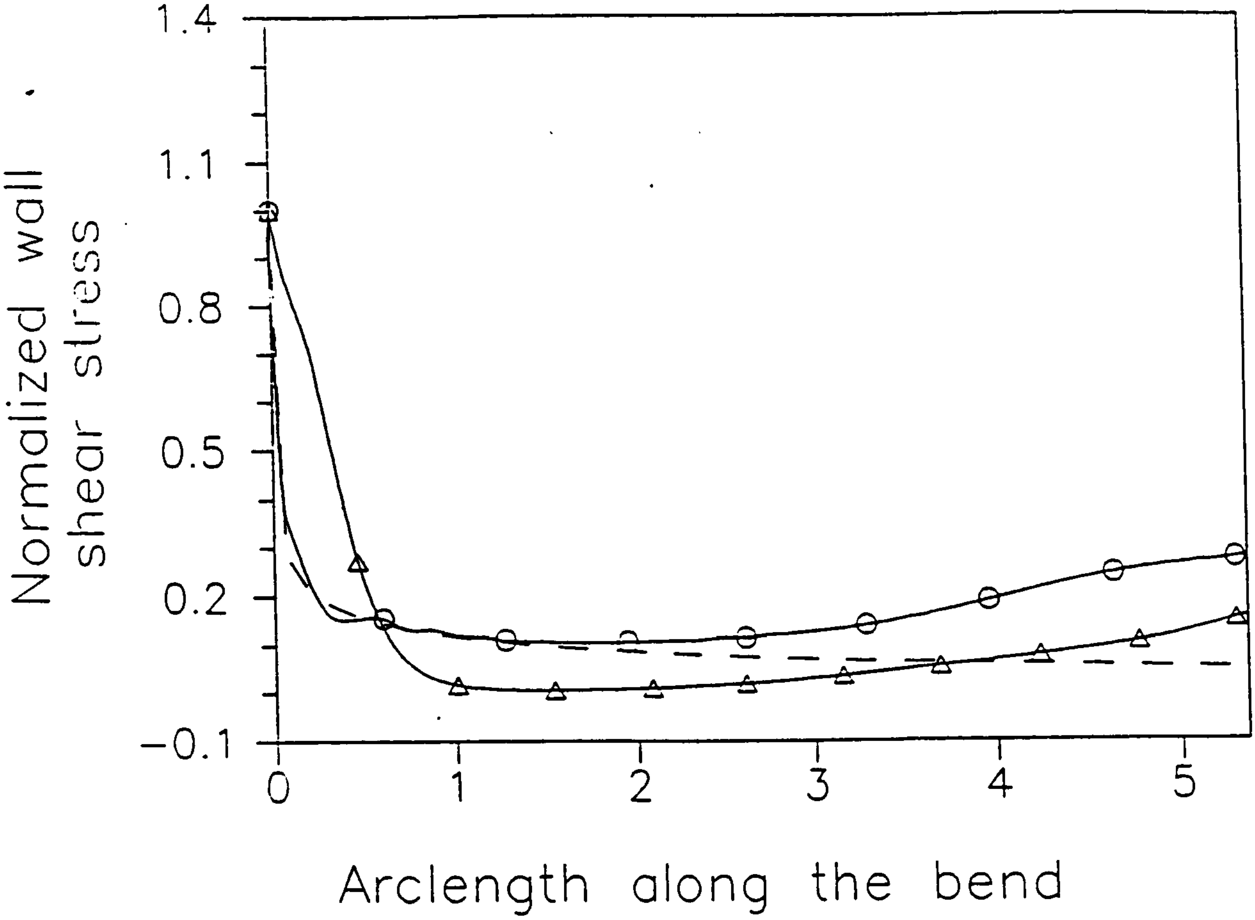

Wall shear stress along the outer wall, Re=100

○ : **Optimum diffusing bend**

△ : **Elliptic diffusing bend**

Dashed Curve : Target distribution

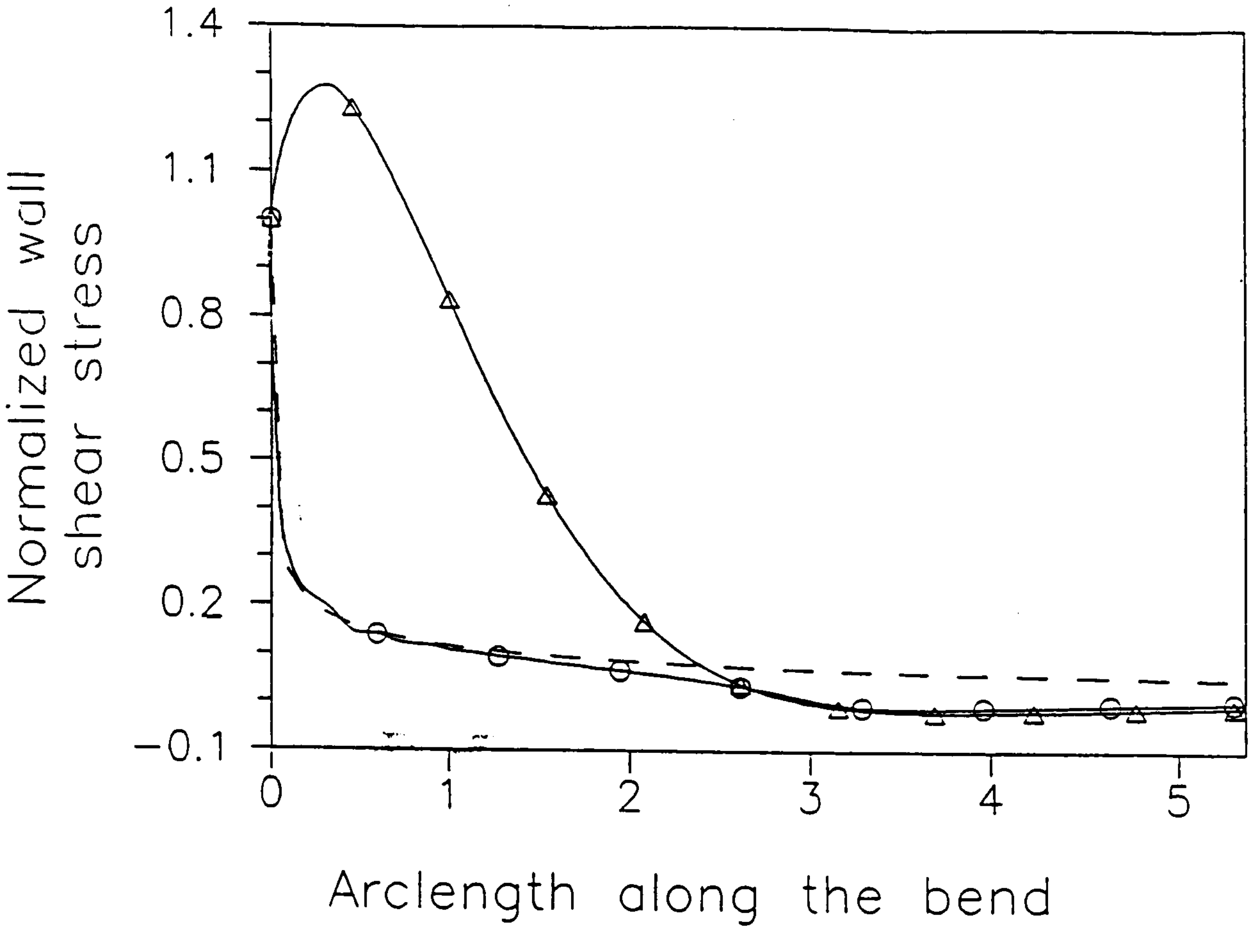

Wall shear stress along the inner wall, Re=100

○ : Optimum diffusing bend

△ : Elliptic diffusing bend

Dashed Curve : Target distribution

Pressure rise along the header (Re=100)

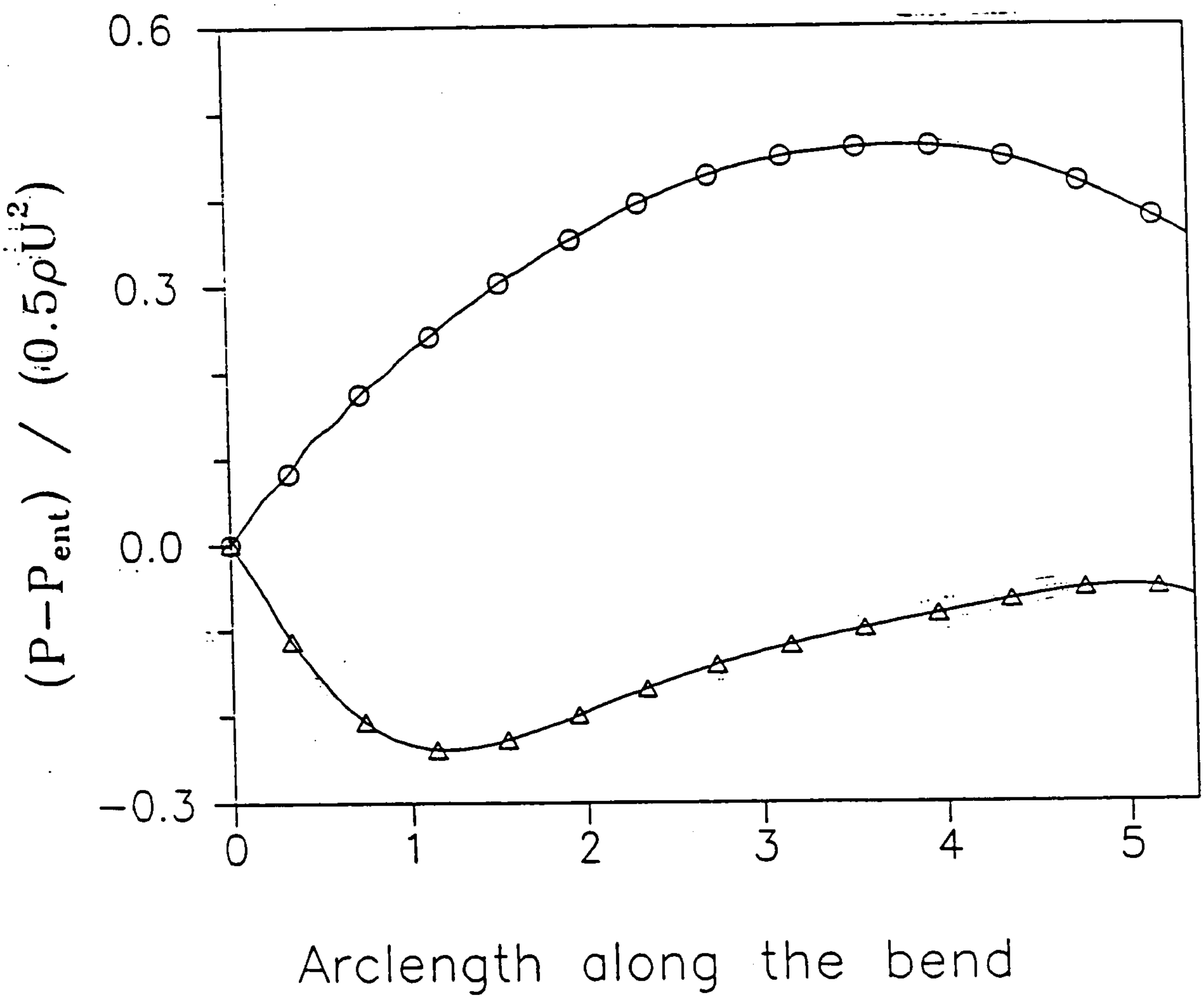

○ : **Optimum header**

△ : **Elliptic header**

Optimum Shapes

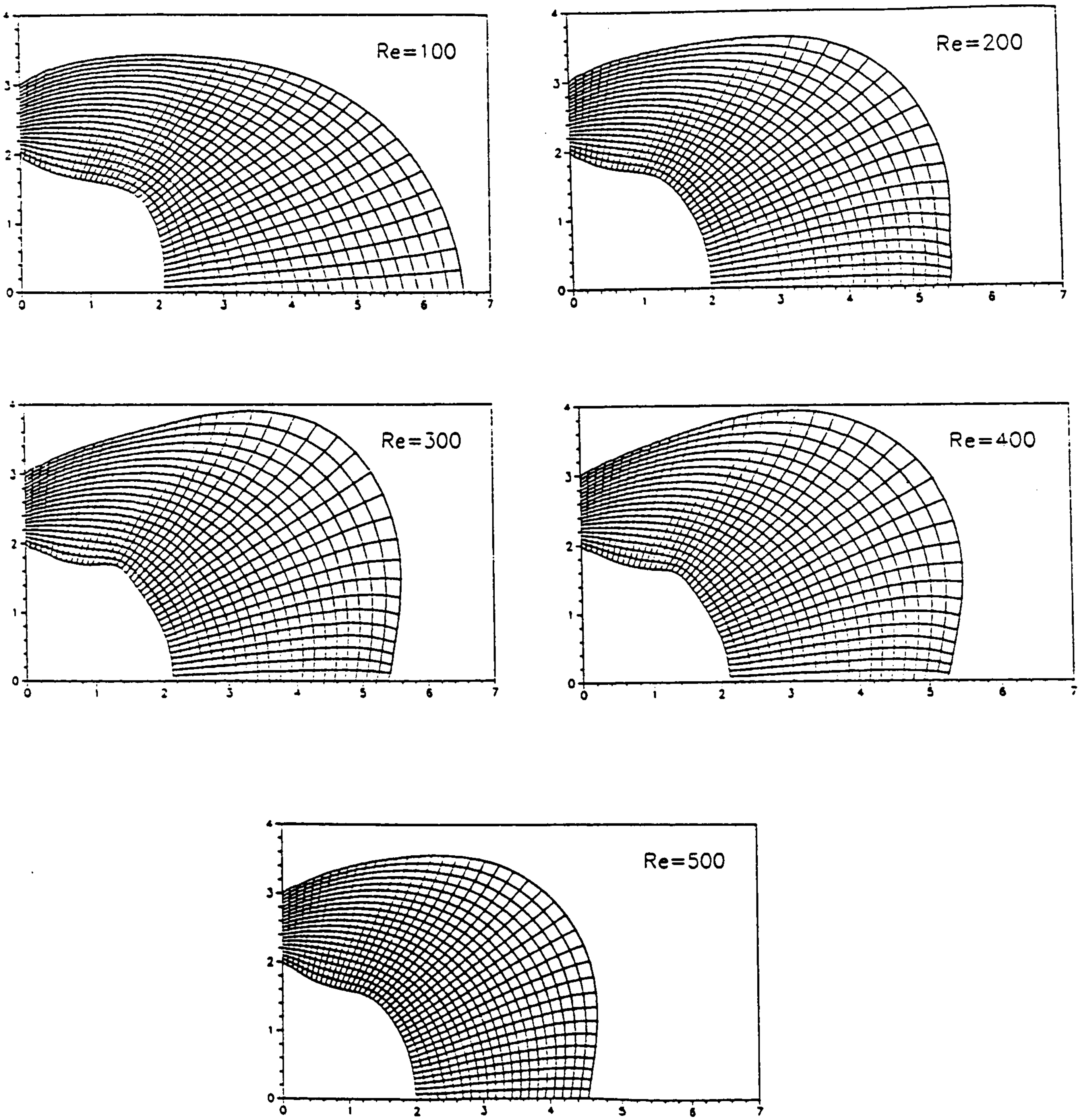

Performance = f(shape)

Possible Applications:

- 90 Degree Bend
- Turn Around Ducts
- Transition Ducts
- S-shaped Ducts
- Straight or Curved Diffusers
- Turbine Blades
- Engine Inlets
- Turning Vanes

CONCLUSIONS

Theory

Theoretical Framework for Design with Navier-Stokes equations

Determine $\rho(s)$ from Direct+Adjoint or from Direct alone

Computational

Direct and Adjoint Solvers Validated for Plane Diffusers

Design of 90 degree Bend with Specified Cross-section, Max. Δp

Number of Design Cycles < 10

"Flow" Interpretation of Adjoint Problem

Future Plan

Apply to 3-D turbulent flow

Specify mean line, vary cross-section

Other objectives : Min. Distortion

A Multi-Domain Method for Subsonic Viscous Flows

Daniel C. Chan and Munir M. Sindir
CFD Technology Center
Rocketdyne Division, Rockwell International Corporation
Canoga Park, California

We have developed a Schwarz type domain decomposition method for a pressure base, two- and three-dimensional Navier-Stokes solver. This technique allows one to partition a flow path, which can be characterized by complex geometry and/or complicated flow physics, into smaller sub-domains according to the local geometric simplicity or estimated flow scales. We can, then, sweep the sub-domains in some order and solve the Navier-Stokes equations using as boundary conditions, along the domain interfaces, the Dirichlet conditions which are taken from the most recent update of the solution in the adjacent neighboring domains. With this technique, one can minimize the adverse effects caused by grid skewness and the stiffness problem caused by disparate flow scales.

This code has been successfully applied to complicated engineering problems and the results are presented as separate papers in this conference. Here, we report the results of a few fundamental flow cases to demonstrate that a judicious use of the multi-domain method can offer a significant convergence acceleration over the traditional one-domain method. This method can be extended to exploit the architecture of a parallel computer to further improve the speed.

A MULTI-DOMAIN METHOD FOR SUBSONIC VISCOUS FLOWS

BY
DANIEL C. CHAN AND MUNIR M. SINDIR
CFD TECHNOLOGY CENTER
ROCKETDYNE DIVISION, ROCKWELL INTERNATIONAL

PRESENTED AT THE NASA MARSHALL SPACE FLIGHT CENTER
TENTH WORKSHOP FOR COMPUTATIONAL FLUID DYNAMIC
APPLICATIONS IN ROCKET PROPULSION
APRIL 28-30, 1992

Rockwell International
Rocketdyne Division

AGENDA

- MOTIVATION
- APPROACH
- FUNDAMENTAL TEST CASES
- RESULTS
- CONCLUSIONS

Rockwell International
Rocketdyne Division

MOTIVATION

- **OPTIMIZE THE DESIGN OF ROCKET ENGINE COMPONENTS**
  - CONSISTENCY AND ACCURACY
  - RAPID TURN AROUND
- **CHALLENGES**
  - COMPLEX FLOW PATH GEOMETRY
  - COMPLICATED FLOW PHYSICS
  - DISPARATE FLOW SCALES
  - STRONG COMPONENTS INTERACTIONS
- **OPTIMIZE THE DESIGN OF A ROCKET PUMP**
  - FLANGE-TO-FLANGE ANALYSIS

Rockwell International
Rocketdyne Division

APPROACH

- **PARTITION A COMPLEX FLOW PATH ACCORDING TO**
  - GEOMETRIC CONSTRAINTS
    - SIMPLIFY GRID GENERATION PROCESS
  - INTERACTIVE COMPONENTS
    - LACK OF WELL-DEFINED BOUNDARY CONDITIONS
  - FLOW SCALES
    - LOCALIZED POCKET OF RECIRCULATING FLOW
- **NUMERICAL ISSUES**
  - TRANSFER OF INFORMATION ACROSS INTERFACE
    - ACCURACY AND STABILITY
  - GRID TOPOLOGY
    - SIMPLY CONNECTED
    - MULTIPLY CONNECTED
  - DATA MANAGEMENT
    - NEAREST NEIGHBORS
    - INTERFACIAL CONNECTIVITIES
- **HARDWARE ISSUES**
  - VECTOR LENGTH
  - CORE MEMORY
  - PARALLELISM

Rockwell International
Rocketdyne Division

MULTI-DOMAIN PATCHING ALGORITHM

- **SCHWARZ APPROACH**
  - SWEEP THE SUB-DOMAINS IN A SEQUENTIAL ORDER
  - APPLY DIRICHLET CONDITION ALONG DOMAIN INTERFACES
    - USE MOST RECENT SOLUTION FROM THE NEIGHBORING DOMAINS
  - NO MAJOR MODIFICATION TO BASIC NAVIER-STOKES SOLVER
  - NOT TIME ACCURATE
  - STABILITY COULD DEPEND ON INITIAL CONDITION

- **GREEN'S FUNCTION APPROACH**
  - FOR LINEAR DIFFERENTIAL OPERATORS ONLY
  - STRONG DOMAIN COUPLING
  - MORE WORK PER TIME STEP
  - TIME ACCURATE
  - FULLY PARALLEL

Rockwell International
Rocketdyne Division

FLOW OVER A HALF CIRCLE
SINGLE AND FOUR DOMAIN GRID TOPOLOGY

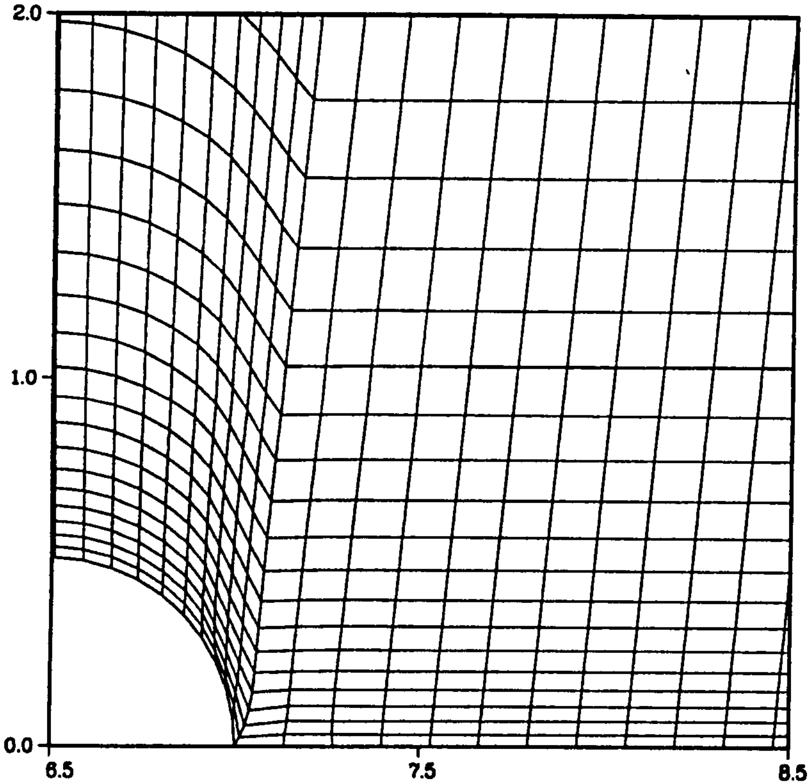

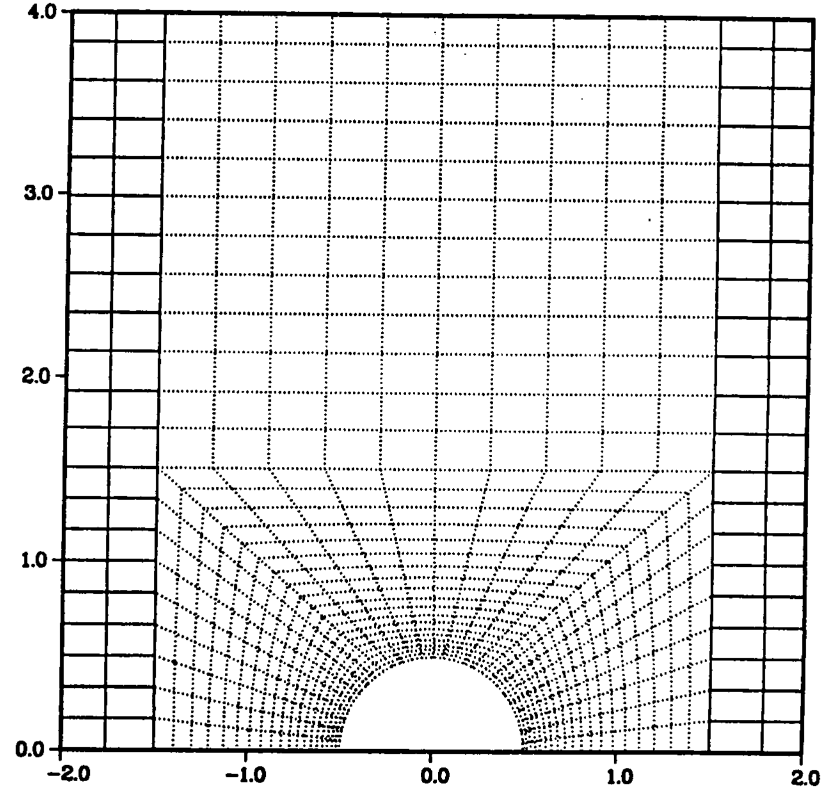

Rockwell International
Rocketdyne Division

DIFFERENT GRID CONNECTIVITY IN COMPUTATIONAL DOMAIN

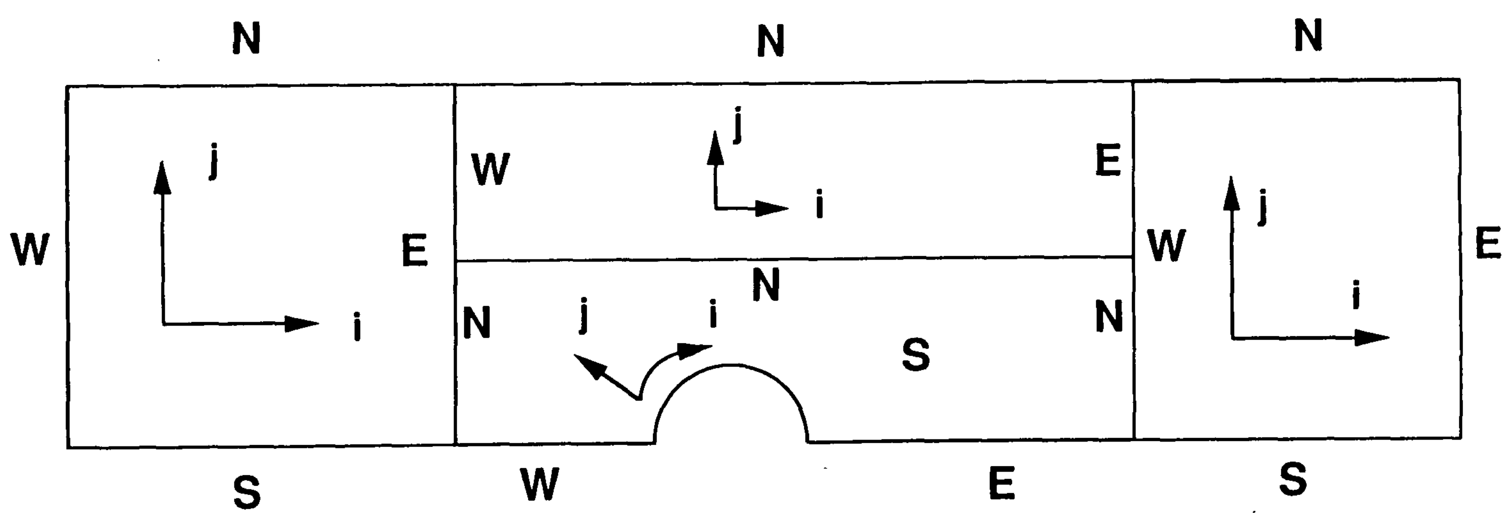

Rockwell International
Rocketdyne Division

FLOW OVER A HALF CIRCLE
SINGLE AND FOUR DOMAIN FLOW SOLUTION
(Re=100)

SINGLE DOMAIN

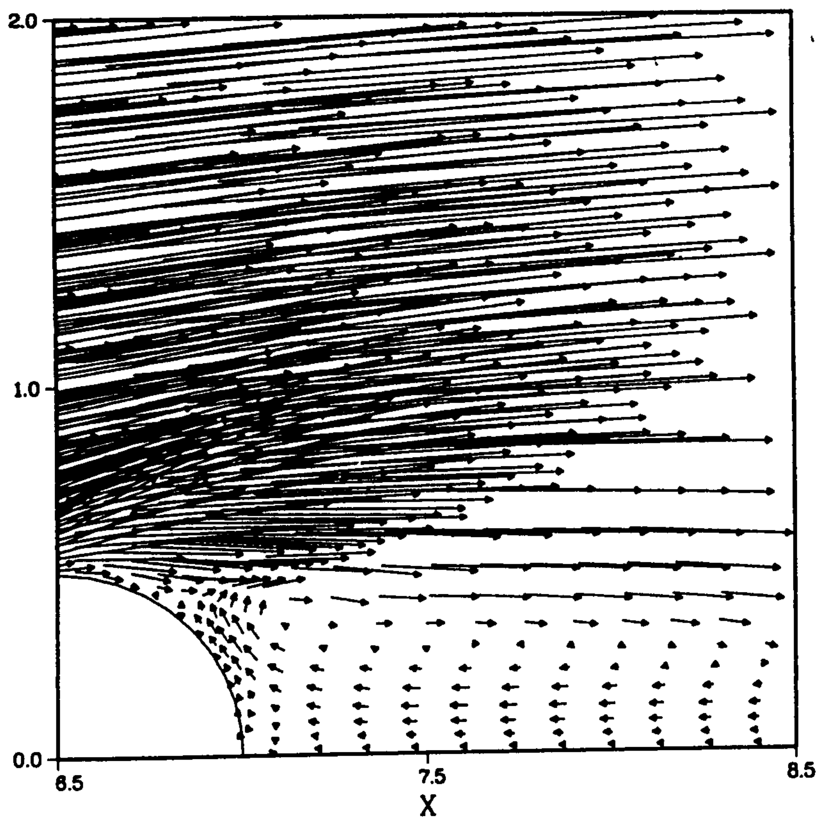

FOUR DOMAINS

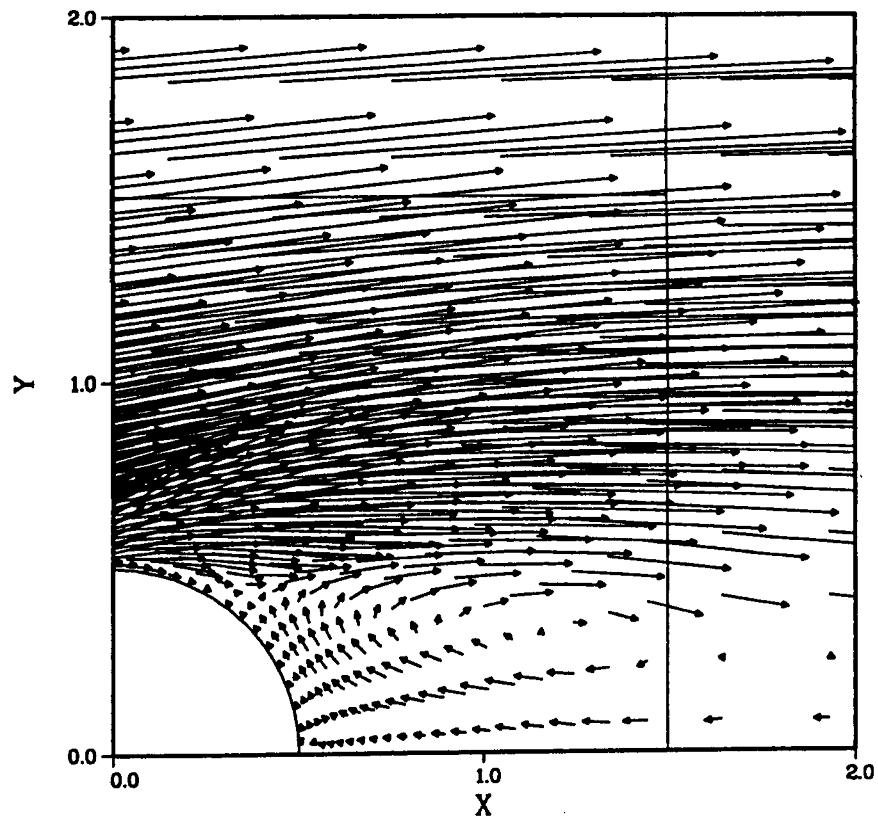

Rockwell International
Rocketdyne Division

GREEN'S FUNCTION MULTI-DOMAIN ALGORITHM
ONE-DIMENSIONAL HELMHOLTZ EQUATION FORMULATION
PULICANI, 1988

- **GOVERNING EQUATION AND BOUNDARY CONDITIONS**

$$U''(x) - \sigma U(x) = f(x), \qquad x \in \Omega =]-1;1[$$

$$U(-1) = g^- \; and \; U(1) = g^+$$

- **ANALYTICAL SOLUTION**

$$for\; f(x) = -2AC^2(\tanh Cx)(1 - \tanh^2 Cx) - \sigma U_e(x)$$

$$U_e(x) = A \tanh Cx + B$$

$$where, A = 0.5, B = 0.5, C = 20, \sigma = 100$$

Rockwell International
Rocketdyne Division

GREEN'S FUNCTION MULTI-DOMAIN ALGORITHM

ONE-DIMENSIONAL HELMHOLTZ EQUATION FORMULATION
PULICANI, 1988

- PARTITION INTO TWO DOMAINS
- CENTRAL DIFFERENCING FOR INTERIOR NODES
- SECOND ORDER BACKWARD DIFFERENCING FOR BOUNDARY NODES

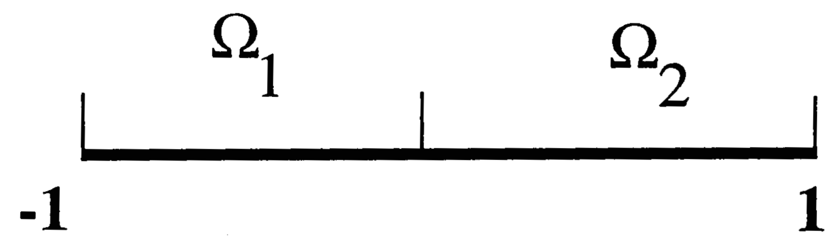

Rockwell International
Rocketdyne Division

GREEN'S FUNCTION MULTI-DOMAIN ALGORITHM

- **SEEK THE SOLUTION IN A FORM OF**

$$U^j = \overline{U}^j + \lambda_{1j} U_1^j + \lambda_{2j} U_2^j \quad where,\ j = 1, \ldots J\ number\ of\ subdomains$$

$$(\overline{U}^j)'' - \sigma \overline{U}^j = f \quad with\ \overline{U}^j(x^{j-1}) = 0\ and\ \overline{U}^j(x^j) = 0$$

$$(\overline{U}_i^j)'' - \sigma \overline{U}_i^j = 0 \quad with\ \overline{U}_i^j(x^{j-1}) = -i + 2\ and\ \overline{U}_i^j(x^j) = i - 1$$

$$i = 1,2$$

- **CONTINUITY AT DOMAIN INTERFACE REQUIRE**

$$U^j(x^j) = U^{j+1}(x^j)$$

$$\frac{d}{dx} U^j(x^j) = \frac{d}{dx} U^{j+1}(x^j)$$

Rockwell International
Rocketdyne Division

ONE-DIMENSIONAL HELMHOLTZ EQUATION
WITH 31 POINTS IN EACH DOMAIN, INTERFACE AT X=0

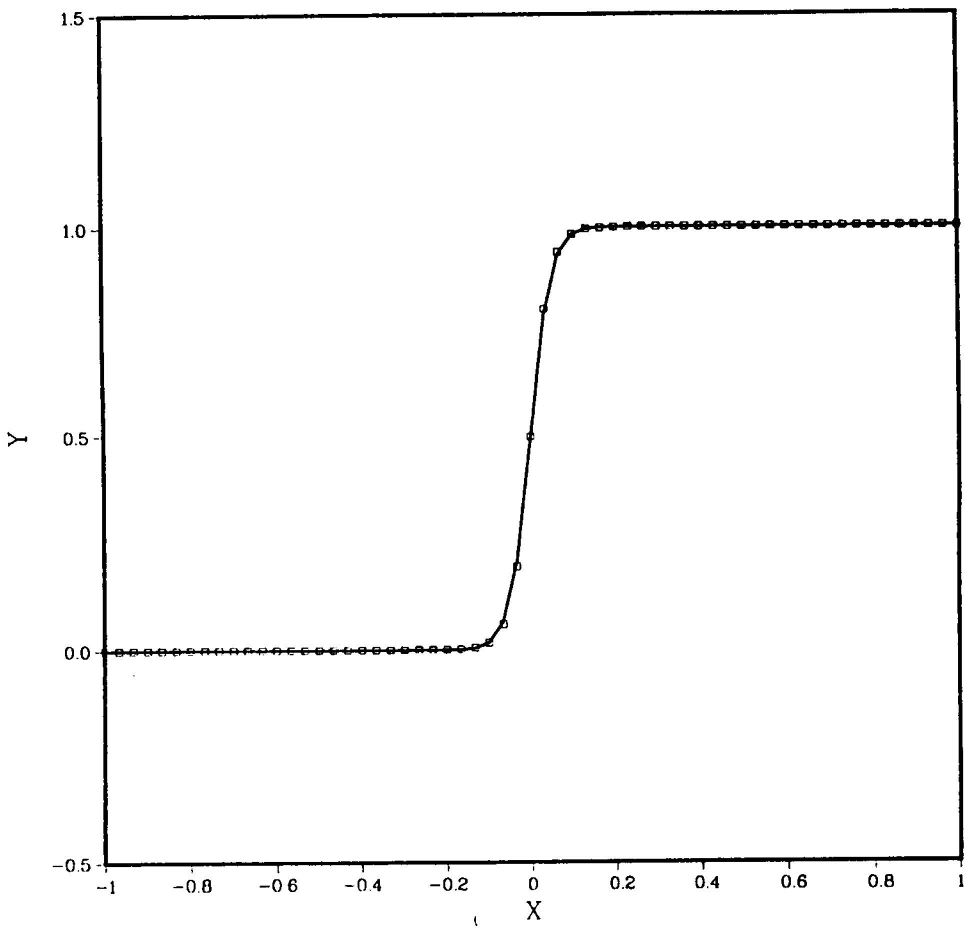

Rockwell International
Rocketdyne Division

ONE-DIMENSIONAL HELMHOLTZ EQUATION
WITH 5 POINTS IN FIRST DOMAIN, 51 POINTS IN SECOND
INTERFACE AT X=-0.1

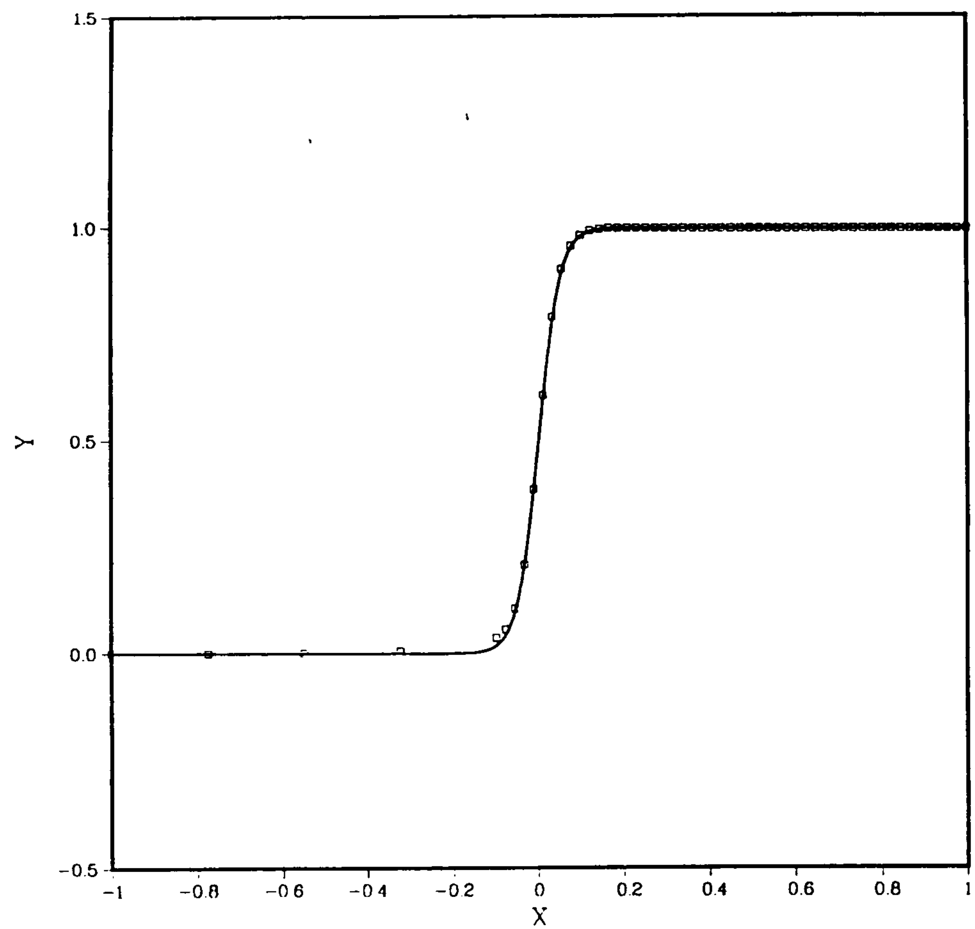

Rockwell International
Rocketdyne Division

ONE-DIMENSIONAL HELMHOLTZ EQUATION
WITH 5 POINTS IN FIRST DOMAIN, 61 POINTS IN SECOND
INTERFACE AT X=-0.4

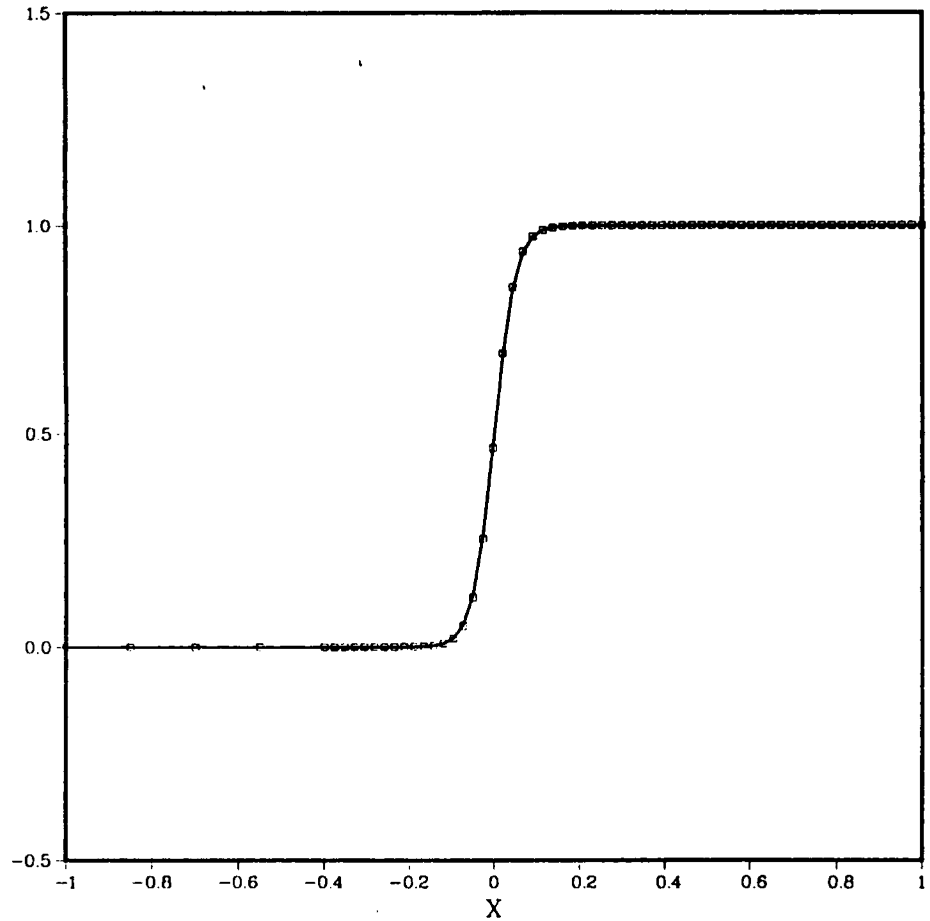

Rockwell International
Rocketdyne Division

FUNDAMENTAL TEST CASES

- **LAMINAR BACKWARD FACING STEP**
  - ARMALY, DURST, PEREIRA AND SCHONUNG, 1983
  - TWO-DIMENSIONAL ANALYSIS FOR REYNOLDS NUMBER RANGING FROM 50 TO 1,500
  - THREE-DIMENSIONAL ANALYSIS FOR REYNOLDS NUMBER OF 1,000
  - TWO COMPUTATIONAL DOMAINS
  - PARABOLIC VELOCITY PROFILE IMPOSED AT INLET PLANE LOCATED AT FOUR STEP HEIGHTS UPSTREAM OF EXPANSION
  - PREDICTED REATTACHMENT LENGTHS COMPARED WITH EXPERIMENTAL MEASUREMENTS

- **LAMINAR DRIVEN CAVITY FLOW**
  - GHIA, GHIA AND SHIN, 1982
  - TWO-DIMENSIONAL ANALYSIS FOR REYNOLDS NUMBER RANGING FROM 1 TO 10,000
  - TWO AND FOUR COMPUTATIONAL DOMAINS
  - INITIALIZE WITH STAGNATING CONDITION

Rockwell International
Rocketdyne Division

2-D LAMINAR BACKWARD FACING STEP
PREDICTED STREAMLINE AT DIFFERENT REYNOLDS NUMBERS

Re=100

Re=389

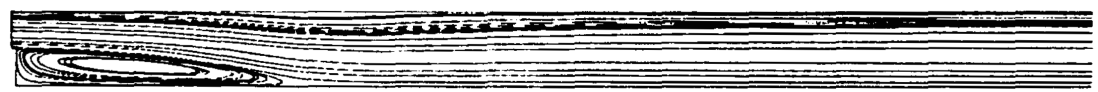

Re=1,000

Rockwell International
Rocketdyne Division

2-D LAMINAR BACKWARD FACING STEP
REATTACHMENT LENGTHS AT DIFFERENT REYNOLDS NUMBERS

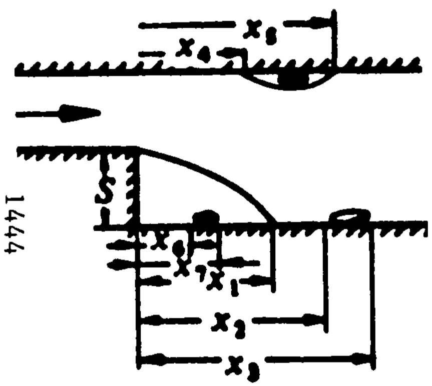

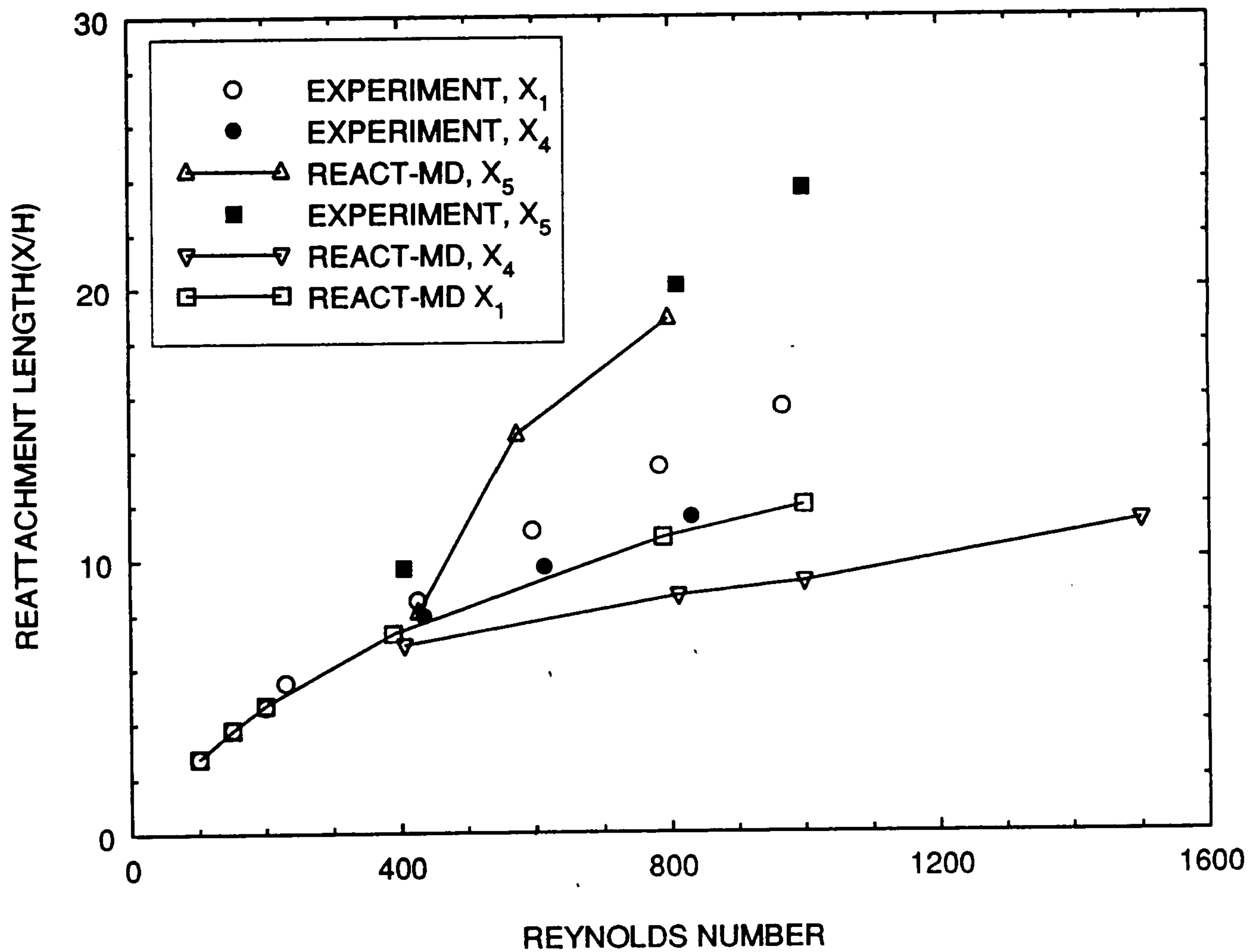

1444

Rockwell International
Rocketdyne Division

2-D DRIVEN CAVITY
FLOW TOPOLOGY AT DIFFERENT REYNOLDS NUMBERS

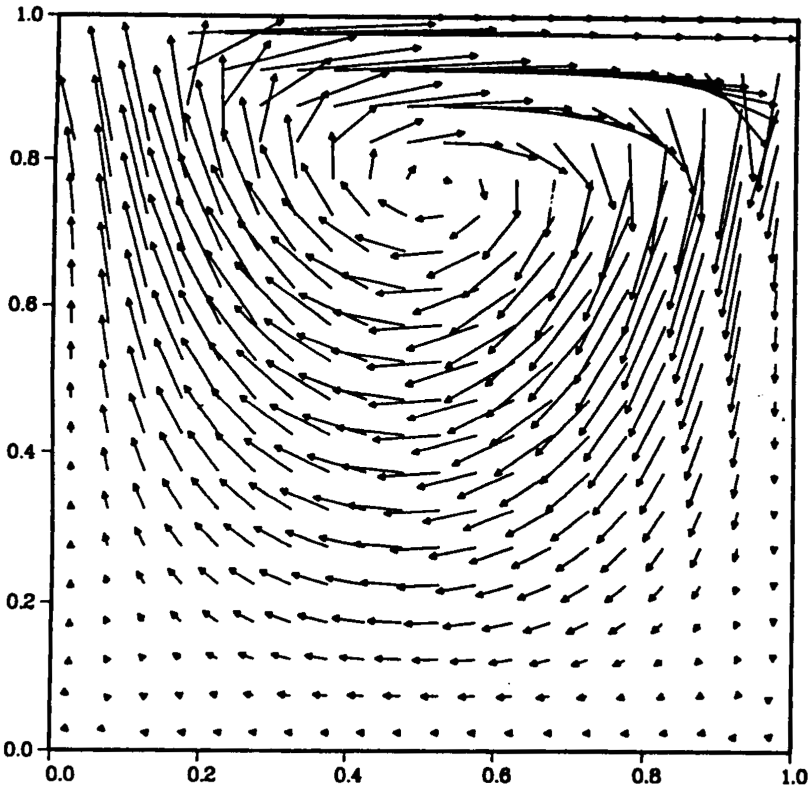

Re=10

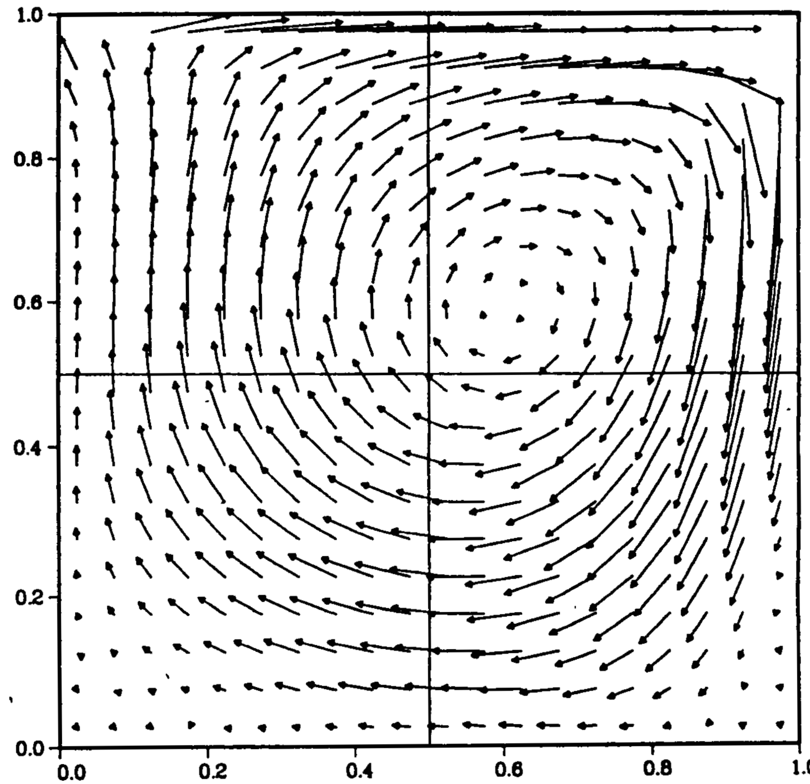

Re=1,000

Rockwell International
Rocketdyne Division

2-D DRIVEN CAVITY
PREDICTED STREAMLINES FOR FOUR DOMAIN COMPUTATIONS USING 81X81 POINTS (Re=10,000)

Present Result (81x81 Grid)

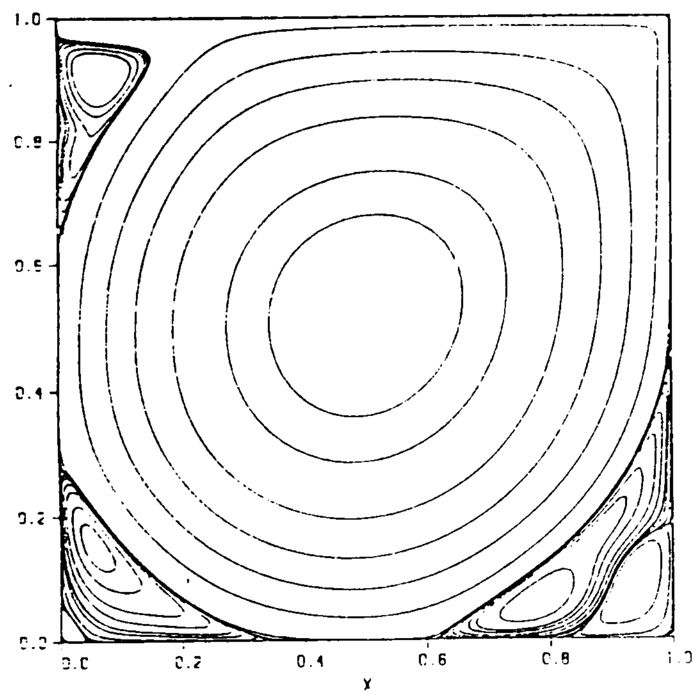

Ghia's Result (257x257 Grid)

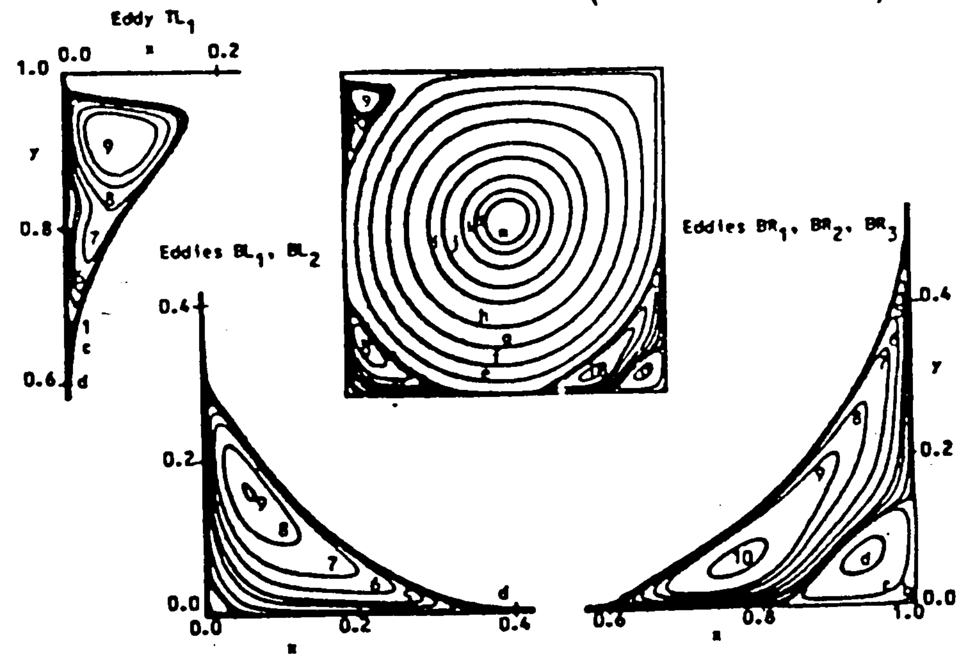

Rockwell International
Rocketdyne Division

2-D DRIVEN CAVITY

CPU TIME REQUIREMENT FOR FOUR AND SINGLE DOMAIN COMPUTATIONS USING 161X161 POINTS

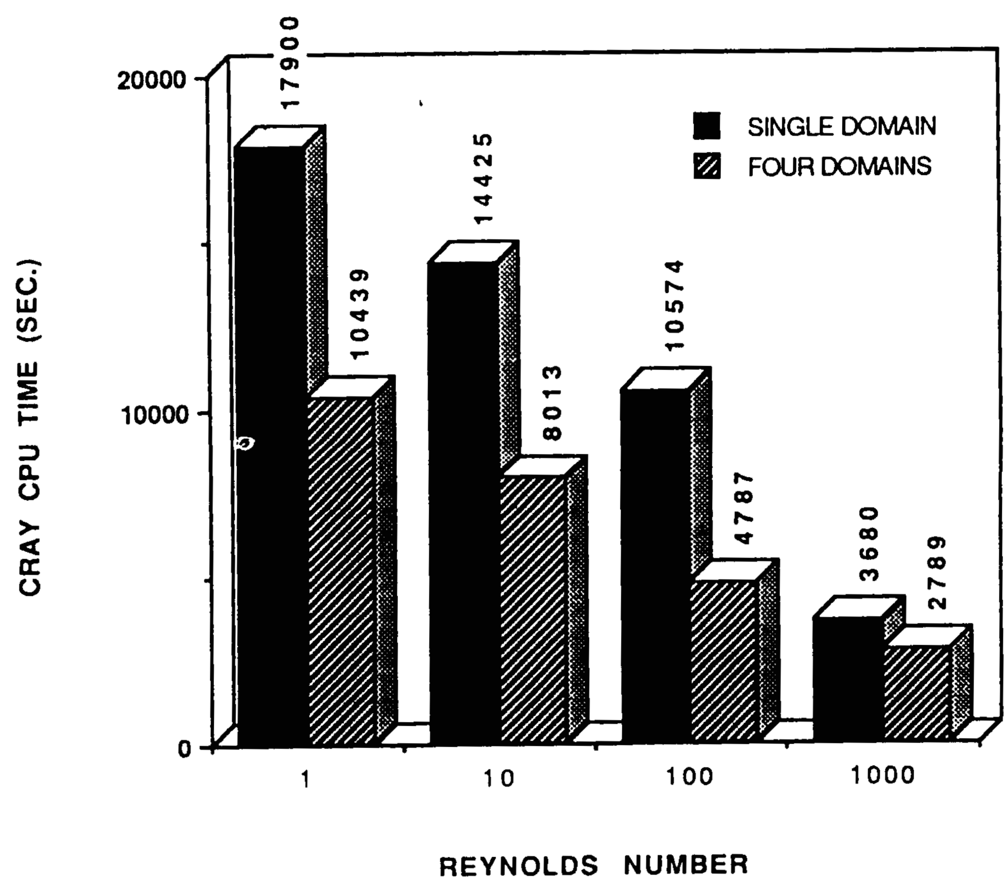

Rockwell International
Rocketdyne Division

2-D CAVITY WITH AN ORIFICE
GRID SYSTEM

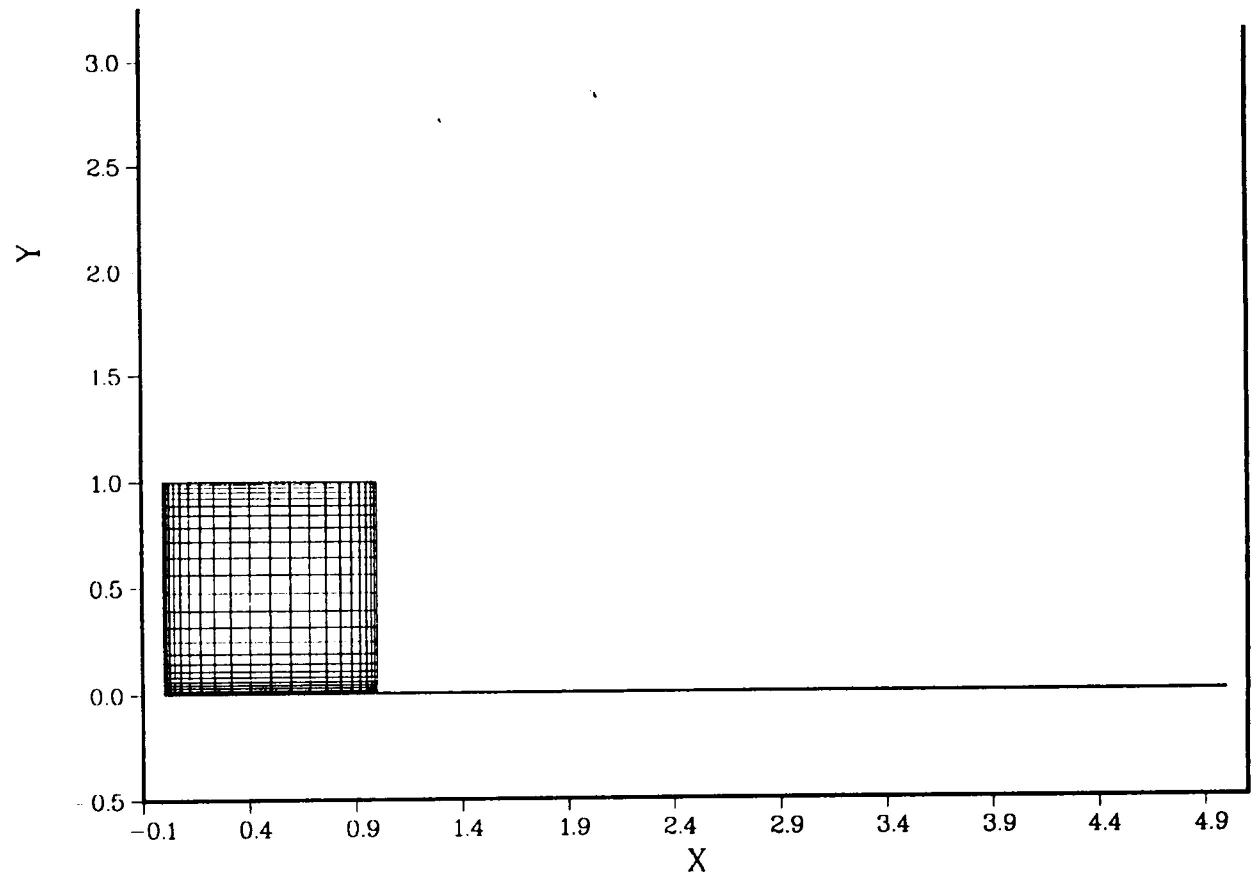

Rockwell International
Rocketdyne Division

2-D CAVITY WITH AN ORIFICE
CONVERGENCE HISTORY AND STREAMLINES FOR TWO-DOMAIN COMPUTATIONS USING 1500 POINTS

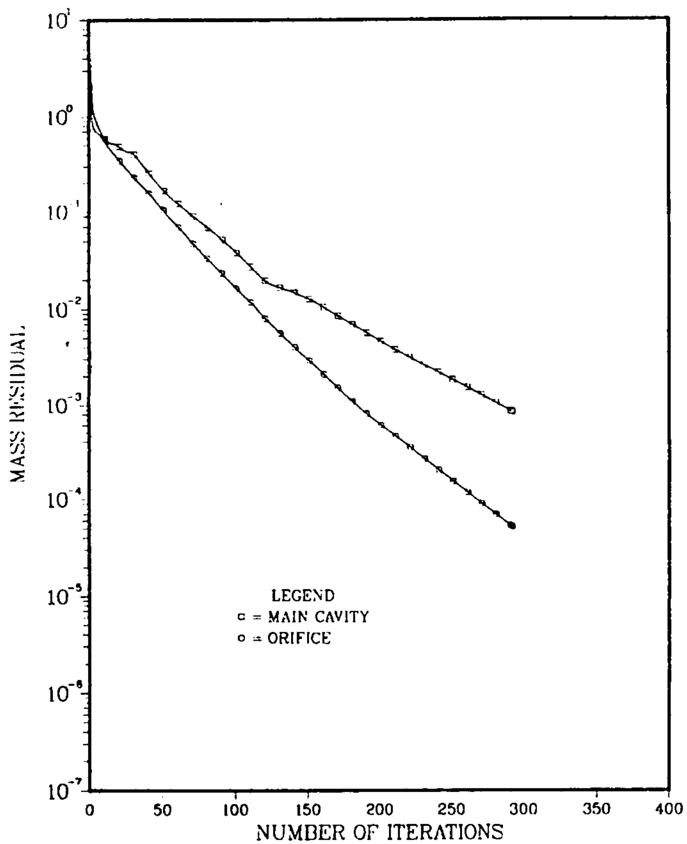

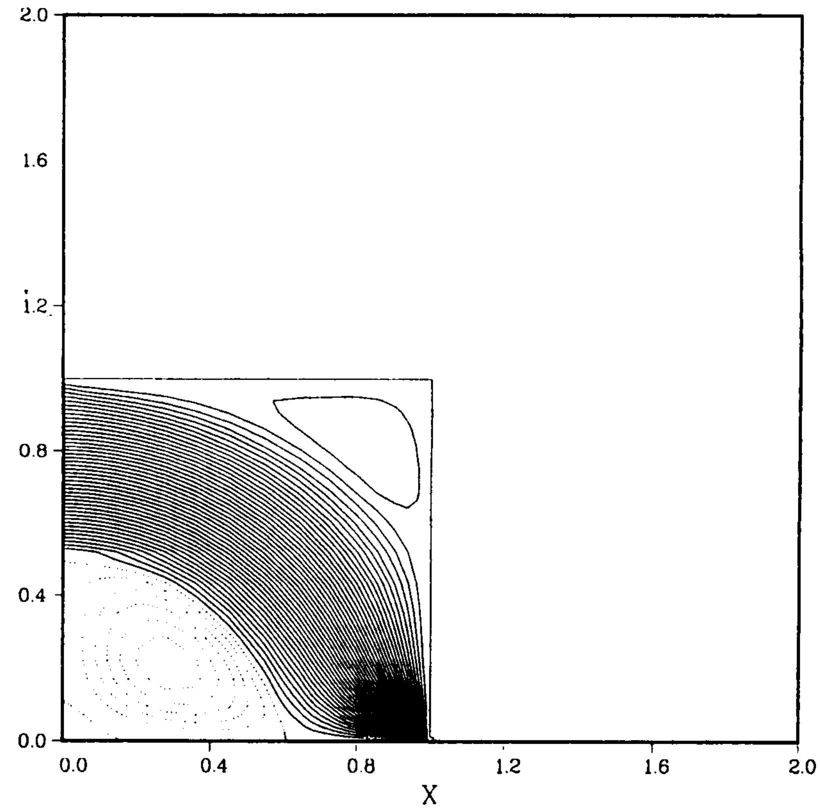

Rockwell International
Rocketdyne Division

2-D CAVITY WITH AN ORIFICE

CPU TIME REQUIREMENT FOR TWO AND SINGLE DOMAIN COMPUTATIONS USING 1500 POINTS

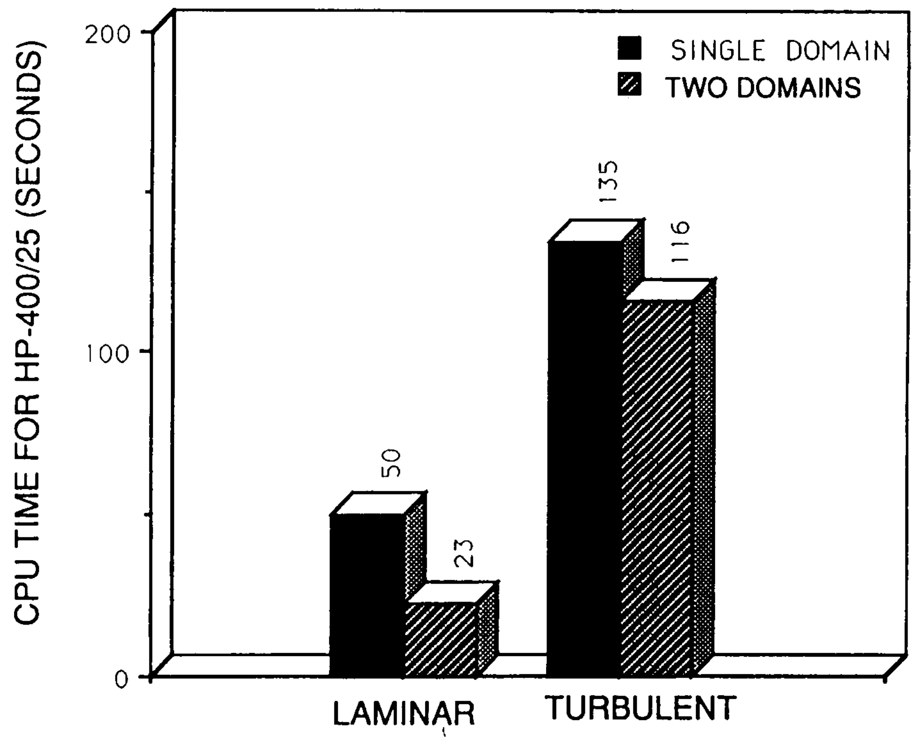

Rockwell International
Rocketdyne Division

SUMMARY

- **MODELING OF COMPLEX FLOW PATHS**
  - GEOMETRIC COMPLEXITY
  - POTENTIAL FOR COMPONENTS COUPLING

- **OFFER CONVERGENCE ACCELERATION**
  - GROUP DISPARATE FLOW SCALE
  - USE CORE MEMORY
  - USE APPROPRIATE VECTOR LENGTH

EXPLOIT PARALLEL COMPUTER ARCHITECTURE
  - **CONCURRENT COMPUTATION OF SUB-DOMAINS ON DIFFERENT CPU'S**

Rockwell International
Rocketdyne Division

LARGE EDDY SIMULATION OF COMPRESSIBLE TURBULENT CHANNEL FLOWS*

Robert A. Beddini and Jeffrey P. Ridder
Department of Aeronautical and Astronautical Engineering, MC 236
University of Illinois at Urbana-Champaign
Urbana, Illinois 61801

Statement of Problem: The development of turbulence within rocket propulsion chamber flows remains a difficult problem to predict. Within solid propellant rockets, for example, the flow can exhibit multiple regions of transition to turbulence, and is susceptible to various modes of aeroacoustic interaction, potentially associated with instability of the combustion/flowfield process.

Objective: To formulate, develop and validate a large eddy simulation (LES) method for compressible channel flows. Additionally, to assess the potential and limitations of the method with regard to predicting flows of interest in realistic systems.

Approach: The LES method separates the resolvable scale motions from the unresolvable (subgrid) scales by applying a spatial filter to the compressible Navier-Stokes equations. The subgrid-scale Reynolds terms are modeled using a compressible extension of an existing incompressible model for wall bounded flows. The equations are solved numerically using a modified four-step Runge-Kutta procedure in time and second or fourth-order finite differences in space.

Results and Conclusions[1]**:** The method has been validated by simulating a low Reynolds number ($Re_b \approx 5400$), low Mach number ($M_c \approx 0.3$) turbulent Poiseuille flow. Various statistical comparisons are made with incompressible experimental and direct simulation data at similar Reynolds numbers, including higher-order statistics and spatial correlations. The results compare favorably with the incompressible data.

A high subsonic Mach number ($M_c \approx 0.3$) turbulent Poiseuille flow is also simulated for comparison with the low Mach number results at nominally constant Reynolds number. The mean velocity profile is seen to depart from the low Mach number profile, corresponding to an expected dependence of the mean density and temperature profiles on Mach number. The turbulence velocity statistics are found to be reasonably independent of Mach number. Pressure fluctuation statistics are also found to scale with the wall shear stress independently of Mach number, although normalized density and temperature fluctuations increase substantially with Mach number. The density and temperature fluctuations, although small in magnitude, are observed not to be isobarically related.

The current simulations have validated the algorithm in the incompressible limit and have demonstrated the ability of the method to simulate high subsonic Mach number flows. The principal impediment in application of the method to practical, high Reynolds number chamber flow problems is the large CPU time requirement of the calculations. At present, this bottleneck is caused in large part by resolution requirements for the turbulence-producing "streaks" in the viscous wall layer. Improvements in the subgrid-scale modeling could greatly reduce CPU requirements, leading to more rapid engineering use.

* Research supported by NASA Marshall Space Flight Center under grant NGT- 50363.

[1] Ridder, J.P.: Large Eddy Simulation Of Compressible Channel Flow, Ph.D. Thesis, U. of Illinois at Urbana-Champaign, January, 1992.

LARGE EDDY SIMULATION OF COMPRESSIBLE CHANNEL FLOWS*

Robert A. Beddini
Jeffrey P. Ridder

Aerothermal Simulations Laboratory
Department of Aeronautical and Astronautical Engineering
University of Illinois at Urbana–Champaign

CFD Applications in Rocket Propulsion
NASA / MSFC
Huntsville, AL
April 28-30, 1992

*Research sponsored by NASA under grant NGT-50383, and by the National Center for Supercomputing Applications, University of Illinois at Urbana–Champaign

MOTIVATION

- SOLID PROPULSION INTERNAL FLOWS UNDERGO TRANSITION TO TURBULENCE WITHIN THE CHAMBER.

- TRANSITIONAL FLOW AND NEAR-SURFACE TURBULENCE HAVE BEEN SHOWN IN PRIOR STUDIES TO AFFECT PROPELLANT COMBUSTION (EROSIVE BURNING & ACOUSTIC RESPONSE).

- PRIOR STUDIES HAVE SHOWN INADEQUACIES IN TURBULENCE MODELS IN PREDICTING TRANSITIONAL FLOW DEVELOPMENT WITH LARGE SURFACE INJECTION RATES.
  - BOTH $k-\varepsilon$ AND FULL REYNOLDS STRESS MODELS REQUIRED SUBSTANTIAL PARAMETER ADJUSTMENT FOR SIMPLEST INTERNAL FLOWS.
  - EFFECTS OF NEAR WALL "PSEUDOTURBULENCE" DIFFICULT TO MODEL.

OBJECTIVES

- FORMULATE AND DEVELOP LARGE-EDDY SIMULATION (LES) METHOD FOR COMPRESSIBLE CHAMBER FLOWS.
  - NO PRIOR SIMULATIONS OF WALL BOUNDED COMPRESSIBLE TURBULENT FLOWS HAVE BEEN REPORTED.

- VALIDATE MODEL & METHOD BY COMPARISON WITH DIRECT SIMULATIONS OF TURBULENT CHANNEL FLOW AT LOW REYNOLDS NUMBERS.

- ASSESS PRACTICALITY AND LIMITATIONS OF LES METHOD FOR PROBLEMATIC FLOWS.

ACTUAL SOLID ROCKET FLOW

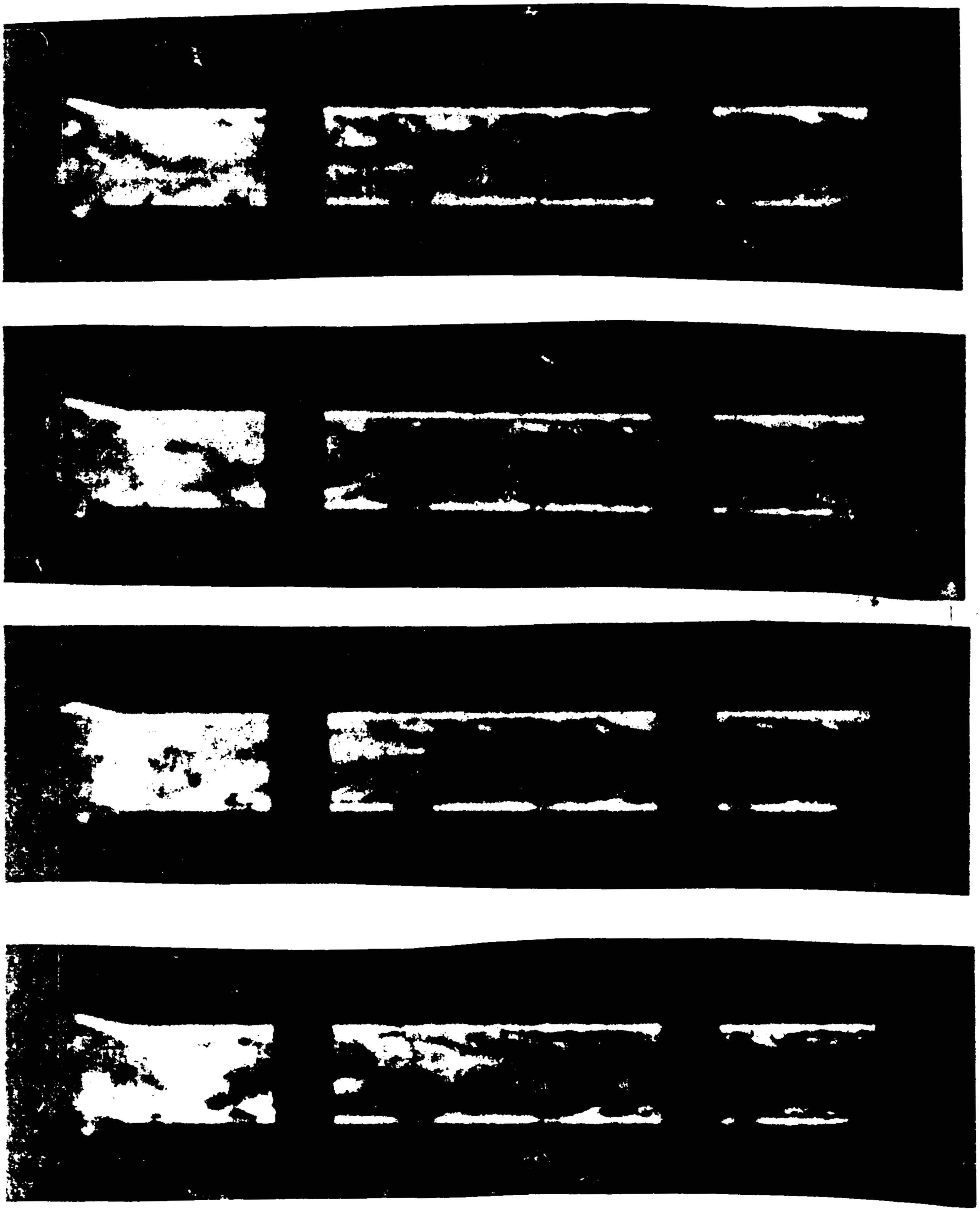

APPROACH

- ADVANTAGES
  - LES APPROACH RESOLVES 3-D TIME-DEPENDENT LARGE SCALE MOTIONS WHICH NATURALLY EXIST IN CHAMBERS.
  - CAN INDICATE POTENTIAL VORTEX/ACOUSTIC INTERACTIONS.
  - CAN PROVIDE TURBULENT LENGTH SCALE INFORMATION NEEDED IN OTHER TURBULENCE MODELS.
  - EMPIRICAL ASSUMPTIONS CONFINED TO SMALLER EDDY SCALES – PRESUMED MORE “UNIVERSAL”.

- DISADVANTAGES
  - EXTENSIVE CPU REQUIREMENTS IMPLY NONROUTINE APPLICATION OF SIMULATIONS AT PRESENT.
  - UNRESOLVED (SUBGRID) SCALES OF TURBULENCE MUST BE EMPIRICALLY MODELLED. (THERE IS NO ALTERNATIVE IF VERY LARGE REYNOLDS NUMBERS ARE CONSIDERED.)

APPROACH - METHOD

- EQUATIONS: 3-D TIME-DEPENDENT COMPRESSIBLE NAVIER-STOKES, FILTERED IN SPACE AND FAVRE AVERAGED.
- SUBGRID REYNOLDS STRESSES AND HEAT FLUX MODELLED USING SMAGORINSKY MODEL (cf MOIN &KIM, '83).
- NUMERICAL METHOD:
  - METHOD DOES NOT ASSUME PERIODIC (SPECTRAL) DECOMPOSITION IN ANY DIRECTION.
  - SECOND AND FOURTH ORDER CENTRAL DIFFERENCES IN SPACE ASSESSED.
  - MODIFIED FOURTH-ORDER TIME DIFFERENCING SCHEME DEVELOPED FOR CELL Re>10. RESULTS IN 40% DECREASE IN CPU TIME.
  - CODE WELL VECTORIZED – 150 MFLOPS ON CRAY Y/MP.

APPLICATION CONDITIONS

- POISEUILLE FLOW - Re~ 5400 (BASED ON AV. U AND HEIGHT)
- THOUGH NOT REQUIRED, PERIODIC BC'S IN ON LENGTH AND DEPTH BOUNDARIES WERE USED TO COMPARE WITH PRIOR STUDIES.
- Mach No. OF 0.3 USED TO VALIDATE METHOD AND ASSESS SUBGRID PARAMETERS
- Mach No. OF 0.7 USED TO ASSESS COMPRESSIBLE FLOW EFFECTS W/O ADDITIONAL SHOCK CAPTURING DISSIPATION TERMS.
- GRID RESOLUTION EFFECTS ASSESSED – BASELINE GRID WAS 32 L x 90 H x 80 D. (=> 4 MW MEMORY REQUIREMENT).

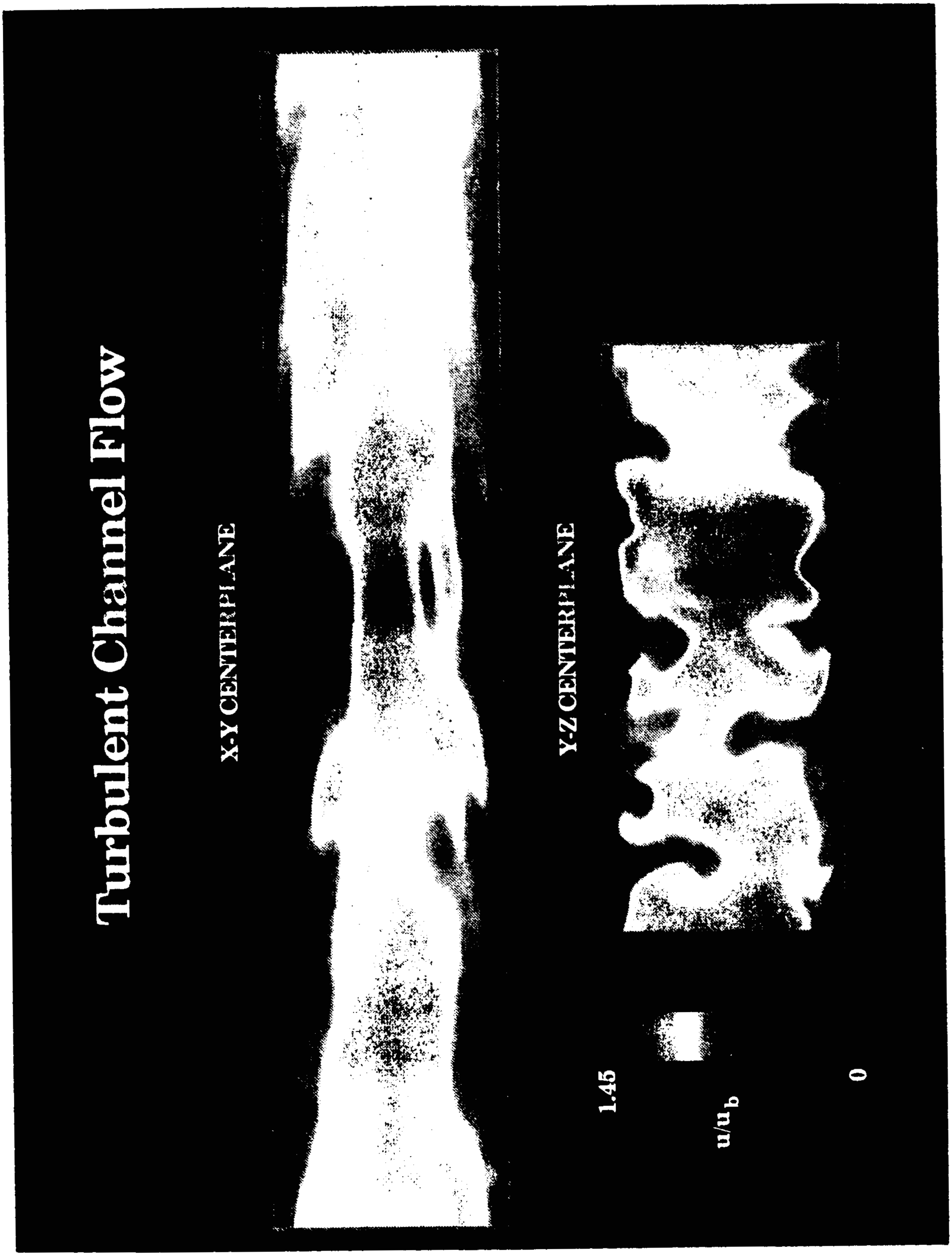
Turbulent Channel Flow
X-Y CENTERPLANE
Y-Z CENTERPLANE
1.45
u/u_b
0

RESULTS (LOW Mach No.)

- SUBGRID CONSTANT C_{mk} MINIMIZED TO PRODUCE LEAST AFFECT ON TURBULENCE.
- MEAN VELOCITY PROFILE AND REYNOLDS SHAER STRESS PROFILE COMPARE FAVORABLY WITH DIRECT N-S STUDIES AND EXPERIMENTAL DATA.
- WALL PRESSURE FLUCTUATIONS COMPARE FAVORABLY WITH DIRECT N-S SOLUTIONS, BUT ARE 1/3 LOWER THAN EXPERIMENTAL DATA.
- MACRO LENGTH-SCALES COMPARE FAVORABLY WITH DIRECT N-S SOLUTIONS, BUT DISSIPATION LENGTH SCALES WERE NOT ADEQUATELY RESOLVED.

RESULTS (HIGH Mach No.)

- AS EXPECTED, MEAN VELOCITY PROFILE AFFECTED BY MEAN DENSITY GRADIENT IN NEAR WALL REGION, BUT FOLLOWS CROCCO SCALING.
- REYNOLDS STRESSES AND PRESSURE FLUCTUATIONS SCALE WELL WITH MEAN VELOCITY AT THIS SUBSONIC MACH NUMBER.
- RMS TEMPERATURE AND DENSITY FLUCTUATIONS FOUND TO SCALE NEARLY AS M^2, BUT ARE NOT ISOBARICALLY RELATED.

MEAN VELOCITY PROFILE COMPARISON

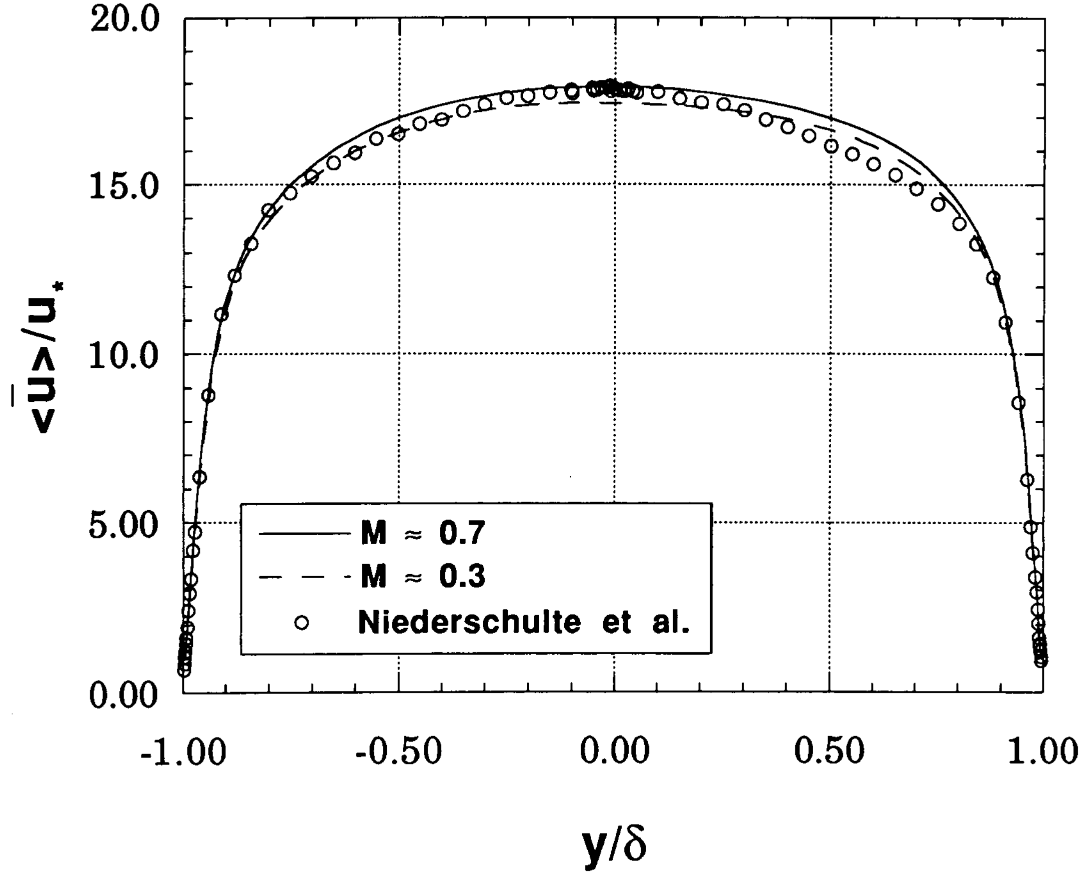

University of Illinois at Urbana - Champaign / Aerothermal Simulations Lab

RESOLVED REYNOLDS SHEAR STRESS COMPARISON

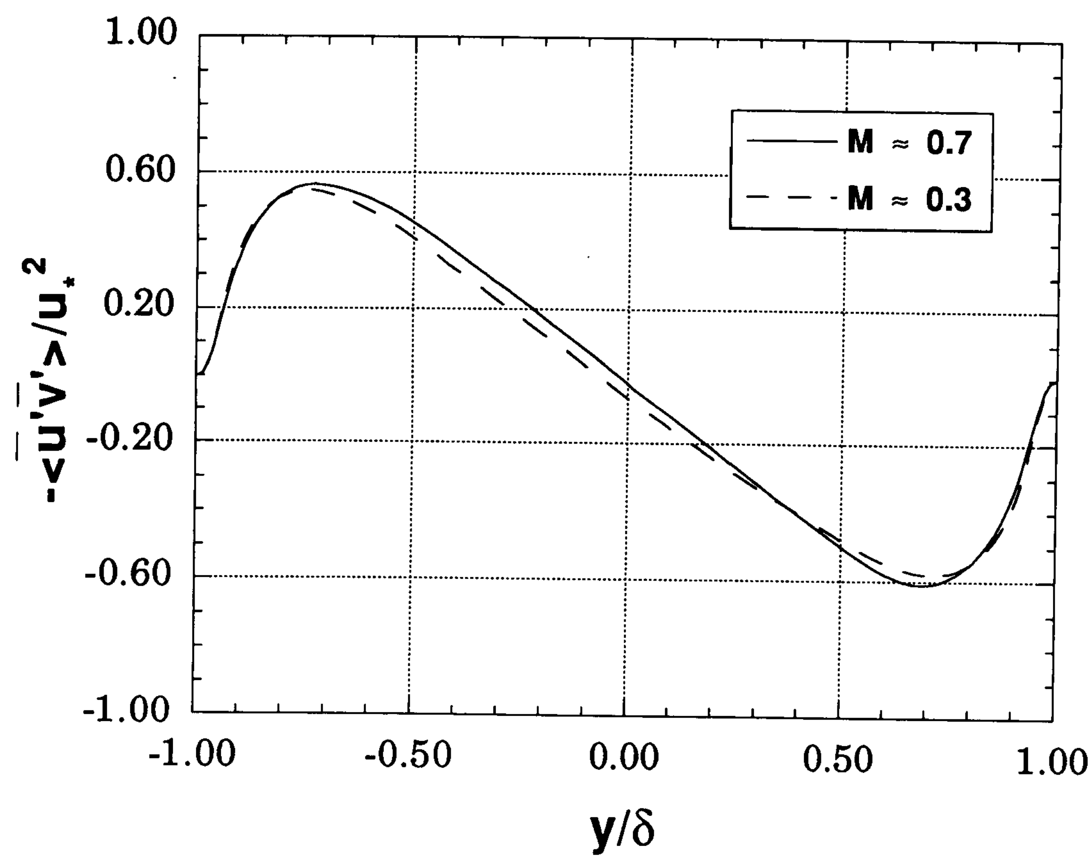

RESOLVED RMS PRESSURE AND TEMPERATURE FLUCTUATIONS

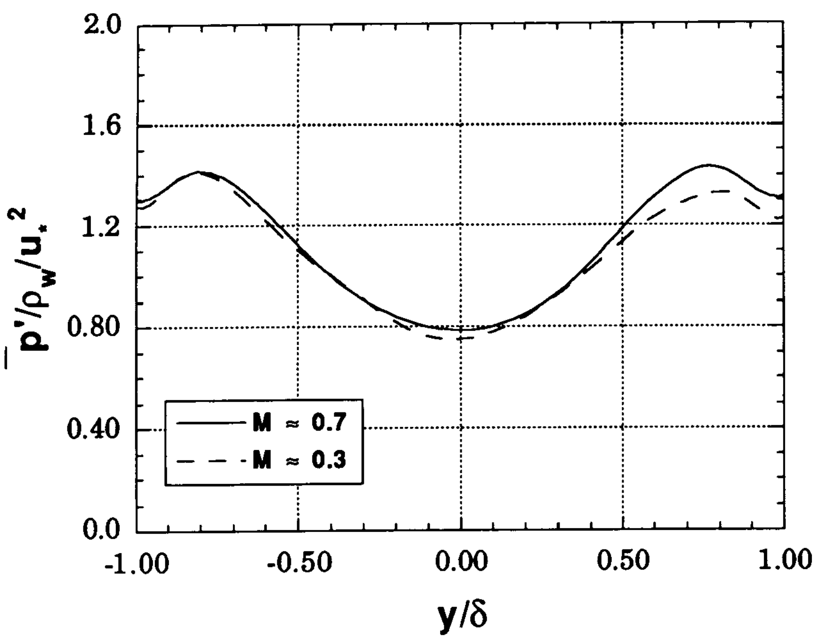

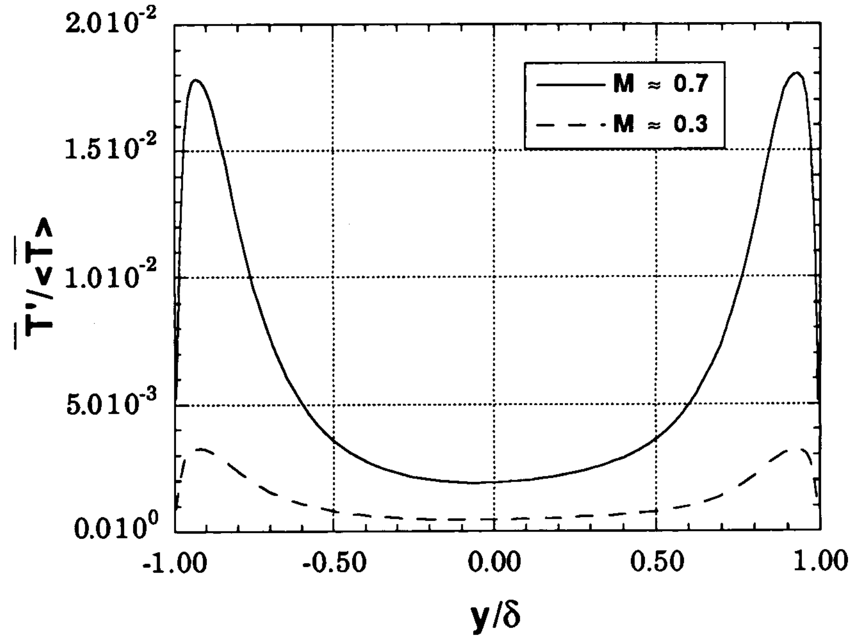

University of Illinois at Urbana - Champaign / Aerothermal Simulations Lab

SUMMARY/CONCLUSIONS

- LES METHOD FOR WALL-BOUNDED COMPRESSIBLE FLOWS DEVELOPED AND VALIDATED.
- FEASIBILITY OF LES SIMULATIONS FOR MORE COMPLEX FLOWS INDICATED PROVIDING MEAN FLOW IS NOMINALLY TWO-D.
- FAVORABLE COMPARISON WITH DIRECT SIMULATION RESULTS AND EXPERIMENTAL DATA AT LOW MACH NO.
  - IMPROVEMENTS REQUIRED IN SUBGRID MODELING.
  - SCALE UP TO VERY-LARGE Re OTHERWIZE LIMITED BY RESOLUTION OF NEAR WALL STREAKS

SUMMARY/CONCLUSIONS (2)

- PRESSURE FLUCTUATION SPECTRA OBTAINED - POTENTIAL FEEDBACK TO PROPELLANT RESPONSE.
- WHY DO DIRECT AND LES METHODS UNDERPREDICT PRESSURE FLUCTUATIONS?
- LENGTH-SCALE DATA OBTAINED - COULD PROVIDE INFORMATION TO TURBULENCE MODELS FOR OTHER APPLICATIONS.
- NORMALIZED REYNOLDS STRESSES AND PRESSURE FLUCTUATIONS NEARLY INDEPENDENT OF MACH NO.
- NORMALIZED TEMPERATURE AND DENSITY FLUCTUATIONS VARY NEARLY AS M^2
  => ARE THESE ACCOUNTED FOR IN HOT WIRE DATA REDUCTION??

N92-32277

Treating Convection in Sequential Solvers

Wei Shyy

Siddharth Thakur

Department of Aerospace Engineering,
Mechanics and Engineering Science
University of Florida, Gainesville, FL

The treatment of the convection terms in the sequential solver, a standard procedure found in virtually all pressure based algorithms, to compute the flow problems with sharp gradients and source terms is investigated. Both scalar model problem and one-dimensional gas dynamics equations have been used to study the various issues involved. Different approaches including the use of nonlinear filtering technique and the adoption of TVD type schemes have been investigated. Special treatments of the source terms such as pressure gradients and heat release have also been devised, yielding insight and improved accuracy of the numerical procedure adopted.

A Proposed Hierarchy of Test Problems

1. Nonlinear scalar wave equation to study capturing of sharp gradient

2. 1-D gas dynamics in a tube ——

(a) to study coupling among u, v, p and ρ

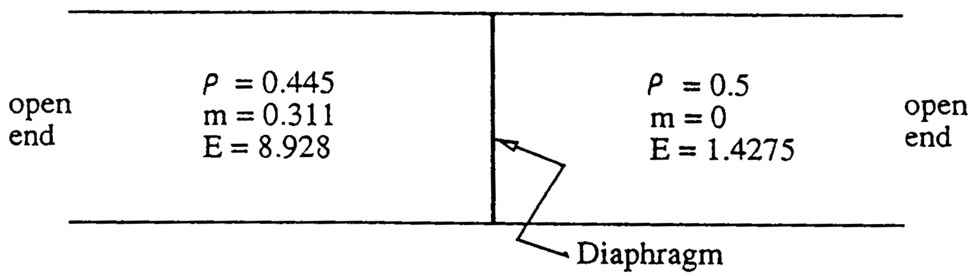

(b) to study interaction with B.C.s and among waves

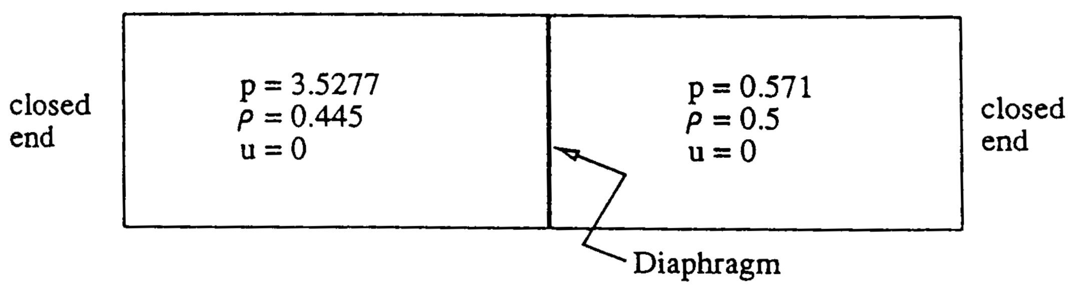

(c) to study formation and propagation of acoustic and entropy waves

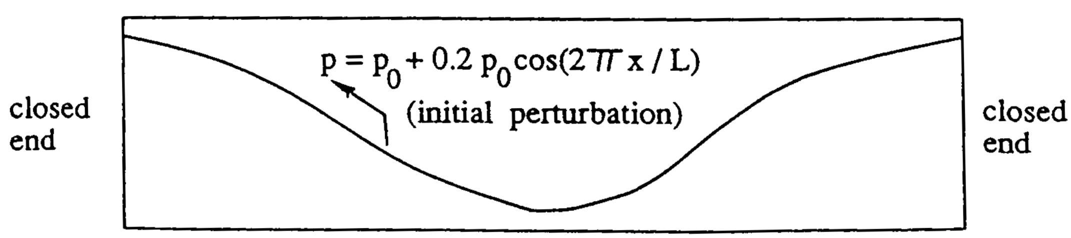

$p_0 = 40$ atm., T = 2800 K, $\gamma = 1.236$

3. 1-D Combusting Flow in a Duct

— to study effect of chemical heat release and its impact on acoustic and entropy waves.

— to study propagation and interaction of nonlinear waves in pressure, thermal and convective fields.

— to understand the longitudinal combustion instability and to devise active control strategy

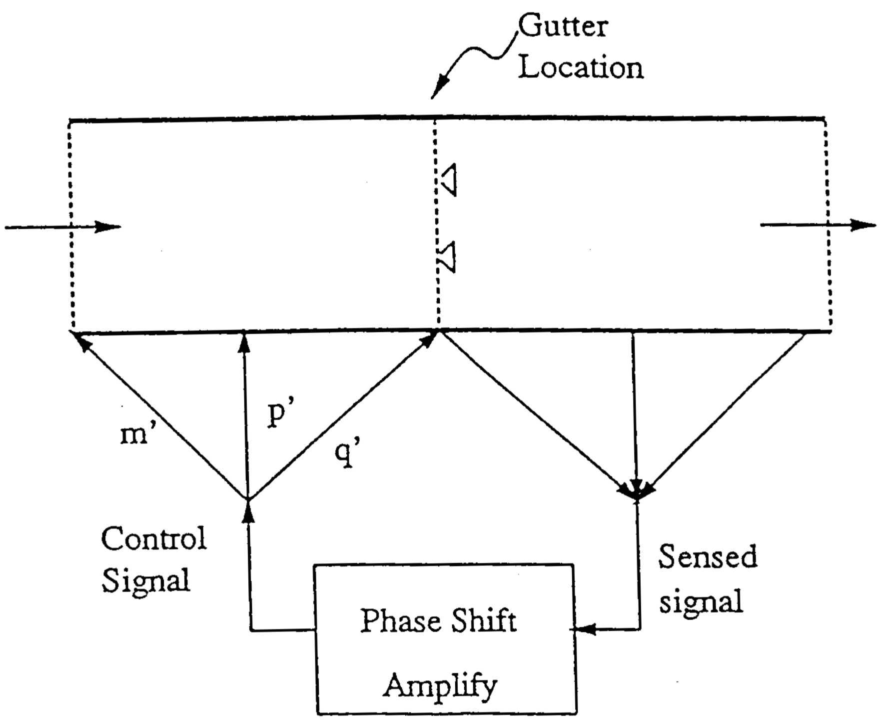

4. Multidimensional Problems

- **For a numerical scheme two features control its performance :**
  - Amplification factor ⟶ numerical damping
  - Phase angle ⟶ numerical dispersion

- **Problems of convection treatment :**
  - First order upwind scheme ⟶ excessive damping
    dispersion problem suppressed
  - Higher order schemes ⟶ no excessive damping
    dispersion problem appears

- **Two approaches investigated**
  - Nonlinear filtering
  - TVD type approach with source term treatment and artificial compression

Backward Euler time stepping scheme :

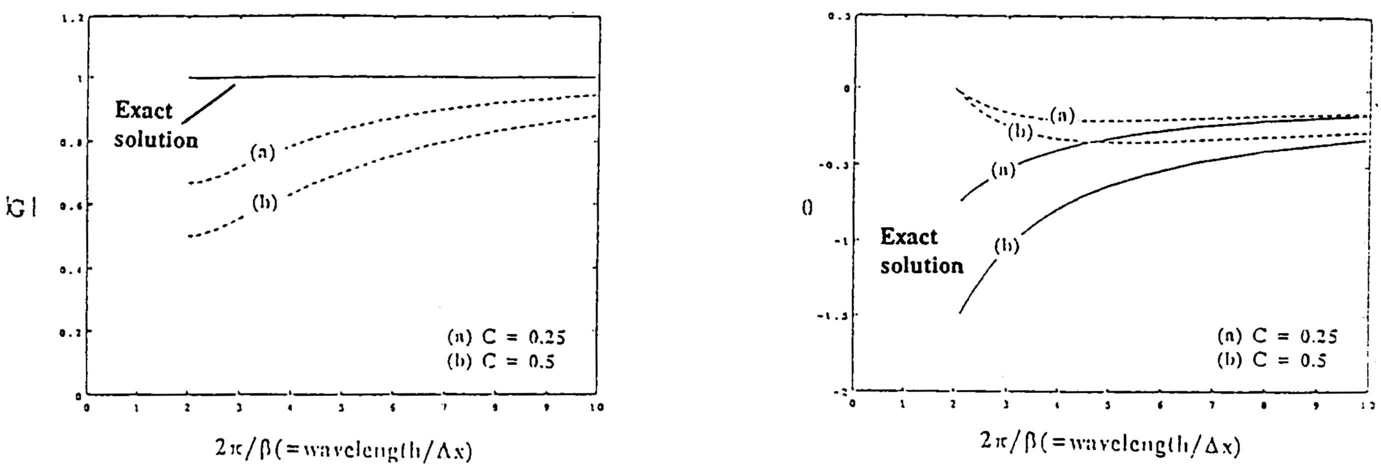

first-order upwind scheme

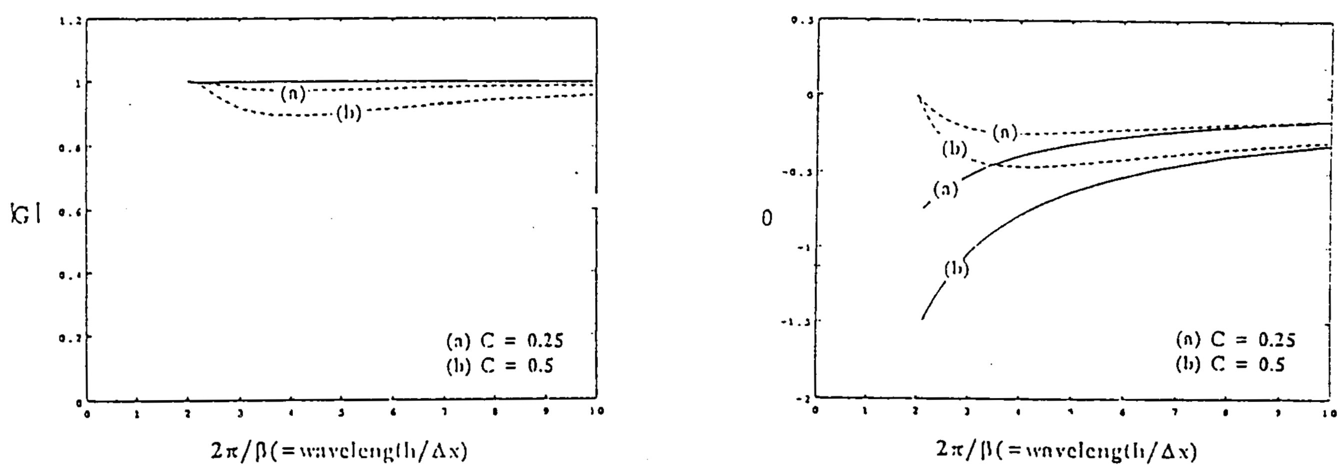

second-order central difference scheme

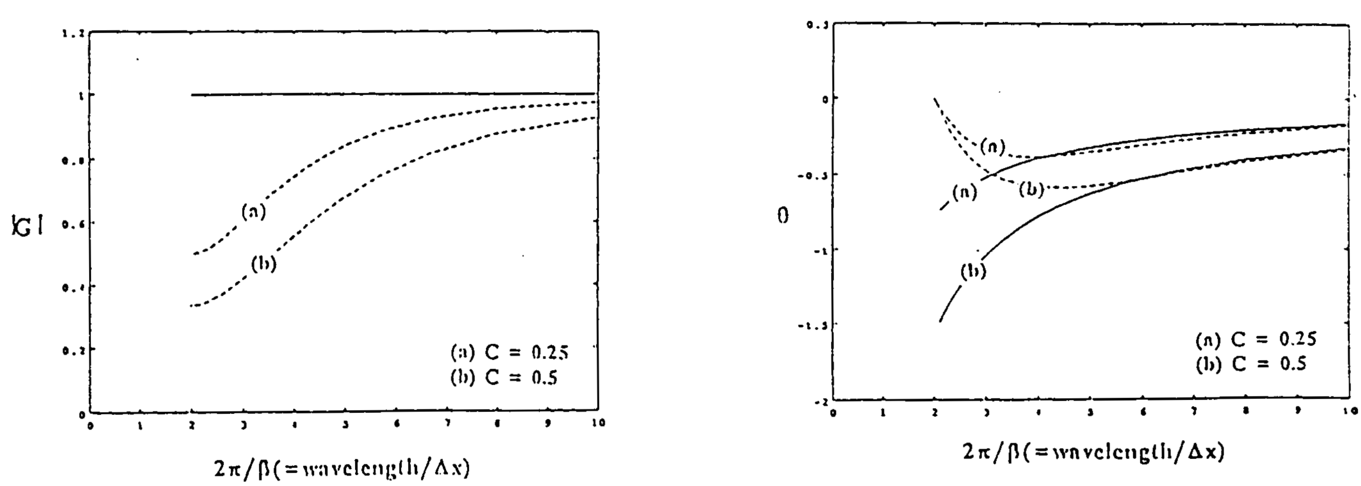

second-order upwind scheme

C-9

Point : A highly dispersive scheme may become a good one if dispersive problems in high wave number can be fixed; or better yet, to make constructive use of these wiggles

A possibility : Nonlinear Filtering

Key elements :

* maintains conservation laws

* utilizes standard schemes as basis

* attempts to eliminate wiggles a posteriori (a geometric approach)

* effective only for short wavelength oscillations (2Δ and 4Δ) & hence can check the filtering effectiveness via grid refinement

Define

--- Energy Content

$$E = \left[\sum_{j}^{N} (\phi_j - \Phi_j)^2 \right]^{1/2}$$

(Φ_j: exact solution; ϕ_j: numerical solution)

--- Area Content

$$A = \sum_{j}^{N} \phi_j$$

--- Goal :

* minimize E

* maintain A

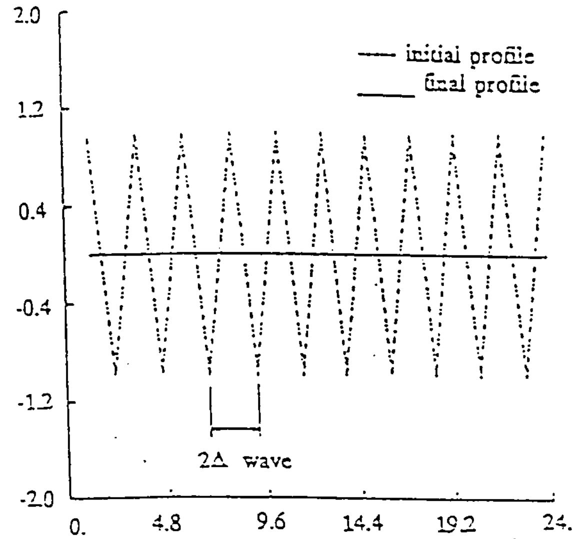

Effect of filtering on oscillations with 2Δ wavelength. For this case one application is sufficient to suppress oscillation completely.

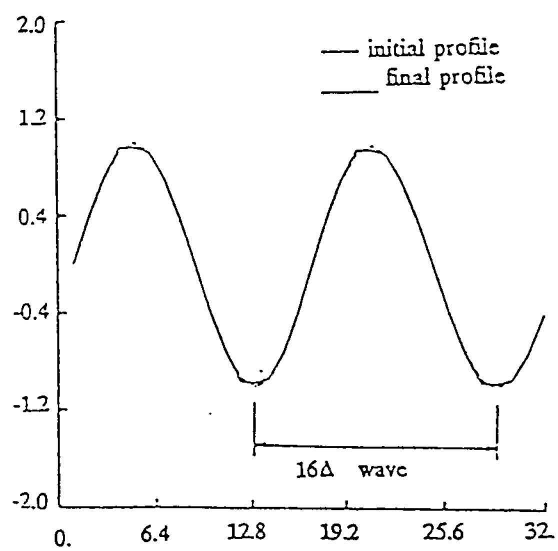

16Δ sine wave is only slightly altered after first filtering. Further application has no effect. E=0.999

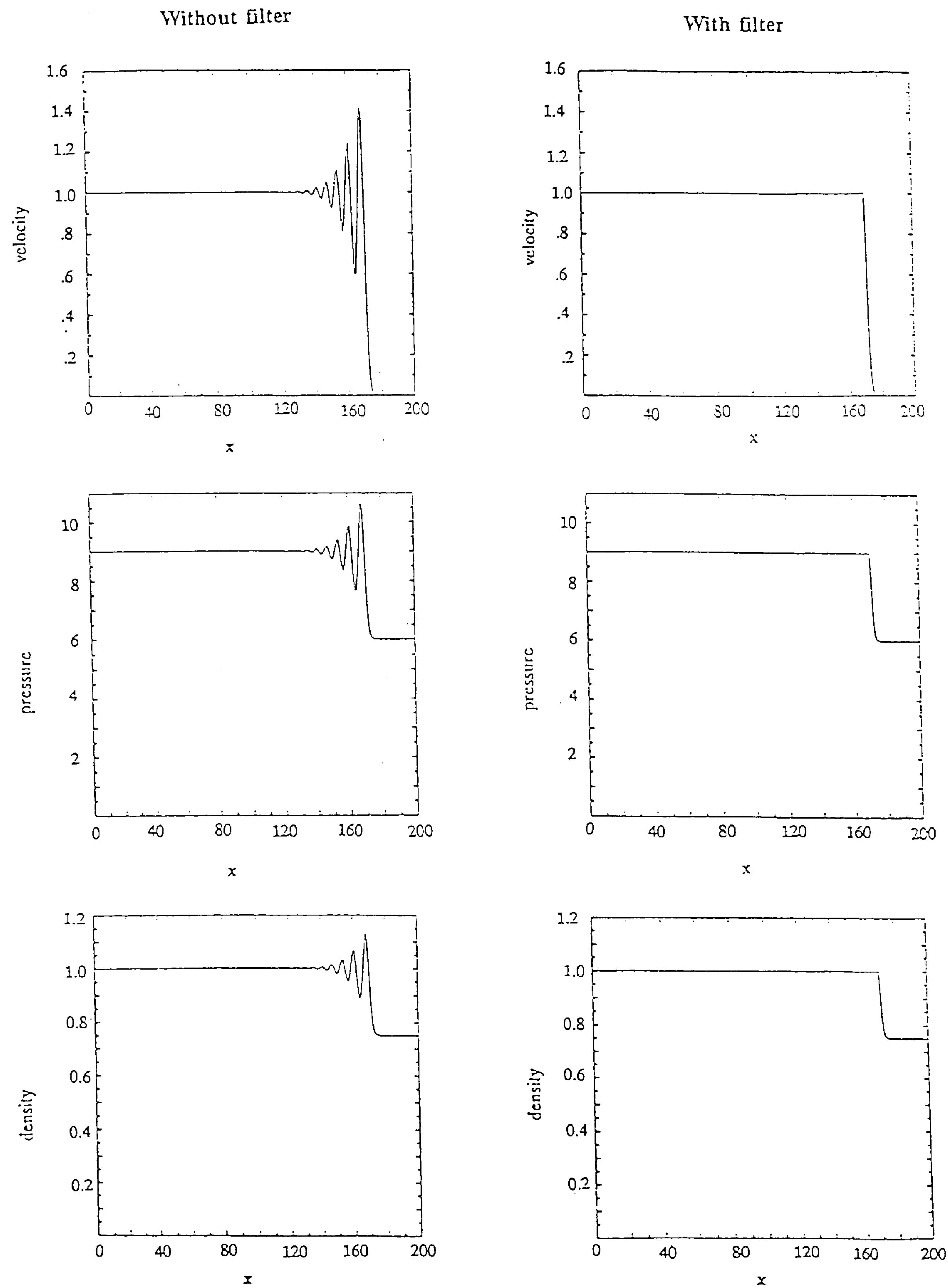

Effect of filtering on a 1-D compressible flow solution.

$Re = 10^4$ time step = 600

Euler Equations as a Simultaneous System

$$\frac{\partial U}{\partial t} + \frac{\partial F(U)}{\partial x} = 0$$

$$U = \begin{bmatrix} \rho \\ m \\ E \end{bmatrix}, \qquad F = \begin{bmatrix} m \\ m^2/\rho + p \\ (E + p)m/\rho \end{bmatrix}$$

Can also write

$$\frac{\partial U}{\partial t} + A(U)\frac{\partial U}{\partial x} = 0, \qquad A(U) = \frac{\partial F(U)}{\partial U}$$

Speed of sound

$$c = \sqrt{\frac{\partial p}{\partial \rho}} = \sqrt{\gamma \frac{p}{\rho}}$$

The eigenvalues of Jacobian matrix are

$$(a^1, a^2, a^3) = (u - c,\ u,\ u + c)$$

Sequential Approach with Coordinated Chracteristics

$$\frac{\partial \rho}{\partial t} + \frac{\partial [\rho u]}{\partial x} = 0$$

$$\frac{\partial m}{\partial t} + \frac{\partial [mu]}{\partial x} = -\frac{\partial p}{\partial x}$$

$$\frac{\partial E}{\partial t} + \frac{\partial [Eu]}{\partial x} = -\frac{\partial (pu)}{\partial x}$$

Pressure terms : source terms

The local characteristic speed : convection speed

$$a_{j+1/2} = \frac{1}{2}\left(u_j + u_{j+1}\right)$$

(same for all equations)

Special Source Term Treatment

Conservation law with a source term $\Psi(u)$

$$u_t + f(u)_x = \psi(u)$$

Examples:

Method I - MacCormack's explicit predictor-corrector method

Method II : Operator splitting (Strang's time-splitting)

$$U^{n+1} = S_\psi(k/2)\, S_f(k)\, S_\psi(k/2)\, U^n$$

where S_f represents the numerical solution operator for the system

$$u_t + f(u)_x = 0$$

and S_ψ is the numerical solution operator for the ODE

$$u_t = \psi(u)$$

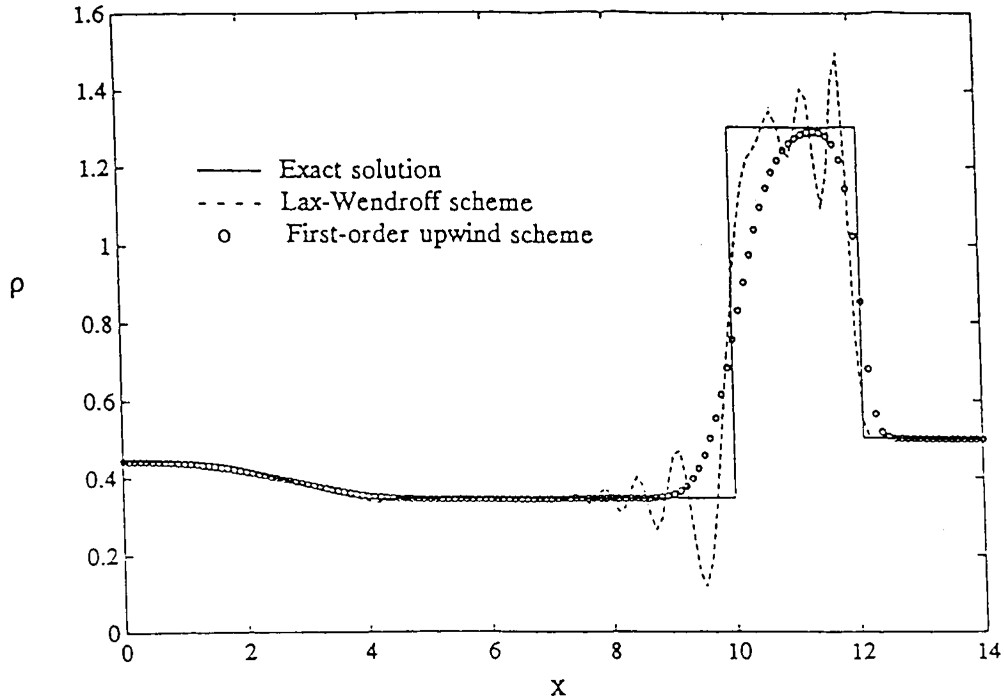

a) First-order upwind and second-order Lax-Wendroff schemes.

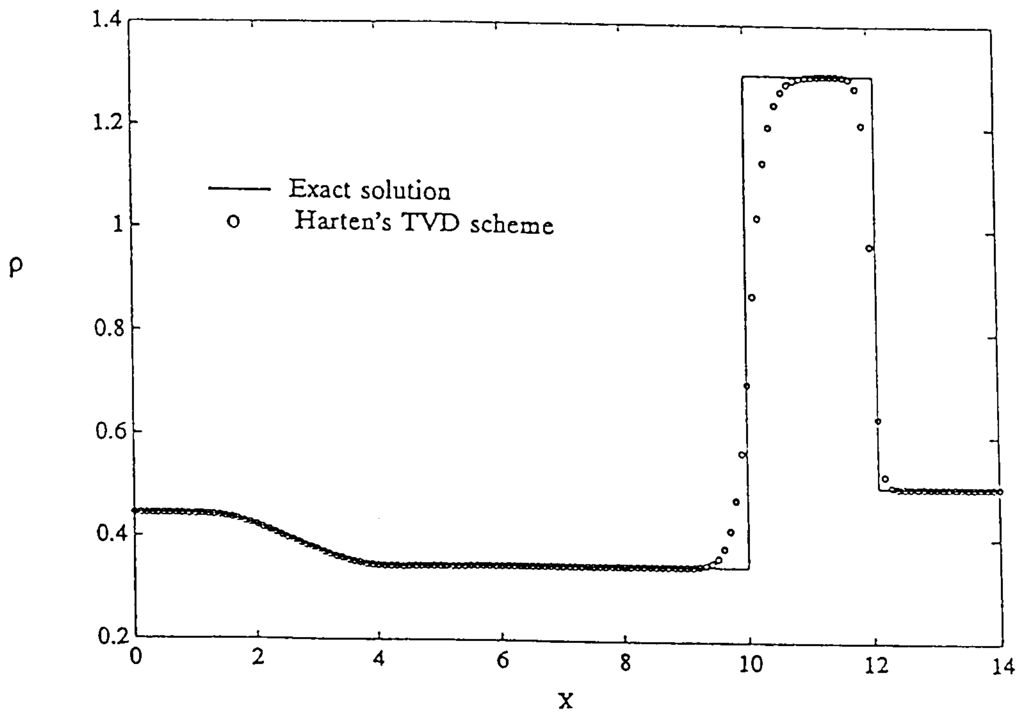

(b) Harten's TVD scheme ($\delta = 0$).

Density profiles using the simultaneous solution approach using different schemes.

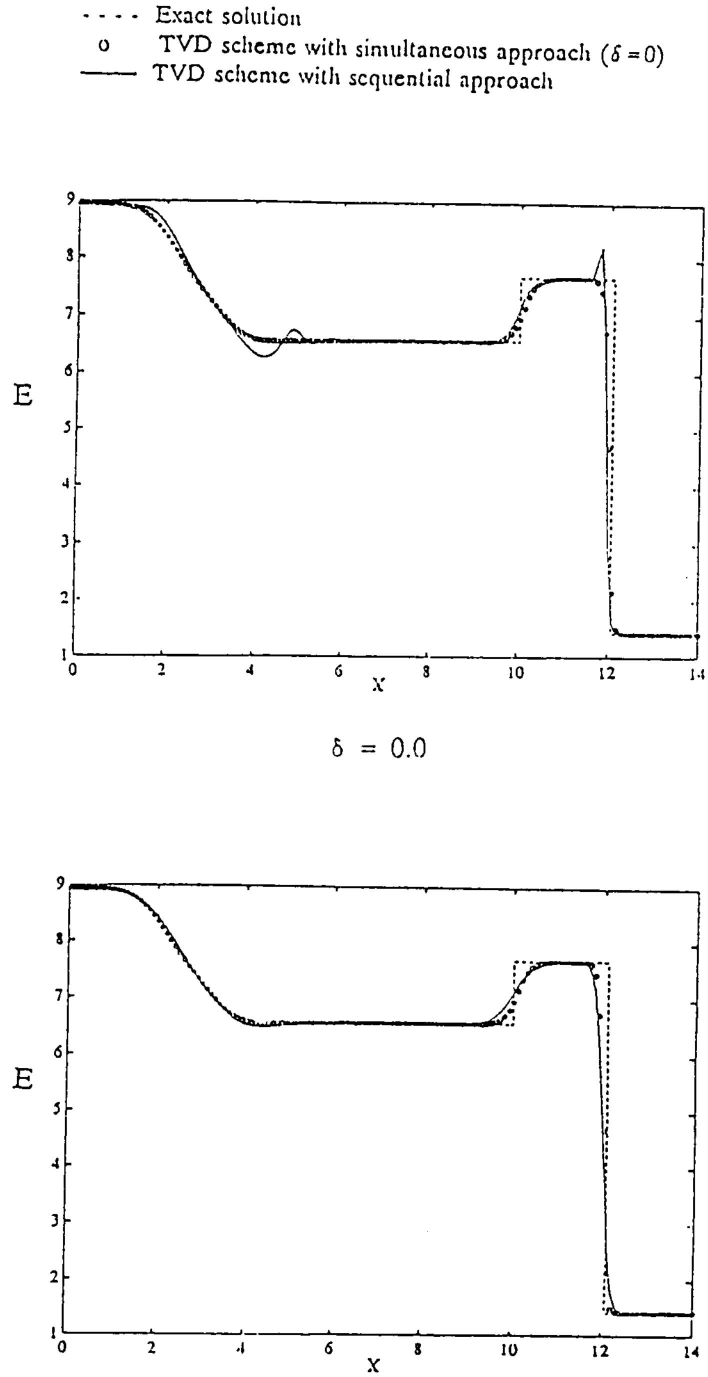

δ = 0.0

δ = 0.8

The standard shock tube (open-ended) problem: density and energy profiles using sequential approach with source term treatment, for different values of δ.

THE RESONANT PIPE PROBLEM

SIMULTANEOUS SOLVER

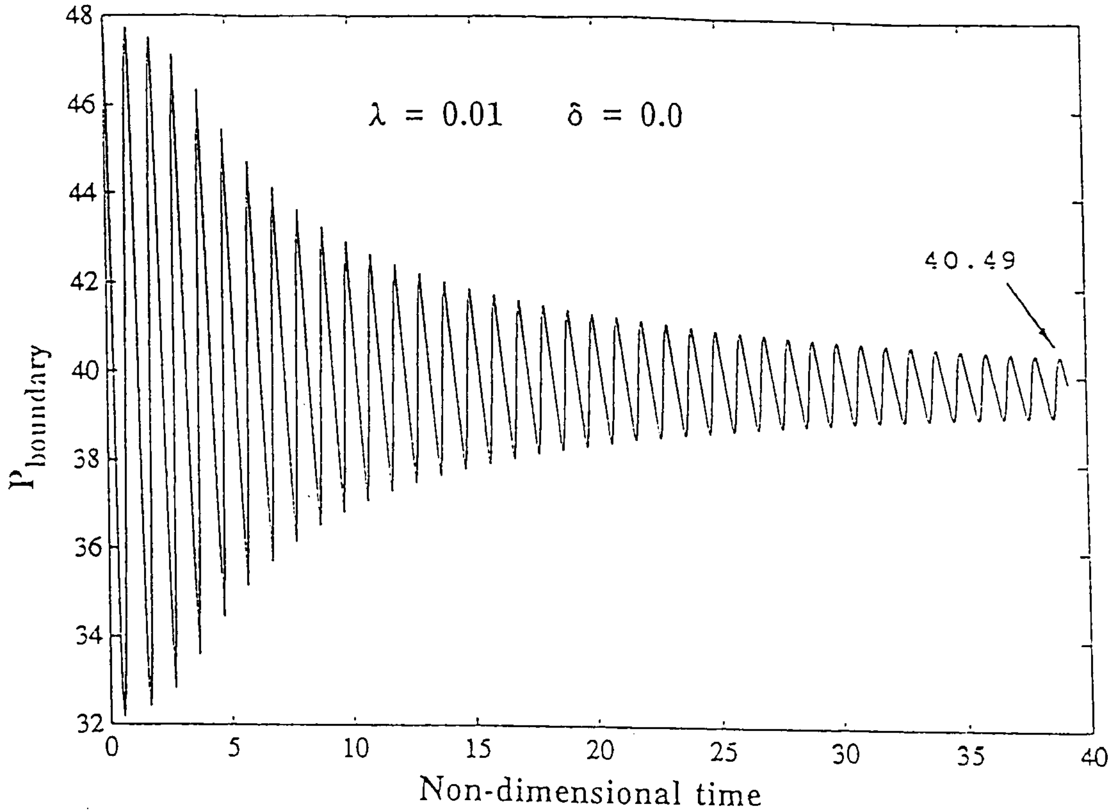

SEQUENTIAL SOLVER

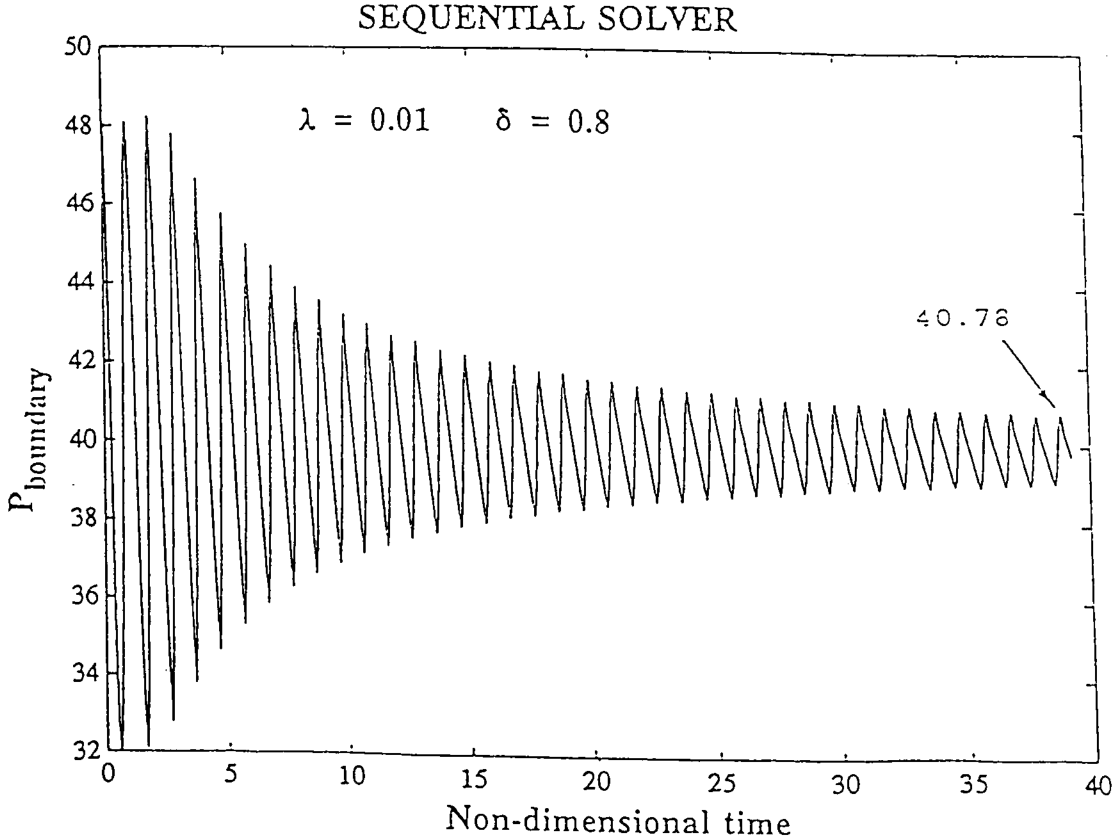

Conclusions

- For sequential solvers, coordination of propagation speed among equations requires extra care.
- Can apply modern TVD type schemes with source term treatment to improve accuracy.
- Can utilize nonlinear filtering techniques to eliminate dispersion problems.
- Several test problems have been investigated; results show promise.

*U.S. GOVERNMENT PRINTING OFFICE: 1992-627-150/60005

REPORT DOCUMENTATION PAGE

Form Approved
OMB No. 0704-0188

1. AGENCY USE ONLY *(Leave blank)*

2. REPORT DATE
July 1992

3. REPORT TYPE AND DATES COVERED
Conference Publication

4. TITLE AND SUBTITLE
Tenth Workshop for Computational Fluid Dynamic Applications in Rocket Propulsion

5. FUNDING NUMBERS

6. AUTHOR(S)
R.W. Williams, Compiler

7. PERFORMING ORGANIZATION NAME(S) AND ADDRESS(ES)
George C. Marshall Space Flight Center
Marshall Space Flight Center, Alabama 35812

8. PERFORMING ORGANIZATION REPORT NUMBER
M-693

9. SPONSORING/MONITORING AGENCY NAME(S) AND ADDRESS(ES)
National Aeronautics and Space Administration
Washington, DC 20546

10. SPONSORING/MONITORING AGENCY REPORT NUMBER
NASA CP-3163, Part 2

11. SUPPLEMENTARY NOTES
Prepared by Structures and Dynamics Laboratory, Science and Engineering Directorate

12a. DISTRIBUTION/AVAILABILITY STATEMENT
Subject Category: 34
Unclassified—Unlimited

12b. DISTRIBUTION CODE

13. ABSTRACT *(Maximum 200 words)*

Conference publication includes 59 abstracts and presentations and three invited presentations given at the Tenth Workshop for Computational Fluid Dynamic Applications in Rocket Propulsion held at George C. Marshall Space Flight Center, April 28–30, 1992. The purpose of the workshop is to discuss experimental and computational fluid dynamic activities in rocket propulsion. The workshop is an open meeting for government, industry, and academia. A broad number of topics are discussed including computational fluid dynamic methodology, liquid and solid rocket propulsion, turbomachinery, combustion, heat transfer, and grid generation.

14. SUBJECT TERMS
Computational Fluid Dynamics, Rocket Propulsion, Liquid Rocket, Solid Rocket, Turbopump, Turbomachinery, Combustion, Methodology, Impeller, Inducer, Heat Transfer, Grid Generation, Nozzle, Plume, Spray, Injector

15. NUMBER OF PAGES
768

16. PRICE CODE
A99

17. SECURITY CLASSIFICATION OF REPORT	18. SECURITY CLASSIFICATION OF THIS PAGE	19. SECURITY CLASSIFICATION OF ABSTRACT	20. LIMITATION OF ABSTRACT
Unclassified	Unclassified	Unclassified	Unlimited